Terms and Conditions of Use of Digitised Theses from Trinity College Library Dublin

Copyright statement

All material supplied by Trinity College Library is protected by copyright (under the Copyright and Related Rights Act, 2000 as amended) and other relevant Intellectual Property Rights. By accessing and using a Digitised Thesis from Trinity College Library you acknowledge that all Intellectual Property Rights in any Works supplied are the sole and exclusive property of the copyright and/or other IPR holder. Specific copyright holders may not be explicitly identified. Use of materials from other sources within a thesis should not be construed as a claim over them.

A non-exclusive, non-transferable licence is hereby granted to those using or reproducing, in whole or in part, the material for valid purposes, providing the copyright owners are acknowledged using the normal conventions. Where specific permission to use material is required, this is identified and such permission must be sought from the copyright holder or agency cited.

Liability statement

By using a Digitised Thesis, I accept that Trinity College Dublin bears no legal responsibility for the accuracy, legality or comprehensiveness of materials contained within the thesis, and that Trinity College Dublin accepts no liability for indirect, consequential, or incidental, damages or losses arising from use of the thesis for whatever reason. Information located in a thesis may be subject to specific use constraints, details of which may not be explicitly described. It is the responsibility of potential and actual users to be aware of such constraints and to abide by them. By making use of material from a digitised thesis, you accept these copyright and disclaimer provisions. Where it is brought to the attention of Trinity College Library that there may be a breach of copyright or other restraint, it is the policy to withdraw or take down access to a thesis while the issue is being resolved.

Access Agreement

By using a Digitised Thesis from Trinity College Library you are bound by the following Terms & Conditions. Please read them carefully.

I have read and I understand the following statement: All material supplied via a Digitised Thesis from Trinity College Library is protected by copyright and other intellectual property rights, and duplication or sale of all or part of any of a thesis is not permitted, except that material may be duplicated by you for your research use or for educational purposes in electronic or print form providing the copyright owners are acknowledged using the normal conventions. You must obtain permission for any other use. Electronic or print copies may not be offered, whether for sale or otherwise to anyone. This copy has been supplied on the understanding that it is copyright material and that no quotation from the thesis may be published without proper acknowledgement.

Design, Synthesis and Photophysical Evaluation of Novel 1,8-Naphthalimide Tröger's Base Derivatives

By

Samantha Murphy

May 2012

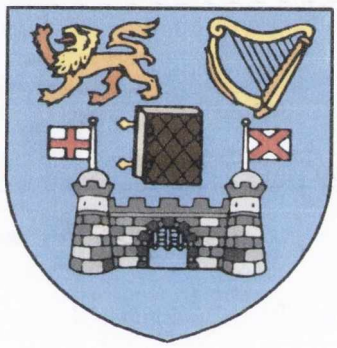

University of Dublin
Trinity College

Based on research carried out under the direction of
Prof. Thorfinnur Gunnlaugsson

A thesis submitted to the School of Chemistry, University of Dublin, Trinity College for the degree of Doctor of Philosophy

Declaration

This thesis is being submitted for the degree of Doctor of Philosophy to the University of Dublin, Trinity College and has not been submitted before for any degree or examination in this or any other University. Other than where acknowledged, all work described herein is original and carried out by the author alone. Permission is granted so that the library may lend or copy this thesis upon request. This permission covers only single copies made for study purposes, subject to normal conditions of acknowledgement.

Summary

This thesis entitled 'Design, Synthesis and Photophysical Evaluation of Novel 1,8-Naphthalimide Based Tröger's Bases' is divided into five chapters. The first chapter provides a brief description of the structure of DNA and the different modes by which molecules may interact with it. In addition, an introduction is given to the discovery and development of 1,8-naphthalimides as anti-cancer agents. Such research represents an important contribution to the design of potent therapeutic agents, some of which have even entered clinical trials. The final section of Chapter 1 reviews the properties of synthetic Tröger's bases which have found use in several areas of research including supramolecular chemistry, molecular recognition and optoelectronics to name but a few, due to the inherent and unique rigid V-shaped structure of the Tröger's base motif. Examples of such applications are reviewed in this chapter which concludes with a description of the ongoing research within the Gunnlaugsson research group and also describes the aims of the research conducted in each of the subsequent chapters.

The second chapter details the design, synthesis and photophysical evaluation of five novel bis-1,8-naphthalimides incorporating the Tröger's base structural motif. These molecules were designed as potential C_2-symmetric DNA binding agents and possess side chains that contain amino functionalities which can be protonated at physiological pH which promotes the aqueous solubility of these molecules as well as enhancing their affinity towards DNA by providing favourable electrostatic interactions with the anionic backbone of DNA. In this chapter, a determination of their p*K*a values and the existence of an ICT excited state will be presented. Following on from this, the affinity of these molecules towards DNA is investigated using absorption and emission techniques where binding constants in the range of 10^6 M^{-1} are determined, an order of magnitude higher than those of their corresponding precursors. The final section of this chapter details the results from linear and circular dichroism studies, which are carried out in order to evaluate the nature by which these molecules bind to DNA.

In chapter three the design and synthesis of amino acid based Tröger's base derivatives derived from both the 3-amino- and 4-amino-1,8-naphthalimide chromophores is presented. Several synthetic pathways are considered for the formation of such derivatives and are detailed in this chapter. Following on from this, the ICT excited state of these novel Tröger's bases is evaluated using absorption and fluorescence emission and excitation techniques providing a basis for their application as potential solvatochromic peptidomimetics.

In chapter four the design and synthesis of tetra-1,8-naphthalimide Tröger's bases is described. The solvatochromic nature of these target compounds and their corresponding precursors is preliminarily investigated and described herein. In the final section of this chapter the preliminary spectroscopic studies investigating the potential of these Tröger's bases to act as hosts for fullerene C_{60} is explored.

Finally, in chapter five, general experimental techniques are outlined and the synthesis and characterisation of each of the compounds discussed is given. Subsequently, literature references are provided and are followed by the appendices which provide spectroscopic and titration data to support the work described in the main text.

For My Family

Acknowledgements

Firstly, I would like to take this moment to formally thank my supervisor Thorri for introducing me to a new world of chemistry in his lab and for his constant support, encouragement and guidance over the last four and a half years.

A huge thank you goes to all the members of the TG group both past and present- Aline, Brian, Celia, Christophe, Cidalia, Danni, Dave, Doireann, Elaine, Esther, Fergus, Gary, Jen, Joe, Komala, Laura, Niamh, Oxana, Rebecca and Rob for all the good times shared. I wish to thank Jon for all his help with the crystal structure data and Steve for all the helpful discussions, jokes and for all his swiss chocolate! A big thank you must go to Emma, Miguel, Swagata and Dawn for all the proof reading, it was really appreciated.

I wish to thank the Rozas group, Aoife, Brendan, Elena, Julian, Daniel and Paddy for all the good times shared in and outside the lab. A special thank you to Caitriona for her support and advice and for always being there for a chat.

A huge thank you must go to Amila who I have been in college with since 2003! So thanks for all the good times, the natters down the back of the lab and all the coffee breaks! Also, I especially want to thank you for all the support and encouragement over the last few months, it was invaluable. I miss not seeing you every day!

I would like to thank Dr. John O' Brien for all he has done for me over the past four and a half years and for his endless patience! Thanks must also go to Dr. Manuel Ruether for all the assistance with the NMR and for letting me skip the queues! Thank you to Dr. Martin Feeney for all the assistance with the mass spectroscopy and Dr. Tom McCabe for getting all the crystal structures. I also wish to thank Mr. Fred Cowzer for all his help and for always changing the nitrogen cylinders even when it was out of hours! A thank you also goes to the technicians Brendan, Peggy, Theresa and Dorothy as well as the secretaries Tess and Helen.

I wish to thank my future in-laws, Deirdre, Kieran, Niamh and Darragh for all their support and encouragement over the past few years, it has been well appreciated.

The biggest thank you must go to my wonderful family especially to my parents James and Louise for all their love, support and encouragement which has been enormous. Thank you to my sisters Carla, Olivia, Ashley, Nicole and Sophia for all the positive talks and encouragement and for all the mad times we have had and that have yet to come! I want to thank my brothers Jordan and Darragh who always know how to make me laugh and who have kept me smiling throughout my PhD experience. Thanks to Thomas, Rob, Dave and

Natalee for all the words of encouragement, the laughs, the fun times at Sunday dinners, the card games and the nights out! A huge thank you must go to my little nephew Teegan who always knows how to put a smile on my face! I look forward to our holiday together in June! A big thank you must almost go to my Granda Eugene and all my family and friends.

Last but certainly not least, thank you Ciaran for sharing this experience with me. All your patience, love and support over the past eight years knows no end. You have been my pillar of strength and I know I could not have done this without you! Now that it is nearly over, I look forward to our future together and the good times to come.

Abbreviations

A	Adenine
AML	Acute myeloid leukemia
Ala	Alanine
app	Apparent
BOP	Benzotriazolyloxy-tris(dimethylamino)hexafluorophosphate
br. s	Broad Singlet
BSA	Bovine serum albumin
C	Cytosine
CNS	Central nervous system
CD	Circular dichroism
CHO	Chinese hamster ovary (cells)
ct	Calf thymus
DCC	*N*, *N'*-Dicyclohexylcarbodiimide
DCM	Dichloromethane
DIEA	*N*,*N*-Diisopropylethyl amine
d	Doublet
dd	Double doublet
DMF	*N*, *N*-Dimethylformamide
DNA	Deoxyribonucleic Acid
EDCI.HCl	*N*-(3-Dimethylaminopropyl)-*N'*-ethylcarbodiimide hydrochloride
eq.	Equivalent
δ	Chemical Shift
G	Guanine
Gly	Glycine
HATU	*O*-(7-Azabenzotriazol-1-yl)-1,1,3,3-tetramethyluronium tetrafluoroborate
HOBt	1-Hydroxybenzatriazole
HMBC	Heteronuclear multiple bond correlation spectrum

HMPA	Hexamethylphosphoramide
HMQC	Heteronuclear multiple quantum coherence spectrum
HPLC	High performance liquid chromatography
HRMS	High resolution mass spectroscopy
HSA	Human serum albumin
ICP	Infinite co-ordination polymers
ICT	Internal charge transfer
IR	Infra-red
J	Coupling constant
Leu	Leucne
LD	Linear Dichroism
LMP	Lysosomal membrane permeabilisation
m	Multiplet
m.p	Melting point
MLCT	Metal to ligand charge transfer
m/z	Mass charge ratio
NAT	*N*-acetyl transferase
NMR	Nuclear magnetic resonance
P/D	Phosphate to dye ratio
Pd/C	Palladium on carbon
ppm	Parts per million
Phe	Phenylalanine
PAT	Poly amine transporter
PBD	Pyrrolo[2,1-c]benzodiazepine
q	Quartet
RT	Room temperature
s	Singlet
t	Triplet

TAP	1,4,5,8-tetraazaphenanthrene
TBTU	*O*-(benzotriazole-1-yl)-1,1,3,3-tetramethyluronium tetrafluoroborate
TEA	Triethylamine
tert	Tertiary
TFA	Trifluoroacetic Acid
T	Thymine
UV	Ultraviolet
Val	Valine
Vis	Visible

Contents

Chapter 1: Introduction

1.1 Preface

The 1,8-naphthalimide structure is a very versatile building block due to its unique photophysical properties and has found application in many areas of chemistry, particularly in the fields of supramolecular and medicinal chemistry.[1,2] The absorption and fluorescence emission spectra of the naphthalimide structure lie within the ultraviolet (UV) and visible (Vis) regions and the photophysical properties can be altered, modulated and fine tuned through facile structural design.[1] Synthetic modifications on either the aromatic ''naphthalene'' group or at the *N*-imide position are possible, allowing for a diverse range of functional groups and structural designs to be incorporated and because of this the 1,8-naphthalimide core has been extensively employed within the dye industry,[3] in the construction of novel therapeutics[2] and in the design of chemical probes,[4] to name just a few applications. Furthermore, the versatility of the 1,8-naphthalimide chromophore extends to colorimetric and fluorescent anion sensing and in the last number of years many examples of naphthalimide based anion sensors have been developed, particularly by researchers such as Tian,[5] Gunnlaugsson[1,6] and Callan.[7] Many others have also explored this field, for instance by conjugating the 1,8-naphthalimide chromophore to known anion recognition moieties either directly or *via* a short covalent spacer.[8,9] In addition, the naphthalimide structure can be tailored to bind to DNA and has played a major role in anti-cancer research.[2] However, this area has been hampered due to the excessive toxicities and lack of selectivity associated with the naphthalimide family.[2]

In this thesis, three approaches have been undertaken to extend the utility of the 1,8-naphthalimide series. Firstly, in order to address the lack of selectivity in targeting specific regions within the DNA structure, a family of bis-1,8-naphthalimides incorporating a unique V-shaped Tröger's base structural motif was investigated. The second area of this thesis deals with incorporating additional chiral centres into the molecular design by developing amino acid based Tröger's bases as potential peptidomimetics. To exploit the unique shape of the Tröger's base structural motif further, the final area of this thesis explored the preliminary design and photophysical investigation of tetra-naphthalimide based Tröger's base derivatives as fullerene C_{60} sensors.

In this introductory chapter, the various topics to be discussed in this thesis will be introduced. Firstly, a description on the structure of DNA and the factors governing its recognition will be given. This will be followed by a discussion on the design and development of 1,8-naphthalimides as cytotoxic agents. The remainder of this chapter will

then deal with a review on the properties and applications of synthetic Tröger's base derivatives.

1.2 DNA Structure and Recognition

DNA is viewed as the central macro-molecule of molecular biology. It is a class of nucleic acid that is encoded with the information that programs all the cells activities, plays a vital role in the transmission, expression and conservation of genetic information and has proved to be essential in the understanding of the processes of mutation/carcinogenesis, drug action and therapeutics.[10] The entire human genome contains 3.2 giga bases of information stored in such a way that it can be passed on from one generation to the next thereby, highlighting the intimate relationship between DNA structure and function.[11]

DNA is a linear biopolymer, composed of two strands running in opposite directions coiled around a common axis to form a double stranded helix. This orientation gives rise to a chiral molecule with distinctive large and small grooves on its exterior surface, termed major and minor grooves, respectively. Each strand consists of a large number of chemical units called nucleotides linked together to form a chain. A nucleotide is composed of three units: a sugar molecule called deoxyribose, a negatively charged phosphate group and one of four different heterocyclic bases divided into two types: the purines – *adenine* (*A*) and *guanine* (*G*) and the pyrimidines – *cytosine* (*C*) and *thymine* (*T*). The nitrogen and oxygen atoms of each base act as hydrogen bond acceptors and donors which allows for two types of specific interaction. The first type is Watson-Crick base pairing which consists of hydrogen bonding between bases on different chains, *guanine* pairs with *cytosine* through three hydrogen bonds and *adenine* with *thymine* through two such bonds. This arrangement is essential to maintaining the specificity of base pairing in DNA as these base pairs provide all the genetic information needed to carry out the cells activities, including the replication of genetic material. These specific hydrogen bonds, although quite weak, collectively stabilise the double helix because of their large numbers in a DNA molecule. As the bases in a DNA molecule are stacked one on top of the other, this extensive stacking results in hydrophobic forces that are the primary means by which the helix is stabilised.[12]

The second kind of specific interaction is Hoogsteen base pairing which occurs with the functional groups that protrude into the major groove, as depicted in Figure 1.1. This type of base pairing is significant for triple helices formation.[13]

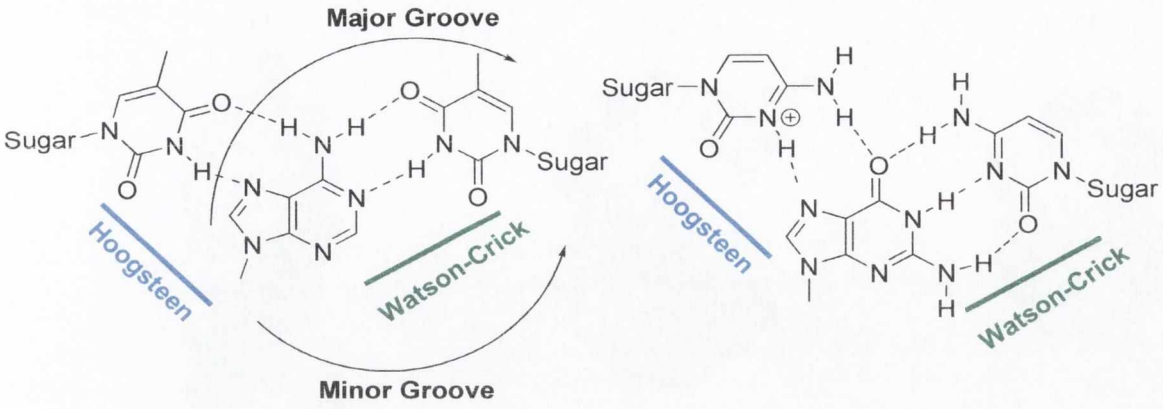

Figure 1.1: *Structures of the DNA bases showing the Watson-Crick and Hoogsteen base pairs and the position of the grooves.*

The configuration of DNA remains constant, whereas, the conformation is dynamic and is highly dependent upon environmental factors such as temperature, pH, salt concentration and humidity.[14] The vast majority of naturally occurring DNA is in the B-form with the Na^+ alkali metal counter ion at a relative humidity of 92%. The structure of B-DNA was elucidated by Watson and Crick to be right handed with the glycosidic bonds in the *anti*-conformation.[15] The ribose sugar units are C2'-endo puckered. This gives a structure with ten base pairs per helix turn, a pitch of 3.4 nm and the formation of a wide major groove and narrow minor groove, both of similar depth. When the relative humidity is reduced to 75%, B-DNA undergoes a reversible conformational change to the right handed A-form and its base pairs are more tilted than perpendicular to the helix axis, resulting in the structure being more compact. This results in the presence of a hole through the centre of the helix, a deep major groove and a very shallow minor groove.[16] The third conformation is Z-DNA which is a left-handed double helix held together by Watson-Crick base pairing. The double helix consists of sequences of alternating pyrimidines and purines with the phosphate backbone having a zigzag appearance. A high salt concentration is required to minimise electrostatic repulsion between the backbone phosphates which are in closer proximity to each other than in A- and B-DNA. The major groove is flat and inaccessible, whereas, the minor groove is deep and narrow.[17] Although the biological role of Z-DNA is still under investigation, Rich *et al.*[18] have shown that the junction of a DNA segment stabilised in the Z-conformation at one end while the other end remains B-DNA containing extruded bases that may act as potential sites for DNA modification. The structural features discussed are depicted in Figure 1.2 and summarised in Table 1.1.

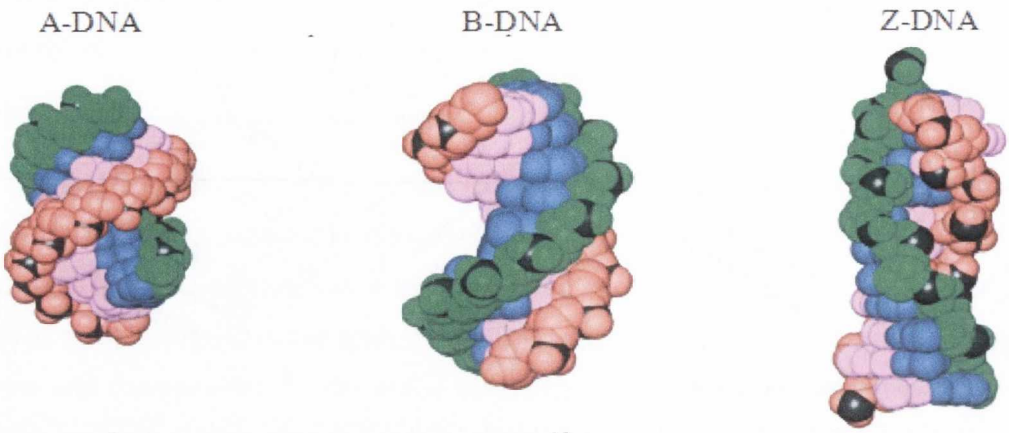

Figure 1.2: *Structutes of A-, B- and Z-DNA.*[13]

Table 1.1: *Structural features of A-, B- and Z-DNA conformations.*[17]

	A-DNA	B-DNA	Z-DNA
Helical sense	Right-handed	Right-handed	Left-handed
Glycosidic Bond	*Anti*	*Anti*	*Anti* for pyrimidines *Syn* for purines
Minor Groove	Wide and shallow	Narrow and deep	Narrow and deep
Major Groove	Narrow and deep	Wide and deep	Flat
Base pairs per helical turn	11.6	10	12 (6 dimers)
Pitch per turn of helix	34 Å	34 Å	44 Å
Base tilt to helix axis	20°	6°	7°
Sugar pucker	C3′ endo	C2′ endo	C2′endo (pyrimidines) C3′ endo (purines)
Helix diameter	~ 26 Å	~20 Å	~ 18 Å
Rise per base pair	2.9 Å	3.4 Å	7.4 Å (per dimer)
Helical twist per base pair	31°	36°	9° for pyrimidine-purine step 51° for purine-pyrimidine step

The presence of DNA in living cells and its association with a vast amount of life processes has lead to DNA being recognised as a valuable target for the development of novel drug therapies. However, DNA is a complex drug design target. In humans, a unique DNA sequence consists of 15-16 bases which can only be read from the exterior of the helical structure, four from the major groove and two from the minor groove, thus, a reading molecule with high specificity must be large and have a unique shape to read the bases. Such molecules are large proteins and complimentary strands of DNA or RNA.[19] Smaller

molecules with less complex shapes have dominated a considerable amount of research, however, the drawback here is the lack of specificity and high toxicity, thus, the challenge of designing small specific DNA interactive molecules remains an integral part of current drug design.[20,21]

Drug-DNA interactions can be categorised as the following; **(a)** minor groove binding, **(b)** major groove binding, **(c)** electrostatic binding, **(d)** covalent attachment and **(e)** intercalation. The grooves are a very important facet of DNA structure as the grooves expose the edges of bases providing sites where molecules can interact with DNA. Molecules may be designed to bind in either the minor or major groove, making use of the differences in electrostatic potential, hydrogen bonding characteristics, steric effects and hydration between the two.[22] Minor groove binders are positively charged molecules that contain linked rather than fused aromatic/hetero-aromatic rings that typically bind the *A·T* region displacing the 'spine of hydration' and causing little distortion to the DNA backbone. Van der Waals and hydrophobic interactions with the grooves play a significant role in the overall stability upon ligand binding, whereas, directed hydrogen bonding is responsible for ensuring binding to particular sites and sequences. Their crescent shape complements the convex surface of the minor groove in a process known as '*isohelicity*'. The combination of these features has given rise to the preferential binding of important minor groove binders such as the natural products netropsin **1** and distamycin A **2** which have been shown to interact with the groove through hydrogen bonding. Studies on this class of compound has lead to the development of synthetic polyamides containing pyrrole and imidazole groups that target DNA sequences with high affinity and specificity which can be directed through appropriate design.[22,23]

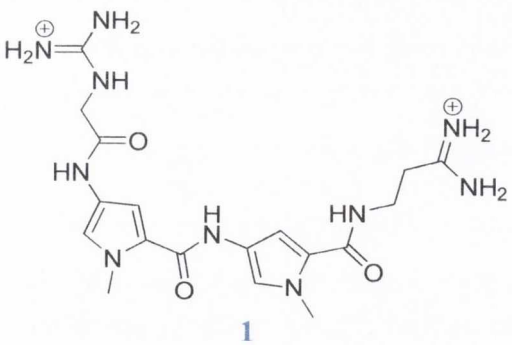

1

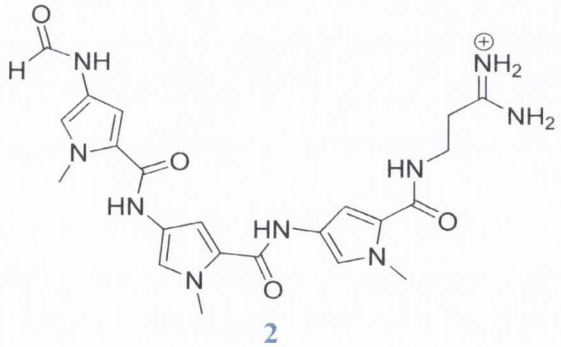

2

Due to their smaller size synthetic molecules tend to bind in the minor groove of DNA and thus, there are few proven cases of major groove binding. One such molecule that targets the major groove is methyl green **3**.[24] A more complex example of a major groove binder comes in the form of the phenothiazinium dye, methylene blue **4**. At low binding ratios with

[poly (dA-dT)]$_2$ methylene blue binds *via* intercalation, whereas, in the case of [poly (dG-dC)]$_2$ and natural DNA a fraction of bound dye will occupy the major groove and this fraction grows with increasing ionic strength.[25,26]

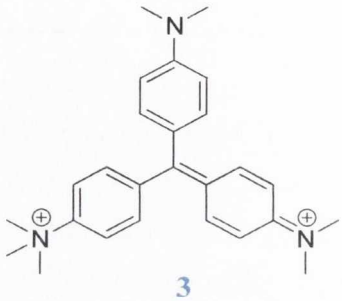

3

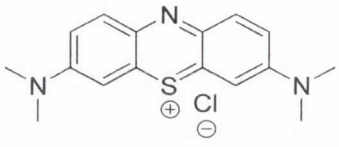

4

Proteins frequently accomplish DNA sequence recognition in the major groove by forming specific hydrogen bonds to the edges of the base pairs. This sequence recognition is possible because of the size of the groove and the greater number and variation in pattern of hydrogen bond donor and acceptor units to which the protein can bind. Particular successes have been achieved with helix-turn-helix structures, zinc fingers and leucine zippers.[12,22] Oligonucleotides and peptide nucleic acids are also capable of major groove recognition which is achieved through Hoogsteen binding leading to the formation of triple stranded DNA, known as triplex DNA. Such recognition is sequence specific and triplex formation has been used to regulate gene expression.[27]

The sugar phosphate backbone is another potential target on the DNA helix due to its hard oxygen rich poly-anion surface which has the ability to interact with group I and II alkali cations.[20] Such electrostatic binding molecules include the natural polyamines spermine and spermidine.[22] For instance, the interaction of a tri-nuclear Pt (II) compound with DNA was evaluated and found to form multiple hydrogen bonds with the phosphate oxygens. The complex can either track along the phosphate backbone or stretch across the minor groove making contacts with the phosphate backbones on either side.[28]

Another important DNA binding mode is covalent attachment through nucleophillic reactions. The first DNA-interactive anti-cancer drugs to be developed were the alkylating nitrogen mustards which were highly toxic. Analogues such as chlorambucil (Leukeran®) **5**, *L*-phenylalanine mustard (Alkeran®) **6** and cyclophosphamide **7** were developed and still find use against some cancers.[22, 29]

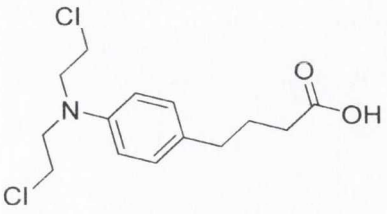

5

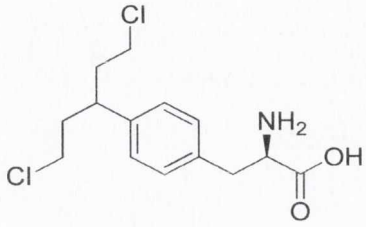

6

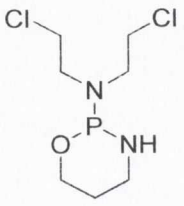

7

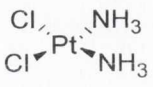

8

Metal based anti-cancer drugs such as cisplatin **8** and its analogues also fall into this category. Cisplatin binds mostly to purines, the *N*7 position of guanine in particular and forms covalent strand cross links which interfere with the normal function of DNA within cells and ultimately lead to cell death.[30]

Intercalators are molecules that insert perpendicularly into DNA without the formation of covalent bonds. The intercalation hypothesis was first proposed by Lerman,[31] a process which results in the separation of base pairs with a lengthening and unwinding of the double helix. The forces involved that stabilise DNA-intercalator complexes are van der Waals, hydrogen bonding, hydrophobic and/or charge transfer forces. Intercalators appear to reach saturation at a maximum of one intercalator per two base pairs. This is known as the 'neighbour exclusion principle'.[22] Classical intercalators consist solely of an intercalating chromophore which may carry a positive charge on the ring system, such as proflavine **9** and ethidium bromide **10**.

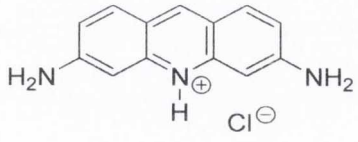

9

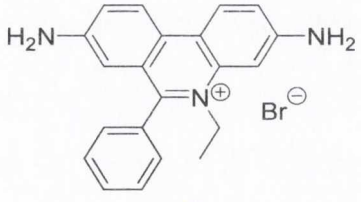

10

More complex intercalators have attached groups such as side chains, sugar rings or peptide units, including actinomycin D **11** and DACA **12**. In addition to intercalation, the cationic end of the dimethylaminoethyl side chain of **12** hydrogen bonds in the major groove , whereas in the case of **11** the peptide groups lie in the minor groove.[22]

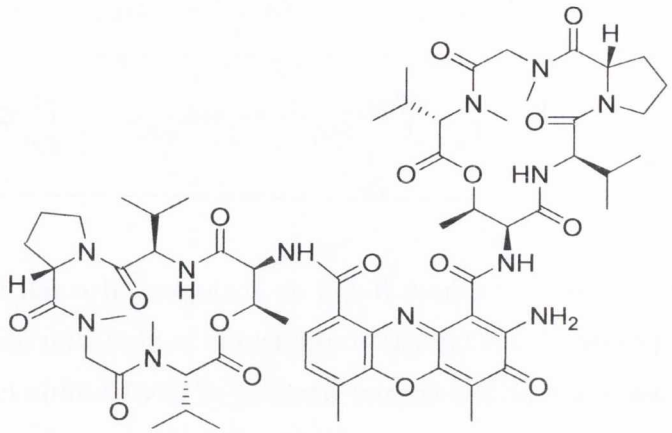

11

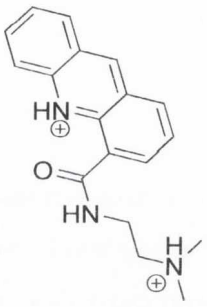

12

Threading intercalators such as naphthalene-bisimide **13** and nogalamycin **14** insert between the base pairs and contain cationic substituents directed into both the major and minor grooves of a duplex simultaneously.[22]

A further type of DNA intercalation appears through the sequence specific non-classical intercalator DAPI **15**. For instance, DAPI binds very strongly to three or more consecutive *A·T* base pairs in a minor groove complex, however, when a lesser amount of *A·T* base pairs are present and especially in pure *G·C* regions, DAPI binds *via* intercalation with binding constants comparable to well known DNA intercalators. [22]

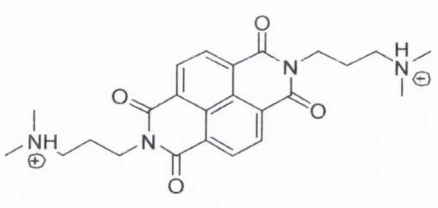

13

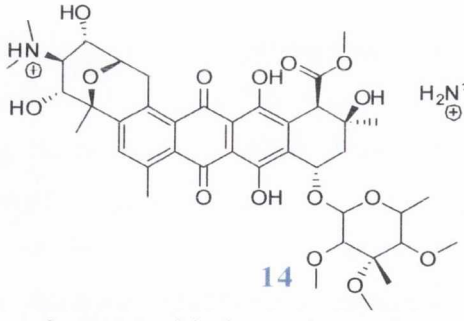

14

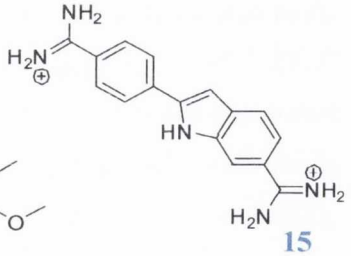

15

Among these categories of DNA binders, intercalators such as the 1,8-naphthalimides are a very important class of compounds which exhibit strong cytotoxic activity and have the potential to act as chemotherapeutic agents.

1.3 Mono-naphthalimides as Anti-Cancer Agents

The development of the naphthalimide class of anti-cancer compounds was initiated by Braña *et al.*[32] by combining structural components of several anti-tumour compounds into a single molecule: the β-nitronaphthalene of aristocholic acid, the glutarimide rings of cycloheximide and CG-603 and the basic side chain of tilorone and CG-603 as shown in Figure 1.3.

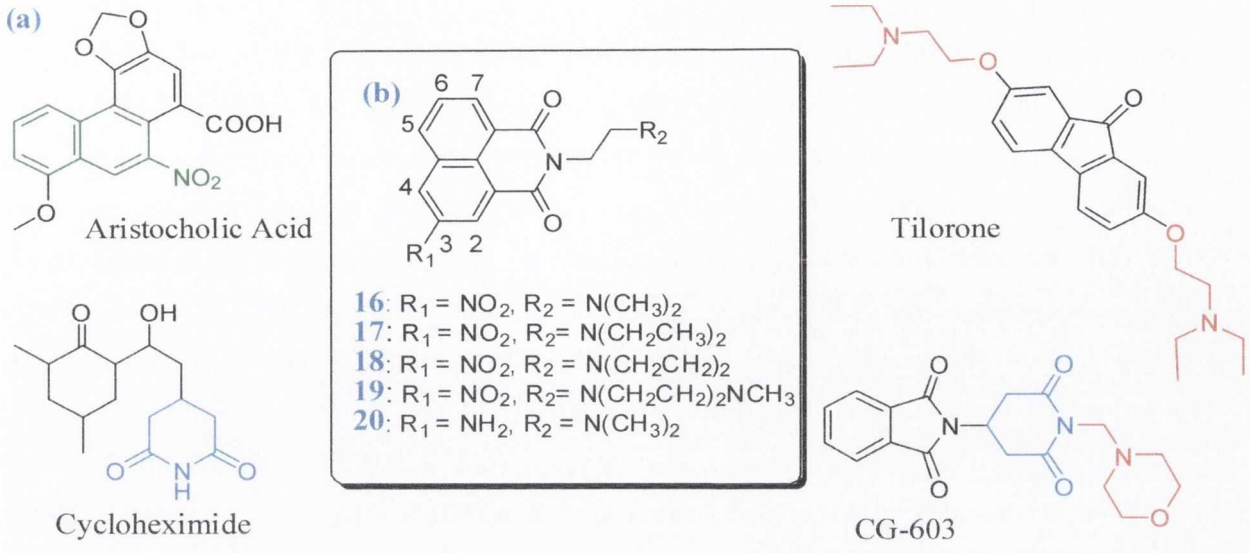

Figure 1.3: **(a)** *Cytotoxic compounds considered in the design of napthalimides.* **(b)** *Series of naphthalimides synthesised for possible anti-tumour activity.* [32]

In the beginning, Braña *et al.*[32] synthesised four different 3-nitronaphthalimides as shown in Figure 1.3, where the basic side chain was varied. These compounds were shown to possess strong cytotoxic activity and inhibit DNA synthesis. Waring *et al.*[33] further investigated the ability of compounds **16** and **17** to bind to double-helical DNA. The shifts observed in the absorption spectra, the magnitude of the binding constants, the removal and the reversal of the supercoiling of circular DNA and the increase in the length of sonicated DNA were all indicative characteristics of intercalation.

In view of the significant anti-tumour activity of these compounds, Braña *et al.*[34] synthesised a larger series of naphthalimides varying both the basic side chain and the naphthalimide ring substituent and found the following criteria essential in achieving cytotoxic activity: **(a)** the presence of a basic terminal group in the side chain, **(b)** the nitrogen atom in the basic side chain should be separated from the ring nitrogen by two methylene groups, **(c)** the terminal nitrogen should not have many substituents and **(d)** substitution should occur at position 3 on the naphthalic ring. The latter was confirmed by Wilson *et al.*[35] who synthesised a series of naphthalimides containing a 3-(dimethylamino)propyl group on the imide nitrogen and varied substituents on the naphthalimide ring and analysed the interaction of such substituted naphthalene monoimides with DNA. It was found that the 3-nitro analogue interacted more strongly with DNA in comparison to the 4-nitro derivative. It is postulated that the difference is due to steric effects, whereby, the 4-nitro substituent is rotated out of the mono-imide plane resulting in perturbed stacking in the intercalated complex.

In the Braña series, the two most active naphthalimides were found to be mitonafide **16** and amonafide **20** which exhibit IC_{50} values (concentration of a drug needed to inhibit 50% of cell growth) of 0.47 μM and 8.80 μM against HeLa cells, respectively.[2(a),36] Their binding mechanism involves intercalation of the naphthalimide chromophore to DNA with the subsequent inhibition of Topoisomerase II activity. It is thought that the side chain interacts sterically with the enzyme active site in the ternary complex.[2(b)] Mitonafide **16** has been shown to inhibit DNA synthesis and induce strand breaks in Chinese Hamster Ovary (CHO) cells.[36] This mechanism of action is different to amonafide **20** which induces single and double strand breaks in addition to producing DNA protein crosslinks through a Topoisomerase II mediated reaction.[37] Furthermore, **16** was studied in Phase I and II clinical trials but was associated with central nervous system (CNS) toxicity.[2(a)] Amonafide **20** has completed many clinical trials and at times its clinical development has been hampered by the unpredictable toxicity caused by the toxic *N*-acetyl metabolite resulting from the polymorphic enzyme *N*-acetyl transferase 2 (NAT2), which has been shown to demonstrate differential activity between individuals.[38,39] The clinical development of **20** was temporarily deferred, however, interest in this drug has re-emerged and new clinical trials are ongoing which include amonafide-*L*-malate in combination with cytarabine for the treatment of acute myeloid leukaemia (AML) and secondary AML.[40] Moreover, **20** has been developed as an NAT2 specific probe as the dysfunction of NAT2 has been associated with many diseases such as breast and cervical cancers, bladder tumours, Parkinson's disease, Behcet's disease and diabetes mellitus. This probe can detect NAT2 as low as 1 μg mL^{-1} selectively over NAT1.[41] Following the discovery of the excellent anti-tumour effects of **16** and **20** many different approaches were undertaken to improve the activity of the mono-naphthalimides.

Zee-Cheng and Cheng examined substitution on the naphthalimide ring and synthesised dinitro and diamine derivatives of **16**.[42] They found that compounds with di-substituted naphthalimide rings had increased activity both *in vitro* and *in vivo* against leukaemia and melanoma cells in comparison to the mono-substituted naphthalimides. In view of these interesting results, Braña *et al.*[43] synthesised 3-amino-6-nitronaphthalimides combining both the electron withdrawing effects of the nitro group which favours the formation of a charge transfer complex with the DNA bases and the electron donating ability of the amino group which tends to form hydrogen bonds with the sugar phosphate chain to yield compounds with higher cytotoxicity than both **16** and **20**.

In order to circumvent the toxicity associated with **20**, Kiss *et al.*[44] synthesised a series of naphthalimides by modifying the aryl amino substituent of **20** to render it less

susceptible to interaction with NAT2, by substituting it with functional groups such as amides, ureas, thioureas, imines and amines. This study showed that the lead compound **21**, is a hydrolysis product formed irreversibly without the generation of **20**. In addition, **21** displays superior *in vivo* activity compared to **20** in leukaemia and pancreatic cancer models and enhances the activity of taxol when co-administered.[45] This compound displays a different mode of action in comparison to amonafide **20**. It is a pan-antagonist of CXCL chemokine expression, can interfere *in vivo* with amino acid metabolism and has entered phase I clinical trials.[2(c),44-45]

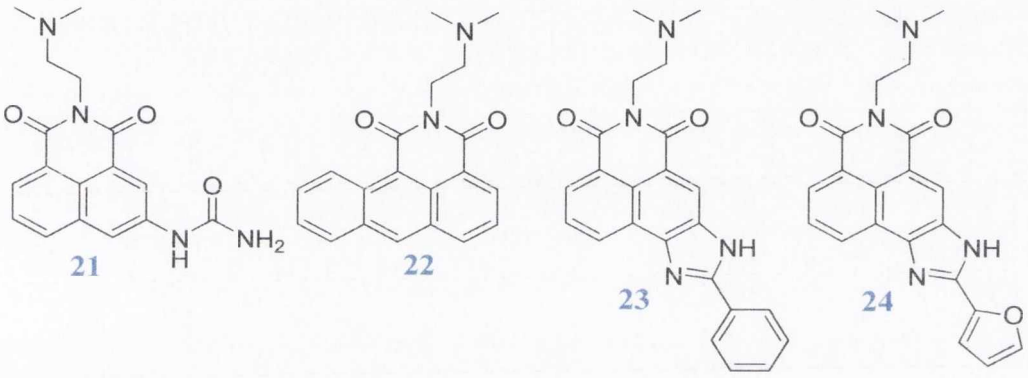

Several attempts have been made to enhance the potency of the mono-naphthalimides. An interesting approach was explored by Remers *et al.*[46] in which the naphthalene chromophore was replaced by an anthracene nucleus to give azonafide **22**. The rationale for this drug design is that formation of the toxic metabolite *N*-acetyl-amonafide will be avoided and the resulting larger chromophore will have increased affinity for DNA. This modification to the naphthalene chromophore proved to be successful as **22** was found to be more active than **20** against a panel of human colon cancer cells. In addition, the anthracene nucleus was replaced by tetrahydroanthracene, phenanthrene and azaphenanthrene moieties, but showed no improvement on the potencies of the anthracenes, highlighting that the linear chromophore is preferred for biological activity.[47]

In order to improve the binding affinity of their naphthalimides, Braña *et al.*[48-50] fused aromatic heterocycles such as imidazole, pyrazine, thiophene and furan with the naphthalene core and observed generally higher *in vitro* cytotoxicity compared to **20** against human colon, cervical and prostate carcinoma cell lines. This synthetic approach has been taken a step further whereby, intercalating agents **23** and **24**, consisting of a naphthalimide moiety fused to an imidazole ring containing an unfused aryl and heteroaryl ring respectively, have been devised to further extend the conjugated chromophore and reinforce DNA binding capacity. This alteration to the naphthalene core appeared successful as in

general, these derivatives displayed an improved cytotoxicity over amonafide **20** under the same experimental conditions.[51]

Inspired by the effect of fusing an aromatic ring to the naphthalimide skeleton Qian *et al.*[52-54] also substituted the 3-amino of the naphthyl chromphore with the introduction of a fused thiol group to yield **25**, which proved to be more cytotoxic than the parent compound **20** with reduced toxicity and equal efficacy in multi-drug resistant cell lines.

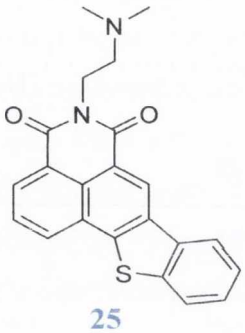

25

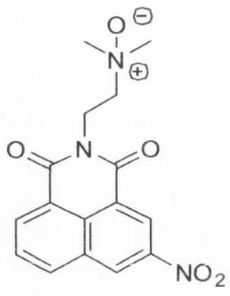

26

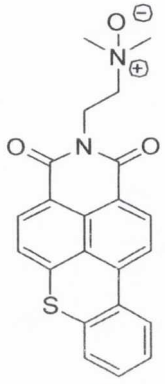

27

This family also consists of the 6-membered thio-analogue, which demonstrated superior cytotoxicty to **20** and also revealed highly efficient DNA photocleavage at a concentration of 50-100 μM on irradiation with visible light at 450 nm.[55] Moreover, further series of heterocyclic fused naphthalimides have been synthesised such as phenazine, thiazole and triazole derivatives which act as intercalative DNA photocleaving agents.[56-61]

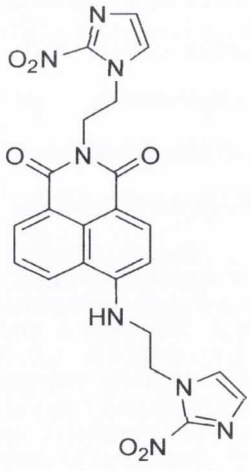

28

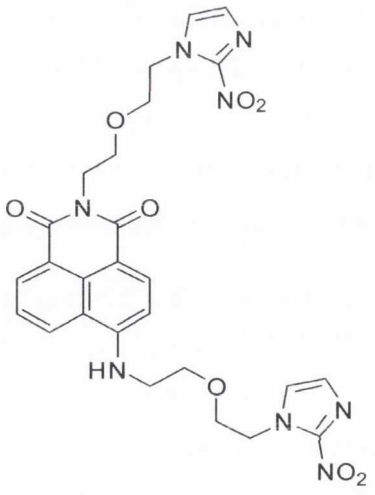

29

In view of the promising biological activity of such naphthalimides, Qian *et al.*[62] synthesised *N*-oxide derivatives such as **26** and **27** as prodrugs against hypoxic solid tumours.

These studies showed that their binding abilities to *ct*-DNA and cytotoxic activities in oxic A375 cell cultures were lower than those of the corresponding amines. However, they proved to be more cytotoxic in hypoxic cell cultures and the results indicated that the N-O group could be bio-reduced to the corresponding amine and lead to the localisation of the active cytotoxins in hypoxic cells. In addition, the bio-reductive efficiency was low in cell and limited by solubility. Other fluorescent markers for hypoxic cells such as **28** and **29** were synthesised containing two 2-nitroimidazole side chains for bio-reductive binding and were found to exhibit high differential fluorescence between hypoxic and oxic V79 cells *in vitro* with **29** showing promising activity in CHO and 95D cells.[63]

In the course of screening for novel anti-cancer compounds, a novel amonafide analogue was generated as a new anti-cancer candidate in the form of **30** which is capable of inducing cell cycle arrest and apoptosis in HL-60, HeLa and MCF-7 cell lines while having a lesser cytotoxic effect on normal cells.[64-66]

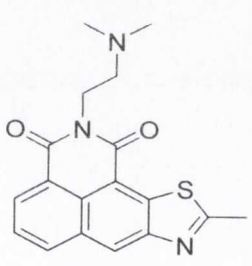

30

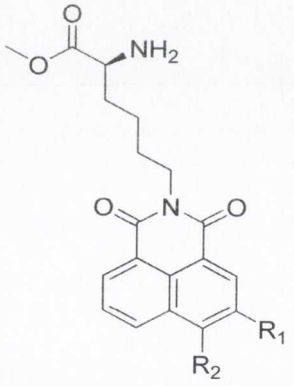

31: $R_1 = R_2 = H$

32: $R_1 = NO_2$, $R_2 = H$

33: $R_1 = H$, $R_2 = NO_2$

Further endeavours to improve the biological activity of naphthalimides have involved incorporating amino acids and polyamines into the core structure. Saito *et al.*[67] reported novel water soluble *L*-lysine derivatives **31-33** possessing a naphthalimide core responsible for inducing efficient and highly sequence selective cleavage of double stranded DNA upon photoirradiation at 320-380 nm. These compounds were investigated for their DNA cleaving properties using supercoiled pBR322 DNA. In each case upon photoirradiation at 0 °C for one hour, single strand and a small amount of double strand breaks were observed at 10 μM drug concentration. This study revealed that lysine derivative **31** induced highly specific DNA cleavage at the 5′ side of 5′-*GG*-3′ steps with a very weak cleavage at the 5′ side of 5′-*GA*-3′ steps after piperidine treatment. However, under the same experimental conditions, it was found that the 3-nitro derivative **32** photonicked the double stranded DNA preferentially at *T* residues, whereas, in the case of the 4-nitro analogue **33**, both 5′-*GG*-3′ and *T* cleavage occurred to an equal extent, thus, by

simply changing the substitution pattern of the naphthalimide ring, the sequence selectivity of the DNA cleavage could be altered.

A further approach involved introducing leucine aryl amine side chains to the sulphur substituted naphthalimide scaffold generating compounds **34**-**36**, which exhibited exclusive anti-tumour activity against the MCF-7 cell line.[68]

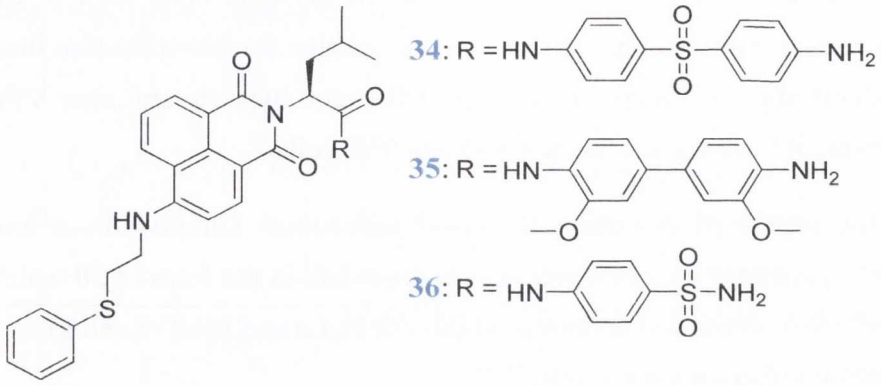

In addition, naphthalimides conjugated to polyamines were designed to harness the active Poly Amine Transporter (PAT) for drug delivery, which has been shown to be beneficial for cancer cell selectivity.[69] This study by Tian *et al.*[70] showed that tri-amine conjugates such as **37** display selectivity for cancer cells over normal cells leading to the conclusion that the PAT mediated process is favourable as cancer cells are associated with increased levels of the transporter. Moreover, the chiral configuration of amino side chains has been revealed to be significant in determining DNA binding activities. For instance, racemic, *R*- and *S*-enantiomers of heterocyclic fused naphthalimides bearing *N*-ethyl-2-(aminomethyl) pyrrolidine side chains were investigated and shown to behave quite differently in terms of cytotoxicity against different cell lines.[71]

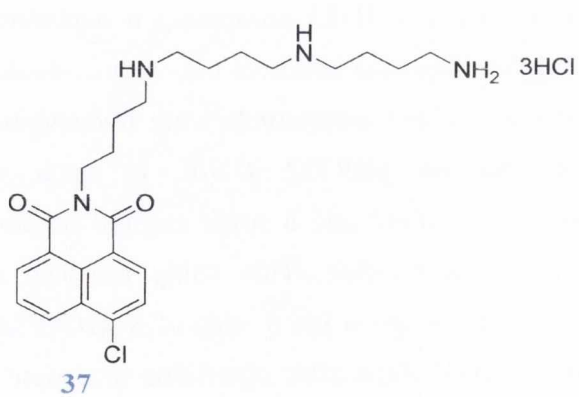

37

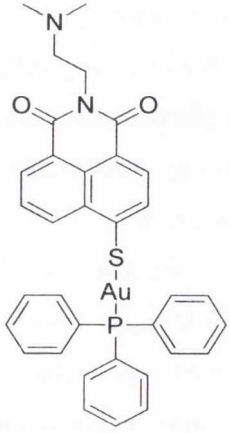

38

Another strategy that has proven successful in yielding systems that possess strong anti-proliferative effects is the synthesis of metallo-drugs such as gold (I) phosphine complexes containing a thio-naphthalimide ligand. For example, **38**, displayed strong cell growth inhibiting potencies in MCF-7 and HT-29 cells, stronger uptake by tumour cells, as well as, enhanced accumulation of gold in the nuclei compared to the naphthalimide free analogue. Furthermore, **38**, was shown to inhibit both angiogenesis in developing zebrafish embryos and tumour-cell induced angiogenesis as a consequence of the presence of the thio-naphthalimide ligand.[72]

So far, the prime efforts have been directed at increasing the binding capacity to DNA, however, no attempts have been made to link the naphthalimides with known minor groove binding agents, such as distamycin **2** or netropsin **1**. On account of this, Gupta *et al.*[73] synthesised and evaluated DNA-directed alkylating agents consisting of naphthalimide, nitrogen mustard and lexitropsin moieties. The results indicated that naphthalimide mustards lacking a lexitropsin group have greater alkylating potential than the lexitropsin bearing compounds. The presence of the lexitropsin group neither enhanced sequence specificity nor increased cytostatic activity.

Following on from this work, many hybrid molecules have been designed and synthesised, including coumarin based naphthalimdes which were evaluated against lung, breast, oral and prostate cancers, with **39** exhibiting cytotoxic activity with IC_{50} values ranging from 0.19 to 31 μM against a broad panel of tumour cell lines.[74]

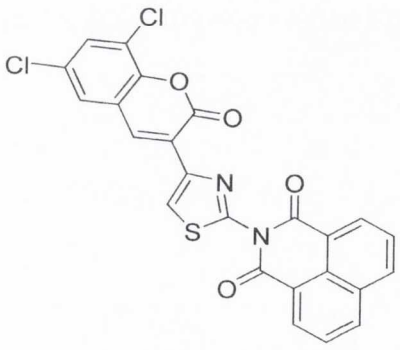

39

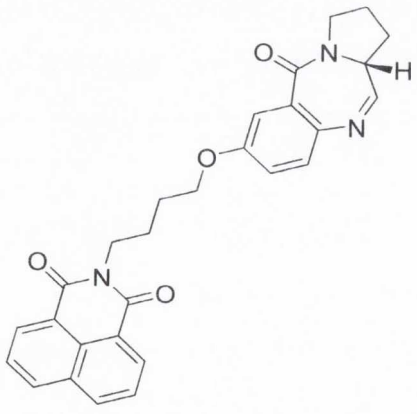

40

Other approaches include incorporating the naturally occurring anti-tumour antibiotic pyrrolo[2,1-c][1,4]benzodiazepine (PBD) family into the design as for molecule **40**. These new conjugates bound DNA *via* intercalation and minor groove interactions. They displayed

cytotoxic activity against a number of cell lines relative to the type of spacer employed to link the two pharmacophores together.[75-79]

Cholody *et al.*[80,81] investigated a series of unsymmetrical bi-functional anti-tumour agents, accomplished by linking an imidazoacridone moiety to the naphthalimide core to give **41**. This compound interacts with DNA *via* intercalation and minor groove binding and has been shown to induce apoptosis in sensitive cells *in vitro* at low nanomolar concentrations. Furthermore, substitution on the naphthalimide ring proved significant in terms of cytotoxicity as a nitro group in position 3 was more active than the corresponding amino in addition to the nitro moiety in position 4 of the naphthalimide ring.[82]

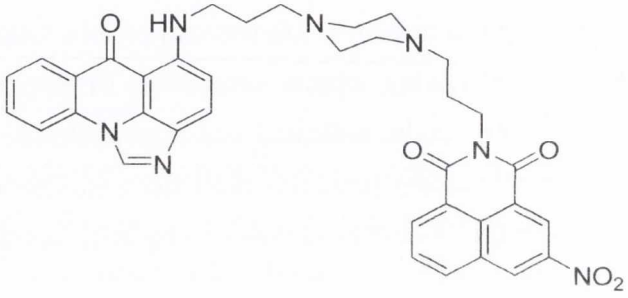

41

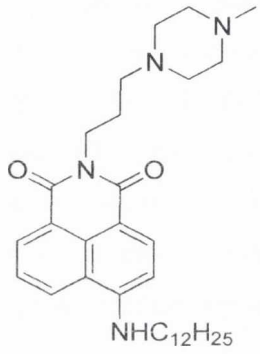

42

More recently, a further series of multi-target naphthalimide based anti-tumour agents were designed featuring lysosomotrophic detergents responsible for lysosomal membrane permeabilisation (LMP), apoptosis and cell death. Such compounds potently inhibited the growth of multiple cancer cell lines. For example **42** was more active than Amonafide **20** in the anti-proliferative cell-based assays, induced apoptosis *via* a mitochondrial pathway and caused LMP.[83]

Furthermore, the effects **42** induces on human Burkitt's lymphoma-derived Raji cells have been investigated. These studies have shown that **42** displays more specificity and sensitivity on Raji cells than normal peripheral blood mononuclear cells and induces apoptosis mediated by a free oxygen radical dependent mitochondrial pathway.[84]

It is evident that mono-naphthalimides as intercalators have been central in anti-cancer research. Over the last forty years improving their binding affinities has proven key in cancer chemotherapy drug design and one of the most important approaches has been the design of bis-naphthalimides and the next section will highlight some of the recent developments made in this area.

1.4 Bis-Naphthalimides

The strategy of dimerising a DNA intercalating agent joined by various cyclic and acyclic linkers was initiated in the late 1980s and is still of current interest for the development of potential anti-cancer drugs. Several series of bis-naphthalimides have been synthesised as a means of increasing their binding to DNA and designed to contain different aromatic substituents and bridges differing in length and the number of amine groups used with the presence of at least one amine group proving essential for significant biological activity, as in the mono-naphthalimide series.[85,86] Many of the bis-naphthalimides showed superior biological activity compared to the parental compounds and certain aromatic substituents were found to increase cytotoxic activity in the following order: CH_3CONH < NH_2 < H < NO_2 for compounds containing the same amino bridge.[85] Selected bis-naphthalimides were tested for efficacy in animal tumour models and *in vivo* with the most active compound being the derivative without any substituents on the naphthalene rings designated LU 79553 as the free base and elinafide **43** as the dimethanesulfonate salt, which exhibited not only tumour inhibition but also tumour regression and tumour free survival against a broad spectrum of tumour types.[87]

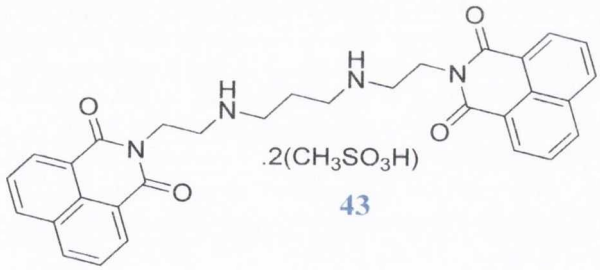

43

Several lines of evidence such as DNA footprinting and photocleaving studies indicate that this bis-naphthalimide intercalates bi-functionally into the double helix *via* the major groove so as to position the polyamine linker there, leaving the minor groove largely undisturbed. This interaction is sequence selective with a preference for the alternating purine-pyrimidine motifs particularly those containing *GpT* (*ApC*) and *TpG* (*CpA*) steps.[88] However, this interaction has proven to be of immense interest as Gallego *et al.*[89] have found it to be more complex through the discovery of a ring flipping process between two bound drug conformations which may be as a result of the orientation of the linker. As the amines that constitute the linker hydrogen bond to the guanine of the hexanucleotide d$(ATGCAT)_2$ the electronegative imide side of the ligand chromophore is forced to stack above the electronegative guanine base and thus, this unfavourable electrostatic stacking interaction may play a role in the rotational flipping motion of the naphthalimide rings.[90] Yet, using a

combination of nuclear magnetic resonance (NMR) spectroscopy, surface plasmon resonance (SPR) and DNA thermal denaturation studies, it was demonstrated that sequences not making direct contact with elinafide **43** modulate the interaction between **43** and its preferred bis-intercalating sites on double stranded DNA. They have established that a two step binding process occurs, one step involving the ligand binding to the duplex DNA and the second step involving ring intercalation which is influenced by the indirect reading. The sequence of base pairs flanking the ligand binding sites have been shown to be important as the most unfavourable sequences oppose intercalation and such complexes exhibit weaker inter- and intra-molecular interactions and increased ring flipping rates.[91]

At the same time, Chen *et al.*[92,93] were working independently on a series of bis-naphthalimides as potential anti-cancer agents. Bisnafide (DMP 840) **44** a dinitrobis-naphthalimide was designed and synthesised and exhibited selectivity *in vivo* for human solid tumours over murine leukaemias. Potent anti-proliferative activity against human, murine and solid tumour cell lines was observed *in vitro* and bisnafide was active against three doxorubicin resistant cell lines at nano range growth inhibitory concentrations. Bisnafide **44**, a topoisomerase II inhibitor, was also shown to induce DNA single strand breaks in a dose dependent manner as well as inhibit DNA and RNA biosynthesis in tumour cells.[94]

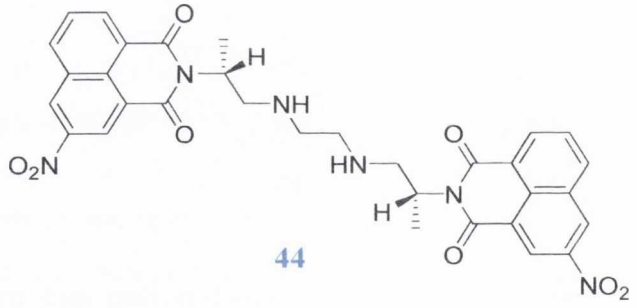

44

The structure of bisnafide **44** differs to that of elinafide **43** due to the presence of nitro substituents on the naphthalene rings and the choice of linker between the two imide functions with the latter feature attributing to their different modes of binding. The amino linker chain of **43** separates the two chromophores by *ca.* 12.3 Å and this inter-chromphore separation is adequate for bis-intercalative binding, whereas, the spacer group in **44** is shorter and insufficient to span two base pairs and subsequently results in mono-intercalation, with the second chromophore lying outside the DNA helix.[88,89,95,96] In general, bis-intercalation occurs in a molecule when the linker chain length is between 9-13 Å, an inter-chromophore distance which permits two planar ring systems to sandwich two base pairs in the intercalated complex.[97]

In view of the encouraging biological activity of these bis-naphthalimides, Pérez *et al.*[98] designed and synthesised the first platinum bound bis-naphthalimide derivatives **45** and **46** which were found to exhibit cytotoxic activity against tumour cell lines sensitive and resistant to cis-platin, an encouraging result for the discovery of novel platinum anti-tumour derivatives.

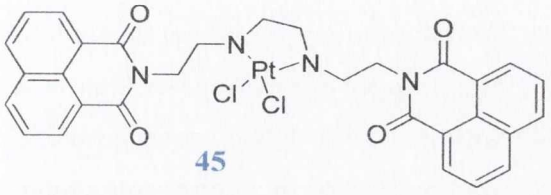

45

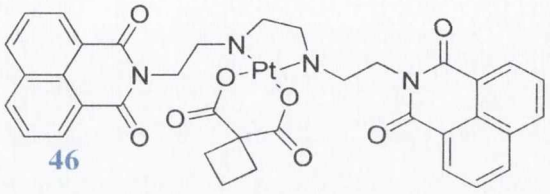

46

A further clue to extend the development of bis-naphthalimides was obtained from the greater activity of azonafide **22** over amonafide **20**.[46] By replacing the naphthalene rings with larger anthracene rings and retaining the same spacer as elinafide **43**, bibenoline **47** emerged. This compound was shown to bind to DNA and alter its gel mobility as well as inhibit Topoisomerases I and II at 5 μM and exhibit similar *in vitro* activity to LU 79553. However, in the M5076 murine tumour model *in vivo*, **47** produced a moderate increase in life span whereas, LU 79553 was inactive, suggesting that these two compounds have some differences in their anti-tumour profiles.[99]

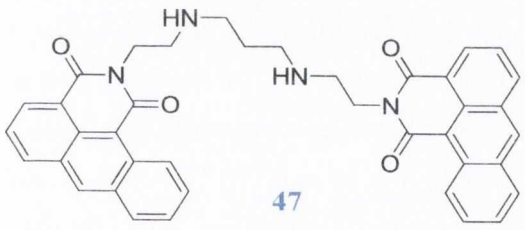

47

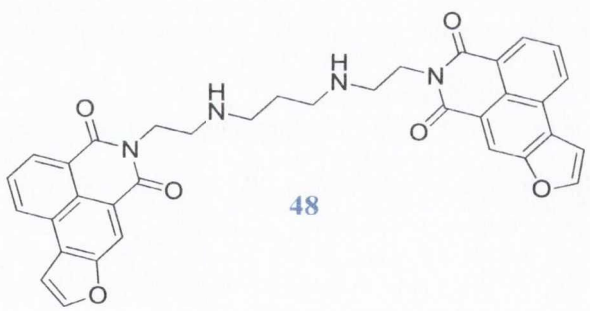

48

To broaden the scope of this kind of compound, bis-furonaphthalimide **48** was designed to incorporate a larger aromatic system in order to improve binding affinity and growth inhibitor potency. Compound **48** is not a topoisomerase inhibitor, yet it possesses the same linker group as **43**. It has a preference for *G·C* rich sequences and can bind *ca.* 1000 times more strongly to DNA than the monomeric parent compound. Although the monomer can accumulate in the nuclei of cells, **48** is more cytotoxic against CEM leukemia cells.[100]

Although the bis-naphthalimides have been reported as a potential class of anti-cancer agents and have entered clinical trials, their development has been hampered by side effects such as neuromuscular toxicity, neutropenia, stomatitis and myelosuppression.[101,102] Another drawback for the development of bis-naphthalimides in particular, is their insolubility in

aqueous solutions making their testing and potential progression into therapeutic agents difficult.[85, 103] Yet, continuous efforts to develop bis-naphthalimide DNA-binding anti-tumour agents are ongoing.

To overcome the toxicity associated with many anti-cancer agents, Suzuki *et al.*[104] attempted to develop compounds that preferentially bind to specific DNA sequences and control the expression of specific genes and thereby, inhibit tumour growth. For example, the strength of binding of **49** was approximately 350 times stronger to *G·C*-repeats than to *A·T* and *A·A*-repeating oligomers. The interaction of **49** with a specific DNA sequence induced p300 gene expression and showed significant anti-cancer activity in human solid tumour xenografts, therefore, showing that DNA binding agents can be sequence specific and have the potential to control transcription of tumour related genes and inhibit tumour growth.

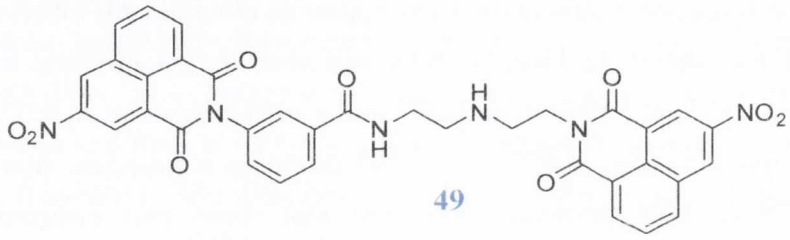

49

In an attempt to drive the development of bis-naphthalimides forward Lin *et al.*[105] have designed and synthesised several series of novel bis-naphthalimidopropyl polyamine derivatives, incorporating natural amines such as spermine and spermidine to aid aqueous solubility. For instance, **50** and **51** were shown to have higher affinities for DNA compared to spermine and spermidine and localise in the nuclei of MCF-7 breast cancer cells with the cytotoxicity of such compounds decreasing with the presence of oxygen atoms in the linker chain.[105,106]

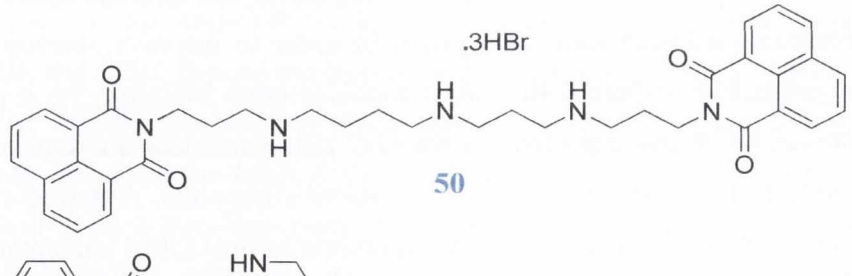

50

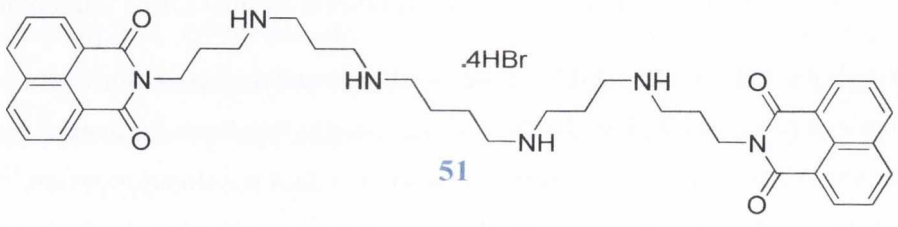

51

Further studies on **50** have shown that this molecule binds to DNA through bis-intercalation *via* the major groove and shows higher cytotoxic activity against Caco-2 colon cancer cells compared to HT-29 cells.[107,108]

In order to develop more active DNA-binding anti-tumour agents and to clarify the influence of the aminoalkyl linker chain on their mode of action, bis-naphthalimides bearing cyclic and acyclic chains of varying length were synthesised. Compounds containing a linear carbon chain were found to be more potent than constrained analogues with the length of the linker chain playing a pivotal role in the ability of these compounds to bind to DNA.[109,110] In fact, bis-quaternary bis-naphthalimide derivatives characterised by the presence of C_3-N_{quat}-$C_{3\text{-}12}$-N_{quat}-C_3 linkers revealed no cytotoxic activity against different cell lines.[111] However, the screening of bis-quaternary bis-naphthalimides against a variety of human pathogens has proved successful. Compounds of this class such as **52** and **53** have been shown to be active against the malaria parasite *Plasmodium falciparum* with anti-malarial activity of 0.66 μM (± 0.03) and 0.40 μM (± 0.18), respectively, combined with no cytotoxicity and more than likely function by interfering with the phosphatidylcholine biosynthetic pathway.[112]

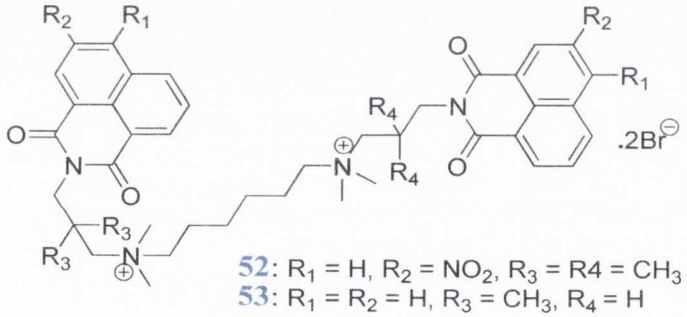

52: R_1 = H, R_2 = NO_2, R_3 = R4 = CH_3
53: R_1 = R_2 = H, R_3 = CH_3, R_4 = H

Moreover, in a recent study by Menzel *et al.*[113] bis-quaternary bis-naphthalimide **52** was found to exhibit strong inhibitory effects against gram positive bacteria *Staphylococcus aureus* (MRSA) and *Staphylococcus pneumoniae* by direct binding to bacterial DNA and thereby preventing DNA replication.

As depicted here, bis-naphthalimides have been reported as versatile compounds with promising results as potential anti-cancer or anti-infective agents. Over the past forty years, the design and development of the naphthalimide core has represented an important contribution from organic and medicinal chemistry, with immense interest still being acquired.

1.5 Advances by Gunnlaugsson *et al.*

Since the late 1990s the design and incorporation of nucleic acid recognition moieties into the naphthalimide structure has played an integral part in the research interests of the Gunnlaugsson group. To date a large number of enantiomerically pure amino acid based 1,8-naphthalimide conjugates have been synthesised using solution phase chemistry in order to achieve a more site specific approach to DNA cleavage. The earliest compounds designed during this research consisted of a basic structure comprising of either a chloro, bromo, nitro or amino substituted naphthalimide core connected to a carbonyl linker prepared from various esters of glycine, *L*-alanine, *L*-leucine and *L*-phenylalanine such as **54**. Such amino acid based naphthalimide derivatives were synthesised by Phelan[114] and tested against the CML HL-60 cell line with the 4-nitro substituted compounds showing the greatest cytotoxicty. For example, the IC_{50} value obtained for the *L*-phenylalanine methyl ester derivative **54** was found to be 1.95 μM, with only a ten-fold decrease in cytotoxicity compared to **16**. Of the peptide derivatives, the most active compound was **55** with an IC_{50} value of 1.57 μM, however, when tested against a more resistant CML cell line such as K562 cells, it remained relatively active with an IC_{50} of 3.49 μM (IC_{50} of **16** = 0.78 μM).

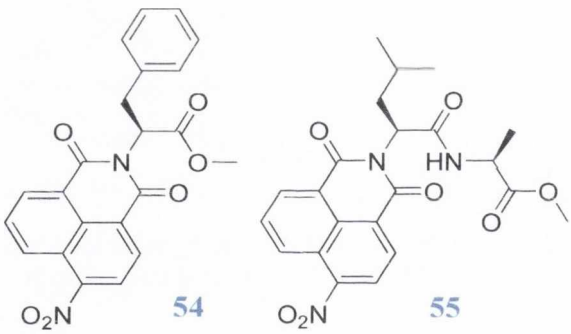

On comparing the activities of the peptide based naphthalimides, the following have been found to be influential in achieving the best anti-tumour activity: **(a)** a larger side chain resulted in a more active compound where for example, leucine and phenylalanine derivatives were more active than glycine and alanine derivatives, **(b)** in the case of the peptide conjugates, leucine should be positioned as the first amino acid when reading from the 1,8-naphthalimide terminus.

Building on this initial work, two approaches were undertaken by Phelan[114] to construct novel bis-naphthalimide structures as anti-cancer compounds. The first approach involved the synthesis of "*Head to Head*" derivatives such as **56** which has an IC_{50} value of 3.46 μM in HL-60 cells. However, when **56** was examined in K562 cells it was found to be

less cytotoxic than both a leucine containing mono-naphthalimide and the peptide derivative **55**.

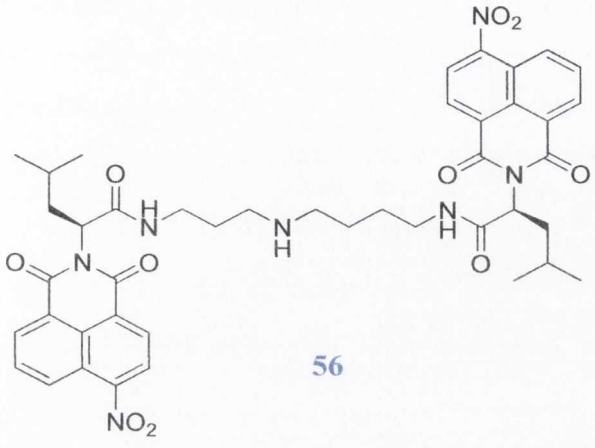

56

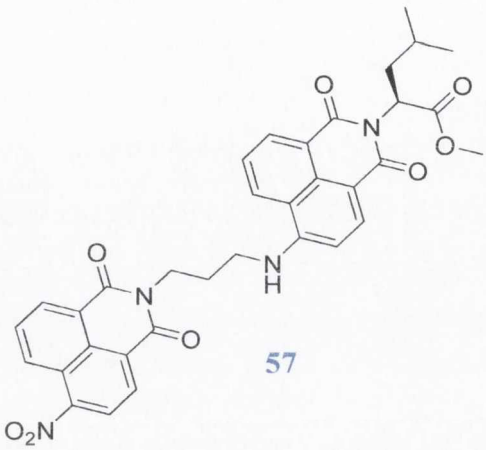

57

The second family of bis-naphthalimides synthesised consisted of "*Head to Tail*" derivatives including **57** which contains a propane linker from the 4-position of one chromophore to the imide position of the other, thus ruling out bis-intercalation as a mode of binding. The IC_{50} value obtained for **57** in HL-60 cells was 1.55 μM, which demonstrated greater activity in comparison to the reference compound mitonafide **16** after 24 hours in the more resistant K562 cell line.[114]

As a direct extension of this work, Hussey[115] developed various amino acid based naphthalimides incorporating *L*-lysine into the design as the lysine moiety can be positively charged at the *N*-imide site and thus, has the potential to mimic the positive nature of **16**, where the most active molecule was the Boc-protected 4-nitro derivative **58** (IC_{50} = 2.0 μM), while the Cbz-*tert*-butyl analogue **59** was the least active (IC_{50} >100 μM). Of the peptide based derivatives, the 1,8-naphthalimide consisting of leucine and Boc-lysine amino acids (IC_{50} = 1.4 μM) was found to be more potent than the phenylalanine and lysine derivative (IC_{50} > 50 μM).

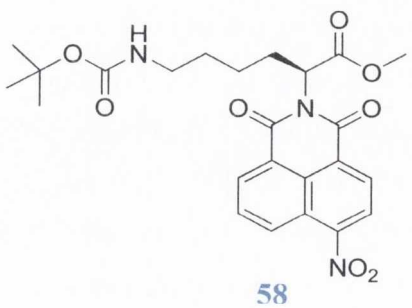

58

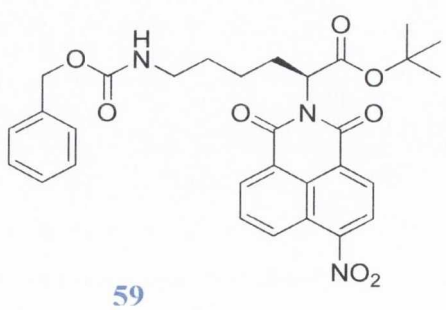

59

Removal of the lysine protecting group to yield a family of charged peptides resulted in an approximate 10-fold decrease in activity in comparison to the protected derivatives. An inability to enter into the cell and cross the hydrophilic membrane was given as a rationale for these unexpected results. Families of bis-naphthalimides consisting of "*Head to Head*" and "*Tail to Tail*" *L*-lysine based derivatives such as **60** and **61**, respectively were also synthesised with IC_{50} values of 4.6 μM and >100 μM, respectively, in HL-60 cells.

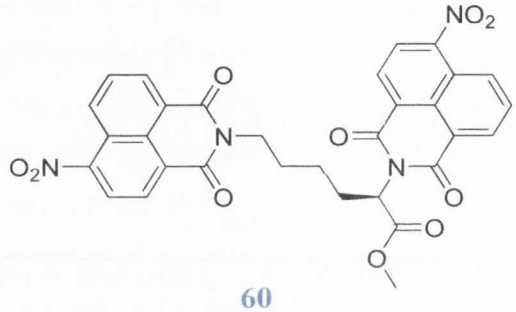

60

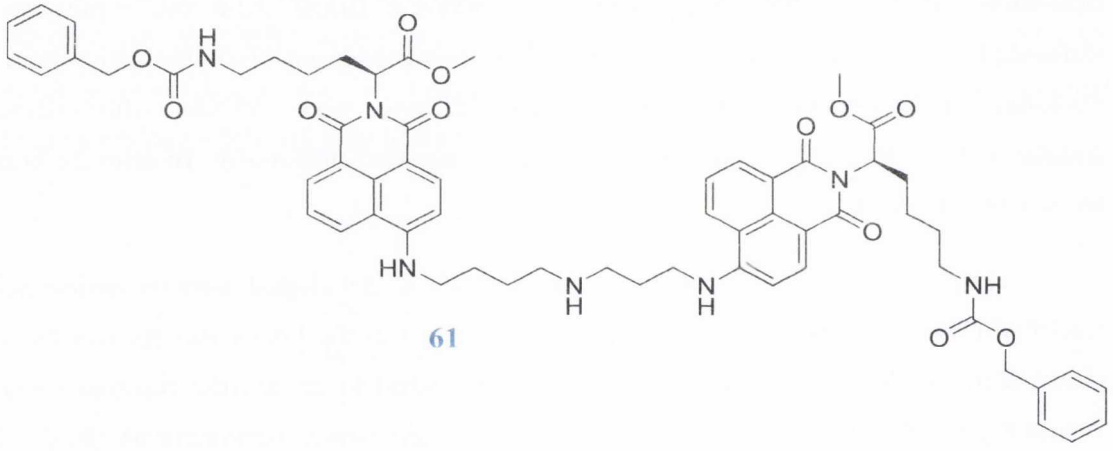

61

To further evaluate the potential of the naphthalimide core, "*Head to Head*" and "*Tail to Tail*" naphthalene di-imide linked bis-naphthalimides were designed as potential anti-cancer compounds. This family was synthesised by Gillespie[116] and on comparing the activity of molecules such as **62** in HL-60 cells, the following proved influential in achieving optimal anti-tumour activity: **(a)** "*Head to Head*" naphthalene linked bis-naphthalimides are more active than the "*Tail to Tail*" derivatives, **(b)** in the case of the peptide derivatives, phenylalanine should be positioned as the first amino acid followed by alanine when reading from the 1,8-naphthalimide terminus, **(c)** the length of the linker chain played a role in the potency of these molecules with the general trend being; hexyl > pentyl > propyl. All of the peptide-based naphthalimide, bis-naphthalimide and the naphthaldiimide derivatives exhibited μM IC_{50} values and have also been shown to inhibit cell cycle arrest and induce apoptosis in HL-60 cells.[117]

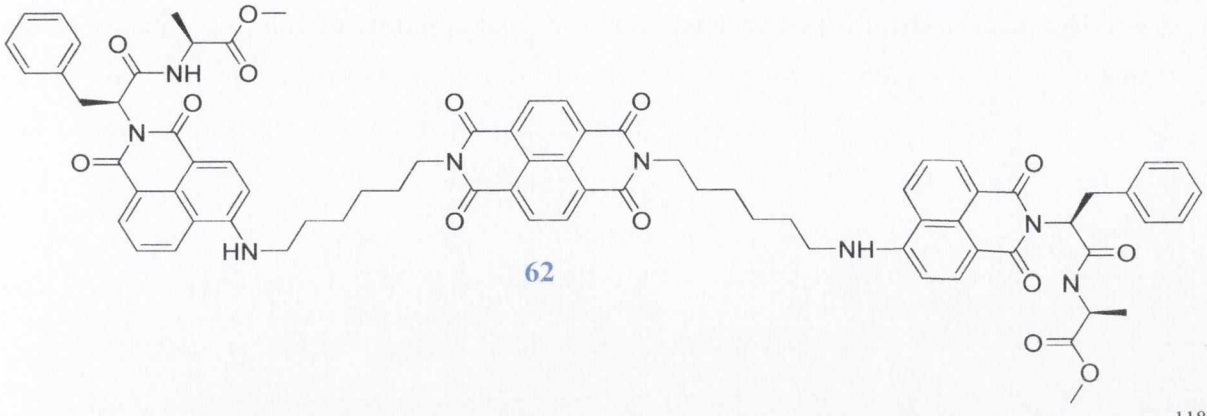

62

In the pursuit of enhanced selectivity and stronger binding affinity to DNA, Ryan[118] developed an alternative approach to DNA targeting by the use of Ru(II) polypyridyl-1,8-naphthalimide conjugates. Complexes **63**-**66** containing both rigidly and flexibly linked 1,8-naphthalimide chromophores were designed to study the effect of variations in substitution and connectivity on DNA binding ability. A *meta* arrangement around the connecting ring of the linker group demonstrated greater affinity for DNA, as well as greater changes in spectroscopic properties due to greater complementarity in the shape of the complex to that of the DNA. Furthermore, all four complexes exhibited highly efficient DNA photo-cleavage and were found to enter cervical cancer HeLa cells and localise within the nucleus.

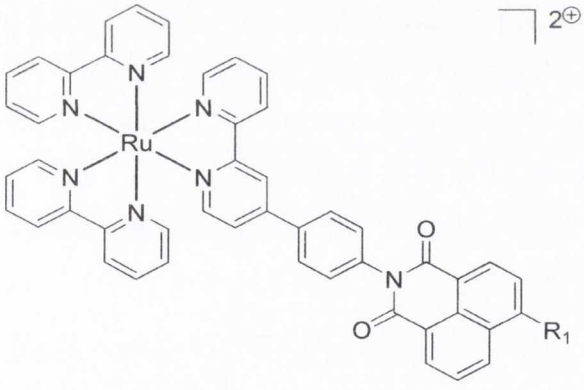

63: $R_1 = NO_2$
64: $R_1 = NH_2$

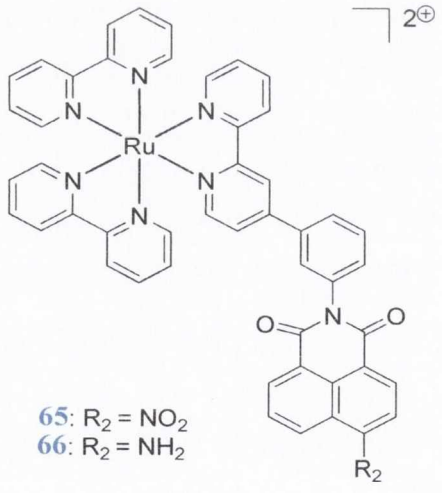

65: $R_2 = NO_2$
66: $R_2 = NH_2$

Following this work, Elmes[119] set out to modify the structures of **65** and **66** in order to incorporate the π-deficient ligand TAP (1,4,5,8 tetra-azaphenanthrene), to yield π-deficient rigid Ru(II)-mono-1,8-naphthalimide conjugates, **67** and **68**. These molecules were designed on the premise that inclusion of two TAP ligands would serve to increase the DNA cleavage efficiency of these systems, the Ru(II) centre would provide interaction through electrostatic association with the double helix or insertion into the grooves of DNA while the 1,8-naphthalimide would contribute to high affinity binding through intercalation, as well as

providing a known set of photophysical properties that could be used to monitor the binding process.

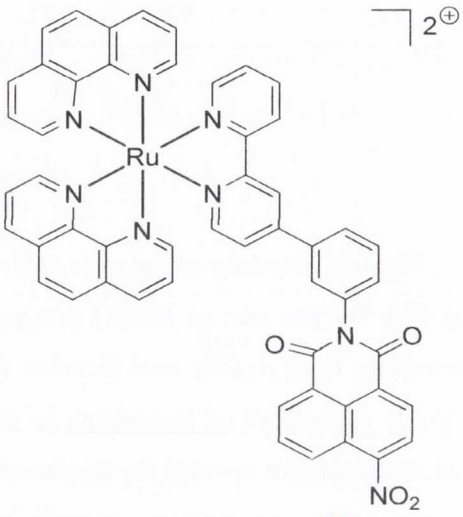

67

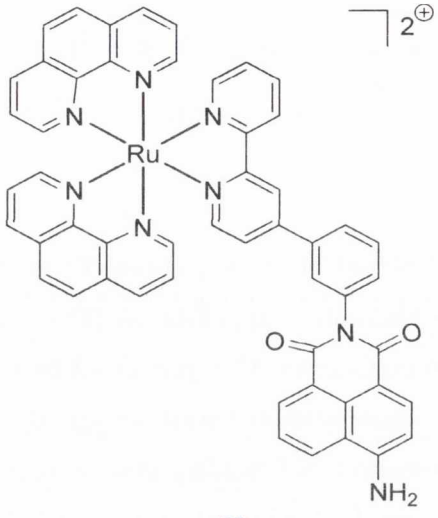

68

Complexes **67** and **68** were shown to possess excellent DNA binding affinities having being evaluated as being of the order of 10^6 M^{-1} and their ability to act as photocleavers was examined where both species were found to cleave supercoiled DNA with much increased efficiencies compared to the Ru(II) polypyridyl-1,8-naphthalimide analogues **65** and **66**. Furthermore, cellular uptake studies showed that both species accumulated in the cytoplasm and nucleus of HeLa cells. In addition, **68** has also been shown to function as a long wavelength emissive fluorescent anion sensor for several anions in organic solution. Fluoride gave rise to the largest changes in the emission spectra through quenching of the metal to ligand charge transfer (MLCT) emission of **68**.[6(a)]

Recently, the DNA binding ability of a novel cationic pyridinium based 4-amino-1,8-naphthalimide derivative was evaluated. Circular dichroism (CD) and linear dichroism (LD) studies revealed that the molecule binds to DNA *via* intercalation while UV-Vis, fluorescence and DNA thermal denaturation studies showed that the compound possesses a strong preference for *A·T* rich sequences demonstrated by the six times larger binding constant determined for poly(d*A*-d*T*)$_2$ than for poly(d*G*-d*C*)$_2$, hence, this molecule may have a therapeutic role in targeting *A·T* rich DNA.[120]

To develop upon the work already carried out in the Gunnlaugsson group, the aim of one of the projects discussed within this thesis is to modify the 1,8-naphthalimide

chromophore by introduction of the Tröger's base structural unit in order to improve upon the biological activity of the naphthalimide family.

1.6 Tröger's Base

The Tröger's base **69** is a rigid V-shaped molecule which has played a considerable role in the field of supramolecular chemistry due to its unique structure featuring two aromatic rings fused to a methano-1,5-diazocine bridge formed from the condensation reaction between *p*-toluidine and formaldehyde in acidic solution.[121,122] The X-ray structure of **69** as shown in Figure 1.4, was reported by Wilcox *et al.*[123] demonstrating that the methano-1,5-diazocine bridge contains two tertiary stereogenic bridge head nitrogen atoms which provide the C_2 symmetry of the structure. The chirality and blocked conformation of these nitrogen atoms makes **69** attractive for use in the area of enantiospecific recognition of molecules. The aromatic rings are orientated approximately perpendicular to each other with a dihedral angle of *ca.* 90°, thus, creating a twist in the molecule.

69

Figure 1.4: *Optimised geometry (left) and structural formula (right) of* **69**.[124]

Dihedral angles ranging from 79° to 104° have since been reported for a number of analogues indicating that the dihedral angle is dependent upon the nature of the substituents present on the aromatic rings.[125] Hence, this rigid V-shaped building block offers the potential for unique molecular designs which have been strongly employed in the fields of molecular recognition and supramolecular chemistry.[126]

1.6.1 Applications of Tröger's Base Analogues

The V-shape and conformationally restricted nature of the Tröger's base make it useful as an armature for the construction of molecular torsional balances,[127] water soluble cyclophanes,[128] chiral solvating agents[129] and molecular tweezers.[130] The cleft like structure of **69** has also been incorporated into macrocycles for the detection of cations.[131] For instance, the bis(crown-ether) analogue of Tröger's base **70** was designed and shown to recognise and detect achiral and chiral primary bis-ammonium salts.[132] Many other structural analogues have also been used to bind biotin, urea, adenine, and amino acids.[133] In particular, Goswami

et al.[134] constructed a family of fluorescent Tröger's base molecular scaffolds including **71** which was shown to selectively bind di-carboxylic acids of various chain lengths demonstrating that the rigidity of the host molecule plays a significant role in the selective binding of di-carboxylic acids.

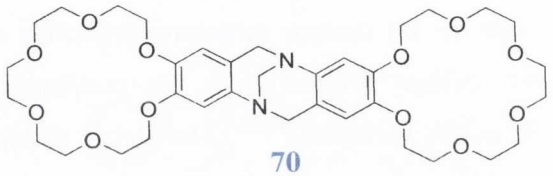

70

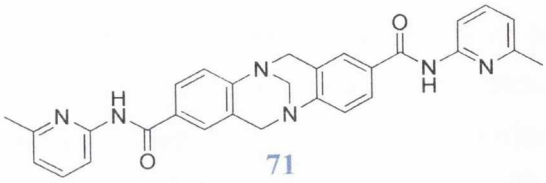

71

Synthetic Tröger's base derivatives have also found use in the field of catalysis. Wu *et al.*[135] have reported on the stereoselective one pot three component Mannich reaction of aldehydes, amines and ketones in aqueous media catalysed by Tröger's base derivative **72**. This catalyst has shown *anti*-selectivity, low catalyst loading and the formation of no by-products such as aldol or deamination products. A Tröger's base functionalised organic nanoporous polymer was designed for heterogeneous catalysis by Wang *et al.*[136] containing the bicovalently-bonded Tröger's base derivative **73** which showed catalytic activity in the addition reaction of diethylzinc to 4-chlorobenzaldehyde with the catalyst still being efficient after three cycles. The Tröger's base structure building motif was also used to generate infinite co-ordination polymers (ICPs) with Zn^{2+} ions which exhibited highly selective H_2 uptake properties in the presence of N_2.[137]

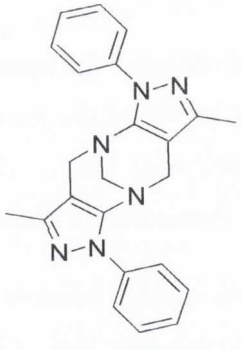

72

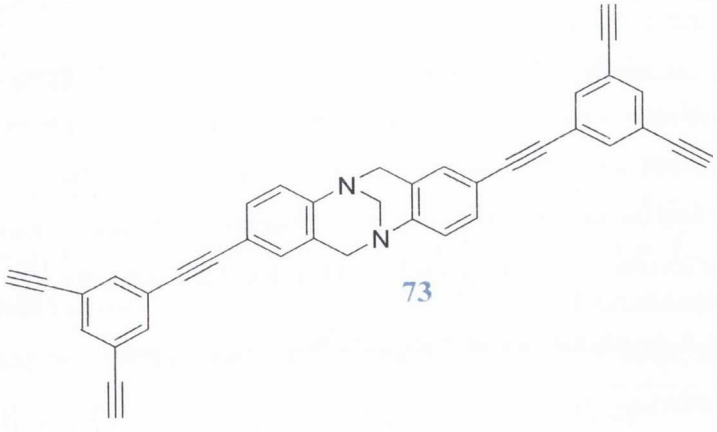

73

Recently, Wu *et al.*[138] modified the Tröger's base scaffold to construct a probe for lysosomal imaging in living cells. Lysosomes were targeted due to their association with oncogenic activation and cancer progression. The two photon fluorescent Tröger's base derived probe **74** showed high specificity and selectivity for lysosomes in HeLa, MRC-5 (normal cells) and NRK (infinite cells) cell lines, with the enantiomers demonstrating no

significant difference in activity. Furthermore, Λ-shaped pyridinium Tröger's base salts have also found use as bio-probes in detecting proteins such as bovine serum albumin (BSA) due to their aggregation induced emission properties.[139]

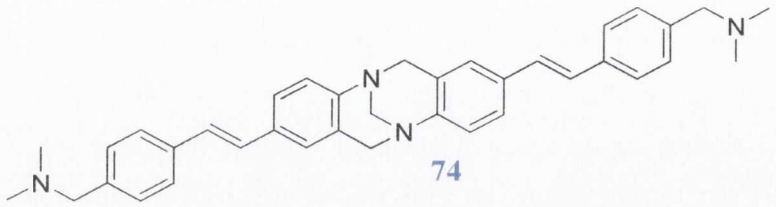

74

In summary, Tröger's base is a well known chiral molecule with a rigid concave shape that makes it highly applicable in several areas of research such as supramolecular chemistry, molecular recognition and optoelectronics.[126,140] In the following section, the modifications to the structural design of **69** and application as novel DNA binding agents will be explored.

1.6.2 Tröger's Base Analogues Targeting DNA

The construction of DNA-binding motifs incorporating the Tröger's base scaffold was initiated by Yashima *et al.*[141] with the preparation of a racemic bis-(1,10-phenanthroline) containing Tröger's base **75**. Circular dichroism measurements showed that **75** interacted with DNA to a higher degree compared to the parent 1,10-phenanthroline. Moreover, it was demonstrated that the copper (I) complex of **75** could cleave DNA by conversion of the covalently closed circular pUC18 plasmid to open circular DNA.

In a similar manner, Demeunynck *et al.*[142] synthesised the acridine substituted Tröger's base derivative **76**. The binding of **76** to DNA was evaluated by UV-Vis measurements and CD studies and shown to be enantiospecific, with the (-)-enantiomer binding preferentially to calf thymus DNA.

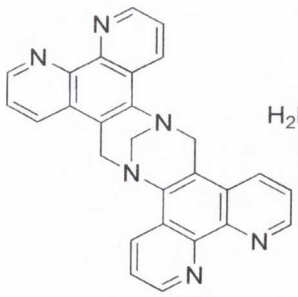

75

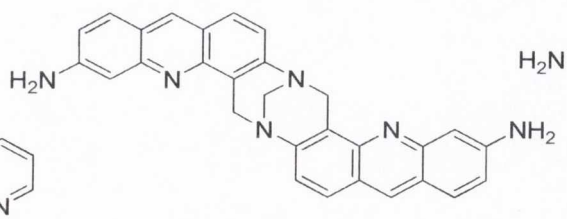

76

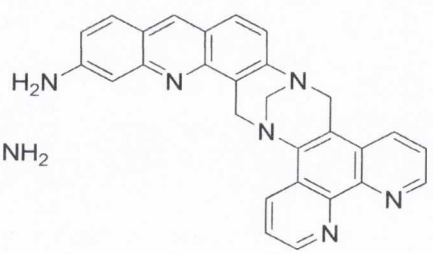

77

In a later study, such binding was shown to be both enantio- and sequence specific. However, due to the symmetric nature of the molecule the exact mode of binding was not elucidated.[143]

In order to circumvent this problem and provide further insight into the binding mode of Tröger's bases to DNA, the asymmetric acridine-phenanthroline Tröger's Base **77** was developed and evaluated using biochemical and biophysical methods.[144] Electric linear dichroism (ELD) and CD measurements indicated a bi-modal binding process, implicating intercalation as the mode of binding for the acridine ring coupled with groove binding of the phenanthroline moiety. Furthermore, the sequence selectivity of **77** was investigated by DNase I footprinting using a ^{32}P-radiolabelled DNA restriction fragment of 117 base pairs and the footprint detected showed that the sequence selectivity of **77** is more similar to the symmetric phenanthroline analogue than to the acridine parent **77**, with the triplet sequences 5′-*GTC*·5′*GAC* providing an optimal binding site for Tröger's base **77**.[144]

To further extend these advances, Kirsch-De Mesmaeker *et al.*[145] have shown that the phenanthroline Tröger's base analogue **75** can act as a bridging ligand in the synthesis of bi-pyridyl containing mono- and bi-metallic ruthenium (II) species **78** and **79**. The interaction of the bi-metallic species with DNA has not yet been reported, conversely, three stereoisomers of the mono-metallic complex **78** have been isolated through crystallography and their interaction with DNA has been explored.[152] The luminescence data suggests that Δ-*S*-**78** possesses a higher binding affinity for DNA than its enantiomer Λ-*R*-**78** and diastereoisomer Λ-*S*-**78** due to a deeper insertion of the metallic unit of Δ-*S*-**78** in the DNA grooves. Moreover, the binding affinity was seen to be controlled by the absolute configuration of the metal centre as opposed to the chirality originating from the Tröger's base scaffold.

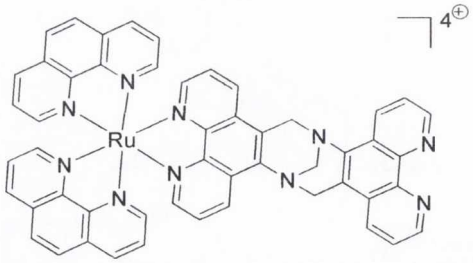

78

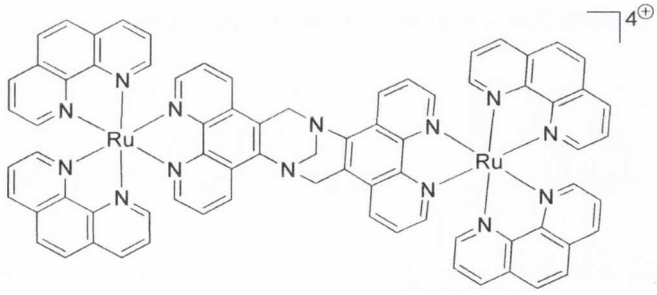

79

To further develop molecular probes to study DNA, Král *et al.*[147] synthesised a series of constrained bis-distamycin analogues **80** possessing the Tröger's base skeleton as enantioselective bi-dentate minor groove binders. As discussed in section 1.3, distamycin A **2** is a naturally occurring antibiotic that binds to the minor groove of DNA with a preference

for *A·T* rich sequences. Conversely, competitive ethidium bromide displacement assays showed that Tröger's base analogues such as **80** have an improved affinity for *G·C* rich sequences. Moreover, the directionality in the binding to DNA is controlled by the stereochemistry of the linker, with the (4*R*,9*R*)-form of **80** displaying an enhanced affinity for DNA and higher discrimination for *A·T* rich sequences compared to the (4*S*,9*S*)-analogue.

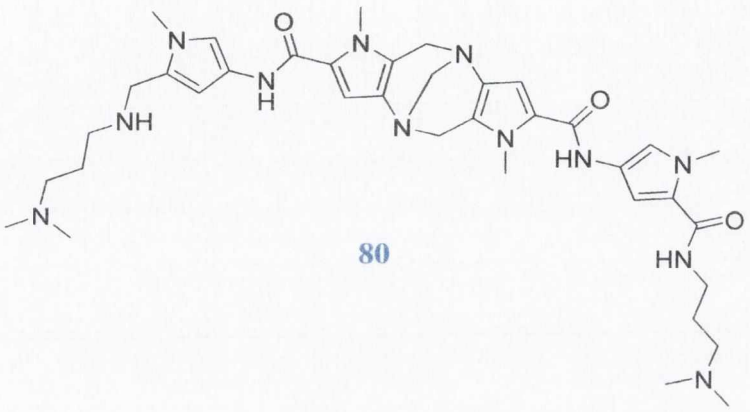

80

In summary, Tröger's base has the potential to be modified in several ways and has been seen to offer itself as a unique building block for development in several areas of research. Hence, the overall theme of this thesis will be to incorporate such structures into the 1,8-naphthalimide unit.

1.6.3 Design of 1,8-Naphthalimides Incorporating the Tröger's Base Framework

The ability to specifically and selectively target nucleic acid structures using small and medium sized molecules has become a highly topical area of research within chemistry. With this in mind Veale *et al.*,[148] developed a series of organic based DNA targeting systems based on 4-amino-1,8-naphthalimide derived Tröger's bases **81**-**83**, designed to be positively charged at physiological pH in order to promote strong electrostatic interactions or binding to the negatively charged phosphate backbone of DNA while the V-shaped geometry would facilitate binding of the naphthalimide units *via* the grooves and/or through intercalation. The interaction of **81**-**83**, with *ct*-DNA was investigated using several techniques such as CD, DNA thermal denaturation studies, ethidium bromide displacement assays and UV-Vis and fluorescence titrations at pH 7.4 in competitive media. Compounds **81** and **83** were found to bind strongly to DNA at pH 7.4 with electrostatic interactions playing a significant role, while **82** which has a p*K*a of 6.0 was not expected to give rise to significant electrostatic interactions possessed a lower binding affinity for DNA. In addition, fluorescent confocal

microscopy imaging studies in the K562 leukaemia cell lines have shown that these molecules accumulate within the nucleus and give rise to apoptotic induced cell death.[149]

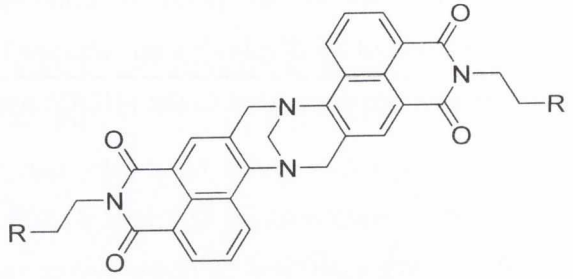

81: R = $N(CH_3)_2$
82: R = $N(CH_2CH_2)_2O$
83: R = $N(CH_2CH_2)_2NCH_3$

The design of **81-83** was modified by Elmes *et al.*[150] to incorporate a bi-pyridyl portion that would allow for the formation of bi-metallic Ru(II)-1,8-naphthalimide containing Tröger's bases **84** and **85**.

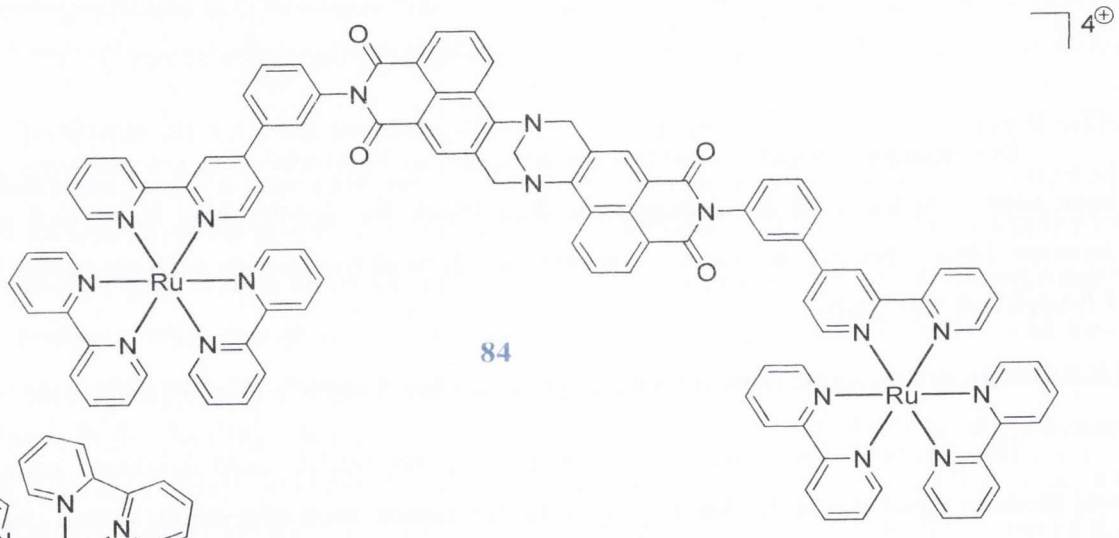

84

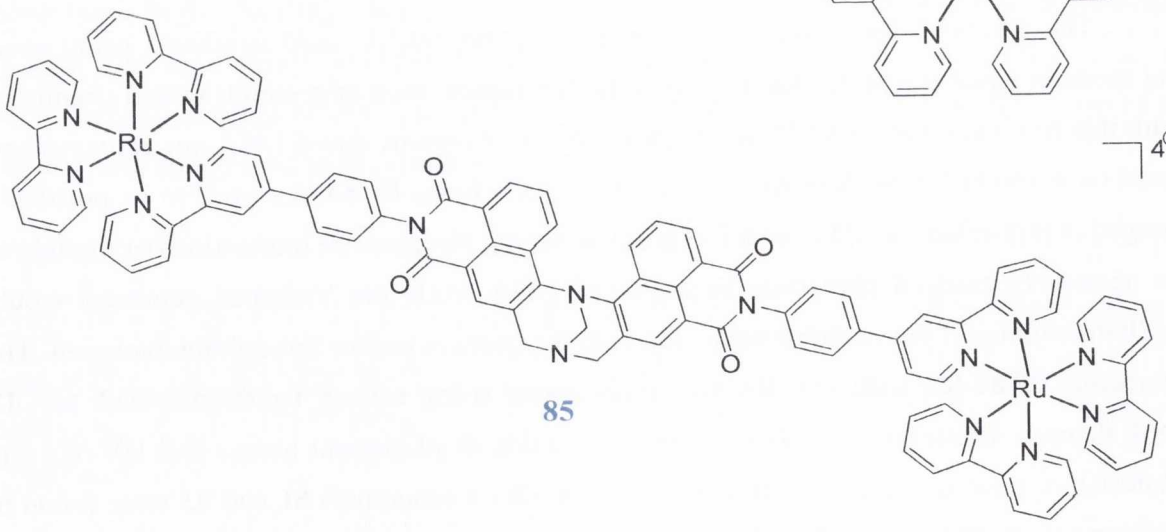

85

As mentioned in Section 1.5, bi-metallic Ru(II) complexes have been shown to interact with DNA quite strongly and have been applied in cellular imaging. The interaction of **84** and **85** with DNA was explored using UV-Vis absorption and fluorescence techniques with both **84** and **85** giving rise to relatively small spectral changes. For example, in the case

of **84**, a minor red shift coupled with 8% hypochromism at 400 nm and 6% hypochroism at 460 nm was observed at high DNA concentrations. Conversely, thermal denaturation studies revealed large stabilisation of the DNA helix upon interaction with both **84** and **85**, where **84** was found to be bound more strongly. Furthermore, highly fluorescent compounds **84** and **85** have been shown to undergo rapid cellular uptake within HeLa cells, being internalised after just two hours. Testing was conducted with a range of concentrations (0.5 to 15 μM) and no concentration dependent effects on cell viability including minimal cytotoxic or proliferative effects on the cell cultures was observed for **85**, hence **85** exhibits promising behaviour as a cellular imaging agent. However, **84** was shown to give rise to membrane blebbing demonstrating its role in apoptosis and potential as a therapeutic agent.

1.7 Work Described Within This Thesis

This research project has been concerned with the modification of the 1,8-naphthalimide chromophore, as it is known to possess unique photophysical properties that have the potential to be tweaked by facile synthetic modification. Building on from the work already carried out in the Gunnlaugsson group, the Tröger's base structural motif was incorporated into the design because of its unique chiral V-shaped structure. The overall aim of the work reported in this thesis is to exploit the versatility of each of these structures by combining the advantageous properties of the naphthalimide species with those of the Tröger's base in order to improve binding to DNA, to develop biological probes for proteins and synthetic sensors for C_{60} detection.

In Chapter 2, the design and synthesis of a novel family of naphthalimide based Tröger's base derivatives is described. Unlike the series synthesised by Veale[148,149] these naphthalimides are substituted with an amino group in the 3-position. It is anticipated that the resulting modified Tröger's base geometry would have the potential to alter and reinforce the binding capacity to DNA. The binding affinity for DNA was investigated using spectroscopic techniques such as UV-Vis and fluorescence spectroscopy, thermal denaturation studies and ethidium bromide displacement assays. Linear dichroism and circular dichroism studies were also employed to understand the nature of the DNA binding interactions.

In Chapter 3, the development of amino acid based Tröger's base derivatives is discussed. Firstly, the synthesis and characterisation of these molecules using CD spectroscopy is described followed by an in depth spectroscopic study of these molecules in solvents of varying polarity, using UV-Vis and fluorescence spectroscopic techniques.

Chapter 4 deals with the design, synthesis and photophysical evaluation of tetra-naphthalimide based Tröger's bases. The first aim of this project was to study these molecules in solvents of varying polarity using UV-Vis and fluorescence techniques including quantum yields and lifetimes and to compare these to the corresponding bis-naphthalimide precursors. The second aim was to evaluate their potential as fullerene receptors. It is envisaged that the unique shape induced by the Tröger's base unit will impose a tweezer like design that will aid in the molecular recognition of the spherical fullerene.

Finally, in Chapter 5, the general experimental procedures used in this thesis and the synthesis and characterisation of novel compounds that will be described are given.

Chapter 2:

Design, Synthesis and Photophysical Evaluation of Novel 1,8-Naphthalimide Based Tröger's Bases as Novel C_2 Symmetric DNA Binding Molecules

2.1 Introduction

The design and development of small molecules which exert their biological activity by interacting with DNA and exhibit photophysical properties that are sensitive to the binding event continue to be the focus of a significant amount of research within the field of medicinal chemistry.[20,60,83,120,148-157] As mentioned in Chapter 1, DNA exhibits many attractive features and a considerable amount of research has focused on the development of small molecules that bind to DNA and interrupt its normal function. These DNA binding modes include **(a)** minor groove binding, **(b)** major groove binding, **(c)** intercalation, **(d)** electrostatic binding and **(e)** covalent attachment. Each mode has been extensively studied with the aim of developing new design principles for the specific recognition of DNA.[22-24,29,31] In addition, several research groups, as discussed in Chapter 1, have investigated the effects of combining two binding motifs within the same molecule to develop new DNA targeting agents with enhanced selectivity and stronger binding affinity.[75-82] In principle, such molecules are designed to possess two binding modes which can include intercalation, bis-intercalation, minor and major groove binding or electrostatic interactions depending on the nature of the chromophore and spacer groups present. For instance, the strategy of dimerising a DNA intercalating agent joined by various cyclic and acyclic linkers to give bis-naphthalimides was discussed in Chapter 1 and the length of the spacer was shown to significantly affect the mode of binding to DNA.[85-113] The work described in this chapter will focus on the development of a series of bis-1,8-naphthalimide agents as potential DNA binders that incorporate the chiral Tröger's base structural motif which due to its V-shaped structure has found extensive use in the fields of molecular recognition and supramolecular chemistry.[126] In order to build upon the work within the Gunnlaugsson group carried out by Veale,[148,149] the aim of this project was to construct several DNA targeting Tröger's bases derived from the 3-amino-1,8-naphthalimide chromophore and to investigate the effect the shape the Tröger's base structural unit has on DNA binding using various photophysical techniques including absorption and fluorescence spectroscopy, thermal denaturation studies as well as linear and circular dichroism spectroscopy. In addition, these results were compared to the 4-amino derived analogues **81-83** and are discussed in the upcoming sections.

2.2 Design of Bis-1,8-Naphthalimide Tröger's Base Derivatives

In the Gunnlaugsson group, the Tröger's base motif has been incorporated into the 4-amino-1,8-naphthalimide skeleton as a means of developing novel bis-1,8-naphthalimide molecules that bind to DNA, exhibiting photophysical properties sensitive to the binding event.[148,149] These compounds were designed to contain basic terminal groups at the *N*-imide sites which were positively charged at physiological pH enhancing the water solubility and interaction of these molecules with DNA.[148,149] In fact, this design was originally put forward by Braña *et al.*[34] and the best anti-cancer activity achieved was observed when the basic terminal group was in the form of a tertiary amine separated from the 1,8-naphthalimide imide nitrogen by two methylene groups. Therefore, such hydrophilic cationic functionalities in the form of alkylaminoethyl side chains were incorporated into the 1,8-naphthalimide based Tröger's base structures, with the side chains differing in the nature of the aminoalkyl substituents. Another aspect which was considered in the design strategy was the fact that the Tröger's base unit is chiral and that the molecules are formed as racemic mixtures.

This work will focus on the design and development of another series of naphthalimide based Tröger's base structures **86-90** derived from the monomeric 3-amino-1,8-naphthalmide chromophore. These potential DNA binding agents are anticipated to be rigid chiral molecules in which the two naphthalimide moieties are held in a well defined position. In terms of an interaction with DNA, bis-intercalation is not anticipated as the Tröger's base unit is not long enough to span the length of two base pairs. Generally, for bis-intercalation to occur, an inter-chromophore distance of 9-13 Å is required.[97] Possible modes of binding envisaged may include a combination of intercalation, groove binding or electrostatic interactions.

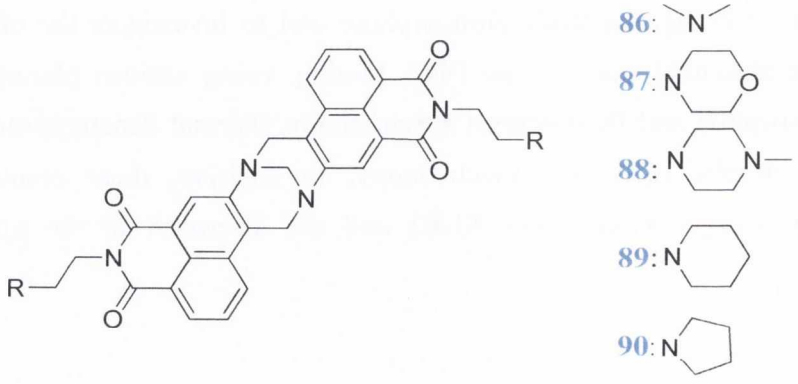

This chapter deals with the synthesis of the target naphthalimide Tröger's bases **86-90** as racemic mixtures and an evaluation of their solvatochromic properties before their interaction with DNA is investigated. Firstly, the general synthesis of the Tröger's base and the mechanism for formation will be discussed in the following section.

2.3 General synthesis of the Tröger's Base 69

The mechanism for the formation of Tröger's base **69** was initially investigated by Wagner *et al.*[158] and found to involve a series of electrophillic aromatic substitution reactions. The reaction proceeds *via* a number of intermediates shown in Scheme 2.1, which have been identified and characterised by Coelho *et al.*[159] using direct infusion electrospray ionisation mass and tandem mass spectrometric experiments (ESI-MS/MS). Interest still surrounds the Tröger's base mechanism of formation and recently, Wan *et al.*[160] identified and isolated a further two intermediates formed during the Tröger's base reaction.

The first step in the reaction sequence as shown in Scheme 2.1, is a condensation reaction between the aromatic amine and formaldehyde which results in the formation of an imine intermediate, which upon protonation and nucleophillic attack by a second aromatic amine gives rise to the methylene-bis-amine **91**.

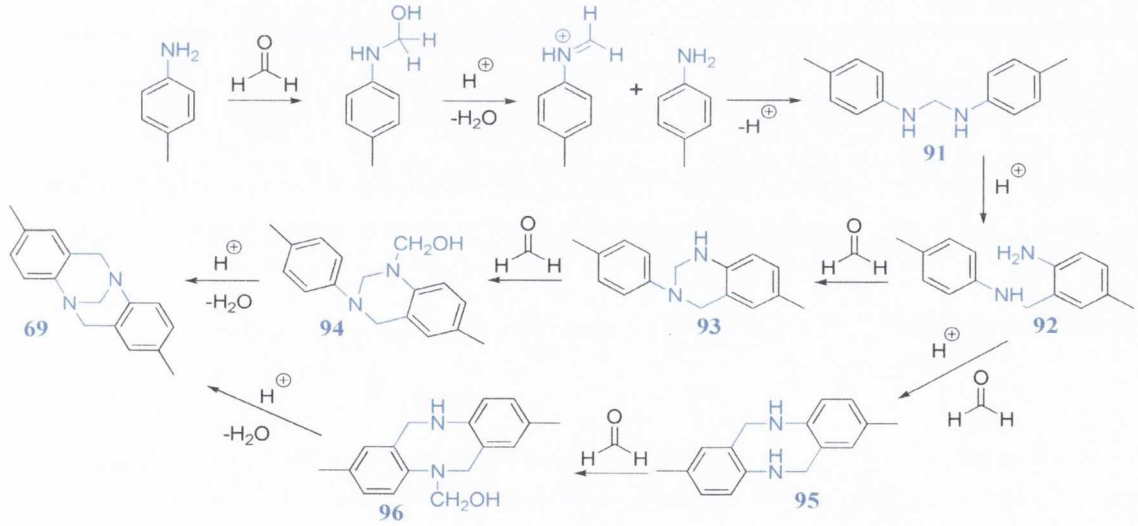

Scheme 2.1: *Reaction scheme for the formation of Tröger's base* **69**.

Subsequent conversion of the methylene-bis-amine **91** to the aminobenzylarylamine **92** is achieved through an acid induced rearrangement, which is shown in Scheme 2.2. Wagner reported that this reaction is not an intramolecular reaction or isomerisation, but can

be recognised as a proton induced cleavage reaction of **91** which yields the anionic and cationic species **97** and **98**, respectively, which couple together and through the loss of a proton to form **92**.[158(d)] According to the mechanism devised by Wagner *et al.*[158] and supported by Coelho *et al.*[159] the aminobenzylarylamine **92** subsequently reacts with formaldehyde in another condensation reaction to firstly form **93** which then undergoes further condensation to form **94**. The elimination of water results in the formation of **69**.

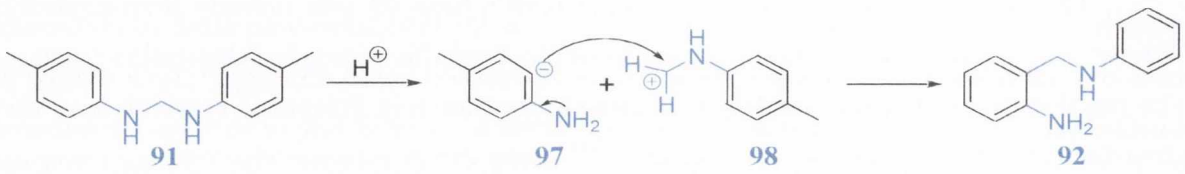

Scheme 2.2: *Conversion of methylene-bis-amine **91** to aminobenzylamine **92**.*[158(d)]

Another reaction pathway leading to the formation of **69** was investigated, as can be seen in Scheme 2.1, where Cooper and Partridge[161] demonstrated that Tröger's base **69** could be obtained *via* **95** which undergoes a condensation reaction to give **96** which upon protonation and the elimination of water generates the desired Tröger's base **69**.

During the formation of **69**, two side reactions are liable to occur: **(i)** conversion of tetrahydroquinazoline **93** to dihydroquinazoline **99** and **(ii)** irreversible conversion of aminobenzyarylamine to dihydroacridine *via* diaminophenylmethane. The formation of dihydroquinazoline has been depicted to form in two ways. The first pathway was devised by Wagner[158(d)] and this is a hydrogenation-dehydrogenation reaction, the elucidation of which explained the presence of methylated amines among the products formed upon reaction of *p*-substituted amines with formaldehyde in the presence of acid as shown in Scheme 2.3.

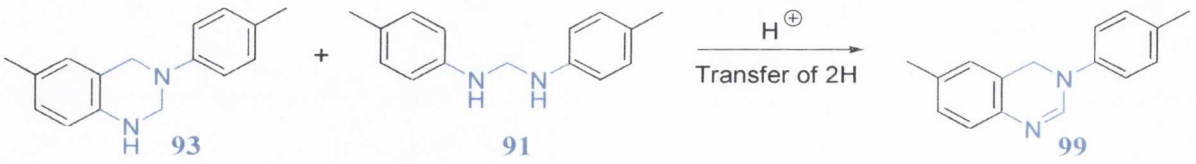

Scheme 2.3: *Conversion of tetrahydroquinazoline **93** to dihydroquinazoline **99**.*[158(d)]

Recently, Wan *et al.*[160] proposed a pathway for the formation of **99** from tetrahydroquinazoline **93** as shown in Scheme 2.4. The first step involves a condensation reaction with formaldehyde to form **94** which subsequently undergoes an elimination reaction to generate **99**.

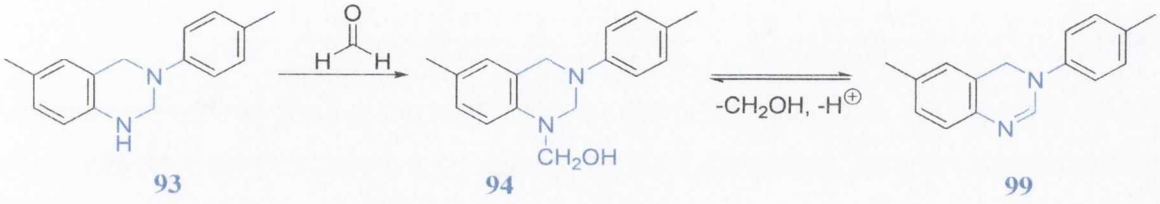

Scheme 2.4: *Synthesis of tetrahydroquinazoline* ***99***.[160]

The formation of dihydroacridine **100**, shown in Scheme 2.5 involves an elimination of ammonia and a subsequent internal ring closure. This reaction is irreversible, slow and partial because the *ortho* hydrogen of the aromatic amine is not readily displaced.[158(d)]

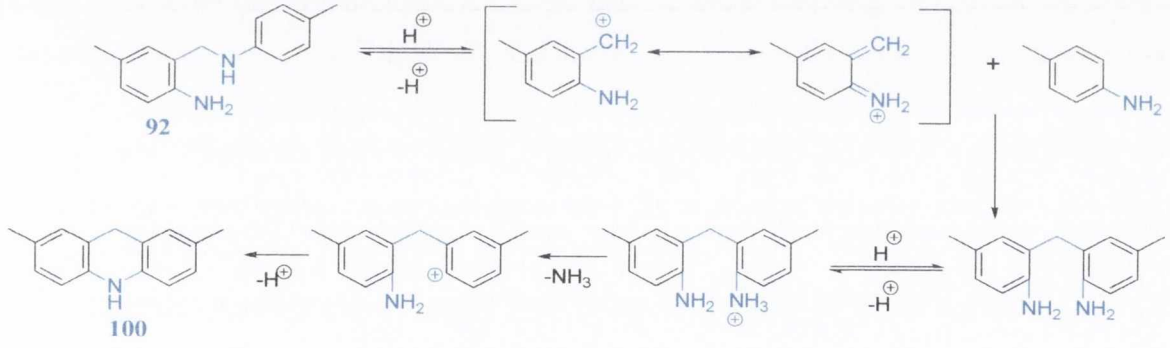

Scheme 2.5: *Conversion of aminobenzylarylamine* ***92*** *to dihydroacridine* ***100***.[158(d)]

The formation of the methano-1,5-diazocine skeleton is based on an acid-induced reaction between an amine and formaldehyde source, with variations in both the acid and formaldehyde sources having been reported. Formaldehyde equivalents including paraformaldehyde,[125(b),162] hexamethylenetetramine,[128(c),163] dimethoxymethane[164] and dimethylsulphoxide[165] have been reported affording varying yields of the Tröger's bases. In addition, varying the acid by using either acetic acid, HCl, trifluoroacetic acid (TFA) or methanesulfonic acid resulted in formation of the Tröger's bases with highly variable success.[125(b),128(c),162-166] Altering reaction conditions such as temperature and length of reaction time also led to the yields of the reaction product differing.[162]

In general, the preparation of the methano-1,5-diazocine skeleton of the Tröger's base can be formed using aromatic amines that are fully substituted except in the *ortho* position which is required for the desired cyclisation reaction to occur. Due to their electronic and steric effects, substituents on the ring have been reported to influence the regiochemistry and yields of such reactions.[125(b),166-171] In addition, to avoid polymerisation occurring, the *para* position on the starting amine must be blocked.[126(c)]

The bis-1,8-naphthalimide containing Tröger's base derivatives **86-90** were prepared as racemates in four steps, beginning with the 3-nitro-1,8-naphthalic anhydride **101**. After preparing **101**, the nitro group was reduced in a hydogenolysis reaction to yield **102**, Subsequently, the *N*-substituted 3-amino-1,8-naphthalimides **20** and **103-106** were synthesised using standard literature procedures which will be discussed in the following section.[42]

2.4. Synthesis of the 1,8-Naphthalic Anhydrides 101 and 102 and 1,8-Naphthalimides 20 and 103-106

Originally, the synthetic pathway leading to the formation of **86-90** began with 3-nitro-1,8-naphthalic anhydride as the starting material. Although 3-nitro-1,8-naphthalic anhydride is commercially available, it was found not to be of the highest purity according to ^{1}H NMR analysis. To establish the identity of the impurity present, the sample prepared for ^{1}H NMR spectroscopy was spiked with 4-nitro-1,8-naphthalic anhydride and the peaks pertaining to the impurity were enhanced. Purification attempts involved refluxing the sample in the presence of activated charcoal in EtOH and filtering through celite, however, this did not lead to any improvement in the ^{1}H NMR spectrum. The sample was recrystallised from toluene multiple times and each time resulted in a slightly improved ^{1}H NMR spectrum as the peaks corresponding to the 4-nitro-1,8-naphthalimide impurity slowly diminished. It was evident that this was not feasible and consequently, the commercially available material was subjected to purification using silica column chromatography with a CH_3OH: CH_2Cl_2 (5: 95) gradient eluent system. Unfortunately, the sample was found to degrade upon the silica column, as deduced by ^{1}H NMR spectroscopy.

Having established that the commercially available material utilised was indeed impure, the nitration of the commercially available 1,8-naphthalic anhydride was attempted. This involved dissolving the anhydride in concentrated H_2SO_4 and stirring the reaction mixture in an ice bath. A solution of HNO_3/ H_2SO_4 (1:10) was then added dropwise, after which the reaction mixture was brought to room temperature and allowed to stir for 90

minutes. The reaction mixture was then poured over an ice/H_2O mixture and filtered off to yield the crude product. Purification involved recrystallisation from glacial acetic acid and gave **101** as beige needles in a 60% yield.[172]

Having obtained **101** in pure form, the next step in the reaction sequence as shown in Scheme 2.6 was the synthesis of **102**. This was achieved by reducing the nitro group of **101** by catalytic hydrogenation in *N,N*-dimethylformaamide (DMF) with 10% Pd/C at 3 atm H_2 after filtration through a celite plug and without the need for further purification.[34] The reaction was also attempted using ethyl acetate as the solvent, however, 50% starting material was recovered according to ^{1}H NMR analysis.[173] This may be due to the insolubility of **101** in ethyl acetate. Therefore, as **102** readily dissolves in DMF and the reaction can be carried out on a large scale (up to 5 g), it remained the solvent of choice for such reactions.

By treating **102** with the relevant alkylamine and refluxing the two components in anhydrous toluene overnight, five 3-amino-1,8-naphthalimides **20** and **103-106** were synthesised and their yields are listed in the Table 2.1.[42]

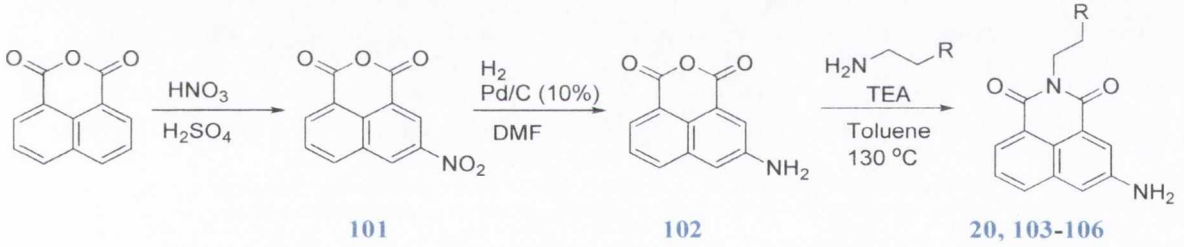

Scheme 2.6: *Synthesis of 1,8-naphthalic anhydrides **101** and **102** and 1,8-naphthalimides **20** and **103-106**.*

Table 2.1: *Methods of purification and the % yields for **20** and **101** - **106***

Cpd.	R	Purification Method	% Yield
101	----------	Recrystallisation with glacial acetic acid	60
102	----------	No purification necessary	92
20		Trituration with $CHCl_3$	74
103	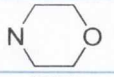	Trituration with CH_3OH	67
104	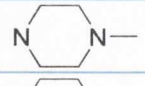	Trituration with EtOAc	76
105	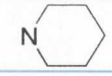	Trituration with CH_3OH	62
106		Recrystallisation with CH_3OH	67

In general, the work-up involved filtering the reaction mixture hot through celite and removing the solvent under reduced pressure. The resulting residue was then dissolved in CH_2Cl_2 and washed once with water, twice with sat. $NaHCO_3$ and twice with brine before the organic layer was dried over $MgSO_4$ and subsequently removed under reduced pressure. The purification of each intermediate is described in Table 2.1.

Single crystals suitable for X-ray diffraction analysis were obtained for **20** and **103-106** and were grown by slow evaporation of CH_2Cl_2 solutions for **20** and **103-105**, while in the case of **106**, brown crystals were obtained after a recrystallisation from CH_3OH. The X-ray diffraction analysis was carried out by Dr. T. McCabe in the School of Chemistry, Trinity College Dublin. The crystal structures were obtained from an analysis of the CIF files (Appendix 1) using Mercury 1.1© and are shown in Figure 2.1.

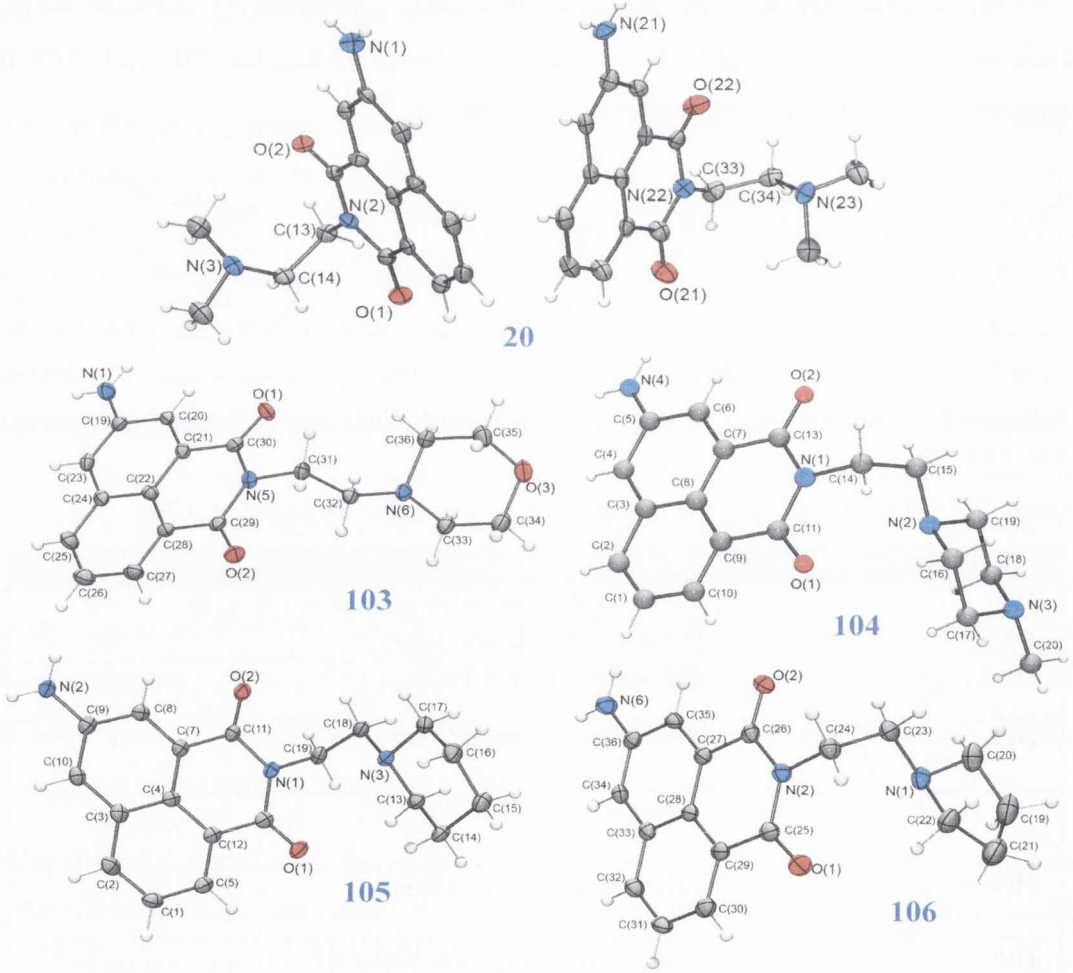

Figure 2.1: *Crystal structures of* ***20*** *and* ***103-106.***

As can be seen in Figure 2.1, **20** contained two crystallographically independent molecules in the asymmetric unit, one of which contained a positional disorder in the *N*-imide group (see Appendix 1 for details). Compound **105** crystallised in the monoclinic space group $P2_1/c$ and contained one molecule in the asymmetric unit. The piperidine moiety adopts a chair like conformation and the dialkyl amino linker adopts a gauche conformation [N(1)-C(19)-C(18)-N(3) torsion angle = 61.9°] resulting in the piperidine moiety being orientated almost perpendicular to the plane of the naphthalimide. The orientation of the piperidine group results in the formation of a complementary hydrogen bonded dimer between the amino protons and the nitrogen atom of the piperidine on a neighbouring symmetry generated molecule [N(2)···N(3) = 3.078 Å and <(N(2)-H(2A)···N(3)) = 153.6°]. The dimer is then linked into a more complex H-bonding array through interactions between the amino group and the carbonyl oxygen atoms on a neighbouring molecule [N(2)···O(2) = 3.018 Å and <(N(2)-H(2B)···O(3)) = 156.5°] (Figure 2.2). Similar torsional angles and hydrogen bonding patterns (Appendix 1) were observed for **20**, **102-104** and **106** are summarised in Table 2.2.

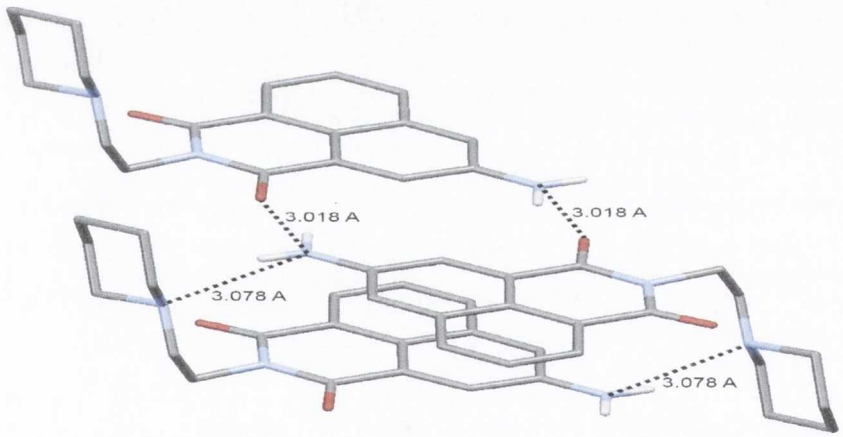

Figure 2.2: *Hydrogen bonding of **105**.*

Table 2.2: *Selected torsional angles for **20**, **103-104** and **106**.*

Cpd.	Bond	Torsional <
20	N(2)-C(13)-C(14)-N(3)	-61.0°
103	N(1)-C(14)-C(15)-N(2)	-68.0°
104	N(1)-C(19)-C(18)-N(3)	61.9°
106	N(2)-C(24)-C(23)-N(1)	-63.0°

In the case of **103**, the morpholine moiety does not adopt a gauche conformation. The torsional angle for [N(5)-C(31)-C(36)-N6] is -173.5° and this results in a different hydrogen bonding pattern being observed as shown in Figure 2.3. No dimers form and hydrogen

bonding was observed between the morpholine oxygen atom and the amino group on an adjacent molecule. In addition hydrogen bonding was observed between the carbonyl oxygen of one molecule and an amino group on an adjacent naphthalimide molecule.

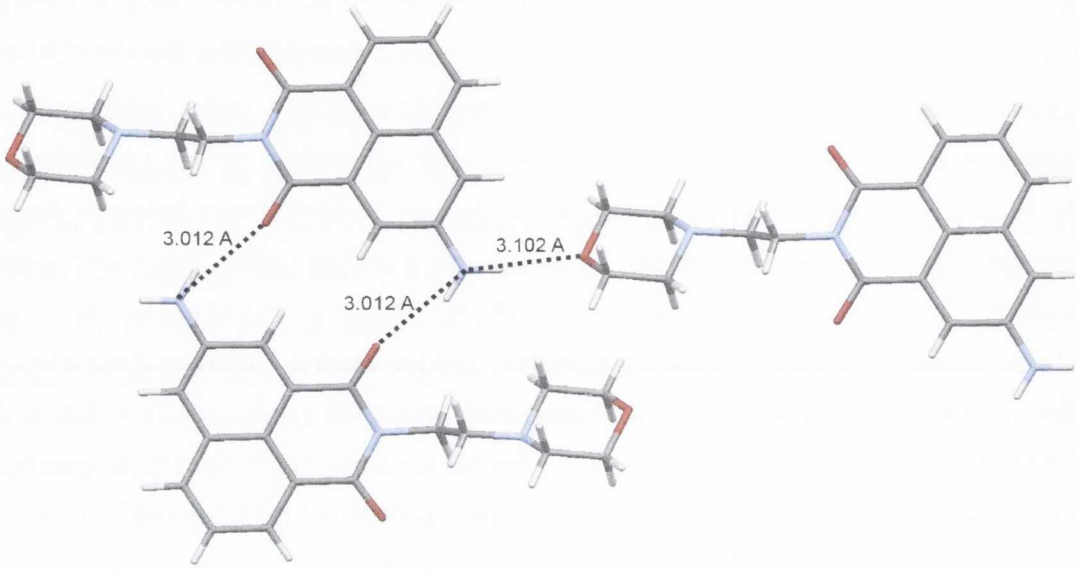

Figure 2.3: *The hydrogen bonding and packing of 103.*

Although the 3-amino-1,8-naphthalimides **20** and **103-106** were prepared by Braña *et al.*[34] and have been shown to bind to DNA, they were characterised by conventional techniques such as ^{1}H and ^{13}C NMR spectroscopy, mass spectroscopy, infra-red (IR) analysis and melting point data as a means of verifying their purity, as these compounds are intended to be used as model compounds for the DNA binding analysis of the target Tröger's bases **86-90**.[61]

2.5 Synthesis of the Tröger's Base Analogues 86-90

The synthetic method developed by Veale *et al.*[148,149] for the synthesis of **81-83** was initially employed for the synthesis of **86-90**, as shown in Scheme 2.7. This method involved stirring the relevant 3-amino-1,8-naphthalimide precursor (1 eq.) in TFA in the presence of formaldehyde (1.5 eq.) at room temperature for twelve hours under an argon atmosphere. Subsequent, work-up involved initially neutralising the reaction mixture before basifying to pH 12 and multiple extractions with CH_2Cl_2. The organic layer was then dried over $MgSO_4$ before being removed under reduced pressure. This reaction was carried out using formaldehyde or paraformaldehyde, both of which yielded similar results.

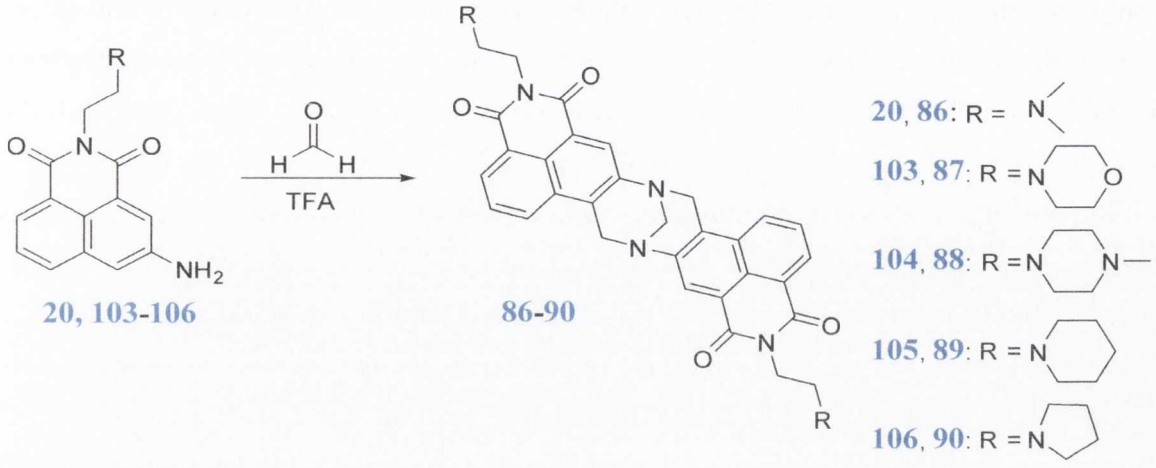

Scheme 2.7: *Synthetic scheme for the formation of* ***86-90***.

The first Tröger's base to be synthesised using this method was **86**. Trituration as a method for purification of **86** was investigated using solvents such as EtOH, CH_3OH and toluene, however, according to ^1H NMR analysis, these purification attempts were unsuccessful as no improvements in the ^1H NMR spectra were observed. Successful purification of **86** was achieved by triturating with CH_3CN, yielding the desired product as a yellow solid in 41% yield.

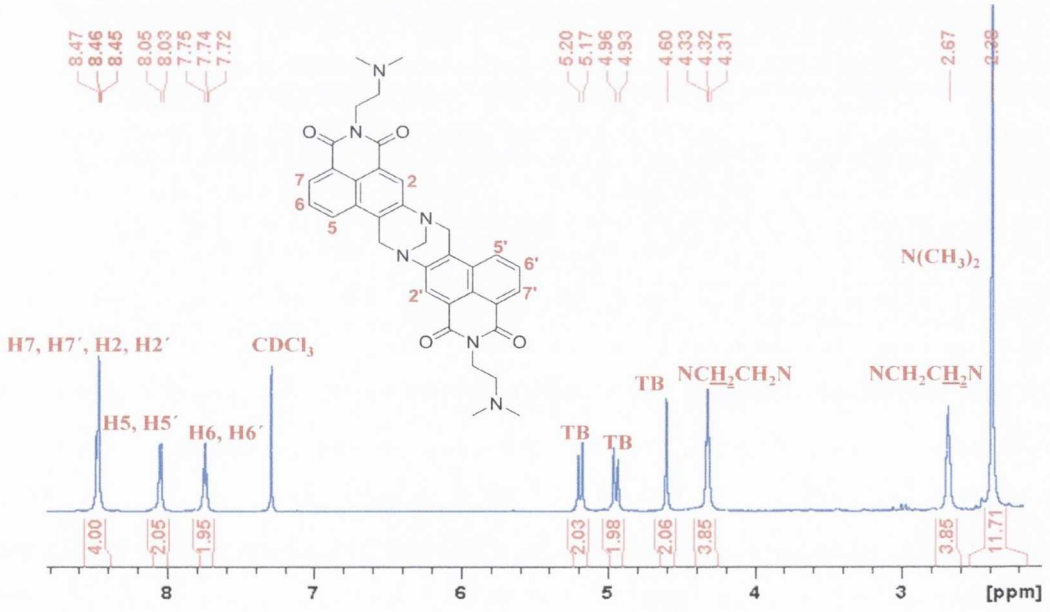

Figure 2.4: *^1H NMR spectrum ($CDCl_3$, 400 MHz) of* **86**.

Tröger's base **86** was fully characterised by ^1H and ^{13}C NMR, HRMS, IR spectroscopy and elemental analysis. The ^1H NMR spectrum ($CDCl_3$, 400 MHz) of **86** is shown in Figure 2.4. The aromatic region is composed of four signals, a singlet, two doublets

and an *apparent* (*app.*) triplet, with each integrating for two protons and pertaining to the aromatic naphthalimide protons. Such integration for the naphthalimide chromophore confirms the symmetric nature of **86**. The methylene groups belonging to the diazocine ring (denoted as TB in spectra) appeared as two doublets and a singlet, respectively, between 4.59 and 5.21 ppm reflecting the C_2-symmetric nature of the molecule. The methylene protons pertaining to the *N*-imide side chain appeared as triplets with coupling constants of 6.5 Hz. The final resonance, which corresponds to the methyl groups was a singlet which appeared at 2.38 ppm, integrating for twelve protons. All of the signal resonances were assigned by ^{1}H-^{1}H-COSY and HMQC experiments. The symmetric nature of **86** was also observed in the ^{13}C NMR spectrum ($CDCl_3$, 150 MHz) by having two more resonances in comparison to the precursor **20**, which pertained to the carbons of the diazocine ring. The HRMS for **86** showed a peak at m/z = 603.2714 $(M+H)^+$ and the IR spectrum showed that the primary amine group which appeared at 3416 and 3323 cm^{-1} for the precursor **20** was no longer present which complemented the assigned structure seen for **86** in Figure 2.4. In addition, **86** was successfully characterised by elemental analysis.

The second compound to be synthesised successfully as part of this 3-amino derived series was **87**, which contains the 4-(2-aminoethyl)-morpholine side chain at the *N*-imide positions. Purification by automated column chromatography on flash silica with a CH_3OH:CH_2Cl_2 (0 to 10%) gradient elution system yielded **87** as a yellow solid in 44% yield.

As with **86**, the aromatic region of the ^{1}H NMR spectrum ($CDCl_3$, 400 MHz) was composed of four signals pertaining to the naphthalimide protons, whilst the methylene protons belonging to the diazocine ring appeared between 4.61 and 5.21 ppm, with the doublets having geminal coupling constants of 17.0 Hz. The methylene protons belonging to the ethylamino side chains appeared as triplets at 4.32 and 2.70 ppm with each integrating for four protons and having coupling constants of 6.5 Hz. Lastly, two broad singlets integrating for eight protons were observed for the methylene protons pertaining to the morpholine functionalities, as can be seen in Figure 2.5. The symmetric nature of this molecule was also confirmed by ^{13}C NMR spectroscopy with the appearance of nineteen signals, two more than that observed for the precursor **103**. The HRMS for **87** showed a peak at m/z = 687.2931 $(M+H)^+$ confirming the molecular formula of the structure shown in Figure 2.5. The elemental analysis was also consistent with the assigned structure shown in Figure 2.5.

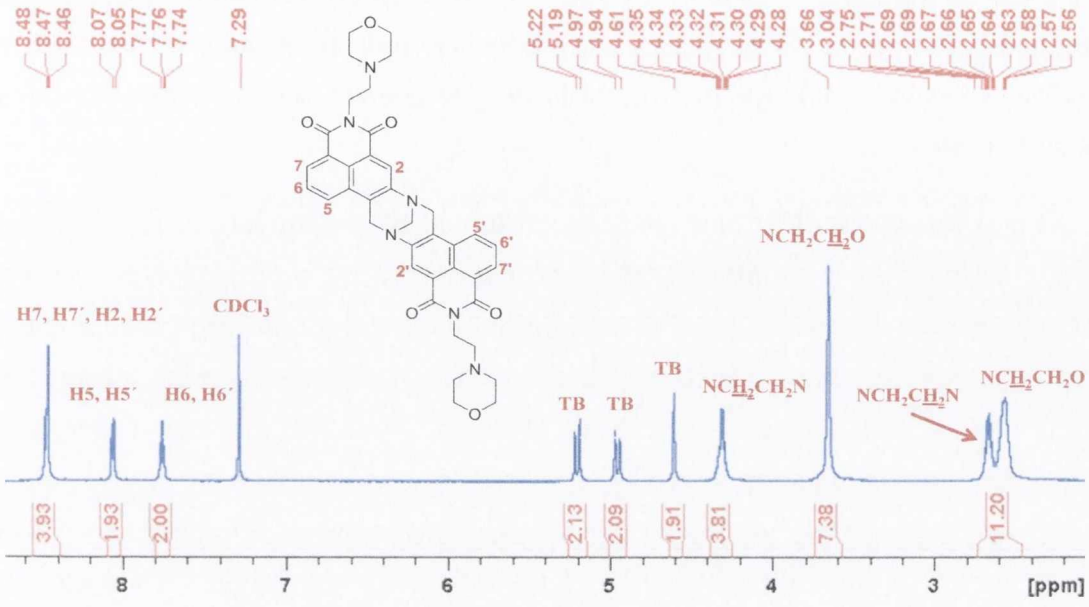

Figure 2.5: *^{1}H NMR spectrum ($CDCl_3$, 400 MHz) of* **87**.

The synthesis of **88-90** was attempted by stirring the relevant naphthalimide (1 eq.) in neat TFA in the presence of paraformaldehyde (1.5 eq.) under an argon atmosphere overnight. After carrying out the usual basic work-up, the resulting molecules were analysed by ^{1}H NMR spectroscopy, where product and the appearance of an unknown additional side product were detected in a 50:50 ratio. In each case, attempts to remove this side-product were carried out using several purification techniques such as trituration, recrystallisation and column chromatography. Unfortunately, it was not possible to remove or isolate this side product. In addition, the identity of this side product remains unknown as it could not be elucidated using NMR or mass spectroscopic techniques.

In order to circumvent this problem, the effects of varying the reaction time and paraformaldehyde equivalents were studied. Firstly, the length of the reaction time was reduced from twelve hours to three hours, however the appearance of this unknown side product was still detected. The reaction was attempted again using a reaction time of three hours and less equivalents of paraformaldehyde (1.1 eq.). These reaction conditions proved successful as this unknown side product was not detected.

As a means of optimising the reaction conditions, another reaction method was investigated which involved **88** (1 eq.) and parafromaldehyde (2 eq.) being added to TFA at -15 °C.[174] The resulting reaction mixture was brought to room temperature slowly and stirred for twenty hours. Subsequently, the reaction mixture was added to ice and an excess of

ammonia was added and extracted with CH_2Cl_2. Unfortunately, the unknown side product was detected again by ^1H NMR spectroscopy and therefore, the former method with the optimised reaction time and reduced paraformaldehyde equivalents was employed for the synthesis of **86-90**.

As previously described, the synthesis of **86** and **87** has already been successfully achieved. Unfortunately, both **86** and **87** were obtained in low yields of 41% and 44%, respectively. In order to improve upon this, the optimised reaction conditions were employed and after basic work up, the crude ^1H NMR spectra ($CDCl_3$, 400 MHz) were obtained and showed a marked improvement over those obtained using the previous experimental conditions described. Trituration with CH_3CN gave **86** as a yellow solid in 78%, almost twice that obtained compared to the first method used. In the case of **87**, these new reaction conditions proved successful as the desired product was obtained in 54% yield after dissolving the crude product in CH_2Cl_2 and precipitating out of CH_3OH.

Formation of **88** was achieved using these optimised conditions and after the basic work-up, **88** was dissolved in a minimal amount of CH_2Cl_2 and precipitated out of diethyl ether to yield the desired product as an orange solid in 61% yield. As seen previously for both **86** and **87**, the symmetric nature of this molecule was evident in the ^1H and ^{13}C NMR spectra. The ^1H NMR spectrum was similar to that obtained for **87** while also showing a sharp singlet at 2.24 ppm pertaining to the methyl protons of the piperazine ring. These signals were assigned using ^1H-^1H-COSY and long range ^1H-^{13}C-COSY experiments. The ^{13}C NMR spectrum ($CDCl_3$, 150MHz) of **88** also confirmed the identity and symmetric nature of this molecule by possessing an additional two carbons pertaining to the diazocine ring in comparison to the mono-naphthalimide precursor **104**. The assigned structure was also complemented by the loss of the primary amine signals observed in the IR spectrum and by the HRMS analysis which exhibited a peak for **88** at m/z = 713.3568 $(M+H)^+$ confirming the molecular formula of **88**. The results obtained from elemental analysis provided further evidence complementing the assigned structure for **88**.

With the latter success, the optimised reaction conditions were employed for the synthesis of **89**, which was obtained in 36 % yield after a recrystallisation from ethyl acetate and fully characterised using standard techniques. The aromatic region of the ^1H NMR spectrum (600 MHz, $CDCl_3$) was similar to that observed for **86-88**, with the aromatic protons resonating between 7.5-8.5 ppm. As is the case with each derivative, the differences

in the *N*-imide groups are relayed in the aliphatic portion of the spectra. In the case of **89**, the methylene protons belonging to the dialkylamino side chains appeared as multiplets, each integrating for four protons at 2.62 and 4.31 ppm, whereas, the methylene protons pertaining to the piperidine moieties appeared as multiplets at 2.52, 1.56 and 1.41, with each integrating for eight, eight and four protons, respectively. These signals were assigned using ^{1}H-^{1}H-COSY and long range ^{1}H-^{13}C-COSY experiments. The ^{13}C NMR spectrum confirmed the symmetric nature of the molecule. In addition, the IR spectral data complemented the assigned structure, as did the HRMS data with a peak at m/z = 683.3332 $(M+H)^+$ confirming the molecular formula of **89**.

The final molecule synthesised as part of this series was **90** which was obtained as a yellow solid in 54% yield after dissolving the crude product in a minimal amount of CH_3OH and precipitating out of diethyl ether. The symmetric nature of this molecule was confirmed by ^{1}H and ^{13}C NMR analysis. The ^{1}H and ^{13}C NMR spectra obtained for **90** were similar to those observed for **89** with the only difference being that **89** contains an additional methylene group, pertaining to the piperidine functionalities. The identity of this molecule was also confirmed by HRMS with a peak being observed at *m/z* = 655.3010 $(M+H)^+$ confirming the molecular formula.

In summary, five new Tröger's bases **86-90** have been designed and synthesised as potential DNA binders. As part of the design strategy, these molecules were derived from the 3-amino-1,8-naphthalimide structure as the amino substituted 1,8-naphthalimide derivatives have been shown to possess an internal charge transfer (ICT) excited state which is sensitive to the polarity of the medium and therefore can be exploited to monitor binding of these ligands to macromolecules such as DNA and proteins, which can have different dielectrics depending on the binding sites.[175-180] In order to ascertain whether or not **86-90** possess this trait, their absorption and emission spectra were investigated in a range of solvents and are discussed in the next section.

2.6 Spectroscopic Evaluation in Solvents of Varying Polarity

The 1,8-napthalimides belong to a class of chromophores for which excited state properties can be significantly altered depending on the nature of the substituent present on the naphthalimide ring.[179] In the case of the 4-amino-1,8-naphthalimide **107**, an internal charge transfer excited state results due to the *''push-pull''* character of the chromophore caused by the electron donating group positioned on the naphthalimide ring and the electron

withdrawing imide groups of the fluorophore, as shown in Figure 2.6. The energy of such an ICT excited state is determined by both the strength of the electron donor and acceptor moieties as well as the solvent polarity and its hydrogen bond donor and acceptor ability. Therefore, ICT is an important design feature as substantial changes can be observed in the absorption and emission spectra, the fluorescence quantum yields and lifetimes when the solvent is varied or when binding to a substrate occurs.[175-180]

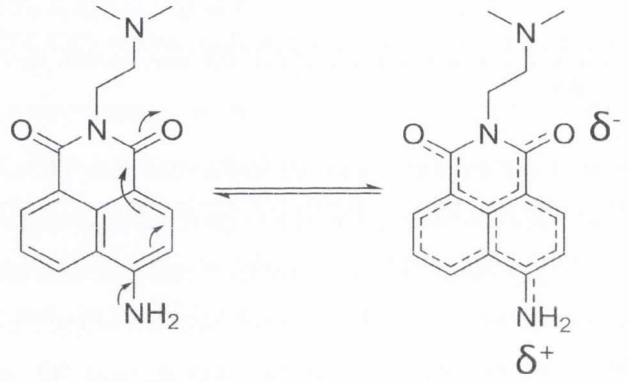

Figure 2.6: *The effect of ICT upon the excited state of* **107**.

Tröger's bases derived from 4-amino-1,8-naphthalimides have been shown to possess ICT character and fluorescence properties dependent on the polarity and hydrogen bonding ability of the medium.[148,149,181] However, due to the incorporation of the rigid V-shaped Tröger's base structural motif, the ability of the amine to participate in the ICT process is significantly reduced in comparison to the corresponding mono-naphthalimide precursors.[148,149,181] In the case of the target Tröger's bases **86-90**, it is anticipated that the ICT character and fluorescence dependence will not be the same as these molecules are derived from the 3-amino-1,8-naphthalimide core which has been shown to have a lower tendency for donating electrons, compared to the 4-amino core.[182,183] Thus, a means of investigating whether **86-90** exhibit an ICT excited state and to what extent, the various spectroscopic properties of these compounds were investigated in protic and aprotic solvents of varying polarity.

The absorption and emission spectra were recorded in a range of solvents and all measurements were carried out at an optical density (OD) of 0.15 at the excitation wavelength which was chosen as the λ_{max} observed in the absorbance spectra. The solvents used in this study were CH_2Cl_2, acetone, CH_3OH, CH_3CN, DMF and H_2O.

2.6.1 Ground State Studies of 86-90 in Solvents of Varying Polarity

The absorption spectrum of **90**, when recorded in CH_3OH, exhibited a high energy transition at *ca.* 238 nm, a lower energy transition at 347 nm with a shoulder with a λ_{maxUV} at *ca.* 390 nm. In general, the absorption spectrum was not significantly affected by the polarity and/or hydrogen bonding ability of the medium as can be seen in Figure 2.7. However, when the absorption spectrum was recorded in water, the shape of the shoulder was altered with the λ_{maxUV} being blue shifted relative to the other solvents. A similar effect was reported by Brown *et al.*[179] for 4-amino-1,8-naphthalimide systems as being due to strong hydrogen bonding with water which resulted in the formation of hydrogen bonding solvated clusters which absorbed at a lower wavelength compared to the other solvents investigated. Similar events were observed for other donor-acceptor systems.[184-186]

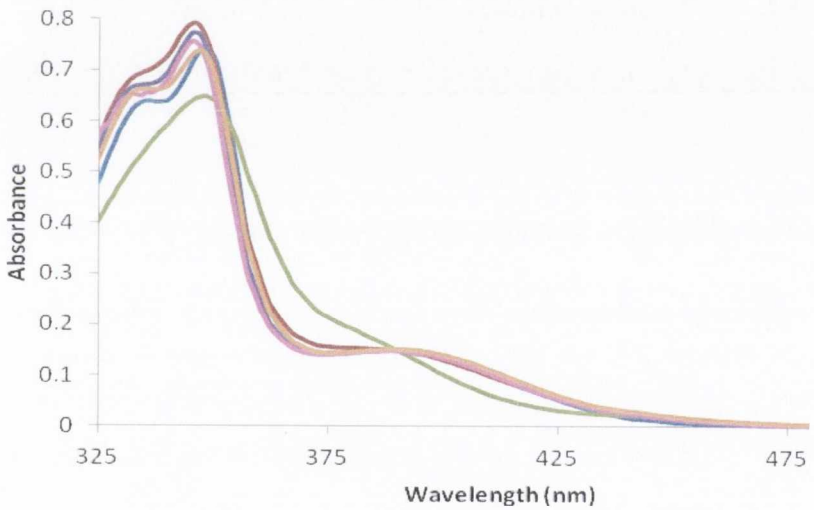

Figure 2.7: *Solvent effects on the absorption properties of* **90** *in* CH_2Cl_2 *(-),* CH_3OH *(-),* H_2O *(-),* CH_3CN *(-), Acetone (-) and DMF (-) with a* λ_{maxUV} *= ca. 390 nm.*

The absorption spectra of the 3-amino-1,8-naphthalimide **106**, which was recorded for comparison purposes, is shown in Figure 2.8. The absorption spectrum of **106** in CH_3OH is characterised by a high energy structural band at 245 nm, whereas, the region between 300 and 500 nm consists of a less intense band at *ca.* 349 nm and a broad band centred at 426 nm. Upon changing the solvent from CH_3OH to CH_2Cl_2, a hypsochromic shift of 17 nm was observed and is characterised as being due to an ICT excited state of the fluorophore. However, when the solvent is changed from CH_3OH to water, the λ_{maxUV} is blue shifted by 18 nm. This effect is similar to that observed for **90**, which has been reported for 4-amino-1,8-

naphthalimides and other donor acceptor systems as being due to the formation and absorbance of water clusters.[179] By comparing these changes with those recorded for **90**, it is evident that incorporation of the Tröger's base structural unit has a significant effect on the ability of the bridgehead nitrogens to participate in the ICT process. Similar results were obtained for the other derivatives **86**-**89** (Appendix 1).

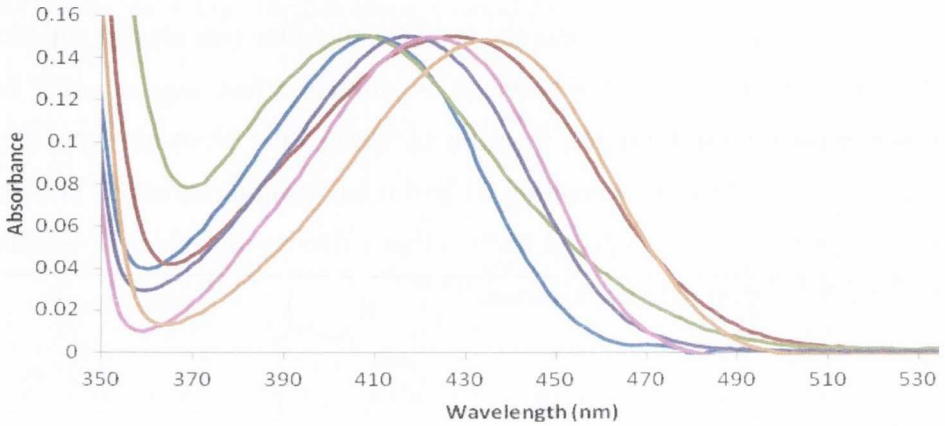

Figure 2.8: *Solvent effects on the absorption properties of* **106** *in* CH_2Cl_2 *(-),* CH_3OH *(-),* H_2O *(-),* CH_3CN *(-), Acetone (-) and DMF (-) where* λ_{maxUV} *= 409, 426, 408, 416, 422 and 434 nm, respectively.*

2.6.2 Excited State Studies of 86-90 in Solvents of Varying Polarity

The influence of solvent polarity on the emission behaviour of **90** and **106** was also studied, using the same solvents as for the absorbance studies above. When excited in CH_2Cl_2, **90** exhibited a broad unsymmetrical band at *ca.* 480 nm that tailed off to longer wavelengths (Figure 2.9). This supports the characterisation of such a band as having contributions from ICT transitions.[175]

As can be seen in Figure 2.9, upon increasing the polarity of the medium, the position of this band was red shifted and the intensity decreased. The largest bathochromic shift, a shift of 67 nm was observed when changing the solvent from CH_2Cl_2 to water. Such a shift was not observed in the absorption spectrum of **90**, therefore, it is evident that the emitting state is more polar than the ground state. A similar effect was observed for **83**.[148,149]

Following on from this, the emission spectra of **106** were investigated in the same range of solvents. When excited in CH_2Cl_2, the emission spectrum of **106** also exhibited a structureless band that tailed off to longer wavelengths. Upon increasing the polarity of the

medium this band was red shifted followed by the emission intensity decreasing, the extent of which depended on both the polarity and hydrogen bonding ability of the solvent. The largest bathochromic shift observed was 100 nm, which occurred when changing the solvent from CH_2Cl_2 to H_2O, as seen in Figure 2.10.

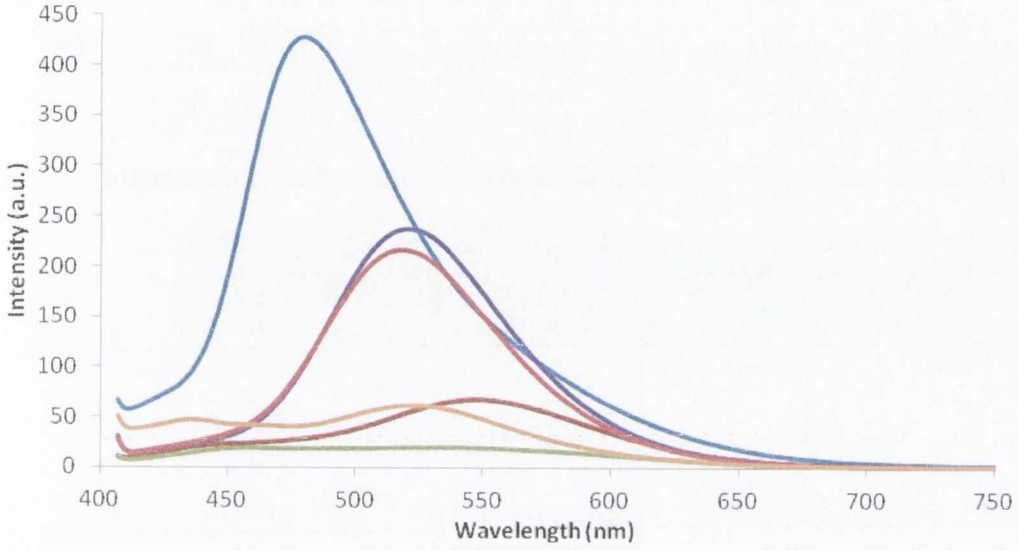

Figure2.9: *Solvent effects on the emission properties of* ***90*** *(λ_{Ex} =. 390 nm) in in CH_2Cl_2 (-), CH_3OH (-), H_2O (-), CH_3CN (-), Acetone (-) and DMF (-) where λ_{maxFLU} = 480, 547, 547*, 520, 518 and 524 nm, respectively. *Describes an approximate value due to the low emission intensity observed.*

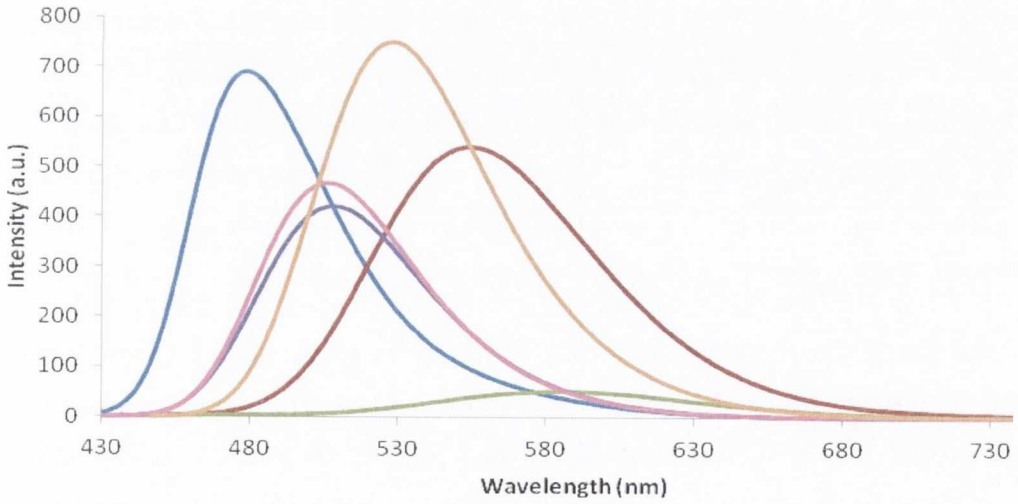

Figure 2.10: *Solvent effects on the emission properties of* ***106*** *(ex. 390 nm) in CH_2Cl_2(-), CH_3OH (-), H_2O (-), CH_3CN (-), Acetone (-) and DMF (-) where λ_{maxFLU} = 481, 555, 591, 505, 503 and 530 nm, respectively.*

The magnitude of this shift was much greater than that observed in the absorption spectrum of **106**, highlighting that the emitting state is more polar than the ground state.[148,149] Furthermore, the magnitude of such spectral shifts was not observed for **90**, which shows that the inherent geometry of the Tröger's base significantly affects the ability of the bridgehead nitrogen atoms to participate in the ICT process. Similar effects were observed for all the Tröger's bases **86-89** (Appendix 1). The photophysical properties of **90** and **106** are summarised in Table 2.3.

Table 2.3: *The photophysical properties of **90** and **106** in solvents of varying polarity.*

Solvent	90:λ_{maxUV} (nm)	90:λ_{maxFLU} (nm)	106:λ_{maxUV} (nm)	106:λ_{maxFLU} (nm)
CH_2Cl_2	390	480	409	481
CH_3OH	390	547	426	555
H_2O	385	547	408	591
CH_3CN	390	520	416	505
Acetone	390	518	422	503
DMF	390	524	434	530

Additional evidence for the presence of an ICT excited state in **90** was gathered by determining the fluorescence quantum efficiencies (ϕ_F), which are a source of information that gives the probability of the excited state being deactivated by fluorescence rather than any other non-radiative mechanism. The fluorescence quantum efficiencies as shown in Table 2.4, are low and were also found to decrease when the polarity of the medium increased. This effect was first reported by Deprez *et al.*[181] and is in agreement with the low fluorescent quantum efficiencies obtained for the bis-naphthalimide based Tröger's base **83** synthesised by Veale.[148, 149]

Firstly, the fluorescence quantum yields of these systems were measured using quinine sulphate (ϕ_F = 0.542 in 0.1M H_2SO_4) as the reference standard and two comparative methods were employed.[187] The first method involved using optically dilute solutions with an OD of 0.03 at the excitation wavelength of 368 nm, so that corrections for self-absorption and of incident and emitted light on the emission intensities were not required. An optically matched solution of the reference standard was used and excited at the same wavelength, so that both the test and reference samples could be considered to be absorbing the same number

of photons. The ϕ_F were calculated by comparing the integrated areas underneath the emission bands of the spectra using equation 2.1,

$$\Phi_x = \Phi_r \cdot A_r/A_x \cdot F_x/F_r \cdot (\eta_x)^2/(\eta_r)^2 \qquad (2.1)$$

where, x, r, A, F and η refer to the test sample, the reference standard, absorbance, integrated area and the solvent refraction index, respectively.[188]

The second method involved acquiring data at a number of different concentrations, where the OD of the solutions ranged from 0.10 to 0.02. Optically matched solutions of both the reference and test samples were used and excited at 368 nm. For this method, the fluorescence quantum efficiencies were determined according to equation 2.2,

$$\Phi_x = \Phi_r \cdot \mathbf{m}_x/\mathbf{m}_r \cdot (\eta_x)^2/(\eta_r)^2 \qquad (2.2)$$

where, x, r, and η refer to the test sample, the reference standard and the solvent refraction index, respectively. The **m** term corresponds to a gradient determined by plotting the integrated fluorescence area *versus* absorbance, where a straight line should be obtained for both the test and reference samples.[189]

The calculated quantum yields from both methods were repeated twice and compared, giving error values of 10 %. As can be seen in Table 2.4, the values determined for **90** were quite low with the ϕ_F being determined for CH_2Cl_2 as being 0.009. In order to ensure the accuracy of these values, these measurements were repeated using **83** (ϕ_F = 0.025 in CH_3CN) as the reference standard and employing both the methods discussed above. The average calculated quantum yields are summarised in Table 2.4.

Table 2.4: *Fluorescence quantum efficiencies determined for* ***90****, using quinine sulphate* and* ***83****** as reference standards.*

Solvent	ϕ_F *(± 10 %)	ϕ_F ** (± 10 %)
CH_2Cl_2	0.009	0.009
CH_3OH	0.003	0.002
H_2O	0.001	0.001
CH_3CN	0.003	0.003
Acetone	0.003	0.003
DMF	0.003	0.003

As can be seen in Table 2.4, the fluorescence quantum yields determined for **90** were found to be quite low in all the solvents investigated as part of this study. However, a trend can be observed as it is evident that these values decrease upon increasing the polarity of the medium. This trend was also observed for 4-amino derived analogues.[148,149,181]

It has been established that **90** exhibits an ICT excited state. This is a very important design element for molecules anticipated to interact with biological macromolecules such as DNA, as the changes in the ICT excited can be indicative of interactions taking place. The next design feature of these molecules to be investigated was the sensitivity of the *N*-imide side chains towards pH and a determination of the p*K*a values of the terminal amines of the ethylamino functionality side chains which are anticipated to interact with DNA and thus, enhance the DNA binding capacity of such molecules.

2.7 Photophysical Studies of 86-90 as a function of pH

In order to ascertain whether the dialkylamino groups could ideally be protonated at physiological pH and thus, allow for the occurrence of electrostatic interactions with DNA, the spectroscopic properties of all the Tröger's bases **86-90** were investigated as a function of pH in water, using 100 mM NaCl as buffer to maintain a constant ionic strength using absorption and fluorescence techniques. For comparison purposes the 3-amino-1,8-naphthalimide precursors **20** and **103-106** were also investigated. Their relevant p*K*a values were determined using the changes observed in the absorbance and/or the emission spectra by fitting the data according to equations 2.3 and 2.4, respectively, which have been derived from the Henderson-Hasselbalch equation,

$$pKa(S_o) = pH - Log[(Abs_{AH}-Abs_A)/(Abs_A-Abs_{A^-})] \quad (2.3)$$

$$pKa(S_1) = pH - Log[(I_{fAH}-I_{fA})/(I_{fA}-I_{fA^-})] \quad (2.4)$$

where, Abs_{AH} and Abs_{A^-} are the absorbance values in acidic and basic solution and Abs_A is the absorbance value at each pH determined in the pH versus A/A_o plot.[190] In the case of equation 2.4, I_{fAH} and I_{fA^-} are the emission intensities in acidic and basic solution and I_{fA} is the emission intensity calculated at each pH in the pH versus I/I_o plot.[190(a)]

Firstly, the effect of pH on the ground states of **86** and **20** was investigated and when recorded at acidic pH, **20** gave rise to a broad absorption band centred at 409 nm (ε_{20} = 4,870 mol^{-1} dm^3 cm^{-1}), whereas, for **86** a broad band was observed at 347 nm (ε_{86} = 19,332 mol^{-1}

dm^3 cm^{-1}). The absorption spectrum of **20** shown in Figure 2.11 exhibited an increase in absorbance between pH 2 and 4, which may be due to protonation of the aryl amino group. Protonation of the 3-amino functionality is possible due to the ICT process being weaker for these derivatives compared to their 4-amino-analogues.[182,183] However, no accurate p*K*a value could be determined from these changes. Furthermore, this ICT band exhibited pH independence from pH 4 to pH 11, as shown in Figure 2.11.

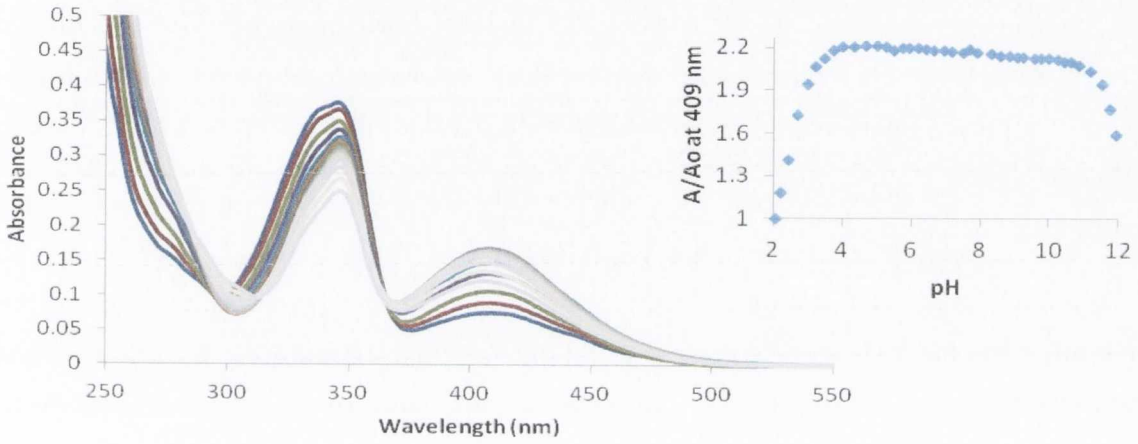

Figure 2.11: *The absorption spectra of* **20** *(15.5. μM) upon a gradual increase in pH. Inset: Changes in A/A_0 vs pH at 409 nm.*

Upon titration with NaOH, the absorption spectrum of **86** exhibited a decrease in absorbance of *ca.* 60 % at λ_{maxUV} = 347 nm, as can be seen in Figure 2.12.

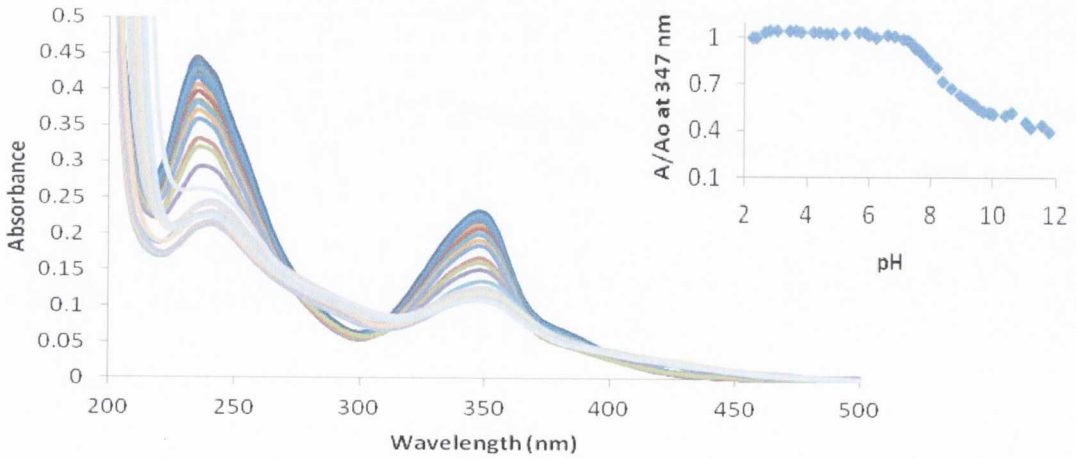

Figure 2.12: *The absorption spectra of* **86** *(11.2 μM) upon a gradual increase in pH. Inset: Changes in A/A_o vs pH at 347 nm.*

A smooth sigmoidal curve was observed between pH 7 and pH 10 giving rise to a p*K*a value of 8.3 (± 0.1). Such behaviour was observed for the 4-amino derived Tröger's base **81** and was postulated as being due to the tendency of the tertiary amine of the dialkylaminoethyl side chain to donate a proton into the naphthalimide structure.[191] The ability of the tertiary amine to donate into the ring is made possible due to the effect of the V-shaped Tröger's base structure on the ICT process, which is weaker and thus, the charge repulsion in **86** is not as strong compared to the 3-amino-1,8-naphthalimides. This effect can also be seen in the pH studies of **20** as protonation of the aryl amino group could occur as the charge repulsion is not strong due to the weak ICT process. Furthermore, this process may be weaker in **86** due to the inherent rigid geometry of the diazocine ring and therefore, the donating of a proton into the naphthalimide structure may occur. Such trends were found to be fully reversible.

The emission of **20** was studied as a function of pH and found to be highly pH dependent. As can be seen in Figure 2.13, a fluorescence enhancement was observed for the ICT emission band at 581 nm between pH 2 and pH 4, perhaps relating to the protonation of the aryl amino group. Unfortunately, no accurate p*K*a value could be determined using equation 2.4. However, as is shown in Figure 2.13, a smooth sigmoidal curve was obtained in the region between pH 6 and 10, and a corresponding p*K*a of 9.03 (± 0.1) was determined for the excited state of **20**.

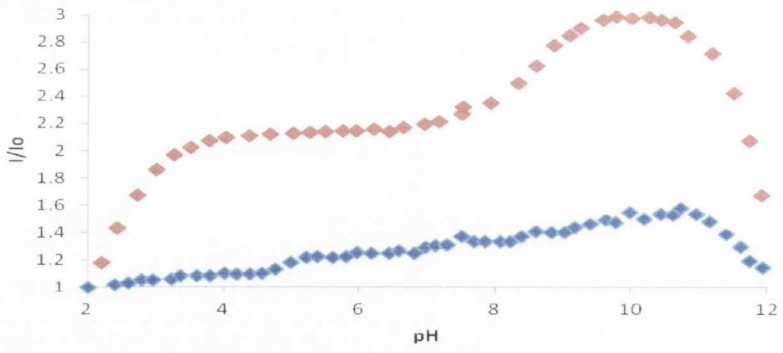

Figure 2.13: *The normalised changes in the emission of **20** (◆) at 581 nm and **86** (◆)*

In the case of **86**, when excited at 347 nm, minimal emission changes were observed between pH 2 and 4, however, fluorescence enhancement was observed between pH 4 and pH 11, however, an accurate p*K*a for **86** could not be determined. The fluorescence enhancement observed in the spectra of both **20** and **86** may be attributed to the loss of the hydrogen bond

that may have formed between the *N*-imide carbonyl oxygen and the protonated amine of the side chain. [192]

The absorbance and emission spectra of **89** and **105** were also investigated as a function of pH. When recorded in acidic solution, **89** gave rise to an absorption spectrum similar to **86**-**88** and **90** with a λ_{maxUV} at 347 nm (ε_{89} = 13,412 mol^{-1} dm^3 cm^{-1}). Upon titration with base, the absorbance spectra of **89** was found to decrease by *ca.* 65 % and these changes were found to be fully reversible (Appendix 1). A plot of the changes in the absorbance with respect to pH showed a sigmoidal step occurring between pH 5 and 9, which has a p*K*a of 7.6 (± 0.1).

When excited at 347 nm, **89** gave rise to an emission spectrum with three bands with λ_{maxFLU} at 436 nm, 463 nm and 499 nm, as shown in Figure 2.14. Upon titration with NaOH, the emission spectra of **89** exhibited a decrease of 98 % at 436 nm and showed a sigmoidal step between pH 4 and 11 from which a p*K*a of 6.7 (± 0.1) was determined. The behaviour observed in the emission spectrum of **89** upon increasing pH is in contrast to that observed for **86**, where a fluorescence enhancement was observed at high pH. As a result of the ICT character being weak, electron transfer from the amine of the side chain may be allowed and upon deprotonation of the piperidine functionality, the fluorescence is quenched.

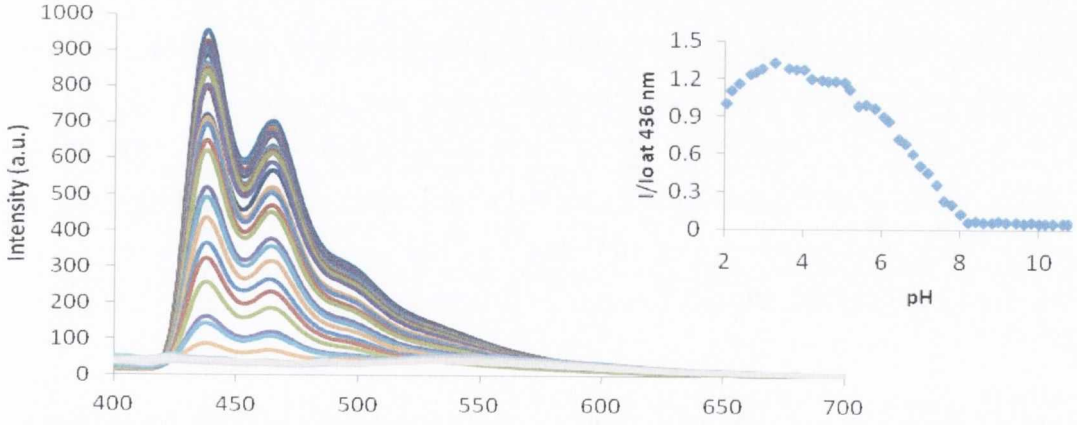

Figure 2.14: *Emission spectrum of* **89** *(9.9 μM) upon a gradual increase in pH with* λ_{Ex} = *347 nm. Inset: Changes in* I/I_o *vs pH at 436 nm.*

In the case of **105**, the absorption spectrum exhibited results similar to those observed for the other naphthalimide precursors such as **20**, with an increase in the absorbance between pH 2 and 4 and pH independence between pH 7 and 10 (Appendix 1). These changes were

fully reversible. When excited at 407 nm, the emission spectrum of **105** consisted of a broad structureless band centred at 587 nm (Figure 2.15).

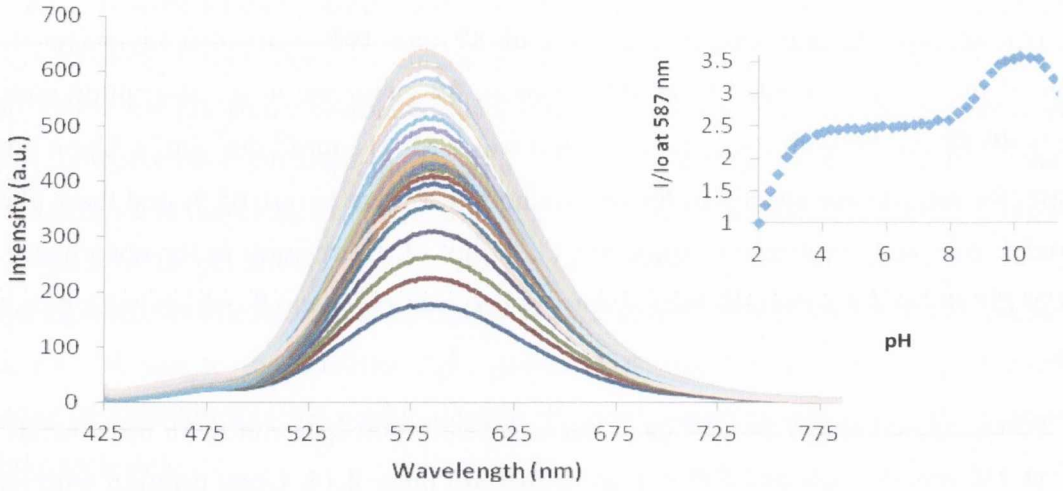

Figure 2.15: *Emission spectrum of **105** (15.5 μM) upon a gradual increase in pH. Inset: Changes in I/I_o vs pH at 587 nm.*

Upon the addition of acid, the emission spectrum exhibited a fluorescence enhancement between pH 2 and 4. At higher pH, a fluorescence enhancement was observed with a sigmoidal step between pH 7 and 10 from which a p*K*a value of 8.4 (± 0.1) was determined. The absorbance and emission properties of **87**, **88** and **90** and their corresponding precursors **103**, **104** and **106** were also examined as a function of pH. At acidic pH the absorption spectrum of **87**, **88** and **90** were found to be similar to that obtained for **86** (Appendix 1). Upon addition of base, the absorbance of each derivative was found to decrease at 347 nm. These changes were large enough to analyse using equation 2.3 and p*K*a values of 6.1 (± 0.1), 7.5 (± 0.1) and 8.1 (± 0.1) were determined for **87**, **88** and **90**, respectively. Again these changes were found to be fully reversible. In addition, the changes observed in the absorption spectra of **103**, **104** and **106** upon the addition of NaOH were similar to those discussed for **20** as a function of pH. These changes are summarised in Table 2.5.

When the emission spectra of **87**, **88** and **90** were studied as a function of pH, similar results were observed as discussed above. Upon excitation at 347 nm, broad unsymmetrical emission bands were observed between 400 and 750 nm, with λ_{maxFLU} of 546 nm, 545 nm and 548 nm for **87**, **88** and **90**, respectively. Upon titration with base, the emission spectra of **87**, **88** and **90** exhibited fluorescence enhancements of *ca.* 13 %, 36 % and 9 %. Again, these changes were fully reversible. Unfortunately, the changes in the emission spectra of **87** and **90** were not

large enough to allow for an accurate calculation of p*K*a values using equation 2.4. However, the pH versus I/I_0 profile for **88** exhibited changes between pH 4 and 11, giving a p*K*a value of 8.9 (± 0.1) (Appendix 1). The emission spectra of **103** and **105-106** showed changes similar to those seen for **20** upon the addition of base (Appendix 1). The changes observed were large enough to determine p*K*a values which are listed in Table 2.5.

Table 2.5: *Summary of properties determined for* ***86-90***, ***20*** *and* ***103-106*** *including pKa (in the ground state) and pKa* (in the excited state).* [a] *Absorbance changes and* [b] *emission changes were too small to permit a reliable determination of pKa values.*

Property	86	87	88	89	90	20	103	104	105	106
Log ε_{max} pH 7.4	4.29	4.17	4.25	4.13	4.17	3.69	3.73	3.63	3.60	3.77
p*K*a (± 0.1)	8.3	6.1	7.5	7.7	8.1	-[a]	-[a]	-[a]	-[a]	-[a]
p*K*a* (± 0.1)	-[b]	-[b]	8.9	6.7	8.6	9.0	6.2	8.2	8.8	9.1

The determination of these p*K*a values were an essential means of ascertaining whether or not the side chain of the relevant bis-1,8-naphthalimide containing Tröger's base derivatives would be protonated at pH 7.4, so that binding of such derivatives to DNA would be facilitated by electrostatic interactions with the negatively charged phosphate backbone of the DNA helix. It was found that **86** and **88-90** will be protonated at physiological pH, whereas, **87** which has a p*K*a of 6.1 (± 0.1) will not be protonated at pH 7.4. However, **87** can act as a model compound for analysing the interactions of **86** and **88-90** with DNA as it is not anticipated to give rise to significant electrostatic interactions with DNA. Having determined the p*K*a values and established the existence of an ICT excited state for **86-90** will aid in the analysis of their DNA binding affinities using various spectroscopic techniques such as absorption and fluorescence spectroscopy, circular dichroism (CD) and linear dichroism (LD), which will be discussed in the following sections.

2.8 DNA Binding Interactions of 86-90

In the work presented herein, each of the Tröger's bases **86-90** were designed to interact with DNA through a combination of modes. Firstly, as discussed in the previous section, the *N*-imide group is protonated at physiological pH and thus, electrostatic interactions with the anionic DNA phosphate backbone were anticipated to take place.

Secondly, binding of the 1,8-naphthalimides to DNA was envisaged to occur *via* intercalation or groove binding or a combination of both as shown in Figure 2.16.

The rationale for the design of the 1,8-naphthalimide containing Tröger's bases **86-90** was similar to that seen for **81-83**.[148,149] It was anticipated that the alteration in the shape of the Tröger's base structural unit as seen in Figure 2.17, by deriving these molecules from the 3-amino-1,8-naphthalimide chromophore, would lead to different DNA binding affinities and binding modes compared to the 4-amino derivatives such as **81** which was found to bind to the grooves of *ct*-DNA (Appendix 2).

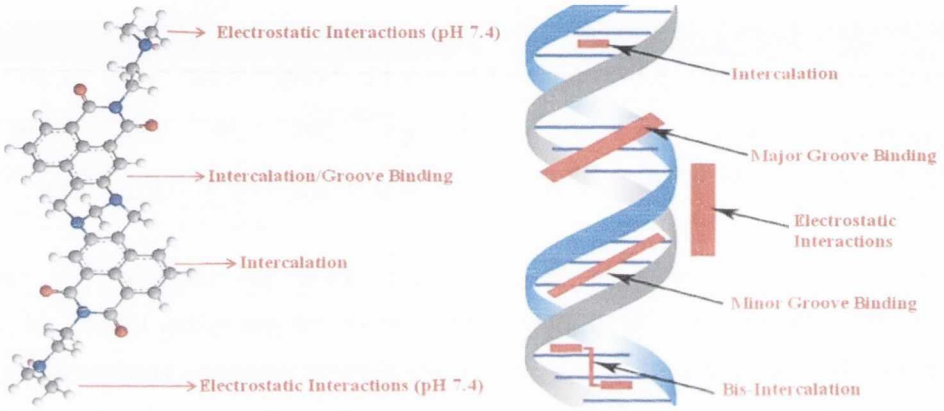

Figure 2.16: *Rationale in the design of **86** as a DNA binding agent and diagram representing the different modes of interaction with the DNA double helix (right).*[193]

With the aim of investigating the potential relationship between the shape of the Tröger's base and its DNA binding mode, the conformations of **81** and **86** were analysed using MM2 molecular mechanics studies in collaboration with Dr. C. Lincheneau (See Appendix 2 for details) and are shown in Figure 2.17. From these studies, dihedral angles of 96° and 72° were determined for the Tröger's base structural units of both **81** and **86**, respectively, and it was anticipated that this difference may play a pivotal role in determining the DNA affinity and DNA binding mode of these molecules.

As a means of evaluating the DNA binding affinity of **86-90**, absorption and fluorescence techniques were employed as interactions with DNA typically result in changes in the electronic spectra of DNA binding molecules. Additional spectroscopic techniques such as LD and CD were also carried out to investigate the nature of the binding of these molecules towards DNA and the results from these studies will be discussed in the following sections.

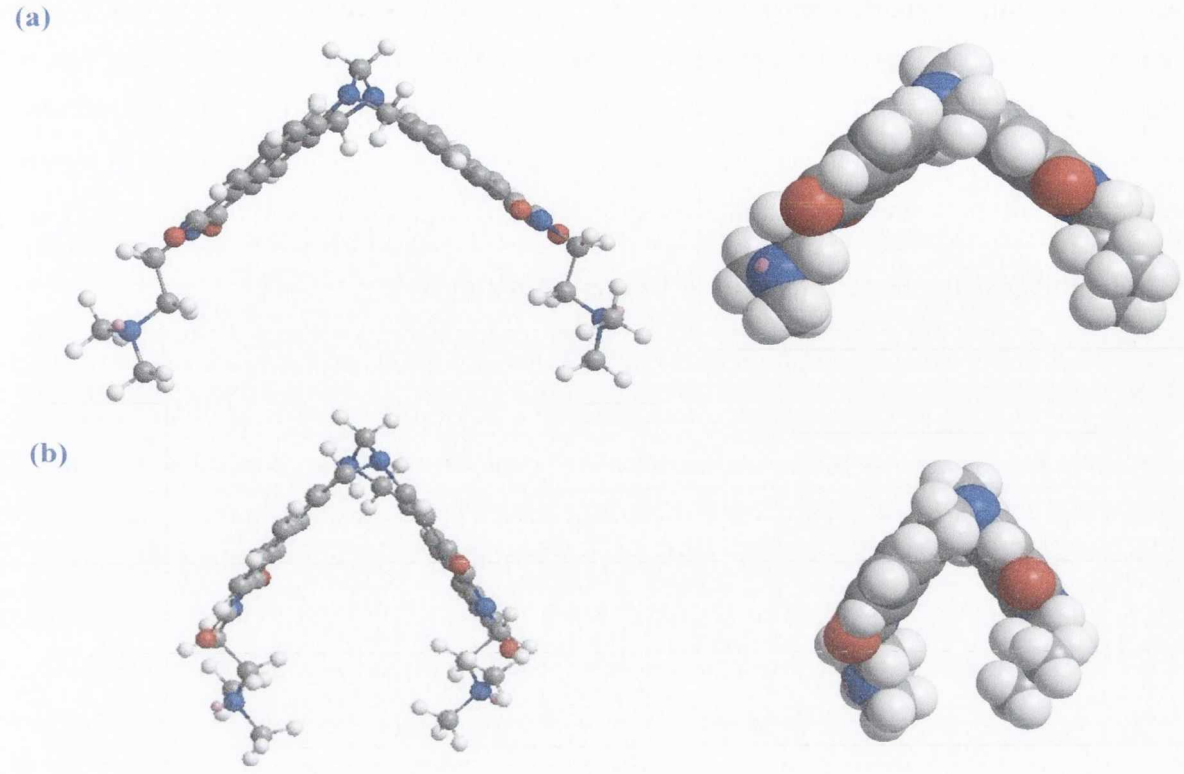

Figure 2.17 *(a) Ball and stick (left) and space filled (right) models of* **81**. *(b) Ball and stick (left) and space filled (right) models of* **86**.

2.8.1 Photophysical Evaluation of the DNA Binding Interaction

As shown in Section 2.6, the naphthalimide chromophores of **86**-**90** absorb in the 300-500 nm region of the electromagnetic spectrum. In contrast, the nucleobases of DNA absorb at *ca.* 250-260 nm and therefore, any changes in the absorption spectra of these DNA targeting molecules can be easily monitored. These changes may include a decrease in the absorbance of the molecule (hypochromism), a shift in the wavelength of the absorption maximum to a longer wavelength (bathochromic shift), or a shift to shorter wavelength (hypsochromic shift). Changes in the emission spectra of **86**-**90** upon the addition of DNA may involve an enhancement or quenching of the fluorescence intensity, a shift of the emission band to longer wavelengths (red shift) or to shorter wavelength (blue shift). When a plateau was reached, it was considered that all the compound was fully bound to DNA and this was regarded as the end point of the titration. All titrations were repeated three times to ensure reproducibility.

The absorption and fluorescence titrations were carried out with *ct*-DNA in aqueous 10 mM phosphate buffer at pH 7.4. At this pH the terminal amine groups of **86** and **88**-**90**

were protonated, whereas, the DNA is largely negatively charged and thus, electrostatic interactions should be maximised between the two. As **87** has a p*K*a value of 6.1 and was not expected to be protonated at physiological pH, this molecule was used as the reference compound in order to evaluate the importance of the cationic side chain in the DNA binding event.

2.8.2 Methods for the Determination of Binding Constants

The absorption and fluorescence spectral changes observed upon the addition of *ct*-DNA to **86-90** were used to estimate their respective binding constants. In order to measure these binding constants, two binding models were considered: **(i)** the Bard model[194] and **(ii)** the McGhee and von Hippel model.[195] Generally, absorbance spectral data may be fitted to the Bard model and/or the McGhee and von Hippel model, whereas, the luminescence data may only be fitted to the McGhee and von Hippel model.[194,195] All titration measurements were conducted a number of times to ensure reproducibility as stated above. The binding constant $\mathbf{K_b}$, described by the Bard model was determined using equations 2.5 and 2.6, which are valid for the assumption of non-cooperative non-specific binding to DNA with the existence of one discreet binding site **n**,

$$\frac{\varepsilon_a - \varepsilon_f}{\varepsilon_b - \varepsilon_f} = \frac{b - (b^2 - \frac{2K_b^2 C_t [DNA]}{n})^{1/2}}{2K_b C_t} \quad (2.5)$$

$$b = 1 + K_b C_t + K_b [DNA]/2n \quad (2.6)$$

where, ε_a, ε_f and ε_b correspond to the apparent extinction coefficient, the extinction coefficient for the free compound and the extinction coefficient for the compound in its fully bound form, respectively.[194] The concentration of DNA in base pairs is [DNA], C_t is the total compound concentration and **n** is the number base pairs occupied by the bound molecule.

$\mathbf{K_b}$ was determined from the luminescence data in accordance to the McGhee and von Hippel model (equation 2.7). The concentration of the bound compound C_b and the free compound C_f at a given concentration were firstly determined using equations 2.8 and 2.9,

$$\frac{r}{C_f} = K_b(1 - nr)\left[\frac{1 - nr}{1 - (n-1)r}\right]^{n-1} \quad (2.7)$$

$$C_b = \frac{I_f - I}{I_f - I_b}C \quad (2.8)$$

$$C_f = C - C_b \quad (2.9)$$

where, I_f and I_b are the fluorescence intensities of the free and bound compound, I is the fluorescence response, C is the total dye concentration, **n** is the binding site size and r = C_b/[DNA] ([DNA] is the concentration of DNA in base pairs).[195] The binding data were plotted in terms of r/C_f versus r and the binding constant and binding site size were determined from the non-linear fit to equation 2.7 using Origin Pro8.

2.8.3 Ground State Studies in Low Ionic Strength Medium (10 mM Phosphate Buffer)

The interaction of **86-90** with *ct*-DNA was first investigated using electronic absorption spectroscopy. Compound **86** was the first to be investigated and its absorption spectrum shown in Figure 2.18 was substantially affected by the successive addition of *ct*-DNA. The initial additions of *ct*-DNA (0-12.4 μM) resulted in a significant hypochromism of *ca.* 34 % for the λ_{maxUV} at 347 nm, with an accompanying bathochromic shift of 2 nm. The significant hypochromism and the concomitant bathochromic shift are indicators of an interaction between **86** and the double stranded *ct*-DNA.[33,196] Upon further addition of *ct*-DNA (14.3-56.1 μM), the absorption spectrum of **86** exhibited a small enhancement of 14 % at 347 nm. Thereafter, no changes were observed upon the addition of *ct*-DNA (42.2-89.0 μM). The changes in the absorbance at 347 nm were plotted with respect to a nucleotide phosphate to dye ratio (P/D) and as can be seen in the insert in Figure 2.18, a bi-phasic DNA binding event was observed for **86**. An initial decrease was observed between P/D 0-2.8 and this was followed by a subsequent absorbance enhancement, with a plateau being reached at a P/D of 12.

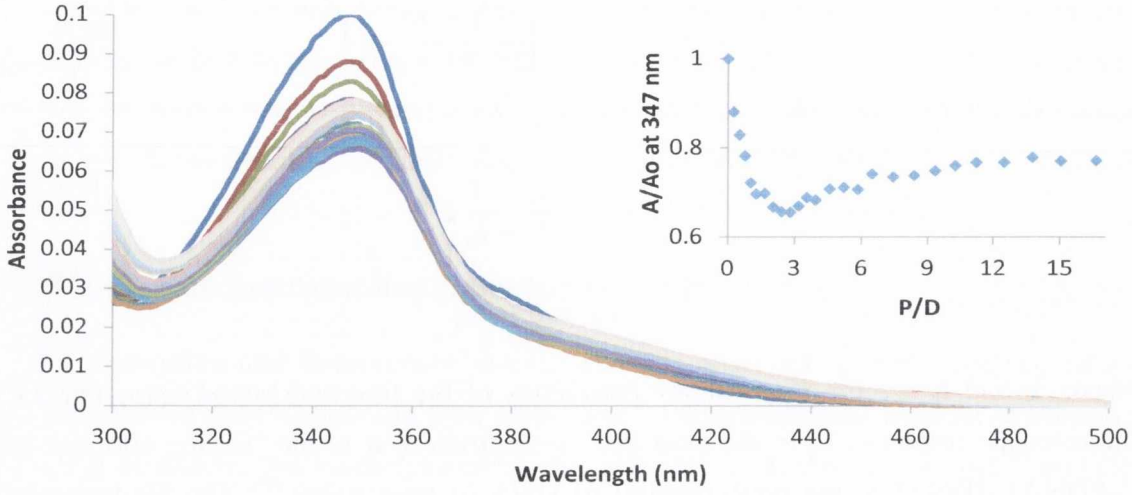

Figure 2.18: *The absorption spectrum of* **86** *(5.2 μM) in 10 mM phosphate buffer (pH 7.4) with increasing concentration of ct-DNA (0 – 89.0 μM). Inset: Plot of changes in the absorption spectrum of* **86** *at 347 nm in the presence of ct-DNA (0 – 89.0 μM).*

Similar results were reported for **81** and **83** and the ruthenium systems **84** and **85** and the bi-phasic behaviour observed was attributed to a ''template directed effect'' where the initial decrease in absorbance was reported to be as a result of DNA induced aggregation of **86**, causing the molecule to stack on the DNA backbone. This was followed by an increase in absorbance due to a de-stacking event and the subsequent redistribution of the species over the length of the DNA polyanion.[119,148,149] In addition, no clear isosbestic point was observed during the course of the titration which is perhaps indicative of more than one mode of binding.[197,198]

The bi-phasic binding behaviour observed for **86** was also observed for **88-90** upon the addition of *ct*-DNA. No clear isosbestic points were observed during the course of the titrations, however, a bathochromic shift of 2 nm was observed for **88**, whereas, for **89** and **90** bathochromic shifts of 3 nm were detected for each. When such changes at λ_{maxUV} = 347 nm were plotted as a function of P/D, similar isotherms were observed for **88** and **90** (Figure 2.19). For instance, **88** exhibits a hypochromism of 35 % between P/D 0-2.8 and upon further addition of *ct*-DNA the absorbance was enhanced by 12 % between P/D 2.4-11.2 with a plateau being reached at a P/D = 14.

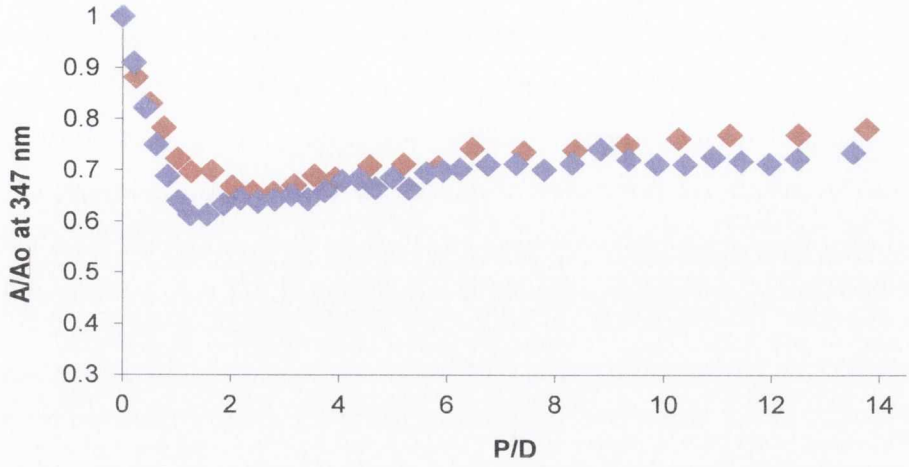

Figure 2.19: *Plot of the changes in the absorption spectra of* ***88*** *(◆) and* ***90*** *(◆) at pH 7.4 at 347 nm in the presence of ct-DNA.*

In the case of **90**, the absorption maximum exhibited a hypochromism of 39 % between P/D of 0-1.25 and a subsequent hyperchromic effect was observed between P/D 1.6 and 8.8.

The largest changes in the absorbance spectra were observed for **89**, where the absorbance maximum showed a hypochromism of 57 % from a P/D of 0-1.1, as shown in Figure 2.20. The subsequent absorbance enhancement of 23 % was observed between P/D 1.1 and 2.0. Thereafter, no changes were observed.

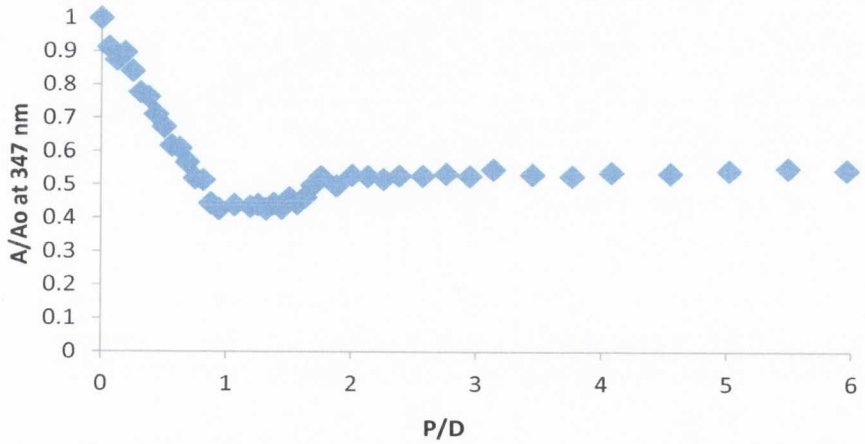

Figure 2.20: *Plot of the changes in the absorption spectra of* ***89*** *at pH 7.4 at 347 nm in the presence of ct-DNA.*

So far, significant changes have been observed in the absorption spectra of the Tröger's bases **86** and **88-90** upon the addition of *ct*-DNA in 10 mM phosphate buffer at pH 7.4. As already mentioned **86** and **88-90** can be protonated at physiological pH and are anticipated to interact with the anionic phosphate backbone through electrostatic interactions. In order to gain an insight as to whether or not the protonated side chains were a necessary feature for achieving stronger DNA binding, the DNA-binding affinity of **87** which has a p*K*a of 6.1 and is not expected to be protonated at physiological pH was investigated in 10 mM phosphate buffer at pH 7.4.

The changes in the absorption spectrum of **87** (10.5 μM) in 10 mM phosphate buffer (pH 7.4) upon the successive addition of *ct*-DNA (0–98.6 μM) were minor and are shown in Figure 2.21. Upon increasing concentration of *ct*-DNA, the absorption maximum at 347 nm exhibited a hypochromism of 7 % between P/D 0-1.1. In addition, no isosbestic point or bathochromic shift was observed. According to a plot of the changes in the absorbance of **87** shown in the inset of Figure 2.21, a bi-phasic binding mode was not observed.

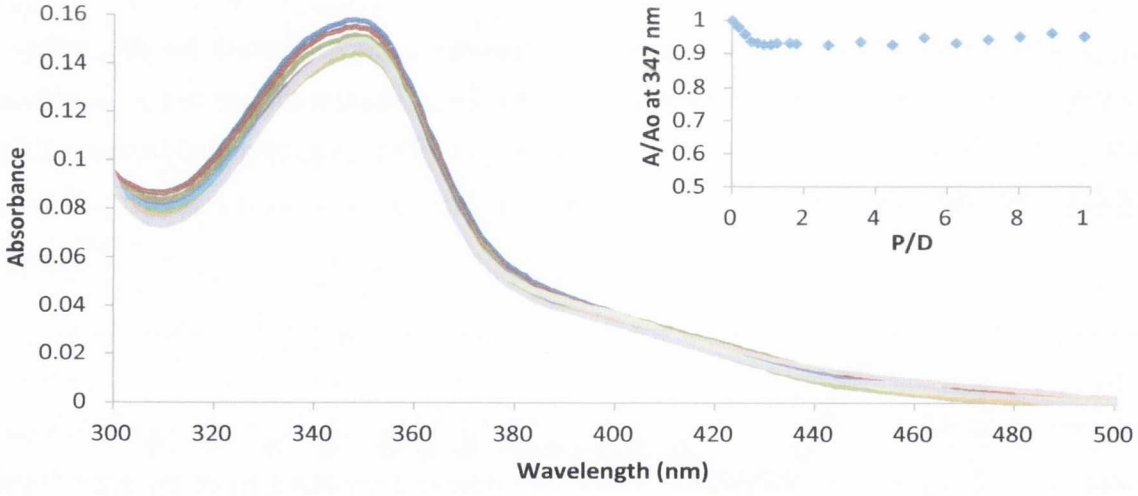

Figure 2.21: *The absorption spectrum of **87** (10.5 μM) in 10 mM phosphate buffer (pH 7.4) with increasing concentration of ct-DNA (0-98.6 μM). Inset: Plot of changes in the absorption spectrum of **86** at 347 nm in the presence of ct-DNA (0-98.6 μM).*

The changes observed in the absorbance spectra of **86-90** are summarised in Table 2.6. The bathochromic shifts and the hypochromic and hyperchromic effects observed in the absorbance spectra for **86** and **88-90** suggest that these molecules bind more strongly to *ct*-

DNA in comparison to **87** implying that the protonated side chain may be a necessary feature in achieving stronger DNA binding. Similar results were also observed for **81-83**.[148,149]

Table 2.6: *Photophysical properties of **86-90** (10 mM phosphate buffer, pH 7.4) in the presence of ct-DNA.* [a] ϵ_F *is the extinction coefficient of the free compound.* [b] λ_{maxF} *is the wavelength of maximum absorbance for the free compound.* [c] λ_{maxB} *is the wavelength of maximum absorbance for the bound compound.*

Property	86	87	88	89	90
ϵ_F (M^{-1} dm^3 cm^{-1}) [a]	19332	14934	16762	13412	14825
λ_{maxF} (nm) [b]	347	347	347	347	347
λ_{maxB}(nm) [c]	349	347	349	350	350
Bathochromic shift (nm)	2	0	2	3	3
Hypochromism (%)	34	7	35	57	39
Hyperchromism (%)	14	0 %	12	23	16

In summary, the affinity of **86-90** towards *ct*-DNA has been investigated by absorption spectroscopy. Analysis of the data in Table 2.6 shows that significant changes occur in the absorption spectra of **86** and **88-90** upon successive addition of *ct*-DNA, whereas, only minor changes occurred for **87**. This was anticipated because the *N*-imide side chains remain unprotonated at physiological pH and no electrostatic interactions can take place. Similar results were reported by Veale *et al.*[148,149] for **81-83** with **82** exhibiting only minor changes upon the addition of *ct*-DNA at pH 7.4.

For comparison purposes, the changes in the absorbance spectra of the 3-amino-1,8-naphthalimide precursors **20** and **103-106** in the presence of *ct*-DNA were also investigated in 10 mM phosphate buffer (pH 7.4). The interaction of *ct*-DNA with **20** is shown in Figure 2.22, where a bathochromic shift of 22 nm of the absorption maxima coupled to a 47 % hypochromism at 408 nm was observed. In addition, an isosbestic point was observed during the course of the titration at 443 nm, indicating the presence of two spectroscopically distinct free and *ct*-DNA bound chromophores. Similar decreases in the absorption spectra have been observed for unsubstituted and 3- and 4-substituted naphthalimides.[33,35,120,191,196,197,199]

The changes observed in the absorbance spectra of **20** were plotted as a function of P/D and as can be seen in the inset in Figure 2.22, no bi-phasic behaviour was observed for **20** upon the addition of *ct*-DNA, showing that there is a significant difference in the binding interactions of **20** and **86** with *ct*-DNA due to the incorporation of the Tröger's base structural unit. Furthermore, this plot shows that **20** is binding to *ct*-DNA at a P/D of 12, whereas, in the case of **86**, the initial binding interaction exhibited by **86** occurred at a much lower P/D of 2.4.

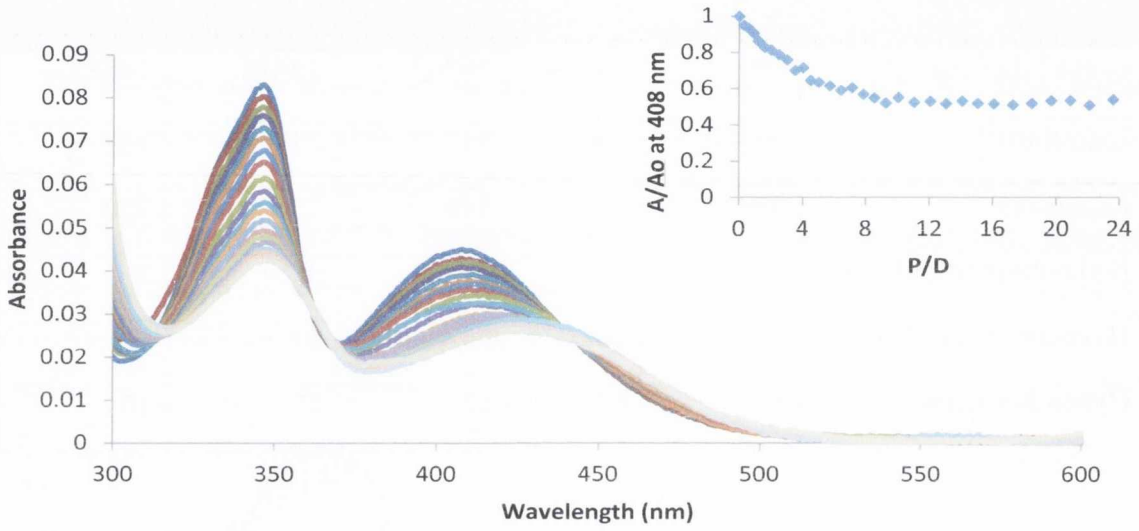

Figure 2.22: *The absorption spectrum of **20** (9.3 μM) in 10 mM phosphate buffer (pH 7.4) with increasing concentration of ct-DNA (0-228.2 μM). Inset: Plot of changes in the absorption spectrum of **20** at 408 nm in the presence of ct-DNA (0-228.2 μM).*

In a similar manner, the absorption spectrum of **103** shown in Figure 2.23, a hypochromic effect of 35 % at λ_{maxUV} = 406 nm was observed accompanied by a bathochromic shift of 17 nm. In addition, an isosbestic point was observed at 437 nm. These changes are plotted as a function of P/D in the inset in Figure 2.23 and are more significant than those observed for the Tröger's base derivative **87**. These spectral changes show the impact of the shape of the Tröger's base unit on the ability of the naphthalimide chromophore to bind to DNA. As only minor changes were observed in the absorption spectra of **87** upon the addition of *ct*-DNA, this suggests that the mode of binding has been altered due to the incorporation of the Tröger's base moiety and that the electrostatic interactions are required for strong DNA binding.

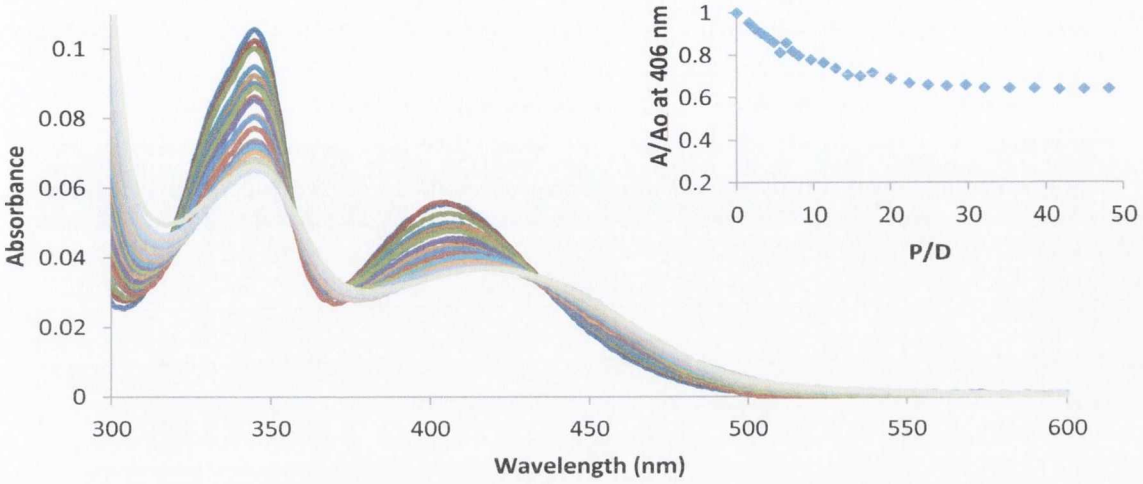

Figure 2.23: *The absorption spectrum of* ***103*** *(10.5 μM) in 10 mM phosphate buffer (pH 7.4) with increasing concentration of ct-DNA (0 – 457.7 μM). Inset: Plot of changes in the absorption spectrum of* ***103*** *at 408 nm in the presence of ct-DNA (0-457.7 μM).*

A plot of A/A_o versus P/D for the changes observed in the absorption spectra of **104-106** is shown in Figure 2.24. Upon the addition of *ct*-DNA to **104-106**, significant decreases in absorbance and shifts to longer wavelengths were observed, in addition to the presence of isosbestic points. Such photophysical behaviour is summarised in Table 2.7.

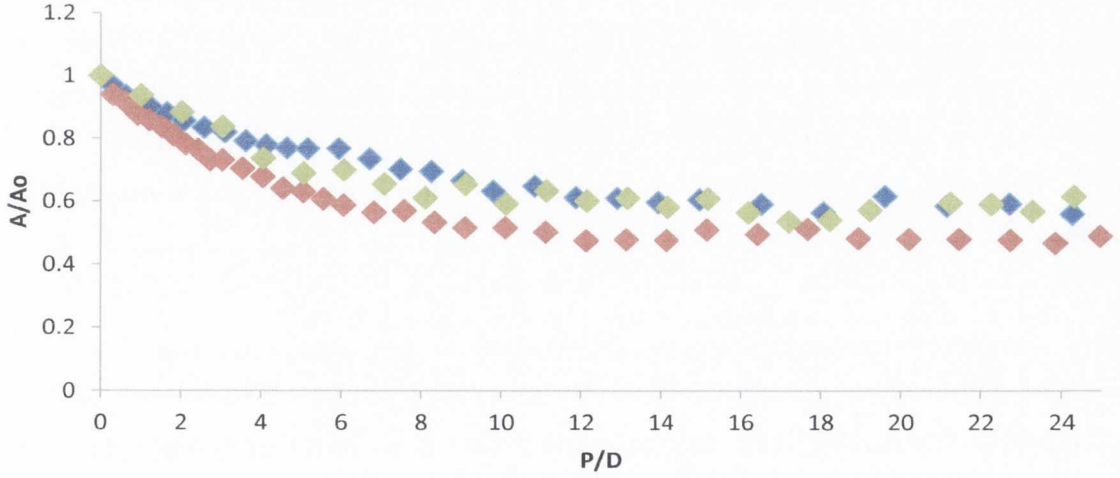

Figure 2.24: *Plot of the changes in the absorption spectra of* ***104*** *(◆), 105 (◆) and 106 (◆) at pH 7.4 in the presence of ct-DNA at 405, 407 and 406 nm, respectively.*

Table 2.7: *Photophysical properties of 20 and 103-106 (10 mM phosphate buffer, pH 7.4) in the presence of ct-DNA.* [a] ϵ_F *is the extinction coefficient of the free compound.* [b] λ_{maxF} *is the wavelength of maximum absorbance for the free compound.* [c] λ_{maxB} *is the wavelength of maximum absorbance for the bound compound.*

Property	20	103	104	105	106
ϵ_F (M^{-1} dm^3 cm^{-1}) [a]	4670	5290	4224	3944	5879
λ_{maxF} (nm) [b]	408	406	405	407	406
λ_{maxB}(nm) [c]	430	423	421	421	429
Bathochromic shift (nm)	22	17	16	14	23
Hypochromism (%)	47	35	39	52	42
Isosbestic point (nm)	433	437	434	438	438

In summary, the ground state investigations have shown that the novel Tröger's bases **86** and **88-90** interact with *ct*-DNA in a bi-phasic binding event, similar to that seen for the 4-amino derived analogues **81** and **83**. Only one mode of binding was observed for the precursors **20** and **103-106** showing that incorporation of the Tröger's base unit impacts on the mode of binding of the naphthalimide chromophore. In order to evaluate the DNA binding interactions, the binding constants were determined and are discussed in the following section.

2.8.4 Binding Constants Determined from the Absorbance Data

The data from the initial changes in the absorption spectra of **86-90** were analysed in order to obtain their binding affinities for *ct*-DNA. Due to the bi-phasic behaviour observed it was not possible to analyse the absorbance data using the Mc Ghee and von Hippel binding model[195] which requires the data from the DNA titrations to be represented as a Scatchard plot which results in the omission of data from the beginning and the end of the titrations. The data points from the first interaction were used to determine the binding parameters for the Bard model[194] and a description of this binding model was previously discussed in Section

2.8.2. However, the errors associated with the binding constants were high and this may be due to the limited number of data points in the plateau region of the first binding interaction.

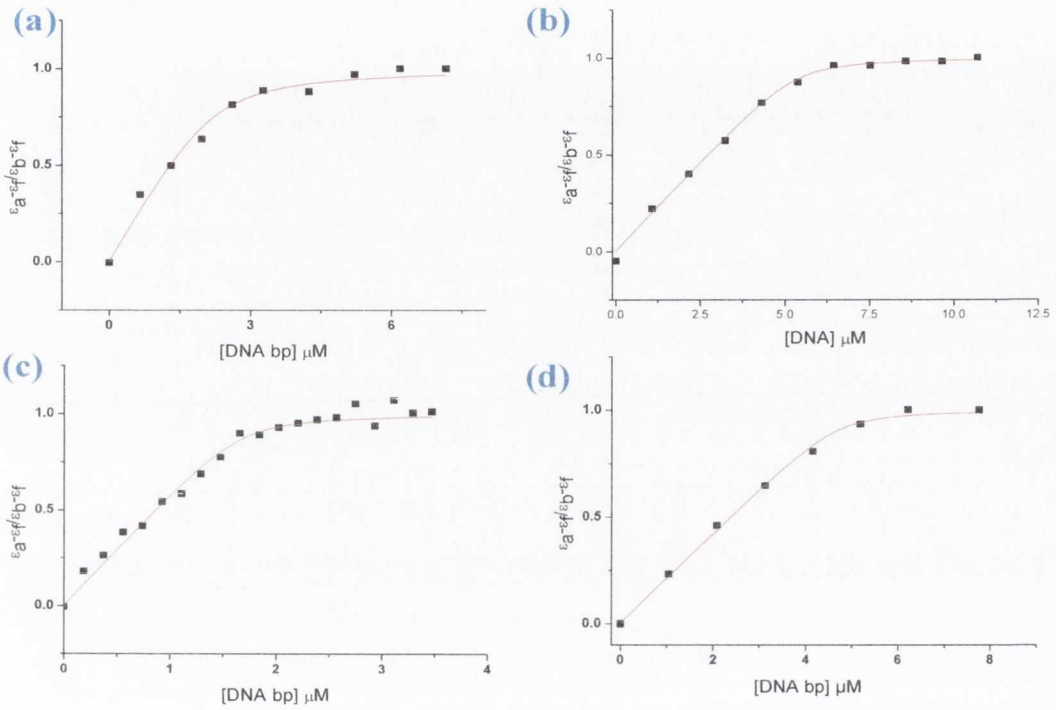

Figure 2.25: *Plot of $(\varepsilon_a-\varepsilon_f)/(\varepsilon_b-\varepsilon_f)$ versus ct-[DNA] for* **86** *(a),* **88** *(b),* **89** *(c) and* **90** *(d) and the corresponding non-linear fits to the Bard model (equation 2.5).*

Binding constants $\mathbf{K_b}$ and binding site sizes **n** were determined for **86** and **88-90** and the representative curves are shown in Figure 2.25. The changes observed in the absorbance spectra of **87** upon the addition of *ct*-DNA were minor and thus, $\mathbf{K_b}$ could not be determined. Binding constants $\mathbf{K_b}$ and binding site sizes **n**, using the Bard binding model are summarised in Table 2.8.[194]

The binding constants determined for **86** and **88-90** were large being in the range of 10^6 M^{-1}. Similar binding affinities were observed for the 4-amino derivatives **81-83**.[148,149] The binding constant values determined for these derivatives were significantly higher than several commonly used anti-tumour agents such as 9-amino acridine (5.3×10^5 M^{-1})[201(a)] and 9-anilinoacridine derivatives.[201(b)] For **87**, the changes in absorbance were relatively small compared to **86**, **88-90** and thus, upon analysis of the data a reasonably good fit using the Bard parameters could not be obtained.[194] The binding site sizes determined as shown in

Table 2.8 were less than unity and this is not in accordance with the ''neighbour exclusion principle''.[200]

Table 2.8: *Binding constants* K_b *and binding site sizes* ***n*** *determined where possible for* **86-90** *bound to ct-DNA in 10 mM phosphate buffer at pH 7.4, using the Bard binding model.*[194] [a] *Changes were too small to determine* K_b.

Compound	K_b ($\times 10^6$ M^{-1})	n (bp)	R^2
86	8.51 (± 5.34)	0.22 (± 0.01)	0.99
87	_____ [a]	_____ [a]	_[a]
88	6.59 (± 2.35)	0.27 (± 0.01)	0.99
89	9.69 (± 3.96)	0.17 (± 0.10)	0.99
90	9.68 (± 4.80)	0.23 (± 0.10)	0.99

Similar binding site sizes were observed for **81-83** which were postulated as being due to the binding interactions of the Tröger's bases occurring in the grooves of the DNA helix.[191] Consequently, investigations were undertaken to elucidate the mode(s) of binding for these compounds using circular and linear dichroism techniques, and the results from these studies will be discussed in Sections 2.8.11 and 2.8.12, respectively.

Quantitative analysis of the absorbance changes for **20** and **103-106** was conducted using both the Bard and McGhee and von Hippel binding models, as shown in Table 2.9.[194,195] The binding constants determined are in the range of 10^5 M^{-1}-10^6 M^{-1} . For instance, the binding constants of **104-106** were found to be an order of magnitude lower than those determined for **87-90** indicating that the incorporation of the Tröger's base structural unit into the design was well founded as the DNA binding affinity of these novel compounds was enhanced.

Table 2.9: *Binding constants K_b and binding site sizes **n** determined where possible for **20** and **103-106** bound to ct-DNA in 10 mM phosphate buffer at pH 7.4, using the Bard and Mc Ghee and von Hippel models.*[194,195] [a] *An accurate K_b could not be determined.*

Compound	Bard		McGhee and von Hippel	
	K_b ($\times 10^5$ M^{-1})	n(bp)	K_b ($\times 10^5$ M^{-1})	n(bp)
20	1.22 (± 0.30)	1.24 (±0.07)	0.37 (± 0.02)	1.82 (±0.06)
103	0.11 (± 0.05)	1.27 (± 0.09)	0.06 (±0.003)	2.69 (±0.08)
104	0.25 (±0.07)	0.90 (± 0.13)	0.14 (± 0.01)	2.21 (±0.01)
105	0.57 (±0.11)	0.78 (± 0. 05)	0.35 (± 0.01)	1.58 (±0.03)
106	_____ [a]	_____ [a]	0.30 (± 0.03)	2.46 (± 0.08)

2.8.5 Excited State Studies in Low Ionic Strength Medium (10 mM Phosphate Buffer)

The interaction of **86-90** with *ct*-DNA was investigated using fluorescence emission and excitation spectroscopy in 10 mM phosphate buffer at pH 7.4. The titrations were performed by exciting the absorbance maximum λ_{maxUV} as no isosbestic points were observed in the absorbance spectra. The fluorescence emission and excitation spectra of **88** and **89** are shown in Figure 2.26.

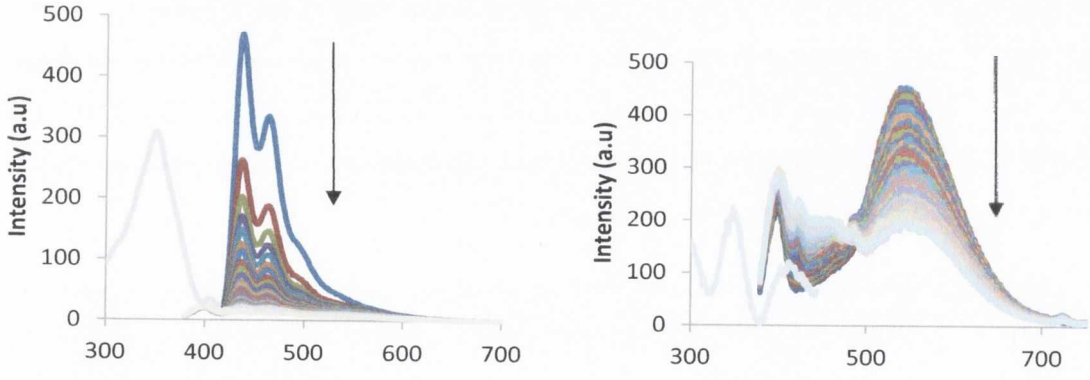

Figure 2.26: *The overlaid excitation (λ_{Em} = 500 nm) and emission spectra (λ_{Ex} = 347 nm) of **89** (left) and **88** (right) in 10 mM phosphate buffer (pH 7.4) upon increasing ct-DNA (0-47.9 μM)*

Upon successive addition of *ct*-DNA, the emission spectrum of **89** was fully quenched and there was no shift in the band position (λ_{maxFLU}). In the case of **88**, a bi-phasic binding phenomenon was observed, as initially there was a dramatic increase in the fluorescence intensity between P/D of 0-0.8, followed by a sharp decrease in the intensity with a plateau being reached at a P/D of 8. However, no shifts in the emission maximum to longer or shorter wavelengths were detected. The changes in the emission spectra of **86** and **88-90** as a function of P/D are shown in Figure 2.27.

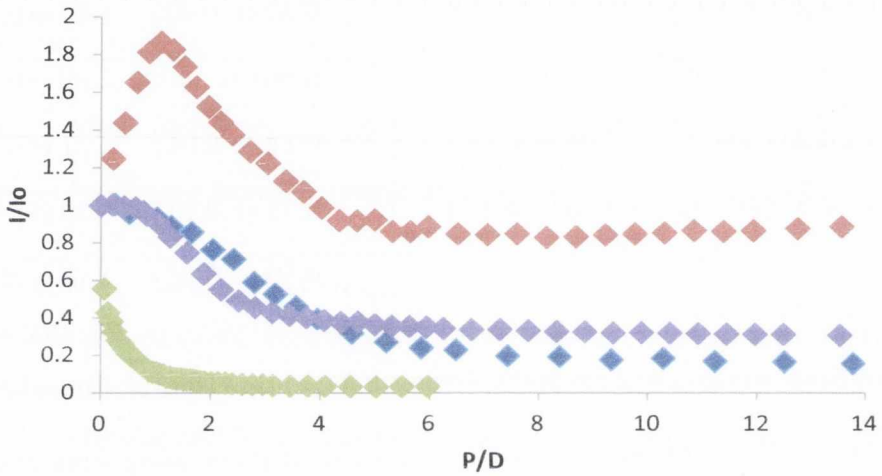

Figure 2.27: *Plot of changes in intensity of* ***86*** *(◆),* ***88*** *(◆),* ***89*** *(◆) and* ***90*** *(◆) vs. P/D in 10 mM phosphate buffer at pH 7.4 at* λ_{Em} *= 538, 545, 464 and 545 nm, respectively.*

When the emission spectrum of **87** in 10 mM phosphate buffer at pH 7.4 was investigated as a function of increasing *ct*-DNA concentration, larger changes were observed in the excited state compared to the ground state as shown in Figure 2.28. In the absence of *ct*-DNA, upon excitation at 347 nm, compound **87** exhibited a broad emission band centred at λ_{maxFLU} at 543 nm. The intensity of this band was significantly quenched by *ca.* 70 % in the presence of increasing concentration of *ct*-DNA.

The substantial fluorescence quenching observed for **86-90** may be attributed to an efficient photo-induced electron transfer (PET) from the DNA bases to the excited state of the naphthalimide chromophore. Similar fluorescence quenching was also observed for the 4-amino derived Tröger's bases **81** and **83**.[191]

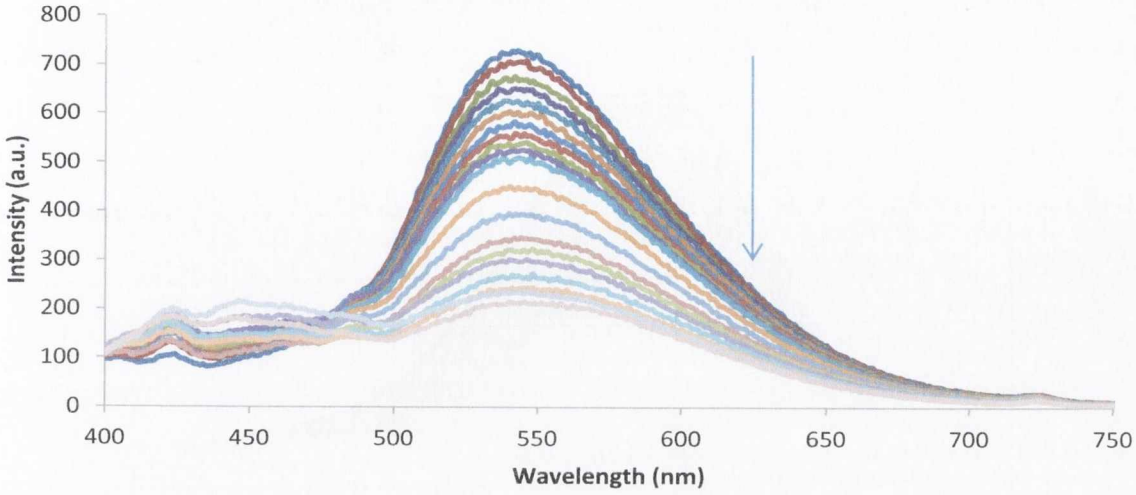

Figure 2.28: *Fluorescence emission spectrum of* **87** *(10.5 μM) (λ_{Ex} = 347 nm) upon increasing ct-DNA concentaration (0-98.6 μM) in 10 mM phosphate buffer at pH 7.4.*

For comparison purposes, the interactions of **20** and **103-106** with *ct*-DNA were investigated using fluorescence emission and excitation spectroscopy in 10 mM phosphate buffer at pH 7.4. The fluorescence emission spectrum of **20** is shown in Figure 2.29. Upon excitation at 408 nm, a broad emission band was observed centred at 582 nm. The intensity of this band was quenched substantially upon increasing concentration of *ct*-DNA (from a P/D of 0 to 20) in addition to a hypsochromic shift of *ca.* 24 nm being observed. Similar changes were observed for **103-106** and these changes are summarised in Table 2.10.

Table 2.10: *Summary of emission properties observed for* **20** *and* **103-106** *upon the addition of ct-DNA in 10 mM phosphate buffer (pH 7.4).* [a] *λ_{maxF} is the wavelength of maximum intensity for the free compound.* [c] *λ_{maxB} is the wavelength of maximum intensity for the bound compound.*

Property	20	103	104	105	106
λ_{maxF} (nm) [a]	582	587	581	583	585
λ_{maxB} (nm) [b]	558	574	552	564	559
Hypochromism (%)	70	64	35	51	56
Hypsochromic Shift	24	13	29	19	26

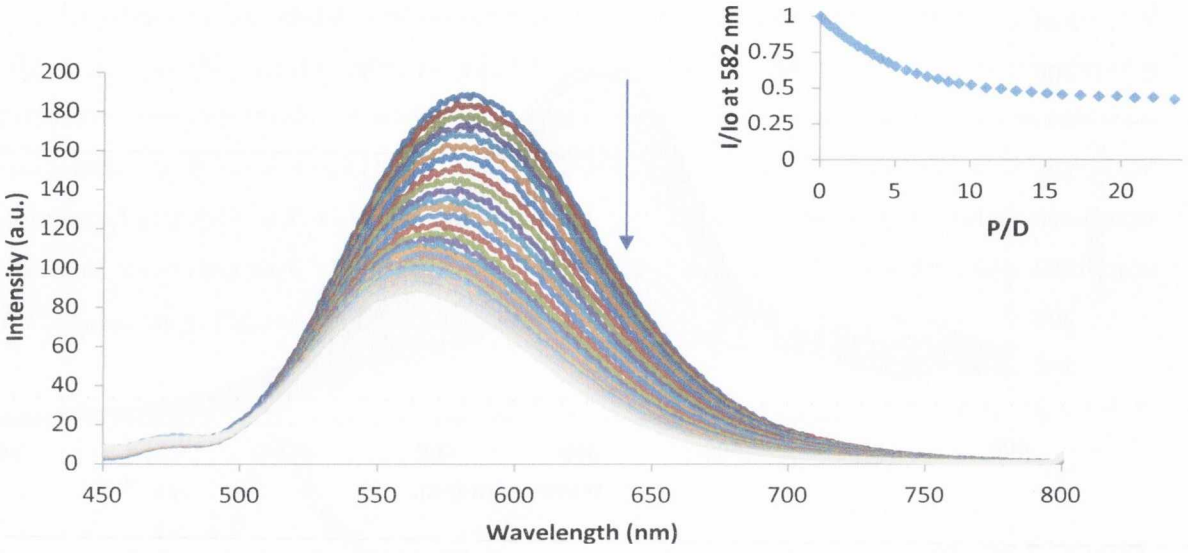

Figure 2.29: *Fluorescence emission spectrum (λ_{Ex} = 408 nm) of* **20** *(9.3 μM) in 10 mM phosphate buffer (pH 7.4) upon successive addition of ct-DNA (0 – 228.2 μM). Inset: Plot of changes in emission spectrum of* **20** *as a function of P/D at 582 nm.*

2.8.6 Binding Constants Determined from the Emission Data

Binding constants $\mathbf{K_b}$ and binding site sizes **n** were determined where possible for **86-90** utilising the McGhee and von Hippel binding model and are summarised in Table 2.11. The binding curves and corresponding fits for the interactions between **87** and **90** and *ct*-DNA are shown in Figure 2.30.

Table 2.11: *Binding constants determined for* **86-90** *where possible using the McGhee and von Hippel binding model.* [a] *Using the data obtained no accurate binding constant could be determined.*

Compound	K_b ($\times 10^6$ M^{-1})	n(bp)	R^2
86	_____ [a]	_____ [a]	____ [a]
87	0.22 (± 0.01)	1.15 (± 0.04)	0.88
88	_____ [a]	_____ [a]	____ [a]
89	5.64 (± 0.24)	0.42 (± 0.01)	0.76
90	0.78 (± 0.02)	1.19 (± 0.03)	0.95

As can be seen in Table 2.11, the R^2 values for the fits for the Scatchard plots were not near unity except for **90** which highlights that the binding constants obtained are not very reliable. This may be because these compounds are binding quite strongly to *ct*-DNA and these changes are happening very quickly. In order to quantify the DNA binding interaction these molecules will be studied in high ionic strength as the strength at which the drug binds is expected to decrease due to a shrinking of the DNA helix.

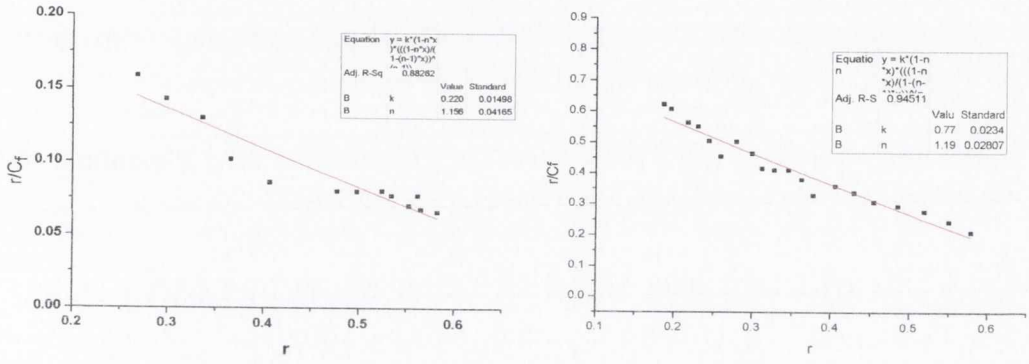

Figure 2.30: *Scatchard plots (■) and best fits (-) of the emission data for **87** (left) and **90** (right) in 10 mM phosphate buffer at pH 7.4.*

The binding constants were determined for the precursors for comparison purposes using the McGhee and von Hippel model and are summarised in Table 2.12. These values are in the range of 10^5 M^{-1}, an order of magnitude lower than that observed for **90** (best fit) showing that the design of these molecules was well founded.

Table 2.12: *Binding constants determined for **20** and **103-106** where possible using the McGhee-von Hippel binding model. [a] Using the data obtained no accurate binding constant could be determined.*

Compound	K_b ($\times 10^5$ M^{-1})	n(bp)	R^2
20	0.22 (± 0.01)	2.41 (± 0.01)	0.98
103	_____ [a]	_____ [a]	0.88
104	0.14 (± 0.01)	2.21 (± 0.10)	0.89
105	0.25 (± 0.01)	1.75 (± 0.05)	0.94
106	0.86 (± 0.03)	0.65 (± 0.01)	0.92

Moreover, the binding site size for the 3-amino-1,8-naphthalimide derivatives **20** and **103-106** were found to close to 2 bp, which is usually observed for intercalating molecules such as proflavin according to the ''Neighbour Exclusion Principle''.[200]

In summary, the newly formed Tröger's bases have been shown to bind to *ct*-DNA with a high affinity and with comparable affinity to the 4-amino derived analogues **81-83**. In addition, **86-90** demonstrate a higher affinity towards *ct*-DNA in comparison to their monomeric counterparts highlighting that the design of these molecules was well founded. In order to further evaluate their binding to *ct*-DNA, these molecules were studied in competitive media and these results are discussed in the following section.

2.8.7 Ground State Studies in High Ionic Strength Medium (10 mM Phosphate buffer + NaCl)

Ligands that bind to double helical DNA through an intercalative mode and/or association with the grooves typically lose their binding affinity as the ionic strength is increased due to a decrease in the phosphate-phosphate repulsion which results in the contraction of the DNA helix.[202,203] According to the polyelectrolyte theory by Manning,[204] sodium and potassium cations interact with DNA through condensation effects that stabilise the polyanionic duplex. As a consequence of this, positively charged DNA binders which would otherwise contribute to charge neutralisation may be displaced by a competitive salt effect in which high concentrations of sodium and potassium cations effectively compete for the negatively charged binding sites.

The Tröger's bases **86-90** studied above contain *N*-imide side chains that are expected to bind to DNA *via* electrostatic interactions, but also contain two 1,8-naphthalimides that are anticipated to either bind in the DNA grooves or *via* intercalative stacking interactions or possibly both. In order to investigate the effect of NaCl on the DNA binding ability of these molecules, their binding affinities were investigated in the presence of 50 mM and 160 mM NaCl. Concentrations of 50 and 160 mM were chosen for NaCl as they mimic the concentrations found within the cell nucleus and standard *in vitro* concentrations, respectively.[202]

The changes in the absorption spectra for the titration of **86** with *ct*-DNA in 50 mM and 160 mM NaCl at pH 7.4 are shown respectively, in Figure 2.31(a) and (b). As can be seen in Figure 2.31(a), the changes observed in the absorption spectrum of **86** (10 mM phosphate

buffer + 50 mM NaCl) upon increasing *ct*-DNA concentration were similar to those observed in the absence of NaCl. A hypochromic effect of 24 % was observed between P/D 0-8, in addition to an absorbance enhancement of 5 % between P/D 8-15 and a slight bathochromic shift of 2 nm was observed for the absorbance maximum at 347 nm.

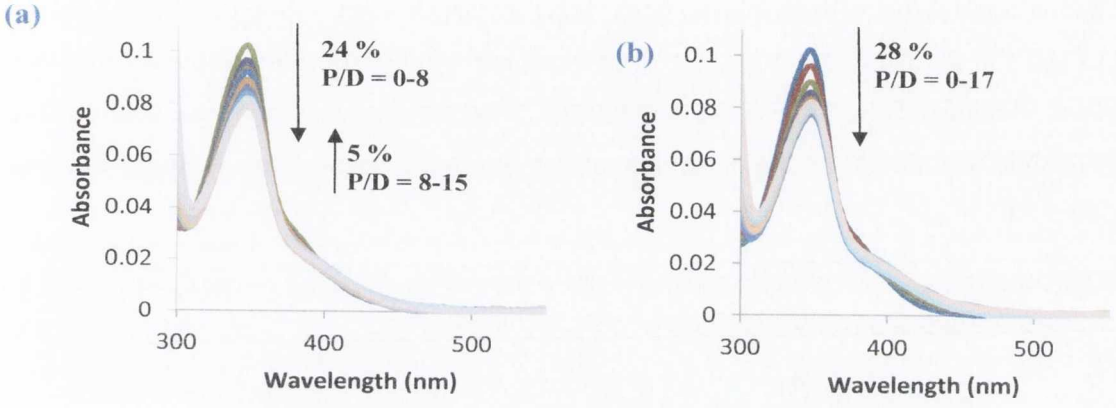

Figure 2.31: *The absorption spectra of* **86** *(5.3 μM) in* **(a)** *10 mM phosphate buffer + 50 mM NaCl and* **(b)** *10 mM phosphate buffer + 160 mM NaCl upon titration with ct-DNA (0 -272 μM).*

Such bi-phasic behaviour was not observed upon the addition of *ct*-DNA at higher ionic strength (10 mM phosphate buffer + 160 mM NaCl), a hypochromism of 28 % was observed between a P/D of 0 to 17. Further additions of *ct*-DNA only produced a negligible effect. A plot of these changes as a function of P/D is shown in Figure 2.32.

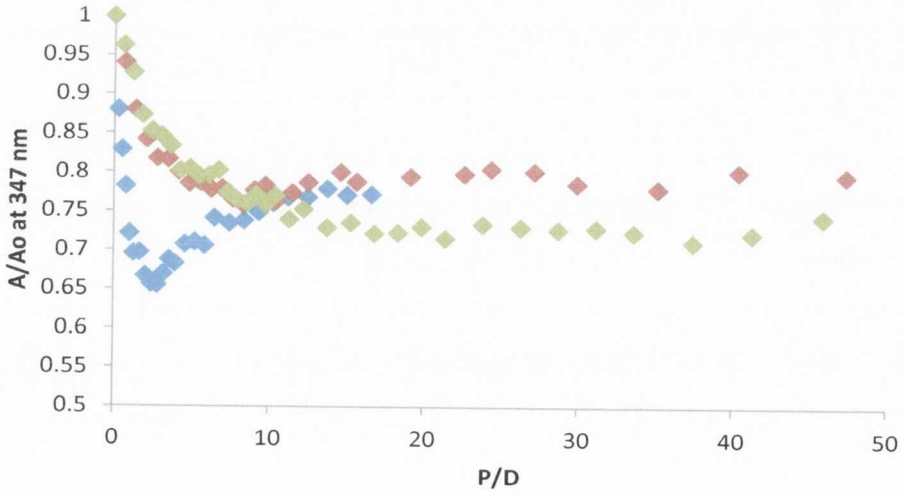

Figure 2.32: *Plot of changes in the absorbance of* **86** *in 10 mM phosphate buffer* (◆), 10 mM phosphate buffer+ *50 mM NaCl* (◆) and *in 10 mM phosphate buffer + 160 mM NaCl* (◆) *versus P/D at 347 nm.*

The results observed here indicated that at high ionic strength (10 mM phosphate buffer + 160 mM NaCl) a single binding interaction prevailed which implied that electrostatic interactions no longer played a major role in the DNA binding event which is unlike that observed for **86** at lower ionic strength (10 mM phosphate buffer + 50 mM NaCl).

The $\mathbf{K_b}$ values were determined from the absorbance data using the Bard binding model and are summarised in Table 2.13. Upon comparing these binding constants to that obtained in the absence of NaCl, it is evident that the presence of NaCl has a significant effect on the DNA binding ability of **86**. A similar effect was observed for the 4-amino derived Tröger's base **81**.

Table 2.13: *Binding constants determined for **86** bound to ct-DNA in 10 mM phosphate buffer and competitive media using the Bard binding model.*[194]

NaCl (mM)	Kb (10^6 M^{-1})	n (bp)	R^2
0	8.51 (± 5.34)	0.22 (±0.01)	0.99
50	2.24 (± 1.09)	0.21 (± 0.02)	0.98
160	0.41 (±0.12)	0.63 (± 0.10)	0.98

The absorbance spectra of **88**-**90** were also recorded in competitive media (corresponding changes in absorbance and the binding isotherms are shown in Appendix 2).

2.8.8 Excited State Studies in High Ionic Strength Medium (10 mM Phosphate buffer + NaCl)

The binding of **86** to *ct*-DNA was evaluated in phosphate buffer at pH 7.4 in the presence of both 50 mM and 160 mM NaCl using fluorescence emission spectroscopy and the representative spectra are shown in Figure 2.33. In 50 mM NaCl, when excited at 347 nm an unsymmetrical band with a λ_{maxFLU} at *ca.* 543 nm was observed and the intensity of this band decreased by *ca* 45 % upon the successive addition of *ct*-DNA and was accompanied by a bathochromic shift of 7 nm as can be seen in Figure 2.33(a). A plateau was reached at a P/D of 20. In the presence of 160 mM NaCl, a λ_{maxFLU} at *ca.* 543 nm was observed when excited at 347 nm. Upon the addition of *ct*-DNA in 160 mM NaCl, a decrease in intensity up to 35 % was observed with a bathochromic shift of 7 nm.

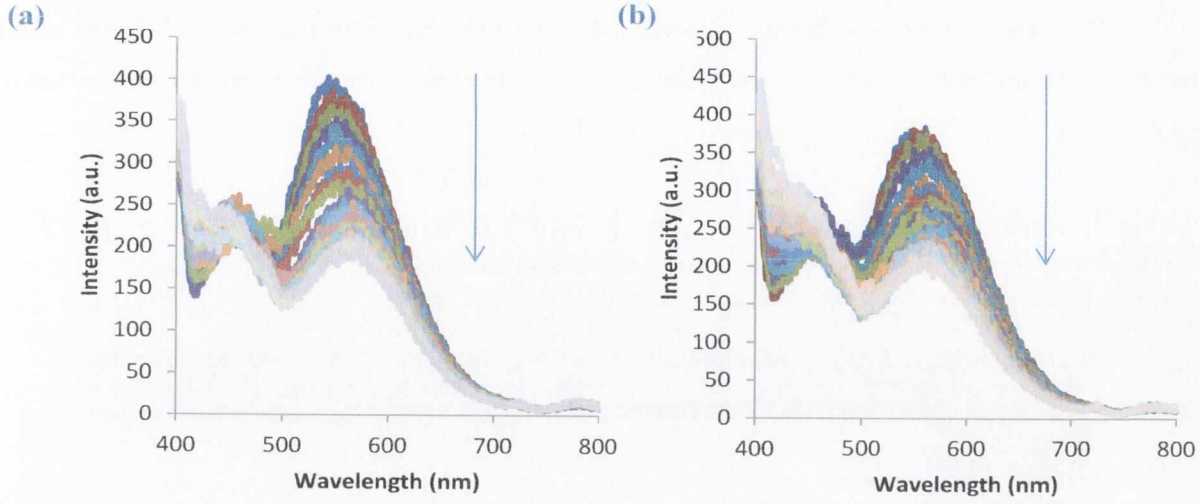

Figure 2.33: *Fluorescence emission spectrum of* **86** *(5.0 μM) (λ_{Ex} = 347 nm) upon increasing ct-DNA concentaration (0-260 μM) in* **(a)** *10 mM phosphate buffer + 50 mM NaCl and* **(b)** *10 mM phosphate buffer + 160 mM NaCl, at pH 7.4.*

In the absence of salt, a hypochromism of 70 % was observed and a plateau was reached at a P/D of 10, showing that the presence of salt clearly affects the binding affinity of **86** towards *ct*-DNA as upon an increase in salt concentration (50 mM NaCl), a hypochromism of *ca.* 45 % was observed for **86** as a function of *ct*-DNA concentration, where a plateau was reached at a P/D of 40, as can be seen in Figure 2.34. Similar behaviour was observed for **88**-**90** (Appendix 2).

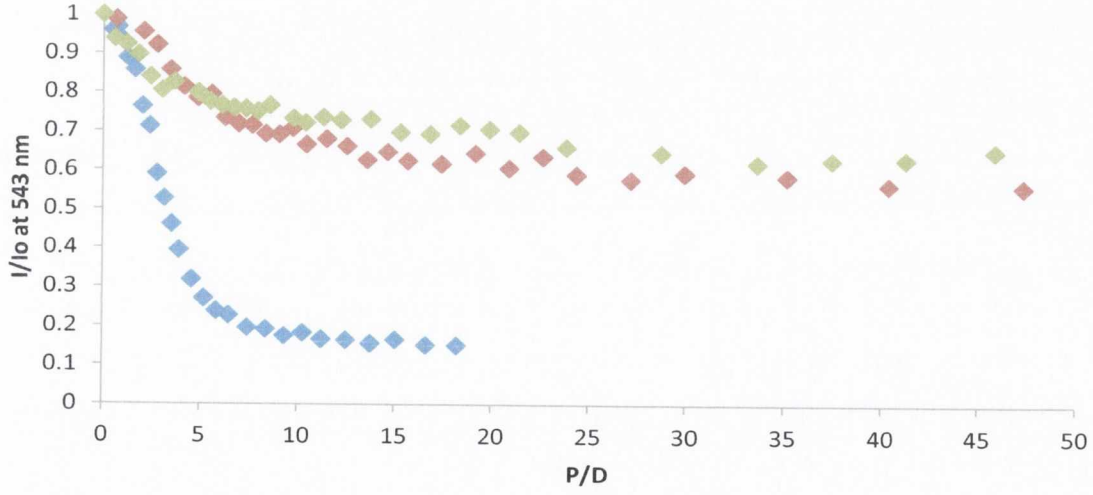

Figure 2.34: *Plot of changes in the emission intensity of* **86** *in 10 mM phosphate buffer* (◆), 10 mM phosphate buffer+ *50 mM NaCl* (◆) and *in 10 mM phosphate buffer + 160 mM NaCl* (◆) *versus P/D at 543 nm.*

As before the emission data was used to determine $\mathbf{K_b}$ values for **86** and **88-90** using the McGhee and von Hippel model and the binding constants are summarised in Table 2.14.[195]

Table 2.14: *K_b and **n** determined for **86** and **88-90** using the McGhee and von Hippel binding model.*[195] *[a]Accurate value could not be determined.*

Compound	50 mM NaCl		160mM NaCl	
	$\mathbf{K_b}$ (10^6 M^{-1})	**n** (bp)	$\mathbf{K_b}$ (10^6 M^{-1})	**n** (bp)
86	0.15 (± 0.01)	2.50 (± 0.21)	0.12 (± 0.01)	1.23 (± 0.12)
88	_____[a]	_____[a]	_____[a]	_____[a]
89	_____[a]	_____[a]	0.034 (±0.007)	0.70 (±0.03)
90	0.67 (± 0.03)	1.79 (±0.05)	0.21 (± 0.004)	1.73 (± 0.04)

In the case of **90**, there was not a considerable difference in the DNA binding affinity when investigated in the presence ($\mathbf{K_b}$ = 0.67 (± 0.03) $\times 10^6$ M^{-1}) and absence ($\mathbf{K_b}$ = 0.78 (± 0.02) $\times 10^6$ M^{-1}) of 50 mM NaCl. However, upon increasing the salt concentration to 160 mM, the affinity for *ct*-DNA was significantly reduced highlighting the involvement of electrostatic interactions in the DNA binding affinity of **86** and **88-90**.

In summary, these spectroscopic investigations have shown that **86** and **88-90** have high *ct*-DNA binding affinities that are comparable to the 4-amino derived analogues **81** and **83**.[148,149] In addition they have enhanced DNA binding affinities compared to their mono-meric counterparts and this indicates that the Tröger's base unit leads to significant changes in the manner in which the naphthalimde chromophore binds to DNA. The next section will further discuss and compare the binding affinities of these molecules, which were analysed from displacement assays using ethidium bromide.

2.8.9 Ethidium Bomide Displacement Assays

The DNA binding affinity of **86-90** was investigated further by carrying out competitive ethidium bromide displacement assays, a technique first introduced by LePecq

and Paoletti[205] that can be used to evaluate the binding selectivity and affinity of both intercalative and non-intercalative drugs.[206] Moreover, the assay is not limited to small molecule assessments and has been used with a variety of ligands including proteins and triplex-forming oligonucleotides.[207] As mentioned in Chapter 1, ethidium bromide is a DNA binder that intercalates between the DNA base pairs and electrostatically interacts with the anionic phosphate groups of the DNA helix. Ethidium bromide is weakly emissive, however, when bound to DNA it becomes highly emissive, as shown in Figure 2.33. Subsequent addition of a DNA binding compound results in a decrease in fluorescence due to displacement of the bound ethidium bromide, where the percentage fluorescence decrease is directly related to the extent of DNA binding providing relative binding affinities.[207] The apparent binding constant K_{app} was calculated according to a competitive model described by Boger *et al.*[207] using equation 2.9,

$$K_{app} = K_{EB}\frac{[EB]}{C_{50}} \qquad (2.9)$$

where, C_{50} is the concentration of the potential DNA binder being tested at 50% reduction in the emission intensity of ethidium bromide, [EB] is the ethidium bromide concentration and K_{EB} is the binding constant for ethidium bromide. The binding constant for ethidium bromide bound to *ct*-DNA is 10×10^6 M^{-1}.[207]

The emission spectrum of ethidium bromide when free and bound to *ct*-DNA in 10 mM phosphate buffer upon titration of **90** is shown in Figure 2.35.

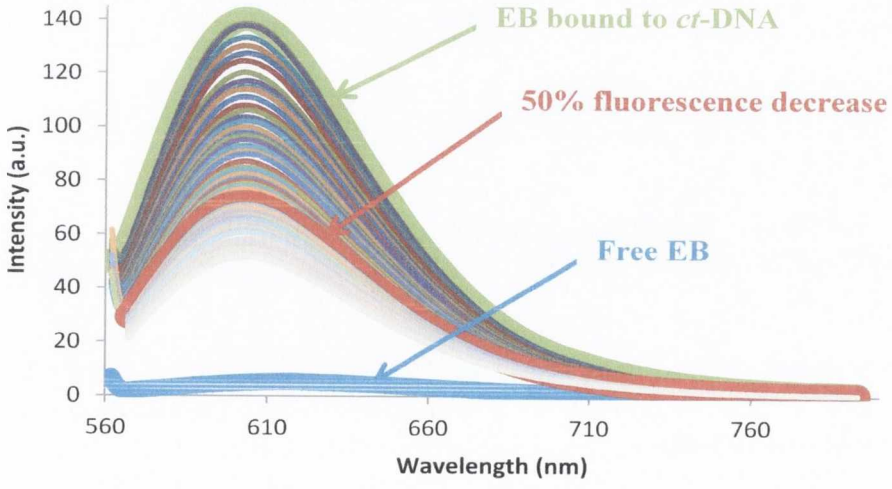

Figure 2.35: *The emission spectra of ethidium bromide (EB) when free and bound to ct-DNA (4.4 μM: 8.8 μM) in 10 mM phosphate buffer upon the addition of* **90** *(0 to 9.1 μM) with* λ_{Ex} *= 545 nm at pH7.4.*

For compounds **86-90** and the precursors **20** and **103-106** which were evaluated for comparison purposes, the spectral data is given in Appendix 2.

The analysis of the emission data from each titration allowed for a determination of the C_{50} values. The plots of the relative decrease in fluorescence intensity (IFrel%) of ethidium bromide/*ct*-DNA against the concentration of **86-90**, **20** and **103-106** added are shown in Figure 2.36.

As can be seen in Figure 2.36, the naphthalimide precursors **20** and **103-106** did not induce fluorescence quenching of ethidium bromide/*ct*-DNA to a large extent, compared to **85** and **88-90**, showing that the V-shaped bis-naphthalimide compounds **86** and **88-90** were more effective at displacing ethidium bromide. The maximum fluorescence quenching induced by the model compound **87** was 16%, compared to 57%, 52%, 40% and 54% determined for **86**, **88**, **89** and **90**, respectively, highlighting the importance of protonation of the terminal amine in improving DNA binding at pH 7.4. For Tröger's bases the displacement capability is in the order of **86** > **90** > **88** > **89** > **87** and the C_{50} values and binding constants for **86-90** are listed in Table 2.15. A binding constant could not be determined for **87** using equation 2.9 as the required 50% emission quenching was not reached over the concentration range investigated.

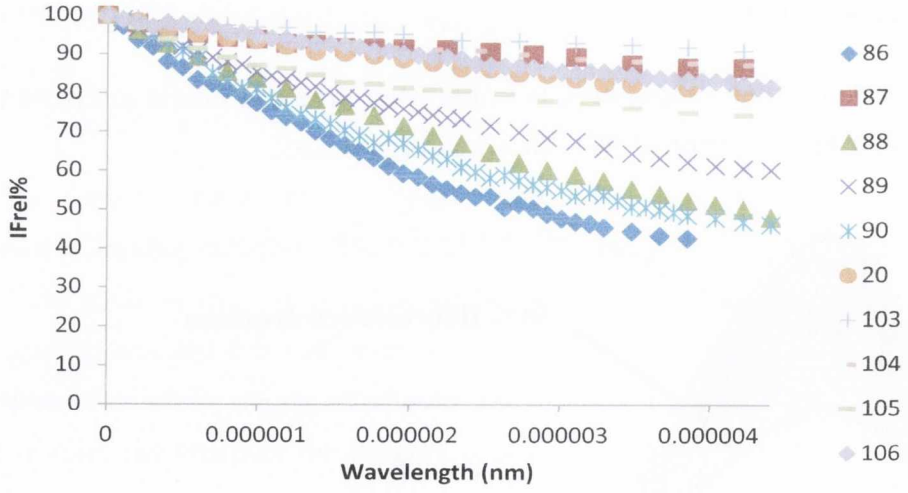

Figure 2.36: *The fluorescence decrease observed for ethidium bromide/ct-DNA (4.4 μM: 8.8 μM) in 10 mM phosphate buffer at 595 nm upon the addition of Tröger's bases* **86-90** *and 3-amino-naphthalimides* **20** *and* **103-106**.

Table 2.15: *C_{50} values and binding constants determined for 86-90.* [a] *Changes were minor and C_{50} values and binding constants could not be determined.*

Compound	C_{50} (μM)	K_{app} ($\times 10^6$)
86	2.81	15.7
87	----------[a]	----------[a]
88	4.22	10.4
89	4.94	7.56
90	3.85	11.5

In summary, the bis-naphthalimide Tröger's base derivatives **86** and **88-90** induce significant emission quenching compared to their mono-naphthalimide derivatives **20** and **104-106**. As can be seen from the binding constants listed in Table 2.15, this is in the order of **86** > **90** > **88** > **89** > **87**, where both **89** and **87** have lower *ct*-DNA binding affinities compared to ethidium bromide. Conversely, **86** displayed higher affinity for *ct*-DNA, the overall affinity being approximately one and a half times that of ethidium bromide. These results show that the *N*-imide side chain plays a role in determining the binding affinities of these molecules for *ct*-DNA. Although no C_{50} values or binding constants were determined for the mono-naphthalimides **20** and **103-106** over the concentration range examined here, it is evident from Figure 2.34 that **86** and **88-90** induce significantly more emission quenching compared to **20** and **103-106** and thus, displace ethidium bromide more efficiently, indicating that the design of these molecules was well founded.

The results from a series of thermal denaturation experiments as well as circular dichroism and linear dichroism studies will be discussed in the following sections. Thermal denaturation experiments were conducted as a means to further compare the binding interactions of **86** and **88-90** with their corresponding precursors **20** and **104-106**. The circular and linear dichroism studies were performed in order to determine the mode of binding of **86** and **88-90** with *ct*-DNA.

2.8.10 Thermal Denaturation Experiments

A thermal denaturation experiment is performed to determine the stability of the DNA structure in the absence and presence of DNA modifying agents. If the temperature of a solution containing double stranded DNA is raised sufficiently, strand separation or ''melting'' can occur. [208] The temperature that marks the midpoint of the transition is called the melting temperature (T_m), as depicted in Figure 2.37. This occurs when half of the nucleic acid exists in the helical state while the other half exists in the single stranded state and the two species are in equilibrium with each other. The melting transitions can be detected by UV-Vis absorbance, circular dichroism, NMR, viscosity, electrophoresis or calorimetry, with UV-Vis spectroscopy being the most commonly used.[208]

Nucleic acids absorb in the UV region with a maximum absorbance at approximately 260 nm. The absorbance increases upon increasing temperature as the double stranded DNA melts into the denatured form. By monitoring this hyperchromicity, a melting curve can be obtained which is sigmoidal in shape and indicative of a co-operative process. The inflection point in this curve is the $\mathbf{T_m}$. The hyperchromic effect is observed because of a reduction of electronic interactions in the stacked form. The absorbance of the single strand approaches that of the nucleic acid taken as monomers where no interactions between the bases occur.[208]

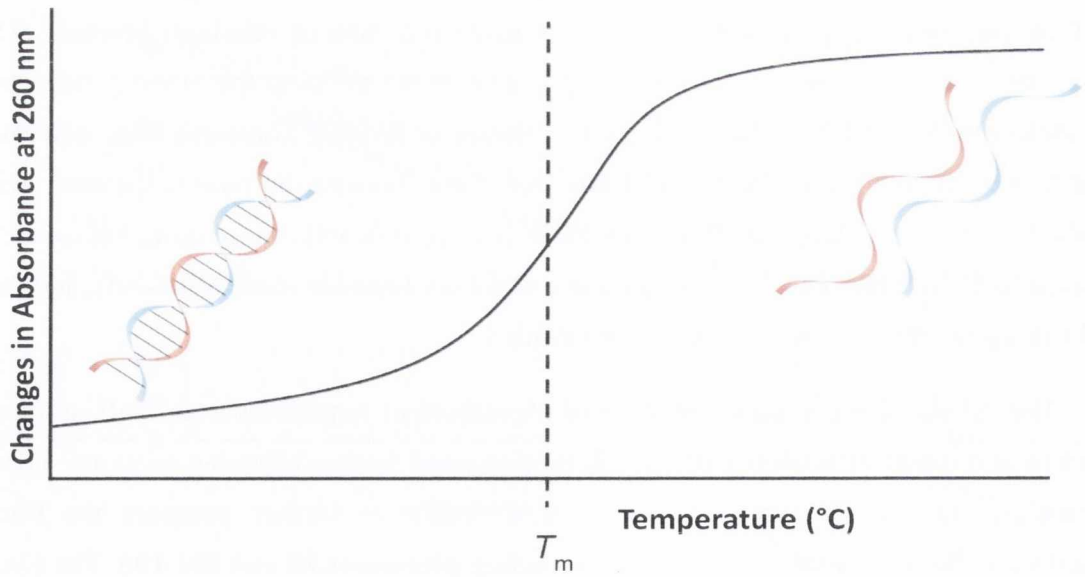

Figure 2.37: *Representative melting curve of DNA showing the changes in the absorbance at λ_{maxUV} = 260 nm as a function of increasing temperature.*[209]

In general, drugs that bind to DNA tend to have a stronger affinity for double stranded DNA over single stranded DNA due to the uniform structural features that favour complex formation. This leads to stabilisation of the double stranded form of DNA and shifting of the equilibrium between the double and single stranded forms with a preference for the former and thus, more energy is required to separate the strands. [208] Stacked bases provide an environment for intercalation of a drug which stabilises the double helix and leads to an increase in the $\mathbf{T_m}$ of the double stranded form of DNA. Minor groove binders have also been shown to stabilise structures and cause increases in the $\mathbf{T_m}$. [208, 210]

The thermal denaturation studies of *ct*-DNA (150 μM) alone and in the presence of **86** and **88-90** at a P/D ratio of 10 were carried out in 10 mM phosphate buffer at pH 7.4. In the absence of compound, the $\mathbf{T_m}$ value for *ct*-DNA was determined to be 68 °C. This value was found to change significantly in the presence of **86** and **88-90**, as shown in Figure 2.38. For comparison purposes the thermal denaturation studies were conducted for *ct*-DNA (150 μM) alone and in the presence of **86** and **88-90** at a P/D ratio of 10 in 10 mM phosphate buffer at pH 7.4.

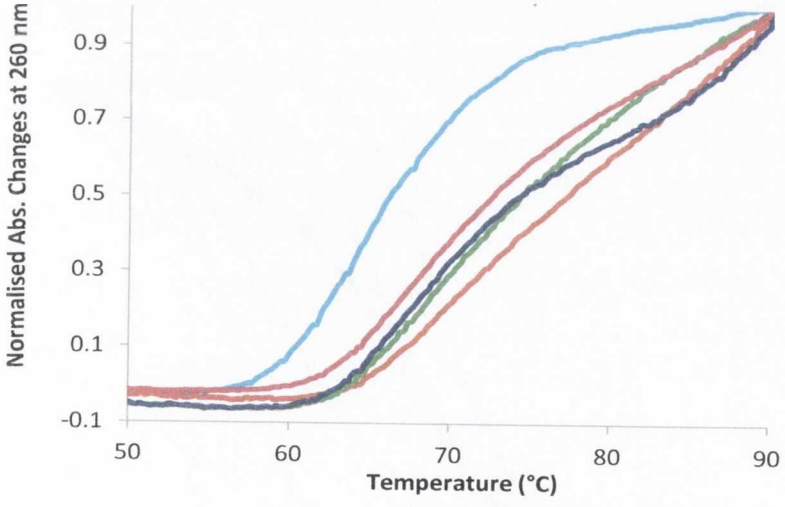

Compound	T_m (°C)
ct-DNA	68
86	>75
88	>75
89	>75
90	>75

Figure 2.38: *Thermal denaturation curves and* $\boldsymbol{T_m}$ *values of ct-DNA (150 μM) in 10 mM phosphate buffer at pH 7.4, in the absence (-) and presence of* **86** *(-),* **88** *(-),* **89** *(-) and* **90** *(-), all at a P/D ratio of 10.*

In general all the molecules stabilised the double stranded DNA structure. However, the $\mathbf{T_m}$ values for **86** and **88-90** did not correlate with the midpoint of the transition curves, as the melting of *ct*-DNA had not finished at 90 °C. The temperature of the sample could not be

increased further due to evaporation and boiling of the buffer. From the results obtained it appears that **86** and **88-90** stabilised the *ct*-DNA structure to a large extent indicating that the design of these molecules was well founded. Similar results were also observed for the 4-amino derived Tröger's bases **81** and **83**.[148-149]

For comparison purposes DNA thermal denaturation studies were carried out for the 3-amino-1,8-naphthalimide precursors **20** and **104-106** and are shown in Figure 2.39, where it can be seen that all the derivatives stabilised the double helix resulting in increases in the $\mathbf{T_m}$ values. In the case of **104**, an increase in the $\mathbf{T_m}$ value of 5 °C was determined whereas, for the remainder of the derivatives the $\mathbf{T_m}$ values did not correlate with the midpoint of the transition curves, as the melting of *ct*-DNA had not finished at 90 °C. These studies show that all the derivatives investigated have a high affinity for *ct*-DNA. This was expected as in Sections 2.8.3-2.8.8 their binding constants were determined and were high being in the range of 10^5-10^6 M^{-1} for the 1,8-naphthalimide derivatives **20** and **104-106** and 10^6 $M^{-1}$for the Tröger's bases **86** and **88-90**.

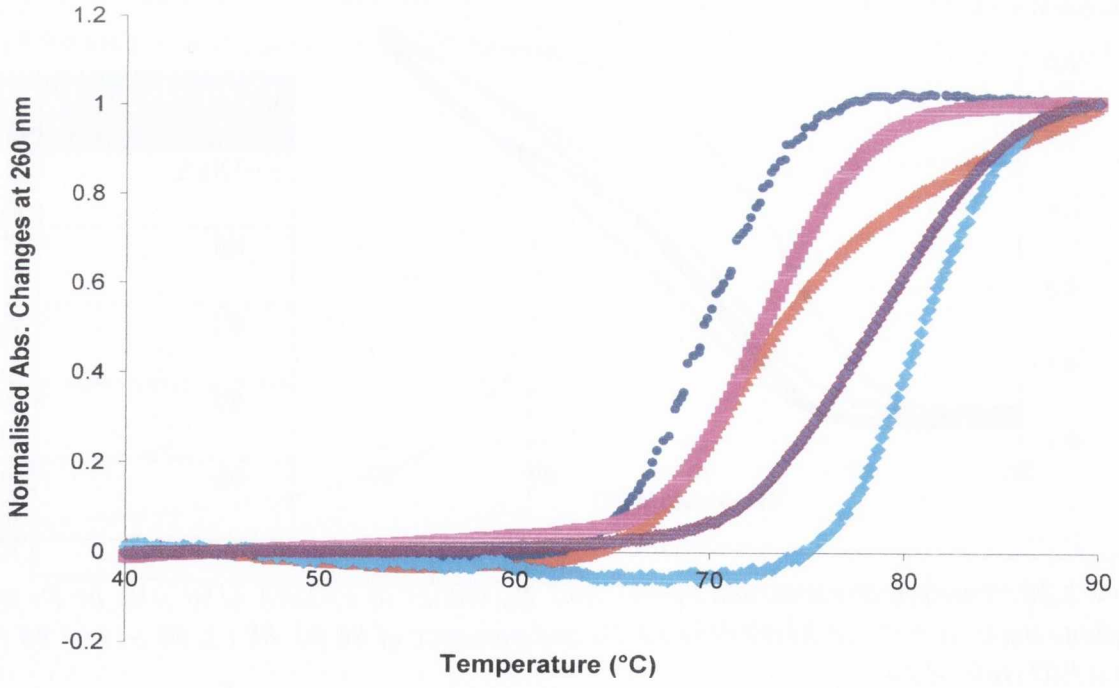

Figure 2.39: *Thermal denaturation curves and* $\boldsymbol{T_m}$ *values of ct-DNA (150 μM) in 10 mM phosphate buffer at pH 7.4 in the absence (◆) and presence of* **20** *(◆),* **104** *(◆),* **105** *(◆) and* **106** *(◆), all at a P/D ratio of 10.*

2.8.11 Circular Dichroism Studies

Circular dichroism is a spectroscopic technique that probes the asymmetry of a system based on the difference in absorption of incident left and right circularly polarised light.[211] This technique has been applied to the conformational and configurational analysis, chiral discrimination and identification of molecules.[212] Moreover, CD can be used as a tool for the study of the structure of DNA and for probing the interactions of DNA with small molecules in solution. The heterocyclic bases of DNA are achiral, however, they become chiral when placed within the framework of the chiral sugar-phosphate backbone.[211] Characteristic CD spectra are observed depending on the sequences and the conformations of the nucleic acids. For instance, the CD spectrum of B-DNA consists of a positive band between 275 and 285 nm due to the base stacking and a negative band between 235-240 nm due to the right handedness of the double helix, whereas, in the case of A-DNA the CD spectrum consists of a strong positive band at 270 nm and a weaker negative band at 240 nm.[213] The B-DNA spectra are distinguishable from the A-DNA spectra in that the 270 nm band is less intense and the 240 nm band is more intensely negative, as depicted in Figure 2.40.[213,214]

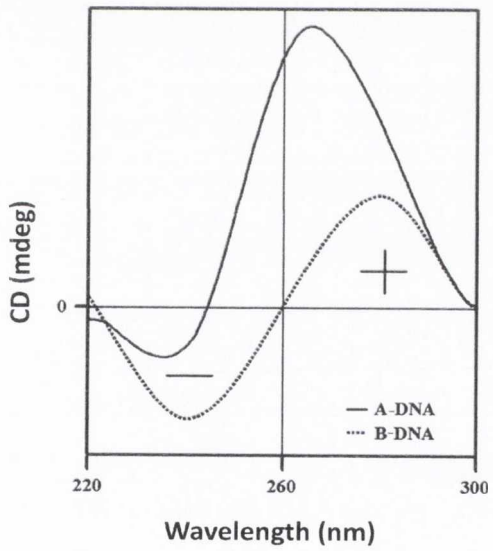

Figure 2.40: *Represenatative CD spectrum of A-DNA and B-DNA.*[214]

Many DNA binding ligands are achiral and thus, optically inactive. However, upon interaction with DNA, a ligand can acquire an induced CD signal through coupling of the electric transition moments of the ligand and the DNA bases. The observation of an induced CD signal within the absorption bands of the achiral ligand is indicative of a ligand-DNA

binding interaction. Equally the interaction of chiral molecules with DNA may cause changes in the CD signal intrinsic to the molecule.[211]

Circular dichroism can be used to determine the binding mode of ligand-DNA interactions where the exact position and orientation of a ligand and the environment within its binding site greatly affect the induced CD signal of a bound ligand. For an intercalator orientated parallel to the base pair long axis a negative induced CD signal is observed while a positive signal would indicate a perpendicular orientation.[211] A strong positive induced CD signal is observed when a molecule is bound to the minor groove, whereas, the sign and magnitude of the induced CD signal for a ligand bound in the major groove is more variable due to the greater number of orientations possible which are facilitated by the width of the major groove. Although assigning of a binding mode from the changes observed in the CD spectrum of a DNA binding event are not definitive, in general, small changes of $< 10\ M^{-1}$ imply intercalation, whereas, larger changes are indicative of groove binding. In addition, only those bands which lie outside the absorption region of DNA are considered when proposing a DNA binding mode as the changes in the DNA region of the spectrum may be due to the induced CD of the ligand as well as the structural changes in the DNA itself resulting from the ligand binding.[211]

Circular dichroism measurements were carried out using **86** and **88-90**, in which the concentration of the *ct*-DNA was kept constant and that of the Tröger's bases **86** and **88-90** was varied to give a range of P/D ratios. The CD spectra resulting from the addition of **90** to *ct*-DNA are shown in Figure 2.41.

From examination of these spectra, it is clear that positive and negative induced signals occur outside the region of absorption of DNA confirming the strong nature of the interaction of **90** with *ct*-DNA. These results also suggest that both intercalation and groove binding take place. Induced CD signals were also observed for **86**, **88** and **89** (Appendix 2), however, no induced signals were observed for the naphthalimide precursors **20** and **104-106** suggesting that the Tröger's bases interact with DNA more strongly compared to their mono-naphthalimide counterparts. Furthermore, the 4-amino-derived Tröger's base analogues **81** and **83** did not exhibit any induced signals outside the absorption region of the DNA at the same P/D ratios, which suggested that the interaction of the 3-amino derived Tröger's bases with DNA was stronger compared to **81** and **83**.[191]

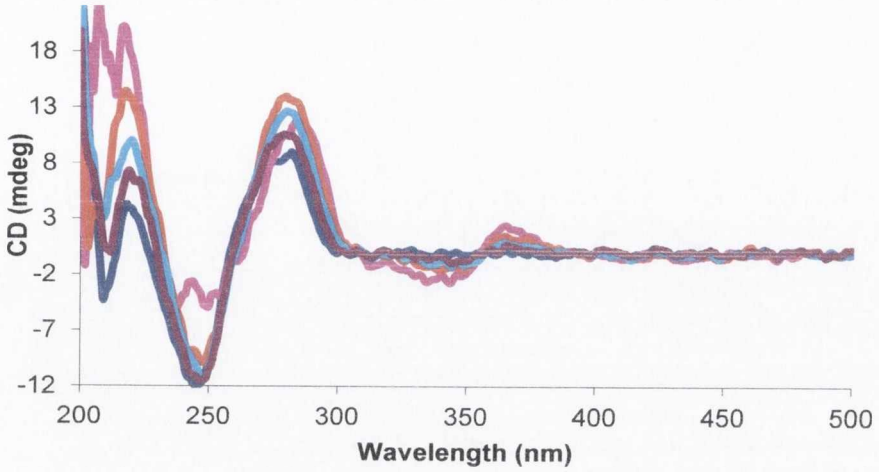

Figure 2.41: *CD spectra of ct-DNA (150 μM) in 10 mM phosphate buffer in the absence (-) and presence of* **90** *at P/D ratios of 2.5 (-), 5 (-), 10 (-) and 20 (-).*

In summary, the CD analysis has shown that this new series of Tröger's bases interacts with *ct*-DNA and interacts quite strongly as the induced signals lying outside the *ct*-DNA absorption region show. Furthermore, the appearance of positive and negative induced signals indicated that two binding modes were observed, such as intercalation and groove binding, further confirming that the design of these molecules was well founded. In order to further analyse the interaction of **86** and **88-90** with *ct*-DNA, linear dichroism measurements were performed.

2.8.12 Linear Dichroism Studies

Linear dichroism (LD) is a spectroscopic technique defined as the differential absorption of light polarised parallel and perpendicular to the orientation direction at a particular wavelength.[215] LD can be observed only provided at least partial alignment of the molecules to be studied can be achieved.[215] The most common applications of LD relate to structural studies of bio-macromolecules such as DNA and probing the interactions of DNA with DNA binding ligands. The observation of an LD signal within the absorption bands of the ligand is indicative of a ligand-DNA binding interaction. From such studies it can be shown that when ligands bind to DNA, they may **(a)** intercalate between the base pairs, **(b)** bind along the minor groove and/or **(c)** associate non-specifically along the DNA backbone.[215] The LD spectrum of B-DNA is negative at 260 nm as the bases are oriented perpendicular to the DNA helical axis and this signal is of the same shape as the absorption spectrum, as shown in Figure 2.42

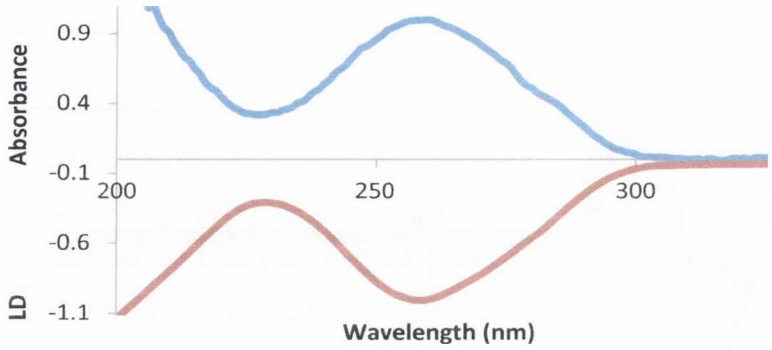

Figure 2.42: *Normalised absorption (-) and LD (-) spectra of B-DNA.*

When the aligned DNA is treated with a DNA binding ligand, the ligand should become oriented in space and be observed to absorb in either the perpendicular or parallel planes as a result of the electronic transitions within the molecule itself. For ligands that intercalate between the DNA bases, their π-π^* transitions are parallel to those of the DNA bases. Their LD signals are negative like those of the local bases except the magnitude of the signal is larger than that of the average base. This is as a result of the stiffening of the DNA induced by the intercalating ligands.[215] The binding of ligands along the minor groove gives rise to positive signals in the absorption region of the ligands as these molecules are absorbing light parallel to the helical axis.[215] For the final binding mode, the LD signal will be very small or equal to zero as the ligands associate non-specifically with the DNA backbone. This is because LD as a characterisation technique requires that the ligands in a ligand-DNA complex are actually bound to DNA. This is one of the major advantages of using such a spectroscopic technique.[215]

Linear dichroism measurements were carried out using **86**-**90**, in which the concentration of *ct*-DNA was kept constant and that of the Tröger's bases was varied to give a range of P/D ratios. The LD spectra resulting from the addition of **90** to *ct*-DNA is shown in Figure 2.43. As can be seen in Figure 2.43, the LD spectra show both a positive signal and negative signal in the absorption region of the Tröger's base **90**. Firstly, this confirms that a DNA binding interaction occurs between DNA and **90** which further supports the DNA binding studies discussed in Section 2.8.3. In particular, the data collected in the LD study complements that of the CD study, as both a positive and negative signal was observed in the absorption region of **90** in the CD spectra indicating strong DNA ligand interactions *via* two modes of binding.

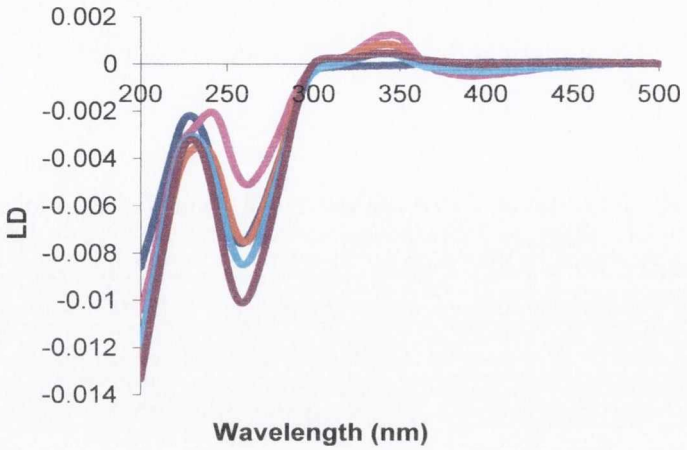

Figure 2.43: *LD spectra of ct-DNA (378 μM) in 10 mM phosphate buffer in the absence (-) and presence of* **90** *at P/D ratios of 2.5 (-), 5 (-), 10 (-) and 20 (-) at pH 7.4.*

Similar results were observed for **86-89** (Appendix 2). For comparison purposes, mono-naphthalimide **106** was studied using LD spectroscopy, as shown in Figure 2.44.

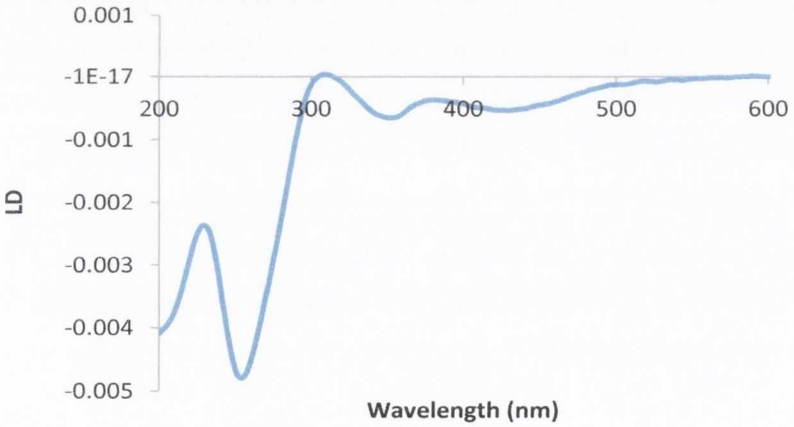

Figure 2.44: *LD spectrum of* **106** *at a P/D ratio of 2.5 in 10 mM phosphate buffer at pH* 7.4.

The negative signal highlights that **106** binds to DNA and does so by intercalating between the DNA base pairs. No other mode of binding for **106** was detected which shows that incorporating the Tröger's base structural unit into the naphthalimide skeleton has a significant effect on the mode of binding of these derivatives.

The most important conclusion that may be drawn from the LD studies carried out here is that incorporation of the Tröger's base motif plays a vital role in determining the mode of binding of these derivatives and in doing so results in both intercalative and groove binding modes being observed. Combining the results obtained here with those collected in

the other DNA binding studies, it is evident that the V-shaped structure of these molecules resulted in enhanced DNA binding compared to their planar monomeric counterparts.

2.9 Conclusion

In this chapter five novel DNA targeting Tröger's base derivatives **86**-**90** were successfully prepared as racemic mixtures in reasonable yields after efficient optimisation of reaction conditions. These molecules were shown to exhibit interesting solvatochromic behaviour due to the presence of an ICT excited state. This photophysical behaviour was studied in a range of solvents and compared to the 3-amino-1,8-naphthalimide precursors using both ground state and excited state spectroscopy. These investigations have shown that in the ground state **86**-**90** were insensitive to the solvent parameters in comparison to their corresponding precursors. Conversely, the fluorescence quantum yields and the positions of the emission bands of **86**-**90** were found to be strongly dependent on the polarity and the H-bonding abilities of the solvents indicating that the excited states of these compounds were more polar than their ground states.

These molecules were designed to be protonated at physiological pH in order to enhance their binding to DNA and thus, their p*K*a values were determined using spectroscopic techniques, where, **86** and **88**-**90** were found to have p*K*a values of 8.3, 7.5, 7.7 and 8.1 (± 0.1) leading to protonation of the alkyl side chains at physiological pH. However, as a p*K*a value of 6.1 was determined for **87**, it would not be protonated at pH 7.4 and would be unable to participate in electrostatic interactions and thus, became the model compound for investigating DNA binding interactions.

The ground state and excited state interactions of **86**-**90** with *ct*-DNA were initially evaluated in 10 mM phosphate buffer at pH 7.4. Upon successive addition of *ct*-DNA, distinct bi-phasic changes were observed in the ground states of **86** and **88**-**90** where the bi-phasic behaviour was attributed to a "template directed effect". The absorbance initially decreased as a result of DNA induced aggregation of the compound causing the compound to stack on the DNA backbone. This was followed by a subsequent increase in absorbance due to a de-stacking event allowing a redistribution of the compound over the length of the DNA backbone. Only minor changes were observed for **87** and this was attributed to the weak affinity of **87** for *ct*-DNA due to the lack of electrostatic interactions. To further evaluate the changes observed in the case of each derivative, binding constants were determined using both the Bard and McGhee and von Hippel binding models.[194,195] The binding constants

obtained were comparable with the 4-amino-derived Tröger's bases and in some cases were an order of magnitude higher than those determined for the 3-amino-precursors as well as several known acridine based DNA binders.

To investigate the importance of the electrostatic interactions, the binding of **86** and **88-90** to *ct*-DNA was evaluated in the presence of NaCl. In the presence of 50 mM NaCl, compounds **86** and **88-90** were found to bind quite strongly (~ 10^6 M^{-1}) to *ct*-DNA and the resulting binding isotherms exhibited similar bi-phasic behaviour to that observed in the absence of salt. Conversely, in the presence of 160 mM NaCl, the binding affinity of **86-90** was significantly reduced highlighting the importance of the electrostatic interactions in the overall affinity of these molecules towards *ct*-DNA.

In order to gain insights into the mode of binding, the interactions of **86-90** with *ct*-DNA were also studied by circular and linear dichroism techniques. CD studies revealed that in the presence of *ct*-DNA, all of the derivatives exhibited bisignate CD signals with a positive band *ca.* 400 nm and a negative band at *ca.* 350 nm, corresponding to the absorption bands of these chromophores in aqueous buffered medium. Such bisignate behaviour is characteristic of bi-modal binding, with one naphthalimide chromophore binding *via* intercalation while the second naphthalimide interacts with the grooves. This dual mode of binding of **86-90** with *ct*-DNA was also observed in the linear dichroism studies. Moreover, **86** and **88-90** were found to stabilise *ct*-DNA to large extents and were comparable with their 3-amino precursors. Such findings were consistent with their high affinity for *ct*-DNA.

Overall, the DNA binding interactions of **86-90** indicated that the rationale for the design of these compounds was well founded. They exhibited a similar affinity for *ct*-DNA in comparison to the 4-amino derived compounds **81-83** and a higher affinity for DNA compared to their naphthalimide precursors. The results obtained here are highly encouraging and indicate that the development of such molecules may find use as potential anti-cancer agents.

Chapter 3:

Design, Synthesis and Photophysical Evaluation of Amino Acid Based Bis-1,8-NaphthalimideTröger's Base Derivatives

3.1 Introduction

The 1,8-naphthalimide structure which consists of a flat planar π-deficient hetero-aromatic system is known to demonstrate a wide range of applications in medicinal and supramolecular chemistry having found extensive use within the dye industry, in the fields of anion and cation sensing and recognition, in the construction of novel cancer therapeutics and the design and development of chemical probes.[1-7] The naphthalimide chromophore possesses unique photophysical properties and one of the main advantages for the use of such a fluorophore is that the absorption and fluorescence spectra which lie within the UV and visible regions can be fine tuned through facile structural design.[1] Synthetic modifications can be easily accommodated on either the aromatic naphthalene moiety or at the *N*-imide site allowing for varieties of structural motifs and functional groups to be incorporated, demonstrating the versatility of the naphthalimide structure. Gunnlaugsson *et al.*[1,6(b),183,216,217] have played a pivotal role in the design and development of the naphthalimide chromophore with the incorporation of anion recognition moieties such as ureas, thioureas and amides, modifications which can be facilitated at both the *N*-imide site and on the aromatic moiety. In addition to being a highly pliable building block for the construction of anion and cation sensors, the 1,8-naphthalimide structure can be derivatised at the *N*-imide site with amino acids and to date several hundred amino acid based 1,8-naphthalimides have been synthesised as potential anti-cancer agents using solution phase peptide chemistry and have been shown to possess significant cytotoxic activity.[114-116,191,218,219] Furthermore, over the past few years, naphthalimides incorporating a variety of functional groups including amino acids have been developed as solvatochromic probes for a wide range of biomolecular interactions.[220,221] Therefore, the amino acid based 1,8-naphthalimide derivatives synthesised within the Gunnlaugsson group by Phelan,[114] Hussey[115] and Veale[191] act as an excellent starting point to further develop the Tröger's base scaffold, which is the main theme of this chapter.

The first part of this chapter deals with the synthesis of amino acid based 1,8-naphthalimides and their corresponding Tröger's base derivatives containing optically active α-amino acids. The synthetic strategy for the design and development of the 1,8-naphthalimide derivatives was initially devised by Phelan[114] and further modified by Hussey.[115] For the formation of Tröger's base naphthalimides incorporating one amino acid residue, the synthetic strategy developed by Veale[191] was utilised. In the case of the peptide based Tröger's bases, two synthetic approaches were considered. The first path explored involved the synthesis of the Tröger's base directly from the peptide based 1,8-naphthalimide

precursor. The second synthetic approach would be to prepare Tröger's base molecules incorporating one amino acid at the *N*-imide terminus and subsequently derivatise the carboxylic acid terminus further with additional amino acids. As a means of achieving this, several coupling agents were investigated and will be discussed in Section 3.3.9.

The second section of this chapter examines the photophysical nature of the novel target molecules which are studied in several solvents by UV-Vis spectroscopy and fluorescence emission and excitation techniques showing that incorporation of the Tröger's base moiety into the skeleton of the 1,-8-naphthalimide unit yields supramolecules that exhibit solvatochromic ICT excited states providing a basis for their use as potential peptide mimics.

3.2 Amino Acids and Peptides

Peptides possess the biocompatibility and chemical diversity found in proteins, however, they are more stable and robust and can be synthesised on a large scale.[222] The fundamental building blocks of polypeptides are the α-amino acids which consist of a central carbon atom known as the α-carbon which has both an amino and carboxylic acid functionality attached. This α-centre also bears a hydrogen atom and a side chain which can be classified as being non-polar, polar or electrically charged. In all, twenty naturally occurring amino acid side chains exist which are responsible for conferring functionality onto polypeptides.[223] With the obvious exception of glycine, α amino acids are chiral, as can be seen with the several examples shown in Figure 3.1.

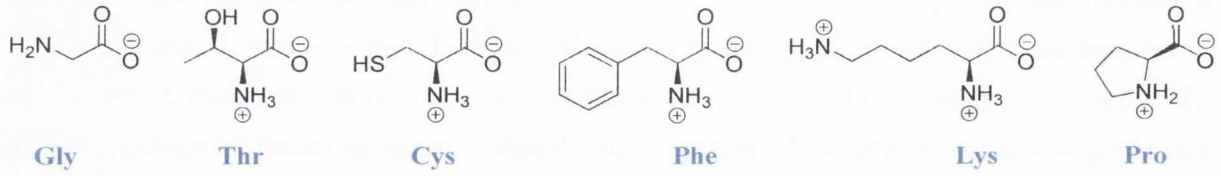

Figure 3.1: *The structures of several S-amino acids including glycine (Gly), threonine (Thr), cysteine (Cys), phenylalanine (Phe), lysine (Lys) and proline (Pro).*

The absolute configuration at the α-carbon is designated by *D* (*dextrorotatory*) and *L* (*laevoratory*) notations, using the compound glyceraldehyde as a standard for defining such configurations, where *D* and *L* are applied to the enantiomers that rotate plane polarised light in clockwise and anti-clockwise directions, respectively. This notation is only used for certain well known natural molecules, where their use is established by tradition, for example, the *L*-amino acids and the *D*-sugars. Using a more modern notation involves applying the Cahn,

Ingold and Prelog (CIP) rules which designates the configuration at a stereocentre as being either *rectus R* or *sinister S*. With the exception of cysteine, all *L*-amino acids have an *S*-configuration at a chiral centre.[224]

The *L*-amino acids are ubiquitous in nature and are the only constituents of proteins. Proteins contain a precisely defined amino acid sequence and serve crucial functions in biological processes. For instance, they can function as catalysts and transporter molecules, they can store molecules such as oxygen, provide mechanical support and immune protection and control growth and differentiation processes.[223] Therefore, to mimic a process that occurs naturally in the human body, *L*-amino acids have been incorporated into the design of novel bio-molecules and structures to facilitate biological recognition. In recent years, many drug-amino acid conjugates have been reported including anthraquinone **108**,[225] doxorubicin,[226] vinblastin,[227] nitrosurea/nitrogen mustard,[228] hydroxymethylacylfulvene **109**,[229] benzothiazole **110**,[230] imidazotetrazines **111**,[231] methionine-enkephalin,[232] camptothecins **112**,[233] 9-hydroxyellipticinium **113**[234] and metal complexes.[235]

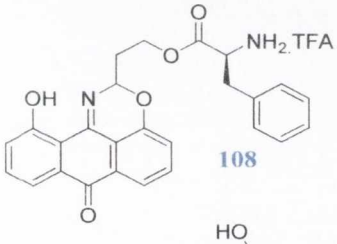

108

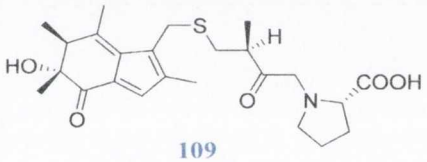

109

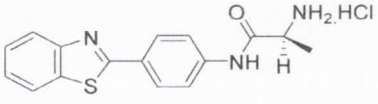

110

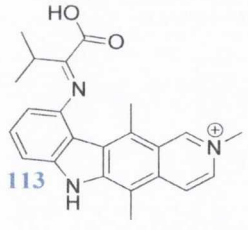

113

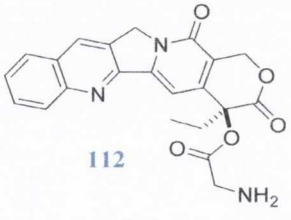

112

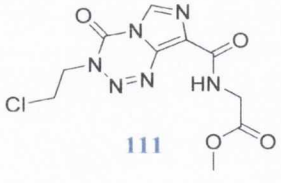

111

In addition, fullerene peptides have also been designed and synthesised and have shown potential anti-microbial and anti-HIV activity.[236] Peptide nanostructures have been applied in the fields of nanoelectronics, tissue and neurological regeneration, diagnostics and bio-sensing.[222] Peptides engineered with appropriate cysteines and histidines have been employed as ligands for producing water soluble quantum dots and for tagging protein ligands and biosensors to quantum dot surfaces. Combining amino acids and quantum dots has also resulted in such structures being transported into cells for intracellular imaging applications.[237] So far, it has been shown that amino acids play a vital role in many different areas of research. To build upon this work, the design and incorporation of amino acid

moieties into the naphthalimide chromophore and their development as potential bio-chemical probes will be discussed.

3.3 Synthesis of Amino Acid and Peptide Based Bis-1,8-Naphthalimide Tröger's Base Derivatives

Tröger's base derivatives incorporating amino acid based 1,8-naphthalimides were prepared starting from the commercially available 3-nitro- and 4-nitro-1,8-naphthalic anhydrides. The synthetic strategy employed involved firstly preparing the *N*-substituted nitro- and amino-1,8-naphthalimide precursors using standard literature procedures, similar to those used and discussed in Chapter 2.[42] During the course of this work, α-amino acid derived Tröger's bases were designed and synthesised as potential peptidomimetics.[238] Exploiting the perpendicular nature of the Tröger's base structural unit, target molecules **114** and **115** were designed with the ability to direct their appended peptides within a 90-100° range potentially mimicking small peptide chains that have been identified to contain 90-100° bends.[238]

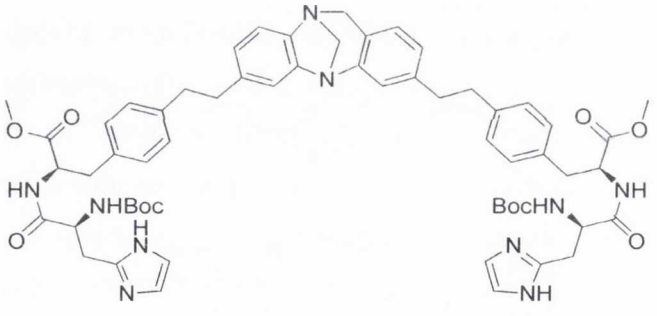

114

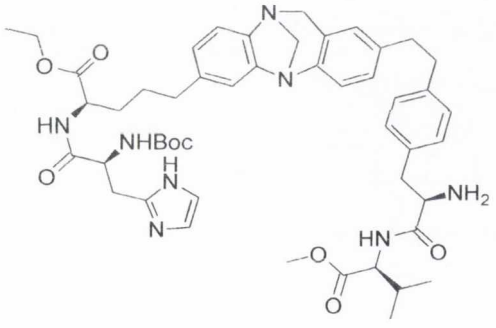

115

3.3.1 Synthesis of α-Amino Acid Based 4-Amino-1,8-Naphthalimides 120, 121 and 124-132

The synthetic strategy employed for the synthesis of *R*-amino acid based 4-amino-1,8-naphthalimides involved four steps as shown in Scheme 3.1, a methodology developed by Phelan.[114] The first step in the reaction sequence involved a condensation reaction between the commercially available 4-nitro-1,8-naphthalic anhydride and the hydrochloric salt of the relevant amino acid which was protected at the carbonyl terminus by either a *tert*-butyl ester or benzyl ester. The reaction was carried out by refluxing the two reagents in anhydrous toluene overnight in the presence of 1.4 equivalents of TEA (a method discussed in Chapter

2) to give **116** as a brown solid and **117-119** as yellow powders in high yields (Table 3.1) without the need for further purification.

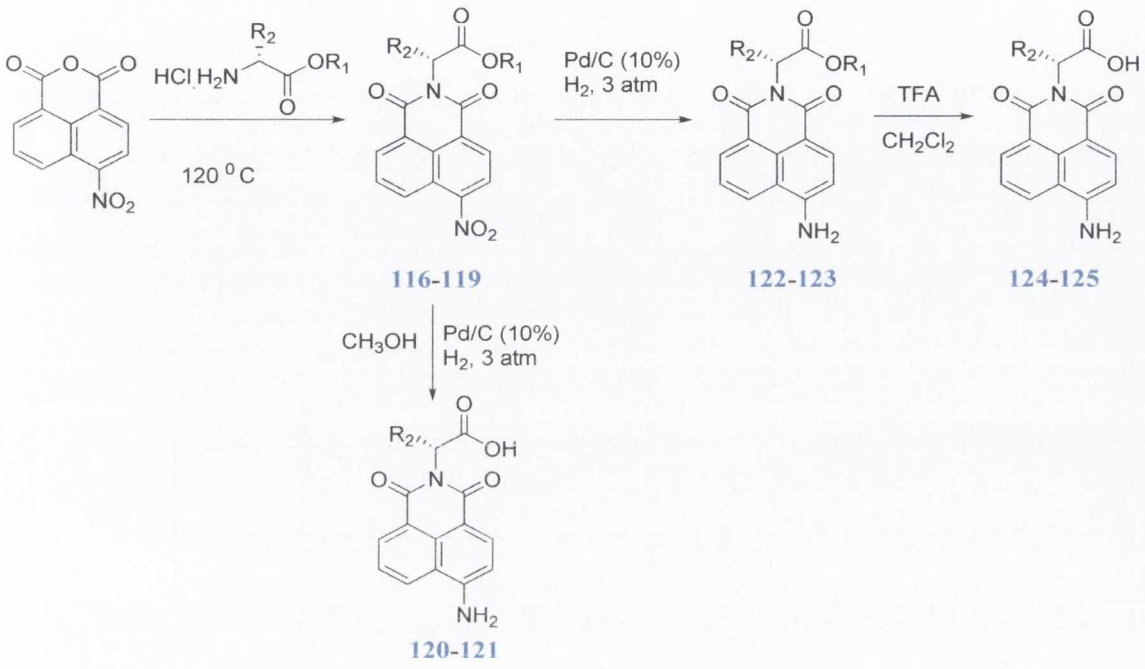

Scheme 3.1: *Synthesis of R-4-nitro and R-4-amino 1,8-naphthalimide derivatives 116-125.*

Table 3.1: *Synthesis of naphthalimide derivatives using* ***Scheme 3.1***.

Cpd.	R_1	R_2	% Yield	Cpd.	R_1	R_2	% Yield
116	CH_2Ph	CH_3	78%	**121**	H	$CH(CH_3)_2$	97%
117	CH_2Ph	$CH(CH_3)_2$	91%	**122**	$C(CH_3)_3$	CH_2Ph	88%
118	$C(CH_3)_3$	CH_2Ph	65%	**123**	$C(CH_3)_3$	$CH_2CH(CH_3)_2$	93%
119	$C(CH_3)_3$	$CH_2CH(CH_3)_2$	98%	**124**	———	CH_2Ph	98%
120	H	CH_3	77%	**125**	———	$CH_2CH(CH_3)_2$	98%

The next step in the reaction pathway involved a hydrogenolysis reaction in CH_3OH in the presence of a palladium catalyst (Pd/C (10 %)). For the benzyl derivatives, this reaction served two purposes as the benzyl group in this reaction was removed in addition to the nitro group being reduced. The work-up involved filtering the reaction mixture through celite and subsequent removal of solvent gave both **120** and **121** as yellow solids. For the *tert*-butyl derivatives, the hydrogenolysis reaction was followed by ester hydrolysis using a

CH_2Cl_2:TFA (2:1) mixture which resulted in the formation of the corresponding acids **124** and **125** without the need for any purification and in high yields as summarised in Table 3.1. Each of the intermediates was characterised by ^1H and ^{13}C NMR studies, mass spectral analysis as well as infra-red spectroscopy. As an example, the ^1H NMR spectrum ($(CD_3)_2SO$, 600 MHz) of **120** is shown in Figure 3.2, where the aromatic region between 6.86 and 8.66 ppm is composed of six signals, made up of four doublets and an *apparent* triplet, all of which integrate for one proton and a broad singlet pertaining to the amino group which integrated for two protons. The α-proton appears as a quartet at 5.56 ppm while the methyl group next to the chiral centre appears as a doublet at 1.50 ppm.

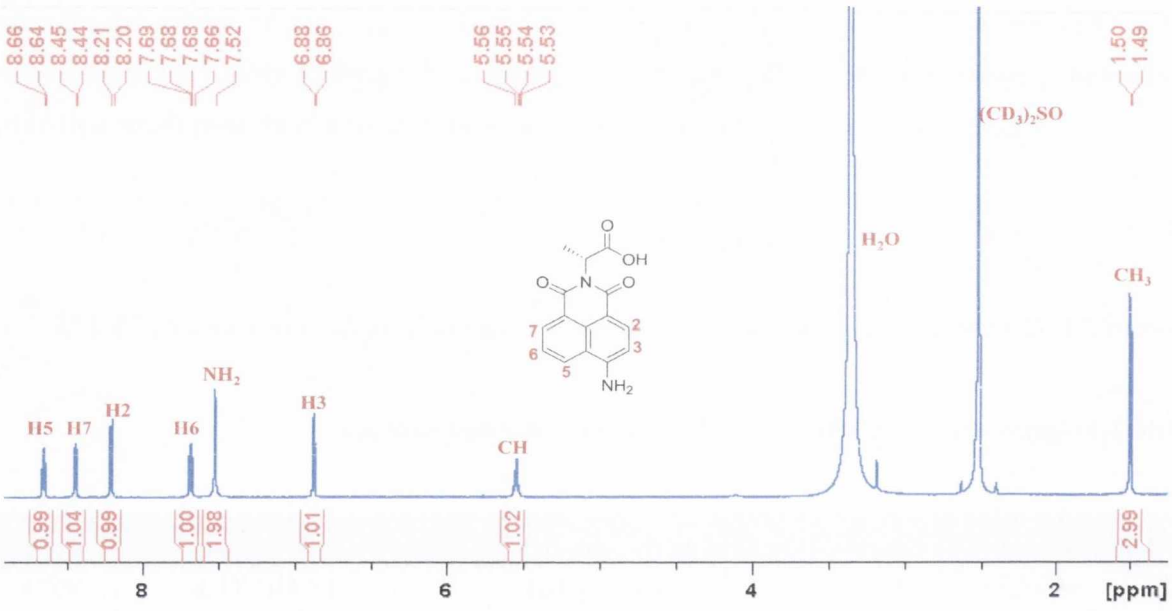

Figure 3.2: *^1H NMR spectrum ($(CD_3)_2SO$, 600 MHz) of **120**.*

The ^{13}C spectrum consisted of fifteen resonances which corresponded to **120**. In addition, the molecular formula was confirmed by mass spectral analysis exhibiting a peak at m/z = 283.0724 in the negative electrospray mode. The IR spectrum also complemented the assigned structure observed in Figure 3.2 with signals at 3438 and 3363 cm^{-1} corresponding to the amine group. The glycine derivative **126** as well as the *L*-amino acid derivatives **127-130** were also synthesised and characterised in a similar manner to that discussed for the preparation of **120-121** and **124-125** above.

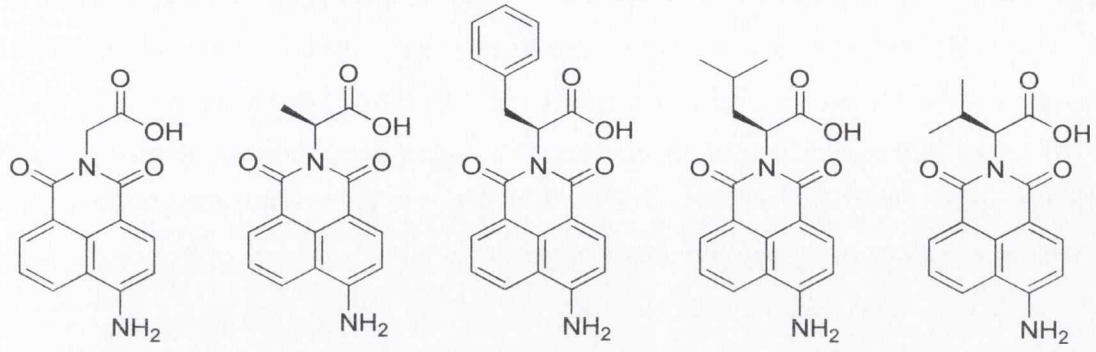

126 **127** **128** **129** **130**

As discussed in Chapter 1, a large number of α-amino acid based 1,8-naphthalimide derivatives were synthesised by both Phelan[114] and Hussey[115] and it was found that all of these molecules retained their chirality. In order to analyse the chirality of the *R*- **120**, **121**, **124** and **125** and *S*- **126-130** analogues, CD measurements were performed in CH_3OH. As can be seen in Figure 3.3, the optical activity of the amino acid naphthalimides **124** and **128** exhibited a distinctive profile for the *R* and *S*-amino acid based naphthalimides, exhibiting a positive signal for the *R*-amino acid based derivative while displaying a negative signal for the *S*-analogue at *ca.* 220 nm.

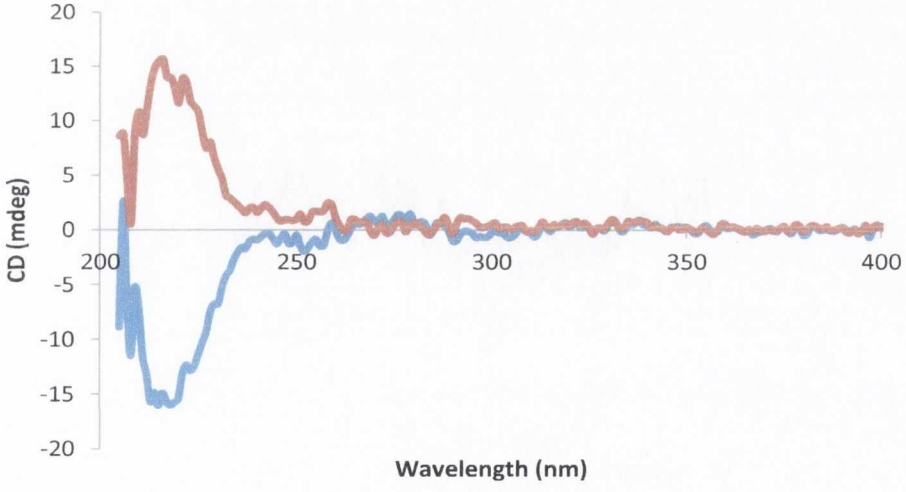

Figure 3.3: *The CD spectra of the **124** (red) and **128** (blue) in CH_3OH.*

Similar results were obtained for derivatives **120**, **121** and **125-130** highlighting that all of these molecules retained their chirality during the synthetic procedures employed.

This previously discussed synthetic route was also employed for the synthesis of the amino acid 1,8-naphthalimide derivatives which are protected at the *C*-terminus by methyl

esters such as **131** and **132** in 98% and 99% yields, respectively. Both **131** and **132** were characterised by ^{1}H NMR and ^{13}C NMR experiments, mass spectroscopy and IR analysis. As an example, the ^{1}H NMR spectrum ($(CD_3)_2SO$, 600 MHz) of **131** was similar to its carboxylic acid derivative **129** except for the appearance of a singlet pertaining to the methoxy group at 3.58 ppm. Analysis of the ^{13}C spectrum showed that **131** possessed an additional carbon in comparison to **129**, pertaining to the methoxy carbon.

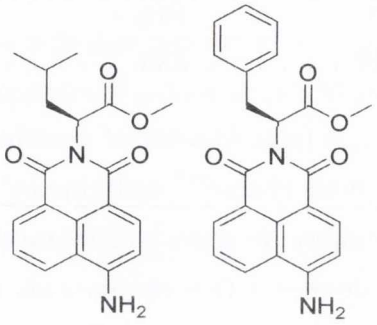

131 **132**

The stereochemistry of these *S*-amino acid-1,8-naphthalimide derivatives were examined in CH_3OH by CD spectroscopy, as can be seen in Figure 3.4 for **132**.

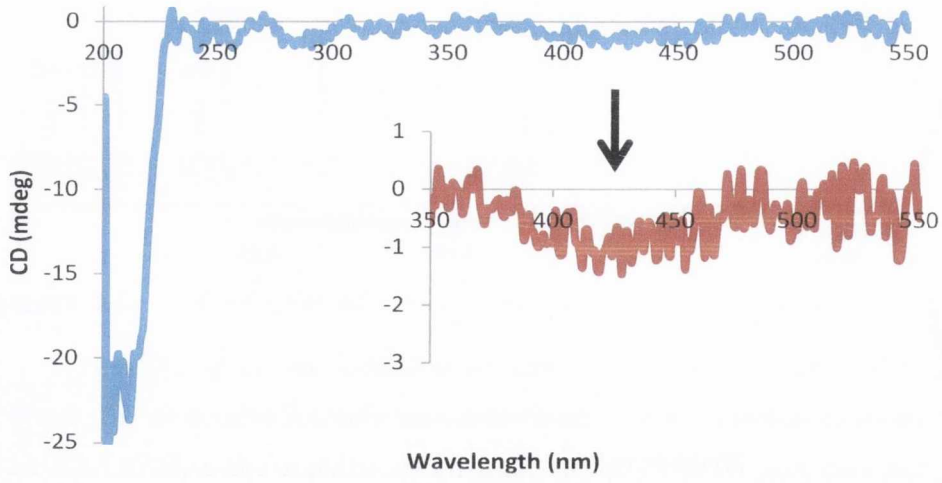

Figure 3.4: *The CD spectrum of **132** in CH_3OH. Inset: Highlighted region of the CD spectrum displaying the observed induced CD signal.*

As expected distinct negative signals were observed at *ca.* 220 nm, confirming once again that the chirality of the amino acids incorporated into these structures was retained. Interestingly, in the case of **132** a very weak induced negative CD signal was observed at *ca.* 430 nm (Figure 3.4) pertaining to the naphthalimide nucleus, demonstrating that attachment

of an achiral aromatic chromophore to a chiral substituent can lead to an induced CD of the chromophore transition. However, in the case of **131**, only a negative signal representing the amino acid moiety was observed.

3.3.2 Synthesis of Peptide Based 4-Amino-1,8-Naphthalimides 138-140

In the previous section, the synthesis of a series of 4-amino-1,8-naphthalimide derivatives incorporating a single amino acid residue in high yields with the retention of chirality was discussed. The next step in the reaction sequence involved modifying these derivatives by functionalising the carboxylic terminus to yield peptide 1,8-naphthalimide conjugates, work pioneered by Phelan[114] which involved considering two synthetic strategies, the stepwise and the anchored approaches, as depicted in Scheme 3.2.

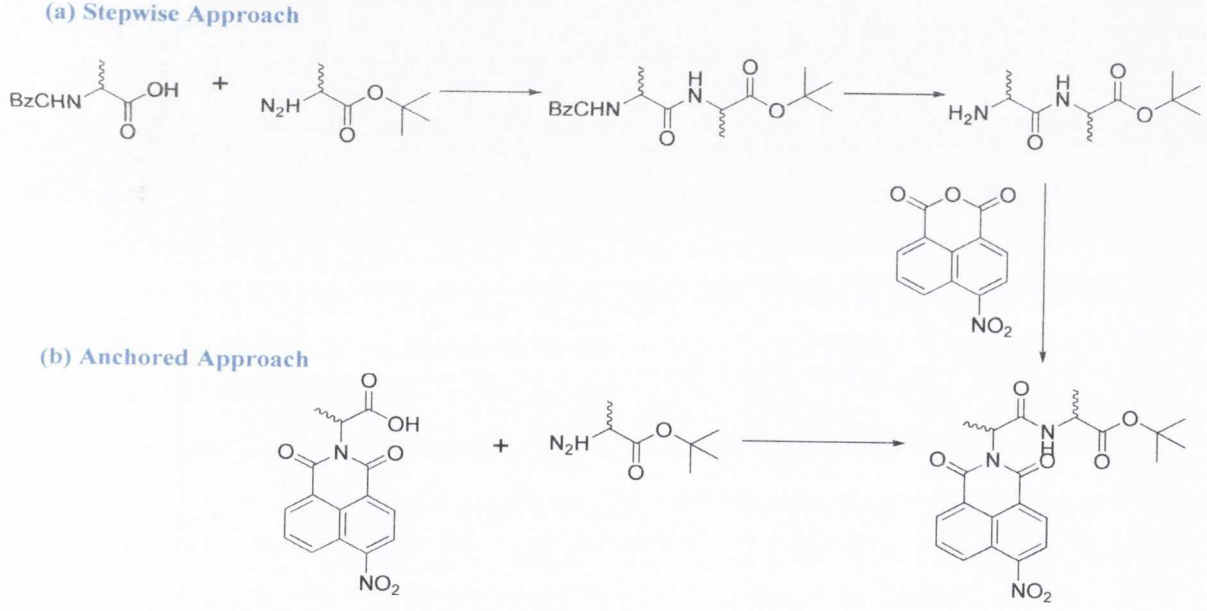

Scheme 3.2: *Two possible routes for the synthesis of the peptide 4-nitro-1,8-naphthalimide conjugates: (a) the stepwise approach and (b) the anchored approach.*

The stepwise method involved the initial formation of the peptide species, followed by condensation of the free peptide with the 1,8-naphthalic anhydride starting material. This was achieved by coupling an *N*-protected amino acid with a carbonyl protected amino acid, subsequent deprotection followed by generation of the free amine which was condensed with the 4-nitro-1,8-naphthalic anhydride starting material forming the carbonyl protected peptide 1,8-naphthalimide conjugates. The alternative synthetic route explored involved coupling a second α-amino ester directly to an amino acid based 1,8-naphthalimide derivative. The

anchored approach was the preferred route of choice since it enabled the derivatives already synthesised in Section 3.3.1 to be used as the building blocks for the peptide derivatives. Furthermore, by using this method, the cyclisation of a Cbz-potected peptide to a acyldiketopiperazine intermediate is inhibited, in addition to the possible formation of a hydantoin intermediate during the ammonolysis step of the peptide.[239,240]

The peptide 4-nitro-conjugates developed by Phelan[114] and incorporated into this project were synthesised using the anchored approach. Two coupling reagents were investigated for use in the formation of peptide functionalised naphthalimides; *N*, *N'*-dicyclohexylcarbodiimide (DCC) **133** and *N*-(3-dimethylaminopropyl)-*N'*-ethylcarbodiimide hydrochloride (EDCI.HCl) **134**.

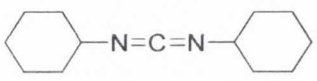

133

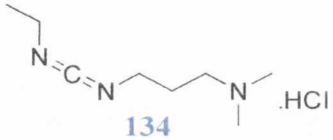

134

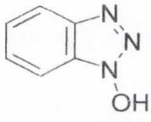

135

Both **133** and **134** are carbodiimide based coupling reagents that exert their mode of action by forming activated esters. This activation process consists of replacing the hydroxyl group of the carboxylic acid with a leaving group, as the acid would otherwise form salts with the incoming amine. One of the main drawbacks associated with the use of these coupling reagents is the tendency for racemisation to occur. To overcome this additives are employed which also have the potential to enhance the reactivity of the coupling reagents. Additives such as 1-hydroxybenzatriazole (HOBt) **135** works by capturing the active species formed between the carboxylic acid and carbodiimide coupling reagent to give the corresponding active ester as depicted in Figure 3.5. As can be seen in Figure 3.5, a water soluble urea is generated as a side product which can be separated by extraction in an acidic aqueous work-up. However, in the case of **133** the dicyclohexyl urea generated is only sparingly soluble and may precipitate incompletely from the reaction mixture, where separation from the desired product in the past has proven difficult.[114] Therefore, utilisation of **134** as a coupling reagent resulted in peptide derivatives of higher yields and greater purity and thus became the agent of choice. To demonstrate the efficiency of the anchored approach, derivative **137** was synthesised from **136** using **134** and **135** in 95% yield.

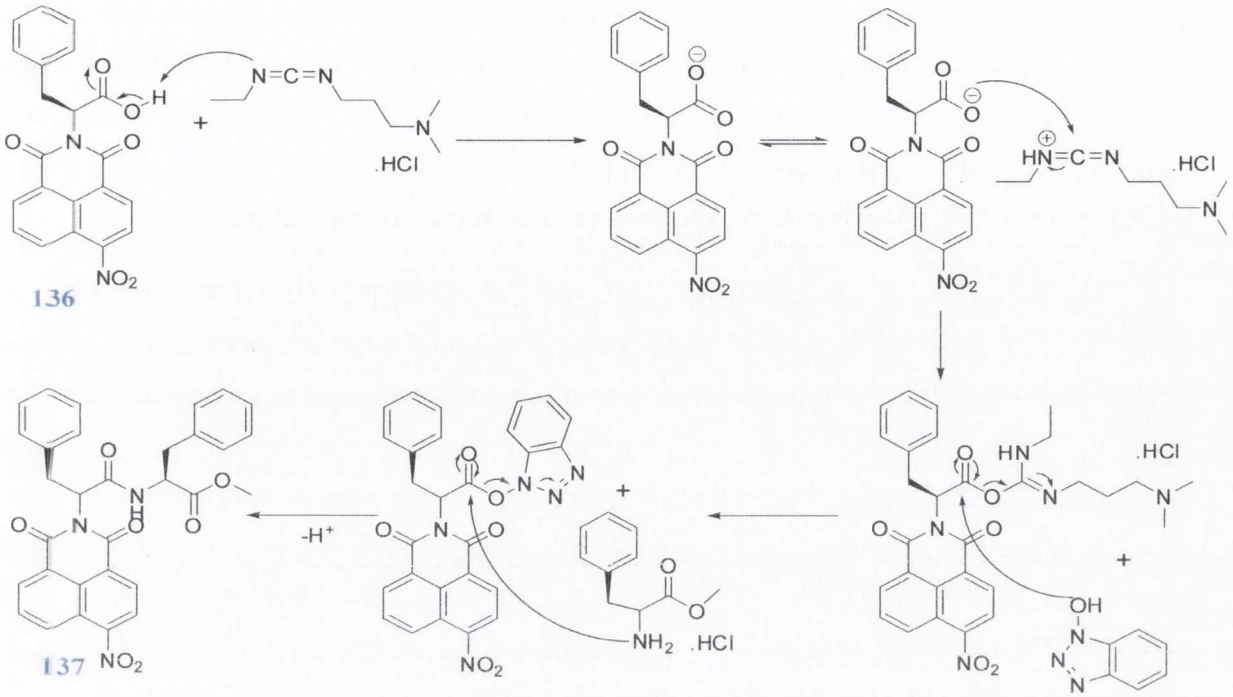

Figure 3.5: *The reaction mechanism of an EDCI.HCl/HOBt mediated coupling yielding 137.*

The ^{1}H NMR ($CDCl_3$, 600 MHz) spectrum of **137** is shown in Figure 3.6.

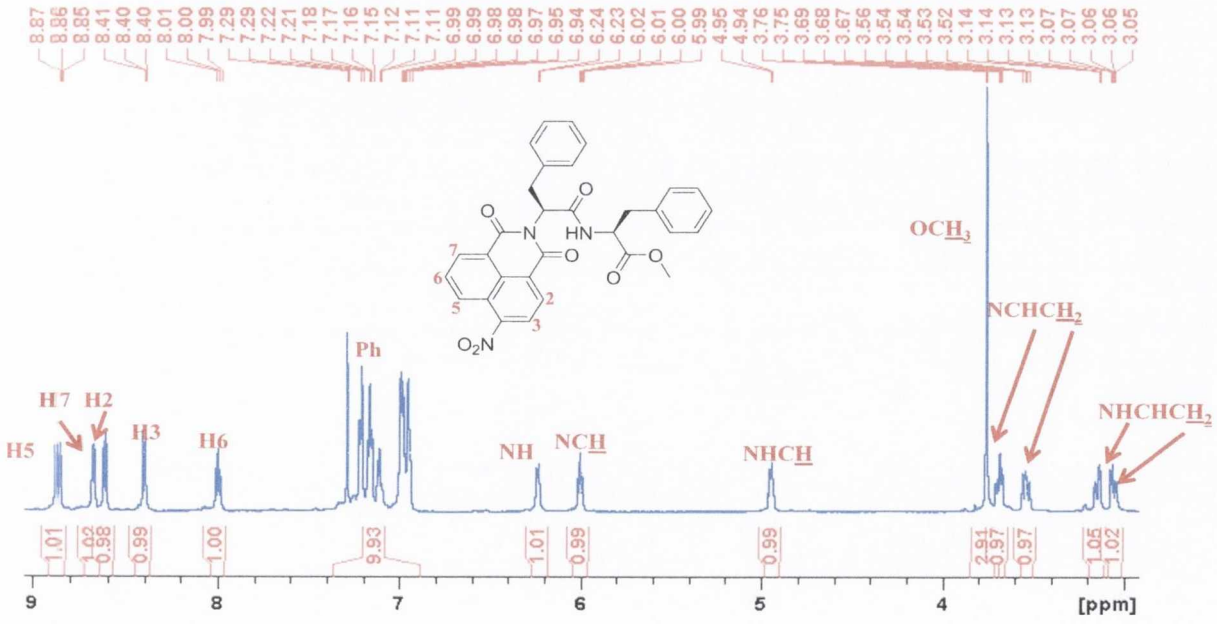

Figure 3.6: *^{1}H NMR ($CDCl_3$, 600 MHz) spectrum of 137.*

The aromatic region is composed of six separate resonances, five of which each integrate for one proton and correspond to the naphthalimide protons and a multiplet which integrates for ten protons pertaining to the two phenyl groups. The amido proton resonates as a doublet at 6.24 ppm with a coupling constant of 6.8 Hz. The presence of the amido proton is significant as it shows that this reaction was successful and a new peptide bond formed.

The remainder of the spectrum is composed of seven signals, which were assigned using HMQC and HMBC experiments. The α-proton belonging to the phenylalanine residue directly attached to the *N*-imide terminus appears at 6.02 ppm, whilst the second α-proton appears at 4.95 ppm. The methoxy group can be seen at 3.76 ppm whilst each of the protons belonging to the methylene groups attached to the α-centres appear as four separate entities, each integrating for one proton. As can be seen in Figure 3.7, assigning these protons was achieved with the aid of a CH-COSY. The appearance of an amide carbonyl stretch at 1666 cm^{-1} in the IR spectrum complemented the assigned structure whereas, mass spectral results confirmed the molecular formula of the assigned structure.

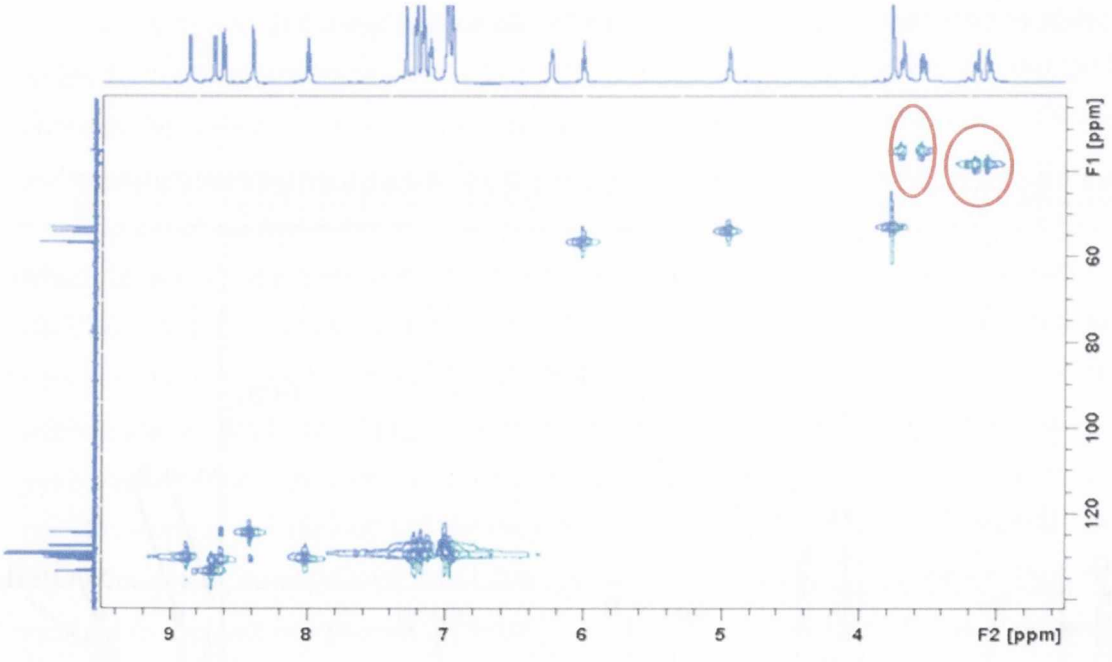

Figure 3.7: *CH-COSY Spectrum ($CDCl_3$) of 137.*

The peptide 4-amino-1,8-naphthalimide conjugates **138-140** were synthesised by hydrogenolysis in EtOH in the presence of Pd/C (10%) at 3 atm H_2 in high yields of 96%, 99% and 98%, respectively, without the need for purification.

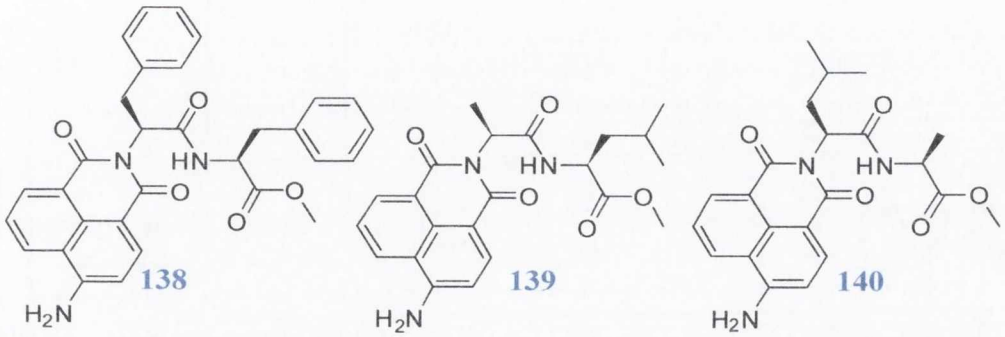

The formation of the desired peptide naphthalimides **138-140** was confirmed by ^{1}H and ^{13}C NMR spectroscopy, whereby the resulting spectra showed the absence of any side-products or starting materials. As can be seen in Figure 3.8, the aromatic region of the ^{1}H NMR ($(CD_3)_2SO$, 600 MHz) spectrum of **140** is defined by seven signals, five of which represent the naphthalimide aromatic protons. The amido proton was found to appear at 8.15 ppm, whereas the amino peak which integrates for two protons and shows that this reaction has been successful appeared as a broad singlet at 7.41 ppm. The remainder of the spectrum consists of nine resonances, two of which represent the α-protons. The *S*-leucine α-proton appears at 5.48 ppm and is followed by the *S*-alanine α-proton at 4.33 ppm and a broad singlet at 3.62 correlating to the methoxy group. In a similar fashion to that seen for **137**, the protons belonging to the methylene group attached to the α-centre of the amino acid residue appear as complex multiplets at 2.08 and 1.94 ppm, each integrating for one proton. These were assigned with the aid of a CH-COSY experiment. Utilising H-H-COSY and long range CH-COSY experiments the methine proton attached to the methyl groups of the *S*-leucine moiety was also assigned and found to appear at 1.33 ppm as a multiplet. These experiments were also used to assign the *S*-alanine methyl group which resides at 1.13 ppm and the methyl groups belonging to the *S* -leucine residue which appeared at 0.89 and 0.80 ppm. Similar methodology was used to characterise derivatives **138** and **139**. In addition, the HRMS and IR spectral analysis also confirmed the assigned structure in Figure 3.8.

The stereochemistry of compounds **138-140** were investigated by CD spectroscopy in CH_3OH, where the characteristic signal for the amino acid moiety was observed confirming that the stereochemistry was retained.

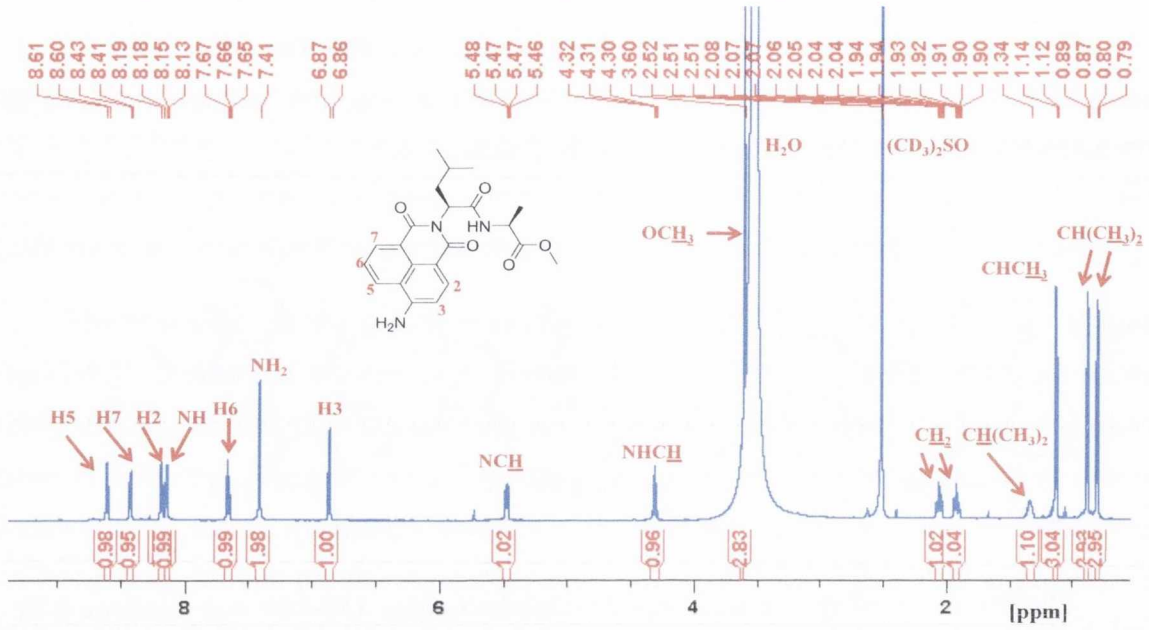

Figure 3.8: *^{1}H NMR spectrum of* ***140***.

3.3.3 Synthesis of α-Amino Acid based 3-Amino-1,8-Naphthalimide Precursors 141-143

A series of α-amino acid based 3-amino-1,8-naphthalimides **141-143** were synthesised in an analogous fashion to those discussed in Section 3.3.1. Once again, the 3-nitro-1,8-naphthalimide derivatives were synthesised by Phelan.[114] As part of this project, the next step in the reaction sequence involved reducing the nitro group. This was achieved by carrying out hydrogenolysis reactions in CH_3OH in the presence of a palladium catalyst at 3 atm H_2, which gave compounds, **141**, **142** and **143** in yields of 98%, 72% and 99%, respectively.

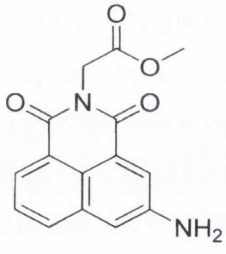

141

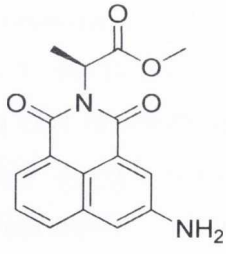

142

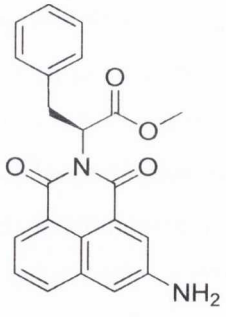

143

Compounds **141-143** were characterised using conventional methods, such as ^{1}H and ^{13}C NMR experiments, mass spectroscopy and IR analysis. For example, the ^{1}H NMR ($(CD_3)_2SO$, 600 MHz), spectrum of **143** is shown in Figure 3.9. Due to the naphthalimide moiety being derivatised with an amino group in the 3-position which appears as a broad

singlet at 6.02 ppm, the naphthalimide protons resonate as four doublets at 8.06, 8.03, 7.84 and 7.30 ppm pertaining to H5, H7, H2 and H4, respectively and an *apparent* triplet at 7.62 ppm belonging to H6. The coupling constants derived for the doublets at 8.06 and 8.03 are 8.3 and 7.1 Hz, respectively, indicating that the protons that are coupling are in close proximity to each other. Conversely the coupling constants calculated for the doublets at 7.84 and 7.30 ppm are 2.1 and 2.3 Hz, respectively, indicating that these protons H2 and H4 are separated by a greater distance compared to H5, H6 and H7. The phenylic protons emerge as a multiplet spanning a 7.04-7.14 ppm range followed by the α-proton which can be found at 5.98 ppm. A distinctive broad singlet at 3.65 ppm correlates to the methoxy group and the protons belonging to the methylene unit appear as two separate multiplets, each integrating for a single proton assigned using a CH-COSY spectrum. The structure assigned here was further supported by ^{13}C NMR with the appearance of twenty resonances. IR analysis confirmed that the amine had formed with signals at 3461 and 3368 cm^{-1}. In addition, mass spectral analysis confirmed the molecular formula of the assigned structure.

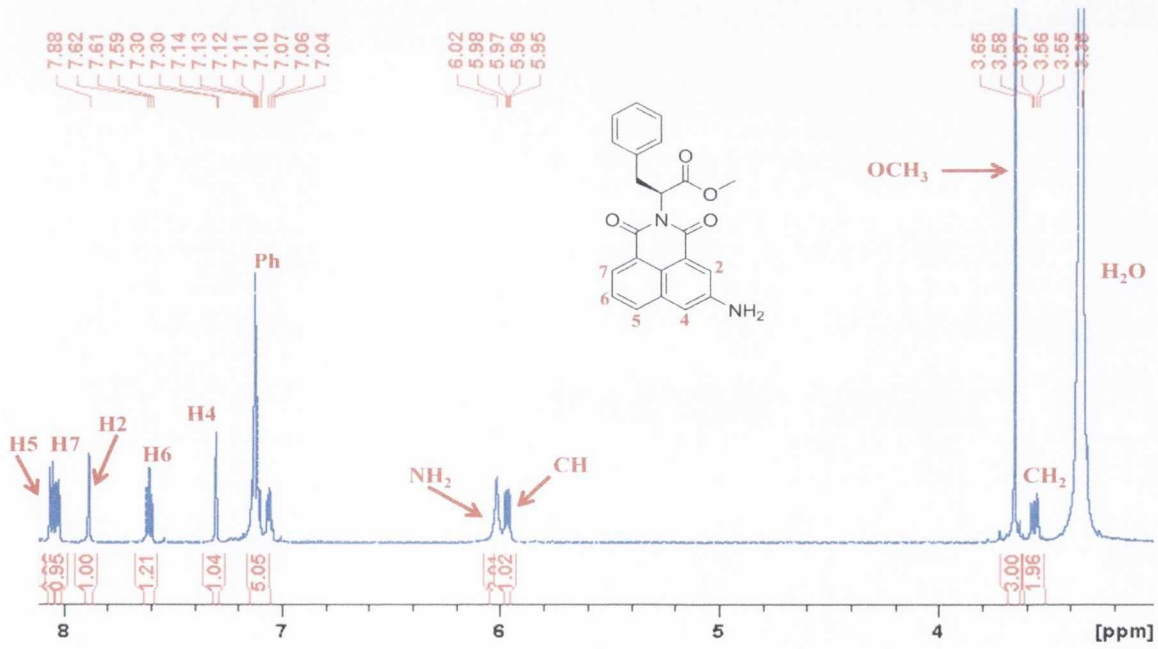

Figure 3.9: ^{1}H NMR ($(CD_3)_2SO$, 600 MHz) spectrum of **143**.

Compounds **142** and **143** were further analysed by carrying out CD experiments in CH_3OH. Negative signals were observed in a 200-240 nm range showing that these molecules retain their chirality during synthesis. No positive or negative induced signals were detected. Conversely, this was not the case for **132**, which is quite similar in structure to **143**, the only

difference being the position of the amino group, which showed a very weak negative induced band.

In summary, seventeen enantiomerically pure amino acid based 1,8-naphthalimide structures with an amino group on either the 3 or 4 positions of the naphthalene ring were synthesised in high yields. With the view of exploring the potential of these enantiomerically pure molecules further, modifications to the naphthalimide aryl ring and/or incorporation of additional synthetic moieties at the *N*-imide site were investigated and are described in the following sections.

3.3.4. Synthesis of Tröger's Base Analogues from 4-Amino-1,8-Naphthalimide Precursors

Formation of the Tröger's base naphthalimides was attempted using the methodology explored by Veale,[148,149] as shown in Scheme 3.3.

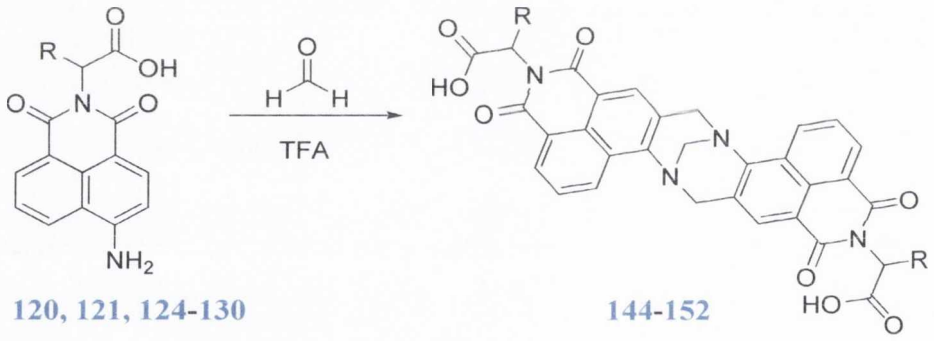

120, 121, 124-130 **144-152**

Cpd.	Cpd.	R	% Yield
126	144	H	76%
127	145	CH_3 (*S*)	91%
120	146	CH_3 (*R*)	91%
128	147	CH_2Ph (*S*)	64%
124	148	CH_2Ph (*R*)	65%
130	149	$CH(CH_3)_2$ (*S*)	71%
121	150	$CH(CH_3)_2$ (*R*)	41%
129	151	$CH_2CH(CH_3)_2$ (*S*)	50%
125	152	$CH_2CH(CH_3)_2$ (*R*)	50%

Scheme 3.3: *Synthesis of 144-152.*

This involved treating the 4-amino-1,8-naphthalimide derivatives with paraformaldehyde (1.5 equivalents) in neat TFA over 12 hours at room temperature. The work-up involved neutralising and further basifying the reaction mixture to pH 12 by the addition of 6M NaOH and extracting the product with CH_2Cl_2. This synthetic protocol was followed however modifications to the work-up procedure were devised depending on the nature of the amino acid present. The synthesis of the Tröger's base derivatives is sub-divided into three sections, starting with the synthesis and characterisation of amino acid conjugates **144-152**, which possess unprotected *C*-termini and will be discussed in the following section.

3.3.5. Synthesis and Characterisation of Tröger's Base Analogues 144-152

The synthesis of **144-152** in moderate to high yields was achieved following Scheme 3.3. The simplest Tröger's base analogue in this series, **144** containing the achiral amino acid glycine, was firstly synthesised as a racemic mixture using the procedure outlined above. The work-up involved removing the TFA by evaporation under reduced pressure in the presence of copious amounts of CH_2Cl_2. Once the crude product was dry, it was subjected to purification by refluxing in CH_3OH in the presence of activated charcoal overnight. The reaction mixture was then filtered while hot through celite and washed with copious amounts of CH_3OH. The filtrate and washings were removed under reduced pressure and the residue was re-dissolved in ethyl acetate and the organic layer was dried over $MgSO_4$ and reduced to dryness to yield the desired product as a yellow powder in 76% yield.

Compound **144** was characterised by standard techniques and Figure 3.10 shows the ^1H NMR spectrum ($(CD_3)_2SO$, 400 MHz) of **144**. As can be seen, the aromatic region is defined by four resonances between 8.80 and 8.17 ppm including two doublets, a singlet and an *apparent* triplet, each integrating for two protons. Such integration for the naphthalimide chromophore confirms the symmetric nature of **144**. The C_2 plane of symmetry is confirmed by the presence of the methylene protons of the diazocine ring which appear between 5.22 and 4.71 ppm as a doublet integrating for two protons and a multiplet integrating for four protons. The methylene protons belonging to the glycine moiety appear as a singlet at 4.66 ppm.

The ^{13}C NMR spectrum ($(CD_3)_2SO$, 150 MHz) of **144** also showed the symmetric nature of the molecule by having two additional signals compared to the naphthalimide precursor **126**, pertaining to the carbons of the diazocine ring. The IR spectrum showed the

loss of the amino group belonging to the precursor at 3364 and 3259 cm^{-1} suggesting that the reaction has taken place. In addition, the molecular formula for **144** was determined by positive electrospray ionisation providing further evidence for the assigned structure.

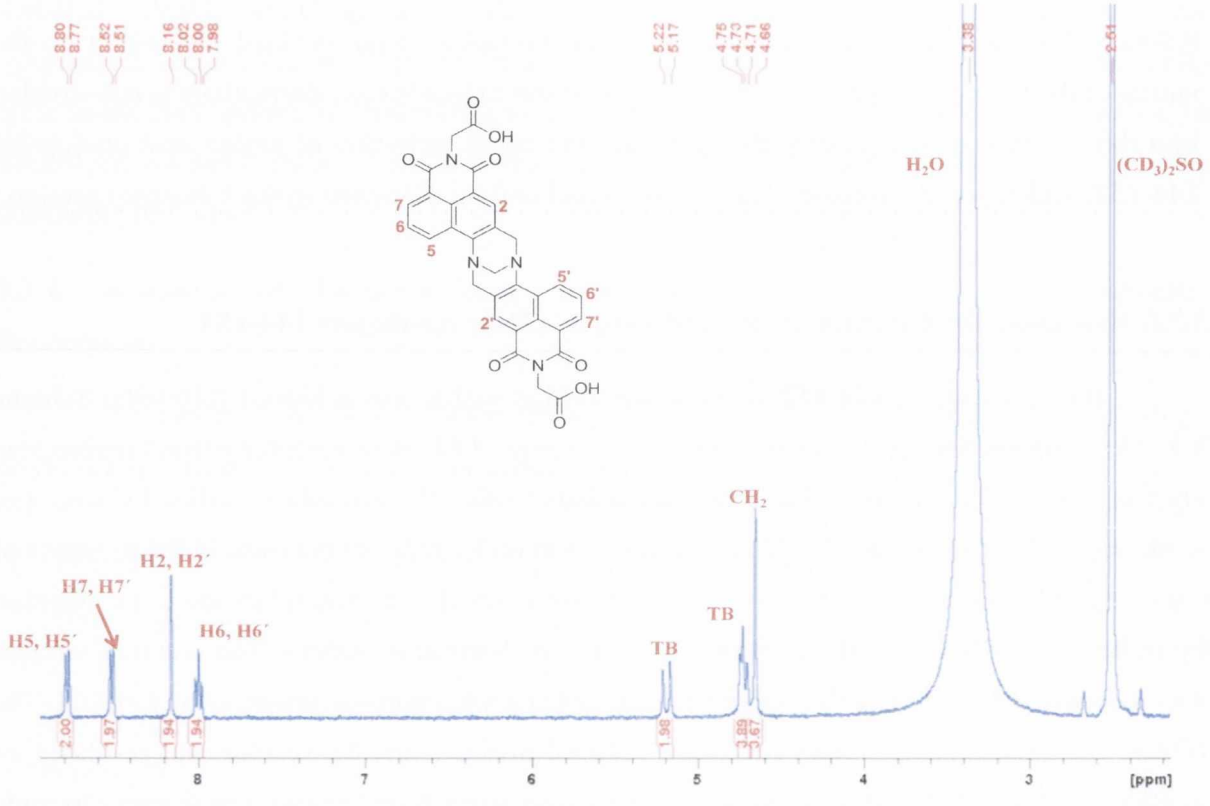

Figure 3.10: *The ^{1}H NMR ($(CD_3)_2SO$, 400 MHz) spectrum of **144**.*

Formation of **145** and **146** from *S*-alanine and *R*-alanine, respectively, was also achieved in high yields using a similar synthetic procedure as for **144** and purified by refluxing in CH_3OH in the presence of activated charcoal. The ^{1}H NMR ($(CD_3)_2SO$, 600 MHz) spectra of **145** and **146** confirmed the formation of the desired bis-1,8-naphthalimide containing Tröger's bases, without the presence of any impurities or starting materials, as shown in Figure 3.11.

The ^{13}C NMR ($(CD_3)_2SO$, 150 MHz) spectra of **145** and **146**, showed that the two methylene carbons of the diazocine ring come into resonance at 66.3 and 57.1 ppm. Interestingly, the doubling of carbon peaks pertaining to the carbonyl, aromatic and aliphatic signals were observed for the diastereoisomers of **145** and **146** formed. For example, the carbon peak pertaining to the methyl group directly bonded to the α-proton is doubled, giving rise to two resonances at 14.8 and 14.7 ppm. According to CH-COSY analysis, these two

resonances correspond to methyl groups, highlighting the effect of combining the chiral α-centre with the chiral Tröger's base structural unit, as no such splitting was observed for the glycine derivative **144**.

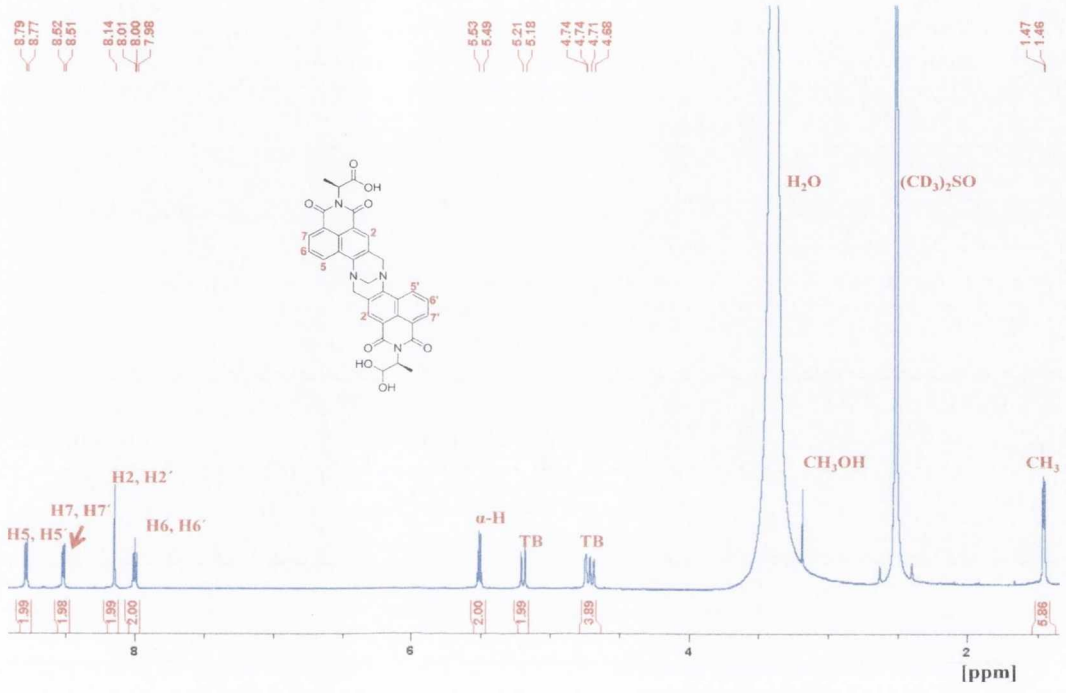

Figure 3.11: *The ^{1}H NMR ($(CD_3)_2SO$, 600 MHz) spectrum of **145**.*

The synthesis of the phenylalanine based molecules **147** and **148** of this series was successfully achieved according to the aforementioned protocol after purification by refluxing in CH_3OH in the presence of activated charcoal. As before, the structure of this compound was confirmed using techniques such as ^{1}H and ^{13}C NMR spectroscopy accompanied by IR and HRMS analysis. In comparison to **144-146**, the ^{1}H NMR ($(CD_3)_2SO$, 600 MHz) spectrum of **147** shown in Figure 3.12 proved to be more complex. Firstly, the aromatic region did not consist solely of two doublets, a singlet and an *apparent* triplet as was the case for the glycine and alanine derivatives, but was composed of what appeared as a triplet, two broad singlets and a doublet of doublets all of which belonged to the naphthalimide moiety. The ten protons belonging to the phenyl rings appeared as a multiplet between 6.91-7.04 ppm. The α-proton appeared at 5.84 integrating for two protons while the remainder of the aliphatic region of the spectrum consisted of the characteristic diazocine ring resonances at 5.14 and 4.68 ppm with the methylene protons situated beside the α-proton resonating as a multiplet at 3.52 ppm. The ^{13}C NMR ($(CD_3)_2SO$, 150 MHz) spectrum of **147**, was also shown to be more complex with

the appearance of multiple signals for carbonyl, aromatic and aliphatic resonances, which indicated the presence of diastereoisomers.

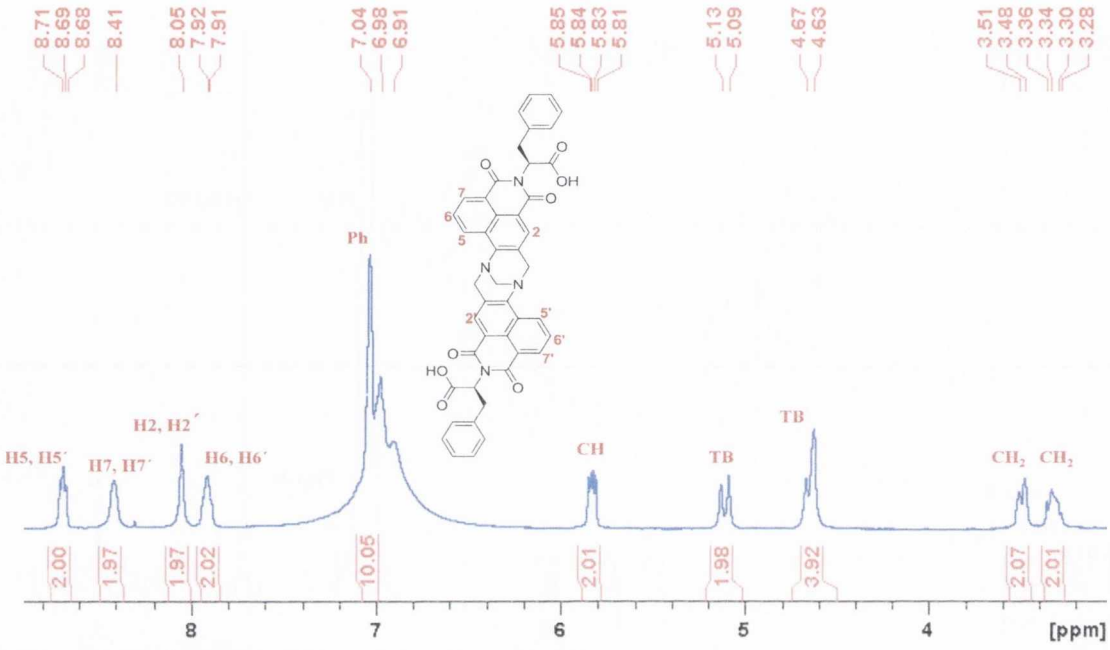

Figure 3.12: *^{1}H NMR ($(CD_3)_2SO$, 400 MHz) of 147.*

Applying the same synthetic procedure lead to the formation of **149** and **150** functionalised with *S*-valine and *R*-valine amino acids, respectively, after refluxing in CH_3OH in the presence of activated charcoal. Formation of **149** and **150** was confirmed by ^{1}H and ^{13}C NMR spectroscopy, HRMS and IR analysis. In comparison to **144-147**, the ^{1}H NMR ($(CD_3)_2SO$, 600 MHz) spectrum of **150** also proved to be more complex suggesting the formation of diastereoisomers. The aromatic region of the ^{1}H NMR ($(CD_3)_2SO$, 600 MHz) spectrum was defined by four resonances belonging to the naphthalimide chromophore composed of a doublet, what appeared as a triplet, two singlets in close proximity and a doublet of triplets. The aliphatic region of the spectrum consisted of a doublet pertaining to the Tröger's base unit with a coupling constant of 17.8 Hz, a doublet representing the α-proton at 5.09 ppm and a multiplet integrating for four protons corresponding to the remainder of the Tröger's base structural unit. In addition, the methine and methyl protons belonging to the valine moiety were represented as a multiplet and two doublets at 2.61, 1.17 and 0.60 ppm, respectively. In a similar way to that seen for the phenylalanine analogues **147** and **148**, the ^{13}C NMR ($(CD_3)_2SO$, 150 MHz) spectrum of **150** was also shown to be more

complex with the appearance of multiple signals, such as carbonyl, aromatic and aliphatic resonances, as seen in Figure 3.13.

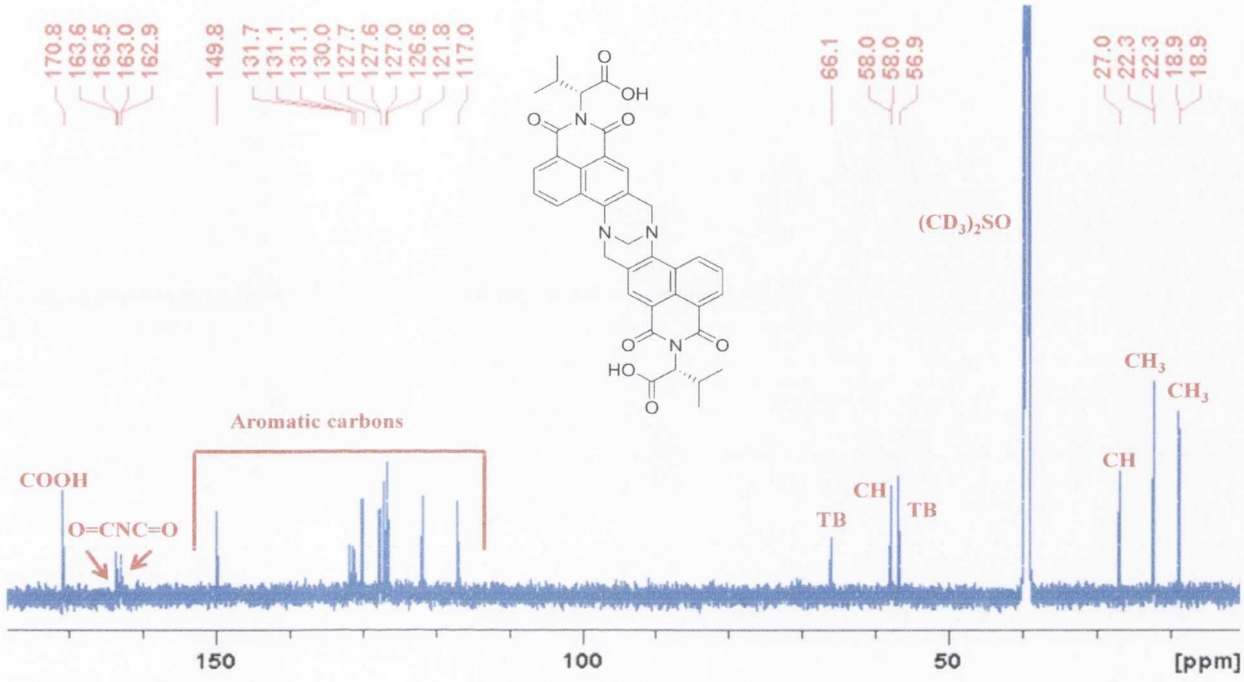

Figure 3.13: *^{13}C NMR spectrum ($(CD_3)_2SO$) of* **150**.

The final compounds in this series, the leucine based molecules **151** and **152**, were synthesised using the same protocol as for **144-150** and demonstrated a complex splitting pattern in the aromatic region of the ^1H NMR ($(CD_3)_2SO$, 600 MHz) spectrum similar to that observed for the phenylalanine and valine analogues **147-148** and **149-150**, respectively. In addition, the aliphatic region of this spectrum particularly the area pertaining to the methyl groups belonging to the leucine moiety showed a more intricate splitting pattern. In this spectrum, the methyl groups appeared as multiplets at 0.87 and 0.77 ppm, whereas, in the case of the precursor **129** they appeared as well defined doublets with coupling constants of 6.5 Hz, further highlighting the effect of combining the enantiomerically pure α-centres with the racemic Tröger's base unit.

In order to confirm that the amino acid Tröger's bases **145-152** synthesised retained their chirality, CD spectroscopy measurements in CH_3OH were carried out as previously described. As can be seen in Figure 3.14, the CD spectrum showed that the phenylalanine amino acid derivatives **147** and **148** retained their chirality, as a negative signal was observed for the *S*-analogue **147** while a positive signal was observed for the *R*-analogue **147**. Furthermore, very weak positive and negative induced signals were observed at longer

wavelengths for **147** and **148**, respectively, which were also observed for their corresponding precursors **128** and **124**. Similar results with the exception of ICD signals were observed for the remainder of amino acid Tröger's bases **145**-**152** synthesised.

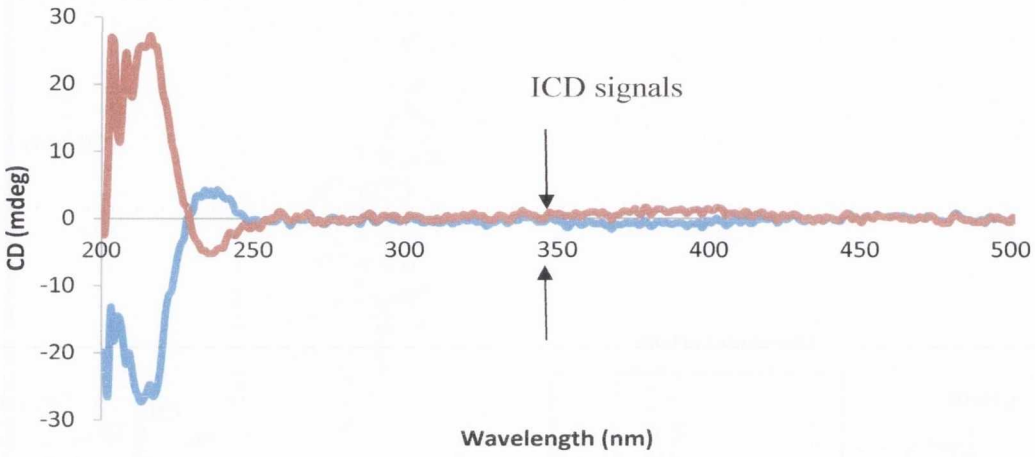

Figure 3.14: *The CD spectra of **148** (red) and **147** (blue) in CH_3OH.*

3.3.6. Synthesis and Characterisation of Tröger's Base Analogues 153 and 154

The synthesis of Tröger's base derivatives **153** and **154** incorporating *S*-leucine methyl esters and *S*-phenylalanine methyl esters, respectively, was achieved by stirring the relevant mono-naphthalimide in TFA in the presence of formaldehyde overnight. After basic work-up, **153** was purified by automated column chromatography using silica and hexane:ethyl acetate (0 to 100%) as eluent followed by trituration from CH_3OH to yield the desired compound as an orange solid in 63% yield. Compound **153** was characterised using conventional methods.

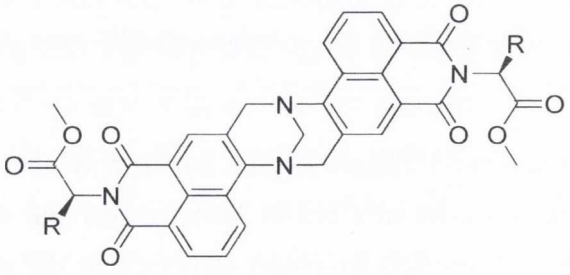

153 R = $CH_2CH(CH_3)_2$
154: R = CH_2Ph

The ^1H NMR ($CDCl_3$, 600 MHz) spectrum of **153** shown in Figure 3.15 shows the presence of the two expected diastereoisomers. The aromatic region of the spectrum consists

of two doublets which are in very close proximity to each other starting at 8.74 ppm pertaining to H5 which integrated for two protons, followed by another pair of doublets integrating for two protons which resonated quite close together at 8.63 ppm belonging to H7. At 8.13 ppm, a resonance consisting of two singlets appeared representing H2. The final resonance in the aromatic region of the spectrum appeared as a doublet of triplets integrating for two protons pertaining to H6. The α-proton appeared as a doublet of doublets at 5.74 ppm with coupling constants of 4.8 and 9.4 Hz. The Tröger's base peaks appeared between 5.18 and 4.63 ppm, where a doublet of doublets appeared at 5.18 ppm which integrated for two protons and had a coupling constant of 4.7 Hz and the characteristic geminal coupling constant of 17.0 Hz. Two singlets in close proximity to one another resonating at 4.72 ppm also belonged to the Tröger's base structural unit in addition to another doublet of doublets at 4.63 ppm with coupling constants of 4.7 Hz and 17.0 Hz. Each methoxy functional group appeared as a separate resonance integrating for three protons at 3.67 and 3.66 ppm. In addition, the methylene groups which are directly attached to the α-centre appeared as two separate resonaces as multiplets between 2.14-2.17 and 2.06-2.09 ppm. Subsequently, the methine protons attached to these methylene protons appeared as one resonance at 1.47 which was followed by the methyl groups which appeared as multiplets between 0.94-0.97 and 0.85-0.87 ppm.

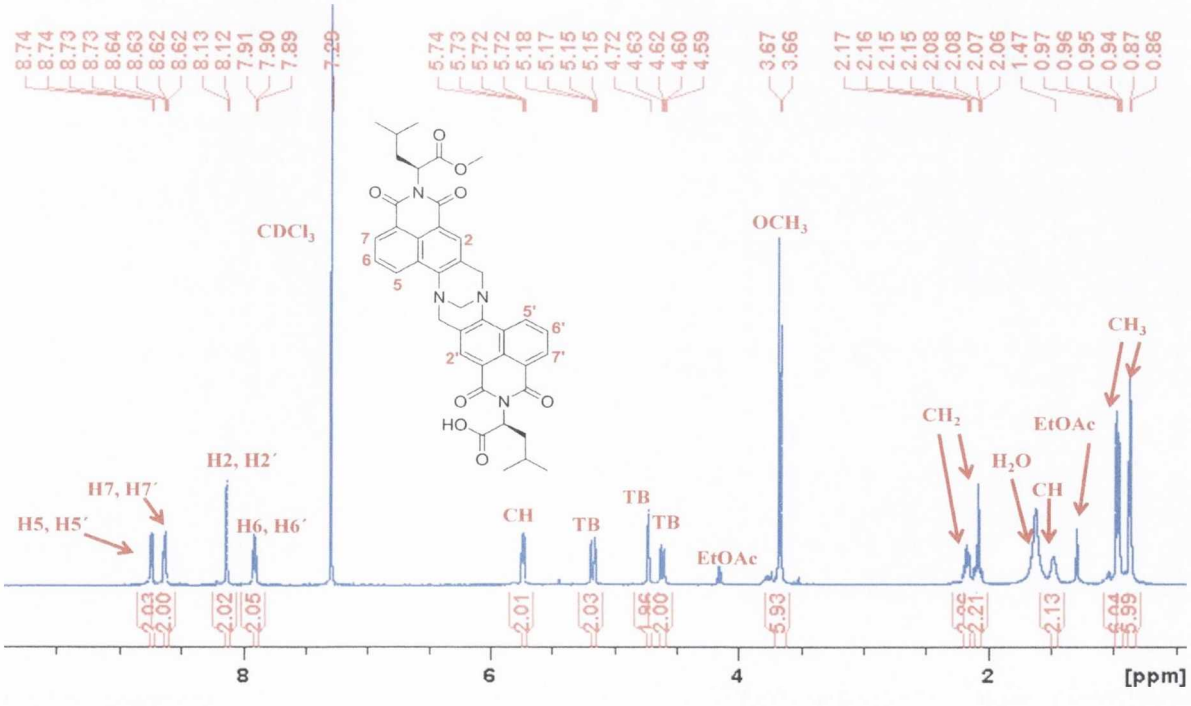

Figure 3.15: *^{1}H NMR ($CDCl_3$, 600 MHz) spectrum of 153.*

Upon comparing the ^{1}H NMR spectra of **153** and its precursor **131**, it was evident that the resonance for the α-proton was not altered upon incorporation of the chiral Tröger's base structural motif, however, those representing the methyl groups were. In the case of its corresponding precursor **131** which is a single enantiomer, the methyl groups appear as well defined doublets with coupling constants of 6.5 Hz. Incorporating the chiral Tröger's base motif led to these signals appearing as multiplets which suggested more complex coupling patterns, such as those that would be seen for a mixture of diastereoisomers.

Additional evidence for the appearance of diastereoisomers was obtained from the ^{13}C NMR ($CDCl_3$, 150 MHz) spectrum of **153** which showed that additional carbon peaks appeared representing carbonyl groups, aromatic and aliphatic carbons.

The CD spectrum of **153** was recorded in CH_3OH and is shown in Figure 3.16. As can be seen, a negative signal at *ca.* 230 nm was observed and can be attributed to the amino acid moiety. At longer wavelengths, a positive induced signal centred at *ca.* 392 nm was detected pertaining to the naphthalimide chromophores. No induced signal was observed for **131**.

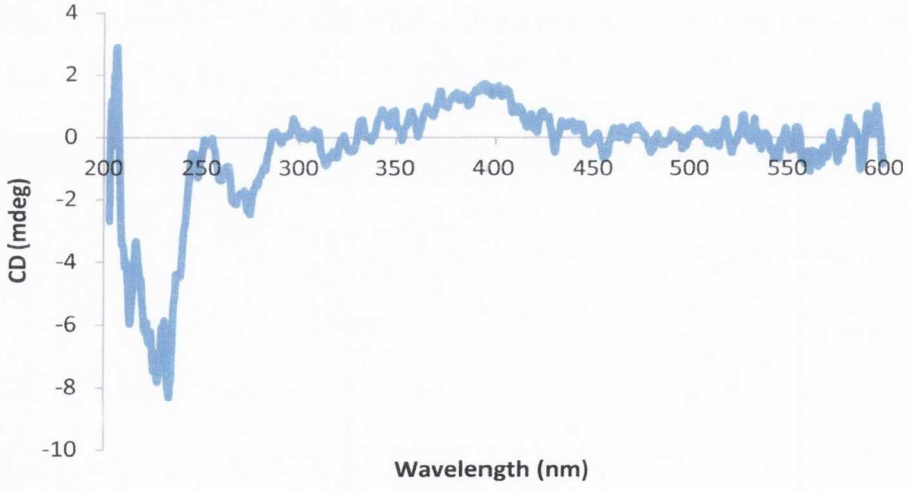

Figure 3.16: *The CD spectrum of the 153 in CH_3OH.*

Compound **154** was synthesised using the same method employed in the synthesis of **153**. Several purification attempts were made and are summarised in Table 3.2. Trituration with several solvents proved unsuccessful as no improvement in the ^{1}H NMR spectra was observed. Other purification techniques were investigated including automated column chromatography using neutral silica as the stationary phase. Two solvent systems were

investigated for the mobile phase (Table 3.2), however, due to poor separation on each of the columns, employing column chromatography as a method for purifying **154** proved unsuccessful. Further attempts included refluxing **154** in either $CHCl_3$ or CH_3OH in the presence of activated charcoal and looking to the data summarised in Table 3.2, it is evident that **attempt 8** was the most efficient method investigated for the purification of **154**, which was obtained in 76% yield.

Table 3.2: *Methods investigated for the purification of 154.*

Attempt	Purification Method	Result
1	Trituration with CH_3OH	Unsuccessful
2	Trituration with ethyl acetate	Unsuccessful
3	Trituration with EtOH	Unsuccessful
4	Trituration with CH_3CN	Unsuccessful
5	Column chromatography Silica:(CH_2Cl_2:CH_3OH, 0-10%)	Unsuccessful
6	Column chromatography Silica: (hexane: ethyl acetate, 0-100%)	Unsuccessful
7	Reflux in $CHCl_3$ with charcoal	Unsuccessful
8	Reflux in CH_3OH with charcoal	Improved ^1H NMR

The successful formation of **154** was confirmed using ^1H and ^{13}C NMR spectroscopy in conjunction with mass spectroscopy and IR analysis. The aromatic region of the ^1H NMR ($CDCl_3$, 600 MHz) spectrum of **154** pertaining to the naphthalimide protons displayed a splitting pattern similar to that described for **154**, as can be seen in Figure 3.17. The phenyl protons belonging to the amino acid residue integrated for ten protons between 7.02 and 7.17 ppm. The α-proton appeared as a doublet of doublets followed by the Tröger's base signals emerging between 4.55-5.15 ppm. As can be seen, the methoxy groups appeared as two separate resonances, as singlets at 3.71 and 3.69 ppm, which was similar to that seen for **149**. Moreover, like **149**, the methylene groups directly attached to the α-centre appeared separately as multiplets between 3.47 and 3.68 ppm. Once again, it was clear that diastereoisomers were present and this was further supported by the data attained from the ^{13}C NMR ($CDCl_3$, 150 MHz) spectrum which is shown in Figure 3.18. For instance, doubling

of carbonyl peaks belonging to the naphthalimide chromophore were observed in addition to the doubling of aromatic and aliphatic signals.

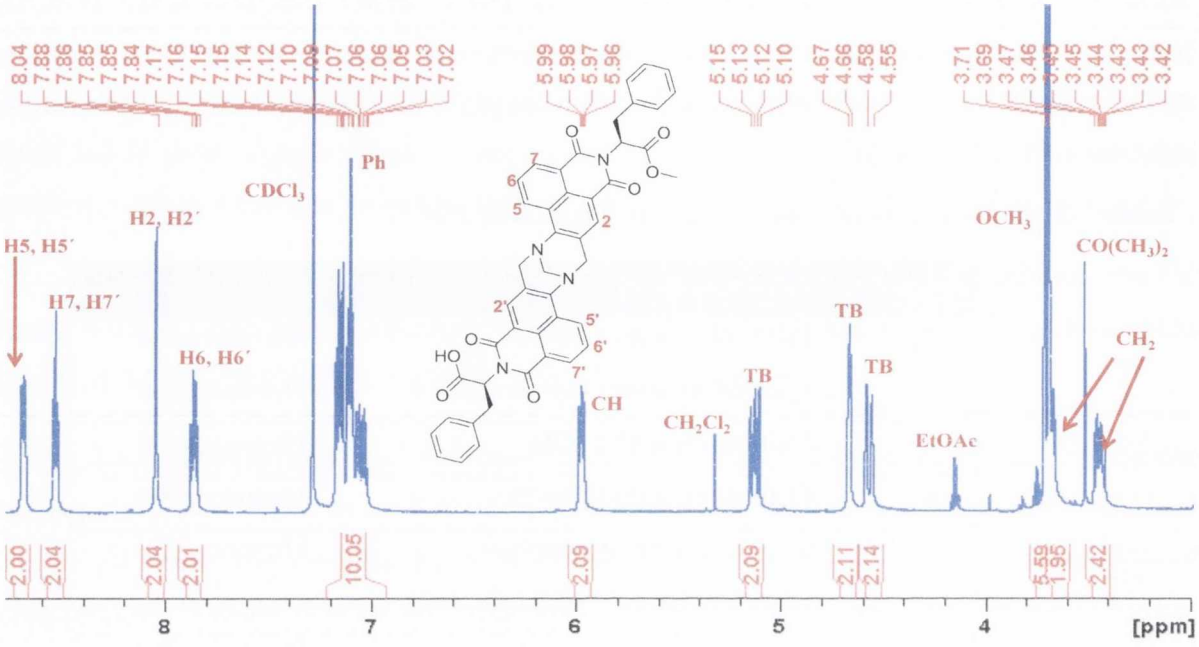

Figure 3.17: *^{1}H NMR ($CDCl_3$, 600 MHz) spectrum of* **154**.

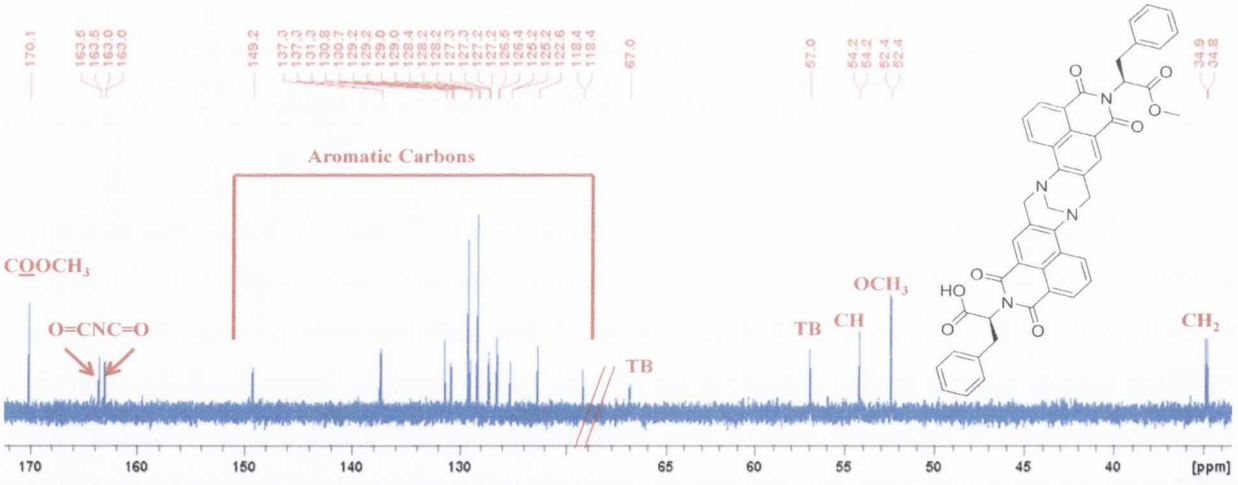

Figure 3.18: *^{13}C NMR ($CDCl_3$, 150 MHz) spectrum of* **154**.

3.3.7. Synthesis and Characterisation of Peptide based Naphthalimide Tröger's Base Analogues 155-157

The peptide based naphthalimide Tröger's bases were synthesised using the methodology developed by Veale,[148,149] which involved stirring the naphthalimide precursors **138-140** and paraformaldehyde in neat TFA overnight. Upon completion of the reaction, the

reaction mixture was initially neutralised and subsequently basified allowing for the crude products to be extracted with CH_2Cl_2 before being dried over magnesium sulphate. Purification was carried out where necessary.

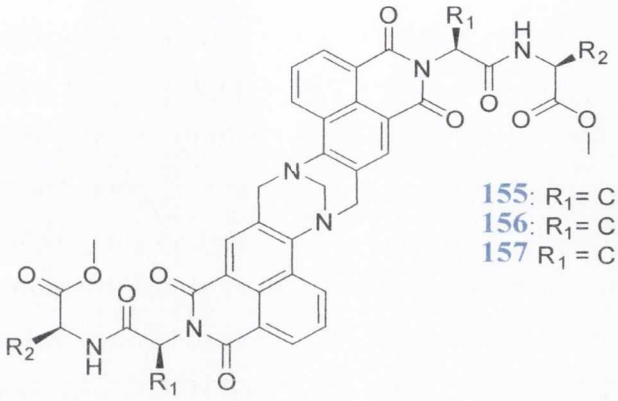

155: R_1= CH_3, R_2= $CH_2CH(CH_3)_2$
156: R_1= $CH_2CH(CH_3)_2$, R_2=CH_3
157 R_1 = CH_2Ph, R_2=CH_2Ph

The first peptide Tröger's base **155** was derived from the 4-amino-1,8-naphthalimide **138**, which bears a peptide moiety consisting of *S*-alanine and *S*-leucine residues with the *S*-alanine residue being directly attached to the *N*-imide terminus. Purification was achieved by a recrystallisation from CH_3OH, yielding the molecule as a yellow solid in 33%. The ^1H NMR ($CDCl_3$, 600 MHz) spectrum of **155** is shown in Figure 3.19.

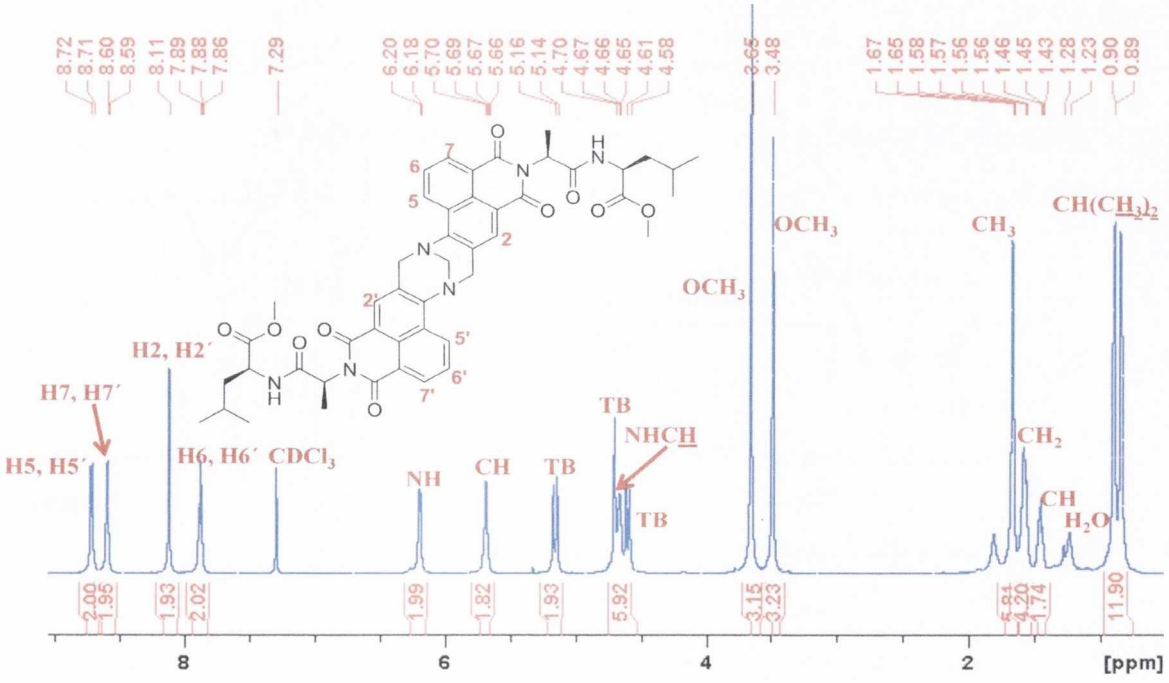

Figure 3.19: *^1H NMR ($CDCl_3$, 600 MHz) spectrum of **155**.*

As can be seen, the aromatic region between 7.19 and 8.72 ppm was composed of five signals, each integrating for two protons. The naphthalimide protons H5 and H7 appear as doublets, H2 as a singlet and H6 as a triplet. The fifth signal in the aromatic region pertains to the amide protons and appeared at 6.19 ppm and had a coupling constant of 7.7 Hz. The α-proton appeared at 5.70 ppm and was followed by the Tröger's base signals emerging as a doublet at 5.16 with a geminal coupling constant of 17.0 Hz, a singlet at 4.70 and another doublet at 4.61 ppm. The methine proton that connects the amide to the ester appeared as a multiplet and the adjacent methoxy group resonated as a singlet at 3.65 ppm. The aliphatic region between 0.84 and 1.67 was composed of five signals. The methyl group belonging to the alanine residue can be found at 1.67 ppm, whereas, the methyl groups belonging to the leucine residues appear as doublets at 0.90 and 0.85 ppm. These methyl groups belonging to each of the amino acid residues were distinguished using HMBC and HMQC experiments.

The ^{13}C NMR ($CDCl_3$, 150 MHz) spectrum of **154** is shown in Figure 3.20 and comprised of twenty-four carbons spanning the spectrum from 10-180 ppm.

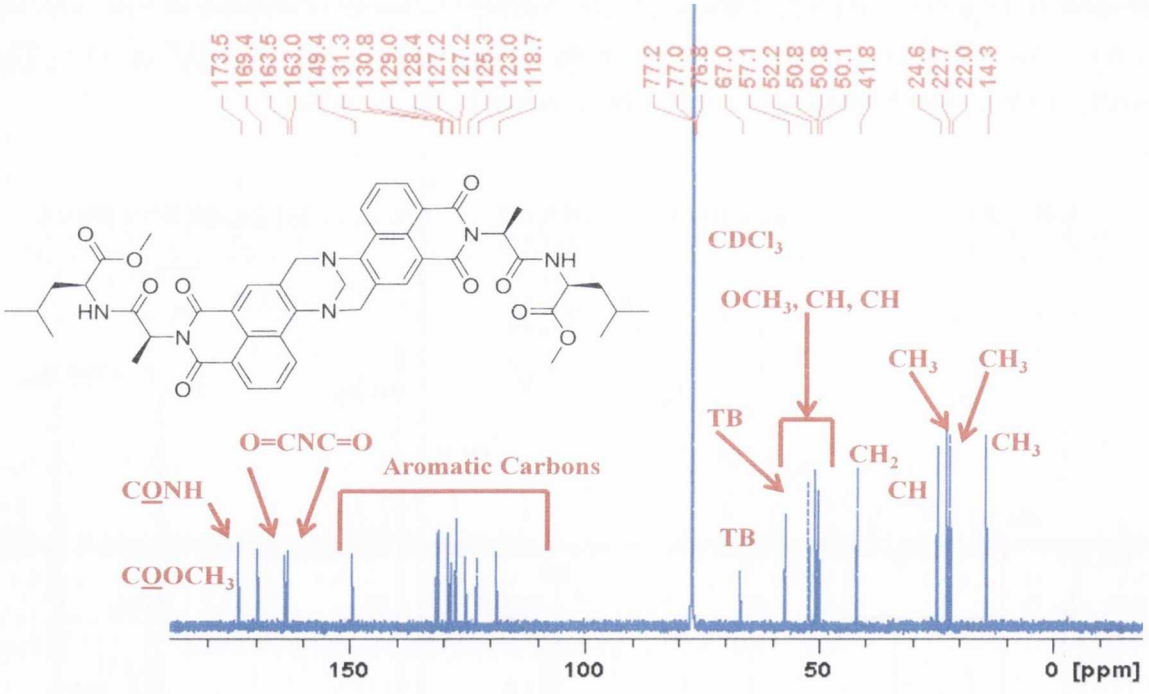

Figure 3.20: *^{13}C NMR ($CDCl_3$, 150 MHz) spectrum of **155**.*

In comparison to the precursor **139**, **155** contains two additional peaks corresponding to the diazocine moiety and highlights the symmetric nature of the Tröger's base. Compound **155** was further analysed by CD spectroscopy in CH_3OH as seen in Figure 3.21 and was found to exhibit a negative signal pertaining to the amino acid residues and a positive induced

signal centred at *ca.* 390 nm which has been attributed to the chiral amino acids inducing chirality into the achiral naphthalimide nucleus, as this effect was also observed for the corresponding precursor **139**, as discussed in Section 3.3.2.

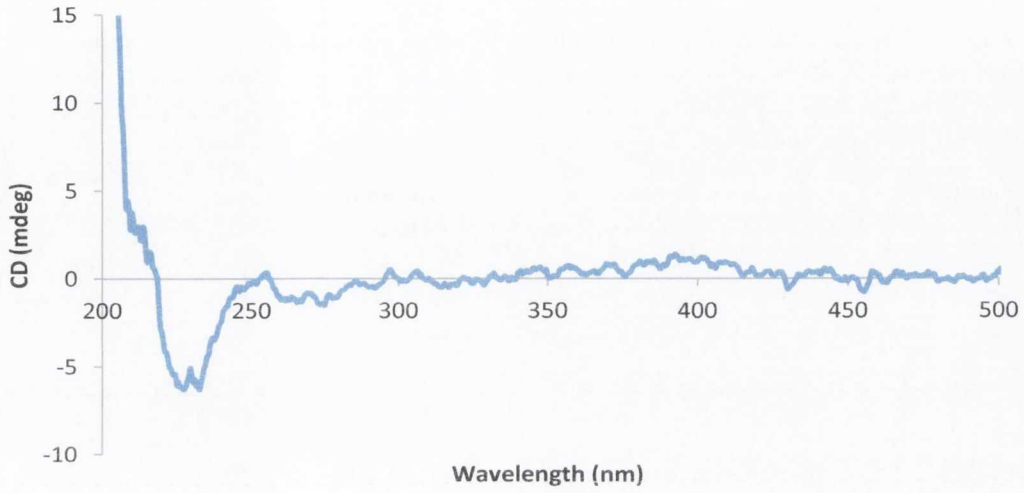

Figure 3.21: *CD spectrum of* ***155*** *in* CH_3OH.

The next peptide Tröger's bases to be synthesised were **156** and **157**. The peptide moiety of **156** is similar to **155** as they are both comprise of *L*-alanine and *L*-leucine residues. However, in the case of **156**, it is the *L*-leucine residue that is directly attached to the *N*-imide terminus and this was shown to have a significant effect on the NMR spectra. Unlike that seen for **155**, the aromatic region of the ^{1}H NMR ($CDCl_3$, 600 MHz) spectrum in relation to the naphthalimide protons is composed of five signals appearing as a doublet, a triplet, two singlets in very close proximity and a multiplet as shown in Figure 3.22. The Tröger's base signals appeared between 4.60 and 5.17 ppm and the methyl groups belonging to the *L*-leucine moiety emerged as multiplets further upfield. The ^{13}C NMR spectrum also shows the presence of multiple signals in the downfield and upfield areas of the spectrum further supporting the formation of diastereoisomers. All of the resonances were assigned using H-H-COSY, CH-COSY and long range CH-COSY techniques. The overall structure of **156** was confirmed by IR analysis and mass spectroscopy.

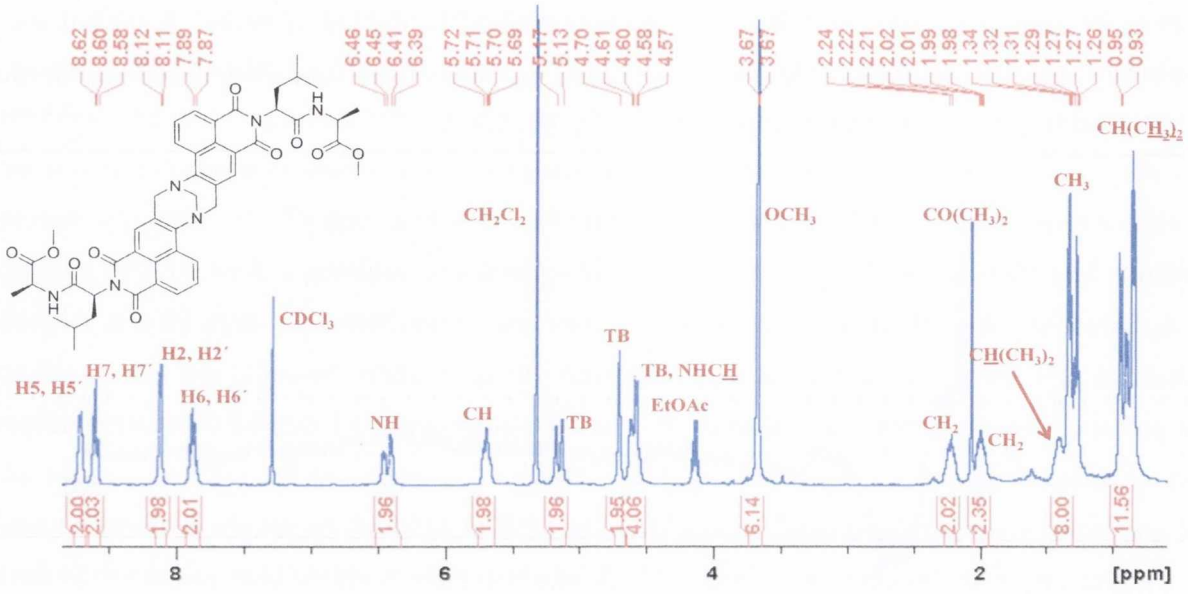

Figure 3.22: *^{1}H NMR ($CDCl_3$, 400 MHz) spectrum of 156.*

Compound **156** was also analysed by CD spectroscopy and in addition to exhibiting a negative signal at *ca.* 228 nm showing that chirality was retained during synthesis, an induced positive band centred at 395 nm was observed suggesting that the chiral moieties of this structure can induce chirality into the achiral counter-parts (Figure 3.23).

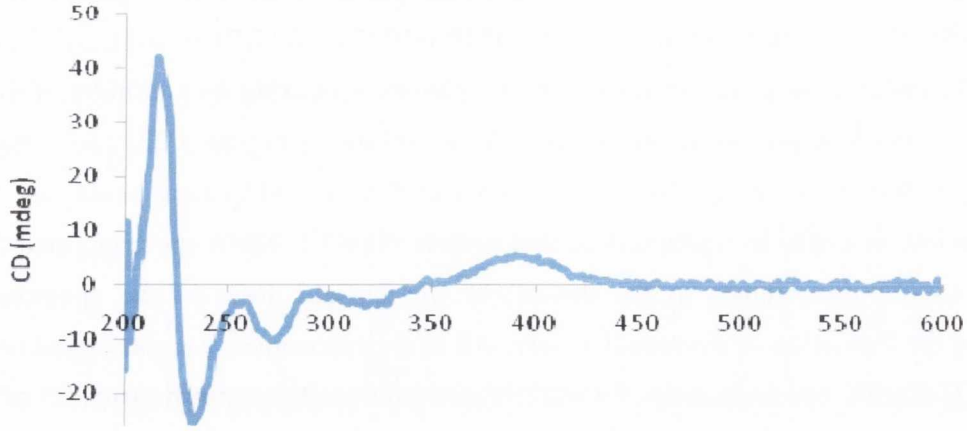

Figure 3.23: *CD Spectrum of 156 in CH_3OH.*

Compound **157** contains a peptide containing two *L*-phenylalanine residues and was purified by recrystallisation from CH_3CN giving the desired product in 79% yield and **157** was fully characterised by conventional techniques. Unlike that seen for **155**, an additional peak was observed in the aromatic region of the ^{1}H NMR ($CDCl_3$, 400 MHz) spectrum (Figure 3.24) which resonated as two doublets in close proximity appearing at 8.70 and 8.54

ppm. Then two singlets at 8.03 and 8.01 pertaining to H2 appeared and together they integrated for two protons. The remaining naphthalimide proton appeared as an *apparent* triplet at 7.87 ppm, before the phenylic protons resonated as a large multiplet between 6.76 and 7.15 ppm integrating for twenty protons. Additional peaks were also observed in the Tröger's base area of the spectrum between 4.58 and 5.14 ppm. The methylene protons directly attached to the α-centres were assigned using H-H COSY, CH-COSY and long range CH-COSY techniques. As a consequence of the formation of diastereoisomers, the ^{13}C NMR ($CDCl_3$, 150 MHz) spectrum showed doubling of carbonyl, aromatic and aliphatic signals. The assigned structure was also confirmed by IR and mass spectral analysis.

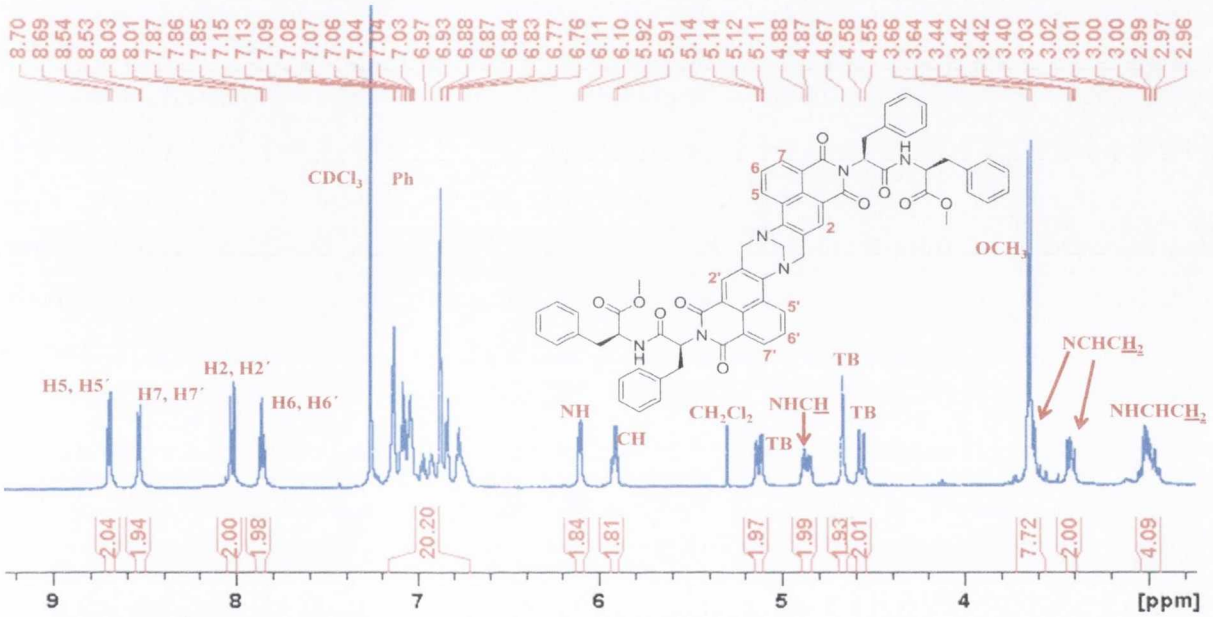

Figure 3.24: *^1H NMR spectrum ($CDCl_3$, 400 MHz) of* **157**.

Compound **157** was also analysed by carrying out CD measurements in CH_3OH and as can be seen in Figure 3.25, a negatively induced signal was observed in the longer wavelength region of the spectrum. However, no induced signals were observed for the naphthalimide precursor **137**. This suggested that perhaps the resulting chirality possessed by the Tröger's base unit after incorporation of the enantiomerically pure α-amino acids can contribute to inducing chirality into the naphthalimide nucleus.

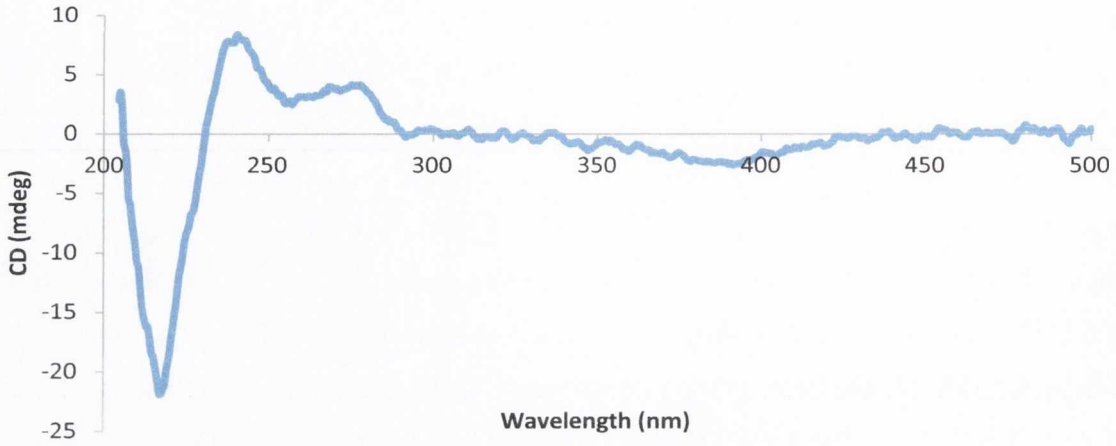

Figure 3.25: *CD spectrum of 157 in CH_3OH.*

In summary, naphthalimide based Tröger's bases incorporating amino acids derived from their 4-amino-counterparts have been synthesised. At the beginning of the synthesis, the amino acids were enantiomerically pure and when combined with a racemic moiety such as the Tröger's Base structural motif, diastereoisomers formed. This is evident from the NMR data discussed. In order to try and separate the diastereoisomers by normal phase column chromatography using silica or reverse phase chromatography using sephadex, many solvent systems were investigated. Unfortunately, separation of the distereoisomers proved unsuccessful. Several of the diastereomeric systems were purified by trituration and recrystallisation. However, differences in the solubilities of the diastereoismers were not observed and thus, the diastereoisomers were not separated *via* these means. Due to time constraints no other methods for separation were investigated.

3.3.8 Synthesis and Characterisation of Tröger's Base Derivatives 158-160 derived from the 3-amino-1,8-naphthalimide chromophore

The synthesis of Tröger's base derivatives **158-160** was achieved using the methodology optimised and discussed in Chapter 2, which involved using shorter reaction times of three hours and only 1.1 equivalents of paraformaldehyde, as shown in Scheme 3.4. The simplest Tröger's base derivative synthesised as part of this family was **158**, which contained glycine methyl ester residues. Upon completion of the Tröger's base reaction, the TFA was removed in the presence of copious amounts of CH_2Cl_2 under vacuum.

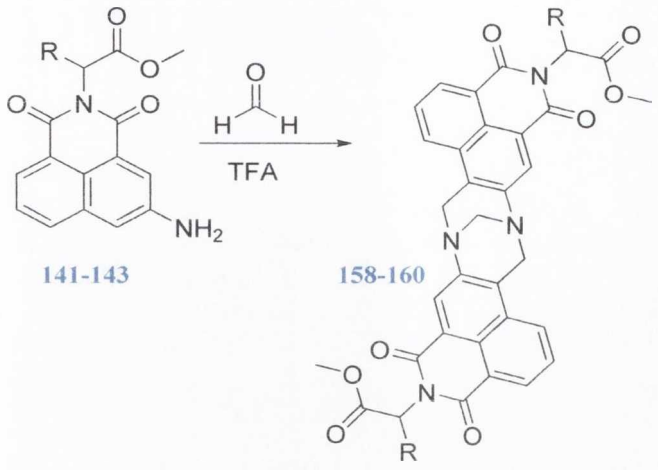

Cpd.	R	% Yield
141/158	H	**158**: 47 %
142/159	CH_3 (*S*)	**159**: 51 %
143/160	CH_2Ph (*S*)	**160**: 47 %

Scheme 3.4: *Synthesis of 158-160.*

Initial purification attempts involved recrystallisation from solvents such as EtOH and CH_3CN. These attempts were unsuccessful according to ^1H NMR spectroscopy. Manual chromatography using neutral alumina and a CH_2Cl_2:CH_3OH (95:5) solvent system was attempted and proved to be fruitless as no improvement could be seen in the ^1H NMR spectrum. The purification of **158** was achieved through recrystallisation from CH_3OH which was carried out twice to yield **158** as an orange solid in 47 % yield.

The identity of **158** was elucidated using conventional techniques such as ^1H and ^{13}C NMR spectroscopy as well as IR and mass spectral analysis. The ^1H NMR spectrum of **158** consisted of nine signals, four in the aromatic region and five in the aliphatic region of the spectrum as can be seen in Figure 3.26. The aromatic region is composed of a singlet, two doublets and an *apparent* triplet where each signal integrates for two protons pertaining to the naphthalimide protons. The characteristic Tröger's base peaks appear as two doublets at 5.31 and 5.02 ppm with germinal coupling constants of 17.3 Hz and a singlet at 4.72 ppm. The glycine methylene and methoxy protons resonate at 4.94 and 3.77 ppm, respectively. The symmetry of the molecule is evident in the ^1H NMR spectrum and is further confirmed in the ^{13}C NMR spectrum which contained two additional signals compared to the precursor **141**, which corresponded to the diazocine ring.

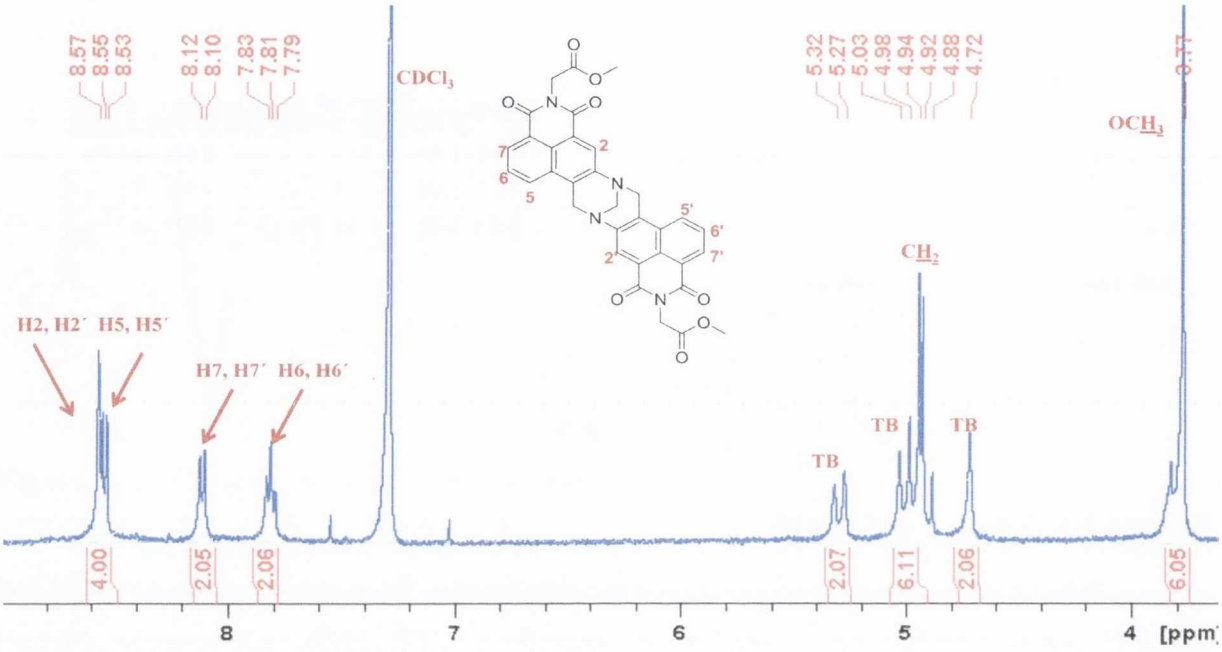

Figure 3.26: *^{1}H NMR spectrum ($CDCl_3$, 400 MHz) of 158.*

The second compound to be synthesised as part of this family was the *L*-alanine derivative **159**, which was purified by refluxing in $CHCl_3$ in the presence of activated charcoal. Unlike that seen in the ^{1}H NMR spectrum of **158**, which contains the achiral amino acid glycine, overlapping peaks were observed in the ^{1}H NMR spectrum ($CDCl_3$, 600 MHz) of **159**. The aromatic region does not consist of a singlet, two doublets and an apparent triplet but a multiplet between 8.48 and 8.50 which integrates for four protons followed by what appears as a triplet and another multiplet, each integrating for two protons. This overlapping of peaks suggests that diastereoisomers have formed and thus the amino acids retain their chirality during synthesis. This overlapping of signals can also be seen for the α-proton which appears as a multiplet, whereas, if diastereoisomers did not form this signal would appear as a quartet, like that seen for the precursor **142**. This overlapping of signals extends to the Tröger's base area of the spectrum with the methylene protons appearing as a doublet at 5.23, a doublet of doublets at 4.98 and two singlets at 4.61 and 4.62 ppm with overlapping signals for the methoxy groups appearing at 3.71 ppm. The overlapping of signals was also observed in the ^{13}C NMR spectrum highlighting that diastereoisomers have been formed. The structure assigned here was further supported by IR and mass spectral analysis. Compound **159** was also studied by CD spectroscopy in CH_3OH and apart from a negative band appearing between 200-240 nm, no other signals were observed.

The final compound in this study was **160** which was synthesised in 47 % yield after purification involving refluxing in CH_3OH in the presence of activated charcoal was carried out. The overlapping of signals was observed in both the ^1H and ^{13}C NMR spectra indicating that diastereoisomers formed during the course of this reaction. Similar to that seen for **159**, the overlapping of signals was observed in the aromatic region of the ^1H NMR spectrum of **160**, as well as for the α-proton and Tröger's base signals. The methoxy protons appear as two separate signals at 3.52 and 3.72 ppm, while the methylene protons bonded to the α-centre were found resonating at 3.47 ppm.

In addition, the overlapping of carbon peaks representing carbonyl, aromatic and aliphatic signals were also observed. The IR and mass spectral data also complemented the assigned structure. Analysis of **160** using CD spectroscopy showed that no induced signals were observed in the naphthalimide region of the spectrum. However, a negative band was detected between 200-240 nm pertaining to the optically active amino acid moiety highlighting that chirality was retained during the course of the reaction.

3.3.9. Synthesis of Peptide Based Tröger's Base Derivatives By Derivatising the *N*-Imide Core Post Tröger's Base Formation

Peptide synthesis relies heavily on reliable and efficient coupling reagents, with a key requirement being inhibition of the racemisation process. A plethora of methods have been reported for the carbon-nitrogen bond forming reactions involved in peptide synthesis, where fast and quantitative reactions are required without side reactions or with easily separated side products.[241-243]

In the work described within this thesis, the synthesis of peptide based Tröger's base derivatives from their corresponding 1,8-naphthalimide precursors was successful with the generation of three novel compounds **155-157**. In order to expand on the synthetic methodology employed here, an alternative route to yield such derivatives was explored which involved coupling a Tröger's base derivative bearing one amino acid at each *N*-terminus with an additional amino acid. As already discussed in Section 3.3.2, one of the most successful amide bond forming approaches has involved activated ester formation.

The coupling of Tröger's base derivative **144** to a second amino acid moiety as depicted in Scheme 3.5 was investigated using several coupling reagents. Using the methodology explored within the Gunnlaugsson group, coupling of the **144** to an additional

amino acid was attempted using EDCI.HCl and HOBt and a slightly varied procedure.[114] To a reaction mixture containing **144** (1 eq.), *S*-leucine methyl ester hydrochloride (2.1 eq.), HOBt (2 eq.) and TEA (2 eq.) in CH_2Cl_2, EDCI.HCl (2.2 eq.) in CH_2Cl_2 was added at 0 °C. The reaction mixture was allowed to stir at 0 °C for 30 minutes, before stirring at room temperature overnight. The work-up involved washing the organic layer with water and sat. $NaHCO_3$ and drying over $MgSO_4$. Removal of solvent and purification involving recystallisation from CH_3OH yielded the desired compound as a yellow solid in 65% yield. In order to improve upon this yield the use of other coupling agents was investigated.

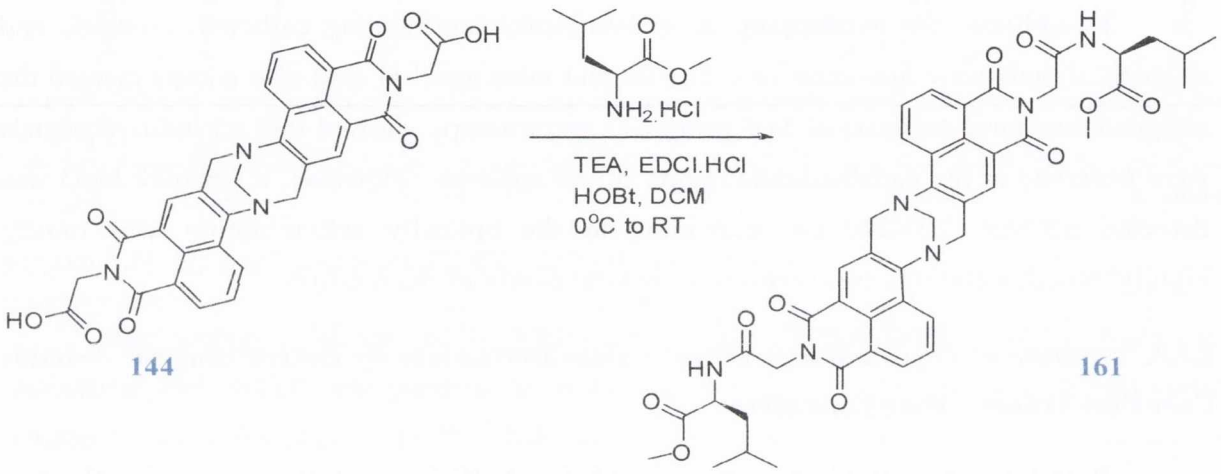

144 **161**

Scheme 3.5: *Synthesis of* **161**.

The second coupling agent to be investigated was ethyl chloroformate, which requires separate activation and aminolysis steps as depicted in Figure 3.27.[243] In the presence of a base such as TEA, a mixed carbonic anhydride is formed in the activation step between the carboxylate and ethyl chloroformate. The resulting activated species is used in its crude form and reacted with the desired amine to give the required amide bond.[243,244] Unfortunately, **161** was synthesised using this reagent in an unimproved yield of 65% after recrystallisation from CH_3OH.

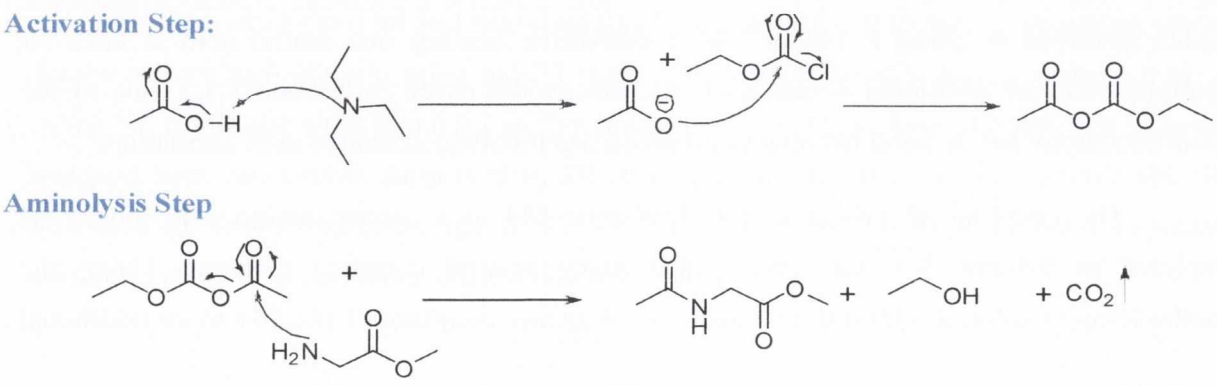

Figure 3.27: *Representative peptide coupling mechanism using ethyl chloroformate.*[243]

The next coupling agent to be considered belongs to the aminium family which incorporates the benzotriazole structure, where the most active reagent is *O*-(7-azabenzotriazol-1-yl)-1,1,3,3-tetramethyluronium hexafluorophosphate (HATU).[241-243] Notably, the use of this reagent is limited due to its vast expense.[243] An alternative to this reagent is *O*-(benzotriazole-1-yl)-1,1,3,3-tetramethyluronium tetrafluoroborate (TBTU) which has found use in the coupling of hindered peptides giving minimum racemisation.[241-243] In solution, TBTU can exist in two forms, as the aminium salt **162a** and the *N*-oxide guanidinium derivative **162b**, as shown in Figure 3.28.[243]

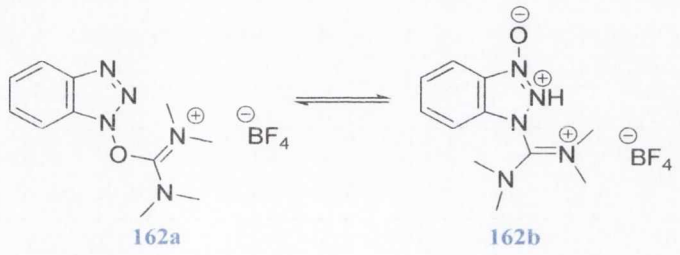

Figure 3.28: *The aminium salt form **162a** and N-oxide guanidinium form **162b** of TBTU.*[243]

The first step in the reaction mechanism involves deprotonation of the carboxylic acid which subsequently interacts with TBTU generating oxybenzotriazole which is free to interact with the newly formed intermediate producing an activated ester. Nucleophillic attack on the activated ester by the incoming amine leads to the formation of the desired amide bond, which is depicted in Figure 3.29.[245] As can be seen, HOBt is generated which is a water soluble by-product.

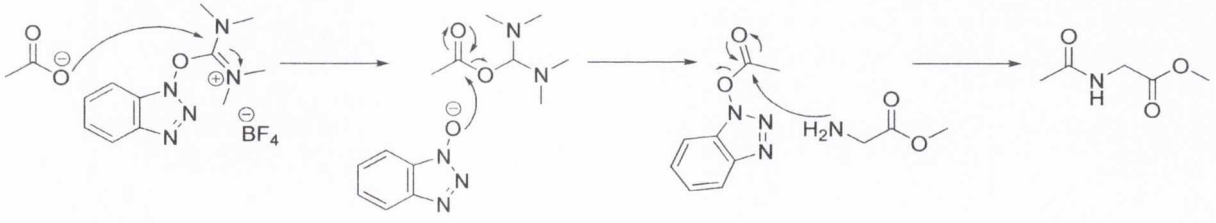

Figure 3.29: *Representative mechanism of TBTU mediated peptide coupling.*[245]

It was found that the synthesis of **161** using TBTU in CH_3CN generated the desired product in 37 % yield. A possible explanation for such a poor yield could be the insolubility of the reagents which occurred during the course of the reaction.

In the quest to obtain the desired peptide based Tröger's base **161** in higher yield, the reaction was attempted using a HOBt based phosphonium coupling reagent known as benzotriazolyoxy-tris(dimethylamino)hexafluorophosphate (BOP), which was designed by Castro[246] in an attempt to avoid the occurrence of racemisation and the unwanted side reactions associated with carbodiimide reagents. However, one of the major downfalls associated with the use of BOP is the generation of the carcinogenic agent hexamethylphosphoramide (HMPA).[243] The coupling mechanism involving BOP requires a tertiary amine to generate the carboxylate anion of the amino acid, which subsequently attacks the BOP coupling reagent in one of two ways, as shown in Figure 3.30. The first mode involved direct nucleophillic attack on the oxybenzotriazole unit which led to the release of HMPA. This is followed by amide formation with the desired amino acid. The second approach comprised of the carboxylate anion attacking the positively charged phosphorus atom on the BOP molecule and releasing the anionic oxybenzotriazole moiety which is free to attack the newly formed intermediate, generating a more active ester and releasing HMPA. Subsequent attack by the incoming amino acid produced the desired amide bond.[243] The synthesis of **161** was successfully achieved by adding BOP to a reaction mixture containing **144**, the required amino acid and DIEA at 0 °C. Following the addition of BOP the reaction mixture was allowed to stir at room temperature overnight.[247] Upon completion of the reaction, ethyl acetate was added to the reaction mixture which was washed successively with 1 M HCl, sat. $NaHCO_3$ and brine before, being dried over $MgSO_4$.

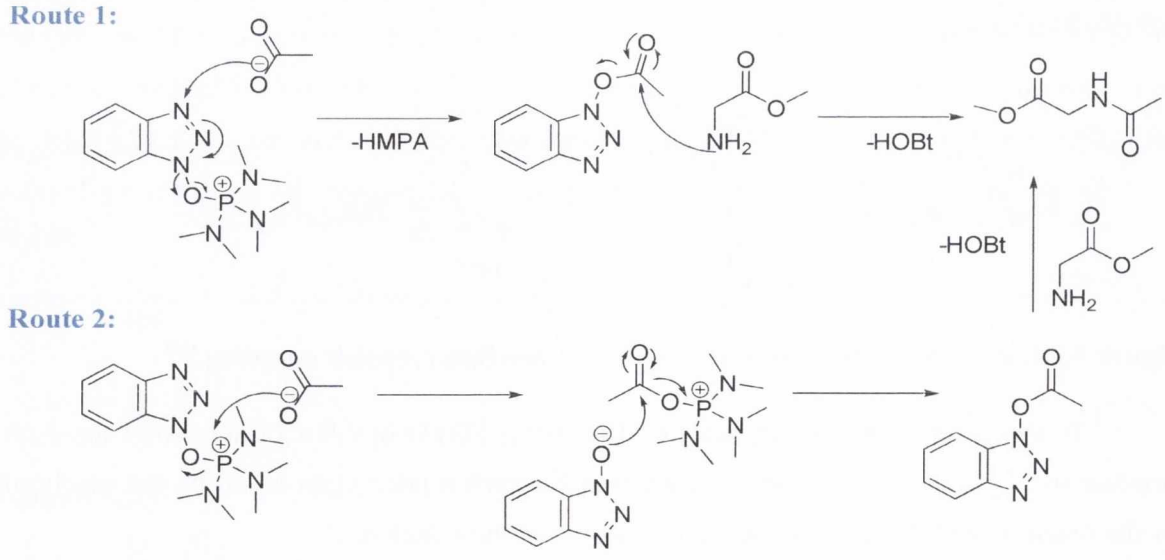

Figure 3.30: *Possible modes of nucleophillic attack on BOP.*[243]

Removal of solvents by evaporation under reduced pressure yielded the desired product in a much improved yield of 96 % after a recrystallisation from CH_3OH. Compound **161** was characterised using ^1H and ^{13}C NMR, mass spectroscopy and IR analysis. The ^1H NMR spectrum ($(CD_3)_2SO$, 400 MHz) of **161** is shown in Figure 3.31. In the ^1H NMR spectrum ($(CD_3)_2SO$, 400 MHz) of **161**, the formation of the peptide bond was confirmed by the presence of amido hydrogens at 8.53 ppm. The remainder of the aromatic region of the spectrum consisted of four peaks representing the naphthalimide protons, which showed overlapping signals highlighting that incorporation of the enantiomerically pure *S*-leucine amino acid into the racemic glycine based naphthalimide Tröger's base skeleton resulted in the formation of diastereoisomers. The rest of the spectrum contained the Tröger's base peaks which appeared as a doublet at 5.20 ppm and as part of a multiplet at 4.59-4.74 ppm, which integrated for eight protons.

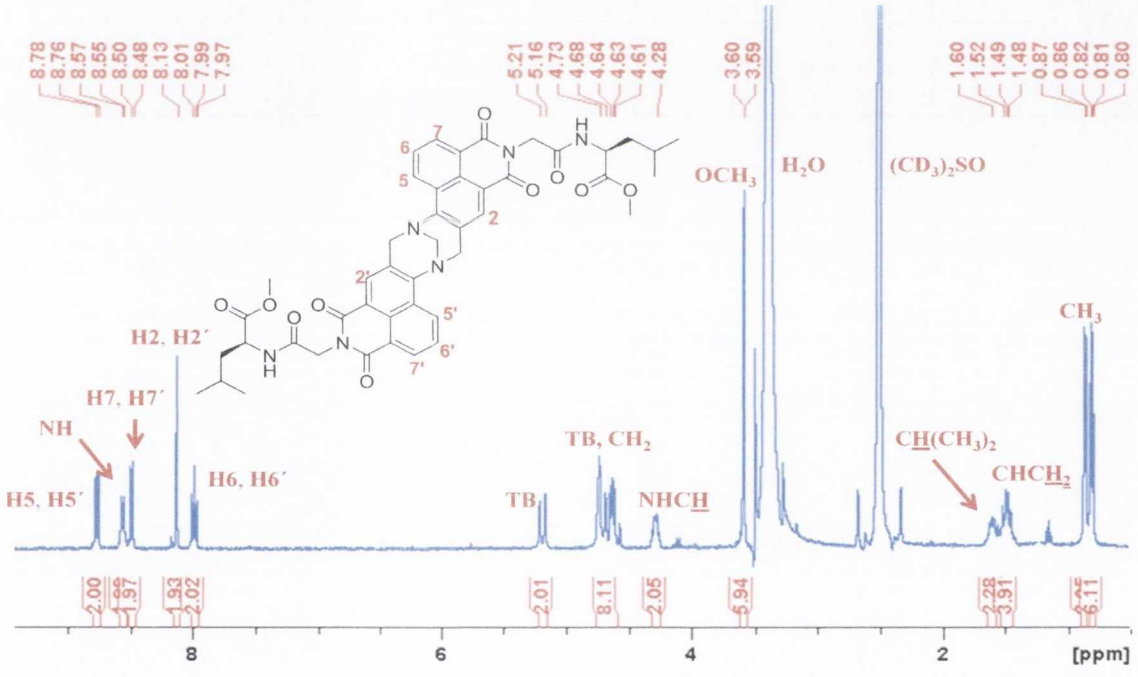

Figure 3.31: *^1H NMR spectrum ($(CD_3)_2SO$, 400 MHz) of **161**.*

According to a CH-COSY experiment, the methylene group pertaining to the glycine moiety also constituted part of this multiplet. The leucine component of this molecule was assigned with the aid of HMBC and HMQC experiments, where it was deduced that the α–proton appeared at 4.30 ppm, the methoxy groups and methylene protons adjacent to the α-centre at 3.60 and 1.47-1.55 ppm, respectively, whereas the methine and methyl protons

showed up at 1.59-1.64 and 0.82-0.88 ppm, respectively. The IR and mass spectral data were also consistent with the assigned structure.

Due to the success of the peptide coupling reactions, the next step in the reaction sequence involved hydrolysis of the methyl ester to give the free carboxylic acid which could potentially be incorporated into the construction of larger peptide Tröger's base derivatives.

The first attempt at cleaving the methyl esters involved refluxing **161** (1 eq.) in the presence of KOH (2.1 eq.) for 48 hours.[248] After washing the reaction mixture with di-ethyl ether, the pH of the solution was slowly adjusted to pH one and extracted with EtOAc. According to ^{1}H NMR analysis, the reaction was unsuccessful as a resonance representing the methoxy groups was present. Conversely, the mass spectroscopy data indicated formation of the desired product. This suggested that only a trace amount of the hydrolysis product formed, as there was no sign of mixtures present by ^{1}H NMR analysis.

The second approach carried out involved attempting to hydrolyse the methyl esters in non-aqueous conditions using CH_2Cl_2:CH_3OH (9:1) as the solvent system and a 2 M methanolic solution of NaOH as the base.[249] The work-up involved removal of the solvents under reduced pressure and re-dissolving the crude residue in H_2O followed by acidifying the solution to pH one and extracting with EtOAc. Disappointingly, both ^{1}H NMR and mass spectroscopy indicated that both starting material and product in a 70:30 ratio were present.

Traditional amino acid methyl ester deprotection using basic conditions has been proven to be difficult, an effect observed by both Phelan[114] and Veale.[191] Therefore, due to the difficulty ensued in attempting to generate the carboxylic acid derivative of **161** by ester hydrolysis, the *tert*-butyl derivative **163** was synthesised using the BOP coupling procedure.

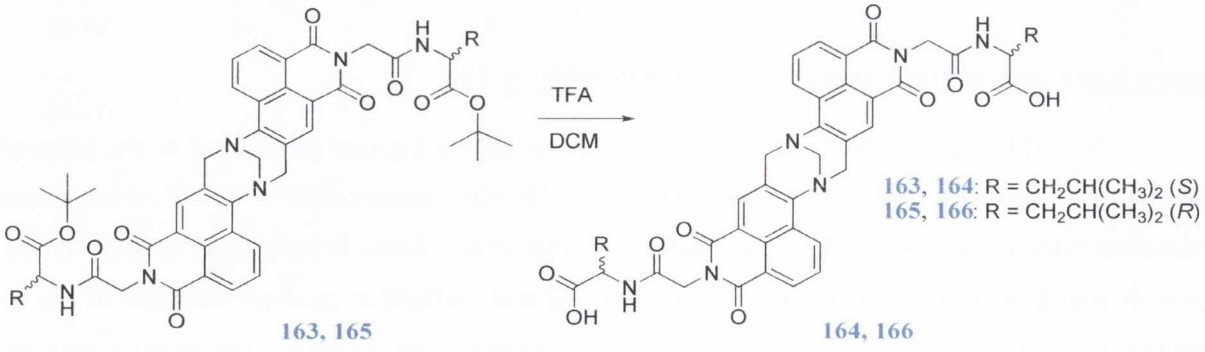

Scheme 3.6: *Synthesis of 163-166.*

Compound **163** was generated in 78% yield after triturating with CH_3OH and cleavage of the *tert*-butyl group was successfully achieved in quantitative yield to give **164** by stirring **163** in TFA:CH_2Cl_2 (1:2) for 3 hours as shown in Scheme 3.6.

For comparison purposes, the *R*-analogues **165** and **166** were also synthesised. Compounds **163-166** were analysed using conventional methods, whereby, ^{1}H NMR and ^{13}C NMR, HRMS and IR analysis confirmed their identity. The ^{1}H NMR spectra of both **163** and **165** were similar to that of **161**, except for the presence of a resonance pertaining to the *tert* butyl ester at 1.36 ppm. The formation of **163** and **165** was also verified in the ^{13}C NMR spectra which contained an additional aliphatic quaternary carbon signal at 27.8 ppm compared to **161**, pertaining to the *tert* butyl moiety. The IR spectra of **163** and **165** exhibited a band at 1595 cm^{-1} confirming that an amide bond had formed and the mass spectral analyses were consistent with the assigned structures.

The disappearance of the *tert* butyl group in the ^{1}H NMR spectra of **164** and **166** confirmed that the ester hydrolysis reactions were successful. In addition, the aliphatic regions of the ^{13}C NMR spectra did not show any signals correlating to the *tert* butyl group. According to the IR spectral data, the carbonyl stretch for the *tert* butyl ester appeared at 1732 cm^{-1}, whereas for the free carboxylic acid it was found at 1701 cm^{-1}. A strong broad band was also observed for the hydroxyl group at 2891 cm^{-1}. Mass spectral analyses also confirmed the identity of the assigned structures. Compounds **164** and **166** were analysed using CD spectroscopy, where a positive signal was observed for **164** and a negative signal for **166** in the 200-240 nm region of the spectrum, showing that racemisation did not occur upon coupling of the leucine amino acids to **144**, using the outlined BOP mediated coupling procedure.

In summary, it is evident from the synthetic methodology employed here that the synthesis of peptide Tröger's base derivatives can be achieved by derivatising the *N*-imide core post Tröger's base formation, without the occurrence of racemisation. In addition, the amino acid *C*-termini can be deprotected yielding the free carboxylic acid with the potential for further modification.

3.4 Summary

The synthesis of amino acid based Tröger's bases has proven to be a versatile one where additional amino acids can be incorporated onto the *N*-imide terminus before or after

the formation of the Tröger's base structural unit. This has resulted in the synthesis of twenty-two novel Tröger's bases derived from both the 3- and 4-amino-1,8-naphthalimide chromophores in moderate to high yields, with the potential for many more to be designed and synthesised. In addition, removal of the protecting groups at the *C*-termini generates the free carboxylic acids which can be further derivatised and modified in several ways leaving these molecules with ample synthetic possibilities.[250]

3.5 Spectroscopic Evaluation of Solvent Dependent Fluorophores

Fluorescence spectroscopy has become one of the most valuable tools for the development of new innovative probes for biochemical research, having found extensive use in the monitoring of ions, small molecules and biological processes.[251-254] Organic fluorophores such as naphthalimides belong to a class of chromophores for which the excited state properties can be drastically altered by the addition of a substituent present on the aromatic ring.[175,255] As already mentioned in Section 2.6, the introduction of electron withdrawing or donating substituents induces an internal charge transfer excited state, where substantial changes in the fluorescence spectrum, quantum yield and lifetime are observed as the solvent is varied.[175,255] Environment-sensitive fluorophores exhibit low quantum yields in aqueous solution and become highly fluorescent in non-polar solvents and based on these changes, they have been used for the selective sensing of nucleoside polyphosphates, studying membrane micro-environments and hydrophobic domains on proteins as well as the dynamics and conformational changes of macromolecules.[256-259] For instance, Hamilton *et al.*[260] synthesised and developed solvatochromic molecules **167** and **168** and studied the influence of solvent polarity on their photophysical behaviour using UV-visible and fluorescence spectroscopy. Both **167** and **168** exhibited solvent dependence where their absorbance and fluorescent spectra were shifted to shorter wavelengths upon decreasing the polarity of the medium. Equipped with these findings, the interaction between **167** and **168** with human serum albumin (HSA) was investigated and the fluorescence spectra of both **167** and **168** were blue shifted upon binding to HSA.

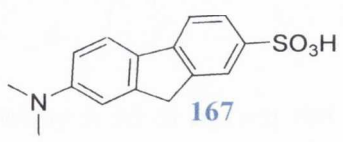

167

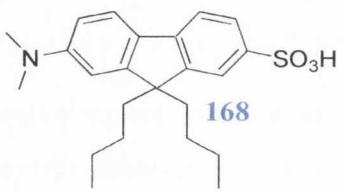

168

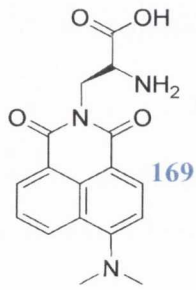

169

Amino acids that possess solvatochromic fluorophores as the side chain group have been developed and investigated for the study of protein interactions.[261] Imperiali *et al.*[221] have contributed greatly to this field with the development of several environment sensitive probes. A 4-*N*,*N*-dimethylamino-1,8-naphthalimide **169** incorporating an unnatural amino acid was developed bearing the same ''switch like'' fluorescent properties that are characteristic to the 4-amino-1,8 naphthalimide structure. Introduction of this molecule into a peptide such as M13 was achieved and binding to calcium-activated calmodulin resulted in a greater than 900 fold enhancement in the fluorescence emission, demonstrating the potential of this molecule as a probe for the study of dynamic protein interactions.[221e]

In a similar manner, 1,8-naphthalimide based Tröger's base derivatives **144-158** and **160-166** were designed, synthesised and analysed using absorption and fluorescence emission and excitation techniques in addition to determining the fluorescence quantum efficiencies and measuring the fluorescent lifetimes. It was anticipated that such compounds would exhibit solvent dependence in their fluorescence spectra indicating that these molecules may have the potential to be used as fluorescent probes. During the course of this work, Λ-shaped Tröger's base pyridinium salts **170-172** which exhibit aggregation induced emission behaviour, where they are non-emissive in solution but highly luminescent in the aggregate state were synthesised as fluorescent probes for the turn-on detection and quantification of proteins.[139] Large spectral shifts were observed when these compounds were found to bind to BSA. Moreover, the plots of luminescence intensity versus BSA concentration exhibited a linear relationship which indicated that quantitative fluorimetric protein detection could be achieved.[139]

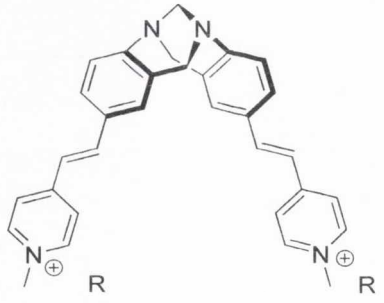

170: R = $NO_3^{\ominus}$

171: R = $I^{\ominus}$

172: R = 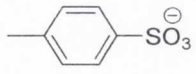

3.6 Photophysical Evaluation of Amino-Acid based Tröger's Base Derivatives in Solvents of Varying Polarity

To determine the excited state character of the naphthalimide based derivatives synthesised and discussed in this chapter, a detailed spectroscopic study was carried out which involved recording the absorption and fluorescence emission and excitation spectra of

Tröger's base derivatives **154**, **155** and **159** and their analogous 1,8-naphthalimide precursors **132**, **139** and **142** in a range of solvents which varied in terms of their polarity and hydrogen bond donor and acceptor capacity. All measurements were carried out using an optical density of 0.15 at the excitation wavelength, which was chosen as the λ_{maxUV} observed in the UV-visible absorption spectrum. The solvents used in this study were toluene, dichloromethane, tetrahydrofuran, chloroform, ethyl acetate, acetone, methanol, ethanol, acetonitrile, dimethylformamide, dimethyl sulphoxide and water and the results from these studies will be discussed in the following sections.

3.6.1 Spectroscopic Evaluation of Amino-Acid based Tröger's Base Derivatives in Solvents of Varying Polarity

As a means of investigating whether the amino acid based bis-1,8-naphthalimide containing Tröger's base derivatives exhibit an ICT excited state and to what extent, the absorption and fluorescence emission and excitation spectra of these derivatives were recorded in protic and aprotic solvents of varying polarity. Derivatives **144**-**152** which possess free carboxylic acid functional groups were omitted from this study due to their limited solubility. As can be seen in Figure 3.32, when recorded in $CHCl_3$, the absorption spectrum of Tröger's base derivative **156** derived from the 4-amino-1,8-naphthalimide precursor **140** was composed of a broad absorption band in the region between 280-450 nm with maxima at *ca.* 346 and 386 nm. Upon excitation of λ_{maxUV}, a broad emission band was exhibited centred at 479 nm for **156**. The fluorescence excitation spectra were also recorded and were identical to the corresponding absorption spectra.

In order to examine the effect of a polar protic solvent, the absorption and fluorescence emission and excitation spectra of **156** were recorded in CH_3OH. No significant changes were observed in the absorption spectra, however, a bathochromic shift of 41 nm was observed in the emission spectrum of **140**. Subsequently, the fluorescence excitation spectrum in CH_3OH was recorded and found not to be identical to the corresponding absorbance spectrum. Instead, the fluorescence excitation spectrum was characterised by two bands appearing at 354 and 420 nm and when compared to the absorbance spectral data they were shown to be shifted to longer wavelengths by 9 and 20 nm, respectively, as seen in Figure 3.33.

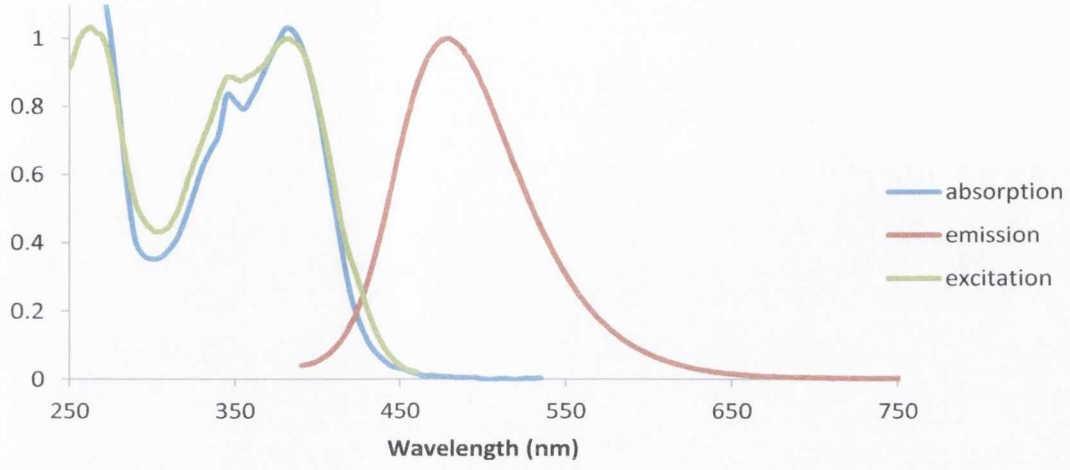

Figure 3.32: *Normalised absorption, fluorescence emission (ex. 385 nm) and excitation (exc. 48 nm) spectra of* **156** *recorded in* $CHCl_3$.

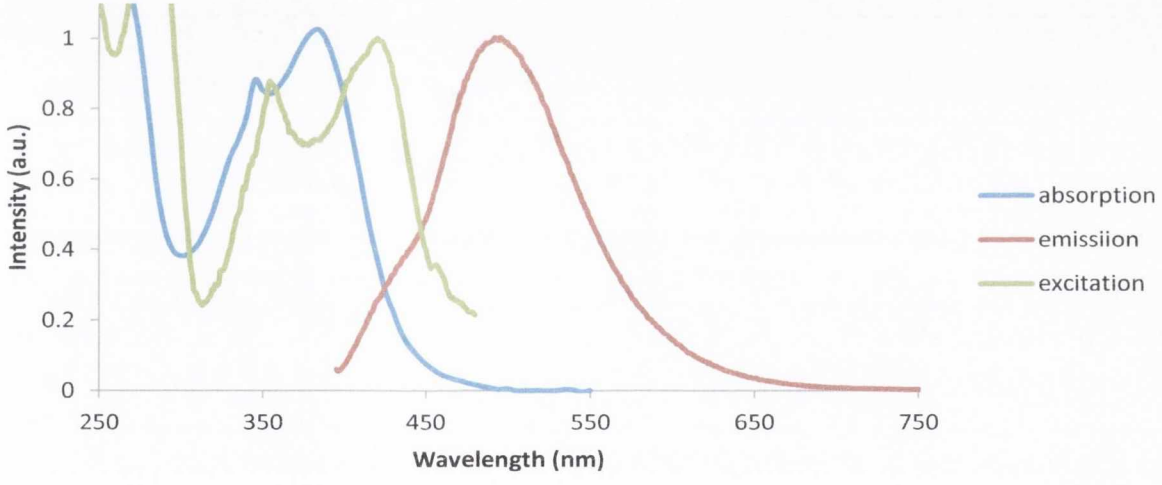

Figure 3.33: *Normalised absorption, fluorescence emission (ex. 385 nm) and excitation (exc. 493 nm) spectra of* **156** *recorded in* CH_3OH.

In an attempt to understand this behaviour exhibited in CH_3OH, the absorption and fluorescence emission and excitation spectra of **156** were recorded in solvents of varying polarity and hydrogen bonding ability. In Figure 3.34, it can be seen that the excitation spectra were not identical to the absorption spectra when recorded in highly polar solvents such as CH_3CN and DMF. However, in non-polar solvents such as toluene, this was not the case. This behaviour was seen for other Tröger's bases such as **153**, **158** and **160** and not for their corresponding counterparts, **131**, **141** and **143**, respectively.

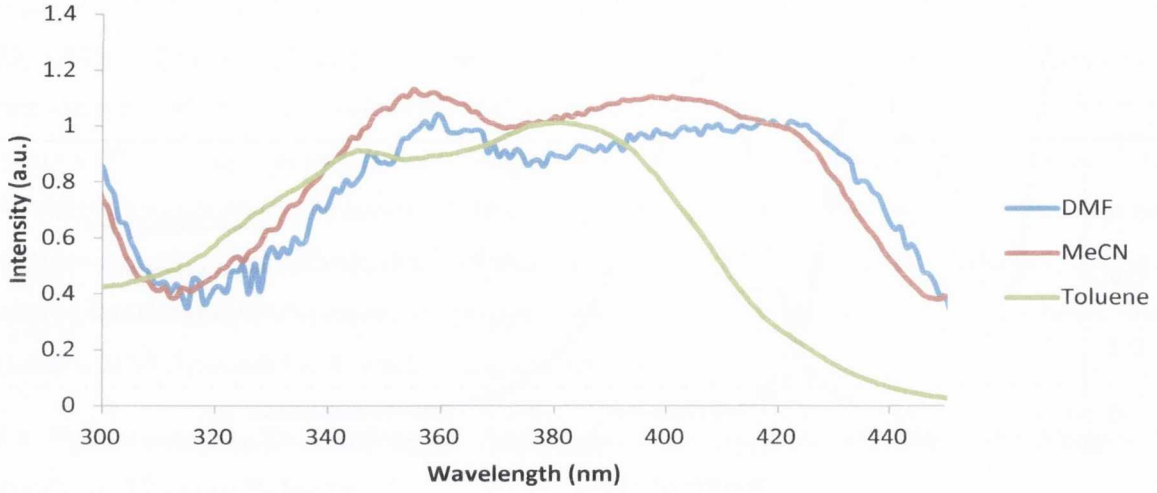

Figure 3.34: *Normalised fluorescence excitation spectra of* **156** *in DMF (exc. 488 nm), CH_3CN (exc. 485 nm) and toluene (exc. 473 nm).*

Upon further examination of these solvents it was found that the excitation spectra did not match the absorption spectral data in solvents where the fluorescence quantum efficiencies were at their lowest, which suggested that what was giving rise to these excitation spectra was more fluorescent than the Tröger's base compounds and present in very dilute and minute quantities. As a consequence of the dilute nature of the excited species present, removal and isolation of this fluorescent entity was unattainable in certain cases using chromatography, recrystallisation and precipitation techniques. However, successful removal without isolation of this fluorescent species was achieved for a number of compounds and the photophysical evaluation of these compounds in a range of solvents is discussed in the following sections.

3.6.2 Spectroscopic Evaluation of 154 in Solvents of Varying Polarity

The first comprehensive spectroscopic solvent study was carried out for Tröger's base derivative **154** which incorporates *S*-phenylalanine methyl ester residues at the *N*-imide termini. A typical UV-Vis absorption spectrum of **154** consists of two bands at *ca.* 230 nm and 265 nm, whilst the region between 280 and 450 nm is composed of a broad absorption band with maxima at *ca.* 346 and 386 nm. The high energy band at *ca.* 230 nm is characteristic of the π-π^* transition belonging to the naphthalimide chromophore whereas, the band at 265 nm represents the phenylalanine moiety, while the less intense region between 280 and 450 nm is attributed to the ICT transitions of the naphthalimide fluorophores. The latter regions of the absorption spectra were significantly affected upon changing the polarity

or the hydrogen-bonding ability of the medium. For instance, the absorption spectrum of **154** when recorded in CH_2Cl_2, exhibited an intense broad band between 280 and 450 nm centred at *ca.* 387 nm, as shown in Figure 3.35. A change of the solvent from CH_2Cl_2 to DMSO resulted in a 9 nm bathochromic shift of the absorption maximum and this is unlike that seen for the 4-amino-1,8-naphthalimides, which, in general, show a much greater bathochromic shift when the polarity or the hydrogen bonding ability of the medium is increased which is indicative of a positive solvatochromic effect. Nevertheless, the magnitude of the shift in the absorbance spectrum to longer wavelengths observed for **154** indicates that the polar solvents are strongly hydrogen-bonded causing a decrease in the energy gap between the ground state and the excited state. Therefore, the bathochromic shift observed for **154** with increasing solvent polarity is characteristic of an ICT band. An exception in this trend was observed when the λ_{maxUV} in DMF and DMSO was compared to the hydrogen-bonding solvent water, where the absorption maximum is located at 389 nm, displaying hypsochromic shifts of 4 nm and 7 nm compared to DMF and DMSO, respectively. Water is a strong hydrogen bonding solvent and may form hydrogen-bonded solvated clusters which may absorb at ~389 nm.[179,185] Similar observations have been reported in the literature for several donor-acceptor systems.[186]

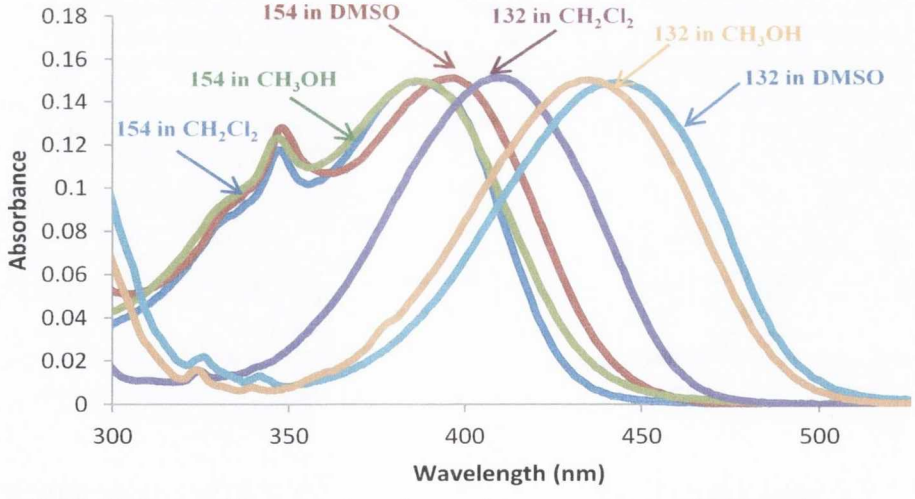

Figure 3.35: *Solvent effects on the absorption properties of **154** and **132**.*

The absorption spectra of the 4-amino-1,8-naphthalimide precursor **132** was recorded in several solvents for comparison purposes, where the longest wavelength absorption of this system is depicted by an intense broad band with the maximum appearing between 325 and 525 nm and can be well characterised as being due to the ICT excited state of the fluorophore. As an example, in CH_3OH, the absorption spectrum of **132** featured a broad band centred at

435 nm and upon a decrease in the polarity and the hydrogen bond donor ability of the medium, the ICT absorption band exhibited a hypsochromic shift of 28 nm when the solvent was changed to toluene. By comparing the changes observed in the absorption spectra of **132** and **154**, it was evident that smaller shifts in λ_{maxUV} were recorded for **154** and it is postulated that this may be due to the inherent geometry of the Tröger's base derived from the V-shaped structure of the methano-1,5-diazocine ring which may have the potential to effect the ability of the amine to donate electrons into the naphthalimide chromophore and thus, participates in ICT to a lesser extent, compared to its 4-amino-1,8-naphthalimide precursor.

The influence of solvent polarity on the photophysical behaviour of **132** and **154** was also examined using fluorescence emission and excitation spectroscopy, as shown in Figure 3.36.

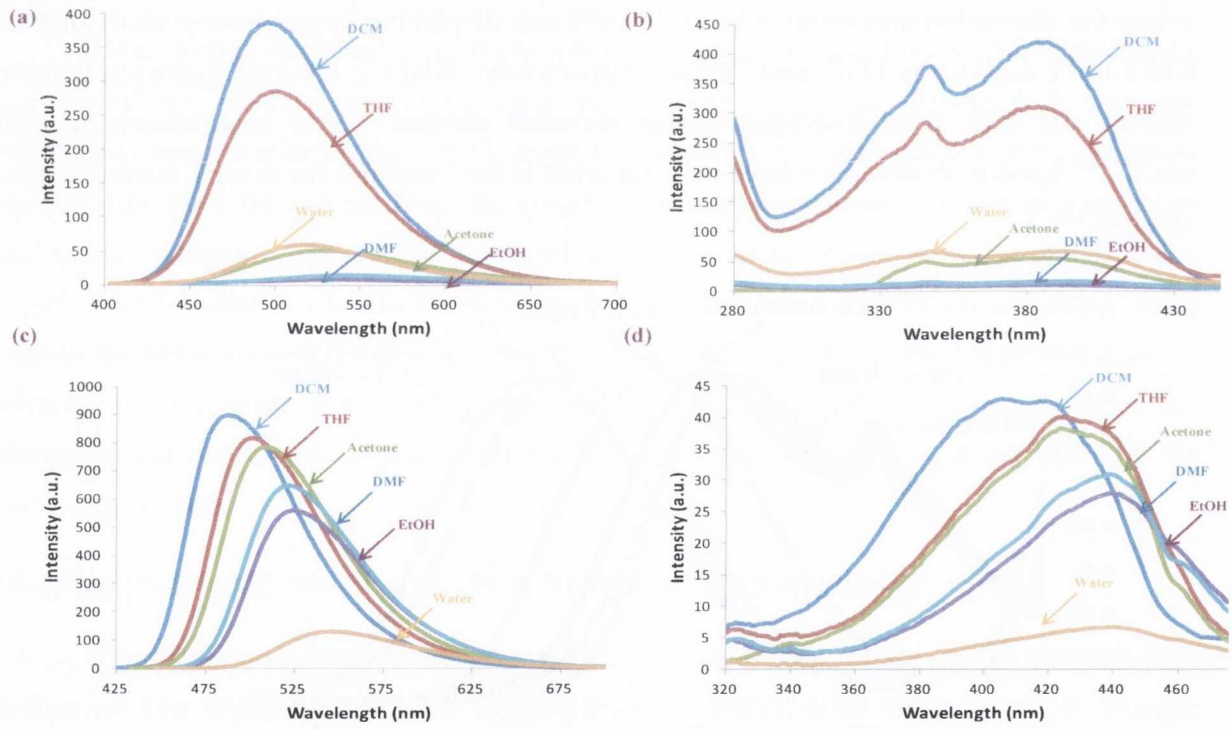

Figure 3.36: *The fluorescence emission spectra of* ***154*** ***(a)*** *and* ***132*** ***(c)*** *and the excitation spectra of* ***154*** ***(b)*** *and* ***132*** ***(d)*** *in solvents of varying polarity. The excitation and emission wavelengths are summarised in Table 3.3.*

When recorded in EtOH, **154** and **132** were excited at λ_{maxUV} 387 and 437 nm, respectively, where they both exhibited maximums at 534 and 524 nm, respectively. Each band was not particularly symmetrical and tailed off to longer wavelengths, which supports

the characterisation of the excitation bands of **154** and **132** as having contributions from ICT transitions. As can be seen in Figure 3.36, upon increasing the solvent polarity, from CH_2Cl_2 to DMF, the fluorescence maximum of **154** exhibited a decrease in the emission intensity and a bathochromic shift of 46 nm. The magnitude of this spectral shift was over seven times greater in the fluorescence spectrum compared to the absorption spectrum which indicates that the excited state is more polar than the ground state. Similarly, the emission spectrum of **132** also displayed a decrease in the emission intensity and a clear bathochromic shift upon an increase in the hydrogen bond donor ability and polarity of the medium highlighting that the excited state of **132** is significantly polar and supporting the characterisation of the emission as ICT. Similar behaviour has previously been reported for related 4-amino-1,8-naphthalimides which suggest that the excited states possess significant ICT character.[148,149,181] In addition, the sensitivity of λ_{maxFLU} to the polarity of the medium was also investigated by fluorescence excitation spectroscopy. As can be seen in Figure 3.36, the intensity of the ICT band increased and hypsochromic shifts were observed when the polarity of the medium decreased providing further evidence that **154** possesses an ICT excited state character. Furthermore, the excitation spectra highlight that **154** is spectroscopically pure in a vast range of solvents. All of the relevant spectral parameters recorded are summarised in Table 3.3.

The fluorescence quantum efficiencies (ϕ_F) were calculated to provide further evidence for the presence of an ICT excited state in **154** using optically dilute solutions and quinine sulphate (ϕ_F = 0.542 in 0.1M H_2SO_4) as the primary reference standard as described in section 2.6.[187,188] As can be seen in Table 3.4, the ϕ_F are low and were found to decrease upon increasing the polarity of the medium. This trend has previously been reported and is in agreement with the low ϕ_F of the alkyl based Tröger's base naphthalimide derivatives reported by Deprez *et al.*,[181] as well as the low ϕ_F depicted for the *N*-substituted 1,8-naphthalimide series synthesised by Veale.[148-149] In addition, the ϕ_F of **132** were determined using fluorescein (ϕ_F = 0.9 in 0.1M NaOH) as the reference standard and although the ϕ_F were larger for **132** in comparison to **154**, an overall trend was observed similar to that seen for **154**.[262]

Table 3.3: *Absorption and emission spectral data for 154 and 132 recorded in a range of* solvents.

Solvent	154:λ_{maxUV} (nm)	154:λ_{maxFLU} (nm)	132:λ_{maxUV} (nm)	132:λ_{maxFLU} (nm)
Toluene	385	470	407	479
DCM	387	496	410	487
THF	385	499	423	502
Chloroform	385	481	409	479
Ethyl Acetate	384	504	419	498
Acetone	387	528	423	510
MeOH	386	530	435	530
EtOH	387	534	437	524
MeCN	388	542	421	513
DMF	393	542	437	522
DMSO	396	543	443	528
Water	389	516	437	546

Table 3.4: *The fluorescence quantum efficiencies and lifetimes measured for 154 and 132.*

Solvent	154: Φ_F (±10%)	154: τ (χ^2)	132: Φ_F (±10%)	132: τ (χ^2)
Toluene	0.374	6.43 ns (1.2)	0.744	9.5 ns (1.2)
DCM	0.170	5.78 ns (1.1)	0.854	11.1 ns (1.2)
THF	0.126	4.72 ns (1.3)	0.684	10.5 ns (1.2)
Chloroform	0.292	6.41 ns (1.2)	0.896	10.2 ns (1.2)
Ethyl Acetate	0.066	4.12 ns (1.5)	0.665	10.6 ns (1.2)
Acetone	0.025	n/a*	0.598	10.2 ns (1.2)
MeOH	0.003	n/a*	0.330	7.5 ns (1.0)
EtOH	0.007	n/a*	0.452	8.9 ns (1.2)
MeCN	0.011	n/a*	0.643	11.2 ns (1.1)
DMF	0.011	n/a*	0.580	10.17 ns (1.2)
DMSO	0.008	n/a*	0.519	10.1 ns (1.2)
Water	0.022	n/a*	0.115	3.3 ns (1.2)

n/a*-τ was too short and could not be measured accurately.

In order to study the photophysical properties of **154** in more detail, singlet excited state lifetime (τ) measurements were carried out in several solvents using the time correlated single photon counting (TCSPC) technique and the decays were fitted to a single exponential decay model. The luminescence lifetime is defined as the time required by a population of excited fluorophores for their intensity to decrease exponentially *via* the loss of energy through fluorescence and other non-radiative processes.[263] The lifetime of photophysical processes vary significantly from tens of femtoseconds for internal conversion, to nanoseconds for fluorescence and microseconds or seconds for phosphorescence. The effect of polarity on the fluorescence lifetime is very similar to what is observed for the fluorescence quantum yields, where an increase in the polarity of the medium resulted in a shortening of the lifetime as shown in Table 3.4.[177-179] As can be seen, the longest lifetime calculated for **154** was in toluene, the least polar solvent examined as part of this study and was shorter in comparison to the 4-amino-1,8-naphthalimide precursor. Upon increasing the polarity of the medium the lifetime was found to decrease. However, in polar solvents the fluorescence decay could not be fitted to a single exponential function very accurately and precise determination of the fluorescence lifetimes could not be achieved, which is presumably due to poor quantum yields of emission in these solvents and the lifetimes were below the limit of detection of the excitation source (~1.2 ns). This was highlighted when the lifetimes were measured in THF and ethyl acetate, where the chi squared values (χ^2) were found to lie outside the accepted range of 0.8 and 1.2.[177-179] Furthermore, due to the fact that the fluorescence quantum yields recorded in more polar solvents such as DMSO and water were extremely low and following this trend, fluorescence lifetimes for **154** could not be determined in such media. The same decreasing pattern was observed for the naphthalimide precursor **132** however, **132** had longer lifetimes and could be measured in all the solvents used as part of this study. From the results shown in Table 3.4, it is evident that the fluorescent lifetimes decrease upon increasing the polarity and hydrogen bond donor ability of the medium, a trend well characterised as being due to the ICT excited state of the fluorophore.[177-179]

In summary, this study has shown that changing the polarity of various solvents has a significant effect on the photophysical characteristics of the 4-amino-1,8-naphthalimide derived Tröger's base **154** and its analogous precursor **132**, where both the absorption and fluorescence emission spectra of each compound exhibited positive solvatochromic effects as observed with the considerable bathochromic shifts recorded when increasing the polarity and

hydrogen bond donor ability of the medium. In addition, the fluorescence quantum yields followed the trends reported in the literature for molecules that possess ICT excited state character.[66,148-149] Owing to the fact that the lifetime values that could be measured for **154** were very short in the solvents examined and were accompanied by high χ^2 values, no luminescent lifetimes were measured for the other molecules which make up part of this study. Furthermore, it has been highlighted that the luminescent lifetimes for Tröger's base **154** are very short in polar solvents and may lie in the picosecond range. Unfortunately, the available apparatus was not suitable to measure such luminescent lifetimes.

3.6.3. Spectroscopic Evaluation of 159 in Solvents of Varying Polarity

The second molecule to be spectroscopically analysed in several solvents was **159**, which is derived from the 3-amino-1,8-naphthalimide precursor **142** incorporating an *S*-alanine methyl ester residue at the *N*-imide terminus. A typical UV-Vis absorption spectrum of **159** is defined by a high energy band centred at *ca.* 235 nm pertaining to the naphthalimide chromophore. The region between 300 and 500 nm is composed of a band centred at *ca.* 340 nm with an adjoining shoulder that absorbs at *ca.* 390 nm and is assigned to the ICT transitions of the naphthalimide chromophores as can be seen for **159** in CH_3CN as shown in Figure 3.37.

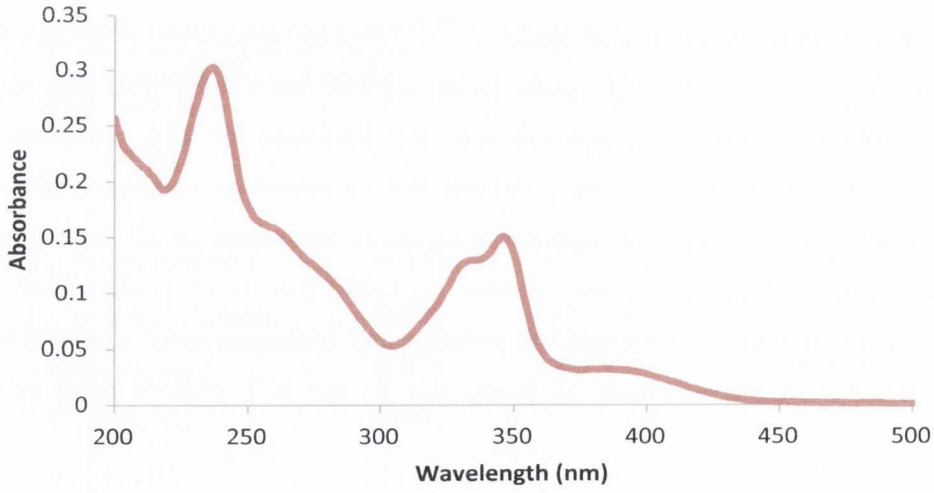

Figure 3.37: *Absorption spectrum of 159 in CH_3CN.*

The absorption spectrum of **159** in CH_2Cl_2 exhibited maxima at *ca.* 347 nm and 385 nm. Upon changing the solvent to DMF and therefore increasing the polarity of the medium, the maxima appeared at *ca.* 348 nm and 389 nm. In general, the absorption spectrum was not

significantly altered by the polarity and or the hydrogen bond donor ability of the medium and these results are summarised in Table 3.5. However, the ICT nature of **159** is evident due to the peak position being slightly affected by the polarity of the medium. Conversely, large changes were observed in the absorption spectra of **142** indicating that polarity and or the hydrogen bond donor ability of the solvent significantly affects peak position. For instance, the longer wavelength region of the absorption spectrum of **142** in toluene is composed of a broad band centred at 411 nm. Upon increasing the polarity of the medium by changing the solvent to DMF, a bathochromic shift of 33 nm is observed. The magnitude of this shift is much greater than any shift recorded for the Tröger's base derivative **159** further highlighting the effect the rigid V-shaped structure imposes on the ability of the amine to donate electrons into the naphthalimide ring and its capacity to participate in the ICT process. In addition, the spectral changes recorded for **142** are smaller than those observed for a 4-amino-1,8-naphthalimide derivative such as **132**, highlighting the difference in the electronic donor ability of the 3- versus 4-amino moiety in such structures.[183] Subsequent incorporation of the Tröger's base structural motif is expected to further affect such electronic donor abilities.

Table 3.5: *The photophysical characteristics of **159** and **142**.*

Solvent	159:λ_{maxUV} (nm)	159:λ_{maxFLU} (nm)	159:Φ_F (±10%)	142:λ_{maxUV} (nm)	142:λ_{maxFLU} (nm)	142:Φ_F (±10%).
Toluene	348/388	481	0.061	411	470	0.617
DCM	347/387	517	0.031	412	475	0.642
THF	346/386	499	0.025	427	503	0.609
Chloroform	347/387	498	0.043	410	468	0.603
Ethyl Acetate	345/385	508	0.015	422	497	0.543
Acetone	345/385	448	0.013	426	512	0.520
MeOH	346/386	455	0.007	429	544	0.175
EtOH	346/386	448	0.010	432	550	0.283
MeCN	346/386	450	0.011	421	513	0.486
DMF	348/386	452	0.010	438	534	0.434
DMSO	349/386	484	0.005	444	546	0.392
Water	348/386	511	0.011	409	584	0.025

Additional evidence for the presence of an ICT excited state in **159** was obtained by studying the influence of solvent polarity using fluorescence emission and excitation spectroscopy studies. As an example, the fluorescence emission spectrum of **159** was recorded in CH_2Cl_2 and consisted of a broad unsymmetrical band that tailed off to longer wavelengths and had a λ_{maxFLU} at 517 nm, as shown in Figure 3.38. The emission intensity decreased and a hypsochromic shift of 69 nm was measured when the solvent was changed to CH_3OH, whereas, a smaller hypsochromic shift of 8 nm was observed when recorded in water. The emission spectra were recorded by exciting at various wavelengths and they each yielded identical results which indicated that the molecule was spectroscopically pure. Furthermore, the fluorescence excitation spectra were identical to the absorption spectra in each of the solvents studied showing that the molecule alone is responsible for the negative fluorosolvatochromism observed.

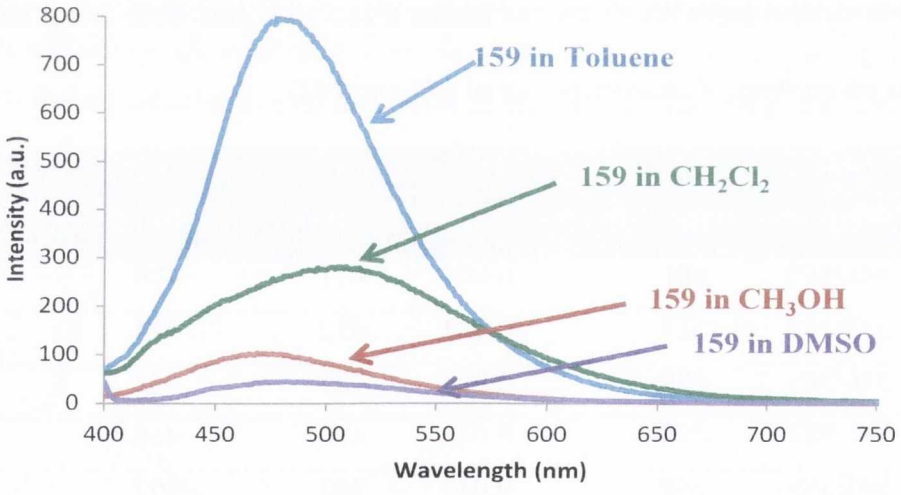

Figure 3.38: *Fluorescence emission spectrum of **159** in solvents of varying polarity. Excitation wavelengths are summarised in **Table 3.5.***

Negative solvatochromism and fluorosolvatochromism have been reported for many systems where the sign of the solvatochromism depends on the difference in the dipole moment between the ground and excited states of the fluorophore.[264-266] Bathochromic shifts have been reported in non-polar solvents for cationic dyes which exhibit instant stabilisation attributed to the fast rearrangement of polarisable electrons during excitation or emission.[264-266] Conversely, the corresponding precursor **142** exhibited bathochromic shifts upon

increasing the polarity of the medium which are well characterised as being due to the ICT excited state.

In order to study the spectral properties of **159** in more detail, ϕ_F were calculated to provide further evidence for the presence of an ICT excited state in **159**. For comparison purposes the ϕ_F were also measured for the precursor **142** and are summarised in Table 3.5. The ϕ_F determined were low and followed a trend similar to that seen for **154** and for similar systems previously reported.[148,149,181]

3.6.4. Spectroscopic Evaluation of 155 in Solvents of Varying Polarity

The influence of solvent polarity and hydrogen bond donor ability on the photophysical behaviour of the peptide Tröger's base **155** was evaluated using absorption and fluorescence emission and excitation spectroscopy. The peptide moiety consists of *S*-alanine and *S*-leucine residues with the *S*-alanine residue being directly attached to the *N*-imide termini. The absorption spectrum of **155** was similar to that described for **154**, consisting of a high energy band centred at *ca.* 230 nm pertaining to the naphthalimide chromophores while the longer wavelength region between 280 and 450 nm can be defined by a broad absorption band with maxima at *ca.* 346 and 386 nm. A look to the data in Table 3.6 shows that in the case of **155** positive solvatochromism was observed when the polarity of the medium was increased. For instance, a bathochromic shift of 9 nm was recorded when changing the solvent from ethyl acetate to DMSO and this is well characterised as being due to an ICT excited state of the fluorophore. Comparing the spectral data collected for **155** with that of its precursor **139**, shows that larger shifts in peak positions were observed for **139** when parameters such as the polarity and hydrogen bond donor ability of the medium was altered. This behaviour is similar to that described for **154** and its corresponding precursor **132** and may be due to the presence of the Tröger's base structural unit which affects the ability of the nitrogen atom to donate electrons into the naphthalimide ring and thus, its contribution in the ICT process. The ϕ_F were calculated for **155** and provide further evidence for the presence of an ICT excited state in **155**, as they were found to be low and to decrease upon increasing the polarity of the solvent. These results are in accordance with the low fluorescent quantum yields previously reported for *N*-substituted 1,8-naphthalimide derivatives. All the relevant spectral data collected is summarised in Table 3.6.

Table 3.6: *The photophysical characteristics measured for 155 and 139.*

Solvent	155:λ_{maxUV} (nm)	155:λ_{maxFLU} (nm)	155:Φ_F (±10%)	139:λ_{maxUV}) (nm)	139:λ_{maxFLU} (nm)	139:Φ_F (±10%).
Toluene	384	476	0.373	404	483	0.621
DCM	386	497	0.182	403	488	0.810
THF	384	499	0.133	418	502	0.560
Chloroform	384	482	0.259	402	481	0.725
Ethyl Acetate	381	502	0.085	412	501	0.586
Acetone	384	530	0.023	415	510	0.478
MeOH	384	520	0.003	429	531	0.252
EtOH	385	530	0.007	436	526	0.319
MeCN	385	535	0.012	414	514	0.655
DMF	387	535	0.013	430	520	0.466
DMSO	390	543	0.009	435	526	0.389
Water	389	520	0.035	427	545	0.091

3.7 Summary

As already mentioned, many examples have been reported whereby systems incorporating naphthalimides because of their solvatochromic response have been designed to study protein interactions.[221] The amino acid Tröger's bases **154**, **155** and **159** synthesised as part of this project have been shown to exhibit positive and negative solvatochromism providing a basis for their use as potential peptidomimetics. In addition, this response may have the potential to be fine tuned as the quantum efficiencies of these compounds vary depending on the solvent parameters but also on the type of naphthalimide present. For instance, Tröger's bases derived from 4-amino-1,8-naphthalimides have been shown above to have higher quantum efficiencies compared to their 3-amino-1,8-naphthalimide derivatives.

3.8 Conclusion

The first section of this chapter dealt with the synthesis of twenty-two novel bis-1,8-naphthalimide based Tröger's bases incorporating amino acids at the *N*-imide termini in moderate to high yields. This involved investigating two main synthetic strategies. The first

approach dealt with the synthesis of 3- or 4-amino-1,8-naphthalimides incorporating either one or two amino acids at the *N*-imide terminus. This was achieved by carrying out condensation reactions between the 3- or 4-nitro-1,8-naphthalic anhydride and the relevant amino acid. The synthesis of 4-nitro-1,8-naphthalimides incorporating two amino acids was carried out using the anchored approach using carbodiimide coupling reagents EDCI.HCl and HOBt. These coupling and condensation reactions were achieved using enatiomerically pure amino acids which retained their chirality during synthesis. Subsequently, the nitro groups were reduced to their amino counter-parts and the Tröger's base reaction followed.

The second strategy involved the initial formation of Tröger's bases incorporating one amino acid at each *N*-imide terminus, followed by peptide bond formation generating derivatives incorporating two amino acids at the *N*-termini post Tröger's base formation. This reaction was investigated using several coupling reagents such as TBTU, ethyl chloroformate, EDCI.HCl and BOP with the latter yielding the desired product in the highest yield. All twenty two molecules were fully characterised using conventional techniques. From analysing the ^{1}H and ^{13}C NMR spectra, it was evident that two species existed in solution. As a consequence of the achiral 1,8-naphthalimide chromophore incorporating both enantiomerically pure amino acids at one end and a chiral racemic centre at the other, diastereoisomers were formed. The ^{1}H and ^{13}C NMR spectra can be described as having overlapping signals or multiple signals due to the presence of the diastereoisomers. Unfortunately, the diastereoisomers could not be separated by column chromatography or recrystallisation techniques. The Tröger's bases and their corresponding amino precursors were analysed using CD spectroscopy in CH_3OH. In the case of the Tröger's bases derived from their 4-amino-1.8-naphthalimide precursors as seen above, induced CD signals were observed in the long wavelength range of the spectra in certain cases highlighting that chirality can be induced into the achiral naphthalimide core. This effect was not observed for the 3-amino-1,8-naphthalimide derivatives investigated as part of this study.

The second section of this chapter dealt with the photophysical evaluation of these novel Tröger's bases which was determined in a range of solvents of varying polarity and hydrogen-bonding ability and compared to their corresponding precursors, using both ground state and excited state spectroscopy. This photophysical evaluation started with an initial screening of the molecules by recording their absorption and fluorescence emission and excitation spectra in CH_3OH and $CHCl_3$ where soluble. No significant changes were observed in the absorption spectra when changing the solvent form $CHCl_3$ to CH_3OH. However larger

changes were measured in the emission spectra when increasing the solvent polarity of the medium. Subsequently, the excitation spectra were measured and found to be identical to the absorption spectrum when measured in $CHCl_3$. However, in the case of CH_3OH the absorption and excitation spectra did not match. By carrying out these studies in more solvents, it was observed that the excitation spectra deviated from that of the absorption spectra when measured in polar solvents such as CH_3OH and DMF, in the solvents where the fluorescence quantum efficiencies are at their lowest. It was predicted that what would give rise to the excitation spectrum in these polar solvents was present in a very minute amount, as it was only observed for solvents at the higher end of the polarity table. Unfortunately, removal and isolation of this fluorescence impurity in each case was not accomplished due to the dilute nature of this unknown entity. Therefore, the identity of this species was not elucidated, however, according to mass spectral analysis and the ^{1}H and ^{13}C NMR experiments conducted, this fluorescence species was not the 3- or 4-amino-1,8-naphthalimide precursor.

Compounds that were optically pure in polar solvents were synthesised and evaluated using a range of twelve solvents of varying polarity and hydrogen bond donor and acceptor ability. It was found that incorporation of the Tröger's base moiety into the skeleton of the 3- and 4-amino-1,8-naphthalimide skeleton altered the ICT excited state of the naphthalimide fluorophore. Compared to their naphthalimide precursors the Tröger's bases analysed did not exhibit large changes when the polarity of the medium was altered. Nevertheless, the magnitude of the bathochromic shifts observed when increasing the polarity of the solvent are indicative and characteristic of an ICT excited state. However, from these studies it is evident that the ICT excited state character is weaker for the Tröger's bases compared to their precursors and this is attributed to the rigid V-shaped geometry imposed on the naphthalimide upon incorporation of the Tröger's base structural unit which affects the ability of the amine to donate electrons into the naphthalimide core and thus, participates in the ICT process to a lesser extent. Furthermore, this effect was found to be more pronounced for the Tröger's bases derived from the 3-amino-1,8-naphthalimide chromphore.

The influence of solvent polarity on the fluorescence emission behaviour was investigated using the same solvents. In the case of the 4-amino-1,8-naphthalimide derived Tröger's bases, increasing the solvent polarity resulted in large red shifts, the magnitude of which were not observed in their absorption spectra. This is typical of solvent stabilisation of more polar excited states and the greater comparable shifts supports the characterisation of the emission as being due to the ICT process. Conversely, in the case of **159**, a Tröger's base

derived from the 3-amino-1-8-naphthalimide **142**, a large blue shift with a decrease in the emission intensity was recorded when changing the solvent from CH_2Cl_2 to CH_3OH. These results clearly show that the naphthalimide based Tröger's bases incorporating amino acids possess ICT character and are capable of generating either positive or negative solvatochromic effects in response to changes in polarity and or the hydrogen bonding capabilities of the medium, which provides a basis for their use as potential peptidomimetics.

Overall, the functionalisation of the Tröger's base skeleton which was the purpose of this work was achieved using facile and versatile synthetic approaches and generated twenty-two new Tröger's base derivatives. Deprotection at the *C*-termini can be achieved yielding the free carboxylic acids which have the potential to be further derivatised and modified in a number of ways. Furthermore, exploitation of their photophysical properties may lend these molecules to the fields of fluorescent bio-sensing and protein detection.

Chapter 4:
Design, Synthesis and Photophysical Evaluation of Tetra-1,8-Naphthalimide Tröger's Base Derivatives as Potential Receptors for Fullerene C_{60}

4.1 Introduction

The fullerenes are a family of molecules that are completely composed of carbon and are in the forms of spheres, ellipsoids or tubes.[267] As fullerenes lack any functionality other than carbon, this in combination with their geometry makes them hard neutral polarised species.[268] The parent of the fullerenes is the buckminster fullerene C_{60}, also known as the ''bucky ball'' and represents a third form of crystalline carbon, the other two being graphite and diamond. C_{60} is in the form of a truncated icosahedron, a molecular ''soccer ball'' with sixty vertices and thirty-two faces consisting of twelve pentagons and twenty hexagons.[267] A diagrammatic representation of C_{60} is shown in Figure 4.1.

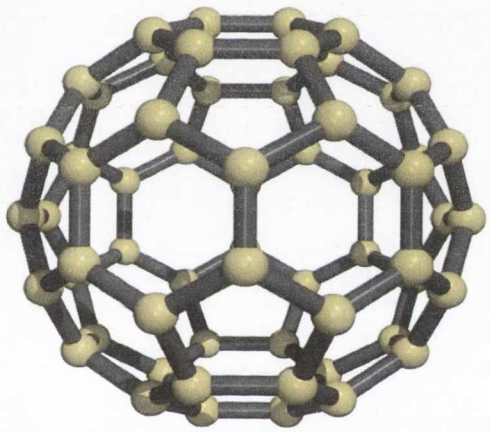

Figure 4.1: *Diagrammatic representation of C_{60}.*[269]

Since the discovery of fullerenes, a new field of synthesis has emerged where fullerenes have been applied extensively in many areas of research as superconducting devices,[270] non-linear optical materials[271] and pharmaceutical agents.[236(a),272] For instance, a fullerene C_{60} based fluorescent probe was developed by Tang *et al.*[273] as a probe for trypsin. The probe consisted of two moieties, one moiety being fluorescein which performed as the fluorophore and electron donor with the other being C_{60} which acted as the electron acceptor. In the presence of trypsin, a fluorescence enhancement was induced as the photoinduced electron transfer process from fluorescein to fullerene was blocked. This probe was highly selective for trypsin over other enzymes and proteins including lipase and bovine serum albumin.

Fullerenes have also played a role in the field of supramolecular chemistry as many host molecules for the inclusion of fullerenes have been developed.[274,275] Research into the non-covalent binding of fullerenes is driven by the interest in finding and developing new and

simpler methods for the purification of a specific fullerene from fullerene soot or a mixture of fullerenes. In addition, research into fullerenes is topical due to the growing interest in the control of the nanometric organisation of electroactive materials for organic solar cells.[268]

A class of efficient receptors for spherical guests are rigid molecular tweezers which are able to employ their two jaws to bind to the desired target.[276] For example Li *et al.*[277] designed and synthesised zinc porphyrin based tweezers such as **173** for the complexation of fullerene C_{60}, as shown in Figure 4.2.

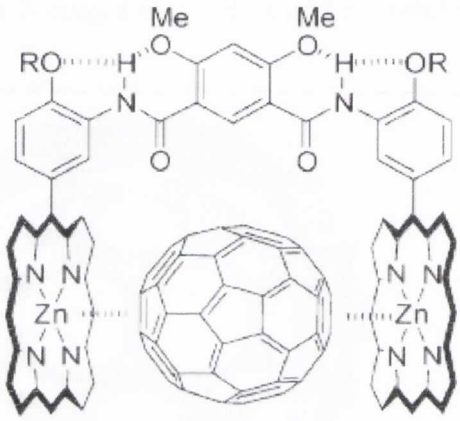

173: R = CH_3

Figure 4.2: *The binding mode for* ***173***.C_{60}.[277]

Wärnmark *et al.*[278] have incorporated the Tröger's base unit to construct the metallo-macrocycle **174** as a potential fluorescent sensor for the detection of C_{60}. Techniques such as NMR, absorption and fluorescence spectroscopy were utilised to study the interaction between the host and guest molecules. The NMR data obtained suggested that the C_{60} was bound weakly to **174** as no changes in the proton or phosphorus resonances were observed relative to **174** alone, although a slight shift in the ^{13}C carbon spectrum of C_{60} was observed compared to C_{60} alone. The spectra were dominated by C_{60} and uncomplexed **174** indicating that either the cavity was too small to host C_{60} or the methyl arms at the rim impeded the binding process. In addition, no changes were observed in the absorption spectrum however, the fluorescence intensity of **174** was quenched in the presence of C_{60}, although no shifts to shorter or longer wavelengths were observed. When the luminescence data was further analysed, a static component in the dynamic quenching of the fluorescence was observed and this supported the picture with the main interaction being with the outside of the cavity.

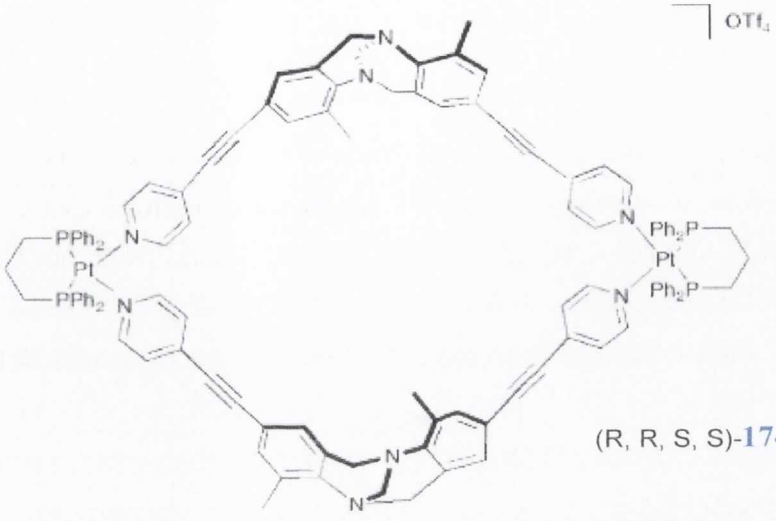

(R, R, S, S)-**174**

In order to build upon this work, 1,8-naphthalimide based Tröger's base derivatives **175** and **176** were developed as potential molecular tweezers for binding to C_{60}. As discussed in Chapter 1, the presence of the Tröger's base moiety results in a cleft like structure, which has been widely explored in the field of supramolecular chemistry.[126] Moreover, as discussed in Chapters 2 and 3, the photophysical properties of the bis-1,8-naphthalimide derivatives incorporating the Tröger's base moiety are largely dependent on the polarity and H-bonding ability of the medium. Therefore, these derivatives can have potential application in the field of sensor development, where the binding of the "guest" molecules can be conveniently monitored by the changes in the photophysical properties of these "hosts". The design, synthesis and interaction of these molecules with C_{60} are discussed in the following sections.

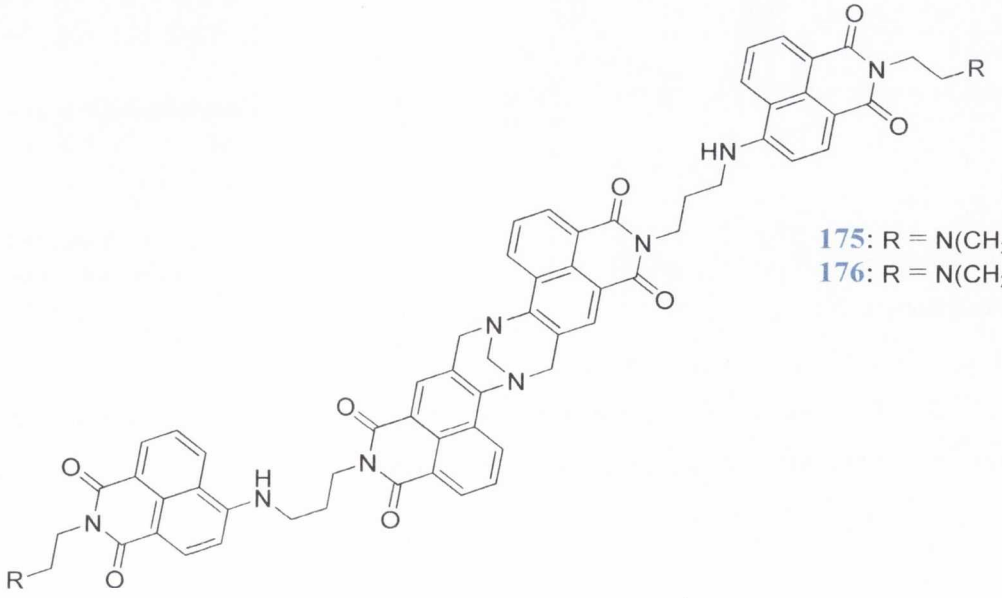

175: R = $N(CH_2)_4$
176: R = $N(CH_2)_5$

4.2 Design and Synthesis of Tetra-1,8-Naphthalimide Tröger's Bases 175 and 176

Before the design strategy for **175** and **176** was developed the potential of a bis-1,8-naphthalimide Tröger's base as a C_{60} receptor was evaluated. For this preliminary study, **153** was chosen as a representative of the bis-1,8-naphthalimide family containing the Troger's base unit. The effect of successive additions of C_{60} in chlorobenzene (0-473 μM) on **153** in DMF (8.7 μM) was monitored using absorption and fluorescence techniques. The absorption spectrum of C_{60} in chlorobenzene is shown in Figure 4.3 and as can be seen, it encompasses a large range of the electromagnetic spectrum, whereas, in the case of **153** the band to be monitored can be found in the 300 to 450 nm region of the spectrum. In Figure 4.3, there is an overlap in the absorbance between **153** and C_{60} and upon increasing the concentration of C_{60}, the ICT band of **153** at 381 nm cannot be monitored. It has been reported that when C_{60} is detected significant changes are observed in the absorbance spectrum such as a decrease in the absorbance of the ligand coupled to the formation of a new band.[279-281] If such changes were to occur for **153** they would not be detectable due to the strong absorbance of C_{60} in the bis-1,8-naphthalimide spectral range.

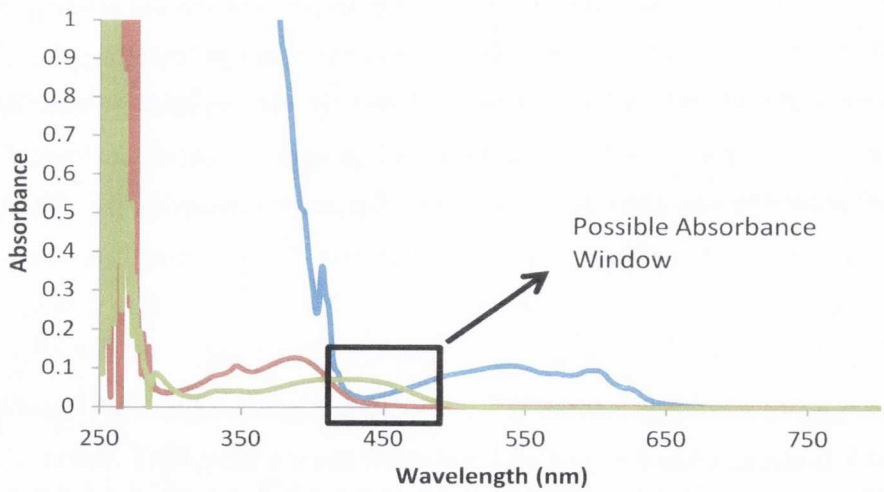

Figure 4.3: *Absorption spectra of C_{60} (-), **153** (-) and the possible absorbance window showing the absorbance band of **175** (-) with the potential to be monitored upon increasing C_{60} concentration.*

After studying the absorption spectrum shown in Figure 4.3, it became apparent that it may be possible to monitor the absorption spectrum upon the addition of C_{60} by constructing a sensor that absorbs at higher wavelength, perhaps in the range of 425-460 nm. In an attempt

to achieve this, the tetra-1,8-naphthalimides **175** and **176** were designed. It was anticipated that the 1,8-naphthalimide not directly bound to the Tröger's base moiety would absorb at longer wavelength in the desired window. This new series of Tröger's bases were synthesised according to Scheme 4.1 shown below. The first step in the synthetic scheme involved a condensation reaction between the 4-chloro-1,8-naphthalic anhydride (1 eq.) **177** and the desired amine (1.4 eq.). This was performed by refluxing the two components in toluene in the presence of TEA overnight. The work-up involved filtering the reaction mixture whilst hot through celite and upon cooling the organic layer was removed under reduced pressure. The crude residue was dissolved in CH_2Cl_2 and washed once with water, brine and sat. $NaHCO_3$. The organic layer was subsequently dried over $MgSO_4$ and removed under reduced pressure to yield the desired products **178** and **179** without the need for further purification, in 99 and 89 % yield, respectively. These compounds were characterised using ^1H and ^{13}C NMR spectroscopy, IR and mass spectral analysis.

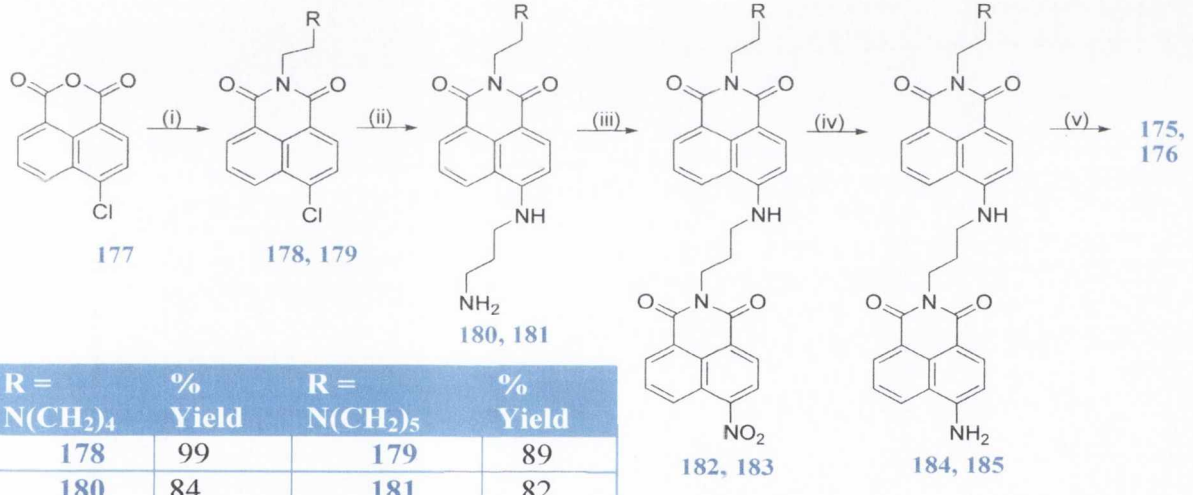

R = $N(CH_2)_4$	% Yield	R = $N(CH_2)_5$	% Yield
178	99	**179**	89
180	84	**181**	82
182	65	**183**	71
184	96	**185**	99
175	56	**176**	70

Scheme 4.1: *Synthesis of Tröger's bases **175** and **176**. Reagents and conditions: (i) 1-(2-aminoethyl)-pyrrolidine to yield **178** and 1-(2-aminoethyl)-piperidine to yield **179** toluene, TEA, reflux. (ii) diaminopropane, reflux (iii) 4-nitro-1,8-naphthalic anhydride, toluene, TEA, reflux (iv) Pd/C (10 %), H_2, 3 atm, CH_2Cl_2, CH_3OH (v) paraformaldehyde, TFA. Table in **Scheme 4.1** showing the % yields obtained.*

The next step in the synthetic pathway involved a nucleophillic aromatic substitution reaction achieved by refluxing both **178** and **179** separately in neat 1,3-diaminopropane overnight generating **180** and **181**, respectively. Upon cooling, CH_2Cl_2 was added to the

reaction mixtures and the newly formed organic layers were washed twice with water and dried over $MgSO_4$ before being removed by evaporation under reduced pressure to yield the desired products without the need for purification. Again, these intermediates were characterised using conventional methods.

Another condensation reaction followed, as **180** and **181** were both treated with 4-nitro-1,8-naphthalic anhydride using the experimental conditions described above. An analogous work-up was also utilised, however, upon cooling both the desired products **182** and **183** precipitated out of their respective toluene solutions and were collected by filtration. In order to ensure that all the TEA was removed each residue was dissolved in CH_2Cl_2 and washed once with water, brine and sat. $NaHCO_3$ and dried over $MgSO_4$. Removal of the organic layer yielded the desired products **182** and **183** as brown powders in 65 and 71 % yield, respectively. The identity of each derivative was confirmed using ^1H and ^{13}C NMR spectroscopy. As an example, the ^1H NMR spectrum ($CDCl_3$, 600 MHz) of **183** is shown in Figure 4.4.

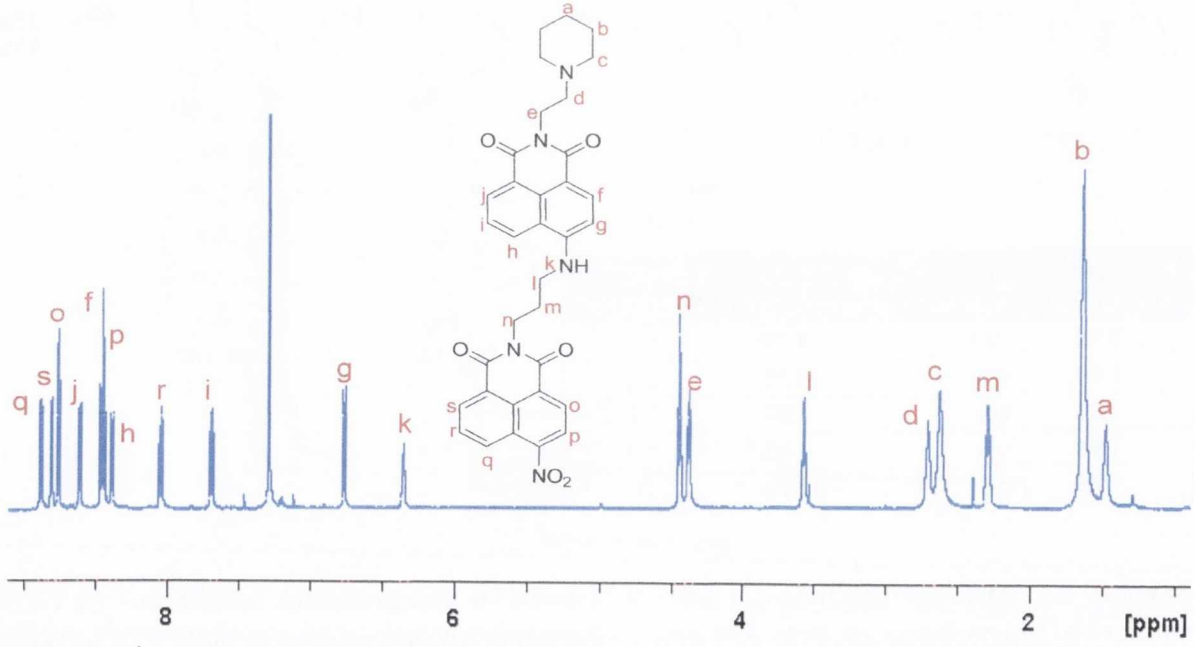

Figure 4.4: *^1H NMR spectrum ($CDCl_3$, 600 MHz) of **183**.*

The aromatic region of the ^1H NMR spectrum ($CDCl_3$, 600 MHz) of **183** is composed of eleven resonances, ten of which pertain to the methine protons belonging to the two 1,8-naphthalimide chromophores. The eleventh aromatic peak belongs to the amido proton which appeared at 6.35 ppm. The aliphatic region of the spectrum is made up of eight resonances,

whereby, the methylene protons of the propane chain appeared at 2.28, 3.56 and 4.43 ppm as two triplets and a multiplet, respectively. The protons belonging to the *N*-imide ethyl linker resonated at 4.37 and 2.70 ppm as triplets. Lastly, the piperidine signals appeared as multiplets at 1.47, 1.63 and 2.61 ppm. The ^{13}C spectrum ($CDCl_3$, 150 MHz) of **183** consisted of thirty-two peaks as expected, highlighting the symmetry of the piperidine functional group. The HRMS data complemented this assigned structure as a peak at m/z = 606.2355 was found and corresponded to the molecular formula of this compound with an additional proton in the positive electrospray mode. Similar spectral data was also used to identify the structure of **182**.

The final step before Tröger's base formation involved reducing the nitro group to the corresponding amino group in a hydrogenolysis reaction. This reduction was carried out using a Parr hydrogen shaker apparatus at 3 atm pressure in the presence of 10 % Pd/C catalyst until no more hydrogen gas was consumed. Using this experimental technique generated **184** and **185** in high yields of 88 and 99 %, respectively. The ^1H NMR spectrum of **185** ($CDCl_3$, 150 MHz) is shown in Figure 4.5.

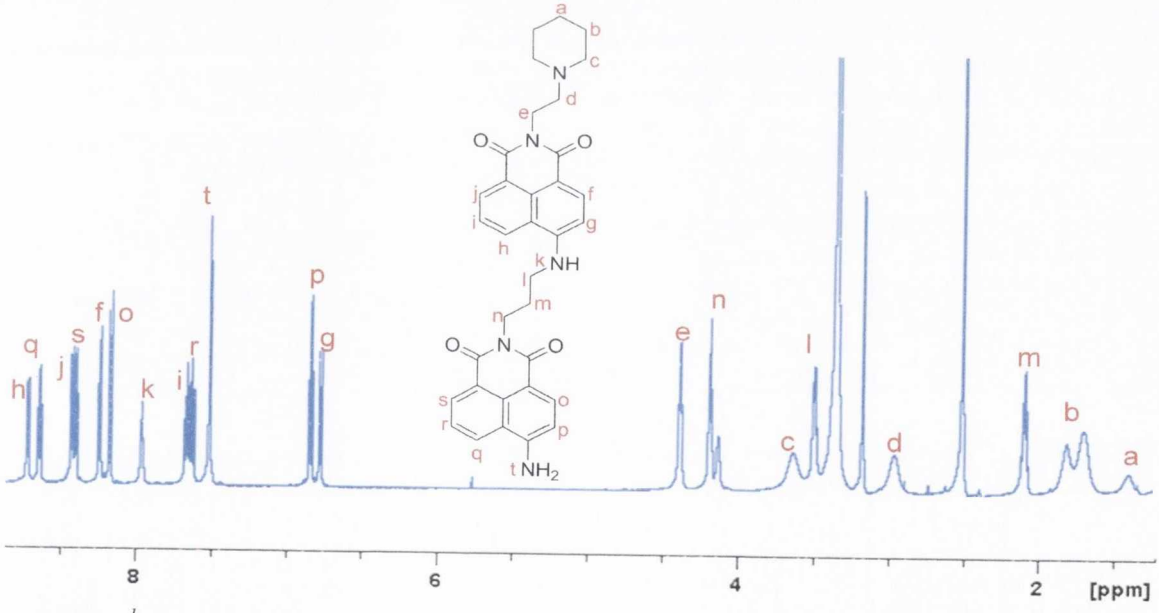

Figure 4.5: *^1H NMR spectrum ($CDCl_3$, 600 MHz) of **185**.*

As can be seen in Figure 4.5, the ^1H NMR spectrum ($CDCl_3$, 600 MHz) of **185** is comprised of twenty resonances, twelve in the aromatic region and eight in the aliphatic portion of the spectrum. There are ten signals that correlated to the aromatic methine protons of the two naphthalimide chromophores. In addition, the primary and secondary amines

appeared at 7.51 and 7.95 ppm, respectively. The protons pertaining to the piperidine group appeared as multiplets at 1.41, 1.76 and 3.64 ppm, whereas, those belonging to the ethyl side chain appeared as triplets with coupling constants of 6.5 Hz. The propane linker protons resonated at 2.09, 3.50 and 4.19 ppm as triplets and a multiplet, respectively. This structural assignment was similar to that conducted for **184**, as **184** and **185** only differ by a methylene group. The ^{13}C spectrum ($CDCl_3$, 150 MHz) of **185** was composed of thirty-two signals as was seen for **183** due to the reaction taking place on the nitro functional group. The loss of signals at 1515 cm^{-1} and 1388 cm^{-1} in the IR spectrum of **183** pertaining to the nitro moiety complemented the structure assigned using NMR spectroscopy, as signals corresponding to the newly formed amino group emerged. In addition, this assignment was further supported by the HRMS data collected which confirmed the molecular formula as being $C_{34}H_{33}N_5O_4$.

The remaining step in the reaction pathway is the synthesis of Tröger's bases **175** and **176**, which were achieved using the methodology described in Chapter 3, which involved stirring the 4-amino-1,8-naphthalimide derivative (1 eq.) in neat TFA in the presence of paraformaldehyde overnight (shown in Scheme 4.1). Upon completion of the reaction, the reaction mixture was initially neutralised and subsequently basified before extracting with CH_2Cl_2. After drying over $MgSO_4$ and removing the solvent under reduced pressure, the crude solids were collected. Trituration with CH_3OH yielded both **175** and **176** as orange solids in good yields of 56 and 70 % respectively. The ^1H NMR spectrum of **175** is shown in Figure 4.6.

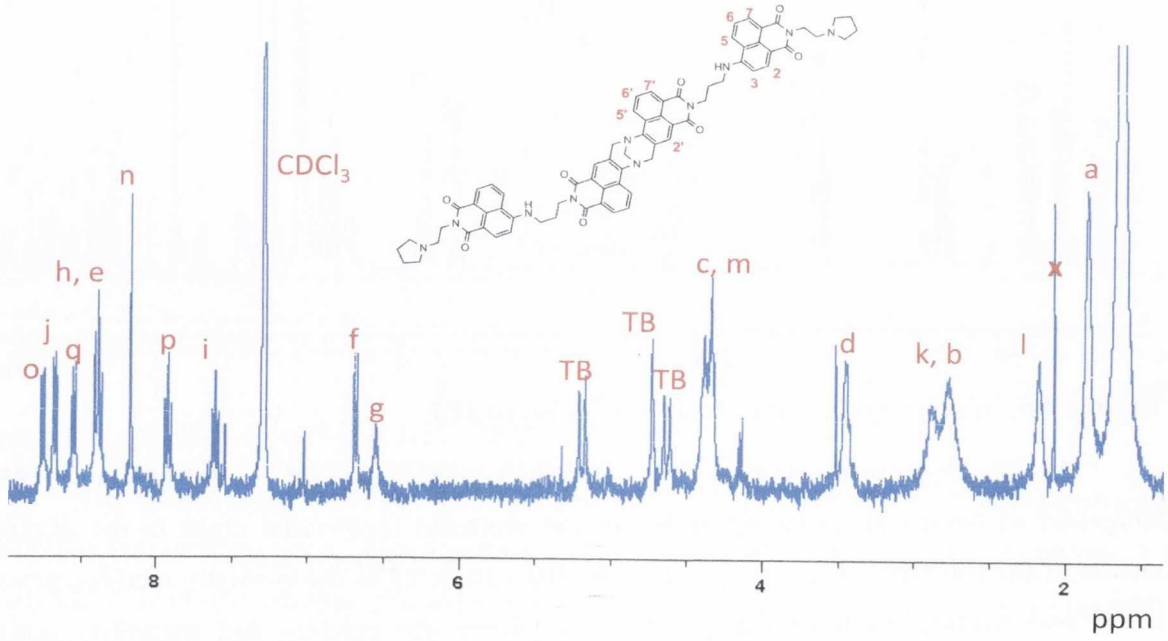

Figure 4.6: *^1H NMR spectrum ($CDCl_3$, 600 MHz) of **175**.*

The symmetric nature of **175** is evident from the ^{1}H NMR spectrum ($CDCl_3$, 600 MHz) of **175** shown in Figure 4.6. The aromatic region consisted of ten resonances which pertained to the naphthalimide protons and the amide proton. These were assigned with the aid of CH-COSY, HH-COSY and long range CH-COSY experiments. The characteristic Tröger's base peaks appeared as a singlet and two doublets with geminal coupling constants of 17.0 Hz. The remainder of the aliphatic region was composed of the methylene protons belonging to pyrrolidine and diaminopropane moieties. The ^{13}C NMR spectrum also confirmed the C_2-symmetric nature of **175** and the molecular formula of this structure was determined by mass spectroscopy. The elemental analysis was also consistent with the assigned structure. The structure of **176** was assigned using similar methodology.

4.3 Spectroscopic Studies In Solvents of Varying Polarity

In order to evaluate the nature of the ground and excited states of the newly formed bis- and tetra-1,8-naphthalimide derivatives (**182-185** and **175-176**) they were studied in a range of solvents that varied by polarity in addition to their hydrogen bonding ability in a manner similar to that previously described for the Tröger's base derivatives in Chapters 2 and 3. Firstly, the 4-nitro-1,8-naphthalimides **182** and **183** were investigated. As can be seen in Figure 4.7, the absorption spectrum of **183**, when recorded in CH_2Cl_2 exhibited a high energy band at 228 nm, two minor bands at 260 and 285 nm, in addition to two broad bands centred at 352 and 430 nm. The broad band at 352 nm can be assigned to the 4-nitro-1,8-naphthalimide chromophore, while the band at 430 nm is characteristic of a 1,8-naphthalimide with an electron donating substituent such as an amine at the 4-position.[175]

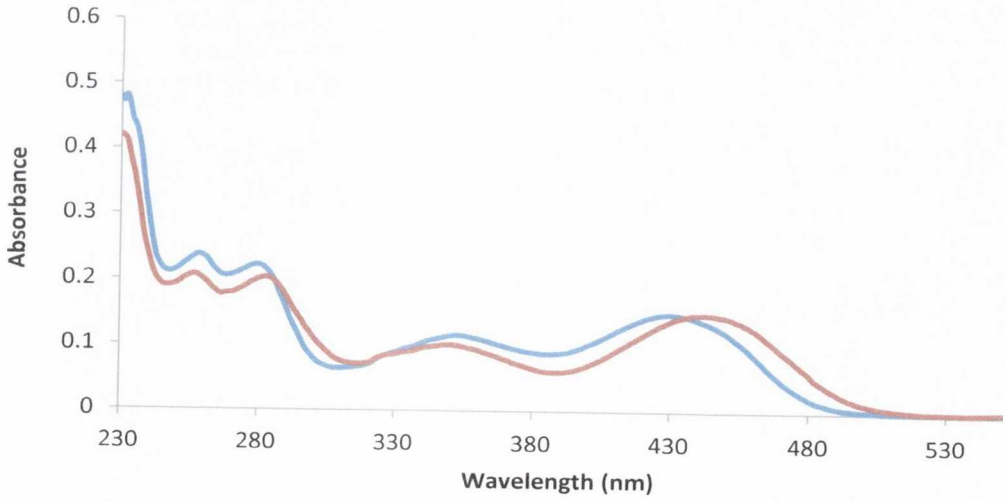

Figure 4.7: *Absorption spectra of **183** in CH_3OH (-) and CH_2Cl_2 (-).*

Upon changing the solvent to CH_3OH, a bathochromic shift of 12 nm was observed for the band at 430 nm, whereas the band at 352 nm did not show any significant shift with varying solvent polarity. The largest bathochromic shift of 30 nm was observed for the absorption band at 430 nm, when changing the solvent from chlorobenzene to water. This positive solvatochromism observed when increasing the polarity of the media for the 430 nm absorption band indicated the involvement of a solvent dependent ICT ground state characteristic of 4-amino-1,8-naphthalimides.[177] These changes are summarised in Table 4.1.

After establishing the presence of the ICT state in the ground state, **183** was investigated using fluorescence emission, excitation and lifetime techniques. In CH_2Cl_2, when excited at 430 nm, the emission spectrum of **183** displayed a broad structureless band that tailed off to longer wavelengths with a λ_{maxFLU} = 500 nm. Upon changing the solvent to EtOH, a bathochromic shift of 24 nm was observed, as can be seen in Figure 4.8 with the corresponding excitation spectra. Larger changes were observed in the emission spectra highlighting that the excited state is stabilised to a greater extent with respect to the ground state. The photophysical properties are summarised in Table 4.1. Importantly, when **183** was excited at 350 nm (the absorption band of the 4-nitro-1,8-naphthalimide), a broad structureless emission centred at 530 nm characteristic of 4-amino-1,8-naphthalimide was observed indicating efficient intramolecular energy transfer occurring from the 4-nitro-1,8-naphthalimide chromophore to the 4-amino-1,8-naphthalimide moiety.

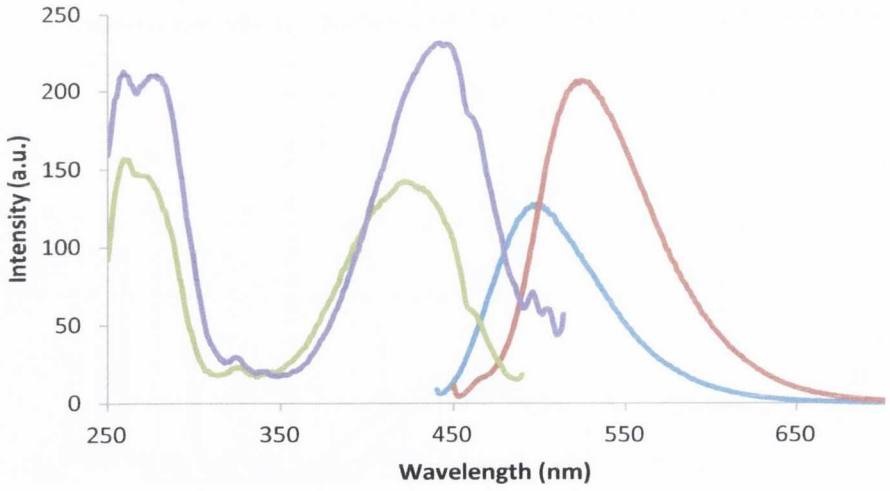

Figure 4.8: *Fluorescence emission spectra of* **183** *in $CHCl_3$ (-) and EtOH (-) excited at 430 and 440 nm, respectively, and excitation spectra in $CHCl_3$ (-) and EtOH (-) recorded at excitation wavelengths of 500 and 524 nm, respectively.*

Table 4.1: *Summary of the photophysical properties of* ***183***. [a] *Lifetimes were determined using a 458 nm nanoled.* [b] *Fluorescein (Φ_F = 0.9, 0.1 M NaOH at 436 nm) was used as the quantum yield reference standard.* [c] *Accurate lifetime value could not be determined.*

Solvent	λ_{maxUV} (nm)	λ_{maxFlu} (nm)	Φ_F (± 10%)[b]	τ (ns)	
				τ_1 (%)	τ_2 (%)
Toluene	419	490	0.033	0.61 (25)	5.87(75)
THF	428	500	0.033	0.98 (19)	7.69 (81)
Chlorobenzene	427	500	0.038	1.39 (20)	7.16 (80)
Ethylacetate	428	502	0.036	1.03 (14)	9.72 (86)
Chloroform	430	500	0.016	0.78 (22)	7.68 (78)
DCM	430	502	0.056	0.42 (42)	8.41 (58)
Acetone	431	511	0.042	1.27 (14)	8.15 (26)
DMF	439	521	0.073	2.45 (70)	8.49 (30)
Acetonitrile	432	517	0.034	1.02 (18)	8.21 (82)
Methanol	442	530	0.054	0.59 (21)	6.59 (79)
Ethanol	440	524	0.03	0.95 (18)	6.95 (82)
DMSO	444	525	0.06	2.56 (20)	8,50 (80)
Water	457	544	0.02	----[c]	-------[c]

As can be seen in Table 4.1, compound **183** exhibited bi-exponential lifetimes in all the solvents studied, with the short lived component presumably representing the 4-nitro-1,8-naphthalimide chromophore while the long lived major component may arise due to the luminescent 4-amino-1,8-naphthalimide moiety.[118,197] Interestingly, the quantum yields were higher in polar protic solvents such as CH_3OH and DMSO in comparison to $CHCl_3$ and toluene. However, no general trend could be established with varying the solvent polarity. This is in contrast with the ICT nature of the excited state observed previously for various 4-amino-1,8-naphthalimide and Tröger's base derivatives as described in Chapters 2 and 3. In addition, the lifetime measurements did not exhibit a clear correlation with solvent polarity either. In regards to the quantum yields a similar effect was observed by Chang *et al.*[282] for a 1,8-naphthalimide based system which showed higher quantum efficiencies in polar solvents compared to non-polar solvents, however, no clear conclusions were drawn from this work in relation to this interesting behaviour except for such compounds exhibiting aggregation

induced emission properties. Similar behaviour was also observed in the case of **182** (Appendix 3).

In an attempt to try and understand this behaviour better, the amino derivative **185** was studied as a function of solvent polarity to compare to **182** and **183**. Compound **185** exhibited a broad structureless absorption band centred at 410 nm in CH_2Cl_2 which is characteristic of 4-amino-1,8-naphthalimide derivatives.[177] Positive solvatochromism was observed for this absorption band when the polarity of the solvent was increased (Figure 4.9(b)). For instance, a bathochromic shift of 24 nm for **185** was recorded when changing the solvent from CH_2Cl_2 to EtOH, establishing the presence of the ICT character. These changes are summarised in Table 4.2.

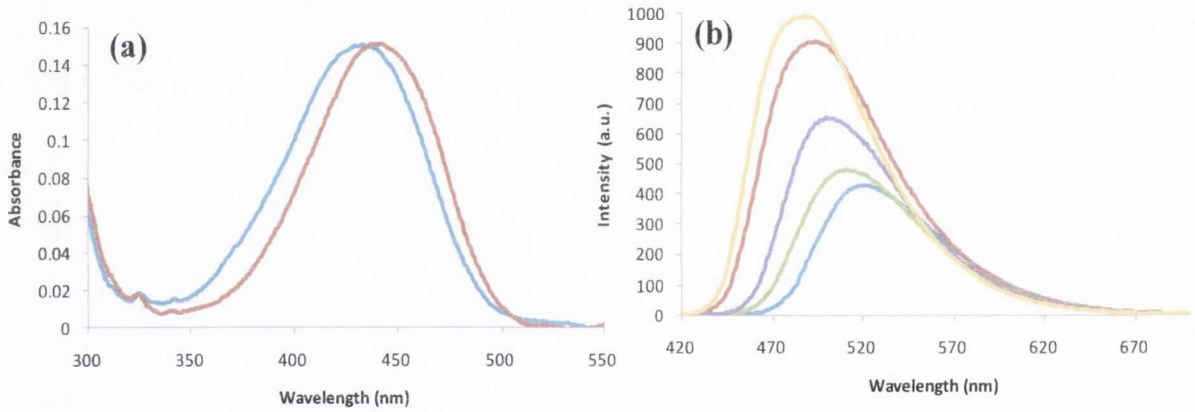

Figure 4.9: *(a) Absorption spectra of 13 in CH_2Cl_2 and CH_3OH* (b) *Fluorescence emission spectra of **185** in CH_2Cl_2 (-), DMF (-),acetone (-), THF (-), $CHCl_3$ (-) with excitations at 433, 410, 422, 422 and 407 nm, respectively.*

Analysing the data in Table 4.2, it can be seen that the quantum yields and lifetimes of **185** vary as a function of the solvent polarity. For instance, when changing the solvent from $CHCl_3$ to DMSO the quantum yield was reduced from 0.481 to 0.184. In all the solvents studied, compound **185** showed bi-exponential decay, where the short lived lifetime presumably corresponds to the 4-*N*-propyl substituted naphthalimide and the long lived component represents the 4-amino substituted 1,8-naphthalimide.[177] Upon changing the solvent from $CHCl_3$ to DMSO, both of these lifetimes were shortened. This behaviour is characteristic of the ICT nature of the singlet excited state. This behaviour is unlike that observed for the nitro derivatives **182**-**183**.

Table 4.2: *Summary of the photophysical properties of* ***184***. [a] *Fluorescein* (Φ_F = *0.9, 0.1 M NaOH at 436 nm) was used as the quantum yield reference standard.* [b] *Lifetimes were determined using a 458 nm nanoled.*

Solvent	λ_{maxUV} (nm)	λ_{maxFlu} (nm)	Φ_F (± 10%)[a]	τ (ns)[b]	
				τ_1 (%)	τ_2 (%)
Toluene	406	481	0.317	0.64 (20)	8.13 (80)
THF	422	500	0.251	1.84 (31)	8.47 (69)
Chlorobenzene	410	489	0.449	4.41 (29)	9.57 (71)
Ethylacetate	418	502	0.250	2.80 (39)	9.22 (61)
Chloroform	407	487	0.481	3.96 (27)	9.59 (73)
DCM	410	494	0.369	3.53 (34)	10.37 (66)
Acetone	422	512	0.184	2.37(48)	8.88 (52)
DMF	433	521	0.179	2.22 (42)	8.66 (58)
Acetonitrile	418	516	0.158	2.41 (50)	9.12 (50)
Methanol	434	532	0.121	2.40 (55)	6.84 (45)
Ethanol	436	527	0.171	2.93 (54)	7.19 (46)
DMSO	439	527	0.184	2.28 (41)	8,59 (59)
Water	439	546	0.015	2.42 (57)	4.66 (43)

The Tröger's base **176** was also studied in several solvents using ground and excited state techniques. The absorption spectrum of **176** in CH_2Cl_2 as shown in Figure 4.10 consisted of a high energy band at *ca.* 242 nm and two small undefined broad like bands at *ca.* 252 and 282 nm. At longer wavelength a broad band was observed between 330-530 nm, centred at 428 nm. Increasing the polarity of the solvent resulted in bathochromic shifts as shown in Figure 4.10 and summarised in Table 4.3. Once again, such positive solvatochromism exhibited upon changing the polarity of the medium indicated the presence of ICT character, although smaller shifts were observed in comparison to the free amine **185**, highlighting the effect of incorporating the Tröger's base moiety.

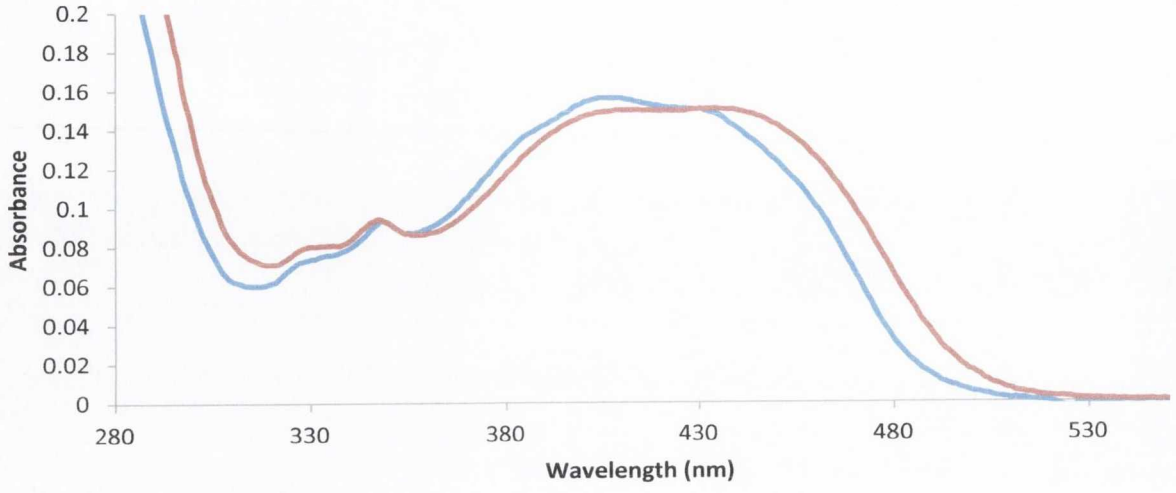

Figure 4.10: *Absorption spectrum of* **176** *in $CHCl_3$ (-) and DMSO (-).*

The fluorescence and excitation spectra were subsequently analysed as a function of solvent. Behaviour similar to the nitro derivative **176** was observed where red shifts occurred when increasing the polarity and hydrogen bonding ability of the solvent. In addition, **176** was found to be more emissive in polar solvents such as DMF compared to toluene. This can be seen in Figure 4.11, with the corresponding excitation spectra.

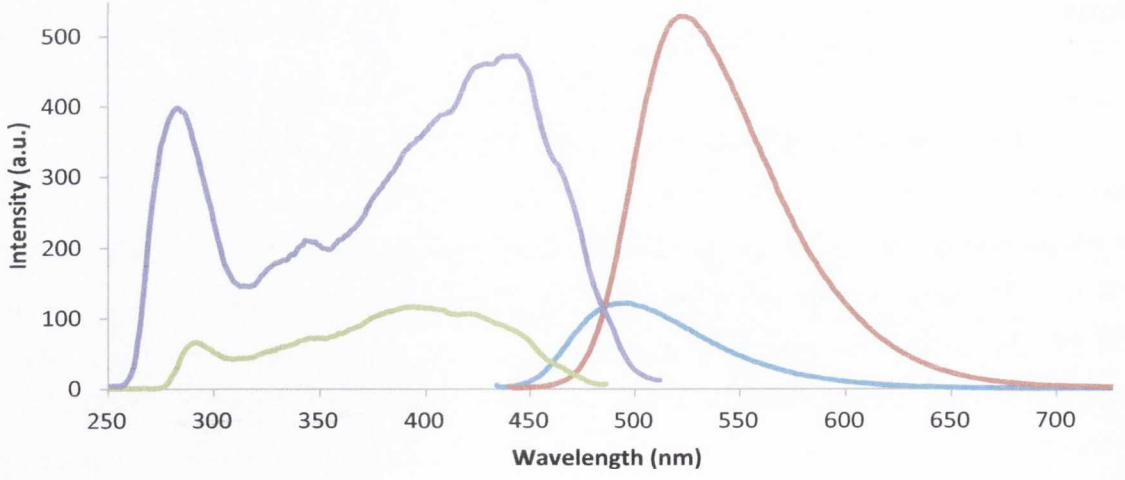

Figure 4.11: *Fluorescence emission spectra of* **176** *in DMF (-) and toluene (-) excited at λ_{max} = 430 and 424 nm, respectively and fluorescence excitation spectra in DMF (-) and toluene (-) with excitation wavelengths at 522 and 496 nm, respectively.*

The fluorescence quantum efficiencies were shown to be greater in polar solvents such as CH_3OH and EtOH in comparison to non-polar solvents such as CH_2Cl_2, toluene and chlorobenzene as summarised in Table 4.3. Fluorescence lifetime measurements showed that, the lifetimes of **176** were longer in polar solvents compared to non-polar solvents. Similar effects were also observed for **175** (Appendix 3).

Table 4.3: *Summary of the photophysical properties of **176**. [a] Fluorescein (Φ_F = 0.9, 0.1 M NaOH at 436 nm) was used as the quantum yield reference standard. [b] Lifetimes were determined using a 458 nm nanoled. [c] An accurate value could not be determined utilising these experimental conditions.*

Solvent	λ_{maxUV} (nm)	λ_{maxFlu} (nm)	Φ_F (± 10%)[a]	τ (ns)[b]	
				τ_1 (%)	τ_2 (%)
Toluene	424	496	0.02	0.99 (49)	6.94 (51)
THF	422	506	0.059	1.32 (56)	7.78 (44)
Chlorobenzene	416	502	0.027	1.28 (44)	7.41 (56)
Ethylacetate	423	512	0.049	1.98 (32)	9.90 (68)
Chloroform	429	507	0.034	1.35 (46)	8.14 (55)
DCM	428	514	0.038	1.72 (45)	5.37 (55)
Acetone	429	516	0.06	1.36 (56)	8.37 (44)
DMF	430	522	0.102	2.34 (68)	8.02 (32)
Acetonitrile	427	522	0.06	1.37 (45)	8.90 (55)
Methanol	436	534	0.079	2.24 (32)	6.72 (68)
Ethanol	432	528	0.069	2.79 (33)	7.73 (67)
DMSO	434	528	0.118	2.48 (60)	7.74 (40)
Water	436	548	0.003	--------[c]	--------[c]

In summary, the bis- and tetra 1,8-naphthalimide derivatives exhibit very interesting solvatochromic behaviour. Shifts to longer wavelengths are observed in both the absorption and emission spectra when the polarity of the solvent is increased indicating the involvement of solvent polarity dependent ICT states. Evidence for the ICT nature of the excited state is usually obtained when carrying out fluorescent lifetime and quantum efficiency measurements, where short lifetimes and low quantum efficiencies are expected in polar solvents such as CH_3OH and water. For four of the six naphthalimide derivatives investigated

here this was not the case as no clear relationship between lifetime or quantum efficiency and solvent dependence could be determined.

4.4 Spectroscopic Titrations of 175 and 176 with Fullerene C_{60}

In order to evaluate the potential of **174** and **175** as C_{60} hosts, their interaction with C_{60} was preliminarily investigated using absorption and fluorescence emission, excitation and lifetime techniques. As discussed earlier in Section 4.2, **174** and **175** were designed to absorb at higher wavelengths with respect to **152**, in an attempt to investigate the ground state interactions of 1,-8-naphthalimide Tröger's bases with C_{60}. As can be seen in Figure 4.12, C_{60} spans the absorption spectrum from 200-680 nm and thus overlaps with the fluorescence spectra of many luminescent molecules. However, the singlet and triplet electronically excited states of C_{60} lie below the emitting levels of these compounds on the energy scale.[283]

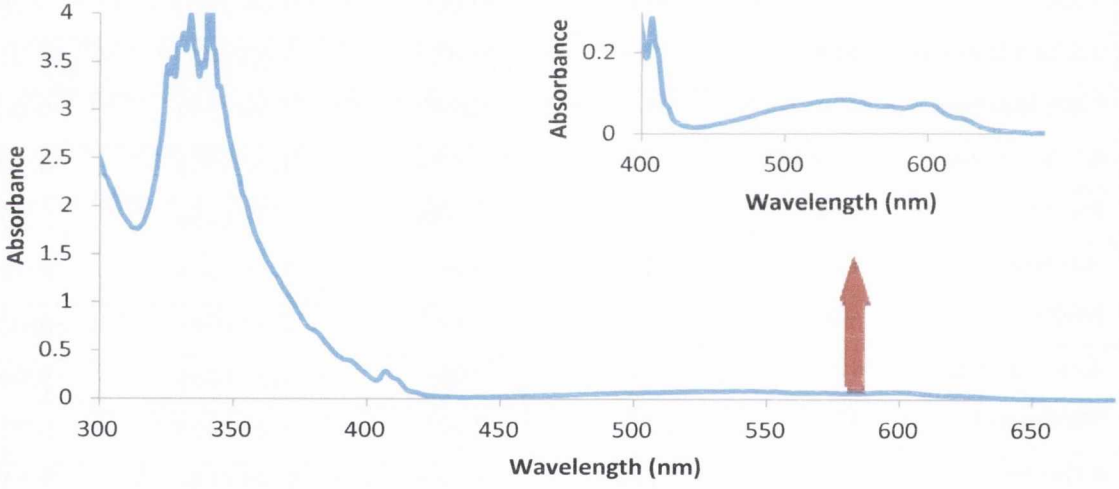

Figure 4.12: *Absorption spectrum of C_{60} (80.6 μM) in chlorobenzene.*

The interaction between **175** (5 μM) in PhCl:DMF (86 %: 14%) and C_{60} (0-728 μM) in PhCl was the first to be preliminarily investigated by absorption spectroscopy. PhCl was chosen as the medium according to previous studies.[279,280] DMF was used for solubility purposes. Upon initial addition of C_{60} (0-26.6 μM) as shown in Figure 4.13(a), no significant decrease in absorbance was observed for the ICT band at 429 nm. Moreover, in the presence of increasing concentration of C_{60}, no new band appeared at the lower energy end of the spectrum (*ca.* 480 nm), which has been reported for several C_{60} host systems and assigned to the 1:1 complex of fullerene with the host.[279,280] Further addition of C_{60} to the solution of **175** resulted in the absorption spectrum being dominated by C_{60} absorption bands (Figure 4.13(b)). Consequently, it was not possible to monitor and follow the absorption spectra as a

function of C_{60} concentration. The same effect was also observed for **176** (4.9 μM) in PhCl:DMF (98 %: 2 %).

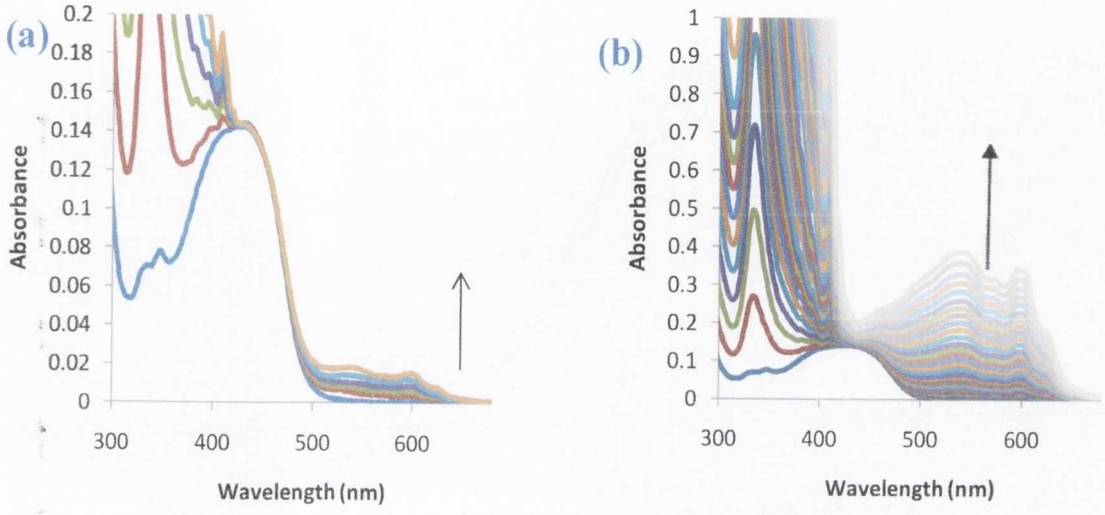

Figure 4.13: *Absorption spectra of* **175** *(5 μM) in* **(a)** *the presence of C_{60} (0-26.6 μM) at low concentration and* **(b)** *the presence of C_{60} (0-728 μM) at high concentration.*

The molar extinction coefficients of **175** and **176** are large with respect to C_{60} and this renders it possible to excite the fluorophores **175** and **176** preferentially, keeping the concentration of **175** and **176** at a much lower level in comparison to C_{60}.[284] The steady state fluorescence emission and excitation spectra of **175** and **176** were studied as a function of C_{60} concentration and these spectra are shown in Figure 4.14 and Figure 4.15, respectively. As can be seen, in the case of **175**, when excited at λ_{maxUV} = 429 nm (the ICT absorption band) a broad structureless emission band centred at 518 nm formed. Successive addition of C_{60} resulted in fluorescence quenching and this was accompanied by a blue shift of *ca.* 3 nm. The excitation spectra showed a decrease in intensity upon addition of C_{60} as well as a blue shift of 4 nm.

When **176** was excited at the absorption maximum of 427 nm, a band centred at 515 nm formed. Similar to that observed for **175**, the intensity of this band decreased significantly upon the addition of C_{60} and this was accompanied by a blue shift of 7 nm, as seen in Figure 4.15. The changes in the fluorescence excitation spectra were also similar to that seen for **175**, with a decrease in intensity and a shift to shorter wavelengths. The fluorescence quenching and the blue shifts in the presence of increasing concentration of C_{60} indicated that an interaction had taken place between C_{60} and the derivatives **175**-**176**.

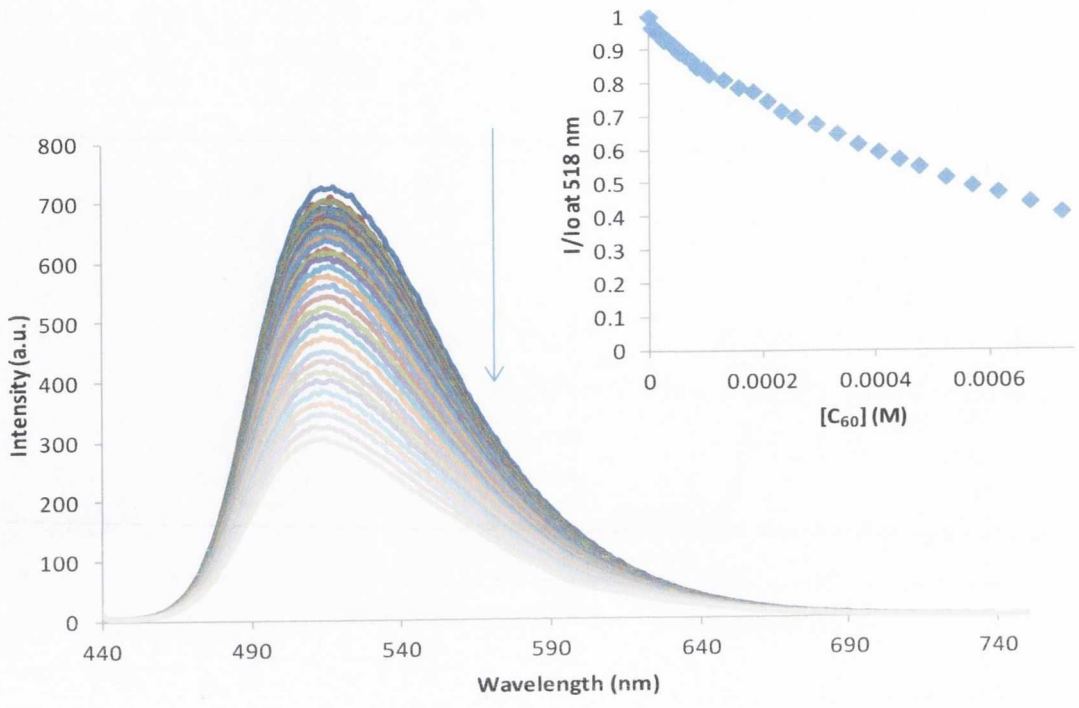

Figure 4.14 *Fluorescence Spectrum of* **175** *(5 μM) upon successive addition of C_{60}. (0-728 μM). λ_{Ex} = 429 nm. Inset: Plot of changes in emission vs. [C_{60}].*

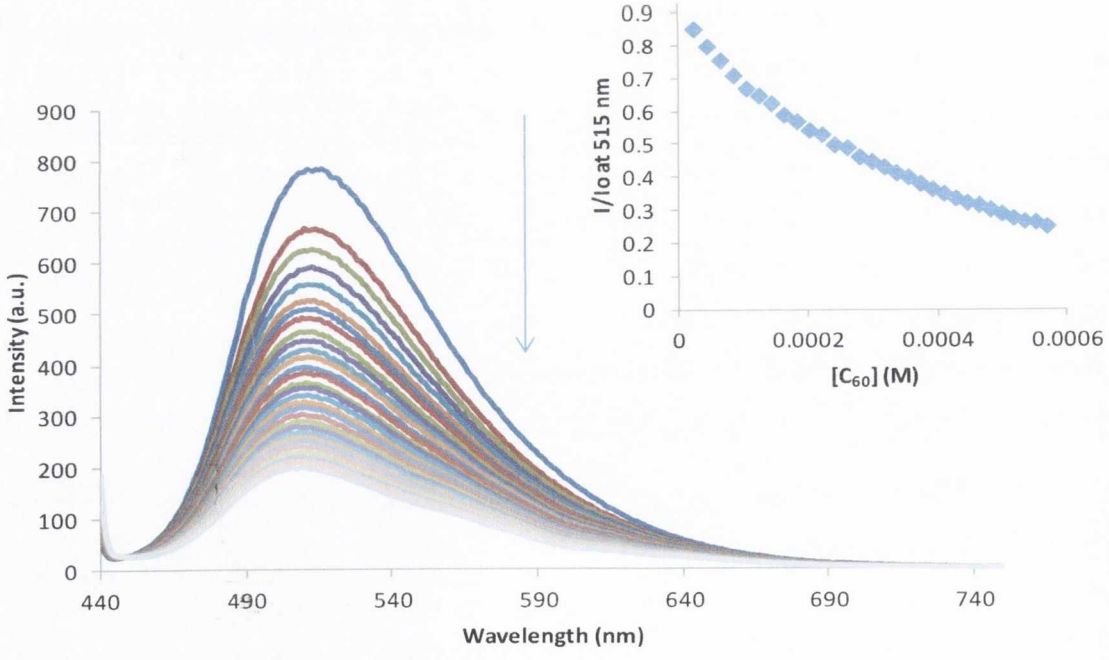

Figure 4.15: *Fluorescence Spectrum of* **176** *(4.9 μM) upon successive addition of C_{60}. (0-567 μM). λ_{ex} = 427 nm. Inset: Plot of changes in emission vs. [C_{60}].*

To account for this quenching, several mechanisms were considered including (i) static quenching through the formation of a non-fluorescent ground state complex, (ii) ´´Sphere of Action´´ static quenching, (iii) dynamic quenching or (iv) Förster Resonance Energy Transfer (FRET).

In order to investigate the mechanism of quenching, single state lifetime measurements were conducted because static and dynamic quenching effect the average lifetime differently. For instance, if static quenching occurs, the decay time will not be shortened because only the uncomplexed fluorophores are excited.[285] However, dynamic quenching results from the collisional encounter between the fluorophore and the quencher and acts on the entire excited state population resulting in the decrease of the mean decay time upon the addition of the quencher.[285] In the presence of increasing concentration of C_{60} the average lifetime of both **175** and **176** remain unchanged (Table 4.4) and thus, the possibility of dynamic quenching as a prevailing quenching mechanism can be ruled out.

Table 4.4: *Fluorescence Lifetime of **176** as a function of [C_{60}]. Lifetimes were determined using a 458 nm nanoled.*

[C_{60}]	τ_1(ns) (%)	τ_2 (ns) (%)
0	1.36 (70)	5.76 (30)
3.331×10^{-6} M	1.28 (68)	5.47 (32)
9.980×10^{-6} M	1.28 (68)	5.53 (32)
3.311×10^{-5} M	1.31 (69)	5.51 (31)
6.579×10^{-5} M	1.33 (68)	5.51 (32)
1.613×10^{-4} M	1.30 (66)	5.47 (34)
4.545×10^{-4} M	1.41 (62)	5.51 (38)

The possibility of FRET between the Tröger's base derivatives **175-176** and C_{60} was also considered as a possible mechanism of fluorescence quenching. For FRET to occur, the fluorescence spectrum of the fluorophore and the absorption spectrum of the quencher must overlap adequately. Moreover, the efficiency of FRET is also governed by the extinction coefficient of the acceptor and the quantum yield of emission of the donor as described below (equation 4.1).[285] Even though the absorption spectra of C_{60} and the fluorophores **175-176**

overlap, C_{60} has very small extinction coefficients of 912 and 798 mol^{-1} cm^{-1} at 515 and 570 nm, respectively and thus the efficiency of FRET is considered to be quite low.[285,286] In addition, these measurements were carried out in PhCl where both **175** and **176** were found to have quantum efficiencies of 0.027 and 0.012, respectively. Therefore, the efficiency of FRET should be low and cannot account for the observed fluorescence quenching. However, at very high concentration of C_{60}, the absorbance at wavelengths > 500 nm becomes quite high (*ca.* 0.4), therefore the possibility of FRET cannot be completely ruled out at such high concentrations.

$$R_0^6 = \frac{9000(ln10)K^2 Q_D}{128\pi^5 N n^4} \int_0^\infty F_D(\lambda)\epsilon_A(\lambda)\lambda^4 \, d\lambda \qquad (4.1)$$

where, Q_D is the quantum yield of the donor in the absence of acceptor, n is the refractive index of the medium, N is Avogadro's number, r is the distance between the donor and the acceptor and $F_D(\lambda)$ is the corrected fluorescence intensity of the donor in the wavelength region λ to $\lambda+d\lambda$, with the total intensity normalised to unity. The extinction coefficient of the acceptor is $\varepsilon_A(\lambda)$ and K^2 is the relative orientation of the transition dipoles of the donor and acceptor in space and is usually assumed to be 2/3 considering random dynamic averaging.[285]

As the average fluorescence lifetime of **175** and **176** remained essentially unchanged over the entire concentration range of C_{60} this suggested that static quenching was responsible for the quenching observed upon the addition of C_{60} to fluorophores **175** and **176**. However, as mentioned before, there was no evidence of ground state complexation from the absorption spectra at lower concentrations of C_{60} (0-26.6 μM), suggesting that either C_{60} interacts very weakly with the hosts **175** and **176** or there is no ground state interaction at all. However, at higher concentrations of C_{60} the interaction between **175** (or **176**) and C_{60} could not be followed by absorption spectroscopy due to strong absorbance of C_{60} at wavelengths > 450 nm, and therefore, no conclusion could be drawn on this type of quenching from the absorbance data. Similar behaviour has been previously observed for the ''molecular box'' **174** containing Pt (II) coordinated to the Tröger's base containing ligands by Wärnmark and co-workers.[278] Such weak interactions between **174** and C_{60} were reported to be due to the inability of the ''molecular box'' **174** to cage C_{60} efficiently. As discussed earlier, this may be due to the size of the cavity not being large enough to host C_{60} or due to the presence of the methyl arms which may impede the binding process. However, the fluorescence intensity of

174 was significantly quenched in the presence of C_{60} in a manner similar to that observed for the interaction of **175** (and **176**) with C_{60} (*cf.* Figures 4.14 and 4.15). The fluorescence quenching of **174** was thought to be due to the weak interaction of C_{60} with the outer surface of the cage, which may also be the possible mode of interaction between the bis-naphthalimides **175-176** described herein. In order to gain further insight into the mechanism of quenching the fluorescence data was analysed in terms of the Stern Volmer equation (equation 4.2),

$$I_o/I = 1 + \mathbf{Ks}[Q] \qquad (4.2)$$

where, I_o is the intensity of the free fluorophore, I is the intensity of the fluorophore in the presence of the quencher, [Q] denotes quencher concentration and **Ks** refers to the association constant.[287] The curves obtained for **175** and **176** in accordance to equation 4.2 are shown in Figure 4.16 (a) and 4.16 (b), respectively.

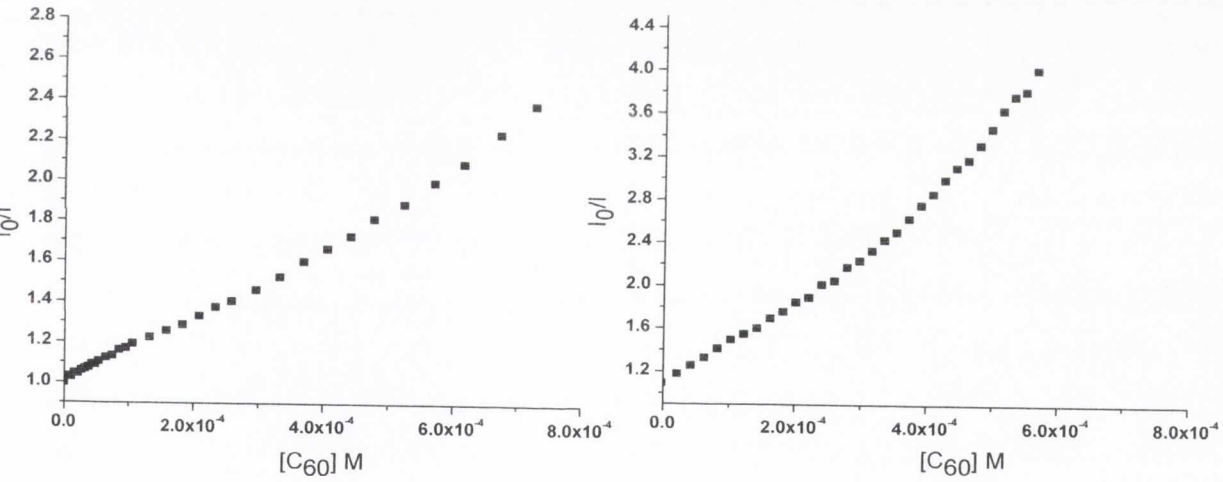

Figure 4.16: *Plot of I/I_0 vs $[C_{60}]$ for* **175** *(left) and* **176** *(right).*

Figure 4.16 reveals that for both of the hosts **175** and **176**, the plots of I/I_0 versus $[C_{60}]$ exhibited positive deviations from linearity at higher concentrations of C_{60}. This deviation was found to be more pronounced for **176**. Such upward curvature in the Stern Volmer plot is indicative of a combination of static and dynamic quenching. The static component was also reflected in the singlet state lifetime measurements, where the mean fluorescence lifetime was essentially unaffected in the presence of increasing concentration of C_{60}. The dynamic component observed at higher concentration of C_{60} can result from the collisional encounter of

C_{60} with the outer surfaces of the hosts **175** and **176**. Alternatively, the fluorescence quenching can also result from the "Sphere of Activation" mechanism[286] if the C_{60} molecules are located adjacent to the fluorophore at the moment of excitation and will quench the fluorescence without forming a ground state complex.[278]

4.5 Conclusion

The work in this chapter has demonstrated that the tetra-1,8-naphthalimide Tröger's bases **175** and **176** synthesised display varying spectroscopic responses towards solvent polarity and hydrogen bonding ability. However, no specific trend could be established for the variation of the photophysical properties with respect to solvent polarity and the H-bonding properties. The interaction of **175** and **176** with C_{60} has been investigated using absorption and fluorescence spectroscopy. The absorption spectra of **175** and **176** remained unchanged at low concentrations of C_{60} and no new band was observed to indicate the formation of a host:guest complex. Unfortunately, the interaction could not monitored at higher concentrations of C_{60} due to the strong absorbance of the molecule at wavelengths > 450 nm. Preliminary studies suggested that the singlet excited states of **175** and **176** were significantly quenched in the presence of C_{60}. Analysis of the fluorescence data in terms of a Stern-Volmer plot showed that the quenching involves a combination of static and dynamic mechanisms. The static component was also reflected in the fluorescence lifetime measurements of **175** and **176** in the presence of varying concentrations of C_{60}, which remained largely unchanged over the entire concentration range of the quencher. Several possibilities have been postulated to account for the dynamic component, which can result from the collisional encounter of the quencher with the outer surface of the cleft shaped host molecules. Alternatively, the close proximity of C_{60} molecules to the fluorophore at the moment of excitation can also result in the quenching of the fluorescence without forming a ground state complex through the "Sphere of Activation" mechanism. Moreover, the efficiency of FRET from the singlet state of **175** or **176** to C_{60} seems to be very low due to the low extinction coefficients of C_{60} at wavelengths > 500 nm. However, at the very high concentrations of C_{60}, due to strong absorbance of C_{60} at wavelengths > 500 nm, the possibility of FRET cannot be completely ruled out. These preliminary titration studies suggest that **175-176** posses potential as sensors for C_{60} and the efficient fluorescence quenching can be utilised (for *e.g* linear region of the Stern-Volmer plots in Figure 4.16(a) and (b)) for the quantitative detection of C_{60}. Therefore, these interactions need to be further evaluated by other physical measurements such as ^{1}H NMR spectroscopy, mass spectroscopy,

dynamic light scattering etc. Moreover, the initial studies suggested that **175-176** interact very weakly with the outer surface of the hosts instead of binding to the "cleft" of these molecules. This needs to be further evaluated and quantitative estimations of these interactions will be carried out in the future.

4.6 Overall Conclusions and Future Perspectives

The overall theme of this thesis was to derivatise the 1,8-naphthalimide chromophore. This was achieved through the incorporation of the racemic Tröger's base structural unit at the 3 and 4 positions on the naphthalimide rings and by modifying the *N*-imide termini. In Chapter 2, Tröger's base derivatives **86-90** were developed as C_2-symmetric DNA binders and were derived from the 3-amino-1,8-naphthalimide chromophore. These molecules as racemic mixtures were shown to bind to *ct*-DNA quite strongly and possess two modes of binding. In view of these encouraging results, the next step will be to separate the enantiomers through chiral resolution and to evaluate their affinity for DNA as single enantiomers. In addition, it is known that these molecules bind to the grooves of DNA, however, it is unknown if these molecules bind to the major or minor grooves of DNA. In order to gain further insight into the DNA binding abilities of these molecules this mode of binding needs to fully elucidated. This will also provide more information on the design of these molecules which may contribute to the future construction and development of 1,8-naphthalimide based Tröger's base derivatives as potential DNA binders. In order to compare **86-90** with the 4-amino derived analogues to the fullest extent the cytotoxic activities of these molecules will be determined in both HL-60 and K562 cell lines. Future work will include conducting Alamar Blue assays in order to study cell proliferation as well as further studies using confocal microscopy.

Chapter 3 dealt with the synthesis of amino acid based Tröger's base derivatives. These molecules were shown to exhibit solvent dependence due to the presence of an internal charge transfer excited state and it was concluded that such molecules may have potential to behave as peptide mimics. In order to evaluate these molecules as potential peptidomimetics, their interaction with proteins such as HSA and BSA will be investigated. Furthermore, the corresponding mono-1,8-naphthalimide precursors were originally designed and evaluated as DNA binders with the premise being that specificity may be achieved by incorporating amino acid and peptide sequences. By incorporating the Tröger's base motif the DNA binding affinities of these molecules may be enhanced as was the case in Chapter 2, thus the

interactions of these molecules with DNA will be investigated using absorption and fluorescence techniques. Moreover, these molecules were formed as diastereoisomers and separation of these will be attempted using high performance liquid chromatography.

The final chapter detailed the design, synthesis and preliminary photophysical investigations of tetra-1,8-naphthalimide Tröger's base derivatives using absorption and fluorescence techniques. In order to gain a better understanding of the interactions discussed in Chapter 4, techniques such as NMR and mass spectroscopy will be employed. In addition, dynamic light scattering may also provide further information on the behaviour exhibited during the course of the titrations.

Chapter 5: Experimental

5.1 General Experimental Techniques

All NMR spectra were recorded using a Brüker DPX-400 Avance spectrometer, operating at 400.1 MHz for ^{1}H NMR and 100.6 MHz for ^{13}C NMR, or a Brüker AV-600 spectrometer operating at 600.1 MHz for ^{1}H NMR and 150.2 MHz for ^{13}C NMR. Shifts are referenced relative to internal solvent signals. Electrospray mass spectra were recorded on a Micromass LCT spectrometer, running Mass Lynx NT V 3.4 on a Waters 600 controller connected to a 996 photodiode array detector with HPLC grade methanol or chloroform. High resolution mass spectra were determined by a peak matching method, using leucine Enkephalin, (Tyr-Gly-Gly-Phe-Leu) as the standard reference (m/z = 556.2771). Melting points were determined using an IA9000 digital melting point apparatus. Infrared spectra were recorded on a Perkin Elmer Spectrum One FT-IR spectrometer fitted with a Universal ATR Sampling Accessory. Elemental analysis was conducted at the Microanalytical Laboratory, School of Chemistry and Chemical Biology, University College Dublin. X-Ray diffraction studies were carried out by Dr. Thomas McCabe (School of Chemistry, Trinity College Dublin) using a Brüker SMART APEX single crystal CD diffractometer.

UV-visible absorption spectra were recorded on a Varian Cary 50 spectrometer. Emission spectra were recorded on a Cary Eclipse Luminescence spectrometer. Solutions were measured in 3 cm (10 mm x 10 mm) cuvettes. Linear and circular dichroism spectra were recorded at concentrations corresponding to optical densities of approximately 2.5 and 1.0, respectively, on a J-815 Circular Dichroism Spectropolarimeter equipped with a Linear Dichroism Accessory (LD) or a Jasco J-810-150S CD spectropolarimeter (CD). Ethidium bromide displacement assays were performed in 10 mM phosphate buffer solution (pH 7.4) according to the procedure of Boger *et al.*[207] The fluorescence of ethidium bromide was initially measured at λ_{Ex} = 545 nm and normalised to 0 % relative fluorescence. An appropriate amount of *ct*-DNA was then added at a ratio of ethidium bromide to *ct*-DNA (base pairs) of 2:1. At this ratio it could be estimated that all interaction sites were occupied and the fluorescence was measured again and normalised to 100 % relative fluorescence. The changes in the emission spectra of ethidium bromide to *ct*-DNA were then monitored upon successive additions of the appropriate DNA binding molecule. The titrations were continued until the decrease in the emission reached saturation and remained constant. Thermal denaturation experiments were performed on a thermoelectrically coupled Perkin Elmer LAMBDA 25 UV/Vis Spectrophotometer.The temperature in the cell was ramped from 30 to 90 °C at a rate of 1 °C per minute and the absorbance at 260 nm was measured every 0.2 °C. For these studies, semi-micro UV-Vis cuvettes were used (path length of 1 cm and window

width of 4 mm). All solutions were thoroughly degassed before the experiment. Fluorescence lifetime experiments were carried out on a Horiba Scientific Fluorolog – Modular Spectrofluorimeter equipped with Time Correlated Single Photon Counting (TCSPC) capability. A nanoled with λ_{Ex}= 458 nm was used as the excitation source. Emission decays were recorded at λ_{Em} depending on the solvent using a slit width of 2 nm. All the decay traces were corrected for using a dilute solution of colloidal silica.

Titrations were carried out by monitoring changes in the absorption and emission spectra of the dye at pH 7.4 in 10 mM phosphate buffer upon successive additions of aliquots of *ct*-DNA. The results are quoted using the concentration of ct-DNA expressed as a nucleotide phosphate to dye ratio (P/D ratio).

5.2 Materials

All reagents and solvents were purchased commercially from Sigma-Aldrich, Fluka, TCI and Apollo Ltd. and unless specified, were used without the need for further purification. Anhydrous solvents were prepared using standard procedures according to Vögel, with distillation under argon prior to each use.[288] Chromatographic columns were run using Silica gel 60 (230-400 mesh ATSM). Analytical TLC was performed using Merck Kieselgel 60 F_{254} silica gel plates. Solutions of *ct*-DNA in 10 mM phosphate buffer pH 7.4 gave a ratio of UV absorbance at 260 and 280 nm of 1.85:1, indicating that the *ct*-DNA was sufficiently free of protein. The concentration of the ct-DNA was determined spectrophotometrically using the molar extinction coefficient of 6600 M^{-1} cm^{-1} at 260 nm.

5.3 General Experimental Techniques For Chapter 2.

5.3.1 Procedure 1: Formation of the 3-Amino-1,8-Naphthalimide Derivatives[42]

3-Amino-1,8-naphthalic anhydride (1 eq.), the appropriate dialkylaminoethylamine (1.4 eq.) and triethylamine (2 eq.) in toluene were stirred at reflux for 24 hours under an argon atmosphere. Upon completion of the reaction the reaction mixture was immediately filtered while hot through celite, washing several times with toluene. The filtrate and washings were removed under reduced pressure and the residue dissolved in CH_2Cl_2. The organic solution was washed twice with sat. $NaHCO_3$, twice with H_2O and once with brine. The organic layer was dried over $MgSO_4$ and evaporated under reduced pressure to dryness. Purification was carried out where necessary.

5.3.2 Procedure 2: Formation of the Bis-1,8-Naphthalimide Tröger's Base Derivatives

A mixture of the relevant 3-amino-1,8-naphthalimide (1 eq.) and paraformaldehyde (1.1 eq.) in neat TFA were stirred at room temperature for 3 hours under an argon atmosphere. The reaction was initially neutralised and further basified using 6 M NaOH. The aqueous solution was extracted several times with CH_2Cl_2. The organic extracts were combined and the solvent was removed under reduced pressure. The crude product was purified and dried under vacuum.

3-Nitro-1,8-Naphthalic Anhydride 101[172]

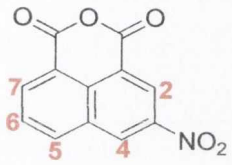

1,8-Naphthalic anhydride (2.50 g, 12.6 mmol) was dissolved in sulphuric acid (10 mL) and cooled in an ice bath. A solution of nitric acid (0.5 mL) in sulphuric acid (5 mL) was added slowly to the cooled naphthalic anhydride solution with stirring. After completion of the addition, the ice bath was removed and the reaction mixture was allowed to warm to room temperature and stir for 90 min. The reaction mixture was poured into ice water and the solid was collected by suction filtration. The crude residue was recrystallised from glacial acetic acid to yield beige needles (1.84 g, 60 %). m.p. 251-253 °C (ref.[172] 249° C); δ_H (400 MHz, $(CD_3)_2SO$), 9.54 (1H, d, J = 2.0 Hz, H2), 8.93 (1H, d, J = 2.5 Hz, H4), 8.84 (1H, d, J = 8.0 Hz, H5), 8.72 (1H, d, J = 7.5 Hz, H7), 8.11 (1H, *app*. t, H6); δ_C (150 MHz, $(CD_3)_2SO$), 159.8 (C=O), 159.6 (C=O), 145.8 (C), 137.2 (Ar-CH), 135.3 (Ar-CH), 131.7 (C), 130.9 (C), 130.6 (Ar-CH), 129.5 (Ar-CH), 124.1 (Ar-CH), 121.4 (C), 119.9 (C); ν_{max} (neat sample)/cm^{-1} 1776, 1733, 1541, 1455, 1341.

3-Amino-1,8-Naphthalic Anhydride 102[34,173]

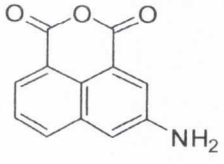

Compound **101** (1.70 g, 6.9 mmol) was shaken with 10 % palladium on carbon in DMF (100 mL) in the presence of hydrogen at 3 atm for 2 hr at room temperature in a Parr shaker. The reaction mixture was filtered through celite and washed with DMF/toluene. The solvent was removed azeotropically with toluene under reduced pressure to yield the product as an orange solid (1.35 g, 92 %). m.p. 304-306°C (ref.[34] > 300°C); HRMS: 214.0504 $([M+H]^+$. $C_{12}H_7NO_3$ requires 214.0496); δ_H (600 MHz, $(CD_3)_2SO$), 8.14 (1H, d, J = 8.3 Hz, H5), 8.11 (1H, d, J = 7.2 Hz, H7), 7.97 (1H, d, J = 2.2 Hz, H2), 7.68 (1H, *app* t, H6), 7.37 (1H, d, J = 2.3 Hz, H4), 6.10 (2H, br. s, NH_2); δ_C (150 MHz, $(CD_3)_2SO$), 161.0 (C=O), 160.9 (C=O), 148.1 (C), 133.6 (C), 132.6 (Ar-CH), 127.3 (Ar-CH), 127.1 (Ar-CH), 123.1 (Ar-CH), 122.9 (C), 119.2 (C),

118.5 (C), 112.6 (Ar-CH); δ_N (60.8 MHz, $(CD_3)_2SO$), 66.3 (NH_2); ν_{max} (neat sample)/cm^{-1} 3465, 3365, 1750, 1717, 1515.

_N_-[1-Dimethylamino-ethyl]-3-amino-1,8-naphthalimide 20

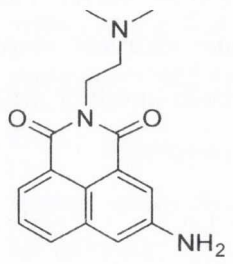

Compound **20** was synthesised by reacting *N,N*-dimethylethylenediamine (210 mg, 0.32 mL, 2.98 mmol), **102** (455 mg, 2.13 mmol) and TEA (431 mg, 0.60 mL, 4.26 mmol) in toluene (100 mL) according to **Procedure 1**, to yield the product as yellow needles (448 mg, 74 %) after triturating with $CHCl_3$. m.p. 171 °C (ref.[34] 169-171 °C); HRMS: 284.1400 ($[M+H]^+$. $C_{16}H_{18}N_3O_2$ requires 284.1399); δ_H (600 MHz, $(CD_3)_2SO$), 8.08 (1H, d, J = 7.2, H7), 8.04 (1H, d, J = 7.9, H5), 7.97 (1H, d, J = 2.3 Hz, H2), 7.63 (1H, *app*.t, H6), 7.29 (1H, d, J = 2.3, H4), 5.98 (2H, br. s, NH_2), 4.14 (2H, t, J = 6.8, $NC\underline{H_2}CH_2N(CH_3)_2$), 2.49 (2H, t, J = 7.2, $NCH_2C\underline{H_2}N(CH_3)_2$), 2.09 (6H, s, $NCH_2CH_2N(C\underline{H_3})_2$); δ_C (150 MHz, $(CD_3)_2SO$), 163.6 (C=O), 163.5 (C=O), 147.8 (C), 133.5 (C), 131.4 (Ar-CH), 126.9 (Ar-CH) 125.4 (Ar-CH), 122.5 (Ar-CH), 122.5 (C), 121.7 (C), 120.5 (C), 111.7 (Ar-CH), 56.5 (CH_2), 45.3 (CH_3), 38.0 (CH_2); δ_N (60.8 MHz, $(CD_3)_2SO$), 65.4 (NH_2); ν_{max} (neat sample)/cm^{-1} 3415, 3322, 1692, 1656, 1445.

_N_-[1-Morpholino-ethyl]-3-amino-1,8-naphthalimide 103

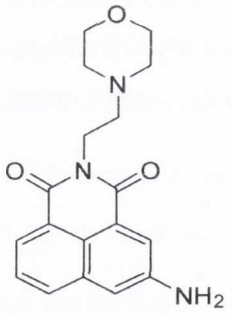

Compound **103** was synthesised by reacting 4-(2-aminoethyl)-morpholine (119 mg, 0.12 mL, 0.20 mmol) with **102** (140 mg, 0.65 mmol) and TEA (132 mg, 018 mL, 1.30 mmol) in toluene (100 mL) according to **Procedure 1**, to yield the product as yellow solid (143 mg, 67 %) after triturating with CH_3OH. m.p. 230 °C (ref.[34] 228 °C); HRMS: 326.1520 ($[M+H]^+$. $C_{18}H_{20}N_3O_3$ requires 326.1505); δ_H (600 MHz, $(CD_3)_2SO$), 8.08 (1H, d, J = 7.14 Hz, H7), 8.04 (1H, d, J = 7.9 Hz, H5), 7.97 (1H, d, J = 2.3 Hz, H2), 7.62 (1H, *app.* t, H6), 7.29 (1H, d, J = 2.3 Hz, H4), 5.98 (2H, br. s, NH_2), 4.17 (2H, t, J = 7.1, $NC\underline{H_2}CH_2N(CH_2)_2(CH_2)_2O$), 3.54 (4H, s, $NCH_2CH_2N(C\underline{H_2})_2(CH_2)_2O$), 2.56 (2H, s, $NCH_2C\underline{H_2}N(CH_2)_2(CH_2)_2O$), 2.47 (4H, s, $NCH_2CH_2N(CH_2)_2(C\underline{H_2})_2O$); δ_C (150 MHz, $(CD_3)_2SO$), 163.7 (C=O), 163.5 (C=O), 147.8 (C), 133.5 (C), 131.4 (Ar-CH), 126.9 (Ar-CH), 125.4 (Ar-CH), 122.5 (C), 121.7 (Ar-CH), 121.7 (C) 120.5 (C), 111.7 (Ar-CH), 66.2 (CH_2), 55.6 (CH_2), 53.4 (CH_2), 36.7 (CH_2); δ_N (60.8 MHz, $(CD_3)_2SO$), 65.5 (NH_2); ν_{max} (neat sample)/cm^{-1} 3455, 3355, 1689, 1653, 1446, 1110.

_N_-[1-Methyl-piperazino-ethyl]-3-amino-1,8-naphthalimide 104

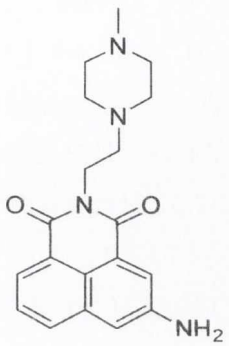

Compound **104** was synthesised by reacting 1-(2-aminoethyl)-4-methylpiperazine (480 mg, 0.50 mL, 3.35 mmol) with **102** (511 mg, 2.39 mmol) and TEA (484 mg, 0.68 mL, 4.79 mmol) in toluene (180 mL) according to **Procedure 1**, to yield the desired product as a yellow powder (616 mg, 76 %) after triturating with ethyl acetate. m.p. 187-189 °C; HRMS: 339.1814 $([M+H]^+$. $C_{19}H_{23}N_4O_2$ requires 339.1821); δ_H (600 MHz, $(CD_3)_2SO$), 8.08 (1H, d, J = 7.5, H7), 8.04 (1H, d, J = 7.9, H5), 7.97 (1H, d, J = 2.3 H2), 7.63 (1H, *app.* t, H6) 7.29 (1H, d, J = 2.2, H4), 5.98 (2H, br. s, NH_2), 4.15 (2H, t, J = 7.1 Hz, $NC\underline{H_2}CH_2N(CH_2)_2(CH_2)NCH_3$), 2.54 (2H, t, J = 7.1 Hz, $NCH_2C\underline{H_2}N(CH_2)_2(CH_2)NCH_3$), 2.47 (4H, br s, $NCH_2CH_2N(C\underline{H_2})_2(CH_2)NCH_3$), 2.28 (4H, br s, $NCH_2CH_2N(CH_2)_2(C\underline{H_2})_2NCH_3$), 2.13 (3H, s, $NCH_2CH_2N(CH_2)_2(CH_2)NC\underline{H_3}$); δ_C (150 MHz, $(CD_3)_2SO$), 163.7 (C=O), 163.5 (C=O), 147.8 (C), 133.5 (C), 131.9 (Ar-CH), 127.4 (Ar-CH), 125.9 (Ar-CH), 122.5 (C), 122.2 (Ar-CH), 121.7 (C), 120.6 (C), 112.2 (Ar-CH), 55.1 (CH_2), 54.7 (CH_2), 52.7 (CH_2), 45.7 (CH_3), 37.0 (CH_2); δ_N (60.8 MHz, $(CD_3)_2SO$), 65.1 (NH_2); ν_{max} (neat sample)/cm^{-1} 3408, 3314, 1693, 1653, 1449.

_N_-[1-Piperidino-ethyl]-3-amino-1,8-naphthalimide 105

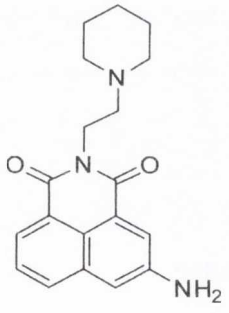

Compound **105** was synthesised using 1-(2-aminoethyl)-piperidine (155 mg, 0.17 mL, 1.21 mmol) according to **Procedure 1** and was yielded as a bright yellow solid (173 mg, 62 %) after trituration with CH_3OH. m.p. 184-186 °C (ref.[34] 180-182 °C); HRMS: 324.1710 $[M+H]^+$. $C_{19}H_{22}N_3O_2$ requires 324.1710); δ_H (600 MHz, $(CD_3)_2SO$), 8.08 (1H, d, J = 7.1 Hz, H7), 8.04 (1H, d, J = 8.3 Hz, H5), 7.97 (1H, d, J = 2.3 Hz, H2), 7.63 (1H, *app.* t, Ar-H6), 7.29 (1H, d, J = 2.3 Hz, H4), 5.98 (2H, br. s, NH_2), 4.16 (2H, t, J = 7.1 Hz, $NC\underline{H_2}CH_2N(CH_2)_2(CH_2)_2CH_2$), 2.53 (2H, t, J = 7.1 Hz, $NCH_2C\underline{H_2}N(CH_2)_2(CH_2)_2CH_2$), 2.45 (4H, s, $NCH_2CH_2N(C\underline{H_2})_2(CH_2)_2CH_2$), 1.47 (4H, s, $NCH_2CH_2N(CH_2)_2(C\underline{H_2})_2CH_2$), 1.37 (2H, s, $NCH_2CH_2N(CH_2)_2(CH_2)_2C\underline{H_2}$); δ_C (150 MHz, $(CD_3)_2SO$), 163.7 (C=O), 163.5 (C=O), 147.8 (C), 133.5 (C), 131.5 (Ar-CH), 126.9 (Ar-CH), 125.4 (Ar-CH), 122.5 (C), 121.7 (C), 121.7 (Ar-CH), 120.5 (C), 111.7 (Ar-CH), 55.7 (CH_2), 54.2 (CH_2), 37.0 (CH_2), 25.6 (CH_2), 23.9 (CH_2); δ_N (60.8 MHz, $(CD_3)_2SO$), 65.4 (NH_2). ν_{max} (neat sample)/cm^{-1} 3406, 3314, 1692, 1654, 1460.

_N_-[1-Pyrrolidino-ethyl]-3-amino-1,8-naphthalimide 106

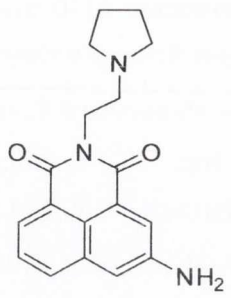

Compound **106** was synthesised using 1-(2-aminoethyl)-pyrrolidine (153 mg, 0.17 mL, 1.3 mmol) according to **Procedure 1** and was yielded as a yellow solid (198 mg, 67 %) after trituration with CH_3OH. m.p. 191-193 °C (ref.[34] 195 - 197 °C); HRMS: 310.1557 ($[M+H]^+$. $C_{18}H_{20}N_3O_2$ requires 310.1556); δ_H (600 MHz, $(CD_3)_2SO$), 8.08 (1H, d, J = 7.1 Hz, H7), 8.04 (1H, d, J = 8.3 Hz, H5), 7.97 (1H, d, J = 2.3 Hz, H2), 7.62 (1H, *app.* t, H6), 7.29 (1H, d, J = 2.2 Hz, H4), 5.98 (2H, br. s, NH_2), 4.17 (2H, t, J = 7.1 Hz, $NC\underline{H_2}CH_2N(CH_2)_2(CH_2)_2$), 2.67 (2H, t, J = 7.1 Hz, $NCH_2C\underline{H_2}N(CH_2)_2(CH_2)_2$), 2.54 (4H, s, $NCH_2CH_2N(C\underline{H_2})_2(CH_2)_2$), 1.66 (4H, s, $NCH_2CH_2N(CH_2)_2(C\underline{H_2})_2$); δ_C (150 MHz, $(CD_3)_2SO$), 163.7 (C=O), 163.5 (C=O), 147.8 (C), 133.5 (C), 131.4 (Ar-CH), 126.9 (Ar-CH), 125.4 (Ar-CH), 122.5 (C), 121.7 (Ar-CH), 121.7 (C), 120.5 (C), 111.7 (Ar-CH), 53.7 (CH_2), 53.0 (CH_2), 38.5 (CH_2), 23.1 (CH_2); δ_N (60.8 MHz, $(CD_3)_2SO$), 65.6 (NH_2); ν_{max} (neat sample) /cm^{-1} 3406, 3314, 1693, 1653, 1451.

Bis-{N-[1-Dimethylamino-ethyl]}-9,18,-methano-1,8-naphthalimido[b,f][1,5]-diazocine 86

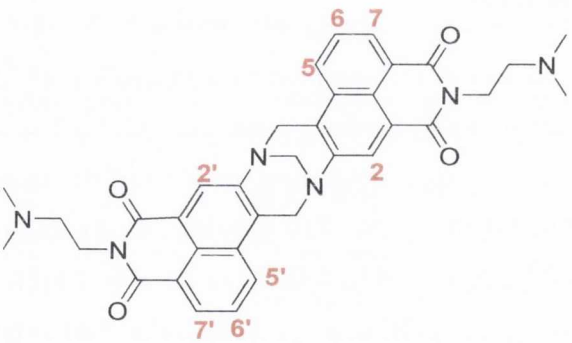

Compound **86** was synthesised by reacting **20** (650 mg, 2.29 mmol) with paraformaldehyde (73 mg, 2.42 mmol) in TFA (4 mL) in accordance to **Procedure 2**, to yield the desired product as an orange solid after trituration with CH_3CN (548 mg, 79 %). m.p. 219-221°C; Calculated for $C_{35}H_{34}N_6O_4.1.5.CH_2Cl_2$: C, 60.05; H, 5.11; N, 11.51. Found C, 59.36; H, 4.84; N, 11.54; HRMS: 603.2714 ($[M+H]^+$.$C_{35}H_{35}N_6O_4$ requires 603.2720); δ_H (600 MHz, $CDCl_3$), 8.47 (2H, d, J = 8.0 Hz, H7, H7'), 8.46 (2H, s, H2, H2'), 8.04 (2H, d, J = 8.0 Hz, H5, H5'), 7.74 (2H, *app.* t, H6, H6'), 5.21 (2H, d, J = 17.0 Hz, TB), 4.97 (2H, d, J = 17.0 Hz, TB), 4.59 (2H, s, TB), 4.36 (4H, t, J = 6.5 Hz, $NC\underline{H_2}CH_2N(CH_3)_2$), 2.67 (4H, t, J = 6.5 Hz, $NCH_2C\underline{H_2}N(CH_3)_2$), 2.38 (12H, s, $NCH_2CH_2N(C\underline{H_3})_2$); δ_C (150 MHz, $CDCl_3$), 164.0 (C=O), 163.9 (C=O), 146.5 (C), 130.1 (C), 129.8 (Ar-CH), 129.6 (Ar-CH), 128.8 (C), 127.6 (Ar-CH), 127.4 (Ar-CH), 125.6 (C), 123.0 (C), 122.7 (Ar-CH), 66.5 (CH_2), 56.8 (CH_2), 56.2 (CH_2), 45.7 (CH_3), 38.0 (CH_2); ν_{max} (neat sample)/cm^{-1} 2947, 2770, 1697, 1653, 1338.

Bis-{N-[1-Morpholino-ethyl]}-9,18,-methano-1,8-naphthalimido[b,f][1,5]-diazocine 87

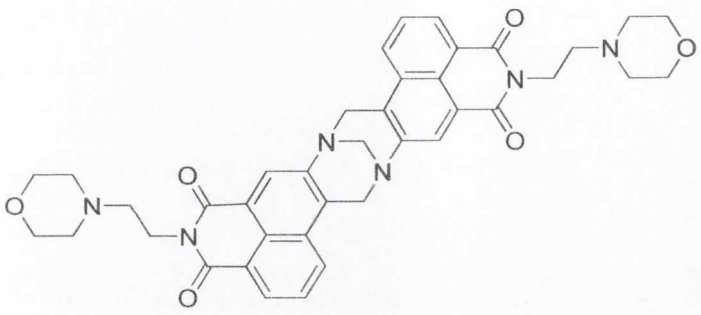

Compound **87** was synthesised by reacting **103** (273 mg, 1.64 mmol) with paraformaldehyde (28 mg, 0.84 mmol) in TFA (3.5 mL) in accordance to **Procedure 2**, to yield the product as a yellow solid (154 mg, 54 %) after trituration with CH_3OH. m.p. 189-190 °C; Calculated for $C_{39}H_{38}N_6O_6.0.75.CH_2Cl_2$: C, 63.62; H, 5.31; N, 11.20. Found C, 64.02; H, 5.01; N, 11.28; HRMS: 687.2931 ($[M+H]^+$. $C_{39}H_{39}N_6O_6$ requires 687.2906); δ_H (600 MHz, $CDCl_3$), 8.48 (2H, d, J = 8.0 Hz, H7, H7'), 8.45 (2H, s, H2, H2'), 8.07 (2H, d, J = 8 .0 Hz, H5, H5'), 7.76 (2H, *app.* t, H6, H6'), 5.21 (2H, d, J = 17.0 Hz, TB), 4.69 (2H, d, J = 17.0 Hz, TB), 4.61 (2H, s, TB), 4.32 (4H, t, J = 6.5 Hz, $NC\underline{H_2}CH_2N(CH_2)_2(CH_2)_2O$), 3.08 (8H, br s, $NCH_2CH_2N(CH_2)_2(C\underline{H_2})_2O$), 2.70 (4H, t, J = 6.5 Hz, $NCH_2C\underline{H_2}N(CH_2)_2(CH_2)_2O$), 2.60 (8H, br s, $NCH_2CH_2N(\underline{CH_2})_2(CH_2)_2O$); δ_C (150 MHz, $CDCl_3$), 163.4 (C=O), 163.2 (C=O), 145.8 (C), 129.7 (Ar-CH), 129.6 (C), 129.5 (Ar-CH), 128.3 (C), 127.7 (Ar-CH), 127.4 (Ar-CH), 125.2 (C), 122.6 (C), 122.1 (C), 67.0 (CH_2), 66.6 (CH_2), 56.1 (CH_2), 55.8 (CH_2), 37.0 (CH_2); ν_{max} (neat sample)/cm^{-1} 2955, 2850, 1698, 1655, 1339.

Bis-{N-[1-Methyl-pyperazino-ethyl]}-9,18,-methano-1,8-naphthalimido[b,f][1,5]-diazocine 88

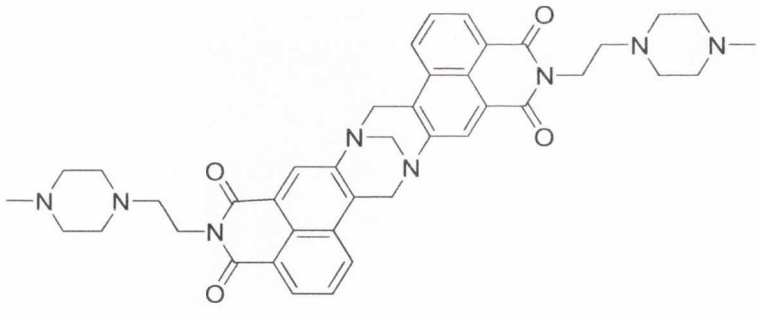

According to **Procedure 2** **88** was synthesised by stirring both **104** (1.32 g, 3.90 mM) and paraformaldehtde (152 mg 5.07 mM) in TFA (4 mL) to yield the desired product as an orange solid (852 mg, 61 %) after dissolving in CH_2Cl_2 (2 mL) and precipitating from diethyl ether (50 mL). m.p. 191-192°C; Calculated for $C_{41}H_{44}N_8O_4.0.8.CH_2Cl_2$: C, 64.30; H, 5.89; N, 14.35. Found C, 63.95; H, 5.77; N, 14.73; HRMS: 713.3568 ($[M+H]^+$.$C_{41}H_{45}N_8O_4$ requires 713.3564); δ_H (600 MHz, $CDCl_3$), 8.44 (2H, d, J = 7.3 Hz, H7, H7'), 8.42 (2H, s, H2, H2'), 8.02 (2H, d, J = 8.5 Hz, H5, H5'),

7.73 (2H, *app.* t, H6, H6'), 5.18 (2H, d, J = 17.4 Hz, TB), 4.93 (2H, d, J =17.4 Hz, TB), 4.57 (2H, s, TB), 4.29 (4H, m, $NC\underline{H_2}CH_2N(CH_2)_2(CH_2)_2NCH_3$), 2.68 (12H, m, $NCH_2CH_2N(C\underline{H_2})_2(CH_2)_2NCH_3$, $NCH_2C\underline{H_2}N(CH_2)_2(CH_2)_2NCH_3$), 2.40 (8H, br. s, $NCH_2CH_2N(CH_2)_2(C\underline{H_2})_2NCH_3$), 2.24 (6H, s, $NCH_2CH_2N(CH_2)_2(CH_2)_2NC\underline{H_3}$); δ_C (150 MHz, $CDCl_3$), 163.9 (C=O), 163.7 (C=O), 146.4 (C), 130.1 (C), 129.7 (Ar-CH), 129.5 (Ar-CH), 128.7 (C), 127.7 (Ar-CH), 127.3 (Ar-CH), 125.6 (C), 123.1 (C), 122.7 (C), 66.5 (CH_2), 56.1 (CH_2), 55.5 (CH_2), 55.1 (CH_2), 53.2 (CH_2), 45.9 (CH_3), 37.5 (CH_2); ν_{max} (neat sample)/cm^{-1} 2935, 2794, 1699, 1598, 1336.

Bis-{N-[1-Piperidino-ethyl]}-9,18,-methano-1,8-naphthalimido[b,f][1,5]-diazocine 89

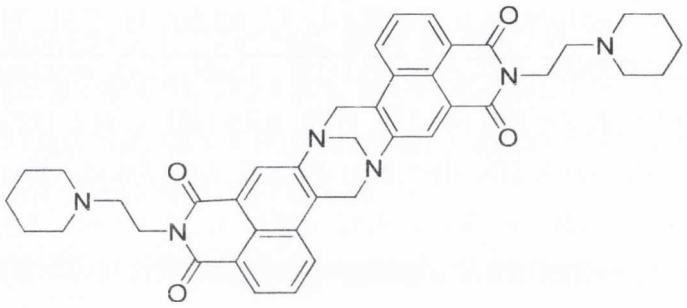

Compound **89** was synthesised by reacting **105** (670 mg, 2.07 mmol) with paraformaldehyde (68 mg, 2.28 mmol) in TFA (4 mL) in accordance to **Procedure 2**, to yield the product as a yellow solid (254 mg, 36 %) after purification from trituration with ethyl acetate. m.p. 234-235°C; HRMS: 683.3332 ($[M+H]^+$.$C_{41}H_{43}N_6O_4$ requires 683.3346); δ_H (600 MHz, $CDCl_3$), 8.45 (2H, d, J = 8.1 Hz, H7, H7'), 8.43 (2H, s, H2, H2'), 8.03 (2H, d, J = 9.3 Hz, H5, H5'), 7.73 (2H, *app.* t, H6, H6'), 5.18 (2H, d, J = 17.3 Hz, TB), 4.94 (2H, d, J = 17.3 Hz, TB), 4.58 (2H, s, TB), 4.31 (4H, m, $NC\underline{H_2}CH_2N(CH_2)_2(CH_2)_2CH_2$), 2.62 (4H, m, $NCH_2C\underline{H_2}N(CH_2)_2(CH_2)_2CH_2$), 2.52 (8H, br.s, $NCH_2CH_2N(C\underline{H_2})_2(CH_2)_2CH_2$), 1.56 (8H, m, $NCH_2CH_2N(CH_2)_2(C\underline{H_2})_2CH_2$), 1.41 (4H, m, $NCH_2CH_2N(CH_2)_2(CH_2)_2C\underline{H_2}$); δ_C (150 MHz, $CDCl_3$), 163.9 (C=O), 163.7 (C=O), 146.4 (C), 130.1 (C), 129.7 (Ar-CH), 129.5 (Ar-CH), 128.7 (C), 127.7 (Ar-CH), 127.3 (Ar-CH), 125.6 (C), 123.1 (C), 122.7 (C), 66.6 (CH_2), 56.3 (CH_2), 56.1 (CH_2), 54.7 (CH_2), 37.6 (CH_2), 25.9 (CH_2), 24.3 (CH_2); ν_{max} (neat sample)/cm^{-1} 2866, 2717, 1658, 1618, 1347.

Bis-{N-[1-Pyrrolidino-ethyl]}-9,18,-methano-1,8-naphthalimido[b,f][1,5]-diazocine 90

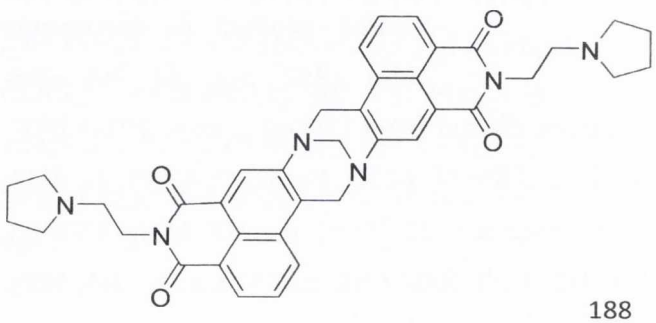

According to Procedure 2 **90** was synthesised by stirring both **106** (630 mg, 2.04 mmol) and paraformaldehyde (67 mg, 2.23 mmol) in TFA (4 mL) to yield **90** as a red solid (359 mg, 54 %) after

dissolving the crude residue in CH_3OH (0.5 mL) and precipitating from diethyl ether (25 mL). m.p. 210-211°C; HRMS: 655.3010 ($[M+H]^+$. $C_{39}H_{38}N_6O_4$ requires 655.3033); δ_H (600 MHz, $CDCl_3$), 8.49 (2H, d, J = 7.3 Hz, H7, H7'), 8.47 (2H, s, H2, H2'), 8.06 (2H, d, J = 8.8 Hz, H5, H5'), 7.76 (2H, *app.* t, H6, H6'), 5.21 (2H, d, J = 17.6 Hz, TB), 4.97 (2H, d, J = 16.9 Hz, TB), 4.61 (2H, s, TB), 4.35 (4H, t, J = 7.3 Hz, $NC\underline{H_2}CH_2N(CH_2)_2(CH_2)_2$), 2.78 (4H, m, $NCH_2C\underline{H_2}N(CH_2)_2(CH_2)_2$), 1.79 (8H, m, $NCH_2CH_2N(C\underline{H_2})_2(C\underline{H_2})_2$); δ_C (150 MHz, $CDCl_3$), 163.9 (C=O), 163.8 (C=O), 146.4 (C), 130.1 (C), 129.7 (Ar-CH), 129.5 (Ar-CH), 128.7 (C), 127.7 (Ar-CH), 127.3 (Ar-CH), 125.6 (C), 123.1 (C), 122.7 (C), 66.6 (CH_2), 56.1 (CH_2), 54.3 (CH_2), 53.6 (CH_2), 39.3 (CH_2), 23.6 (CH_2); ν_{max} (neat sample)/cm^{-1} 2970, 2707, 1695, 1617, 1342.

5.4 General Experimental Techniques For Chapter 3.

5.4.1 Procedure 1: Formation of the 4-Nitro-1,8-Naphthalimide Derivatives[42]

4-nitro-1,8-naphthalic anhydride (1 eq.), the appropriate amino acid (1.4 eq.) and triethylamine (2 eq.) in toluene were stirred at reflux for 24 hours under an argon atmosphere. Upon completion the reaction mixture was immediately filtered while hot through celite, washing several times with toluene. The filtrate and washings were removed under reduced pressure and the residue dissolved in CH_2Cl_2. The organic solution was washed twice with sat. $NaHCO_3$, twice with H_2O and once with 1 M HCl. The organic layer was dried over $MgSO_4$ and evaporated under reduced pressure to dryness. Purification was carried out where necessary.

5.4.2 Procedure 2: Formation of the 3- and 4-Amino-1,8-Naphthalimide Derivatives

The reduction reaction of the relevant 3- or 4-nitro-1,8-naphthalimide in CH_3OH or EtOH was carried out using a Parr hydrogen shaker apparatus at 3 atm pressure, in the presence of 10 % Pd/C catalyst until no more hydrogen gas was consumed. The reaction mixture was filtered through celite, washing with either CH_3OH or EtOH. The filtrate and washings were evaporated under reduced pressure and further dried under vacuum.

5.4.3 Procedure 3: Formation of the Bis-1,8-Naphthalimide Trőger's Base Derivatives Synthesised from the 4-amino-1,8-naphthalimide precursors[148,149]

A mixture of the relevant 4-amino-1,8-naphthalimide (1. eq) and paraformaldehyde (1.5 eq.) in neat TFA were stirred at room temperature overnight. The subsequent work-up depended on the *N*-imide group present. Purification was carried out where necessary.

5.4.4 Procedure 4: Formation of the Bis-1,8-Naphthalimide Trőger's Base Derivatives Synthesised from the 3-amino-1,8-naphthalimide precursors

A mixture of the relevant 3-amino-1,8-naphthalimide (1.0 eq.) and paraformaldehyde (1.1 eq.) in neat TFA were stirred at room temperature for 3 hours under an argon atmosphere. The reaction was then initially neutralised and subsequently basified using 6 M NaOH. The aqueous solution was extracted several times with CH_2Cl_2. The organic extracts were combined and the solvent was removed under reduced pressure. The crude product was purified and dried under vacuum.

5.4.5 Procedure 5: Coupling of amino acid Tröger's Base with second amino acid using the BOP coupling reagent

To a solution containing the Tröger's base (1 eq.) and relevant amino acid (2.1 eq), DIEA (8 eq.) was added at 0 °C. This was followed by the addition of BOP (3 eq.). The reaction mixture was allowed to stir at 0 °C for 30 minutes and then at room temperature overnight. Upon completion of the reaction, ethyl acetate was added and the reaction mixture was washed twice with 1 M HCl, twice with sat. $NaHCO_3$ and once with brine before being dried over $MgSO_4$. The organic layer was removed by evaporation under reduced pressure. Purification was carried out where necessary.

The Tröger's base derivatives synthesised using **Procedures 3** and **5** were in the form of diastereoisomers. As a consequence of the mixtures present, the overlapping of resonances was observed in the ^1H NMR spectra and thus coupling constants were not determined for such resonances.

_N_-[(1_R_)-Benzyloxycarbonyl-ethyl]-4-nitro-1,8-naphthalimide 116

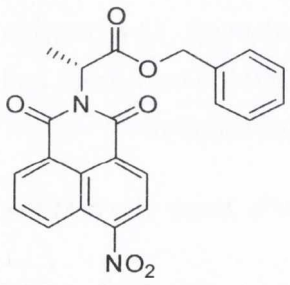

116 was synthesised by reacting *R*-alanine benzyl ester hydrochloride (639 mg, 1.819 mmol) and 4-nitro-1,8-naphthalic anhydride (316 mg,1.230 mmol) in toluene (100 mL) according to **Procedure 1**, to yield the product as a yellow solid (412 mg, 78%). No further purification was necessary. m.p. 88-90 °C; HRMS: 427.0891 ($[M+Na]^+$. $C_{22}H_{16}N_2O_6Na$ requires 427.0906); δ_H ($(CD_3)_2SO$, 600 MHz), 8.75 (1H, d, J = 7.9 Hz, H5), 8.67 (1H, d, J = 7.5 Hz, H7), 8.65 (1H, d, J = 8.1 Hz, H2), 8.58 (1H, d, J = 8.1 Hz, H3), 8.14 (1H, *app. t*, H6), 7.26 (5H, s, $OCH_2\underline{Ph}$), 5.76 (1H, q, J = 6.9 Hz, CH), 5.16 (2H, s, $OC\underline{H_2}Ph$), 1.61 (3H, d, J = 7.0 Hz, CH_3); δ_C ($(CD_3)_2SO$, 150 MHz), 169.9 ($\underline{C}OOCH_2Ph$), 162.8 (C=O), 162.0 (C=O), 149.8 (C), 136.0 (C), 132.6 (Ar-CH),

130.6 (Ar-CH), 130.6 (Ar-CH), 129.7 (Ar-CH), 128.7 (C), 128.6 (Ph), 128.3 (Ph), 128.0 (Ph), 126.3 (C), 124.7 (Ar-CH), 123.1 (C), 122.5 (C), 66.6 (CH_2), 49.4 (CH), 14.5 (CH_3); ν_{max} (neat sample)/cm^{-1} 2958, 1742, 1665, 1530.

_N_-[(1*R*)-*tert*-Butoxycarbonyl-2-ethylphenyl]-4-nitro-1,8-naphthalimide 118

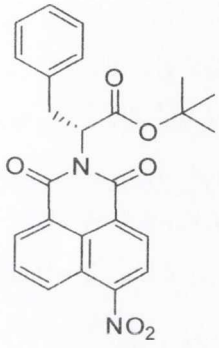

118 was synthesised by refluxing *R*-phenylalanine *tert*-butyl ester hydrochloride (499 mg, 1.934 mmol) with 4-nitro-1,8-naphthalic anhydride (336 mg, 1.381 mmol) and TEA (279 mg, 0.385 mL, 2.762 mmol) according to **Procedure 1** in toluene (100 mL) to yield the product as a yellow solid (402 mg, 65%) after refluxing in CH_3OH in the presence of activated charcoal. m.p. 137-139 °C (ref. [114] 137-139 °C); HRMS: 469.1361 ($[M+Na]^+$. $C_{25}H_{22}N_2O_6Na$ requires 469.1376); δ_H ($CDCl_3$, 600 MHz), 8.84 (1H, d, J = 8.8 Hz, H7), 8.68 (1H, d, J = 6.8 Hz, H5), 8.63 (1H, d, J = 8.0 Hz, H2), 8.39 (1H, d, J = 8.2 Hz, H3), 7.99 (1H, *app.* t, H6), 7.08-7.19 (5H, m, Ph), 5.97 (1H, dd, J = 5.7, 10.2 Hz, CH), 3.68-3.71 (1H, m, C$\underline{H}_2$), 3.49-3.53 (1H, m, C$\underline{H}_2$), 1.48 (9H, s, C(C$\underline{H}_3$)$_3$); δ_C ((CD_3Cl, 150 MHz), 167.9 (C$\underline{O}$OOC(CH_3)$_2$), 162.6 (C=O), 161.8 (C=O), 149.5 (C), 137.2 (C), 132.5 (Ar-CH), 129.8 (Ar-CH), 129.8 (Ar-CH), 129.4 (Ar-CH), 129.3 (C), 128.9 (Ph), 128.4 (Ph), 128.2 (Ph), 126.9 (Ph), 126.4 (Ph), 126.3 (C), 123.7 (Ar-CH), 123.5 (C), 122.4 (C), 82.3 (C), 55.4 (CH), 34.7 (CH_2), 27.8 (CH_3); ν_{max} (neat sample)/cm^{-1} 2978, 2934, 1732, 1670, 1497.

_N_-[(1*R*)-*tert*-Butoxycarbonyl-3-methylbutyl]-4-nitro-1,8-naphthalimide 119

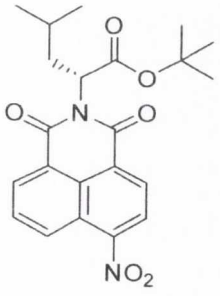

118 was synthesised by refluxing *R*-leucine *tert*-butyl ester hydrochloride (543 mg, 2.427 mmol) with 4-nitro-1,8-naphthalic anhydride (422 mg, 1.735 mmol) and TEA (351 mg, 0.484 mL, 3.470 mmol) according to **Procedure 1** in toluene (100 mL) to yield the product as a brown solid (702 mg, 98%). No further purification was necessary. m.p. 266-267 °C; HRMS: 435.1526 ($[M+Na]^+$. $C_{22}H_{24}N_2O_6Na$ requires 435.1532); δ_H ($CDCl_3$, 600 MHz), 8.88 (1H, d, J = 8.6 Hz, H7), 8.78 (1H, d, J = 7.2 Hz, H5), 8.73 (1H, d, J = 6.0 Hz, H2), 8.44 (1H, d, J = 6.0 Hz, H3), 8.04 (1H, *app.* t, H6), 5.69 (1H, dd, J = 5.0, 9.2 Hz, CH), 2.19-2.24 (1H, m, CH_2), 2.07-2.12 (1H, m, CH_2), 1.53-1.59 (1H, m, C$\underline{H}$(CH_3)$_2$) 1.44 (9H, m, C(C$\underline{H}_3$)$_3$), 1.03 (3H, d, J = 6.0 Hz, CH(C$\underline{H}_3$)$_2$), 0.95 (3H, d, J = 6.0 Hz, CH(C$\underline{H}_3$)$_2$); δ_C ((CD_3Cl, 150 MHz), 168.8 (C$\underline{O}$OOC(CH_3)$_2$), 163.0 (C=O), 162.2 (C=O), 149.7 (C), 132.7 (Ar-CH), 130.1 (Ar-CH), 130.0 (Ar-CH), 129.5 (Ar-CH), 129.2 (C), 126.8 (C), 123.9 (Ar-CH),

123.7 (C), 122.8 (C), 82.0 (C), 53.3 (CH), 38.0 (CH_2), 27.9 (CH_3), 25.6 (CH), 23.1 (CH_3), 22.0 (CH_3); ν_{max} (neat sample)/cm^{-1} 3030, 1735, 1668, 1527.

_N_-[*(1R)*-Carboxy-ethyl)-4-amino-1,8-naphthalimide 120

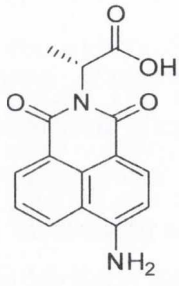

120 was synthesised from **116** (121 mg, 0.299 mmol) and 10% Pd/C in CH_3OH according to **Procedure 2**, to yield the product as an orange solid (66 mg, 78%). No further purification was necessary. Decomposed at 305-307 °C; HRMS: 283.0724 ([M-H]$^-$. $C_{15}H_{11}N_2O_4$ requires 283.0719); δ_H ($(CD_3)2SO$, 600 MHz), 8.66 (1H, d, J = 8.6 Hz, H5), 8.45 (1H, d, J = 7.5, H7), 8.21 (1H, d, J = 8.3, H2), 7.69 (1H, *app.* t, H6), 7.52 (2H, br. s, NH_2), 6.88 (1H, d, J = 8.3, H3), 5.55 (1H, q, J = 6.8 Hz, CH), 1.50 (3H, d, J = 6.8, CH_3); δ_C ($(CD_3)_2SO$, 150 MHz), 172.1 (COOH), 163.6 (C=O), 162.7 (C=O), 153.4 (C), 134.6 (Ar-CH), 131.6 (Ar-CH), 130.1 (C), 129.9 (Ar-CH), 124.4 (Ar-CH), 121.9 (C), 119.7 (C), 108.6 (Ar-CH), 107.5 (C), 48.3 (CH), 15.0 (CH_3); ν_{max} (neat sample)/cm^{-1} 3438, 3363, 3262, 1653, 1308.

_N_-[*(1R)*-Carboxy-3-methyl)-4-amino-1,8-naphthalimide 121

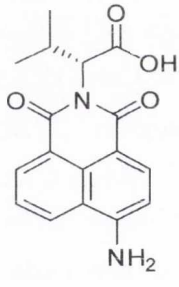

121 was synthesised from **117** (397 mg, 0.918 mmol) and 10% Pd/C in CH_3OH according to **Procedure 2**. The crude product was purified by refluxing in CH_3OH in the presence of charcoal. The resulting solution was filtered through celite, washing with CH_3OH. The filtrate and washings were evaporated under reduced pressure and further dried under vacuum to yield the product as an orange solid (281 mg, 98%). m.p. 277-279 °C; HRMS: 311.1044 ([M-H]$^-$. $C_{17}H_{15}N_2O_4$ requires 311.1032); δ_H ($(CD_3)_2SO$, 600 MHz), 8.65 (1H, d, J = 9.9 Hz, H5), 8.46 (1H, d, J = 8.3 Hz, H7), 8.21 (1H, d, J = 8.3 Hz, H2), 7.69 (1H, *app.* t, H5), 7.53 (2H, s, NH_2), 6.89 (1H, d, J = 8.3 Hz, H3), 5.12 (1H, d, J = 8.8 Hz, CH), 2.66 (1H, m, C<u>H</u>$(CH_3)_2$), 1.19 (3H, d, J = 6.6 Hz, CH(C<u>H</u>$_3)_2$), 0.65 (3H, d, J = 6.6 Hz, CH(C<u>H</u>$_3)_2$; δ_C ($(CD_3)_2SO$, 150 MHz), 171.5 (COOH), 164.1 (C=O), 163.1 (C=O), 153.5 (C), 134.8 (Ar-CH), 131.9 (Ar-CH), 130.2 (C), 130.1 (Ar-CH), 124.6 (Ar-CH), 121.5 (C), 119.6 (C), 108.7 (Ar-CH), 107.1 (C), 57.8 (CH), 27.1 (CH), 22.5 (CH_3), 19.2 (CH_3); ν_{max} (neat sample)/cm^{-1} 3360, 1630, 1717, 1479, 1306.

_N_-[(1*R*)-*tert*-Butoxycarbonyl-3-methylbutyl]-4-amino-1,8-naphthalimide 123

123 was synthesised from **119** (628 mg, 1.523 mmol) and 10% Pd/C in CH_3OH according to **Procedure 2**. The crude product was purified by refluxing in CH_3OH in the presence of charcoal. The resulting solution was filtered through celite, washing with CH_3OH. The filtrate

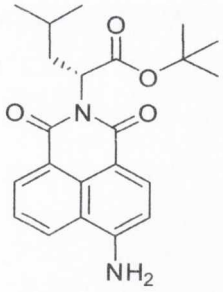

and washings were evaporated under reduced pressure and further dried under vacuum to yield the product as a brown solid (578 mg, 94%). HRMS: 381.1820 ([M-H)$^-$. $C_{22}H_{25}N_2O_4$ requires 381.1814); δ_H ($(CD_3)_2SO$, 600 MHz), 8.67 (1H, d, J = 8.3 Hz, H5), 8.47 (1H, d, J = 7.2 Hz, H7), 8.23 (1H, d, J = 8.4 Hz, H2), 7.70 (1H, *app.* t, H6), 7.55 (2H, br. s, NH_2), 6.88 (1H, d, J = 8.4 Hz, H3), 5.55 (1H, dd, J = 5.5, 8.4 Hz, CH), 1.94-2.00 (2H, m, CH_2), 1.36-1.43 (1H, m, $\underline{CH}(CH_3)_2$), 1.32 (9H, s, $C(\underline{CH_3})_3$), 0.93 (3H, d, J = 6.5 Hz, $CH(\underline{CH_3})_2$), 0.85 (3H, d, J = 6.5 Hz, $CH(\underline{CH_3})_2$); δ_C ($(CD_3)_2SO$, 150 MHz), 169.5 ($\underline{CO}OC(CH_3)_3$), 164.0 (C=O), 163.0 (C=O), 153.4 (C), 134.7 (Ar-CH), 131.8 (Ar-CH), 130.1 (C), 130.0 (Ar-CH), 124.5 (Ar-CH), 121.6 (C), 119.6 (C), 108.7 (Ar-CH), 107.2 (C), 80.9 (C), 51.9 (CH), 38.1 (CH_2), 27.9 (CH_3), 27.8 (CH), 23.5 (CH_3), 22.5 (CH_3); ν_{max} (neat sample)/ cm^{-1} 3358, 3250, 2932, 1728, 1685, 1636, 1463, 1367.

_N_-[(1*R*)-Carboxy-2-ethylphenyl]-4-amino-1,8-naphthalimide 123

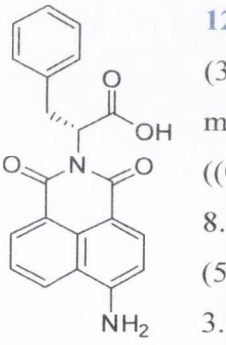

123 was prepared using **121** (480 mg, 1.153 mmol), TFA (1 mL) and CH_2Cl_2 (3 mL) according to **Procedure 2**, to yield the product as an orange solid (407 mg, 98%). HRMS: 383.1027 ($[M-Na)^+$. $C_{21}H_{16}N_2O_4Na$ requires 383.1008); δ_H ($(CD_3)_2SO$, 600 MHz), 8.62 (1H, d, J = 8.3 Hz, H5), 8.37 (1H, d, J = 6.8, H7), 8.13 (1H, d, J = 8.3, H2), 7.63 (1H, *app.* t, H6), 7.49 (2H, br. s, NH_2), 7.11 (5H, m, Ph), 6.83 (1H, d, J = 8.3, H3), 5.87 (1H, dd, J = 5.3, 10.0 Hz, CH), 3.50 (1H, m, CH_2), 3.38 (1H, m, CH_2); δ_C ($(CD_3)_2SO$, 150 MHz), 171.8 (COOH), 163.5 (C=O) 162.5 (C=O), 153.0 (C), 138.2 (Ar-CH), 134.2 (Ar-CH), 131.3 (Ar-CH), 129.7 (Ar-CH), 129.6 (C), 129.0 (Ph), 128 (Ph), 126.1 (Ph), 124.1 (Ar-CH), 121.3 (C), 119.3 (C), 108.3 (Ar-CH), 106.9 (C), 53.3 (CH), 34.4 (CH_2); ν_{max} (neat sample)/cm^{-1} 3363, 2500, 1497, 1631, 1246.

_N_-[*(1R)*-Carboxy-3-methylbutyl]-4-amino-1,8-naphthalimide 125

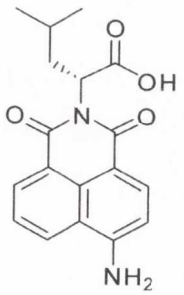

125 was synthesised by stirring *N*-[*(1R)-tert*-butoxycarbonyl-3-methylbutyl]-4-amino-1,8-naphthalimide **123** (519 mg, 1.357 mmol) in TFA:CH_2Cl_2 (1:3) for 3 hours. The resulting solution was reduced to dryness under vacuum to yield the product as an orange solid (362 mg, 82%). m.p. 156-157 °C; HRMS: 325.1181 ([M-H)$^-$. $C_{18}H_{17}N_2O_4$ requires 325.1188); δ_H ($(CD_3)_2SO$, 400 MHz), 8.67 (1H, d, J = 8.3 Hz, H5), 8.47 (1H, d, J = 8.3 Hz, H7), 8.23 (1H, d, J = 8.4 Hz, H2), 7.70 (1H, *app.* t, H6), 7.55 (2H, br. s, NH_2), 6.88 (1H, d, J = 8.4 Hz, H3), 5.55 (1H, dd, J = 5.5, 8.4 Hz, CH), 2.00 (2H, m, CH_2), 1.41-1.47 (1H, m, $\underline{CH}(CH_3)_2$), 1.32 (9H, s,

C($\underline{CH_3}$)$_3$), 0.93 (3H, d, J = 6.5 Hz, CH($\underline{CH_3}$)$_2$), 0.85 (3H, d, J = 6.5 Hz, CH($\underline{CH_3}$)$_2$)); δ_C ((CD$_3$)$_2$SO, 150 MHz) 171.8 (COOH), 163.6 (C=O), 162.7 (C=O), 153.1 (C), 134.4 (Ar-CH), 131.5 (Ar-CH), 129.9 (C), 129.7 (Ar-CH), 124.1 (Ar-CH), 121.4 (C), 119.3 (C), 108.4 (Ar-CH), 107.0 (C), 50.8 (CH), 37.7 (CH$_2$), 25.0 (CH), 23.1 (CH$_3$), 22.0 (CH$_3$); ν_{max} (neat sample)/cm^{-1} 3366, 3251, 2923, 1630, 1463, 1371.

_N_-(1-Carboxy-methyl)-4-amino-1,8-naphthalimide 126

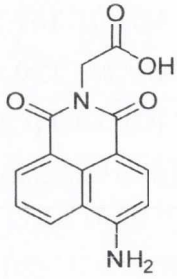

126 was synthesised from _N_-(benzyloxycarbonyl-methyl)-4-nitro-1,8-naphthalimide (293 mg, 0.751 mmol) and 10% Pd/C in CH$_3$OH under 3 atm of pressure according to **Procedure 2**, to yield the product as an orange powder (193 mg, 95%). No further purification was necessary. Decomposed at 308-310 °C; HRMS: 269.0558 ([M-H]$^-$. $C_{14}H_9N_2O_4$ requires 269.0562); δ_H ((CD$_3$)$_2$SO, 600 MHz), 8.67 (1H, d, J = 7.9 Hz, H5), 8.46 (1H, d, J = 6.4, H7), 8.22 (1H, d, J = 8.3, H2), 7.70 (1H, *app*. t, H6), 7.51 (2H, br. s, NH$_2$), 6.88 (1H, d, J = 8.3, H3), 4.66 (2H, s, CH$_2$); δ_C ((CD$_3$)$_2$SO, 150 MHz), 169.8 (COOH), 163.6 (C=O) 162.6 (C=O), 153.1 (C), 134.2 (Ar-CH), 131.3 (Ar-CH), 129.9 (Ar-CH), 129.7 (C), 124.1 (Ar-CH), 121.5 (C), 119.4 (C), 108.3 (Ar-CH), 107.1 (C), 41.1 (CH$_2$): ν_{max} (neat sample)/cm^{-1} 3364, 3259, 1637, 1571, 1376.

_N_-[*(1S)*-Carboxy-ethyl)-4-amino-1,8-naphthalimide 127

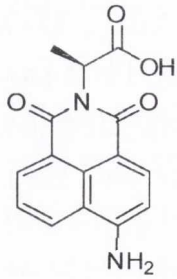

127 was synthesised from _N_-[*(1S)*-Benzyloxycarbonyl-ethyl)-4-nitro-1,8-naphthalimide (110 mg, 0.273 mmol) and 10% Pd/C in CH$_3$OH under 3 atm of pressure according to **Procedure 2**, to yield the product as an orange solid (75 mg, 97%). No further purification was necessary. Decomposed at 305-307 °C; HRMS: 283.0719 ([M-H)$^-$. $C_{15}H_{11}N_2O_4$ requires 283.0719); δ_H ((CD$_3$)2SO, 600 MHz), 8.66 (1H, d, J = 8.6 Hz, H5), 8.45 (1H, d, J = 7.5, H7), 8.21 (1H, d, J = 8.3, H2), 7.69 (1H, *app*. t, H6), 7.52 (2H, br. s, NH$_2$), 6.88 (1H, d, J = 8.3, H3), 5.55 (1H, q, J = 6.8 Hz, CH), 1.50 (3H, d, J = 6.8, CH$_3$); δ_C ((CD$_3$)$_2$SO, 150 MHz), 172.1 (COOH), 163.6 (C=O), 162.7 (C=O), 153.4 (C), 134.6 (Ar-CH), 131.6 (Ar-CH), 130.1 (C), 129.9 (Ar-CH), 124.4 (Ar-CH), 121.9 (C), 119.7 (C), 108.6 (Ar-CH), 107.5 (C), 48.3 (CH), 15.0 (CH$_3$): ν_{max} (neat sample)/cm^{-1} 3438, 3362, 3262, 1653, 1479, 1308.

_N_-[*(1S)*-Carboxy-ethylphenyl)-4-amino-1,8-naphthalimide 128

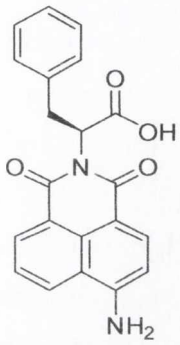

128 was synthesised from _N_-[*(1S)*-carboxy-2-ethylphenyl)-4-nitro-1,8-naphthalimide (405 mg, 1.040 mmol) and 10% Pd/C in MeOH under 3 atm of pressure according to **Procedure 2**, to yield the product as a yellow solid after refluxing in CH_3OH in the presence of activated charcoal (309 mg, 82%). HRMS: 383.1130 ($[M+Na]^+$. $C_{21}H_{16}N_2O_4Na$ requires 383.1134); δ_H ($(CD_3)_2SO$, 600 MHz), 8.62 (1H, d, J = 8.3 Hz, H5), 8.37 (1H, d, J = 6.8, H7), 8.13 (1H, d, J = 8.3, H2), 7.63 (1H, *app.* t, H6), 7.49 (2H, br. s, NH_2), 7.04-7.11 (5H, m, Ph), 6.83 (1H, d, J = 8.3, H3), 5.87 (1H, dd, J = 5.3, 10.0 Hz, CH), 3.50-3.53 (1H, m, CH_2), 3.38 (1H, m, CH_2); δ_C ($(CD_3)_2SO$, 150 MHz), 171.8 (COOH), 163.5 (C=O) 162.5 (C=O), 153.0 (C), 138.2 (Ar-CH), 134.2 (Ar-CH), 131.3 (Ar-CH), 129.7 (Ar-CH), 129.6 (C), 129.0 (Ph), 128 (Ph), 126.1 (Ph), 124.1 (Ar-CH), 121.3 (C), 119.3 (C), 108.3 (Ar-CH), 106.9 (C), 53.3 (CH), 34.4 (CH_2); ν_{max} (neat sample)/cm^{-1} 3363, 2500, 1497, 1631,1246.

_N_-[*(1S)*-Carboxy-3-methylbutyl]-4-amino-1,8-naphthalimide 129

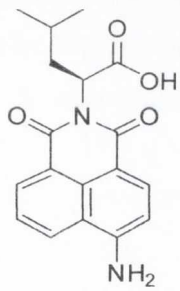

129 was synthesised from _N_-[*(1S)*-carboxy-3-methylbutyl)-4-nitro-1,8-naphthalimide (606 mg, 0.863 mmol) and 10% Pd/C in CH_3OH under 3 atm of pressure according to **Procedure 2**, to yield the product as an orange solid after refluxing in CH_3OH in the presence of activated charcoal (484 mg, 87%). m.p. 266-267 °C (Ref.[114] 266-267 °C); HRMS: 349.1155 ($[M+Na]^+$. $C_{18}H_{18}N_2O_4Na$ requires 349.1164); δ_H ($(CD_3)_2SO$, 600 MHz) 8.66 (1H, d, J = 8.2 Hz, H5), 8.45 (1H, d, J = 7.2 Hz, H7), 8.22 (1H, d, J = 8.5 Hz, H2), 7.69 (1H, *app.* t, H6), 7.54 (2H,br. s, NH_2), 6.88 (1H, d, J = 8.5 Hz, H3), 5.62 (1H, t, J = 7.1 Hz, CH), 2.03 (2H, *app.* t, CH_2), 1.44 (1H, m, $\underline{CH}(CH_3)_2$), 0.92 (3H, d, J = 6.6 Hz, $CH(\underline{CH_3})_2$), 0.84 (3H, d, J = 6.6 Hz, $CH(\underline{CH_3})_2$): δ_C ($(CD_3)_2SO$, 150 MHz) 171.8 (COOH), 163.6 (C=O), 162.7 (C=O), 153.1 (C), 134.4 (Ar-CH), 131.5 (Ar-CH), 129.9 (C), 129.7 (Ar-CH), 124.1 (Ar-CH), 121.4 (C), 119.3 (C), 108.4 (Ar-CH), 107.0 (C), 50.8 (CH), 37.7 (CH_2), 25.0 (CH), 23.1 (CH_3), 22.0 (CH_3); ν_{max} (neat sample)/cm^{-1} 3360, 3248, 2955, 1684, 1631, 1466, 1367.

_N_-[*(1S)*-Carboxy-3-methyl)-4-amino-1,8-naphthalimide 130

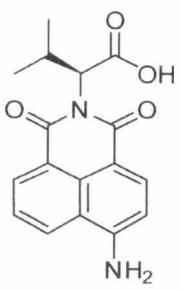

130 was synthesised from _N_-[*(1S)-tert*-butoxycarbonyl-3-methyl)-4-nitro-1,8-naphthalimide (344 mg, 1.701 mmol) and 10% Pd/C in CH_3OH under 3 atm of pressure according to **Procedure 2**. The crude product was dissolved in CH_3OH and refluxed in the presence of activated charcoal. The reaction

mixture was filtered through celite and washed with CH_3OH. The filtrate and washings were evaporated under reduced pressure and further dried under vacuum. The crude product was dissolved in TFA:CH_2Cl_2 (1:3) and stirred at room temperature for 3 hrs. The resulting solution was reduced to dryness under reduced pressure to yield the product as an orange solid (265 mg, 98%). No further purification was necessary. m.p. 277-279 °C; HRMS: 335.1006 ($[M+Na]^+$. $C_{17}H_{16}N_2O_4Na$ requires 335.1008); δ_H ($(CD_3)_2SO$, 600 MHz), 8.67 (1H, d, J = 7.6 Hz, H5), 8.46 (1H, d, J = 6.8 Hz, H7), 8.22 (1H, d, J = 8.4 Hz, H2), 7.70 (1H, *app.* t, H5), 7.55 (2H, s, NH_2), 6.88 (1H, d, J = 8.4 Hz, H3), 5.14 (1H, d, J = 9.4 Hz, CH), 2.62-2.70 (1H, m, C<u>H</u>$(CH_3)_2$), 1.21 (3H, d, J = 6.6 Hz, CH(C<u>H</u>$_3)_2$), 0.67 (3H, d, J = 6.6 Hz, CH(C<u>H</u>$_3)_2$; δ_C ($(CD_3)_2SO$, 150 MHz), 171.1 (COOH), 163.8 (C=O), 162.8 (C=O), 153.2 (C), 134.5 (Ar-CH), 131.6 (Ar-CH), 129.9 (C), 129.8 (Ar-CH), 124.2 (Ar-CH), 121.3 (C), 119.7 (C), 108.4 (Ar-CH), 106.8 (C), 57.5 (CH), 26.9 (CH), 22.3 (CH_3), 19.0 (CH_3); ν_{max} (neat sample)/cm^{-1} 3356, 3248, 2977, 1718, 1625, 1717, 1479, 1374, 1308.

N-[*(1S)*-Methoxycarbonyl-3-methylbutyl]-4-amino-1,8-naphthalimide 131

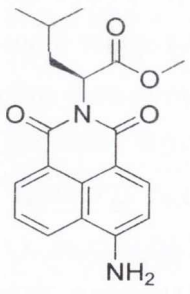

131 was synthesised using *N*-[*(1S)*-methoxycarbonyl-3-methylbutyl]-4-nitro-1,8-naphthalimide (601 mg, 1.623 mmol) in EtOH according to **Procedure 2** and was yielded as an orange solid (541 mg, 98%). No further purification was necessary. m.p. 110-112 °C (Ref.[114] 110-112 °C); (HRMS: 363.1337 ($[M+Na)^+$. $C_{19}H_{20}N_2O_4Na$ requires 363.1321); δ_H ($(CD_3)_2SO$, 600 MHz), 8.66 (1H, d, J = 8.3 Hz, H5), 8.46 (1H, d, J = 7.2 Hz, H7), 8.21 (1H, d, J = 8.4 Hz, H2), 7.69 (1H, *app.* t, H6), 7.67 (2H, br. s, NH_2), 6.88 (1H, d, J = 8.4 Hz, H3), 5.66 (1H, dd, J = 5.0, 9.1 Hz, CH), 3.58 (3H, s, OCH_3), 1.96 (2H, m, CH_2), 1.45 (1H, m, C<u>H</u>$(CH_3)_2$), 0.92 (3H, d, J = 6.5 Hz, CH(C<u>H</u>$_3)_2$), 0.84 (3H, d, J = 6.5 Hz, CH(C<u>H</u>$_3)_2$); δ_C ($(CD_3)_2SO$, 150 MHz), 170.9 ($COOCH_3$), 163.7 (C=O), 162.7 (C=O), 153.4 (C), 134.7 (Ar-CH), 131.8 (Ar-CH), 130.0 (C), 129.9 (Ar-CH), 124.3 (Ar-CH), 121.3 (C), 119.4 (C), 108.6 (Ar-CH), 106.8 (C), 52.2 (OCH_3), 50.8 (CH), 37.8 (CH_2), 24.9 (CH), 23.1 (CH_3), 22.1 (CH_3); ν_{max} (neat sample)/cm^{-1} 3362, 3252, 2954, 1731, 1685, 1632, 1462, 1367.

***N*-[*(1S)*-Methoxycarbonyl -ethylphenyl)-4-amino-1,8-naphthalimide 132**

132 was synthesised from *N*-[*(1S)*- methoxycarbonyl-ethylphenyl)-4-nitro-1,8-naphthalimide (516 mg, 1.276 mmol) and 10% Pd/C in EtOH under 3 atm of pressure according to **Procedure 2**, to yield the product as an brown powder (473 mg, 99%). No further purification was necessary. m.p. 117-118 °C (Ref.[114] 117-118 °C); HRMS: 397.1161 ($[M+Na)^+$. $C_{22}H_{18}N_2O_4Na$ requires 397.1164); δ_H ($(CD_3)_2SO$, 600 MHz), 8.63 (1H, d, J = 8.0 Hz, H5),

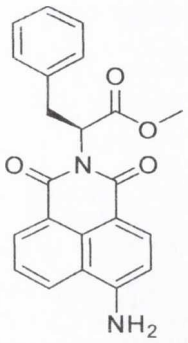

8.36 (1H, d, J = 8.0 Hz, H7), 8.12 (1H, d, J = 8.1 Hz, H2), 7.65 (1H, *app.* t, H6), 7.51 (2H, s, NH_2), 7.05-7.13 (5H, m, Ph), 6.83 (1H, d, J = 8.1 Hz, H3), 5.96 (1H, dd, J = 6.0, 10.0 Hz, CH), 3.64 (3H, s, OCH_3), 3.56 (1H, dd, J = 6.0, 14.0 Hz, C$\underline{H}_2$), 3.36 (1H, dd, J = 10.0, 14.0 Hz, C$\underline{H}_2$); δ_C ($(CD_3)_2SO$, 150 MHz), 170.6 ($\underline{C}OOCH_3$), 163.8 (C=O), 163.5 (C=O), 153.5 (C), 138.0 (C), 134.7 (Ar-CH), 131.8 (Ar-CH), 130.2 (Ar-CH), 130.2 (C), 128.9 (Ph), 128.1 (Ph), 126.7 (Ph), 124.4 (Ar-CH), 121.4 (C), 119.0 (C), 108.6 (Ar-CH), 106.9 (C), 53.5 (CH), 52.4 (CH_3), 34.6 (CH_2); ν_{max} (neat sample)/cm^{-1} 3359, 3247, 1739, 1631, 1572, 1526, 1479, 1368, 1305.

_N_-[(1*S*)-[(2*S*)-Methyl-3-phenylpropanamido-3-phenylpropanoate]-4-nitro-1,8-naphthalimide 137[114]

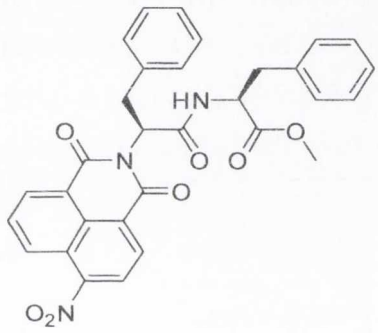

137 was synthesised by stirring (*S*)-phenylalanine methyl ester hydrochloride (306 mg, 1.420 mmol), HOBt (174 mg, 1.291 mmol), TEA (143 mg, 0.197 mL, 1.420 mmol), *N*-[*(1S)*-carboxy-ethylphenyl)-4-nitro-1,8-naphthalimide (504 mg, 1.291 mmol) in THF (50 mL) at -10°C before EDCI.HCl (272 mg, 1.420 mmol) was added. The reaction mixture was left to stir at -10 °C for 30 mins and at room temperature overnight. The reaction mixture was filtered through celite and the solvent was removed under reduced pressure. The resulting residue was re-dissolved in CH_2Cl_2 and washed twice with 1 M HCl, sat. $NaHCO_3$ and once with H_2O. The organic layer was dried over MgSO4 and reduced to dryness under vacuum to yield the product as a yellow solid (674 mg, 95%). No further purification was necessary. m.p 90-92°C (Ref[114] 90-92 °C); HRMS: 574.1595 ($[M+Na]^+$. $C_{31}H_{25}N_3O_7Na$ requires 574.1590); δ_H ($CDCl_3$, 600 MHz), 8.87 (1H, d, J = 8.7 Hz, H5), 8.68 (1H, d, J = 7.1 Hz, H7), 8.62 (1H, d, J = 8.0 Hz, H2), 8.41 (1H, d, J = 8.0 Hz, H3), 8.01 (1H, *app.* t, H6), 7.22 (10H, m, Ph), 6.24 (1H, d, J = 6.8 Hz, NH), 6.02 (1H, m, N$\underline{C}$HCH_2Ph), 4.95 (1H, m, $\underline{C}$HCOOCH_3), 3.76 (3H, d, J = 2.8 Hz, OCH_3), 3.70 (1H, m, NCH$\underline{CH_2}$Ph), 3.56 (1H, m, NCH$\underline{CH_2}$Ph), 3.16 (1H, m, NHCH$\underline{CH_2}$Ph), 3.07 (1H, m, NHCH$\underline{CH_2}$Ph); δ_C ($CDCl_3$, 150 MHz), 171.7 ($COOCH_3$), 168.0 (CONH), 163.0 (C=O), 162.1 (C=O), 149.7 (C), 136.7 (C), 135.6 (C), 132.8 (Ar-CH), 130.2 (Ar-CH), 129.9 (Ar-CH), 129.6 (Ar-CH), 129.1 (Ar-CH), 129.0 (Ph), 128.7 (Ph), 128.3 (Ph), 127.0 (Ph), 126.8 (Ph), 126.4 (C), 123.8 (Ph), 123.6 (C), 122.4 (C), 55.9 (CH), 53.4 (OCH_3), 52.4 (CH), 37.7 (CH_2), 34.6 (CH_2); ν_{max} (neat sample)/ cm^{-1} 3372, 2947, 1735, 1711, 1666, 1584, 1526, 1455, 1340.

_N_-[(1_S_)-[(2_S_)-Methyl-3-phenylpropanamido-3-phenylpropanoate]-4-amino-1,8-naphthalimide 138

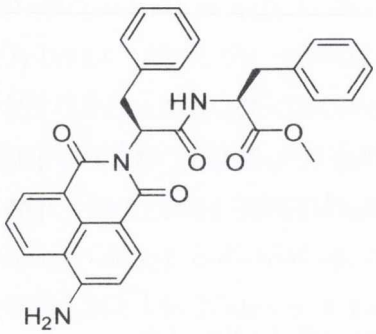

138 was synthesised from **137** (420 mg, 0.763 mmol) and 10% Pd/C in CH_3OH under 3 atm of pressure according to **Procedure 2**, to yield the product as an orange solid (381 mg, 96%). No further purification was necessary. m.p. 191-193 °C; HRMS: 544.1853 ($[M+Na)^+$. $C_{31}H_{27}N_3O_5Na$ requires 544.1848); δ_H ($CDCl_3$, 600 MHz), 8.56 (1H, d, J = 8.1 Hz, H5), 8.30 (1H, d, J = 7.2 Hz, H7), 8.24 (1H, d, J = 7.4 Hz, NH), 8.08 (1H, d, J = 8.1 Hz, H2), 7.64 (1H, *app*. t, H6), 7.35 (2H, s, NH_2), 7.00-7.12 (10H, m, Ph), 6.84 (1H, d, J = 8.3 Hz, H3), 5.73 (1H, dd, J = 5.3, 10.0 Hz, NC<u>H</u>CH_2Ph), 4.45 (1H, q, J = 7.3 Hz, NHC<u>H</u>), 3.64 (3H, s, OCH_3), 3.23-3.27 (2H, m, NCHC<u>H</u>$_2$Ph), 2.85-2.87 (2H, m, NCHC<u>H</u>$_2$Ph); δ_C ($CDCl_3$, 150 MHz), 172.6 (<u>C</u>$OOCH_3$), 169.8 NHCO, 164.2 (C=O), 163.2 (C=O), 152.9 (C), 138.5 (C), 137.7 (C), 134.4 (Ar-CH), 131.5 (Ar-CH), 130.2 (C), 129.5 (Ar-CH), 129.4 (Ph), 129.2 (Ph), 128.5 (Ph), 128.3 (Ph), 126.7 (Ph), 126.5 (Ph), 124.4 (Ar-CH), 122.3 (C), 119.6 (C), 108.4 (Ar-CH), 108.2 (C), 54.6 (CH), 54.5 (CH), 52.3 (OCH_3), 36.4 (CH_2), 34.3 (CH_2); ν_{max} (neat sample)/cm^{-1} 3358, 1745, 1631, 1576, 1454, 1368, 1306.

_N_-[*1S*-[*(2S)*-4-Methyl-pentanoic acid methyl ester]carboxamido-ethyl]-4-amino-1,8-naphthalimide 139

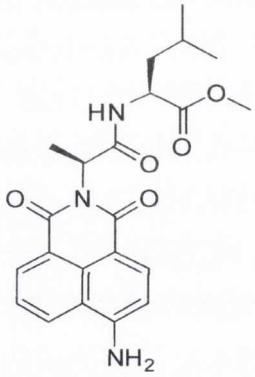

139 was synthesised using _N_-[*1S*-[*(2S)*-4-methyl-pentanoic acid methyl ester]carboxamido-ethyl]-4-nitro-1,8-naphthalimide (245 mg, 0.555 mmol) in EtOH according to **Procedure 2** and was yielded as a light brown solid (228 mg, 100%). m.p. 231-232 °C; HRMS: 434.1711 ($[M+Na)^+$. $C_{22}H_{25}N_3O_5Na$ requires 434.1692); δ_H ($(CD_3)_2SO$, 600 MHz), 8.58 (1H, d, J = 8.3Hz, H5), 8.40 (1H, d, J = 7.3 Hz, H7), 8.17 (1H, d, J = 7.0 Hz, NH), 8.16 (1H, d, J = 8.5 Hz, H2), 7.67 (1H, *app*.t, H6), 7.37 (2H, br. s, NH_2), 6.84 (1H, d, J = 8.5 Hz, H3), 5.42 (1H, q, J = 6.8 Hz, C<u>H</u>CH_3), 4.28 (1H, m, NHC<u>H</u>$CH_2CH(CH_3)_2$), 3.67 (3H, s, OC<u>H</u>$_3$), 2.54 (2H, m, NHCHC<u>H</u>$_2$$CH(CH_3)_2$), 1.46 (1H, m, $NHCHCH_2C$<u>H</u>$(CH_3)_2$), 1.43 (3H, d, J = 6.8 Hz, CHC<u>H</u>$_3$), 0.78 (3H, d, J = 6.4 Hz, $NHCHCH_2CH(C$<u>H</u>$_3)_2$), 0.68 (3H, d, J = 6.4 Hz, $NHCHCH_2CH(C$<u>H</u>$_3)_2$); δ_C ($(CD_3)_2SO$, 150 MHz), 174.0 ($COOCH_3$), 170.5 (CONH), 164.1 (C=O), 163.2 (C=O), 153.0 (C), 134.2 (Ar-CH), 131.4 (Ar-CH), 130.3 (C), 129.5 (Ar-CH),

124.6 (Ar-CH), 122.8 (C), 119.8 (C), 108.6 (C) 108.5 (Ar-CH), 52.3 (OCH_3), 51.0 (CH), 49.2 (CH), 33.7 (CH_2), 24.2 (CH), 23.2 (CH_3), 21.3 (CH_3), 14.8 (CH_3); ν_{max} (neat sample)/cm^{-1} 3331, 2953, 1730, 1629, 1575, 1462, 1367.

_N_-[*1S*-[*(2S)*-Propionic acid methyl ester]carboxamido-3-methylbutyl]-4-amino-1,8-naphthalimide 140

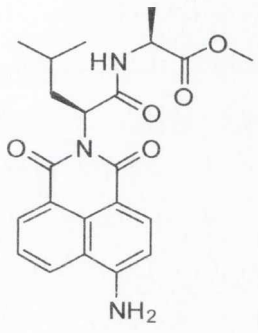

140 was synthesised using _N_-[*1S*-[*(2S)*-propionic acid methyl ester]carboxamido-3-methylbutyl]-4-nitro-1,8-naphthalimide (127 mg, 0.288 mmol) in EtOH according to **Procedure 2** and was yielded as a light brown solid (116 mg, 98%). m.p. 226-227°C (Ref.[114] 226 -227 °C); HRMS: 434.1697 ($[M+Na]^+$. $C_{22}H_{25}N_3O_5Na$ requires 434.1692); δ_H ($(CD_3)_2SO$, 600 MHz), 8.61 (1H, d, J = 8.0 Hz, H5), 8.43 (1H, d, J = 7.20 Hz, H7), 8.19 (1H, d, J = 8.4 Hz, H2), 8.15 (1H, d, J = 7.0 Hz, NH), 7.67 (1H, *app.* t, H6), 7.41 (2H, br. s, NH_2), 6.87 (1H, d, J = 8.40, H3), 5.48 (1H, dd, J = 4.6, 9.6 Hz, CH), 4.33 (1H, m, $NHC\underline{H}CH_3COOCH_3$), 3.62 (3H, s, $NHCHCH_3COOC\underline{H_3}$), 2.08 (1H, m, $NCHC\underline{H_2}CH(CH_3)_2$), 1.94 (1H, m, $NCHC\underline{H_2}CH(CH_3)_2$), 1.33 (1H, m, $NCHCH_2C\underline{H}(CH_3)_2$), 1.13 (3H, d, J = 7.3 Hz, $NHCHC\underline{H_3}COOCH_3$), 0.89 (3H, d, J = 6.7 Hz, $NCHCH_2CH(\underline{CH_3})_2$), 0.80 (3H, d, J = 6.7 Hz, $NCHCH_2CH(\underline{CH_3})_2$); δ_C ($(CD_3)_2SO$, 150 MHz), 173.6 ($COOCH_3$), 170.0 (CONH), 164.4 (C=O), 163.5 (C=O), 152.9 (C), 134.3 (Ar-CH), 131.4 (Ar-CH), 130.3 (C), 129.4 (Ar-CH), 124.4 (Ar-CH), 122.6 (C), 119.6 (C), 108.4 (Ar-CH), 108.3 (C), 52.1 (OCH_3), 51.9 (CH), 48.1 (CH), 37.5 (CH_2), 25.1 (CH_3), 23.5 (CH_3), 22.2 (CH_3), 17.0 (CH_3): ν_{max} (neat sample)/cm^{-1} 3354, 3330, 2954, 2849, 1730, 1690, 1651, 1576, 1364, 1341.

_N_-(*1*-Methoxycarbonyl-methyl)-4-amino-1,8-naphthalimide 141

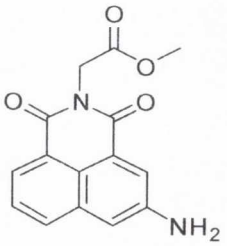

141 was synthesised using N-(*1*-methoxycarbonyl-methyl)-3-nitro-1,8-naphthalic anhydride (302 mg, 0.961 mmol) in EtOH according to **Procedure 2** and was yielded as an orange solid (268 mg, 98%). m.p. 229-230°C (Ref.[114] 229-230 °C); HRMS: 307.0695 ($[M+Na]^+$. $C_{15}H_{12}N_2O_4Na$ requires 307.0695); δ_H ($(CD_3)_2SO$, 400 MHz), 8.11 (1H, d, J = 7.5 Hz, H5), 8.10 (1H, d, J = 9.6 Hz, H7), 7.80 (1H, d, J = 2.0 Hz, H2), 7.67 (1H, *app.*t, H6), 7.34 (1H, d, J = 2.0 Hz, H4), 6.06 (2H, br. s, NH_2), 4.81 (2H, s, CH_2), 2.51 (3H, s, OCH_3); δ_C ($(CD_3)_2SO$, 150 MHz), 168.8 ($COOCH_3$), 163.5 (C=O), 163.4 (C=O), 148.0 (C), 133.7 (C), 132.2 (Ar-CH), 127.2 (Ar-CH), 126.0 (Ar-CH), 122.0 (Ar-CH), 122.0 (C), 121.2 (C), 120.7

(C), 112.4 (Ar-CH), 52.3 (OCH_3), 41.2 (CH); ν_{max} (neat sample)/cm^{-1} 3460, 3368, 2959, 1741, 1697, 1656, 1451, 1380, 1323.

_N_-[*(1S)*-Methoxycarbonyl-ethyl)]-3-nitro-1,8-naphthalimide 142

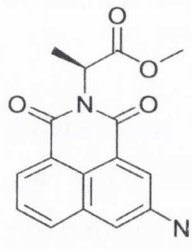

142 was synthesised using N-[*(1S)*-methoxycarbonyl-ethyl)]-3-nitro-1,8-naphthalimide (222 mg, 0.676 mmol) in CH_3OH according to **Procedure 2** and was yielded as an orange solid (145 mg, 72%). m.p. 194-195 °C; HRMS: 321.0854 ($[M+Na)^+$. $C_{16}H_{14}N_2O_4Na$ requires 321.0851); δ_H ($(CD_3)_2SO$, 400 MHz), 8.12 (1H, d, J = 7.0 Hz, H7), 8.11 (1H, d, J = 8.3 Hz, H5), 7.99 (1H, d, J = 2.0 Hz, H2), 7.67 (1H, *app.* t, H6), 7.34 (1H, d, J = 2.2 Hz, H4), 6.06 (2H, br. s, NH_2), 5.69 (1H, q, J = 7.0 Hz, CH), 3.61 (3H, s, OCH_3), 1.54 (3H, d, J = 7.0 Hz, CH_3); δ_C ($(CD_3)_2SO$, 150 MHz), 170.6 ($\underline{C}OOCH_3$), 163.2 (C=O), 163.0 (C=O), 148.0 (C), 133.6 (C), 132.0 (Ar-CH), 127.1 (Ar-CH), 125.9 (Ar-CH), 122.1 (C), 122.0 (Ar-CH), 121.3 (C), 120.5 (C), 112.2 (Ar-CH), 52.1 (OCH_3), 48.2 (CH), 14.5 (CH_3): ν_{max} (neat sample)/cm^{-1} 3446, 3365, 1739, 1699, 1655, 1598, 1375, 1305.

_N_-[*(1S)*-Methoxycarbonyl-2-ethylphenyl)]-4-nitro-1,8-naphthalimide 143

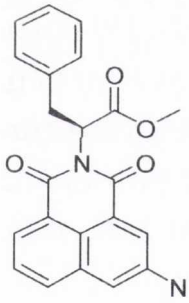

143 was synthesised using *N*-[*(1S)*-Methoxycarbonyl-2-ethylphenyl)]-4-nitro-1,8-naphthalimide (430 mg, 1.063 mmol) in CH_3CH_2OH according to **Procedure 2** and was yielded as an orange solid (395 mg, 99%). m.p. 95 -96 °C (Ref.[114] 95-96 °C); HRMS: 397.1172 ($[M+Na)^+$. $C_{22}H_{18}N_2O_4Na$ requires 397.1164); δ_H ($(CD_3)_2SO$, 600 MHz), 8.06 (1H, d, J = 8.3 Hz, H5), 8.03 (1H, d, J = 7.1 Hz, H7), 7.89 (1H, d, J = 2.1 Hz, H2), 7.62 (1H, *app.* t, H6), 7.30 (1H, d, J = 2.3 Hz, H4), 7.14 (5H, m, Ph), 6.02 (2H, br. s, NH_2), 5.98 (1H, dd, J = 5.5, 10.0 Hz, CH), 3.65 (3H, s, OCH_3), 3.58 (1H, d, J = 5.40 Hz, CH_2), 3.56 (1H, d, J = 5.4 Hz, CH_2); δ_C ($(CD_3)_2SO$, 150 MHz), 169.9 ($\underline{C}OOCH_3$), 163.3 (C=O), 163.1 (C=O), 148.0 (C), 137.4 (C), 133.5 (C), 132.1 (Ar-CH), 129.0 (Ph), 128.1 (Ph), 127.1 (Ar-CH), 126.4 (Ph), 126.0 (Ar-CH), 122.1 (Ar-CH), 121.6 (C), 120.9 (C), 120.4 (C), 112.3 (Ar-CH), 53.5 (CH), 52.3 (OCH_3), 34.1 (CH_2); ν_{max} (neat sample)/cm^{-1} 3461, 3368, 2952, 1740, 1696, 1657, 1377.

Bis-{*N*-(1-Carboxy-methyl)}-9,18-methano-1,8-naphthalimido[b,f][1,5]-diazocine 144

144 was synthesised by reacting **126** (236 mg, 0.873 mmol) with paraformaldehyde (39 mg, 1.299 mmol) in TFA (2 mL) according to **Procedure 3**. The crude product was dissolved in CH_3OH and refluxed in the presence of activated charcoal. The reaction mixture was filtered

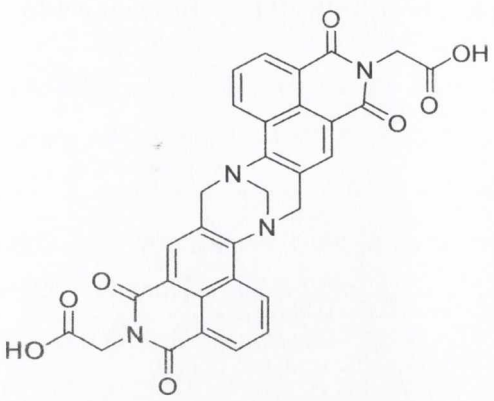

through celite, washing with CH_3OH. The filtrate and washings were evaporated under reduced pressure and the residue was dissolved in ethyl acetate and the organic layer was dried over $MgSO_4$ and evaporated under reduced pressure and further dried under vacuum to yield the product as a yellow powder (192 mg, 76%). Decomposed at 300-301 °C; HRMS: 599.1179 ($[M+Na]^+$. $C_{31}H_{20}N_4O_8Na$ requires 599.1193); δ_H ($(CD_3)_2SO$, 400 MHz), 8.80 (2H, d, J = 8.4 Hz, H5, H5′), 8.53 (2H, d, J = 7.3 Hz, H7, H7′), 8.17 (2H, s, H2, H2′), 8.02 (2H, *app.* t, H6, H6′), 5.22 (2H, d, J = 15.9, TB), 4.74 (4H, m, TB), 4.67 (2H, s, $N\underline{CH_2}$); δ_C ($(CD_3)_2SO$, 150 MHz), 169.2 (COOH), 163.2 (C=O), 162.5 (C=O), 149.6 (C), 131.1 (Ar-CH), 130.5 (Ar-CH), 129.6 (Ar-CH), 127.5 (C), 127.3 (Ar-CH), 126.9 (C), 126.4 (C), 121.9 (C), 117.1 (C), 65.9 (CH_2), 56.7 (CH_2), 41.0 (CH_2); ν_{max} (neat sample)/cm^{-1} 2925,1697,1656, 1597, 1459.

Bis-{*N-(1S)*-[Carboxy-ethyl)}- 9,18-methano-1,8-naphthalimido[b,f][1,5]-diazocine 145

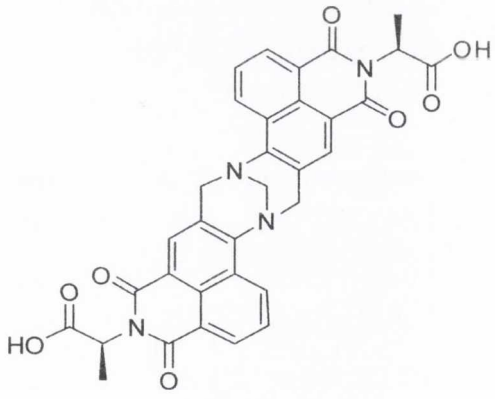

145 was synthesised according to **Procedure 3** from **127** (414 mg, 1.456 mmol) and paraformaldehyde (66 mg, 2.198 mmol) in TFA (3 mL) to yield the product as a brown powder (400 mg, 91%). Decomposed at 300-301 °C; Calculated for $C_{33}H_{24}N_4O_8.0.5CH_2Cl_2$: C, 62.19; H, 3.89; N, 8.66. Found C, 62.63; H, 4.33; N, 8.08; HRMS: 627.1502 ($[M+Na]^+$. $C_{33}H_{24}N_4O_8Na$ requires 627.1492); δ_H ($(CD_3)_2SO$, 600 MHz), 8.79 (2H, d, J = 8.6 Hz, H5, H5′), 8.52 (2H, d, J = 6.4 Hz, H7, H7′), 8.14 (2H, s, H2, H2′), 8.01 (2H, *app.* t, H6, H6′), 5.53 (2H, q, J = 6.8 Hz, CH), 5.21 (2H, d, J = 17.3 Hz, TB), 4.74 (1H, s, TB), 4.74 (1H, s, TB), 4.71 (2H, d, J = 17.3 Hz, TB), 1.47 (6H, dd, J = 3.2, 7.0 Hz, CH_3); δ_C ($(CD_3)_2SO$, 150 MHz), 171.4 (COOH), 163.0 (C=O), 162.3 (C=O), 149.5 (C), 131.2 (Ar-CH), 130.6 (Ar-CH), 129.6 (Ar-CH), 127.5 (Ar-CH), 127.3 (C), 126.8 (C), 126.4 (C), 122.1 (C), 117.3 (C), 66.0 (CH_2), 56.8 (CH_2), 48.3 (CH), 14.5/14.5 (CH_3); ν_{max} (neat sample)/cm^{-1} 2500, 1655, 1594, 1371.

Bis-{*N*-*(1R)*-[Carboxy-ethyl)}- 9,18-methano-1,8-naphthalimido[b,f][1,5]-diazocine 146

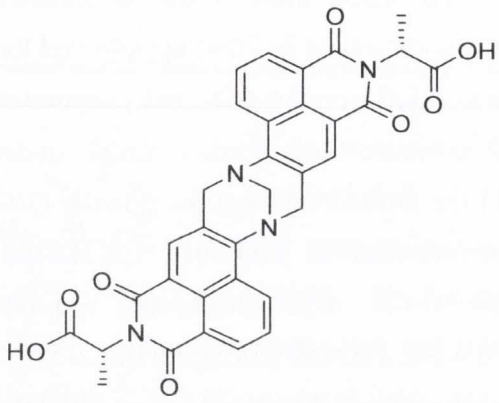

146 was synthesised by reacting **120** (50 mg, 0.176 mmol) with paraformaldehyde (7.9 mg, 0.263 mmol) in TFA (1 mL) according to **Procedure 3**. The resulting solution was reduced to dryness and dried further under vacuum to yield the product as a yellow powder (48 mg, 91%). Decomposed at 300 °C. Calculated for $C_{33}H_{24}N_4O_8.0.75CH_2Cl_2$: C, 60.66; H, 3.85; N, 8.38. Found C, 60.90; H, 3.49; N, 7.86; HRMS: 603.1507 ($[M-H]^-$. $C_{33}H_{23}N_4O_8$ requires 603.1516); δ_H ($(CD_3)_2SO$, 600 MHz), 8.79 (2H, d, J = 8.3 Hz, H5, H5′), 8.51 (2H, d, J = 7.3 Hz, H7, H7′), 8.13 (2H, s, H2, H2′), 8.00 (2H, *app*.t, H6, H6′), 5.52 (2H, q, J = 6.8 Hz, CH), 5.20 (2H, d, J = 17.0 Hz, TB), 4.73 (2H, s, TB), 4.69 (2H, d, J = 17.0 Hz, TB), 2.52 (6H, s, CH_3); δ_C ($(CD_3)_2SO$, 150 MHz), 171.7(COOH), 163.3 (C=O), 162.7 (C=O), 149.8 (C), 131.4 (Ar-CH), 131.0(Ar-CH), 129.9 (Ar-CH), 127.8 (Ar-CH), 127.7 (C), 127.1 (C), 126.6 (C), 122.4 (C), 117.6 (C), 66.3 (CH_2), 57.1 (CH_2), 48.6 (CH), 14.8/14.7 (CH_3); ν_{max} (neat sample)/cm^{-1} 2968, 1655, 1596, 1374.

Bis-{*N*-[(1*S*)-Carboxy-2-ethylphenyl]}-9,18-methano-1,8-naphthalimido[b,f][1,5]-diazocine 147

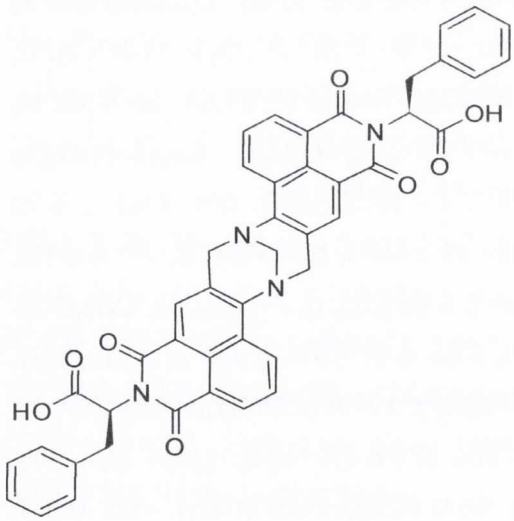

147 was synthesised by reacting **128** (292 mg, 0.810 mmol) with paraformaldehyde (36 mg, 1.215 mmol) in TFA (2 mL) according to **Procedure 3**. The crude product was purified by refluxing in CH_3OH in the presence of charcoal. The resulting solution was filtered through celite, washing with CH_3OH. The filtrate and washings were evaporated under reduced pressure and the residue was dissolved in ethyl acetate and the organic layer was dried over $MgSO_4$ and evaporated under reduced pressure and further dried under vacuum to yield the product as an orange solid (247 mg, 81%). Decomposed at 207-208 °C; HRMS: 779.2082 ($[M-Na]^-$. $C_{45}H_{31}N_4O_8$ requires 755.2142); δ_H ($(CD_3)_2SO$, 600 MHz), 8.72 (2H, t, H5, H5′), 8.42 (2H, br. s, H7, H7′), 8.06 (2H, br.s, H2, H2′), 7.93 (2H, dd, J = 7.3, 12.5 Hz, H6, H6′), 7.07 (10H, m, Ph), 5.84 (2H, dd, J = 4.0, 8.0 Hz, CH), 5.14 (2H, d, J = 17.1 Hz, TB), 4.69 (4H, m, TB), 3.52 (2H, m,

CH_2), 3.36 (2H, m, CH_2); δ_C ($(CD_3)_2SO$, 150 MHz), 170.6/170.6 (COOH), 163.0 (C=O), 162.4/162.4 (C=O), 149.9 (C), 137.7/137.7 (C), 131.2 (Ar-CH), 130.6 (Ar-CH), 129.5 (Ar-CH), 128.8/128.8 (Ph), 128.0/128.0 (C), 127.2/127.2 (Ar-CH), 127.0 (C), 126.8 (Ph), 126.3/126.3 (Ph), 126.2/126.1 (C), 121.6 (C), 116.8 (C), 65.8 (CH_2), 56.4 (CH_2), 53.8 (CH), 34.2/34.1 (CH_2); ν_{max} (neat sample)/cm^{-1} 2956, 2929, 2830, 1723, 1660, 1258.

Bis-{*N*-[(1*R*)-Carboxy-2-ethylphenyl]}-9,18-methano-1,8-naphthalimido[b,f][1,5]-diazocine 148

148 was synthesised by reacting **124** (403 mg, 0.968 mmol) with paraformaldehyde (43.5 mg, 1.449 mmol) in TFA (2.5 mL) according to **Procedure 3**. The crude product was purified by refluxing in CH_3OH in the presence of charcoal. The resulting solution was filtered through celite, washing with CH_3OH. The filtrate and washings were evaporated under reduced pressure and the residue was dissolved in ethyl acetate and the organic layer was dried over $MgSO_4$ and evaporated under reduced pressure and further dried under vacuum to yield the product as an orange solid (237 mg, 65%). Decomposed at 207-208 °C; HRMS: 779.2082 ($[M+Na]^+$. $C_{45}H_{32}N_4O_8Na$ requires 779.2118); δ_H ($(CD_3)_2SO$, 600 MHz), 8.74 (2H, t, H5, H5′), 8.42 (2H, *m*, H7, H7′), 8.05 (2H, s, H2, H2′), 7.95 (2H, m, H6, H6′), 7.35 (10H, m, Ph), 5.83 (2H, dd, J = 4.0, 8.0 Hz, CH), 5.15 (2H, d, J = 18.0 Hz, TB), 4.68 (4H, m, TB), 3.52 (2H, m, CH_2), 3.36 (2H, m, CH_2); δ_C ($(CD_3)_2SO$, 150 MHz), 170.6/170.6 (COOH), 163.0 (C=O), 162.4/162.4 (C=O), 149.9 (C), 137.7/137.7 (C), 131.2 (Ar-CH), 130.6 (Ar-CH), 129.5 (Ar-CH), 128.8/128.8 (Ph), 128.0/128.0 (C), 127.2/127.2 (Ar-CH), 127.0 (C), 126.8 (Ph), 126.3/126.3 (Ph), 126.2/126.1 (C), 121.6 (C), 116.8 (C), 67.1 (CH_2), 57.0 (CH_2), 54.1 (CH), 34.2/34.1 (CH_2); ν_{max} (neat sample)/cm^{-1} 2956, 2929, 2830, 1723, 1660, 1258.

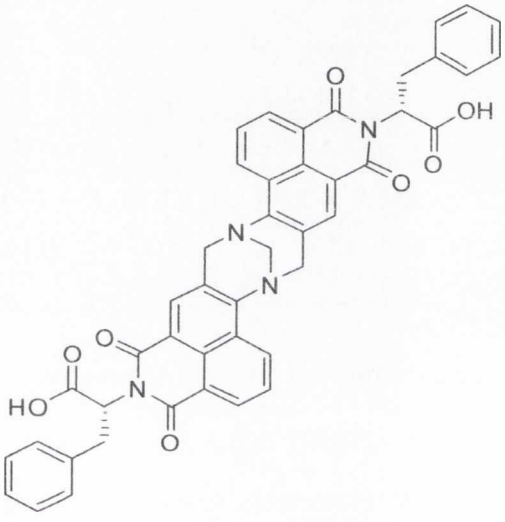

Bis-{*N*-[(1*S*)-Carboxy-3-methyl]}-9,18-methano-1,8-naphthalimido[b,f][1,5]-diazocine 149

149 was synthesised by reacting **130** (266 mg, 0.852 mmol) with paraformaldehyde (38 mg, 1.265 mmol) in TFA (2.5 mL) according to **Procedure 3**. The crude product was purified by refluxing in CH_3OH in the presence of charcoal. The resulting solution was filtered through celite, washing with CH_3OH. The filtrate and washings were evaporated under reduced

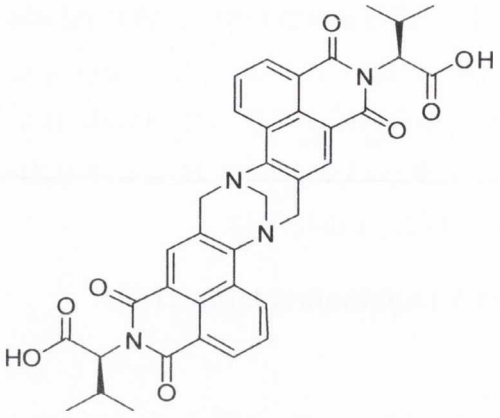

pressure and the residue was dissolved in CH_2Cl_2 and the organic layer was dried over $MgSO_4$ and evaporated under reduced pressure and further dried under vacuum to yield the product as a yellow solid (115 mg, 41%). Decomposed at 224-225 °C; HRMS: 683.2117 ($[M+Na)^+$. $C_{37}H_{32}N_4O_8Na$ requires 683.2118); δ_H ($(CD_3)_2SO$, 600 MHz), 8.78 (2H, d, J = 8.3 Hz, H5, H5′), 8.53 (2H, t, H7, H7′), 8.15 (1H, s, H2), 8.15 (1H, s, H2′) 8.00 (2H, t, H6, H6′), 5.20 (2H, d, J = 17.8 Hz, TB), 5.09 (2H, d, J = 9.4 Hz, CH), 4.73-4.75 (4H, m, TB), 2.59-2.61 (2H, m, $\underline{CH}(CH_3)_2$), 1.15-117 (6H, d, J = 5.6 Hz, $CH(\underline{CH_3})_2$), 0.58-0.60 (6H, d, J = 5.6 Hz, $CH(\underline{CH_3})_2$); δ_C ($(CD_3)_2SO$, 150 MHz), 170.8/170.8 (COOH), 163.6/163.5 (C=O), 163.0/162.9 (C=O), 149.9/149.9 (C), 131.7/131.6 (Ar-CH), 131.1/131.1 (Ar-CH), 130.0 (Ar-CH), 127.7/127.7 (Ar-CH), 127.6/127.6 (C) 127.0 (C), 126.6 (C), 121.8 (C), 117.0 (C), 66.1 (CH_2), 58.0/58.0 (CH), 56.9 (CH_2), 27.0/27.0 (CH), 22.3/22.3 (CH_3), 18.9/18.9 (CH_3); ν_{max} (neat sample)/cm^{-1} 2924, 1659, 1596, 1459, 1373, 1340.

Bis-{*N*-[(1*R*)-Carboxy-3-methyl]}-9,18-methano-1,8-naphthalimido[b,f][1,5]-diazocine 150

150 was synthesised by reacting **121** (266 mg, 0.852 mmol) with paraformaldehyde (38 mg, 1.265 mmol) in TFA (2.5 mL) according to **Procedure 3**. The crude product was purified by refluxing in CH_3OH in the presence of charcoal. The resulting solution was filtered through celite, washing with CH_3OH. The filtrate and washings were evaporated under reduced pressure and the residue was dissolved in CH_2Cl_2 and the organic layer was dried over $MgSO_4$ and evaporated under reduced pressure and further dried under vacuum to yield the product as a yellow solid (115 mg, 41%). Decomposed at 224-225 °C; HRMS: 683.2117 ($[M+Na)^+$. $C_{37}H_{32}N_4O_8Na$ requires 683.2118); δ_H ($(CD_3)_2SO$, 600 MHz), 8.78 (2H, d, J = 8.3 Hz, H5, H5′), 8.53 (2H, t, H7, H7′), 8.15 (1H, s,, H2), 8.15 (1H, s, H2′) 8.00 (2H, *app.* t, H6, H6′), 5.20 (2H, d, J = 17.8 Hz, TB), 5.09 (2H, d, J = 9.4 Hz, CH), 4.75 (4H, m, TB), 2.61 (2H, m, $\underline{CH}(CH_3)_2$), 1.17 (6H, d, J = 5.6 Hz, $CH(\underline{CH_3})_2$), 0.60 (6H, d, J = 5.6 Hz, $CH(\underline{CH_3})_2$);

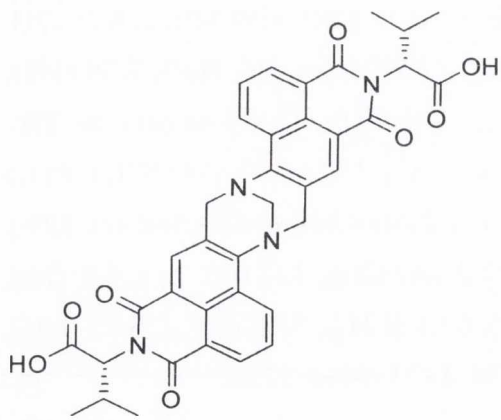

δ_C ($(CD_3)_2SO$, 150 MHz), 170.8/170.8 (COOH), 163.6/163.5 (C=O), 163.0/162.9 (C=O), 149.9/149.9 (C), 131.7/131.6 (Ar-CH), 131.1/131.1 (Ar-CH), 130.0 (Ar-CH), 127.7/127.7 (Ar-CH), 127.6/127.6 (C) 127.0 (C), 126.6 (C), 121.8 (C), 117.0 (C), 66.1 (CH_2), 58.0/58.0 (CH), 56.9 (CH_2), 27.0/27.0 (CH), 22.3/22.3 (CH_3), 18.9/18.9 (CH_3); ν_{max} (neat sample)/cm^{-1} 2927, 1697, 1655, 1595, 1404, 1374.

Bis-{*N*-[*(1S)*-Carboxy-3-methylbutyl]}-9,18-methano-1,8-naphthalimido[b,f][1,5]-diazocine 151

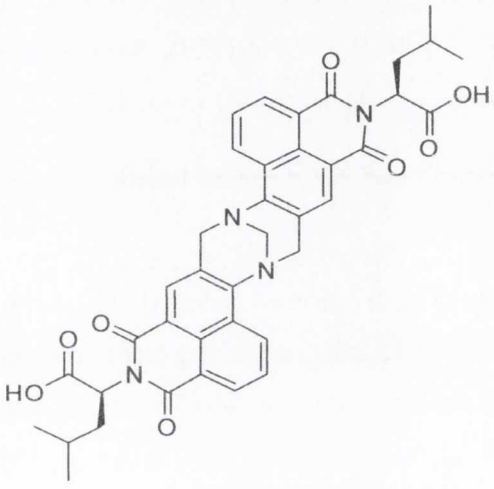

151 was synthesised by reacting **129** (281 mg, 0.861 mmol) with paraformaldehyde (39 mg, 1.299 mmol) in TFA (2 mL) according to **Procedure 3**. The crude product was dissolved in CH_2Cl_2 and refluxed in the presence of activated charcoal. The solution was filtered through celite, washing with CH_2Cl_2. The filtrate and washings were evaporated under reduced pressure yielding the product as a yellow solid (142 mg, 50%). Decomposed at 232-233 °C; HRMS: 711.2419 ($[M+Na]^+$. $C_{39}H_{36}N_4O_8Na$ requires 711.2431); δ_H ($(CD_3)_2SO$, 600 MHz), 8.80 (2H, dd, J = 6.3, 8.3 Hz, H5, H5′), 8.54 (2H, *app.* t, H7, H7′), 8.17 (1H, s, H2), 8.17 (1H, s, H2′), 8.01 (2H, m, H6, H6′), 5.53 (2H, dd, J = 5.7, 8.3 Hz, CH), 5.21 (2H, d, J = 17.0 Hz, TB), 4.74 (4H, m, TB), 2.00 (4H, m, $CH\underline{CH_2}$), 1.35 (2H, m, $\underline{CH}(CH_3)_2$), 0.87 (6H, m, $CH(\underline{CH_3})_2$), 0.77 (6H, m, $CH(\underline{CH_3})_2$); δ_C ($(CD_3)_2SO$, 150 MHz), 171.3 (COOH), 163.3/163.2 (C=O), 162.7/162.6 (C=O), 149.5 (C), 131.4/131.3 (Ar-CH), 130.8/130.7 (Ar-CH), 129.6 (Ar-CH), 127.5 (C), 127.3 (Ar-CH), 126.7 (C), 126.4 (C), 121.9/121.8 (C), 117.1/117.0 (C), 66.0 (CH_2), 56.7 (CH_2), 51.1 (CH), 37.4/37.3 (CH_2), 24.8 (CH), 23.0 (CH_3), 21.7 (CH_3): ν_{max} (neat sample)/cm^{-1} 2924, 1698, 1655, 1595, 137, 1354.

Bis-{*N*-[*(1R)*-Carboxy-3-methylbutyl]}-9,18-methano-1,8-naphthalimido[b,f][1,5]-diazocine 152

152 was synthesised according to **Procedure 3** by stirring **125** (349 mg, 1.07 mmol) and paraformaldehyde (48 mg, 1.60 mmol) in TFA (2.5 mL). The crude product was dissolved in CH_2Cl_2 and refluxed in the presence of activated charcoal. The solution was filtered through celite, washing with CH_2Cl_2. The filtrate and washings were evaporated under reduced pressure yielding the product as a yellow solid (184 mg, 50%). Decomposed at 232-233 ° C; HRMS: 711.2416 ($[M+Na]^+$. $C_{39}H_{36}N_4O_8Na$ requires 711.2431); δ_H ($(CD_3)_2SO$, 600 MHz),

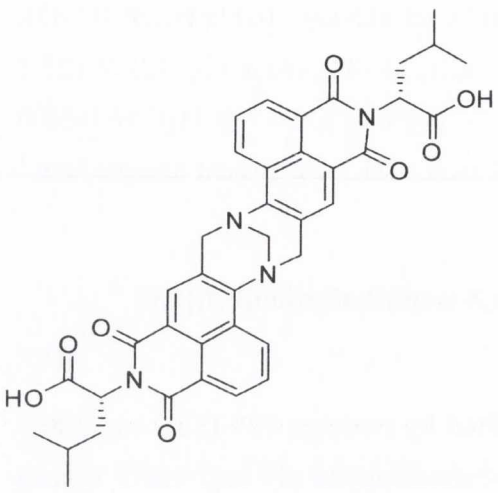

8.78 (2H, d, J = 8.3 Hz, H5, H5′), 8.53 (1H, t, H7, H7′), 8.15 (1H, d, H2, H2′), 8.00 (2H, t, H6, H6′), 5.52 (2H, dd, J = 6.0, 8.5 Hz, CH), 5.20 (2H, d, J = 17.8 Hz, Ha), 4.74 (4H, m, TB), 1.98 (4H, m, CH$\underline{CH_2}$), 1.35 (2H, m, $\underline{CH}(CH_3)_2$), 0.85 (6H, m, CH($\underline{CH_3}$)$_2$), 0.76 (6H, m, CH($\underline{CH_3}$)$_2$); δ_C ($(CD_3)_2SO$, 150 MHz), 171.2 (COOH), 163.3 (C=O), 162.6 (C=O), 149.5 (C), 134.4 (Ar-CH), 130.8 (Ar-CH), 129.8 (Ar-CH), 129.6 (C), 127.5 (C), 127.3 (Ar-CH), 126.8 (C), 126.4 (C), 124.0 (C), 66.1 (CH_2), 56.9 (CH_2), 51.2 (CH), 37.5 (CH_2), 24.9 (CH) 23.0 (CH_3), 21.7 (CH_3); ν_{max} (neat sample)/cm^{-1} 2925, 1698, 1658, 1595, 1373.

Bis-{*N*-[*(1S)*-Methoxycarbonyl-3-methylbutyl]}-9,18-methano-1,8-naphthalimido [b,f][1,5]-diazocine 153

153 was synthesised by reacting **131** (104 mg, 0.306 mmol) with paraformaldehyde (13.7 mg, 0.456 mmol) in TFA (1 mL) according to **Procedure 3**. Upon completion the reaction mixture was basified to pH 14 and extracted with CH_2Cl_2. The crude product was purified using automated column chromatography using flash silica and ethyl acetate: hexane (0 – 100%) to yield the product as an orange solid after trituration with CH_3OH (69 mg, 63%). HRMS: 739.2759 ([M+Na)$^+$. $C_{41}H_{40}N_4O_8Na$ requires 739.2744); δ_H ($CDCl_3$, 600 MHz), 8.74 (2H, dd, J = 1.9, 8.4 Hz, H5, H5'), 8.63 (2H, dd, J = 3.9 Hz, 6.5 Hz, H7, H7'), 8.13 (1H, s, H2), 8.13 (1H, s, H2′), 7.92 (2H, *app.* m, H6, H6′), 5.74 (2H, dd, J = 4.8 Hz, 9.4 Hz, CH), 5.18 (2H, dd, J = 4.7 Hz, 17.0 Hz, TB), 4.72 (2H, d, J = 2.8 Hz, TB), 4.63 (2H, dd, J = 4.7 Hz, 17.0 Hz, TB), 3.67 (3H, s, OCH_3), 3.66 (3H, s, OCH_3), 2.17 (2H, m, CH_2), 2.09 (2H, m, CH_2), 1.47 (2H, m, CH), 0.97 (6H, m CH_3), 0.87 (6H, t, CH_3); δ_C ($CDCl_3$, 150 MHz), 171.0 ($\underline{C}OOCH_3$), 164.0/163.9 (C=O), 163.5/163.4 (C=O), 149.5 (C), 131.6/131.6 (Ar-CH), 131.1/131.0 (Ar-CH), 129.2/129.2 (C), 128.7 (Ar-CH), 127.5/127.5 (C), 127.4/127.4 (Ar-CH), 125.5/125.5 (C), 123.1/123.0 (C), 118.8/118.7 (C), 67.3/67.3 (CH_2), 57.4/57.4 (CH_2), 52.5 (OCH_3), 52.0 (CH), 38.1/38.0 (CH_2), 25.4 (CH), 23.3 (CH_3), 22.2 (CH_3); ν_{max} (neat sample)/cm^{-1} 2930, 1698, 1660, 1458, 1374, 1256.

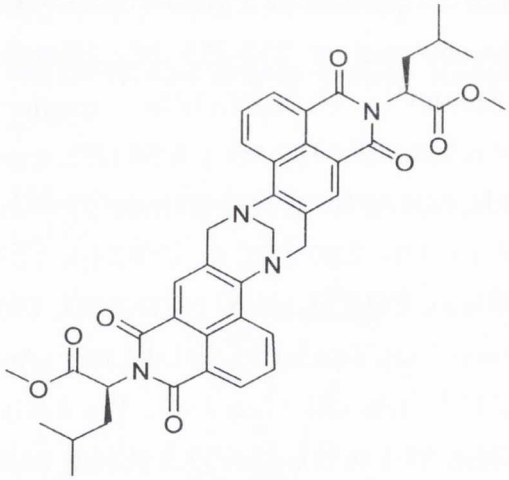

Bis-{*N*-[*(1S)*-Methoxycarbonyl-ethylphenyl]}-9,18-methano-1,8-naphthalimido[b,f][1,5]-diazocine 154

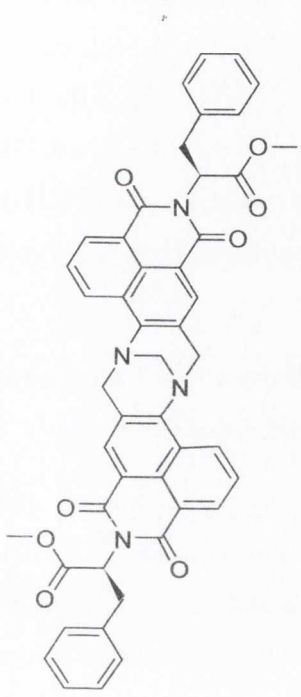

154 was synthesised by reacting **132** (248 mg, 0.662 mmol) with paraformaldehyde (30 mg, 0.999 mmol) in TFA (1.5 mL) according to **Procedure 3**. The crude product was dissolved in CH_3OH and refluxed in the presence of activated charcoal. The reaction mixture was filtered through celite, washing with CH_3OH. The filtrate and washings were evaporated under reduced pressure to yield the product as an orange solid (191 mg, 76%). m.p. 210-211 °C; Calculated for $C_{47}H_{36}N_4O_8$.: C, 71.93; H, 4.62; N, 7.14. Found C, 71.10; H, 4.67; N, 6.65; HRMS: 807.2410 ($[M+Na)^+$. $C_{47}H_{36}N_4O_8Na$ requires 807.2431); δ_H ($CDCl_3$, 600 MHz), 8.70 (2H, m, H5, H5′), 8.55 (2H, t, H7, H7′), 8.05 (1H, s, H2), 8.05 (1H, s, H2′), 7.88 (2H,m, H6, H6′), 7.17 (10H, m, Ph), 5.99 (2H, dd, J = 5.4, 9.7 Hz, CH), 5.15 (2H, d, J = 17.2 Hz, TB), 4.67 (2H, *app.* d, TB), 4.58 (2H, d, J = 17.2 Hz, TB), 3.71 (3H, s, OCH_3), 3.69 (3H, s, OCH_3), 3.68 (2H, m, CH_2), 3.47(2H, m, CH_2); δ_C ($CDCl_3$, 150 MHz), 170.1 ($COOCH_3$), 163.6/163.5 (C=O), 163.0/163.0 (C=O), 149.2 (C), 137.4/137.3 (C), 131.3 (Ar-CH), 130.8/130.7 (Ar-CH), 129.2/129.2 (Ar-CH), 129.0/129.0 (Ph), 128.4 (Ph), 128.2 (C), 127.3/127.2 (Ar-CH), 126.5 (C), 126.4 (Ph), 125.2/125.2 (C), 122.6 (C), 118.4 (C), 67.0 (CH_2), 57.0 (CH_2), 54.2/54.2 (CH), 52.4 (OCH_3), 34.9/34.8 (CH_2); ν_{max} (neat sample)/cm^{-1} 2949, 1742, 1662, 1597, 1198.

Bis-{*N*-[*(1S)*-4-Methyl-pentanoic acid methyl ester]carboxamido-ethyl]}-9,18-methano-1,8-naphthalimido[b,f][1,5]-diazocine 155

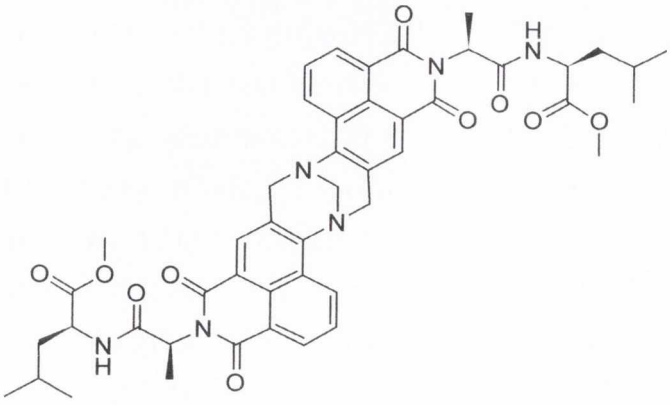

155 was synthesised by reacting **139** (92 mg, 0.224 mmol) with paraformaldehyde (10 mg, 0.333 mmol) in TFA (1 mL) according to **Procedure 3.** After basic work-up the crude residue was recrystallised from CH_3OH yielding the product as a yellow solid (35 mg, 33%). Calculated for $C_{47}H_{50}N_6O_{10}$: C, 62.83; H, 5.67; N, 9.24. Found C, 62.99; H, 5.08; N, 8.82; HRMS: 881.3471 ($[M+Na)^+$. $C_{47}H_{50}N_6O_{10}Na$ requires 881.3486); δ_H

($CDCl_3$, 600 MHz), 8.72 (2H, d, J = 8.3 Hz, H5, H5′), 8.60 (2H, d, J = 7.1 Hz, H7, H7′), 8.11 (2H, s, H2, H2′), 7.89 (2H, *app.* t, H6, H6′), 6.19 (2H, d, J = 7.7 Hz, NH), 5.70 (2H, q, J = 6.8 Hz, C<u>H</u>CH_3), 5.16 (2H, d, J = 17.0 Hz, TB), 4.70 (2H, s, TB), 4.67 (2H, m, NHC<u>H</u>), 4.61 (2H, d, J = 17.0 Hz, TB), 3.65 (6H, s, OCH_3), 1.67 (6H, d, J = 6.8 Hz, $CHC\underline{H}_3$), 1.58 (2H, m, C<u>H</u>$(CH_3)_2$), 1.44 (4H, m, $NHCHC\underline{H}_2$), 0.90 (6H, d, J = 5.7 Hz, $CH(C\underline{H}_3)_2$), 0.85 (6H, d, J = 5.7 Hz, $CH(C\underline{H}_3)_2$); δ_C ($CDCl_3$, 600 MHz), 173.5 (<u>C</u>$OOCH_3$), 169.4 (CONH), 163.5 (C=O), 163.0 (C=O), 149.4 (C), 131.3 (Ar-CH), 130.8 (Ar-CH), 129.0 (Ar-CH), 128.4 (Ar-CH), 127.2 (C), 127.1 (C) 125.3 (C), 123.0 (C), 118.7 (C), 67.0 (CH_2), 57.1 (CH_2), 52.2 (OCH_3), 50.8 (CH), 50.1 (CH), 41.8(CH_2), 24.6 (CH), 22.7 (CH_3), 22.0 (CH_3), 14.3 (CH_3); ν_{max} (neat sample)/cm^{-1} 2953, 1731, 1703, 1662, 1597, 1459, 1369, 1256.

Bis-{*N*-[*(1S)*-Propionic acid methyl ester]carboxamido-3-methylbutyl]}-9,18-methano-1,8-naphthalimido[b,f][1,5]-diazocine 156

156 was synthesised according to **Procedure 3** using **140** (234 mg, 0.57 mmol) and paraformaldehyde (26 mg, 0.85 mmol) in TFA (2 mL). Upon completion of the reaction, the reaction mixture was basified and extracted with CH_2Cl_2. Removal of the organic layer and subsequent automated flash chromatography using a CH_2Cl_2: CH_3OH (0-10 %) eluent system yielded the desired product as a yellow solid (165 mg, 68 %). m.p. 167-168 °C; HRMS: 859.3585 ($[M+H]^+$. $C_{47}H_{51}N_6O_{10}$ requires 859.3667); δ_H ($CDCl_3$, 600 MHz), 8.71 (2H, t, H5, H5′), 8.62 (2H, t, H7, H7′), 8.12 (1H, s, H2), 8.12 (1H, s, H2′), 7.85-7.89 (2H, m, H6, H6′), 6.41 -6.46 (2H, m, NH), 5.70-5.72 (2H, m, $NHC\underline{H}CH_2CH(CH_3)_2$), 5.16 (2H, d, J = 16.8 Hz, TB), 4.70 (2H, s, TB), 4.58-4.61 (4H, m, $NHC\underline{H}CH_3$, TB), 3.69 (6H, s, OCH_3), 2.19-2.25 (2H, m, $NCHC\underline{H}_2CH(CH_3)_2$), 1.98-2.03 (2H, m, $NCHC\underline{H}_2CH(CH_3)_2$), 1.41-1.45 (2H, m, $NCHCH_2C\underline{H}(CH_3)_2$), 1.28-1.35 (6H, m, $NHCHC\underline{H}_3COOCH_3$), 0.85-0.95 (12H, m, $NCHCH_2CH(C\underline{H}_3)_2$); δ_H ($CDCl_3$, 600 MHz), 173.7 (<u>C</u>$OOCH_3$), 169.4 (CONH), 164.2/164.1 (C=O), 163.7/163.6 (C=O), 149.5 (C), 131.7 (C), 131.5 (Ar-CH), 131.2/131.1 (Ar-CH), 129.2/129.2 (Ar-CH), 128.7 (C), 127.4/127.3 (Ar-CH), 125.5/125.5 (C), 123.0/123.0 (C), 118.7/118.7 (C), 67.2 (CH_2), 57.3 (CH_2), 53.4/53.3 (CH), 52.5 (OCH_3), 48.4 (CH), 37.5/37.4 (CH_2), 25.6 (CH), 23.4 (CH_3), 22.1 (CH_3), 18.5 (CH_3); ν_{max} (neat sample)/cm^{-1} 2925, 2855, 1701, 1659, 1571, 1458, 1170.

Bis-{*N*-[*1S-f(2S)*-Methyl-3-phenylpropanamido-3-phenylpropanoate]-9,18-methano-1,8-naphthalimido[b,f][1,5]-diazocine 157

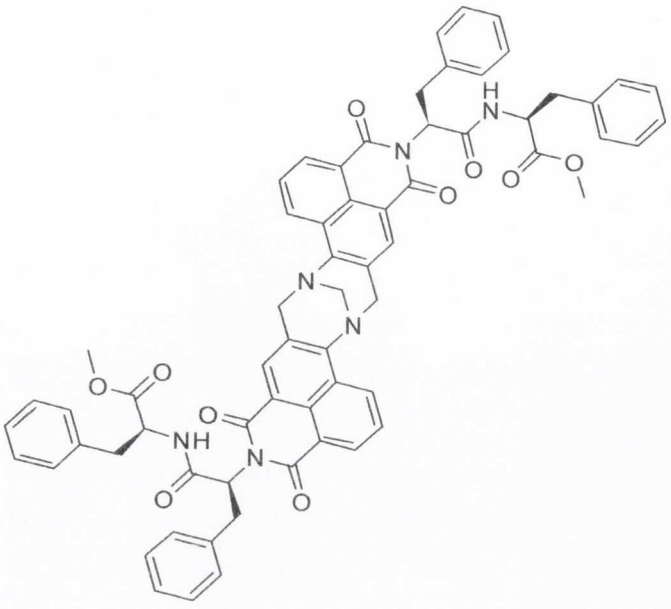

157 was synthesised by reacting **138** (169 mg, 0.324 mmol) with paraformaldehyde (15 mg, 0.486 mmol) in TFA (2 mL) according to **Procedure 3** After basic work-up, a recrystallisation from CH_3CN gave the product as a yellow powder (138 mg, 79%). m.p. 170-171 °C; HRMS: 1101.3779 ($[M+Na)^+$. $C_{65}H_{54}N_6O_{10}Na$ requires 1101.3799; δ_H ($CDCl_3$, 400 MHz), 8.73 (2H, d, J = 8.2 Hz, H5, H5'), 8.56 (2H, d, J = 7.2 Hz, H7, H7'), 8.06 (1H, s, H2,), 8.03 (1H, s, H2') 7.90 (2H, *app.* t, H6, H6'), 6.77-7.17 (20H, m, Ph), 6.16 (2H, d, J = 4.0, 7.2 Hz, NH), 5.91- 5.96 (2H, m, NC$\underline{H}CH_2Ph$), 5.17 (2H, d, J = 17.7 Hz, TB), 4.87-4.91 (2H, m, NHC$\underline{H}CH_2Ph$), 4.69 (2H, s, TB), 4.61 (2H, d, J = 17.7 Hz, TB), 3.67 (3H, s, OCH_3), 3.66 (3H, s, OCH_3), 3.62-3.64 (2H, m, NCHC$\underline{H_2}$Ph), 3.41-3.47 (2H, m, NCHC$\underline{H_2}$Ph), 2.98-3.05 (4H, m, NHCHC$\underline{H_2}$Ph)): δ_H ($CDCl_3$, 150 MHz), 171.7/171.7 ($\underline{C}OOCH_3$), 168.5 (CONH), 163.7/163.7 (C=O), 163.2/163.2 (C=O), 149.4/149.4 (C), 137.3 (C), 135.6 (C), 131.4/131.4 (Ar-CH), 130.9 (Ar-CH), 129.1 (Ph), 129.0 (Ph), 129.0 (Ph), 129.0 (Ar-CH), 128.4/128.4 (Ph), 128.2/128.1 (Ph), 127.2/127.2 (Ar-CH), 126.7 (C), 126.5 (Ph), 126.6/126.5 (C), 125.3/125.3 (C) 122.7/122.6 (C), 118.4/118.3 (C), 67.0 (CH_2), 57.1 (CH_2), 55.5/55.5 (CH), 53.3 (CH), 52.2/52.2 (OCH_3), 37.7/37.7 (CH_2), 34.6/34.5 (CH_2); ν_{max} (neat sample)/cm^{-1} 2951, 1735, 1703, 1661, 1597, 1457.

Bis-{*N*-(1-Methoxycarbonyl-methyl]-9,18-methano-1,8-naphthalimido[b,f][1,5]-diazocine 158

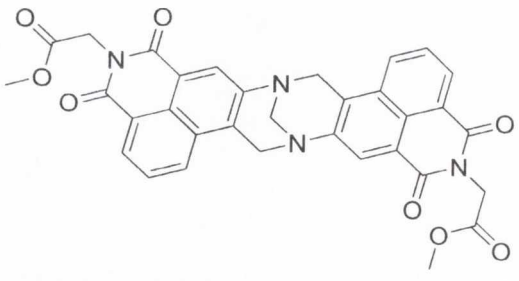

158 was synthesised by reacting **141** (111 mg, 0.391 mmol) with paraformaldehyde (13 mg, 0.433 mmol) in TFA (1 mL) according to **Procedure 4**. Recrystallisation from CH_3OH yielded the product as an orange solid (56 mg, 47%). Decomposed at 204 °C; HRMS: 627.1487 ($[M+Na)^+$. $C_{33}H_{24}N_4O_8Na$ requires 627.1492); δ_H ($CDCl_3$, 400 MHz), 8.57 (2H, s, H2, H2'), 8.55 (2H, d, J = 7.3 Hz, H7, H7'), 8.12 (2H, d, J = 8.3 Hz, H5,

H5'), 7.83 (2H, *app.* t, H6, H6'), 5.32 (2H, d, J = 17.3 Hz, TB), 5.03 (6H, m, TB, CH_2), 4.71 (2H, s, TB), 3.77, (6H, s, OCH_3); δ_C ($CDCl_3$, 150 MHz), 167.7 ($\underline{C}OOCH_3$), 163.4 (C=O), 162.7 (C=O), 146.3 (C), 130.2 (Ar-CH), 129.8 (Ar-CH), 129.3 (C), 128.9 (C), 127.6 (Ar-CH), 127.5 (Ar-CH), 127.1 (C), 125.3 (C), 121.8 (C), 66.3 (CH_2), 55.9 (CH_2), 52.2 (OCH_3), 40.8 (CH_2); ν_{max} (neat sample)/cm^{-1} 2956, 1747, 1660, 1618, 1598, 1354, 1324.

Bis-{*N*-[*(1S)*-Methoxycarbonyl-ethyl]}-9,18-methano-1,8-naphthalimido[b,f][1,5]-diazocine 159

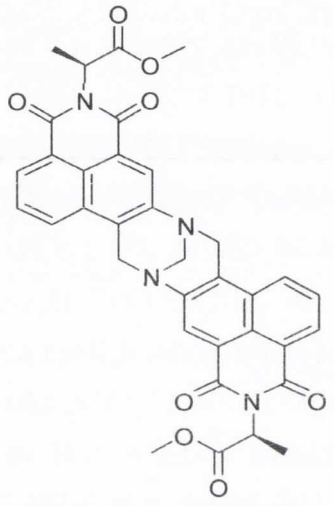

159 was synthesised by reacting **142** (121 mg, 0.406 mmol) with paraformaldehyde (13 mg, 0.433 mmol) in TFA (2 mL) according to **Procedure 4**. The crude product was refluxed in $CHCl_3$ in the presence of activated charcoal. The reaction mixture was filtered through celite, washing with $CHCl_3$. The filtrate and washings were evaporated under reduced pressure and the residue was further purified by trituration with CH_3OH to yield the product as a yellow solid (66 mg, 51%). Decomposed at 235 °C; Calculated for $C_{35}H_{28}N_4O_8$: C, 63.73; H, 4.74; N, 8.49. Found C, 63.59; H, 4.34; N, 8.09; HRMS: 655.1794 ($[M+Na)^+$. $C_{35}H_{28}N_4O_8Na$ requires 655.1805); δ_H ($CDCl_3$, 600 MHz), 8.50 (4H, m, H2, H2′, H7, H7′), 8.10 (2H, t, H5, H5′), 7.79 (2H, m, H6, H6′), 5.74 (2H, m, CH), 5.23 (2H, d, J = 17.6 Hz, TB), 4.98 (2H, dd, J = 11.0 Hz, 17.6 Hz, TB), 4.62 (1H, s, TB), 4.62 (1H, s, TB), 3.71 (3H, s, OCH_3), 3.71 (3H, s, OCH_3), 1.68 (3H, s, CH_3), 1.67 (3H, s, CH_3); δ_C ($CDCl_3$, 150 MHz), 170.8 ($\underline{C}OOCH_3$), 163.3 (C=O), 163.1(C=O), 146.3 (C), 130.1/130.1 (Ar-CH), 129.8/129.8 (Ar-CH), 129.1/129.1 (C), 127.8 (Ar-CH), 127.7 (C), 127.7 (Ar-CH), 125.7 (C), 122.8/122.8 (C), 122.5 (C), 66.6/66.5 (CH_2), 56.2/56.1 (CH_2), 52.4/52.4 (OCH_3), 49.1/49.1 (CH), 14.7/14.7 (CH_3); ν_{max} (neat sample)/cm^{-1} 2947, 1743, 1660, 1617, 1597, 1342.

Bis-{*N*-[*(1S)*-Methoxycarbonyl-2-ethylphenyl]}-9,18-methano-1,8-naphthalimido[b,f][1,5]-diazocine 160

160 was synthesised by reacting **143** (105 mg, 0.281 mmol) with paraformaldehyde (9 mg, 0.300 mmol) in TFA (2 mL) according to **Procedure 4**. The crude product was dissolved in CH_3OH and refluxed in the presence of activated charcoal. The reaction mixture was filtered through celite, washing with CH_2Cl_2. The filtrate and washings were evaporated under reduced pressure to yield the product as a yellow solid (52 mg, 47%). m.p. 210-211 °C; Calculated for $C_{47}H_{36}N_4O_8$.: C, 71.93; H, 4.62; N, 7.14. Found C, 71.23; H, 4.74; N, 6.85;

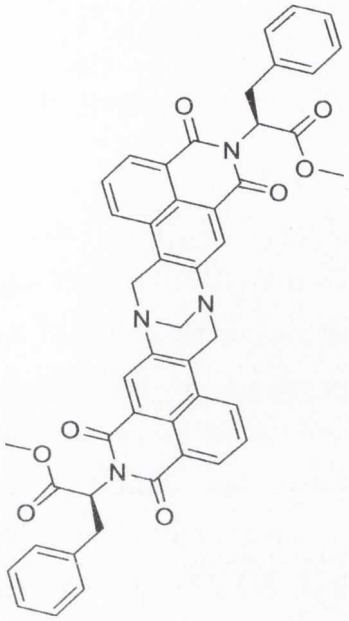

HRMS: 807.2416 ($[M+Na]^+$. $C_{47}H_{36}N_4O_8Na$ requires 807.2431); δ_H ($CDCl_3$, 600 MHz), 8.43 (2H, m, H7), 8.39 (2H, s, H2), 8.06 (2H, d, J = 7.9 Hz, H5), 7.76 (2H, *app.* t, H6), 7.08-7.19 (10H, m, Ph), 6.02 (2H, m, CH), 5.20 (2H, d, J = 17.3 Hz, TB), 4.95 (2H, dd, J = 12.2, 17.3 Hz, TB), 4.59 (1H, s, TB), 4.59 (1H, s, TB), 3.75 (4H, m, CH_2), 3.72 (3H, m, OCH_3), 3.52 (3H, m, OCH_3); δ_C ($CDCl_3$, 150 MHz), 170.0/170.0 ($\underline{C}OOCH_3$), 163.3/163.3 (C=O), 163.2 (C=O), 14.8/145.8 (C), 137.3/137.3 (C), 130.3/130.2 (Ar-CH), 130.0 (C), 129.7 (Ar-CH), 129.2 (Ph), 129.9/128.9 (C), 128.3/128.3 (Ph), 127.8 (Ar-CH), 127.7/127.6 (Ar-CH), 126.5/126.5 (Ph), 125.8/1225.7 (C), 122.6/122.6 (C), 122.3/122.3 (C), 66.4 (CH_2), 56.0/56.0 (CH_2), 54.4/54.3 (CH), 52.5/52.5 (CH_2), 34.9/34.9 (OCH_3); ν_{max} (neat sample)/cm^{-1} 2948, 1742, 1702, 1662, 1597, 1341.

Bis-{*N*-[*(1S)*-4-Methyl-pentanoic acid methyl ester]carboxamido-methyl]}-9,18-methano-1,8-naphthalimido[b,f][1,5]-diazocine 161[247]

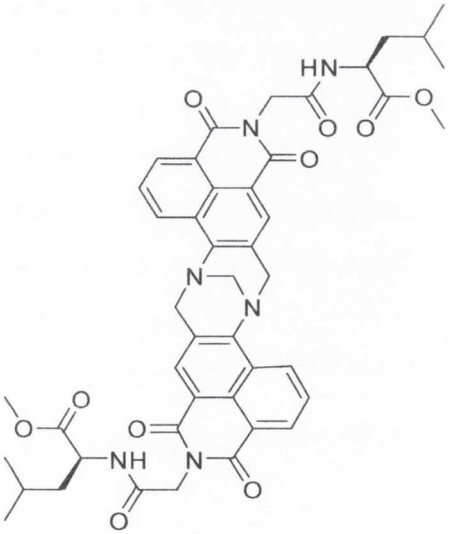

161 was synthesised by stirring **144** (60 mg, 0.104 mmol) and *S*-leucine methyl ester hydrochloride (40 mg, 0.219 mmol) in anhydrous CH_2Cl_2 at 0 °C. DIEA (108 mg, 0.15 mL, 0.832 mmol) was subsequently added followed by the slow addition of BOP (138 mg, 0.312 mmol) according to **Procedure 5** where a recrystallisation from CH_3OH yielded the desired product as a yellow solid (82 mg, 95 %). Decomposed at 254 °C; HRMS: 853.3193 ($[M+Na]^+$. $C_{45}H_{46}N_6O_{10}Na$ requires 853.3173; δ_H ($(CD_3)_2SO$, 400 MHz), 8.78 (2H, d, J = 8.0 Hz, H5, H5′), 8.57 (2H, d, J = 8.0 Hz, NH), 8.50 (2H, d, J = 8.0 Hz, H7, H7′), 8.13 (2H, s, H2, H2′), 8.01 (2H, *app.* t, H6, H6′), 5.21 (2H, d, J = 17.0 Hz, TB), 4.61-4.73 (8H, m, TB, CH_2), 4.28 (2H, m, NH$\underline{CH}$), 3.60 (6H, s, OCH_3), 1.60 (2H, m, $\underline{CH}(CH_3)_2$), 1.52 (4H, m, $CH\underline{CH_2}$), 0.87 (6H, d, J = 6.5 Hz, $CHCH_2CH(\underline{CH_3})_2$), 0.82 (6H, d, J = 6.5 Hz, $CHCH_2CH(\underline{CH_3})_2$); δ_C ($(CD_3)_2SO$, 150 MHz), 172.8 ($\underline{C}OOCH_3$), 166.6 (CONH), 163.1 (C=O), 162.6 (C=O), 149.2 (C), 131.2 (Ar-CH), 130.6 (Ar-CH), 130.3 (C), 129.8 (Ar-CH), 127.6 (Ar-CH), 126.7 (C), 126.2 (C), 122.2 (C), 107.0 (C), 66.4 (CH_2), 57.1 (CH_2), 52.2

(OCH_3), 50.0 (CH), 42.6 (CH_2), 40.2 (CH_2), 24.5 (CH), 23.0 (CH_3), 21.8 (CH_3); ν_{max} (neat sample)/cm^{-1} 2953, 1731, 1703, 1662, 1597, 1571, 1459.

Bis-{*N*-[*(1S)*-4-Methyl-pentanoic acid *tert* butyl ester]carboxamido-methyl]}-9,18-methano-1,8-naphthalimido[b,f][1,5]-diazocine 163[247]

163 was synthesised according to **Procedure 5** by stirring **144** (99 mg, 0.172 mmol) and *S*-leucine *tert*-butyl ester hydrochloride in anhydrous CH_2Cl_2 (10 mL) at 0 °C. DIEA (137 mg, 0.24 mL, 1.374 mmol) was added followed by BOP (229 mg, 0.518 mmol) at 0 °C. The reaction mixture was left to stir at room temperature overnight and the product was yielded as an orange solid (122 mg, 77 %) after trituration with CH_3OH. Decomposed at 281-283 °C; HRMS: 915.4293 ($[M+H]^+$. $C_{51}H_{59}N_6O_{10}Na$ requires 915.4293; δ_H ($(CD_3)_2SO$, 400 MHz), 8.76 (2H, d, J = 8.6 Hz, H5, H5′), 8.45 (2H, d, J = 7.1 Hz, NH), 8.41 (2H, d, J = 7.1 Hz, H7, H7′), 8.12 (2H, s, H2, H2′), 7.99 (2H, *app.* t, H6, H6′), 5.18 (2H, d, J = 17.0 Hz, TB), 4.55-4.75 (8H, m, TB, CH_2), 4.10-4.17 (2H, m, NHC<u>H</u>), 1.34 (9H, br.s, $OC(CH_3)_3$), 0.78-0.87 (12H, m, $NHCHCH_2CH(\underline{CH_3})_2$); δ_C ($(CD_3)_2SO$, 150 MHz), 172.2 ($\underline{C}OOC(CH_3)_3$), 166.2 (CONH), 163.9 (C=O), 163.3 (C=O), 149.6 (C), 131.3 (Ar-CH), 130.9 (Ar-CH), 129.0 (Ar-CH), 128.5 (C), 127.4 (C), 127.1 (Ar-CH), 125.3 (C), 122.9 (C), 118.8 (C), 82.2 (C), 67.1 (CH_2), 42.8 (CH_2), 51.9 (CH_2), 51.7 (CH), 42.3 (CH_2), 28.0 (CH_3), 24.5 (CH), 22.8 (CH_3), 22.3 (CH_3); ν_{max} (neat sample)/cm^{-1} 3356, 2958, 1732, 1706, 1664, 1597, 1571, 1458, 1369.

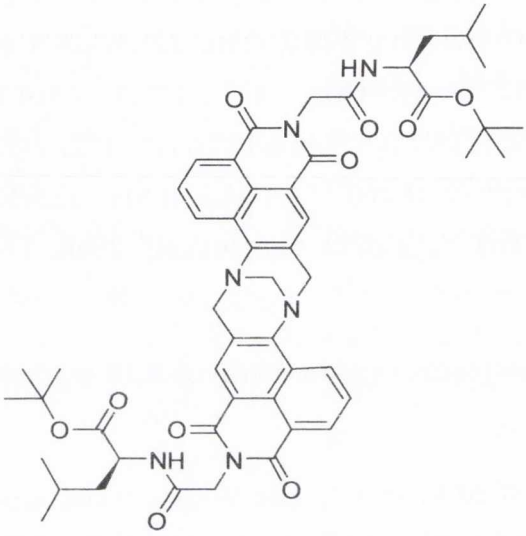

Bis-{*N*-[*(1S)*-4-Methyl-pentanoic acid] carboxamido-methyl]}-9,18- methano-1,8-naphthalimido[b,f][1,5]-diazocine 164[247]

164 was synthesised by stirring **163** (252 mg, 0.275 mmol) in TFA:CH_2Cl_2 (2:1) for three hours and removing the solvents by evaporation under reduced pressure to yield **163** as an orange solid. No purification was necessary. HRMS: 825.2855 ($[M+Na]^+$. $C_{43}H_{42}N_6O_{10}Na$ requires 825.2860; δ_H ($(CD_3)_2SO$, 600 MHz), 8.73 (2H, d, J = 8.0, H5, H5′), 8.62 (2H, d, J = 8.0, H7, H7′), 8.15 (2H, s, H2, H2′), 7.88 (2H, d, J = 8.0, H6, H6′), 5.18 (2H, d, J = 17.0 Hz, TB), 4.71 (2H, s, TB), 4.61 (2H, d, J = 17.0 Hz, TB), 4.52 (2H, m, NHC<u>H</u>), 4.28 (4H, s, CH_2), 1.69 (2H, m, $NHCHCH_2\underline{CH}(CH_3)_2$), 1.54 (4H, $NHCH\underline{CH_2}CH(CH_3)_2$), 0.93 (6H, m,

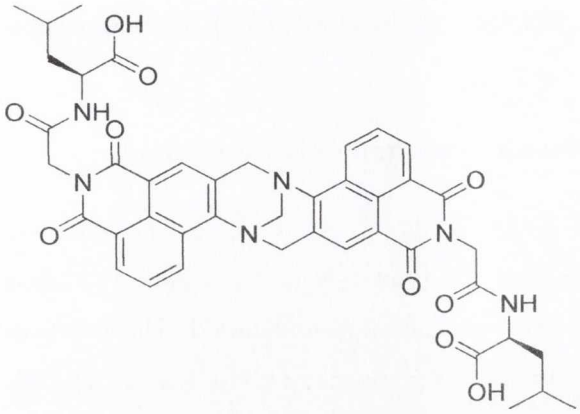

NHCHCH$_2$CH(C$\underline{H}_3$)$_2$), 0.92 (6H, m, NHCHCH$_2$CH(C$\underline{H}_3$)$_2$); δ_C ((CD$_3$)$_2$SO, 150 MHz), 171.8 (C$\underline{O}$OCH$_3$), 166.2 (CONH), 163.6 (C=O), 162.6 (C=O), 153.0 (C), 131.3 (Ar-CH), 130.8 (Ar-CH), 129.0 (Ar-CH), 128.5 (C), 127.4 (C), 127.1 (Ar-CH), 125.3 (C), 122.9 (C), 106.9 (C),67.1 (CH$_2$), 57.0 (CH$_2$), 51.5 (CH), 42.7 (CH$_2$), 42.1 (CH$_2$), 24.7 (CH), 22.8 (CH$_3$), 22.3 (CH$_3$); ν_{max} (neat sample)/cm^{-1} 2980, 1702, 1655, 1595, 1459.

5.5 General Synthetic Procedures for Chapter 4

5.5.1 Procedure 1: Formation of the 4-Chloro-1,8-Naphthalimide Derivatives[42]

4-Chloro-1,8-naphthalic anhydride (1 eq.), the appropriate dialkylaminoethylamine (1.4 eq.) and triethylamine (2 eq.) in toluene were stirred at reflux for 24 hours under an argon atmosphere. After completion of the reaction the solution mixture was immediately filtered while hot through celite, washing several times with toluene. The filtrate and washings were removed under reduced pressure and the residue dissolved in CH_2Cl_2. The organic solution was washed twice with sat. $NaHCO_3$, twice with H_2O and once with brine. The organic layer was dried over $MgSO_4$ and evaporated under reduced pressure to dryness.

5.5.2 Procedure 2: Formation of the 4-Amino Functionalised 1,8-Naphthalimide Derivatives

The relevant 4-chloro-1,8-naphthalimide derivative was refluxed in an excess of 1,3-diamino-propane. Upon cooling CH_2Cl_2 was added to the reaction mixture. The organic layer was washed twice with H_2O, dried over MgSO4 and evaporated under reduced pressure to dryness, to yield the desired product.

5.5.3 Procedure 3: Formation of the 4-Nitro-Bis-1,8-Naphthalimide Derivatives

The relevant 4-amino functionalised 1,8-naphthalimide derivative (1.05 eq.), 4-nitro-1,8-naphthalic anhydride (1.0 eq.) and triethylamine (2.0 eq.) were stirred at reflux in toluene overnight. Upon completion of the reaction, the reaction mixture was filtered hot through celite and washed with copious amounts of toluene. Upon cooling of the filtrate and washings, the residue precipitated out of solution and was subsequently collected by suction filtration. The residue was re-dissolved in CH_2Cl_2 and washed once with H_2O, sat. $NaHCO_3$

and brine. The organic layer was dried over $MgSO_4$ before being removed by evaporation under reduced pressure.

5.5.4 Procedure 4: Formation of the 4-Amino-Bis-1,8-Naphthalimide Derivatives

Reduction of the relevant 4-nitro-bis-1,8-naphthalimide in CH_2Cl_2:CH_3OH was carried out in the presence of a 10 % palladium on carbon catalyst using a Parr hydrogen shaker apparatus at 3 atm pressure until no more hydrogen gas was consumed. The reaction mixture was filtered through celite and washed with copious amounts of CH_2Cl_2 and CH_3OH. The filtrate and washings were removed under reduced pressure and further dried under vacuum.

5.5.5 Procedure 5: Formation of the Tetra-1,8-Naphthalimide Tröger's Base Derivatives[148,149]

A mixture of the relevant 4-amino-bis-1,8-naphthalimide (1.0 eq.) and paraformaldehyde (1.5 eq.) in neat TFA were stirred at room temperature overnight. The reaction mixture was initially neutralised and further basified by the slow addition of aqueous NaOH (6 M). The aqueous solution was extracted several times with CH_2Cl_2. The organic extracts were combined and the solvent was removed under reduced pressure. The crude product was purified and dried under vacuum.

N-[1-Pyrrolidino-ethyl]-4-chloro-1,8-naphthalimide 178

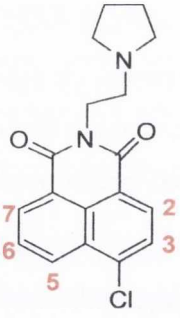

178 was synthesised by condensing 4-chloro-1,8-naphthalic anhydride (623 mg, 2.70 mmol) with 1-(2-aminoethyl)-pyrrolidine (428 mg, 0.472 mL, 3.7 mmol) in toluene (100 mL) in the presence of TEA according to **Procedure 1**, yielding the desired product as a light brown solid (887 mg, 99 %). No purification was necessary. Decomposed at 214-215 °C; HRMS: 329.1052 ($[M+H]^+$.$C_{18}H_{18}N_2O_2Cl$ requires 329.1057); δ_H ($(CD_3)_2SO$, 600 MHz), 8.67 (1H, d, J =8.3 Hz, H5), 8.63 (1H, d, J = 7.1 Hz, H7), 8.48 (1H, d, J = 7.9 Hz, H2), 8.09 (1H, d, J = 7.9 Hz, H3), 8.07 (1H, dd, J = 7.5, 8.6 Hz, H6), 4.41 (2H, t, J = 6.0 Hz, $NC\underline{H_2}CH_2N(CH_2)_2(CH_2)_2$), 3.65 (2H, m, $NCH_2CH_2N(CH_2)_2(C\underline{H_2})_2$), 3.54 (2H, t, J = 6.0 Hz, $NCH_2C\underline{H_2}N(CH_2)_2(CH_2)_2$), 3.15 (2H, m, $NCH_2CH_2N(CH_2)_2(\underline{CH_2})_2$), 2.02 (2H, m, $NCH_2CH_2N(C\underline{H_2})_2(CH_2)_2$), 1.88 (2H, t, J = 6.0 Hz, $NCH_2CH_2N(C\underline{H_2})_2(CH_2)_2$); δ_C ($(CD_3)_2SO$, 150 MHz), 163.6 (C=O), 163.3 (C=O), 137.6 (C), 131.7 (Ar-CH), 131.0 (Ar-CH), 130.2 (Ar-CH), 128.7(Ar-CH), 128.6 (C), 128.5 (C), 127.7 (Ar-CH), 123.0 (C), 121.7 (C), 53.5 (CH_2), 51.6 (CH_2), 36.3 (CH_2), 22.7 (CH_2); ν_{max} (neat sample)/cm^{-1} 2952, 1655, 1460, 786.

_N_-[1-Piperidino-ethyl]-4-chloro-1,8-naphthalimide 179

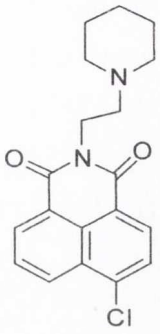

179 was synthesised according to **Procedure 1** by reacting 4-nitro-1,8-naphthalic anhydride (875 mg, 3.76 mmol) with 1-(2-aminoethyl)-piperidine (675 mg, 0.750 mL, 5.27 mmol) in toluene (100 mL) in the presence of TEA (761 mg, 1.0 mL, 7.52 mmol) to yield the product as a beige solid (1.157 g, 89 %). No purification was necessary. Decomposed at 240-241 °C; HRMS: 343.1223 ($[M+H]^+$.$C_{19}H_{20}N_2O_2Cl$ requires 343.1213); δ_H ($(CD_3)_2SO$, 600 MHz), 8.65 (1H, d, J = 8.4 Hz, H5), 8.61 (1H, d, J = 6.8 Hz, H7), 8.47 (1H, d, J = 7.9 Hz, H2), 8.08 (1H, d, J = 7.9 Hz, H3), 8.05 (1H, *app.* t, H6), 4.40 (2H, t, J= 5.7 Hz, $NC\underline{H_2}CH_2N(CH_2)_2(CH_2)_2CH_2$), 3.34 (2H, m, $NCH_2C\underline{H_2}N(CH_2)_2(CH_2)_2CH_2$), 3.02 (2H, m, $NCH_2CH_2N(C\underline{H_2})_2(CH_2)_2CH_2$), 2.74 (2H, m, $NCH_2CH_2N(C\underline{H_2})_2(CH_2)_2CH_2$), 1.74 (4H, m, $NCH_2CH_2N(CH_2)_2(C\underline{H_2})_2CH_2$), 1.54 (2H, m, $NCH_2CH_2N(CH_2)_2(CH_2)_2C\underline{H_2}$); δ_C ($(CD_3)_2SO$, 150 MHz), 163.6 (C=O), 163.3 (C=O), 137.8 (C), 131.8 (Ar-CH), 131.1 (Ar-CH), 130.4 (Ar-CH), 128.8 (Ar-CH), 128.7 (Ar-CH), 128.6 (C), 127.9 (C), 123.0 (C), 121.7 (C), 53.7 (CH_2), 52.7 (CH_2), 34.8 (CH_2),22.6 (CH_2), 21.5 (CH_2); ν_{max} (neat sample)/cm^{-1} 2951, 1655, 1459, 781.

_N_-[1-Pyrrolidino-ethyl]-4-diaminopropane-1,8-naphthalimide 180

180 was synthesised by refluxing **178** (753 mg, 2.29 mmol) in excess diaminopropane (5.942 g, 6.7 mL) according to **Procedure 2**, yielding the product as a brown solid (696 mg, 83 %). No purification was necessary. Decomposed at 205 °C; HRMS: 367.2131 ($[M+H]^+$.$C_{21}H_{27}N_4O_2$ requires 367.2134); δ_H ($(CD_3)_2SO$, 400 MHz), 8.64 (1H, d, J = 8.5 Hz, H5), 8.42 (1H, d, J = 7.04 Hz, H7), 8.25 (1H, d, J = 8.5 Hz, H2), 7.68 (1H, *app.* t, H6), 6.77 (1H, d, J = 8.5 Hz, H3), 4.15 (2H, t, J = 7.0 Hz, $NC\underline{H_2}CH_2N(CH_2)_2(CH_2)_2$), 3.45 (2H, t, J = 6.8 Hz, $NHC\underline{H_2}CH_2CH_2NH_2$), 2.74 (2H,t, J = 6.2 Hz, $NHCH_2CH_2C\underline{H_2}NH_2$), 2.64 (2H, t, J = 7.0 Hz, $NCH_2C\underline{H_2}N(CH_2)_2(CH_2)_2$), 2.51 (4H, m, $NCH_2CH_2N(C\underline{H_2})_2(CH_2)_2$), 1.81 (2H, quin, J = 6.5 Hz, $NHCH_2C\underline{H_2}CH_2NH_2$), 1.65 (2H, m, $NCH_2CH_2N(CH_2)_2(C\underline{H_2})_2$); δ_C ($(CD_3)_2SO$, 100 MHz), 163.7 (C=O), 162.8 (C=O), 150.8 (C), 134.3 (Ar-CH), 130.7 (Ar-CH), 129.4 (C), 128.5 (Ar-CH), 124.2 (Ar-CH), 121.8 (C), 120.1 (C), 107.3 (C), 103.7 (Ar-CH), 53.7 (CH_2), 53.3 (CH_2), 41.2 (CH_2), 38.9 (CH_2), 38.3 (CH_2), 31.1 (CH_2), 23.2 (CH_2); ν_{max} (neat sample)/cm^{-1} 3372, 3296, 2951, 2794, 1677, 1645.

_N_-[1-Piperidino-ethyl]-4-diaminopropane-1,8-naphthalimide 181

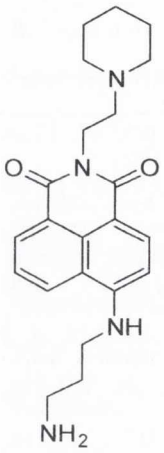

181 was synthesised according to **Procedure 2** by refluxing **179** (301 mg, 0.88 mmol) in excess diaminopropane (2.278 g, 2.6 mL), to yield the desired product as an orange solid (274 mg, 82 %). Decomposed at 223 °C; HRMS: 379.2134 ($[M\text{-}H]^-.C_{22}H_{27}N_4O_2$ requires 379.2134); δ_H ($(CD_3)_2SO$, 400 MHz), 8.67 (1H, d, J = 8.3 Hz, H5), 8.45 (1H, d, J = 7.3 Hz, H7), 8.28 (1H, d, J = 8.5 Hz, H2), 7.71 (1H, dd, J= 7.5, 8.5 Hz, H5), 6.81 (1H, d, J = 8.5 Hz, H3), 4.16 (2H, t, J = 7.3 Hz, $NC\underline{H_2}CH_2N(CH_2)_2(CH_2)_2CH_2$), 3.47 (2H, t, J = 6.9 Hz, $NHC\underline{H_2}CH_2CH_2NH_2$), 2.74 (2H, t, J = 6.4 Hz, $NHCH_2CH_2C\underline{H_2}NH_2$), 2.49 (2H, m, $NCH_2C\underline{H_2}N(CH_2)_2(CH_2)_2CH_2$), 2.47 (4H, m, $NCH_2CH_2N(C\underline{H_2})_2(CH_2)_2CH_2$), 1.82 (2H, m, $NHCH_2C\underline{H_2}CH_2NH_2$), 1.49 (4H, m, $NCH_2CH_2N(CH_2)_2(C\underline{H_2})_2CH_2$), 1.39 (2H, m, $NCH_2CH_2N(CH_2)_2(CH_2)_2C\underline{H_2}$); δ_C ($(CD_3)_2SO$, 100 MHz), 163.7 (C=O), 162.9 (C=O), 150.8 (C), 134.3 (Ar-CH), 130.6 (Ar-CH), 129.5 (C), 128.5 (Ar-CH), 124.3 (Ar-CH), 121.9 (C), 120.1 (C), 107.3 (C), 103.7 (Ar-CH), 56.0 (CH_2), 54.2 (CH_2), 41.3 (CH_2), 39.6 (CH_2), 36.8 (CH_2), 31.2 (CH_2), 25.6 (CH_2), 24.0 (CH_2); ν_{max} (neat sample)/cm^{-1} 3343, 3296, 2939, 1639, 1454.

_N_-[1-Pyrrolidino-ethyl]-1,8-naphthalimide-4_N_-propyl-4-nitro-1,8-naphthalimide 182

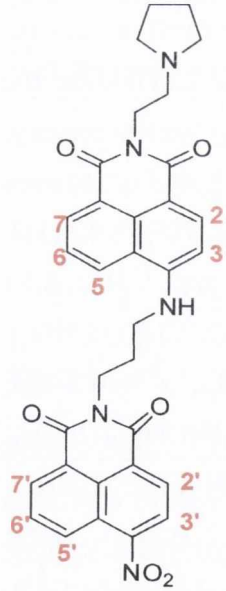

According to **Procedure 3**, **182** was synthesised by condensing **180** (1.472 g, 4.02 mmol) with 4-nitro-1,8-naphthalic anhydride (930 mg, 3.83 mmol) in toluene (150 mL) in the presence of triethylamine (774 mg, 1.060 mL, 7.65 mmol) to give a light brown solid (1.460 g, 65 %). No purification was necessary. Decomposed at 166 °C; HRMS: 592.2193 ($[M+H]^+.C_{33}H_{30}N_5O_6$ requires 592.2196); δ_H ($(CD_3)_2SO$, 600 MHz), 8.61 (1H, d, J = 8.6 Hz, H5'), 8.51 (1H, d, J = 8.0 Hz, H7'), 8.48 (3H, m, H2', H5, H3'), 8.33 (1H, d, J = 7.3 Hz, H7), 8.16 (1H, d, J = 8.6 Hz, H2), 8.01 (1H, *app.* t, H6'), 7.71 (1H, t, J = 5.4 Hz, NH), 7.51 (1H, *app.* t, H6), 6.74 (1H, d, J = 8.6 Hz, H3), 4.26 (2H, t, J = 6.7 Hz, $NHCH_2CH_2C\underline{H_2}N$), 4.15 (2H, m, $NC\underline{H_2}CH_2N(CH_2)_2(CH_2)_2$), 3.55 (2H, m, $NHC\underline{H_2}CH_2CH_2N$), 2.66 (2H, m, $NCH_2C\underline{H_2}N(CH_2)_2(CH_2)_2$), 2.55 (4H, t, m, $NCH_2CH_2N(C\underline{H_2})_2(CH_2)_2$), 2.20 (2H, m, $NHCH_2C\underline{H_2}CH_2N$), 1.68 (4H, m, $NCH_2CH_2N(C\underline{H_2})_2(C\underline{H_2})_2$); δ_C ($(CD_3)_2SO$, 150 MHz), 163.9 (C=O), 163.4 (C=O), 163.1 (C=O), 162.6 (C=O), 150.6 (C), 149.2 (C), 134.4 (Ar-CH), 131.8 (Ar-CH), 130.8 (Ar-CH), 130.2 (Ar-CH), 129.7 (Ar-CH), 129.4 (C), 128.8 (Ar-CH), 128.5 (Ar-CH), 128.5 (C), 126.9

(C), 124.4 (Ar-CH), 124.4 (Ar-CH), 123.0 (C), 122.8 (C), 121.9 (C), 120.3 (C), 107.8 (C), 104.3 (Ar-CH), 54.1 (CH_2), 53.5 (CH_2), 41.2 (CH_2), 38.7 (CH_2), 38.5 (CH_2), 26.1 (CH_2), 23.5 (CH_2); ν_{max} (neat sample)/cm^{-1} 3077, 2981, 1664, 1623, 1530, 1437.

_N_-[1-Pyperidino-ethyl]-1,8-naphthalimide-4_N_-propyl-4-nitro-1,8-naphthalimide 183

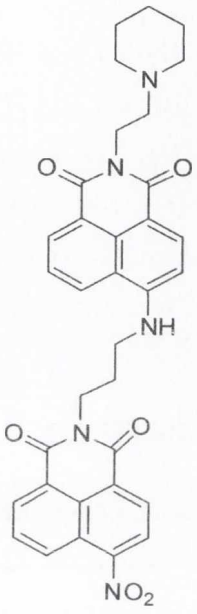

183 was synthesised by refluxing **181** (2.218 g, 5.83 mmol), 4-nitro-1,8-naphthalic anhydride (1.350 g, 5.55 mmol) and triethylamine (1.120 g, 1.5 mL, 1.11 mmol) in toluene (150 mL) according to **Procedure 3**, yielding the desired product as a brown solid (2.374 g, 71 %). No purification was necessary. Decomposed at 214 °C; HRMS: 606.2350 ($[M+H]^+$.$C_{34}H_{32}N_5O_6$ requires 606.2353); δ_H ($(CD_3)_2SO$, 600 MHz), 8.81 (2H, d, J = 8.6 Hz, H7'), 8.76 (2H, d, J = 8.0 Hz, H2'), 8.60 (2H, d, J = 8.0 Hz, H7'), 8.58 (2H, d, J = 8.0 Hz, H5'),8.45 (2H, d, J = 8.0 Hz, H2), 8.44 (2H, d, J = 8.0 Hz, H3'), 8.38 (2H, d, J = 8.0 Hz, H5), 8.04 (2H, *app.* t, H6'), 7.69 (2H, *app.* t, H6), 6.76 (2H, d, J = 8.0 Hz, H3), 6.35 (1H, d, J = 5.4 Hz, NH), 4.43 (2H, t, J = 6.7 Hz, $NHCH_2CH_2C\underline{H_2}N$), 4.37 (2H, m, $NC\underline{H_2}CH_2N(CH_2)_2(CH_2)_2$), 3.56 (2H, m, $NHC\underline{H_2}CH_2CH_2N$), 2.70 (2H, m, $NCH_2C\underline{H_2}N(CH_2)_2(CH_2)_2$), 2.28 (2H, m, $NHC\underline{H_2}CH_2CH_2N$), 2.01 (4H, m, $N(C\underline{H_2})_2(CH_2)_2CH_2$), 1.63 (4H, m, $N(CH_2)_2(C\underline{H_2})_2CH_2$), 1.47 (2H, m, $N(CH_2)_2(CH_2)_2C\underline{H_2}$); δ_C ($(CD_3)_2SO$, 150 MHz), 164.6 (C=O), 164.0 (C=O), 164.0 (C=O), 163.2 (C=O), 149.9 (C), 149.3 (C), 134.4 (Ar-CH), 132.9 (Ar-CH), 131.1 (Ar-CH), 130.3 (Ar-CH), 130.0 (C),130.0 (Ar-CH), 129.8 (Ar-CH), 129.1 (C), 126.5 (C), 126.2 (Ar-CH), 124.9 (Ar-CH), 123.9 (Ar-CH), 123.7 (C), 123.1 (C), 122.6 (C), 120.5 (C), 110.4 (C), 104.1 (Ar-CH), 56.5 (CH_2), 54.7 (CH_2), 40.2 (CH_2), 38.0 (CH_2), 37.3 (CH_2), 26.7 (CH_2), 26.0 (CH_2), 24.4 (CH_2); ν_{max} (neat sample)/cm^{-1} 3356, 2961, 1698, 1655, 1575, 1529, 1437.

_N_-[1-Pyrrolidino-ethyl]-1,8-naphthalimide-4_N_-propyl-4-amino-1,8-naphthalimide 184

184 was synthesised using **182** (105 mg, 0.18 mmol) according to **Procedure 4** and gave the product as an orange solid (96 mg, 95 %). Decomposed at 205 °C; HRMS: 562.2454 ($[M+H]^+$.$C_{33}H_{32}N_5O_4$ requires 562.2454); δ_H ($(CD_3)_2SO$, 600 MHz), 8.69 (1H, d, J = 8.4 Hz, H5), 8.63 (1H, d, J = 8.4 Hz, H5'), 8.41 (1H, d, J = 7.3 Hz, H7), 8.38 (1H, d, J = 7.4 Hz, H7'), 8.22 (1H, d, J = 8.5 Hz, H2), 8.16 (1H, d, J = 8.4 Hz, H2'), 7.93 (1H, t, J = 5.4 Hz NH),7.69 (1H, dd, J = 7.5, 8.1 Hz, H6), 7.62 (1H, dd, J = 7.5, 8.2 Hz, H6'), 7.50 (2H, s, NH_2), 6.83 (1H, d, J = 8.4 Hz, H3'), 6.76 (1H, d, J = 8.7 Hz, H3), 4.35 (2H, t, J = 5.9 Hz, $NC\underline{H_2}CH_2N(CH_2)_2(CH_2)_2$), 4.19 (2H, t, J = 6.9 Hz, $NHCH_2CH_2C\underline{H_2}N$), 3.49 (2H, m,

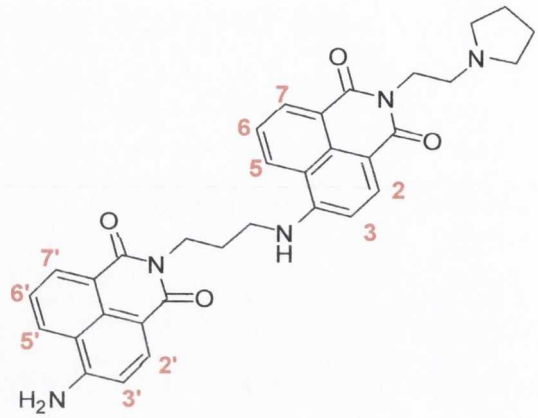

NHC$\underline{H_2}$CH$_2$CH$_2$N), 3.42 (2H, m, NCH$_2$C$\underline{H_2}$N(CH$_2$)$_2$(CH$_2$)$_2$), 3.41 (4H, m, NCH$_2$CH$_2$N(C$\underline{H_2}$)$_2$(CH$_2$)$_2$), 2.09 (2H, m, NHCH$_2$C$\underline{H_2}$CH$_2$N), 1.92 (4H, m, NCH$_2$CH$_2$N(CH$_2$)$_2$(C$\underline{H_2}$)$_2$); δ_C ((CD$_3$)$_2$SO, 150 MHz), 164.2 (C=O), 164.0 (C=O), 163.1 (C=O), 163.0 (C=O), 152.8 (C), 150.7 (C), 134.5 (Ar-CH), 134.0 (Ar-CH), 131.0 (Ar-CH), 130.8 (Ar-CH), 129.8 (C), 129.7 (C), 129.3 (Ar-CH), 128.6 (Ar-CH), 124.7 (C), 124.3 (Ar-CH), 123.9 (Ar-CH), 121.8 (C), 120.2 (C), 119.9 (C), 108.1 (Ar-CH), 107.5 (C), 107.4 (C), 103.7 (Ar-CH), 53.7 (CH$_2$), 52.0 (CH$_2$), 40.9 (CH$_2$), 37.4 (CH$_2$), 35.9 (CH$_2$), 26.7 (CH$_2$), 22.8 (CH$_2$); ν_{max} (neat sample)/cm^{-1} 3657, 3443, 3251, 1700, 1646, 1436.

_N_-[1-Piperidino-ethyl]-1,8-naphthalimide-4_N_-propyl-4-amino-1,8-naphthalimide 185

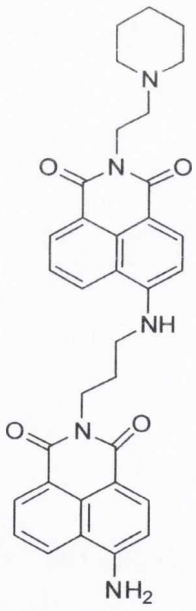

185 was synthesised using **183** (548 mg, 0.91 mmol) according to **Procedure 4** and gave the product as a red solid (519 mg, 99 %). Decomposed at 223 °C; HRMS: 576.2609 ([M+H]$^+$.C$_{34}$H$_{34}$N$_5$O$_4$ requires 576.2611); δ_H ((CD$_3$)$_2$SO, 600 MHz), 8.71 (1H, d, J = 8.4 Hz, H5), 8.63 (1H, d, J = 8.4 Hz, H5'), 8.42 (1H, d, J = 7.3 Hz, H7), 8.39 (1H, d, J = 7.4 Hz, H7'), 8.23 (1H, d, J = 8.5 Hz, H2), 8.16 (1H, d, J = 8.4 Hz, H2'), 7.95 (1H, t, J = 5.4 Hz, NH), 7.65 (1H, dd, J = 7.5, 8.1 Hz, H6), 7.62 (1H, dd, J = 7.5, 8.2 Hz, H6'), 7.51 (2H, s, NH$_2$), 6.84 (1H, d, J = 8.4 Hz, H3'), 6.77 (1H, d, J = 8.7 Hz, H3), 4.39 (2H, t, J = 5.9 Hz, NC$\underline{H_2}$CH$_2$N(CH$_2$)$_2$(CH$_2$)$_2$CH$_2$), 4.19 (2H, t, J = 6.9 Hz, NHCH$_2$CH$_2$C$\underline{H_2}$N), 3.64 (2H, m, NCH$_2$CH$_2$N(C$\underline{H_2}$)$_2$(CH$_2$)$_2$CH$_2$), 3.50 (2H, m, NHC$\underline{H_2}$CH$_2$CH$_2$N), 3.35 (2H, m, NCH$_2$C$\underline{H_2}$N(CH$_2$)$_2$(CH$_2$)$_2$CH$_2$), 2.96 (2H, m, NCH$_2$CH$_2$N(C$\underline{H_2}$)$_2$(CH$_2$)$_2$CH$_2$), 2.09 (2H, m, NHCH$_2$C$\underline{H_2}$CH$_2$N), 1.81 (2H, m, NCH$_2$CH$_2$N(CH$_2$)$_2$(C$\underline{H_2}$)$_2$CH$_2$), 1.76 (2H, m, NCH$_2$CH$_2$N(CH$_2$)$_2$(C$\underline{H_2}$)$_2$CH$_2$), 1.41 (2H, m, NCH$_2$CH$_2$N(CH$_2$)$_2$(CH$_2$)$_2$C$\underline{H_2}$); δ_C ((CD$_3$)$_2$SO, 150 MHz), 164.2 (C=O), 164.0 (C=O), 163.1 (C=O), 163.0 (C=O), 152.8 (C), 150.8 (C), 134.4 (Ar-CH), 134.0 (Ar-CH), 131.0 (Ar-CH), 130.8 (Ar-CH), 129.7 (C), 129.6 (C), 129.4 (Ar-CH), 129.7 (C), 128.8 (Ar-CH), 124.2 (Ar-CH), 123.9 (Ar-CH), 121.7 (C), 121.7 (C), 119.4 (C), 108.2 (Ar-CH), 107.4 (C), 107.3 (C), 103.8 (Ar-CH), 55.9 (CH$_2$), 52.5 (CH$_2$), 40.9 (CH$_2$), 37.5 (CH$_2$), 34.2 (CH$_2$), 26.9 (CH$_2$), 22.5 (CH$_2$), 21.3 (CH$_2$): ν_{max} (neat sample)/cm^{-1} 3443, 3356, 3249, 1698, 1655, 1437.

Tetra-1,8-Naphthalimide based Tröger's Base 175

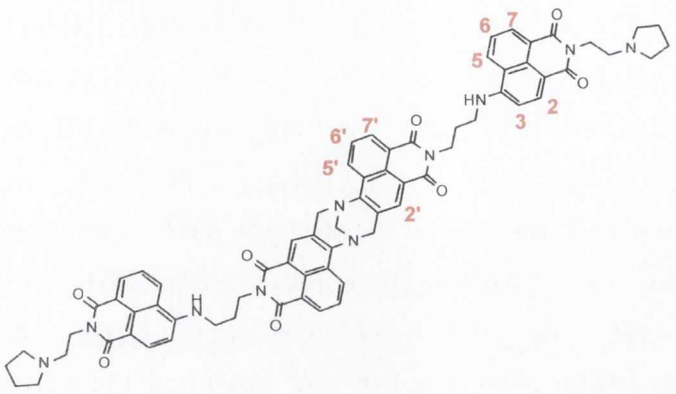

175 was synthesised according to **Procedure 5**, by stirring **184** (200 mg, 0.37 mmol) and paraformaldehyde (16 mg, 0.55 mmol) in TFA (2 mL) at room temperature overnight. Trituration with CH_3OH gave **175** as an orange solid (119 mg, 56 %). Decomposed at 232 °C; Calculated for $C_{71}H_{66}N_{10}O_8$. $CH_2Cl_2.CH_3OH$: C, 66.82; H, 5.37; N, 10.97. Found C, 66.28; H, 4.95; N, 10.60; HRMS: 1159.4821 ($[M+H]^+$.$C_{69}H_{63}N_{10}O_8$ requires 1159.4830); δ_H (COND$(CD_3)_2$, 600 MHz), 8.67 (2H, d, J = 8.0 Hz, H5′), 8.61 (2H, d, J = 8.0 Hz, H7), 8.54 (2H, d, J = 8.0 Hz, H7′), 8.36 (2H, d, J = 8.0 Hz, H5), 8.26 (2H, d, J = 8.0 Hz, H2), 8.06 (2H, s, H2′), 7.91 (2H, *app.* t, H6′), 7.50 (2H, *app.* t, H6), 6.60 (2H, d, J = 8.0 Hz, H3), 5.11 (2H, d, J = 17.0 Hz, TB), 4.69 (2H, s, TB), 4.53 (2H, d, J = 17.0 Hz, TB), 4.48 (4H, m, $N\underline{CH_2}CH_2N(CH_2)_2(CH_2)_2$), 4.23 (4H, m, $NHCH_2CH_2\underline{CH_2}N$), 3.88 (4H, m, $NCH_2\underline{CH_2}N(CH_2)_2(CH_2)_2$), 3.39 (4H, m, $NH\underline{CH_2}CH_2CH_2N$), 3.38 (8H, m, $NCH_2CH_2N(\underline{CH_2})_2(CH_2)_2$), 2.10 (8H, m, $NCH_2CH_2N(CH_2)_2(\underline{CH_2})_2$), 2.09 (4H, m, $NHCH_2\underline{CH_2}CH_2N$); δ_C (COND$(CD_3)_2$, 150 MHz), 164.0 (C=O), 164.0 (C=O), 163.8 (C=O), 163.7 (C=O), 149.2 (C), 149.0 (C), 135.0 (Ar-CH), 131.1 (Ar-CH), 131.0 (Ar-CH), 130.7 (Ar-CH), 129.2 (Ar-CH), 129.0 (Ar-CH), 127.4 (Ar-CH), 124.5 (Ar-CH), 119.5 (C), 107.7 (C), 103.8 (Ar-CH), 66.0 (CH_2), 57.0 (CH_2), 54.5 (CH_2), 52.0 (CH_2), 40.4 (CH_2), 37.6 (CH_2), 35.6 (CH_2), 26.9 (CH_2), 23.0 (CH_2); ν_{max} (neat sample)/cm^{-1} 3657, 3355, 3077, 2897, 1697, 1648, 1576, 1435, 1347.

Tetra-1,8-Naphthalimide based Tröger's Base 176

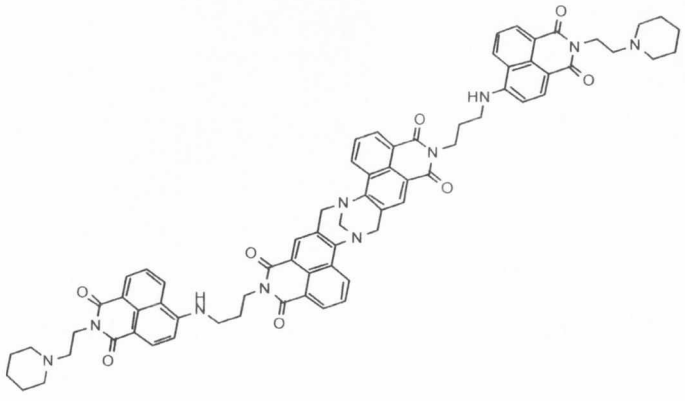

176 was synthesised by stirring **185** (233 mg, 0.41 mmol) and paraformaldehyde (18 mg, 0.61 mmol) in TFA (2 mL) overnight according to **Procedure 5** as an orange solid (168 mg, 70 %) after trituration from CH_3OH. Decomposed at 229-230 °C; Calculated for $C_{71}H_{66}N_{10}O_8$. CH_2Cl_2: C, 77.97; H, 5.42; N, 10.65. Found C,

68.27; H, 5.42; N, 10.65; HRMS: 1187.5088 ($[M+H]^+$.$C_{71}H_{67}N_{10}O_8$ requires 1187.5143); δ_H ($COND(CD_3)_2$, 600 MHz), 8.96 (2H, d, J = 8.0 Hz, H7′), 8.82 (2H, d, J = 8.0 Hz, H7), 8.68 (2H, d, J = 8.0 Hz, H5′), 8.58 (2H, d, J = 8.0 Hz, H5), 8.42 (2H, d, J = 8.0 Hz, H2), 8.31(2H, s, H2′), 8.16 (2H, *app*.t, H6′), 7.74 (2H, *app.* t, Hz, H6), 7.00 (2H, d, J = 8.0 Hz, H3), 5.42 (2H, d, J = 17.0 Hz, TB), 4.99 (2H, s, TB), 4.92 (2H, d, J = 17.0 Hz, TB), 4.48 (4H, m, $N\underline{CH_2}CH_2N(CH_2)_2(CH_2)_2CH_2$), 4.46 (4H, m, $NHCH_2CH_2\underline{CH_2}N$), 3.77 (4H, m, $NH\underline{CH_2}CH_2CH_2N$), 3.77 (8H, m, $NCH_2CH_2N(\underline{CH_2})_2(CH_2)_2CH_2$), 3.67 (4H, m, $NCH_2\underline{CH_2}N(CH_2)_2(CH_2)_2$), 2.38 (4H, m, $NHCH_2\underline{CH_2}CH_2N$), 1.79 (8H, m, $NCH_2CH_2N(CH_2)_2(\underline{CH_2})_2CH_2$), 1.65 (4H, m, $NCH_2CH_2N(CH_2)_2(CH_2)_2\underline{CH_2}$); δ_C ($COND(CD_3)_2$, 164.5 (C=O), 164.3 (C=O), 164.0 (C=O), 163.4 (C=O), 150.9 (C), 134.3 (Ar-CH), 130.8 (Ar-CH), 130.4 (Ar-CH), 129.6 (Ar-CH), 129.3 (Ar-CH), 128.4 (Ar-CH), 127.1 (Ar-CH), 124.3 (Ar-CH), 121.4 (C), 120.0 (C), 108.3 (C), 104 (Ar-CH), 85.3 (C), 67.4 (CH_2), 56.9 (CH_2), 53.8 (CH_2), 42.0 (CH_2), 41.5 (CH_2), 38.2 (CH_2), 36.6 (CH_2), 26.8 (CH_2), 25.2 (CH_2), 23.8 (CH_2); ν_{max} (neat sample)/cm^{-1} 3664, 2981, 2896, 1698, 1654, 1575, 1436.

References

1. Duke, R. M.; Veale, E. B.; Pfeffer, F. M.; Kruger, P. E.; Gunnlaugsson, T. *Chem. Soc. Rev.* **2010**, *39*, 3936-3953.

2. (a) Braña, M. F.; Ramos. A. *Curr. Med. Chem. Anti-Cancer Agents* **2001**, *1*, 237. (b) Braña, M. F.; Cacho, M.; Gradillas, A.; de Pascual-Teresa, B.; Ramos, A. *Curr. Pharm. Des.* **2001**, *7*, 1745. (c) Ingrassia, L.; Lefranc, F.; Kiss, R.; Mijatovic, T. *Curr. Med. Chem.* **2009**, *16*, 1192-213. (d) Lv, M.; Xu, H. *Curr. Med. Chem.* **2009**, *16*, 4797-4813.

3. (a) Grabchev, I.; Bojinov, V.; Petkov, C. *Dyes and Pigments* **2001**, *51*, 1-8. (b) Grabchev, I.; Chovelon, J-M. *Z. Naturforsch.* **2003**, *58a*, 45-50. (c) Gharanjig, K.; Ameri, F.; Dadras, F. S.; Khosravi, A. *Prog. Color Colourants Coat* **2011**, *4*, 27-37.

4. (a) de Silva, A. P.; Rice, T. E. *Chem. Commun.* **1996**, 163-164. (b) Gunnlaugsson, T.; McCoy, C. P.; Morrow, R. J.; Phelan, C.; Stomeo, F. *Arkivoc* **2003**, *8*, 216-228. (c) Parkesh, R.; Lee, T. C.; Gunnlaugsson, T. *Org. Biomol. Chem.* **2007**, *5*, 310-317. (d) Xu, Z.; Xiao, Y.; Qian, X.; Cui, J.; Cui, D. *Org. Lett.* **2005**, *7*, 889-892. (e) Hanaoka, K.; Muramatu, Y.; Urano, Y.; Terai, T.; Nagano, T. *Chem. Eur. J.* **2010**, *16*, 568-572.

5. (a) Tian, H.; Liu, B. *J. Mater. Chem.* **2005**, *15*, 3026-3033. (b) Xu, Z.; Tang, J.; Tian, H. *Chin. Chem. Lett.* **2008**, *19*, 1353-1357. (c) Li, Y.; Cao, L.; Tian, H.; *J. Org. Chem.* **2006**, *71*, 8279-8282.

6. (a) Elmes, R. B. P.; Gunnlaugsson, T. *Tetrahedron Lett.* **2010**, *51*, 4082-4087. (b) Veale, E. B.; Tocci, G. M.; Pfeffer, F. M.; Kruger, P. E.; Gunnlaugsson, T. *Org. Biomol. Chem.* **2009**, *7*, 3447-3454.

7. Singh, N.; Kaur, N.; Dunn, J.; Behan, R.; Malrooney, R. C.; Callan, J. F. *Eur. Polym. J.* **2009**, *45*, 272-277.

8. Bao, X-P.; Wang, L.; Wu, L.; Li, Z-Y. *Supramol. Chem.* **2008**, *20*, 467-472.

9. Pfeffer, F. M.; Seter, M.; Lewcenko, N.; Barnett, N. W. *Tetrahedron Lett.* **2006**, *47*, 5241-5245.

10. Neidle, S., *Nucleic Acid Structure and Recognition*; Oxford University Press Inc.: New York, 2002.

11. International Human Genome Mapping Consortium, *Nature* **2001**, *409*, 934-941.

12. Berg. J. M.; Tymoczko, J. L.; Stryer, L. *Biochemistry*, 5th ed.; W. H. Freeman and Company: New York, 2003.

13. Blackburn, G. M.; Gait, M. J.; Loakes, D.; Williams, D. M. *Nucleic Acids in Chemistry and Biology,* 4th ed.; Royal Society of Cambridge, 2006.

14. Bloomfield, V. A. C.; Tinoco Jr., D. M. *Nucleic Acids: Structures, Properties and Functions*, 1st ed. ; Oxford University Press: Oxford, 2002.

15. Watson, J. D.; Crick, F. H. C. *Nature* **1953**, *171*, 737-738.

16. Neidle, S., *Principles of Nucleic Acid Structure*; Academic Press, 2008.

17. Voet, D.; Voet, J. G. *Biochemistry*; Wiley: New Jersey, 2011.

18. Ha, S. C.; Lowenhaupt, K.; Rich, A.; Kim, Y-G.; Kim, K. K. *Nature* **2005**, *437*, 1183-1186.

19. Propst, C. L.; Penin, T. J. *Nucleic Acid Targeted Drug Design;* Marcel Dekker Inc., New York, 1992.

20. Hannon, M. J. *Chem. Soc. Rev.* **2007**, *36*, 280-295.

21. Schreiber, S. L. *Science* **2000**, *287*, 1964-1969.

22. Neidle, S., *Nucleic Acid Structure and Recognition*, Oxford University Press Inc., New York, 2002.

22. Dervan, P. B.; Poulin-Kerstien, A. T.; Fechter, E. J.; Edelson, B. S. *Top. Curr. Chem.* **2005**, *253*, 1-31.

23. Dervan, P. B.; Edelson, B. S. *Curr. Opin. Struc. Biol.* **2003**, *13*, 284-299.

24. Kim, S. K.; Nordén, B. *FEBS Lett.* **1993**, *315*, 61-64.

25. Tuite, E.; Nordén, E. *J. Am. Chem. Soc.* **1994**, *116*, 7548-7556.

26. Tuite, E.; Kelly, J. M. *Biopolymers*, **1995**, *35*, 419-433.

27. Da Ros, T.; Spalluto, G.; Prato, M.; Saison-Behmoaras, T.; Boutorine, A.; Cacciari, B. *Curr. Med. Chem.* **2005**, *12*, 71-88.

28. Harris, A.; Qu, Y.; Farrell, N.; *Inorg. Chem.* **2005**, *44*, 1196-1198.

29. www.macmillan.org.uk

30. Zhang, C. X.; Lippard, S. J.; *Curr. Opin. Chem. Biol.* **2003**, *7*, 481-489.

31. Lerman, L. S. *J. Mol. Biol.* **1961**, *3*, 18-30.

32. Braña, M. F.; Castellano, J. M.;. Roldán, C. M.; Santos, A.; Vásquez, D.; Jiménez, A. *Cancer Chemother. Pharmacol.* **1980**, *4*, 61-66.

33. Waring, M. J.; González, A.; Jiménez, A.; Vázquez, D. *Nucleic Acids Res.* **1979**, *7*, 217-230

34. Braña, M. F.; Sanz, A. M.; Castellano, J. M.; Roldan, C. M.; Roldan, C. *Eur. J. Med. Chem.- Chim. Ther.* **1981**, *3*, 207-212.

35. Stevenson, K. A., Yen, S. F., Yang, N. C., Boykin, D. W.; Wilson, W. D. *J. Med. Chem.*, **1984**, *27*, 1677-1682.

36. Nishio, A.; Uyeki, E. M. *J. Natl. Cancer Inst.* **1983**, *70*, 1097-1102.

37. Andersson, B. S.; Beran, M.; Bakic, M.; Silberman, L. E.; Newman, R. A.; Zwelling, L. A. *Cancer Res.* **1987**, 47, 1040-1044.

38. Saez, R.; Craig, J. B.; Kuhn, J. G.; Weiss, G. R.; Koeller, J.; Phillips, J.; Havlin, K.; Harman, G.; Hardy, J.; Melink, T. J. *J. Clin. Oncol.* **1989**, *7*, 1351-1358.

39. Ratain, M. J.; Mick, R.; Berezin, F.; Janish, L.; Schilsky, R. L.; Williams, S. F.; Smiddy, J. *Clin. Pharmacol. Ther.* **1991**, *50*, 573-579.

40. (a) ClinicalTrials.gov. Identifier NCT07066494, (b) ClinicalTrials.gov. Identifier NCT00715637.

41. Cui, L.; Zhong, Y.; Zhu, W.; Xu, Y.; Qian, X. *Chem. Commun.* **2010**, *46*, 7121-7123.

42. Zee-Cheng, R. K. Y.; Cheng, C. C. *J. Med. Chem.* **1985**, *28*, 1216-1222.

43. Braña, M. F.; Castellano, J. M.; Morán, M.; Emling, F., Kluge, M.; Schlick, E.; Klebe, G.; Walker, N. *Arzneim.-Forsch.* **1995**, *45*, 1311-1318.

44. Van Quaquebeke, E.; Mahieu, T.; Dumont, P.; Dewelle, J.; Ribaucour, F.; Simon, G.; Sauvage, S.; Gaussian, J-F.; Tuti, J.; El Yazidi, M.; Van Vynckt, F.; Mijatotovic, T.; Lefranc, F.; Darro, F.; Kiss, R. *J. Med. Chem.* **2007**, *50*, 4122-4134.

45. Mijatotovic, T.; Mahieu, T.; Bruyère, C.; De Nève, N.; Dewelle, J.; Simon, G.; Dehoux, M. J. M.; Van der Aar, E.; Haibe-Kains, B.; Bontempi, G.; Decaestecker, C.; Van Quaquebeke, E.; Darro, F.; Kiss, R. *Neoplasia.* **2008**, *10*, 573-586.

46. Sami, S. M.; Dorr, R. T.; Alberts, D. S.; Remers, W. A. *J. Med. Chem.* **1993**, *36*, 765-770.

47. Sami, S. M.; Dorr, R. T.; Alberts, D. S.; Slyom, A. M.; Remers, W. A. *J. Med. Chem.* **1993**, *36*, 765-770.

48. Braña, M. F.; Cacho, M.; García, M. A.; de Pascual-Teresa, B.; Ramos, A.; Acero, N.; Llinares, F.; Muñoz-Mingarro, D.; Abradelo, C.; Rey-Stolle, M. F.; Yuste, M. *J. Med. Chem.* **2002**, *45*, 5813-5816.

49. Braña, M. F.; Cacho, M.; Ramos, A.; Domínguez, M. T.; Pozuelo, J. M.; Abradelo, C.; Rey-Stolle, M. F.; Yuste, M.; Carrasco, C.; Bailly, C. *Org. Biomol. Chem.* **2003**, *1*, 648-654.

50. Braña, M. F.; Cacho, M.; García, M. A.; de Pascual-Teresa, B.; Ramos, A.; Domínguez, M. T.; Pozuelo, J. M.; Abradelo, C.; Rey-Stolle, M. F.; Yuste, M.; Báñez-Coronel, M.; Lacal. J. C. *J. Med. Chem.* **2004**, *47*, 1391-1399.

51. Li, F.; Cui, J.; Guo, L.; Qian, X.; Ren, W.; Wang, K.; Liu, F. *Bioorg. Med. Chem*, **2007**, *15*, 5114-5121.

52. Xu, Y.; Qu, B.; Q. X.; Li, Y. *Bioorg. Med. Chem. Lett.* **2005**, *15*, 1139-1142.

53. Zhu, H.; Huang, M.; Yang, F.; Chen, Y.; Miao, Z-H.; Qian, X.; Xu, Y-F.; Qin, Y-X.; Luo, H-B.; Shen, X.; Geng, M-Y.; Cai, Y-J.; Ding, J. *Mol. Cancer Ther.* **2007**, *6*, 484-495.

54. Zhu, H.; Míao-Z-M.; Huang, M.; Feng, J-M.; Zhang, Z-X.; Lu, J-J.; Cai, Y-J.; Tong, L-J.; Xu, Y-F.; Qian, X.; Ding, J. *Neoplasia* **2009**, *11*, 1226-1234.

55. Qian, X.; Li, Y.; Xu, Y.; Liu, Y.; Qu, B. *Med. Chem. Lett.* **2004**, *14*, 2665-2668.

56. Yang, P.; Yang, Q.; Qian, X.; Cui, J. *Bioorg. Med. Chem.* **2005**, *13*, 5909-5914.

57. Li, Z.; Yang, Q.; Qian, X. *Bioorg. Med. Chem. Lett.* **2005**, *15*, 1769-1772.

58. Li, Z.; Yang, Q.; Qian, X. *Bioorg. Med. Chem.* **2005**, *13*, 4864-4870.

59. Li, Z.; Yang, Q.; Qian, X. *Bioorg. Med. Chem. Lett.* **2005**, *15*, 3143-3146.

60. Li, X.; Lin, Y.; Yuan, Y.; Liu, K.; Qian, X. *Tetrahedron*, **2011**, *67*, 2299-2304.

61. Xie, L.; Cui, J.; Qian, X.; Xu, Y.; Liu, J.; Xu, R. *Bioorg. Med. Chem.* **2011**, *19*, 961-967.

62. Yin, H.; Xu, Y.; Qian, X.; Li, Y.; Liu, J. *Bioorg. Med. Chem. Lett.* **2007**, *17*, 2166-2170.

63. Liu, Y.; Xu, Y.; Qian, X.; Liu, J.; Shen, L.; Li, J.; Zhang, Y. *Bioorg. Med. Chem.* **2006**, *14*, 2935-2941

64. Liang, X.; Xu, Y.; Liu, J.; Qian, X. *Mol. Cancer Res.* **2010**, *8*, 1619-1632.

65. Liang, X.; Wu, A.; Xu, Y.; Xu, K.; Liu, J.; Qian, X. *Invest New Drugs* **2011**, *29*, 646-658.

66. Liang, X.; Xu, K.; Xu, Y.; Liu, J.; Qian, X. *Toxicol. Appl. Pharm.* **2011**, *256*, 52-61.

67. Saito, I.;Takayama, M. *J. Am. Chem. Soc.* **1995**, *117*, 5590-5591.

68. Wu, A.; Xu, Y.; Qian, X. *Bioorg. Med. Chem.* **2009**, *17*, 592-599.

69. Phanstiel, O.; Price, H. L.; Wang, L.; Juusola, J.; Kline, M.; Shah, S. M. *J. Org. Chem.* **2000**, *65*, 5590-5599.

70. Tian, Z.; Xie, S.; Mei, Z.; Zhao, J.; Gao, W.; Wang, C. *Org. Biomol. Chem.* **2009**, *7*, 4651-4660.

71. Yang, Q.; Yang, P.; Qian, X.; Tong, L. *Bioorg. Med. Chem. Lett.* **2008**, *18*, 6210-6213.

72. Bagowski, C. P.; You, Y.; Scheffler, H.; Vlecken, D. H.; Schmitz, D. J.; Ott, I. *Dalton Trans.* **2009**, *48*, 10799-10805.

73. Gupta, R.; Liu, J.; Xie, J.; Lown, J. W. *Anti-Cancer Drug Des.* **1996**, *11*, 581-596.

74. Kamal, A.; Adil, S. F.; Tamboli, J. R.; Siddardha, B.; Murthy, U. S. N. *Lett. Drug Des. Discov.* **2009**, *6*, 201-209.

75. Kamal, A.; Reddy, B. S. N.; Reddy, G. S. K.; Ramesh, G. *Bioorg. Med. Chem. Lett.* **2002**, *12*, 1933-1935.

76. Kamal, A.; Srinivas, O.; Ramulu, P.; Ramesh, G.; Kumar, P. P. *Bioorg. Med. Chem. Lett.* **2003**, *13*, 3577-3581.

77. Kamal, A.; Ramu, R.; Tekumalla, V.; Khanna, G. B. R.; Barkume, M. S.; Juvekar, A. S.; Zingde, S. M. *Bioorg. Med. Chem.* **2008**, *16*, 7218-7224.

78. Rettig, M.; Kamal, A.; Ramu, R.; Mikolajczak, J.; Weisz, K. *Bioorg. Med. Chem.* **2009**, *17*, 919-928.

79. Rettig, M.; Langel, W.; Kamal, A.; Weisz, K.; *Org. Biomol. Chem.* **2010**, *8*, 3179- 3187.

80. Cholody, W. M.; Kosakowska-Cholody, T.; Hollingshead, M. G.; Hariprakasha, H. K.; Michejda, C. J. *J. Med. Chem.* **2005**, *48*, 4474-4481.

81. Kosakowska-Cholody, T.; Cholody, W. M.; Monks, A.; Woynarowska, B. A.; Michejda, C. J. *Mol. Cancer. Ther.* **2005**, *4*, 1617-1627

82. Hariprakasha, H. K.; Kosakowska-Cholody, T.; Meyer, C.; Cholody, W. M.; Stinson, S. F.; Tarasova, N. I.; Michedja, J. *J. Med. Chem.* **2007**, *50*, 5557-5560

83. Chen, Z.; Liang, X.; Zhang, H.; Xie, H.; Liu, J.; Xu, Y.; Zhu, W.; Wang, Y.; Wang, X.; Tan, S.; Kuang, D.; Qian, X. *J. Med. Chem.* **2010**, *53*, 2589-2600.

84. Lin, B.; Chen, Z.; Xu, Y.; Zhang, H.; Liu, J.; Qian, X. *Leukemia Res.* **2011**, *35*, 646-656.

85. Braña, M. F.; Castellano, J. M.; Morán, M. J.; Pérez de Vega, C. R.; Romerdahl, C. R.; Qian, X-D.; Bousquet, P.; Emling, F.; Schlick, E.; Keilhauer, G. *Anti-Cancer Drug Des.* **1993**, *8*, 257-268.

86. Braña, M. F.; Castellano, J. M.; Morán, M. J.; Pérez de Vega, C. R.; Perron, D.; Conlon, D.; Bousquet, P. F.; Romerdahl, C. A.; Robinson, S. P. *Anti-Cancer Drug Des.* **1996**, *11*, 297-309.

87. Bousquet, P.F.; Braña, M. F.; Conlon, D.; Fitzgerald, K. M.; Perron, D.; Cocchiaro, C.; Miller, R.; Moran, M.; George, J.; Qian, X-D.; Keilhauer, G.; Romerdahl, C. A. *Cancer Res.* **1995**, *55*, 11796-1180.

88. Bailly, C.; Braña, M. F.; Waring, M. J. *Eur. J. Biochem.* **1996**, *240*, 195-208.

89. Gallego, J.; Reid, B. R. *Biochemistry* **1999**, *38*, 15104-15115.

90. Gallego, J. *Nucleic Acids Res.* **2004**, *32*, 3607-3614.

91. González-Buines, L.; Gallego, J. *J. Am. Chem. Soc.* **2009**, *131*, 7781-7791.

92. McRipley, R. J.; Burns-Horwitz, P. E.; Czerniak, P. M.; Diamond, R. J.; Diamond, M. A.; Miller, J. L. D.; Page, R. J.; Dexter, D. L.; Chen, S-F.; Sun, J-H.; Behrens, C. H.; Seitz, S. P.; Gross, J. L. *Cancer Res.* **1994**, *54*, 159-164.

93. Kirschenbaum, M. R.; Chen, S-F.; Behrens, C. H.; Papp, L. M.; Stafford, M. M.; Sun, J-H.; Behrens, D. L.; Fredericks, J. R.; Polkus, S. T.; Sipple, P.; Patten, A. D.; Dexter, D.; Seitz, S. P.; Gross, J. L. *Cancer Res.* **1994**, *54*, 2199-2206.

94. Nitiss, J. L.; Zhou, J.; Rose, A.; Hsiung, Y.; Gale, K. C.; Osheroff, N. *Biochemistry* **1998**, *37*, 3078-3085.

95. Gamage, S. A.; Spicer, J. A.; Finlay, G. J.; Stewart, A.J.; Charlton, P.; Baguley, B. C.; Denny, W. A. *J. Med. Chem.* **2001**, *44*, 1407-1415.

96. Cherney, R. J.; Swartz, S. G.; Patten, A. D.; Akamike, E.; Sun, J-H.; Kaltenbach III, R. F.; Seitz, S. P.; Behrens, C. H.; Getahun, Z.; Trainor, G. L.; Vavala, M.; Kirschenbaum, M. R.; Papp, L. M.; Stafford, M. P.; Czerniak, P. M.; Diamond, R. J.; McRipley, R. J.; Page, J.; Gross, J. L. *Bioorg. Med. Chem. Lett.* **1997**, *7*, 163-168.

97. Wright, R. G. McR.; Wakelin, L. P. G.; Fieldes, A.; Acheson, R. M.; Waring, M. J. *Biochemistry* **1980**, *19*, 5825-5836.

98. Pérez, J. M.; López-Solera I.; Montero, E. I.; Braña, M. F.; Alonso, C.; Robinson, S. P.; Navarro-Ranninger, C. *J. Med. Chem.* **1999**, *42*, 5482-5486.

99. Braña, M. F.; Castellano, J. M.; Perron, D.; Maher, C.; Conlon, D.; Bousquet, P. F.; George, J.; Qian, X-D.; Robinson, S. P. *J. Med. Chem.* **1997**, *40*, 449-454.

100. Bailly, C.; Carrasco, C.; Joubert, A.; Bal, C.; Wattez, N.; Hildebrand, M-P.; Lansiaux, A.; Colson, P.; Houssier, C.; Cacho, M.; Ramos, A.; Braña, M. F. *Biochemistry* **2003**, *42*, 4136-4150.

101. (a)Villalona-Calero, M. A.; Eder, J. P.; Toppmeyer, D. L.; Allen, L. F.; Fram, R.; Velagapudi, R.; Myers, M.; Amato, A.; Kagen-Hallet, K.; Razvillas, B.; Kufe, D. W.; Von Hoff, D. D.; Rowinsky, E. K. *J. Clin. Oncol.* **2001**, *19*, 857-869. (b) Awada, A.; Thödtmann, R.; Piccart, M. J.; Wanders, J.; Schrijvers, A. H. G. J.; Von Broen, I-M.; Hanauske, A. R. *Eur. J. Cancer* **2003**, *39*, 742-747.

102. (a) ASCO. Annual Meeting 1995. (b) ASCO. Annual Meeting 1996.

103. Braña, M. F.; Castellano, J. M.; Morán, M.; Pérez de Vega, M. J.; Qian, X-D.; Romerdahl, C. A.; Keilhauer, J. *Eur. J. Med. Chem.* **1995**, *30*, 235-239.

104. Suzuki, K.; Nagasawa, H.; Uto, Y.; Sugimoto, Y.; Noguchi, K.; Wakida, M.; Wierzba, K.; Terada, T.; Asao, T.; Yamada, Y.; Kitazato, K.; Hori, H. *Bioorg. Med. Chem.* **2005**, *13*, 4014-4021.

105. Pavlov, V.; Lin, P. K. T.; Rodilla, V. *Chem-Biol. Interact.* **2001**, *137*, 15-24.

106. Dance, A-M.; Ralton, L.; Fuller, Z.; Milne, L.; Duthie, S.; Bestwick, C. S.; Lin, P. K. T. *Biochem. Pharmacol.* **2005**, *69*, 19-27.

107. Oliveira, J.; Ralton, L.; Tavares, J.; Codeiro-da-Silva, A.; Bestwick, C. S.; McPherson, A.; Lin, P. K. T. *Bioorg. Med. Chem.* **2007**, *15*, 541-545.

108. Ralton, L. D.; Bestwick, C. S.; Milne, L.; Duthie, S.; Lin, P. K. T. *Chem-Biol. Interact.* **2009**, *177*, 1-6.

109. Filosa, R.; Peduto, A.; Di Micco, S.; de Caprariis, P.; Festa, M.; Petrella, A.; Capranico, G.; Bifulco, G. *Bioorg. Med. Chem.* **2009**, *17*, 13-24.

110. Barron, G. A.; Bermano, G.; Gordon, A.; Lin, P. K. T. *Eur. J. Med. Chem.* **2010**, *45*, 1430-1437.

111. Muth, M.; Hoerr, V.; Glaser, M.; Ponte-Sucre, A.; Moll, H.; Stich, A.; Holzgrabe, U. *Bioorg. Med. Chem. Lett.* **2007**, *17*, 1590-1593.

112. Tischer, M.; Sologub, L.; Pradel, G.; Holzgrabe, U. *Bioorg. Med. Chem.* **2010**, *18*, 2998-3003.

113. Menzel, T. M.; Tischer, M.; François, P.; Nickel, J.; Schrenzel, J.; Bruhn, H.; Albrecht, A.; Lehmann, L.; Holzgrabe, U.; Ohlsen, K. *Antimicrob. Agents. Chemother.* **2011**, *55*, 311-320.

114. Phelan, C. *PhD. Thesis*, University of Dublin, Trinity College, 2002.

115. Hussey, G. *PhD. Thesis*, University of Dublin, Trinity College, 2003.

116. Gillespie, L. J. *PhD. Thesis*, University of Dublin, Trinity College, 2007.

117. Frímannsson, D. Ó. *PhD. Thesis*, University of Dublin, Trinity College, 2008.

118. Ryan, G. J.; Quinn, S.; Gunnlaugsson, T. *Inorg. Chem.* 2008, 47, 401-403.

119. Elmes, R. B. P. *PhD. Thesis*, University of Dublin, Trinity College, 2011.

120. Banerjee, S.; Kitchen, J. A.; Gunnlaugsson, T.; Kelly, J. M. *Org. Biomol. Chem.* **2012**, *10*, 3033-3043.

121. (a) Tröger, J. *J. Prakt. Chem.* **1887**, *36*, 225-245. (b)Wagner, E. C.; Eisner, A. *J. Am. Chem. Soc.* **1934**, *56*, 1938-1943. (c) Wagner, E. C., *J. Am. Chem. Soc.* **1935**, *57*, 1296-1298. (d) Wagner, E. C.; Eisner, A. *J. Am. Chem. Soc.* **1937**, *59*, 879-883.

122. Spielman, M. A. *J. Am. Chem. Soc.* **1935**, *57*, 583-585.

123. Wilcox, C. S. *Tetrahedron Lett.* **1985**, *26*, 5749-5752.

124. Khoshbin, M. S.; Ovchinnikov, M. V.; Mirkin, C. A.; Golen, J. A.; Rheingold, A. L. *Inorg. Chem.* **2006**, *45*, 2603-2609.

125. (a) Adrian Jr., J. C.; Wilcox, C. S; *J. Am. Chem. Soc.* **1992**, *114*, 1398-1403. (b) Sucholeiki, I.; Lynch, V.; Phan, L.; Wilcox, C. S. *J. Org. Chem.* **1998**, *53*, 98-104. (c) Lenev, D. A.; Golovanov, D. G.; Lyssenko, K. A.; Kostyanovsky, R. G. *Tetrahedron Asym.* **2006**, *17*, 2191-2194.

126. (a) Webb, T. H.; Wilcox, C. S. *Chem. Soc. Rev.* **1993**, *22*, 383-395. (b) Bag, B. G. *Curr Sci.* **1995**, *68*, 279-288. (c) Valík, M.; Strongin, R. M.; Král, V. *Supramol. Chem.* **2005**, *17*, 347-367. (d) Dolenský, B.; Elguero, J.; Král, V.; Pardo, C.; Valík, M. *Adv. Heterocycl. Chem.* **2007**, *93*, 1-56. (e) Sergeyev, S. *Helv. Chim. Acta* **2009**, *92*, 415-444.

127. (a) Paliwal, S.; Geib, S.; Wilcox, C. S.; *J. Am. Chem. Soc.* **1994**, *116*, 4497-4498. (b) Kim, E. I.; Paliwal, S.; Wilcox, C.S. *J. Am. Chem. Soc.* **1998**, *120*, 11192-11193. (c) Bhayana, B.; Wilcox, C. S. *Angew. Chem. Int. Ed.* **2007**, *46*, 6833-6836. (d) Fischer, F. R.; Schweizer, W. B.; Diederich, F. *Angew. Chem. Int. Ed.* **2007**, *46*, 8270-8273. (e) Hof, F.; Scofield, D. M.; Schweizer, W. B.; Diederich, F. *Angew. Chem. Int. Ed.* **2004**, *43*, 5056-5059. (f) Bhayana, B.; Ams, M. R. *J. Org. Chem.* **2011**, *76*, 3594-3596.

128. (a) Cowart, M. D.; Sucholeiki, I,; Bukownik, R. R.; Wilcox, C. S. *J. Am. Chem. Soc.* **1988**, *110*, 6204-6210. (b) Wilcox, C. S.; Cowart, M. D. *Tetrahedron Lett.* **1986**, *27*, 5563-5566. (c) Webb, T. H.; Suh, H.; Wilcox, C. S. *J. Am. Chem. Soc.* **1991**, *113*, 8554-8555.

129. Wilen, S. H.; Qi, J. Z.; Williard, P. G. *J. Org. Chem.* **1991**, *56*, 485-487. (b) Klein, J.; Hartenstein, H.; Sicker, D. *Magn. Res. Chem.* **1994**, *32*, 727-731.

130. (a) Pardo, C.; Sesmilo, E.; Gutierrez-Puebla, E.; Monge, A.; Elguero, J.; Fruchier, A. *J. Org. Chem.* **2001**, *66*, 1607-1611. (b) Havlík, M. Král, V.; Kaplánek, R.; Dolenský, B. *Org.*

Lett. **2008**, *10*, 4767-4769. (c) Zimmerman, S. C.; Weiming, W. *J. Am. Chem. Soc.* **1989**, *111*, 8054-8055.

131. Manjula, A.; Nagarajan, M. *Tetrahedron* **1997**, *53*, 11859-11868.

132. Hansson, A. P.; Norrby, P-O.; Wärnmark, K. *Tetrahedron Lett.* **1998**, *39*, 4565- 4568.

133. (a) Adrian Jr., J. C.; Wilcox, C.S; *J. Am. Chem. Soc.* **1989**, *111*, 8055-8057. (b) Wilcox, C. S; Adrian Jr., J. C.; Webb, T. H.; Zawacki, F. J.; *J. Am. Chem. Soc.* **1992**, *114*, 10189-10197. (c) Crossley, M. J.; Hambley, T. W.; Mackay, L. G.; Try, A. C.; Walton, E. *J. Chem. Soc., Chem. Commun.* **1995**, 1077-1079. (d) Crossley, M. J.; Mackay, L. G.; Try, A. C. *J. Chem. Soc., Chem. Commun.* **1995**, 1925-1927.

134. (a) Goswami, S.; Ghosh, K.; Dasgupta, S. *J. Org. Chem.* **2000**, *65*, 1907-1914. (b) Goswami, S.; Ghosh, K. *Tetrahedron Lett.* **1997**, *38*, 4503-4506.

135. Wu, H.; Chen, X-M.; Wan, Y.; Ye, L.; Xin, H-Q.; Xu, H-H.; Yue, C-H.; Pang, L-L.; Ma, R.; Shi, D-Q. *Tetrahedron Lett.* **2009**, *50*, 1062-1065.

136. Du, X.; Sun, Y.; Tan, B.; Teng, Q.; Yao, X.; Su, C.; Wang, W. *Chem. Commun.* **2010**, *46*, 970-972.

137. Jeon, Y-M.; Armatas, G. S.; Kim, D.; Kanatzidis, M. G.; Mirkin, C. A. *Small* **2009**, *5*, 46-50.

138. Wu, Z.; Tang, M.; Tian, T.; Wu, J.; Deng, Y.; Dong, X.; Tan, Z.; Weng, X.; Liu, Z.; Wang, C.; Zhou, X. *Talanta* **2011**, *87*, 216-221.

139. Yuan, C-X.; Tao, X-T.; Wang, L.; Yang, J-X.; Jiang, M-H. *J. Phys. Chem. C* **2009**, *113*, 6809-6814.

140. Yuan, C-X.; Xin, Q.; Liu, H-J.; Wang, L.; Jiang, M-H, Tao, X-T. *Sci China Chem.* **2011**, *54*, 587-595.

141. Yashima, E.; Akashi, M.; Miyauchi, N. *Chem. Lett.* **1991**, *20*, 1017-1020.

142. Tatibouët, A.; Demeunynck, M.; Andraud, C.; Collet, A.; Lhomme, J. *Chem. Commun.* **1999**, 161-162.

143. Bailly, C.; Laine, W.; Demeunynck, M.; Lhomme, J. *Biophys. Res. Commun.* **2000**, *273*, 681-685.

144. Baldeyrou, B.; Tardy, C.; Bailly, C.; Colson, P.; Houssier, C.; Charmantray, F.; Demeunynck, M. *Eur. J. Med. Chem.* **2002**, *37*, 315-322.

145. Van Gijte, O.; Tatibouët, A.; Demeunynck, M.; Lhomme, J.; Kirsch-De Mesmaeker, A.; *Tetrahedron Lett.* **1997**, *38*, 1567-1570.

146. Claessens, N.; Pierard, F.; Bresson, C.; Moucheron, C.; Kirsch-De Mesmaeker, A. *J. Inorg. Biochem.* **2007**, *101*, 987-996.

147. Valík, M.; Palivec, L.; Foltynová, J.; Tkadlecová, M.; Urbanová, M.; Brabec, V.; Král, M. *Tetrahedron* **2006**, *62*, 8591-8600.

148. Veale, E. B.; Gunnlaugsson, T. *J. Org. Chem.* **2010**, *75*, 5513-5525.

149. Veale, E. B.; Frímannsson, D. Ó.; Gunnlaugsson, T. *Org. Lett.* **2009**, 11, 4040-4043.

150. Elmes, R. B. P.; Erby, M.; Bright, S. A.; Williams, D. C.; Gunnlaugsson, T. *Chem. Commun.* **2012**, *48*, 2588-2590.

151. Dervan, P. B. *Bioorg. Med. Chem.* **2001**, *9*, 2215-2235.

152. Du, Y. H.; Huang, J.; Weng, X. C.; Zhou, X. *Curr. Med. Chem.* **2010**, *17*, 173-189.

153. Lu, Y-H.; Wu, X-Q.; Zhang-Negerie, D.; Gao, Q. *Mini Rev. Med. Chem.* **2011**, *11*, 611-624.

154. Chang, Y-M.; Chen, C. K-M.; Hou, M-H. *Int. J. Mol. Sci.* **2012**, *13*, 3394-3413.

155. Thompson, M. Bioconjugate Chem. 2006, *17*, 507-13.

156. Ryan, G. J.; Elmes, R. B. P.; Quinn, S. J.; Gunnlaugsson, T. *Supramol. Chem.* **2012**, *24*, 175-188.

157. Thorp-Greenwood, F. L.; Coogan, M. P.; Mishra, L.; Kumari, N.; Rai, G.; Saripella, S. *New. J. Chem.* **2012**, *36*, 64-72.

158. (a) Wagner, E. C. *J. Am. Chem. Soc.* **1934**, *56*, 1938-1943. (b) Wagner, E. C.; Eisner, A. *J. Am. Chem. Soc.* **1937**, *59*, 879-883. (c) Wagner, E. C. *J. Am. Chem. Soc.* **1935**, *57* 1296-1298. (d) Wagner, E. C. *J. Org. Chem.* **1954**, *12*, 1862-1881.

159. Abella, C. A. M.; Benassi, M.; Santos, L. S.; Eberlin, M. N.; Coelho, F. *J. Org. Chem.* **2007**, *72*, 4048-4054.

160. Wan, Y.; Yan, R.; Zhang, W-C.; Shi, Y-H.; Lin, W.; Yin, W.; Bo, R-C.; Shi, J-J.; Hui, W. *Tetrahedron* **2010**, *66*, 3405-3409.

161. Cooper, F. C.; Partridge, M. W. *J. Chem. Soc.* **1955**, 991-994.

162. Hansson, A.; Jensen, J.; Wendt, O. F.; Wärnmark, K. *Eur. J. Org. Chem.* **2003**, *2003*, 3179-3188.

163. Johnson, R. A.; Gorman, R. R.; Wnuk, R. J.; Crittenden, N. J.; Aiken, J. W. J. *Med. Chem.* **1993**, *36*, 3202-3206.

164. Maitra, U.; Bag, B. G.; Rao, P.; Powell, D. *J. Chem. Soc. Perkin Trans. 1* **1995**, 2049-2056.

165. Becker, D. P.; Finnegan, P. M.; Collins, P. W. *Tetrahedron Lett.* **1993**, *34*, 1889-1892.

166. Maitra, U.; Bag, B. G. *J. Org. Chem.* **1992**, *57*, 6979-6981.

167. Crossley, M. J.; Try, A. C.; Walton, R. *Tetrahedron Lett.* **1996**, *37*, 6807-6810.

168. Cudero, J.; Pardo, C.; Ramos, M.; Gutierrez-Puebla, E.; Monge, A.; Elguero, J. *Tetrahedron* **1997**, *53*, 2233-2240.

169. Demeunynck, M.; Fontaine, C.; Lhomme, J. *Magn. Reson. Chem.* **1999**, *37*, 73-76.

170. Valík, M.; Dolenský, B.; Petříčková, H.; Vašek, P.; Král, V. *Tetrahdron Lett.* **2003** *44*, 2083-2086.

171. Kobayashi, T.; Moriwaki, T.; Tsubakiyama, M.; Yoshida, S. *J. Chem. Soc. Perkin Trans.* 1 **2002**, 1963-1967.

172. Ares, J. J.; Kador, P. F, Miller, D. D. *J. Med Chem.* **1986**, *29*, 2384-2389.

173. Middleton, R. W.; Parrick, J.; Clarke, E. D.; Wardman, P. *J. Heterocyclic Chem.* **1986,** *23,* 849-855.

174. Sergeyev, S.; Diederich, F. *Chirality* **2006**, *18,* 707-712.

175. Kucheryavy, P.; Li, G.; Vyas, S.; Hadad, C.; Glusac, K. D. *J. Phys. Chem. A* **2009**, *113*, 6453-6461.

176. Banthia, S.; Samanta, A. *Chem. Lett.* **2005**, *34*, 722-723.

177. Saha, S.; Samanta, S. *J. Phys. Chem. A* **2002**, *106*, 4763-477.

178. de Silva, A. P.; Gunaratne, H. Q. N.; Gunnlaugsson, T.; Huxley, A. J. M.; McCoy, C. P.; Rademacher, J. T.; Rice, T. E. *Chem. Rev.* **1997**, *97*, 1515-1566.

179. Yuan, D.; Brown, R. G. *J. Phys. Chem. A* **1997**, *101*, 3461-3466.

180. Demets, G. J-F.; Triboni, E. R.; Alvarez, E. B.; Arantes, G. M.; Filho, P. B.; Politi, M. J. *Spectrochim. Acta A* **2006**, *63*, 220-226.

181. Deprez, N. R.; McNitt, K. A.; Petersen, M. E.; Brown, R. G.; Lewis, D. E.; *Tetrahedron Lett.* **2005**, *46*, 2149-2153.

182. Martín, E,; Weigand, R. *Chem. Phys. Lett.* **1998**, *288*, 52-58.

183. Duke, R. M.; Gunnlaugsson, T. *Tetrahedron Lett.* **2011**, *52*, 1503-1505.

184. (a) Chakraborty, A.; Kar, S.; Guchhait, N. *Chem. Phys.* **2006**, *320*, 75-83. (b) Chakraborty, A.; Kar, S.; Guchhait, N. *J. Phys. Chem. A* **2006**, *110,* 12089-12095.

185. Singh, R. P.; Mahanta, S.; Kar, S.; Guchhait, N. *J. Lumin.* **2008**, *128*, 1421-1430.

186. (a) Chakraborty, A.; Kar, S.; Guchhait, N. *J. Photoch. Photobio. A* **2006**, *181*, 246-256. (b) Chakraborty, A.; Kar, S.; Guchhait, N. *Chem Phys.* **2006**, *324*, 733-741.

187. Demas, J. N.; Crosby, G. A. *J. Phys. Chem.* **1971**, *75*, 991-1024.

188. Williams, A. T. R.; Winfield, S. A.; Miller, J. N. *Analyst* **1983**, *108*, 1067-1071.

189. www.jobinyvon.com/usadivisions/fluorescence/applications/quantumyieldstrad.pdf

190. (a) de Silva, A. P.; Rice, T. E. *Chem. Commun.* **1999**, *2*, 163-164. (b) Atkins, P.; de Paula, J. *Atkins' Physical Chemistry*, *7th ed.*, Oxford University Press Inc., New York, 2002.

191. Veale, E. *PhD. Thesis*, University of Dublin, Trinity College, 2007.

192. Pardo, A.; Martin, E.; Poyato, J. M. L.; Camacho, J. J. *J. Photochem. Photobiol. A* **1987**, *41*, 69-78.

193. www.invitrogen.com

194. Carter, M. T.; Rodriguez, M.; Bard, A. J. *J. Am. Chem. Soc.* **1989**, *111*, 8901-8911.

195. McGhee, J. D.; von Hippel, P.H. *J. Mol. Biol.* **1974**, 86, 469-489.

196. Rogers, J. E.; Weiss, S. J. Kelly, L. A. *J. Am. Chem. Soc.* **2000**, *122*, 427-436.

197. Ryan, G .J. *PhD. Thesis*, University of Dublin, Trinity College, 2008.

198. Qin, Y.; Pang, J-Y.; Chen, W.H.; Cai, Z.; Jiang, Z-H. *Bioorg. Med. Chem.* **2006**, *14*, 25-32.

199. Yen, S-F.; Gabbay, E. J. ; Wilson, W. D. *Biochemistry* **1982**, *21*, 2070-2076.

200. Rao, S. N.; Kollman, P. A.; *Proc. Natl. Acad. Sci.* **1987**, *84*, 5735-5739.

201(a) Wilson, W. R.; Baguley, B. C.; Wakelin, L. P. G.; Waring, M. *Mol. Pharmacol.* **1981**, *20*, 404-414. (b) Baguley, B. C.; Denny, W. A.; Atwell, G. J.; Cain, B. F.; *J. Med. Chem.* **1981**, *24*, 170-177.

202. Terry, C. A.; Fernández, M-J.; Gude, L.; Lorente, A.; Grant, K. B. *Biochemistry* **2011**, *50*, 10375-10389.

203. Modukuru, N. K.; Snow, K. J.; Perrin, B. S. Jr.; Thota, J.; Kumar, C. V.; *J. Phys. Chem. B* **2005**, *109*, 11810-11818.

204. Manning, G. S. *Biopolymers* **1972**, *11*, 937-949.

205. LePecq, J-B.; Paoletti, C. *J. Mol. Biol.* **1967**, *27*, 87-106.

206. Boger, D. L.; Fink, B. E.; Hedrick, M. P. *J. Am. Chem. Soc.* **2000**, *122*, 6382-6394.

207. Tse, W. C.; Boger, D. L. *Acc. Chem. Res.* **2004**, *37*, 61-69.

208. Wilson, W. D.; Tanious, F. A.; Fernandez-Saiz, M.; Rigl, C. T. *Method. Mol. Biol.* **1997**, *90*, 214-240.

209. www.atdbio.com/content/53/DNA-duplex-stability

210. Pilch, D. S.; Poklar, N.; Baird, E. E.; Dervan, P. B.; Breslauer, K. J. *Biochemistry* **1999**, *38*, 2413-2151.

211. Garbett, N. C.; Ragazzon, P. A.; Chaires, J. B. *Nat. Protocols* **2007**, *2*, 3166-3172.

212. Rodger, A.; Nordén, B. *Circular Dichroism and Linear Dichroism*, Oxford University Press Inc., New York, 1997.

213. Monnot, M.; Mauffret, O.; Lescot, E.; Fermandjian, S. *Eur. J. Biochem.* **1992**, *204*, 1035-1039.

214. Havemann, S. A.; Hoshika, S.; Hutter, D.; Benner, S. A. *Nucleos. Nucleot. Nucl.* **2008**, *27*, 261-278.

215. Nordén, B.; Kurucsev, T. *J. Mol. Recognit.* **1994**, *7*, 141-156.

216. (a) Gunnlaugsson, T.; Kruger, P. E.; Lee, C.; Parkesh, R.; Pfeffer, F. M.; Hussey, G. M. *Tetrahedron Lett.* **2003**, *44*, 6575-6578. (b) Gunnlaugsson, T.; Kruger, P. E.; Jensen, P.; Pfeffer, F. M.; Hussey, G. M. *Tetrahedron Lett.* **2003**, *44*, 8909-8913. (c) Veale, E. B.; Gunnlaugsson, T. *Annu. Rep. Prog.Chem., Sect. B*: *Org. Chem.* **2010**, *106*, 376-406.

217. (a) Duke, R. M.; Gunnlaugsson, T. *Tetrahedron Lett.* **2007**, *48*, 8043-8047.

218. (a) Staneva, D.; Grabchev, I.; Soumillion, J-P.; Bojinov, V. *J. Photoch. Photobio. A.* **2007**, *189*, 192-197. (b) Grabchev, I.; Chovelon, J-M.; Petkov, C. *Spectrochim. Acta A.* **2008**, *69*, 100-104. (c) Okamoto, H.; Satake, K.; Kimura, M. *Arkivoc*, **2007**, *(viii)*, 112-123.

219. (a) 74. Wu, A.; Xu, Y.; Qian, X. *Bioorg. Med. Chem.* **2009**, *17*, 592-599. (b) Bindu, A.; Kelly, L. A. *J. Phys. Chem. B.* **2003**, *107*, 12534-12541.

220. Vázquez, M. E.; Blanco, J. B.; Salvadori, S.; Trapella, C.; Argazzi, R.; Bryant, S. D.; Jinsmaa, Y.; Lazarus, L. H.; Negri, L.; Giannini, E.; Lattanzi, R.; Colucci,M.; Balboni, G. *J. Med. Chem.* **2006**, *49*, 3653-3658.

221. (a) Nitz, M.; Mezo, A. R.; Ali, M. H.; Imperiali, B. *Chem. Commun.* **2002**, 1912-1913. (b) Vázquez, M. E.; Rothman, D. M.; Imperiali, B. *Org. Biomol. Chem.* **2004**, *2*, 1965-1966. (c) Vázquez, M. E.; Blanco, J. B.; Imperiali, B. *J. Am. Chem. Soc.* **2005**, *127*, 1300-1306. (d) Venkatraman, P.; Nguyen, T. T.; Sainlos, M.; Bilsel, O.; Chitta, S.; Imperiali, B.; Stern, L. J. *Nat. Chem. Biol.* **2007**, *3*, 222-228. (e) Loving, G. S.; Imperiali, B. *J. Am. Chem. Soc.* **2008**, *130*, 13630-13638. (f) Loving, G.; Imperiali, B. *Bioconjugate Chem.* **2009**, *20*, 2133-2141. (g) Sainlos, M.; Iskenderlan, W. S.; Imperiali, B. *J. Am. Chem. Soc.* **2009**, *131*, 6680-6682. (h) Loving, G. S.; Sainlos, M.; Imperiali, B. *Trends Biotechnol.* **2010**, *28*, 73-83. (i) Goguen, B. N.; Loving, G. S.; Imperiali, B. *Bioorg. Med. Chem. Lett.* **2011**, *21*, 5058-5061.

222. Gazit, E. *Chem. Soc. Rev.* **2007**, *36*, 1263-1269.

223. Campbell, N. A.; Reece, J. B. *Biology*, *6th ed.*; Benjamin Cummings Publishing Company Inc., University of California, 2002.

224. Clayden, J.; Greeves, N.; Warren, S.; Wothers, P. *Organic Chemistry*, Oxford University Press Inc., New York, 2001.

225. (a) Dias, N.; Goossens, J-F.; Baldeyrou, B.; Lansiaux, A.; Colson, P.; Di Salvo, A.; Bernal, J.; Turnbull, A.; Mincher, D. J.; Bailly, C. *Bioconjugate Chem.* **2005**, *16*, 949-958. (b)

Hsin, L-W.; Wang, H-P.; Kao, P-H.; Lee, O.; Chen, W-R.; Chen, H-W.; Guh, J-H.; Chan, Y-L.; His, C-P.; Wang, M-S.; Li, T-K.; Lee, C-H.; *Bioorg. Med. Chem.* **2008**, *16*, 1006-1014.

226. (a) Paul, A.; Vincent, M. J.; Duncan, R. *Biomacromolecules* **2007**, *8*, 1573-1579. (b) Kline, T.; Torgov, M. Y.; Mendelsohn, B. A.; Cerveny, C. G.; Senter, P. D. *Mol. Pharmaceut.* **2004**, *1*, 9-22.

227. Rao, K. S. P. B.; Collard, M. P. M.; Dejonghe, J. P. C.; Atassi, G.; Hannart, J. A.; Trouet, A. *J. Med.Chem.* **1985**, *28*, 1079-1088.

228. Rodriguez, M.; Imbach, J-L.; Martinez, J. *J. Med. Chem.* **1984**, *27*, 1222-1225.

229. McMorris, T. C.; Yu, J.; Ngo, H-T.; Wang, H.; Kelner, M. J. *J. Med. Chem.* **2000**, *43*, 3577-3580.

230. Hutchinson, I.; Jennings, S. A.; Vishnuvajjala, B. R.;Westwell, A. D.; Stevens, M. F. G. *J. Med. Chem.* **2002**, *45*, 744-747.

231. Arrowsmith, J.; Jennings, S. A.; Clark, A. S.; Stevens, M. F. G. *J. Med. Chem.* **2002**, *45*, 5458-5470.

232. Horvat, Š.; Mlinarić-Majerski, K.; Glavaš-Obrovac.; Jakas, A.; Veljković, J.; Marczi, S.; Kragol, G.; Roščić, M.; Matković, M.; Milostić-Srb, A. *J. Med. Chem.* **2006**, *49*, 3136-3142.

233. Song, L.; Bevins, R.; Anerson, B. D. *J. Med. Chem.* **2006**, *49*, 4344-4355.

234. Auclair, C.; Voisin, E.; Banoun, H.; Paoletti, C.; Bernadou, J.; Meunier, B. *J. Med. Chem.* **1984**, *27*, 1161-1166.

235. (a), Gao, X.; Wang, X.; Ding, J.; Lin, L.; Li, Y.; Guo, Z. *Inorg. Chem. Commun.* **2006**, *9*, 722-726. (b) Vinklárek, J.; Paláčková, H.; Honzíček, J.; Holubová, J.; Holčapek, M.; Císařová, I. *Inorg. Chem.* **2006**, *45*, 2156-2162. (c) Paláčková, H.; Vinklárek, J.; Holubová, J.; Erben, M. *J. Organomet. Chem.* **2007**, *92*, 3758-3764.

236. (a) Bosi, S.; Da Ros, T.; Spalluto, G.; Prato, M. *Eur. J. Med. Chem.* **2003**, *38*, 913-923. (b) Tokuyama, H.; Yamago, S.; Nakamura, E.; Shiraki, T.; Sugiura, Y. *J. Am. Chem. Soc.* **1993**, *115*, 7918-7919. (c) Bianco, A.; Da Ros, T.; Prato, M.; Toniolo, C. *J. Peptide Sci.* **2001**, *7*, 208-219.

237. Zhou, M.; Ghosh, I. *Peptide Sci.* **2007**, *88*, 325-339.

238. Bew, S. P.; Legentil, L.; Scholier, V.; Sharma, S. V. *Chem. Commun.* **2007**, 389-91

239. Goodman, M.; Stueben, K. C. *J. Am. Chem. Soc.* **1962**, *84*, 1279-1283.

240. (a) Fruton, J. S.; Bergmann, M. *J. Biol. Chem.* **1942**, *145*, 253-265. (b) Bodanszky, M.; Sheehan, J. T.; Ondetti, M. A.; Lande, S. *J. Am. Chem. Soc.* **1963**, *85*, 991-997.

241. Valeur, E.; Bradley, M. *Chem. Soc. Rev.* **2009**. *38*, 606-631.

242. Han, S-Y.; Kim, Y-A. *Tetrahedron* **2004**, *60*, 2447-2467.

243. Jouillié, M. M.; Lassen, K. M. *Arkivoc* **2010**, *(viii)*, 189-250.

244. Biron, E.; Voyer, N. *Org. Biomol. Chem.* **2008**, *6*, 2507-2515.

245. Movassagh, B.; Balalaie, S.; Shaygan, P. *Arkivoc* **2007**, *(viii)*, 47-52.

246. (a) Castro, B.; Dormoy, J-R.; Evin, G.; Selve, C. *Tetrahedron Lett.* **1975**, *16*, 1219-1222. (b) Dormoy, J-R.; Castro, B. *Tetrahedron Lett.* **1979**, *20*, 3321-3322. (c) Le-Nguyen, D.; Heitz, A.; Castro, B. *J. Chem. Soc. Perkin Trans 1* **1987**, 1915-1919.

247. Brunel, J. M.; Salmi, C.; Letourneux, Y. *Tetrahedron Lett.* **2005**, *46*, 217-220.

248. Lau, C. K.; Belanger, P. C.; Dufresne, C.; Scheigetz, J.; Therien, M.; Fitzsimmons, B.; Young, R. N.; Ford-Hutchinson, A. W.; Riendeau, D. *J. Med. Chem.* **1992**, *35*, 1299-1318.249.

249. Theodorou, V.; Skobridis, K.; Tzakos, A. G.; Ragoussis, V. *Tetrahedron Lett.* **2007**, *48*, 8230-8233.

250. Goossen, L. J.; Rodríguez, N.; Goossen, K. *Angew. Chem. Int. Ed.* **2008**, *47*, 3100-3120.

251. Zhang, J.; Campbell, R. E.; Ting, A. Y.; Tsien, R. Y. *Nat. Mol. Cell. Biol.* **2002**, *3*, 906-918.

252. (a) Jiang, P.; Guo, Z. *Coord. Chem. Rev.* **2004**, *248*, 205-229. (b) Fabbrizzi, L.; Licchelli, M.; Rabaioli, G.; Taglietti, A. *Coord. Chem. Rev.* **2000**, *205*, 85-108. (c) Valeur, B.; Leray, I. *Coord. Chem. Rev.* **2000**, *205*, 3-40.

253. (a) Chan, P-K.; Liu, H. B.; Chen, Y. W.; Chan, K. C.; Tsang, C-W.; Leung, Y, C.; Wong, K-Y. *J. Am. Chem. Soc.* **2004**, *126*, 4074-4075. (b) Morii, T.; Sugimoto, K.; Makino, K.; Otsuka, M.; Imoto, K.; Mori, Y. *J. Am. Chem. Soc.* **2002**, *124*, 1138-1139.

254. Lippincott-Schwartz, J.; Patterson, G. H. *Science* **2003**, *300*, 87-91.

255. Alexiou, M. S.; Tychopoulos, V.; Ghorbanian, S.; Tyman, J. H. P.; Brown, R. G.; Brittain, P. I. *J. Chem. Soc. Perkin Trans. 2* **1990**, 837-842.

256. (a) Wang, D.; Zhang, X.; He, C.; Duan, C. *Org. Biomol. Chem.* **2010**, *8*, 2923-2925. (b) Singh, N.; Jang, D. O. *Tetrahedron Lett.* **2011**, *52*, 2608-2610.

257. (a) Ojha, B.; Das, G. *Chem. Commun.* **2010**, *46*, 2079-2081. (b) Kudo, K.; Momotake, A.; Nishimura, Y.; Arai, T. *Chem. Commun.* **2011**, *47*, 3867-3869. (c) Zeng, X.; Zhang, X.; Zhu, B.; Jia, H.; Li, Y.; Xue, J. *Analyst* **2011**, *136*, 4008-4012.

258. (a) Sun, W.; Wei, S.; Yin, C.; Liu, L.; Hu, C.; Zhao, Y.; Ye, Y.; Hu, X.; Fan, J. *Bioorg. Med. Chem. Lett.* **2011**, *21*, 3798-3804. (b) Zhang, G.; Zhao, N.; Wang, L. *J. Lumin.* **2011**, *132*, 880-887. (c) Baptista, M. S.; Indig, G. L. *J. Phys. Chem. B* **1998**, *102*, 4678-4688. (d) Ghosh, S. K.; Hossain, S. U.; Bhattacharya, S.; Bhattacharya, S. C. *J. Photoch. Photobio. B* **2005**, *81*, 121-128.

259. Heyduk, T. *Curr. Opin, Biotech.* **2002**, *13*, 292-296.

260. Park, K. K.; Park, J. W.; Hamilton, A. D. *Org. Biomol. Chem.* **2009**, *7*, 4225-4232.

261. (a) Summerer, D.; Chen, S.; Wu, N.; Deiters, A.; Chin, J. W.; Schultz, P. G. *P. Natl. Acad. Sci. USA* **2006**, *103*, 9785-9789. (b) Wang, J.; Xie, J.; Schultz, P. G. *J. Am. Chem. Soc.* **2006**, *128*, 8738-8739. (c) Cohen, B. E.; McAnaney, T. B.; Park, E. S.; Jan, Y. N.; Boxer, S. G.; Jan, L.Y. *Science* **2002**, *296*, 1700-1703. (d) Turcatti, G.; Nemeth, K.; Edgerton, M. D.; Meseth, U.; Talabot, F.; Peitsch, M.; Knowles, J.; Vogel, H.; Chollet, A. *J. Biol. Chem.* **1996**, *271*, 19991-19998. (e) Dufau, I.; Mazarguil, H. *Tetrahedron Lett.* **2000**, *41*, 6063-6066.

262. Olmsted III, J. *J. Phys. Chem.* **1979**, *83*, 2581-2584.

263. Berezin, M. Y.; Achilefu, S. *Chem. Rev.* **2010**, *110*, 2641-2684.

264. Reichardt, C. *Chem. Soc. Rev.* **1992**, *21*, 147-153.

265. Sahoo, D.; Bhattacharya, P.; Chakravorti, S. *J. Phys. Chem. B* **2011**, *115*, 10983-10989.

266. Baheti, A.; Singh, P.; Lee, C-P.; Thomas, K. R. J.; Ho, K-C. *J. Org. Chem.* **2011**, *76*, 4910-4920.

267. Silberberg, M. S. *Chemistry: The Molecular Nature of Matter and Change, 3rd ed.*; McGraw Hill, 2006.

268. Pérez, E. M. *Pure Appl. Chem.* **2011**, *83*, 201-211.

269. www.ornl.gov/

270. (a) Hebard, A. F.; Rosseinsky, M. J.; Haddon, R. C.; Murphy, D. W.; Glarum, S. H.; Palstra, T. T. M.; Ramirez, A. P.; Kortan, A. R. *Nature* **1991**, *350*, 600-601. (b) Tanigaki, K.; Ebbesen, T. W.; Saito, S.; Mizuki, J.; Tsai, J. S.; Kubo, Y.; Kuroshima, S. *Nature* **1991**, *352*, 222-223.

271. Zaleśny, R.; Loboda, O.; Iliopoulos, K.; Chatzikyriakos, G.; Couris, S.; Rotas, G.; Tagmatarchis, N.; Avramopoulos, A.; Papadopoulos, M. G. *Phys. Chem. Chem. Phys.* **2010**, *12*, 373-381.

272. Chawla, P.; Chawla, V.; Maheshwari, R.; Saraf, S. A.; Saraf, K. S. *Mini-Rev. Med. Chem.* **2010**, *10*, 662-677.

273. Xu, K.; Liu, F.; Ma, J.; Tang, B. *Analyst* **2011**, *136*, 1199-1203.

274. Gayathri, S. S.; Wielopolski, M.; Pérez, E. M.; Fernández, G.; Sánchez, L.; Viruela, R.; Ortí, E.; Guldi, D. M.: Martín, N. *Angew. Chem. Int. Ed.* **2009**, *48*, 815-819.

275. Georghiou, P. E.; Dawe, L. N.; Tran, H-A.; Strübe, J.; Neumann, B.; Stammler, H-G.; Kuck, D. *J. Org. Chem.* **2008**, *73*, 9040-9047.

276. Harmata, M. *Acc. Chem. Res.* **2004**, *37*, 862-873.

277. Wu, Z-Q.; Shao, X-B.; Li, C.; Hou, J-L.; Wang, K.; Jiang, X-K.; Li, Z. T. *J. Am. Chem. Soc.* **2005**, *127*, 17460-17468.

278. Arribas, C. S.: Wendt, O. F.; Sundin, A. P.; Carling, C-J.; Wang, R.; Lemieux, R. P.; Wärnmark, K. *Chem. Commun.* **2010**, *46*, 4381-4383.

279. Huerta, E.; Isla, H.; Pérez, E. M.; Bo, C.; Martín, N.; de Mendoza, J. *J. Am. Chem. Soc.* **2010**, *132*, 5351-5353.

280. Pérez, E. M.; Sánchez, L.; Fernández, G.; Martín, N. *J. Am. Chem. Soc.* **2006**, *128*, 7172-7173.

281. Gayathri, S. S.; Wielopolski, M.; Pérez, E. M.; Fernández, G.; Sánchez, L.; Viruela, R.; Ortí, E.; Guldi, D. M.; Martín, N. *Angew. Chem. Int. Ed.* **2009**, *48*, 815-819.

282. Lin, H-H.; Chan, Y-C.; Chen, J-W.; Chang, C-C.; *J. Mat. Chem.* **2011**, *21*, 3170-3177.

283. Bulgakov, R. G.; Galimov, D. I. *Russ. Chem. Bull.* **2007**, *56*, 446-451.

284. Mukherjee, P.; Ray, A.; Bauri, A.; Bhattacharya, A. K. *J. Mol. Liq.* **2009**, *148*, 51-57.

285. Lakowicz, J. R. *Principles of Fluorescence Spectroscopy*, *3rd ed.*; Springer, 2006.

286. Gun'kin, I. F.; Loginova, N. Y. *Russ. J. Gen. Chem.* **2006**, *76*, 1911-1913.

287. Datta, K.; Mukherjee, A. K. *Spectrochim. Acta A* **2006**, *65*, 261-264.

288. Vogel, A. I. *Vogel's Textbook of Practical Organic Chemistry*, Longman, 1989.

289. Allinger, N. L. Burkert, U. *Molecular Mechanics*, American Chemical Society; Washington D.C., 1982.

290. Frey, S. T.; Chang, C. A.; Carvalho, J. F.; Varadarajan, A.; Schultze, L. M.; Pounds, K. L.; Horrocks Jr. W. D. *Inorg. Chem.* **1994**, *33*, 2882-2889.

Appendices

Crystal data and structure refinement for 20.

Empirical formula	$C_{64}H_{68}N_{12}O_8$	
Formula weight	133.30	
Temperature	153(2) K	
Wavelength	0.71073 Å	
Crystal system	Triclinic	
Space group	P-1	
Unit cell dimensions	a = 5.7449(11) Å	α= 71.59(3)°.
	b = 13.716(3) Å	β= 87.71(3)°.
	c = 18.608(4) Å	γ = 82.95(3)°.
Volume	1380.7(5) $Å^3$	
Z	4	
Density (calculated)	1.296 Mg/m^3	
Absorption coefficient	0.089 mm^{-1}	
F(000)	568	
Crystal size	0.30 x 0.20 x 0.10 mm^3	
Theta range for data collection	2.31 to 25.00°.	
Index ranges	-6<=h<=6, -16<=k<=16, -22<=l<=22	
Reflections collected	21388	
Independent reflections	4840 [R(int) = 0.0505]	
Completeness to theta = 25.00°	99.6 %	
Absorption correction	Semi-empirical from equivalents	
Max. and min. transmission	0.9912 and 0.9739	
Refinement method	Full-matrix least-squares on F^2	
Data / restraints / parameters	4840 / 0 / 408	
Goodness-of-fit on F^2	1.982	
Final R indices [I>2sigma(I)]	R1 = 0.1515, wR2 = 0.4779	
R indices (all data)	R1 = 0.1701, wR2 = 0.4863	
Largest diff. peak and hole	0.717 and -0.723 $e.Å^{-3}$	

Hydrogen bonds [Å and °].

D-H...A	d(D-H)	d(H...A)	d(D...A)	<(DHA)
N(1)-H(1B)...N(3)#1	0.88	2.31	3.122(7)	154.4
N(1)-H(1A)...O(2)#2	0.88	2.14	2.997(7)	163.9
N(21)-H(21A)...N(23)#3	0.88	2.14	2.981(8)	160.4

N(21)-H(21B)...O(22)#4	0.88	2.10	2.950(8)	161.6

Single, X-ray quality crystals of **20** were obtained as yellow blocks by the slow evaporation of CH_2Cl_2 and the low temperature (108K) structure determined. Compound **20** crystallised in the triclinic spacegroup P-1 and contained two molecules in the asymmetric unit. The two components differ only in the orientation of the R-group where it is oriented towards a different face of the naphthalimide ring. One of the two crystallographically independent molecules of **20** contains a disordered ethylene diamine group where the two methyl carbon atoms and one of the ethylene carbon atoms are disordered over two sites with relative occupancies of 0.65 and 0.35 for the two parts (Figure A.1). Hydrogen bonding interactions are again similar to those of **104**, **105** and **106** where dimers form through complementary H-bonding interactions between the amino protons H(1B) and H(21A) and the symmetry generated dimethyl amino nitrogen atoms N(3) and N(23) on neighbouring molecules [N(1)···N(3)' = 3.122(7) Å and <(N(1)-H(1B)···N(3)') = 154.4°; N(21)···N(23)' = 2.981(8) Å and <(N(21)-H(21A)···N(23)') = 160.4°]. These dimers then link through further H-bonding interactions between the amino protons H1A and H21B and the carbonyl oxygen atoms O(2) and O(22) on neighbouring molecules [N(1)···O(2)' = 2.997(7) Å and <(N(1)-H(1A)···O(2)') = 163.9°; N(21)···O(22)' = 2.950(8) Å and <(N(21)-H(21B)···O(22)') = 161.6°].

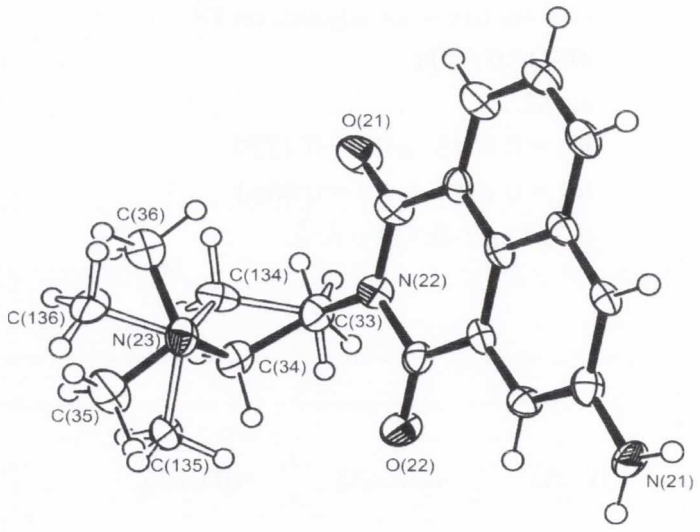

Figure A1.1: *Model of **20** representing disorder of ethylene di-amine group.*

Crystal data and structure refinement for 103.

Empirical formula	$C_{18}H_{19}N_3O_3$	
Formula weight	1224.84	
Temperature	150(2) K	
Wavelength	0.71075 Å	
Crystal system	Monoclinic	
Space group	P2(1)/c	
Unit cell dimensions	a = 5.5440(18) Å	α = 90°.
	b = 23.166(8) Å	β = 102.769(4)°.
	c = 12.365(4) Å	γ = 90°.
Volume	1548.8(9) $Å^3$	
Z	1	
Density (calculated)	1.313 Mg/m^3	
Absorption coefficient	0.094 mm^{-1}	
F(000)	612	
Crystal size	0.20 x 0.20 x 0.10 mm^3	
Theta range for data collection	2.44 to 25.00°.	
Index ranges	-6<=h<=6, -27<=k<=27, -14<=l<=14	
Reflections collected	7067	
Independent reflections	2638 [R(int) = 0.0437]	
Completeness to theta = 25.00°	96.5 %	
Absorption correction	Semi-empirical from equivalents	
Max. and min. transmission	1.0000 and 0.7933	
Refinement method	Full-matrix least-squares on F^2	
Data / restraints / parameters	2638 / 0 / 217	
Goodness-of-fit on F^2	1.123	
Final R indices [I>2sigma(I)]	R1 = 0.0599, wR2 = 0.1700	
R indices (all data)	R1 = 0.0907, wR2 = 0.2225	
Largest diff. peak and hole	0.423 and -0.373 $e.Å^{-3}$	

Crystal data and structure refinement for 104.

Empirical formula	$C_{72}H_0N_{12}O_2$	
Formula weight	676.81	
Temperature	150(2) K	
Wavelength	0.71075 Å	
Crystal system	Triclinic	
Space group	P-1	
Unit cell dimensions	a = 6.851(7) Å	α = 73.30(4)°.

	b = 11.056(12) Å	β = 76.74(5)°.
	c = 12.484(13) Å	γ = 80.35(5)°.
Volume	876.3(16) $Å^3$	
Z	1	
Density (calculated)	1.283 Mg/m^3	
Absorption coefficient	0.086 mm^{-1}	
F(000)	360	
Crystal size	0.35 x 0.20 x 0.06 mm^3	
Theta range for data collection	1.74 to 24.99°.	
Index ranges	-7<=h<=8, -13<=k<=13, -14<=l<=14	
Reflections collected	13762	
Independent reflections	3078 [R(int) = 0.2060]	
Completeness to theta = 24.99°	99.8 %	
Absorption correction	Semi-empirical from equivalents	
Max. and min. transmission	1.0000 and 0.4474	
Refinement method	Full-matrix least-squares on F^2	
Data / restraints / parameters	3078 / 0 / 228	
Goodness-of-fit on F^2	1.304	
Final R indices [I>2sigma(I)]	R1 = 0.1915, wR2 = 0.4022	
R indices (all data)	R1 = 0.3090, wR2 = 0.5288	
Largest diff. peak and hole0.759 and -0.875 e.$Å^{-3}$		

Crystal data and structure refinement for 105.

Empirical formula	C_{76} H_0 N_{12} O_8	
Formula weight	1208.88	
Temperature	150(2) K	
Wavelength	0.71075 Å	
Crystal system	Monoclinic	
Space group	P2(1)/c	
Unit cell dimensions	a = 6.962(2) Å	α = 90°.
	b = 14.046(5) Å	β = 95.843(4)°.
	c = 16.346(6) Å	γ = 90°.
Volume	1590.1(9) $Å^3$	
Z	1	
Density (calculated)	1.262 Mg/m^3	
Absorption coefficient	0.086 mm^{-1}	
F(000)	604	
Crystal size	0.20 x 0.10 x 0.10 mm^3	
Theta range for data collection	2.51 to 24.99°.	

Index ranges	-7<=h<=8, -16<=k<=15, -19<=l<=19
Reflections collected	12869
Independent reflections	2792 [R(int) = 0.0406]
Completeness to theta = 24.99°	99.6 %
Absorption correction	Semi-empirical from equivalents
Max. and min. transmission	1.0000 and 0.7695
Refinement method	Full-matrix least-squares on F^2
Data / restraints / parameters	2792 / 0 / 217
Goodness-of-fit on F^2	1.202
Final R indices [I>2sigma(I)]	R1 = 0.0588, wR2 = 0.1140
R indices (all data)	R1 = 0.0697, wR2 = 0.1191
Largest diff. peak and hole	0.287 and -0.354 e.$Å^{-3}$

Crystal data and structure refinement for 106.

Empirical formula	C_{72} H_{76} N_{12} O_8	
Formula weight	1237.45	
Temperature	150(2) K	
Wavelength	0.71075 Å	
Crystal system	Monoclinic	
Space group	P2(1)/c	
Unit cell dimensions	a = 6.6599(17) Å	α = 90°.
	b = 21.310(5) Å	β = 99.174(4)°.
	c = 11.054(3) Å	γ = 90°.
Volume	1548.7(7) $Å^3$	
Z	1	
Density (calculated)	1.327 Mg/m^3	
Absorption coefficient	0.088 mm^{-1}	
F(000)	656	
Crystal size	0.20 x 0.10 x 0.10 mm^3	
Theta range for data collection	1.91 to 25.00°.	
Index ranges	-7<=h<=7, -24<=k<=25, -13<=l<=12	
Reflections collected	12422	
Independent reflections	2692 [R(int) = 0.0456]	
Completeness to theta = 25.00°	98.8 %	
Absorption correction	Semi-empirical from equivalents	
Max. and min. transmission	1.0000 and 0.7695	
Refinement method	Full-matrix least-squares on F^2	
Data / restraints / parameters	2692 / 0 / 208	
Goodness-of-fit on F^2	1.169	

Final R indices [I>2sigma(I)]	R1 = 0.0583, wR2 = 0.1641
R indices (all data)	R1 = 0.0845, wR2 = 0.1973
Largest diff. peak and hole	0.438 and -0.460 e.Å^{-3}

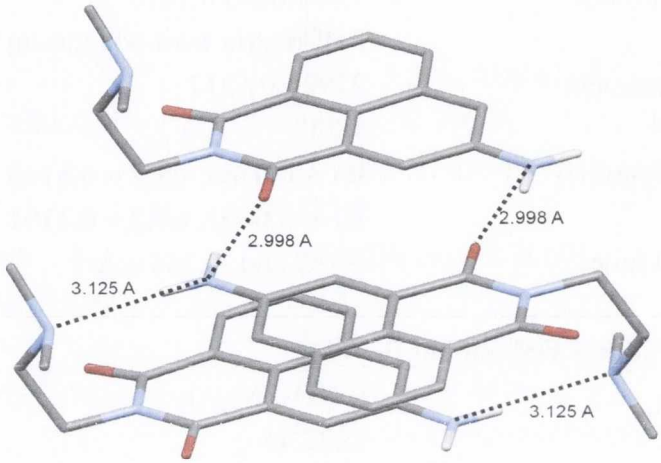

Figure A1.2: *Hydrogen bonding of* ***20****.*

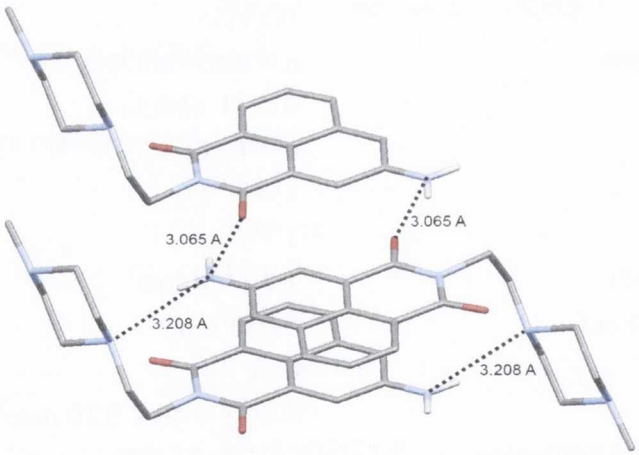

Figure A1.3: *Hydrogen bonding of* ***104****.*

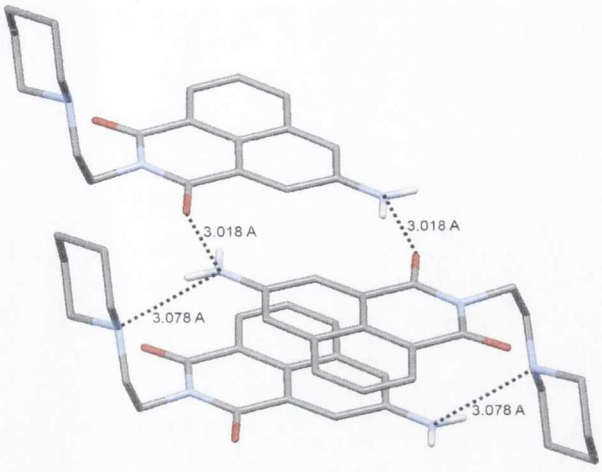

Figure A1. 4: *Hydrogen bonding of* ***105****.*

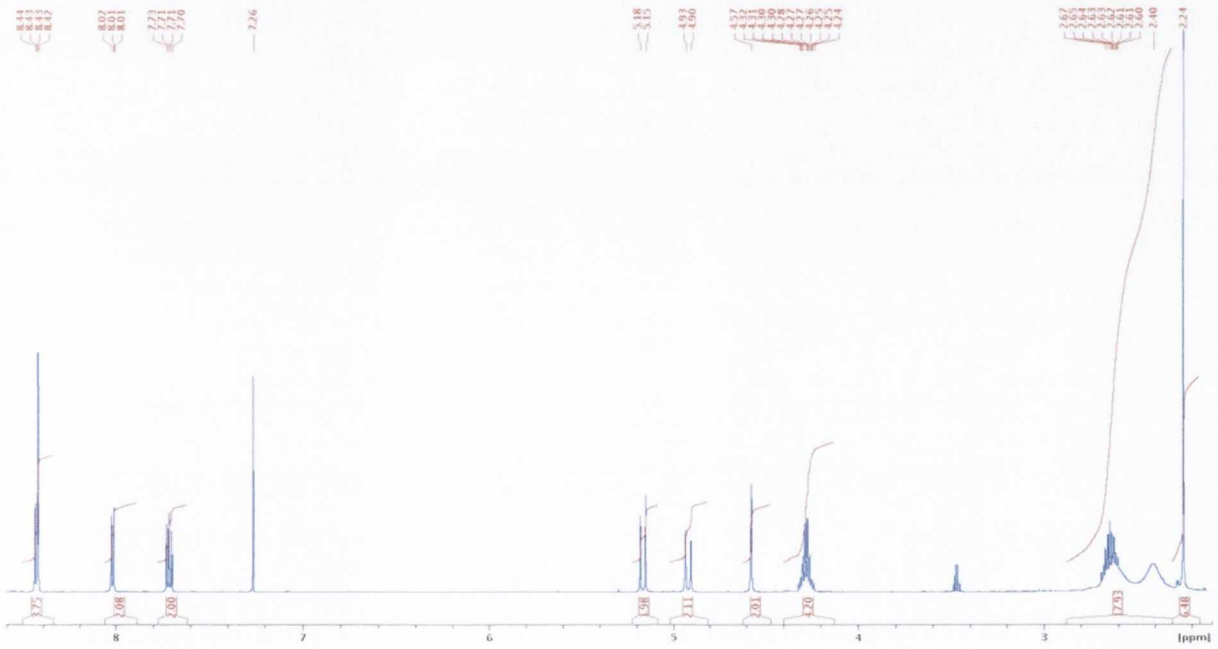

Figure A1.5: *^{1}H NMR spectrum (CDCl3, 600 MHz) of* ***88****.*

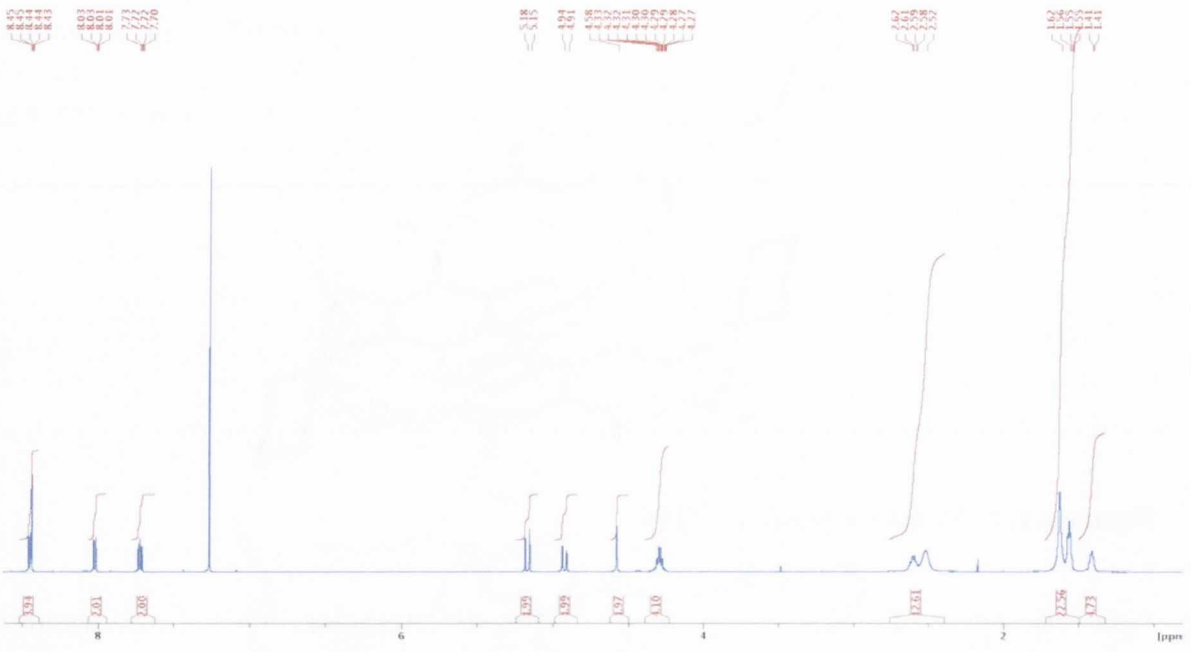

Figure A1.6: *^{1}H NMR spectrum (CDCl3, 600 MHz) of* ***89****.*

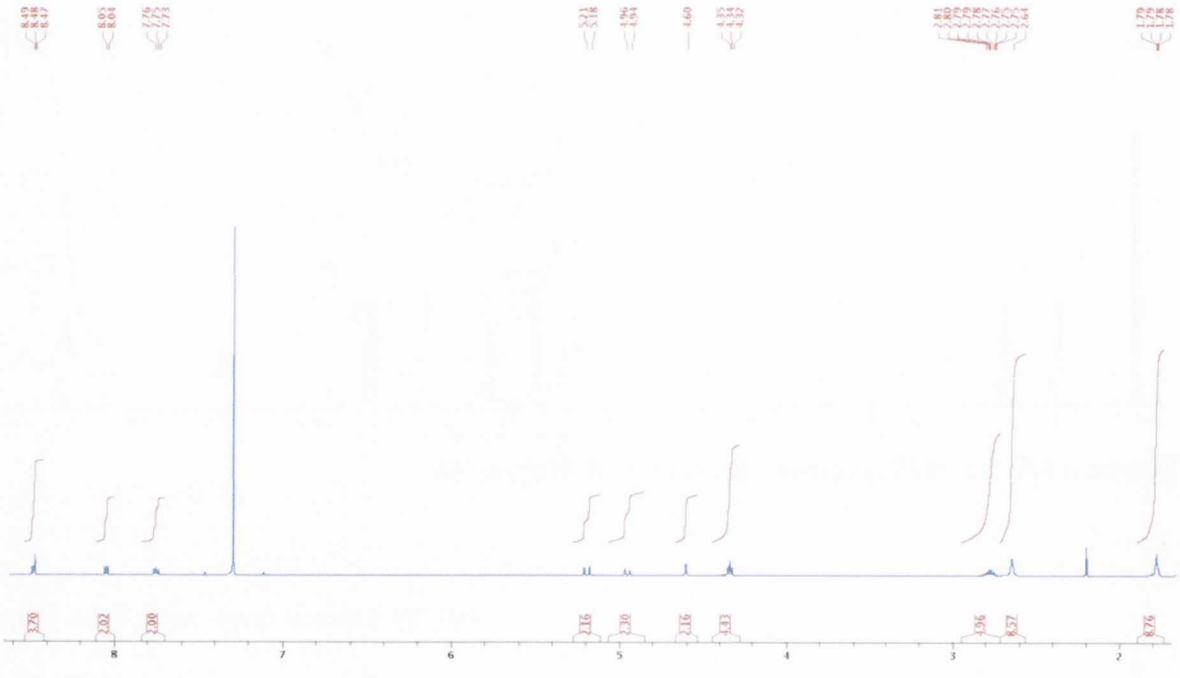

Figure A1.7: *^{1}H NMR spectrum (CDCl3, 600 MHz) of* ***90****.*

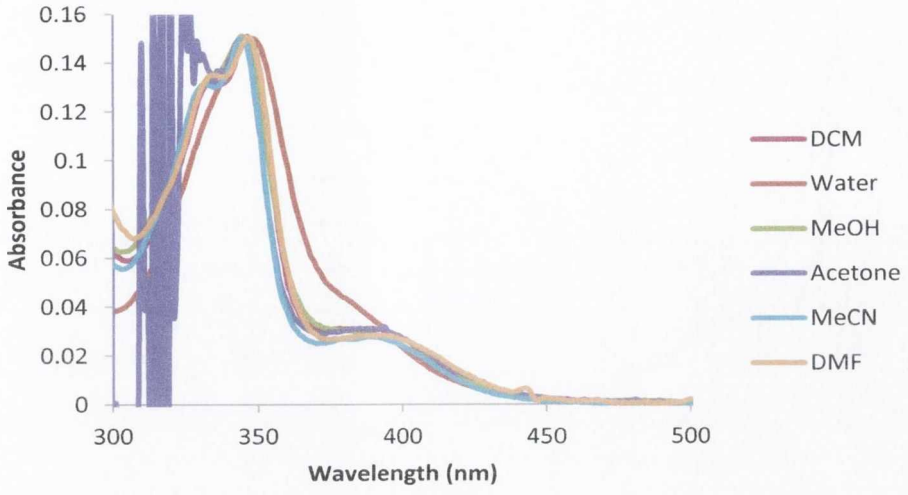

Figure A1.8: *Absorption spectra of* ***86*** *in solvents of varying polarity.*

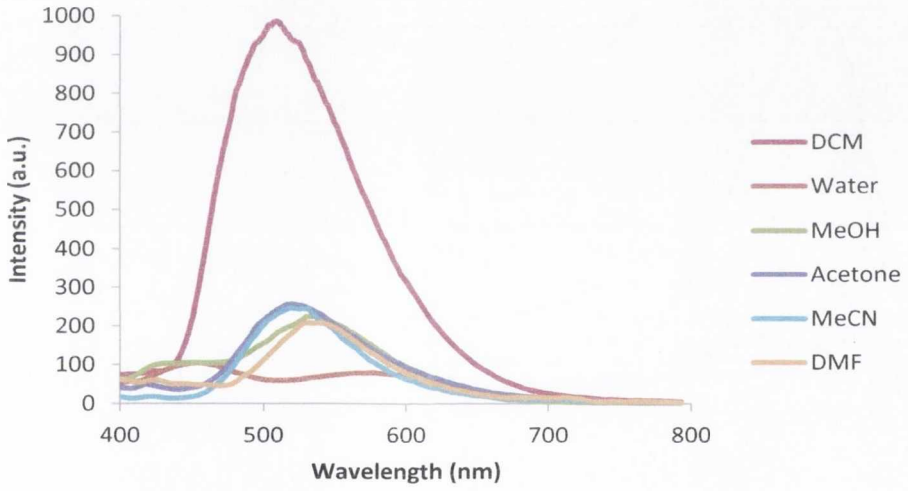

Figure A1.9: *Emission spectra of* ***86*** *in solvents of varying polarity (excitation at 347 nm).*

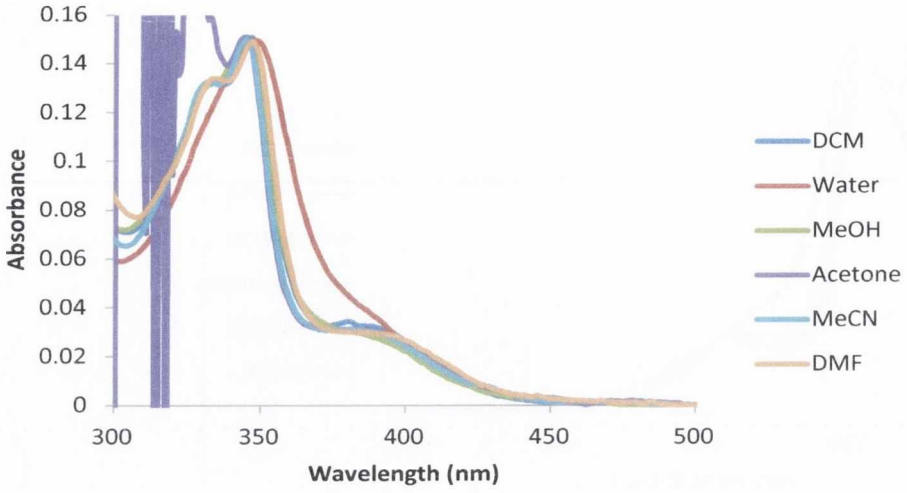

Figure A1.10: *Absorption spectra of 87 in solvents of varying polarity.*

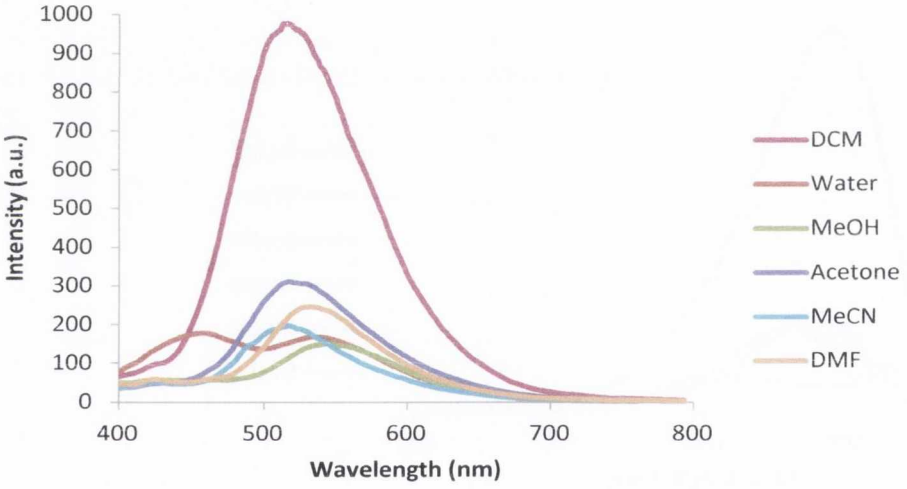

Figure A1.11: *Emission spectra of 87 in solvents of varying polarity (excitation at 347 nm).*

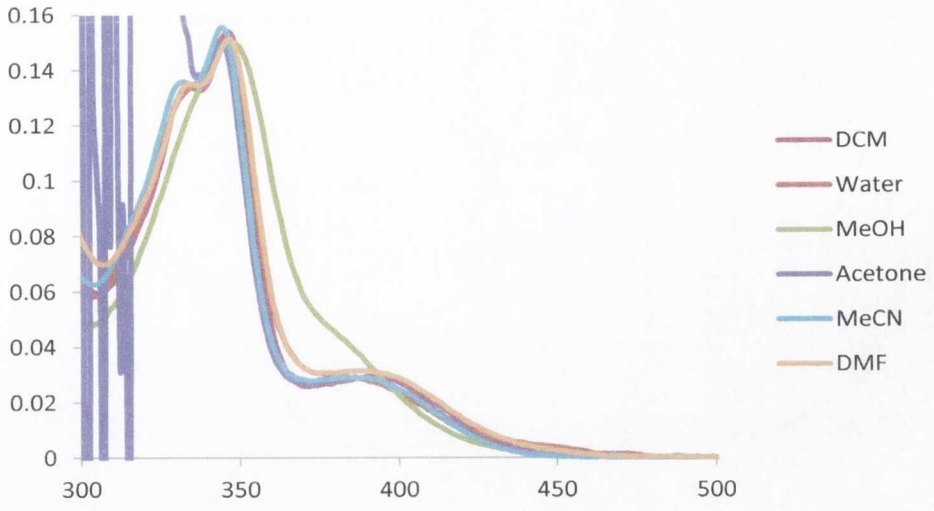

Figure A1.12: *Absorption spectra of* ***88*** *in solvents of varying polarity.*

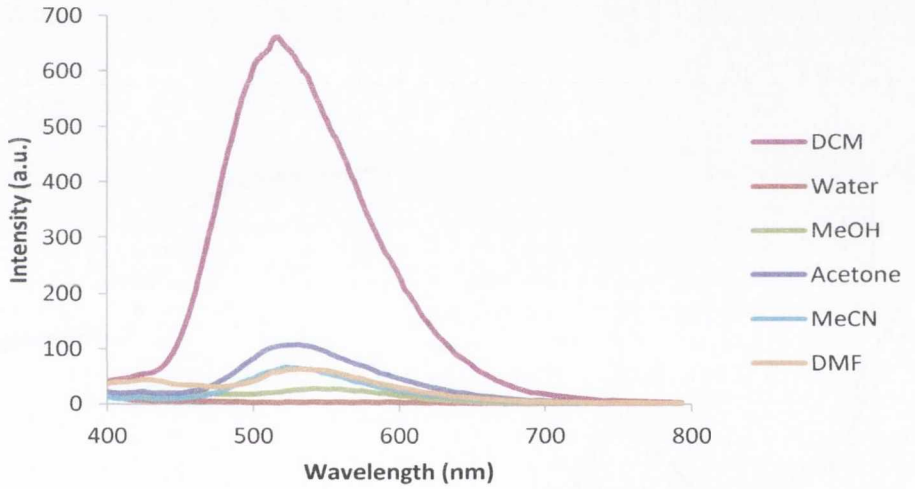

Figure A1.13: *Emission spectra of* ***88*** *in solvents of varying polarity (excitation at 347 nm).*

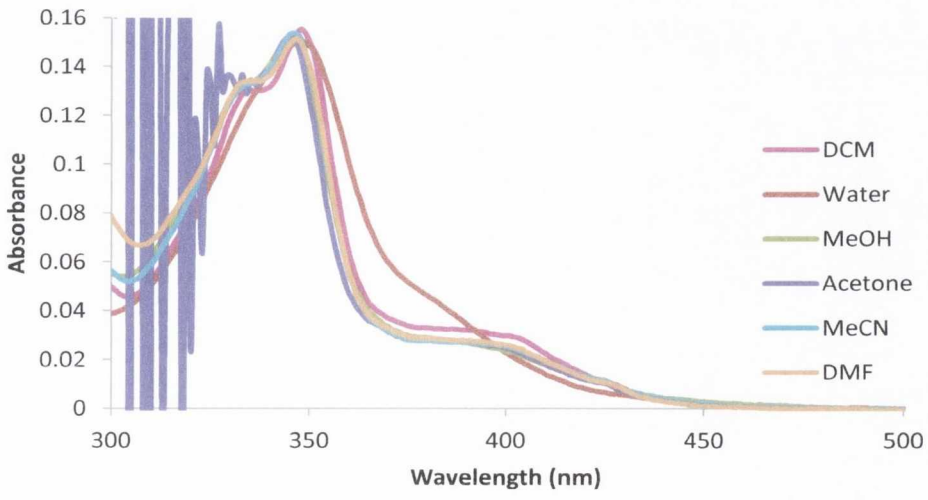

Figure A1.14: *Absorption spectra of* ***89*** *in solvents of varying polarity.*

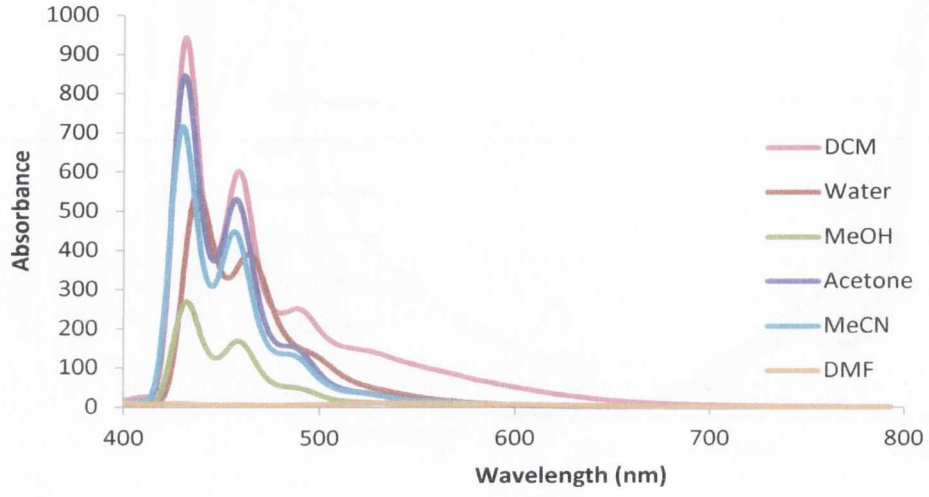

Figure A1.15: *Emission spectra of* ***89*** *in solvents of varying polarity (excitation at 347 nm).*

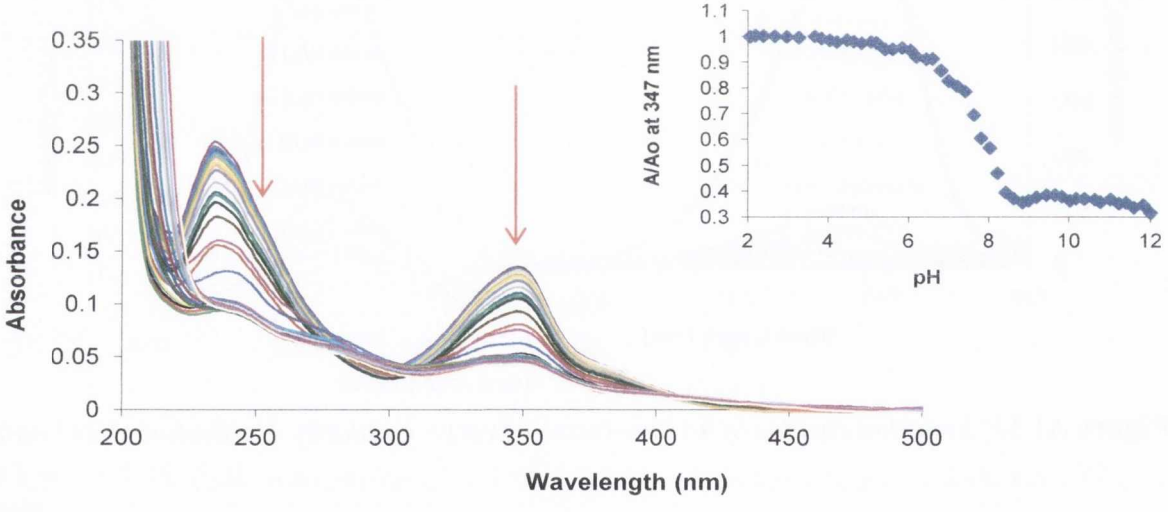

Figure A1.16: *Absorption spectra of* ***89*** *as a function of pH. Inset: Plot of changes in absorbance as a function of pH.*

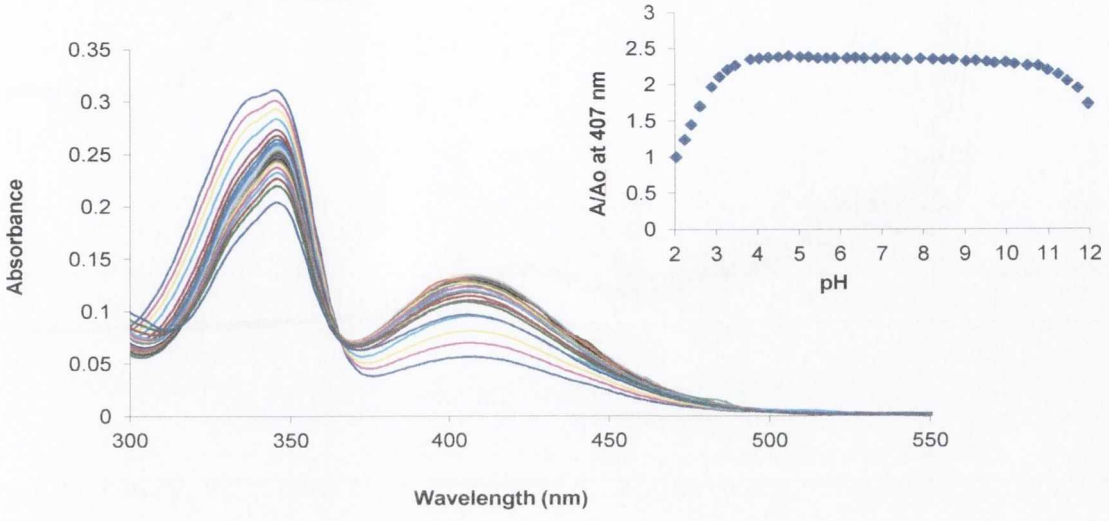

Figure A1.17: *Absorption spectra of* ***105*** *as a function of pH. Inset: Plot of changes in aborbance as a function of pH.*

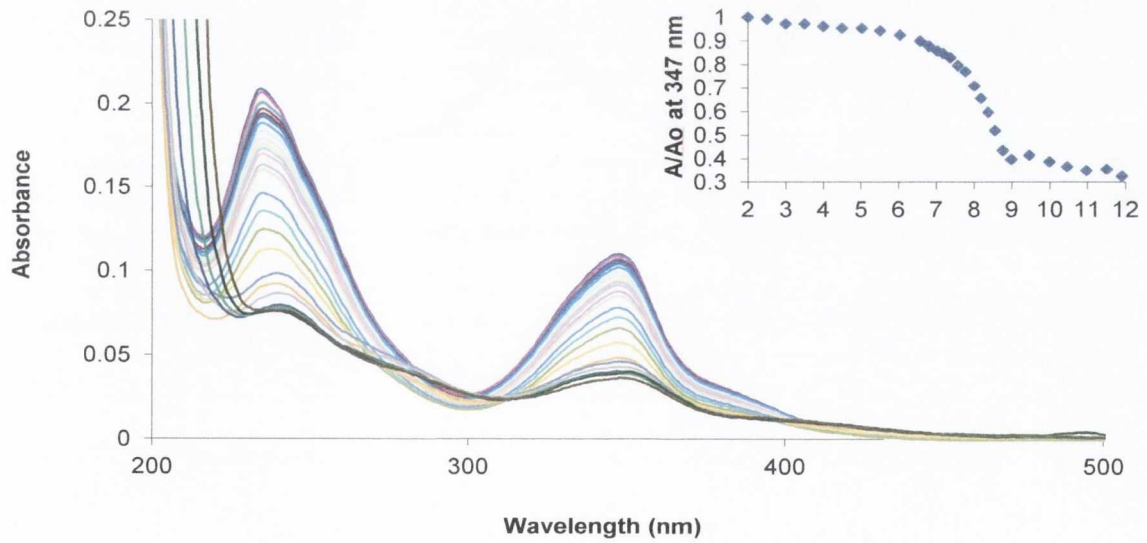

Figure A1.18: *Absorption spectrum of* ***90*** *as a function of pH. Inset: Plot of changes as a function of pH.*

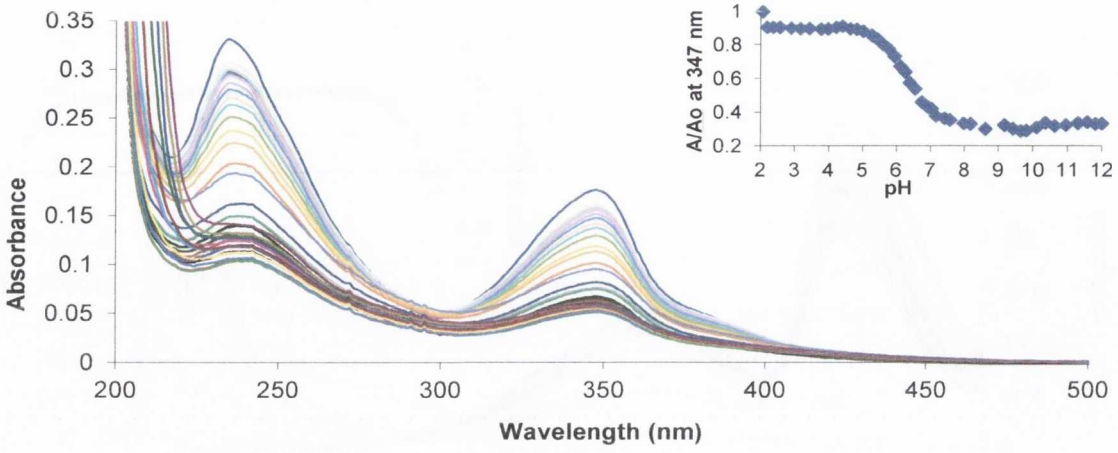

Figure A1.19: *Absorption spectrum of* ***87*** *as a function of pH. Inset: Plot of changes as a function of pH.*

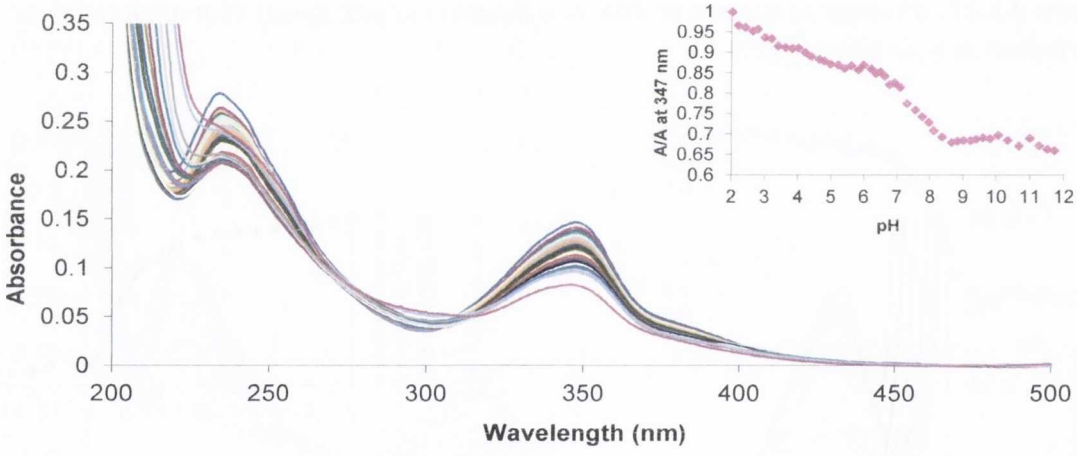

Figure A1.20: *Absorption spectrum of* ***88*** *as a function of pH. Inset: Plot of changes as a function of pH.*

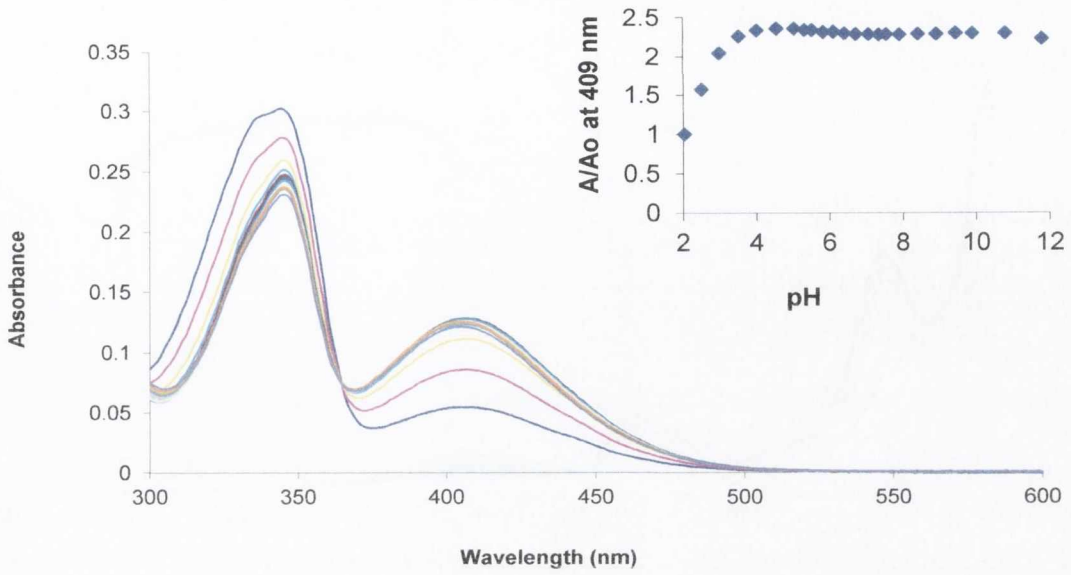

Figure A1.21: *Absorption spectrum of* ***103*** *as a function of pH. Inset: Plot of changes as a function of pH.*

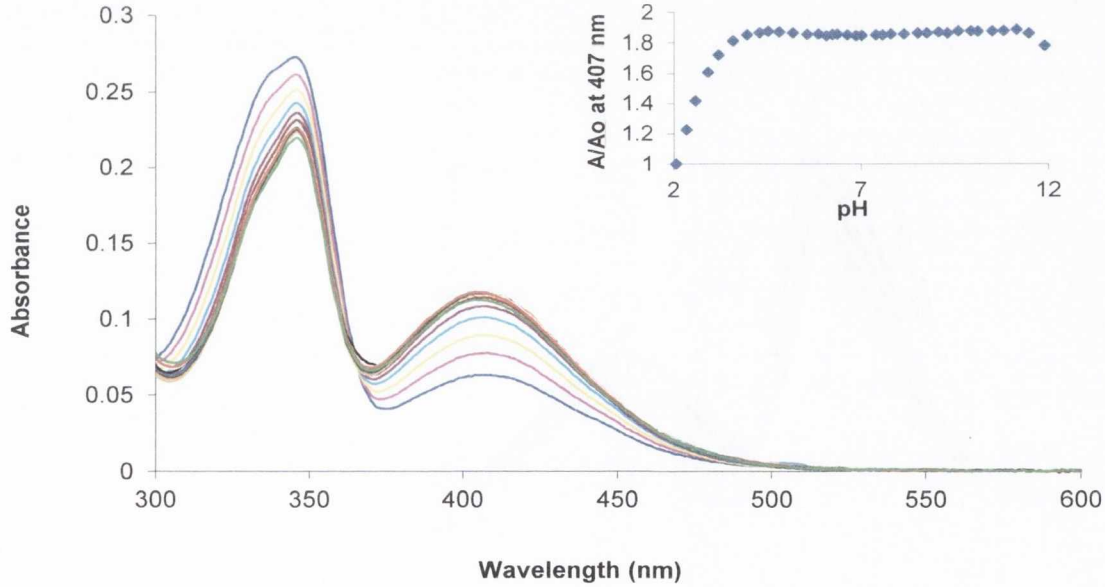

Figure A1.22: *Absorption spectrum of* ***104*** *as a function of pH. Inset: Plot of changes as a function of pH.*

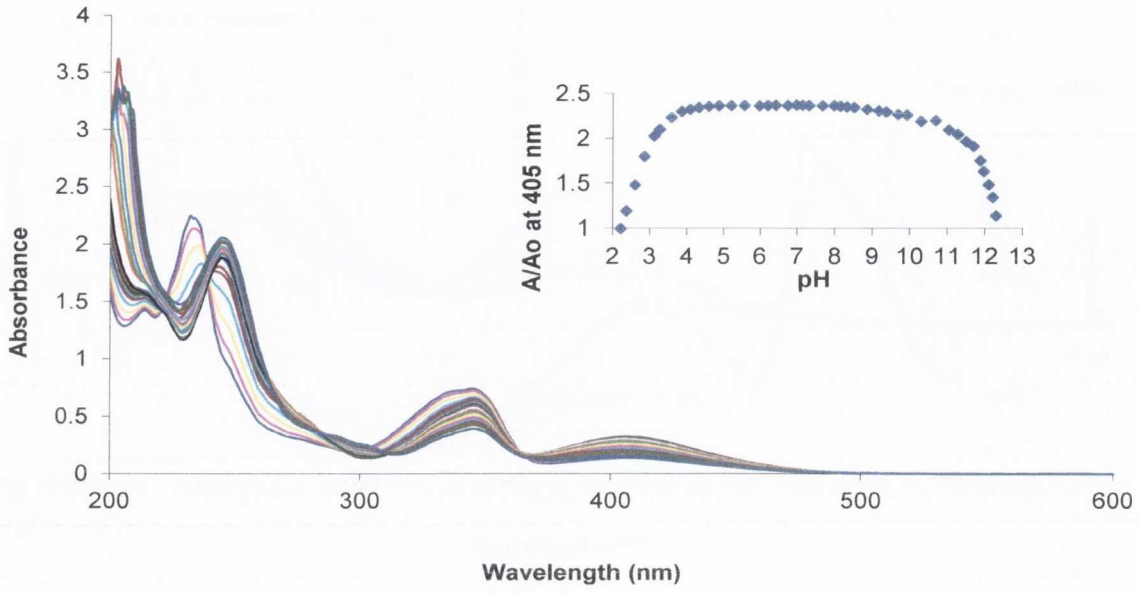

Figure A1.23: *Absorption spectrum of* ***105*** *as a function of pH. Inset: Plot of changes as a function of pH.*

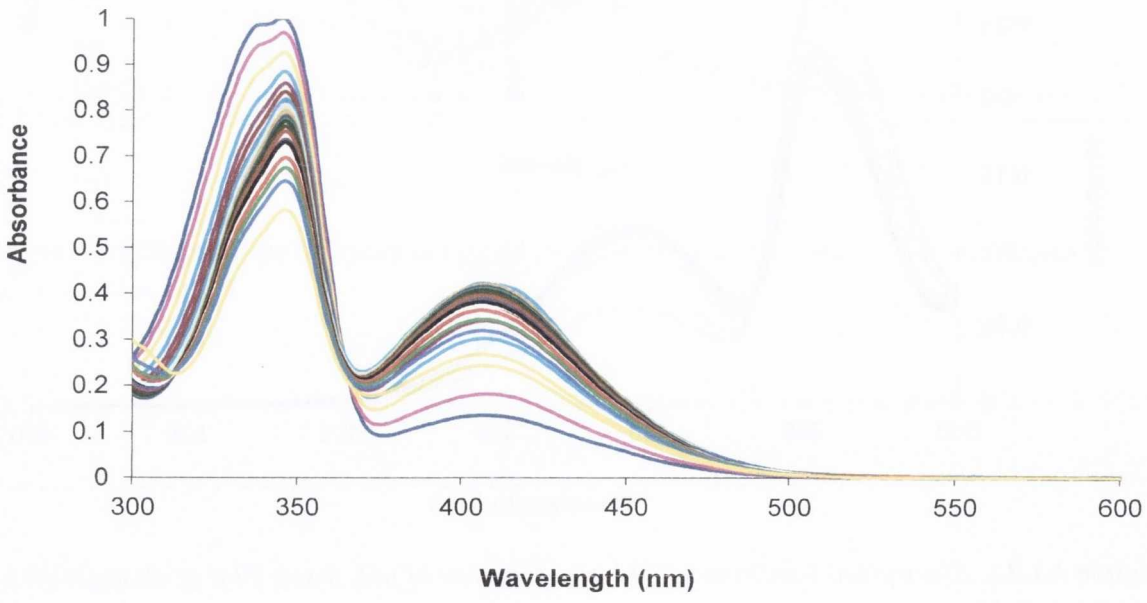

Figure A1.24: *Absorption spectrum of* ***106*** *as a function of pH.*

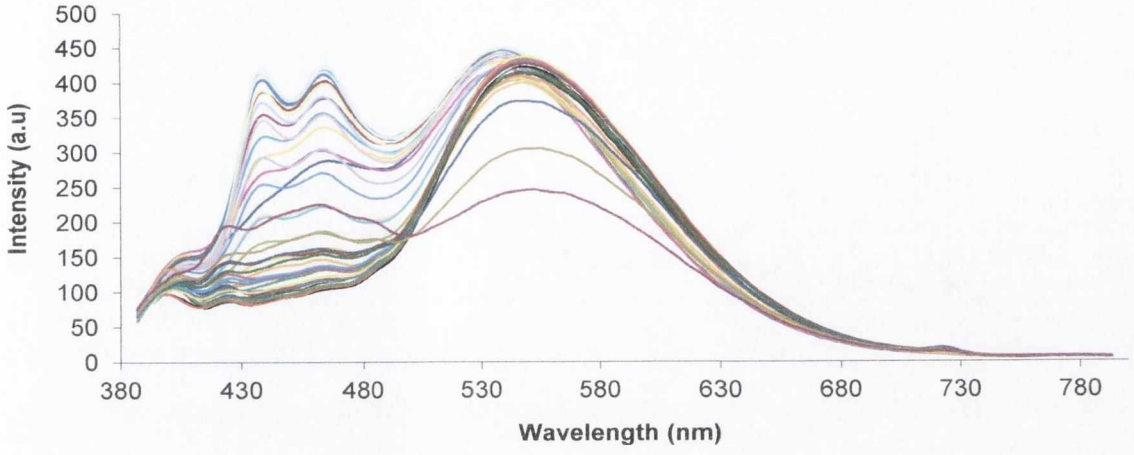

Figure A1.25: *Emission spectrum of* ***87*** *as a function of pH (excitation at 347 nm).*

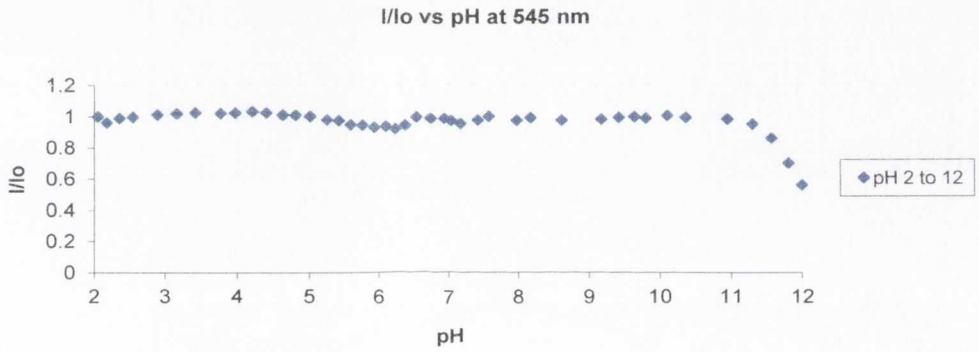

Figure A1.26: *Plot of changes in the emission spectrum of* ***87*** *as a function of pH.*

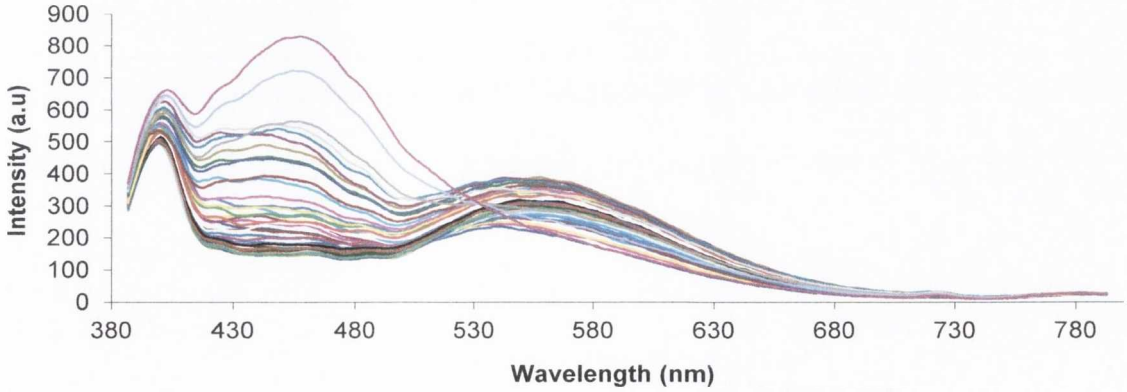

Figure A1.27: *Emission spectrum of* ***88*** *as a function of pH (excitation at 347 nm).*

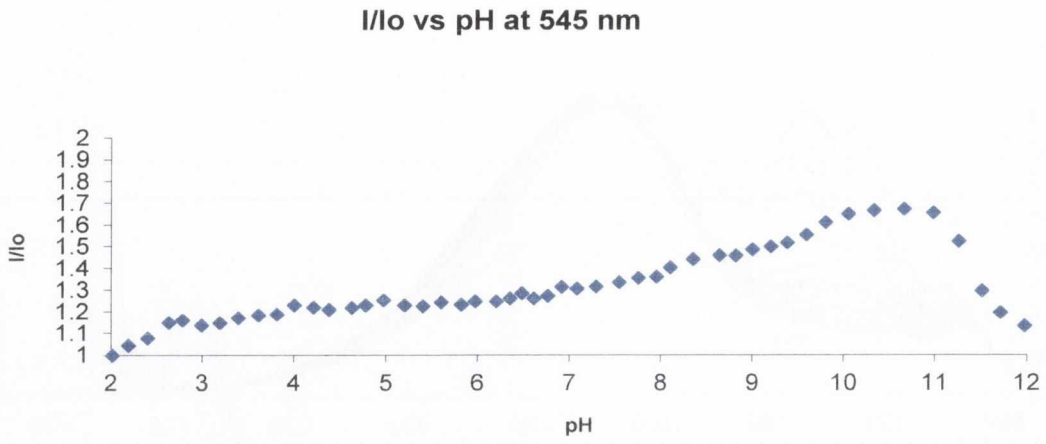

Figure A1.28: *Plot of changes in the emission spectrum of* ***88*** *as a function of pH.*

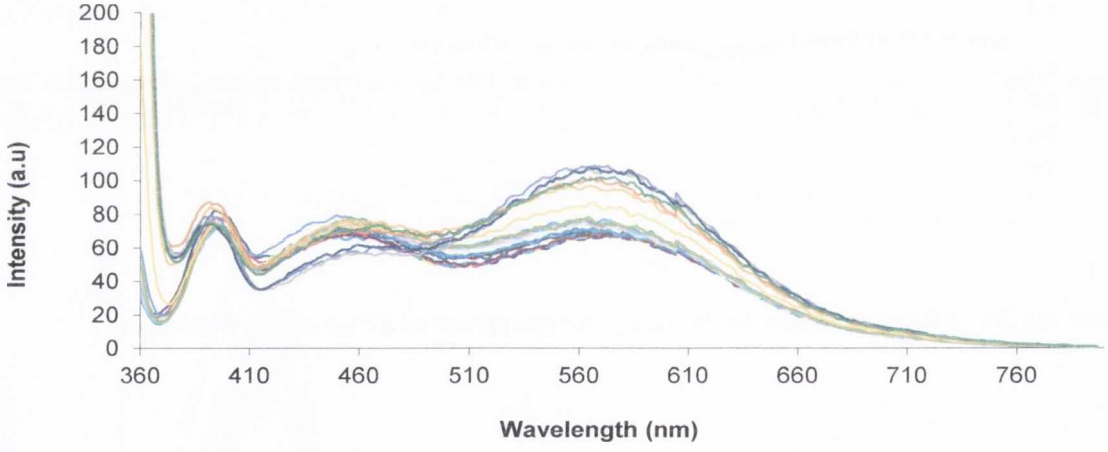

Figure A1.29: *Emission spectrum of* ***90*** *as a function of pH (excitation at 347 nm).*

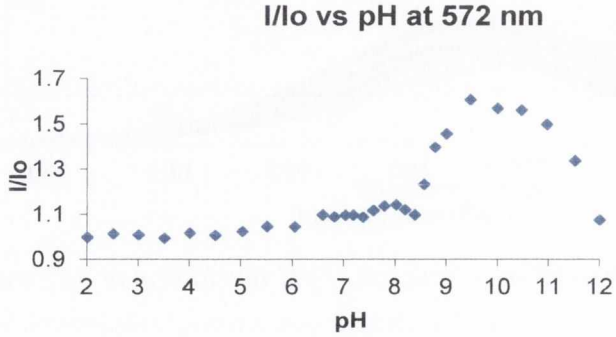

Figure A1.30: Changes in the *emission spectrum of* ***90*** *as a function of pH.*

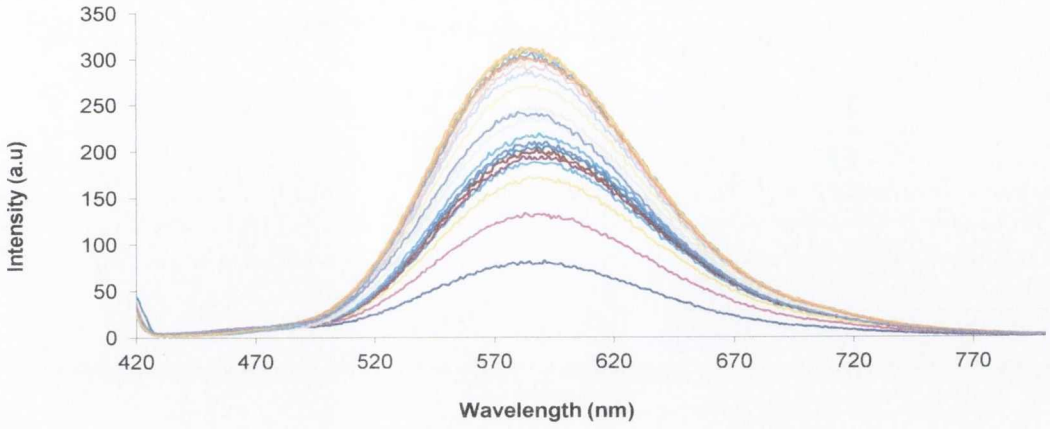

Figure A1.31: Emission spectrum *of* ***103*** *as a function of pH (excitation at 408 nm).*

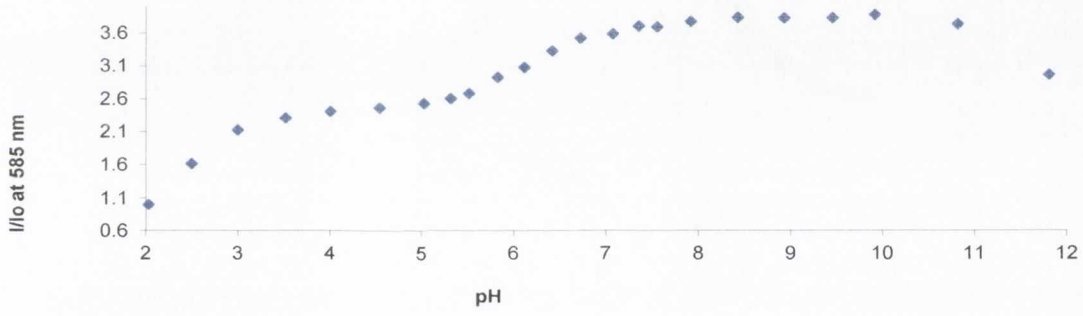

Figure A1.32: Changes in the emission spectrum *of* ***103*** *as a function of pH.*

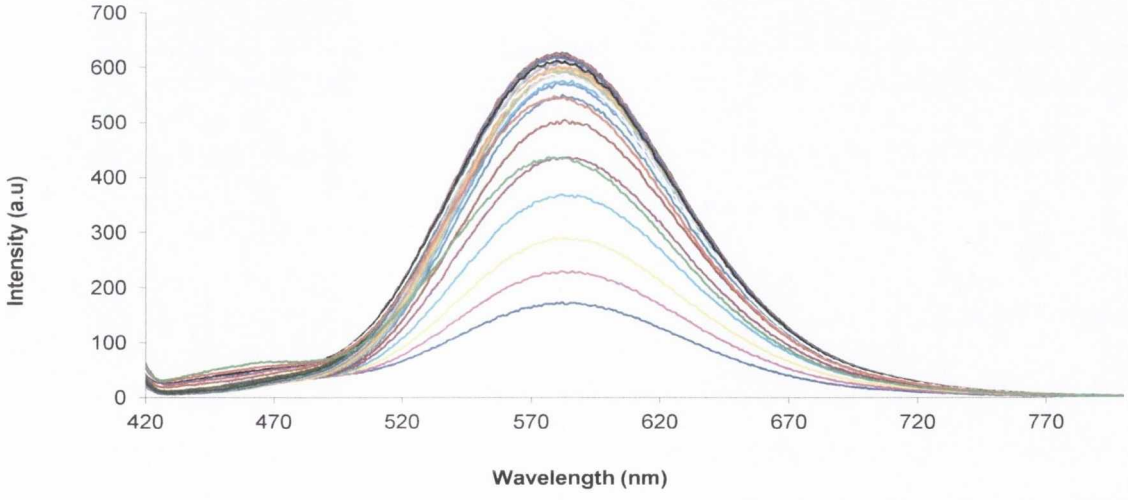

Figure A1.33: *Emission spectrum of* ***104*** *as a function of pH (excitation at 407 nm).*

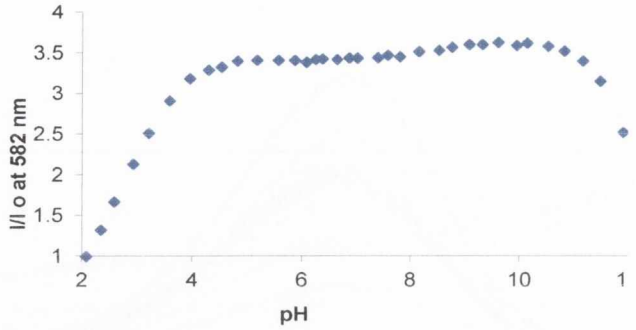

Figure A1.34: *Plot of changes in the emission spectrum of* ***104*** *as a function of pH.*

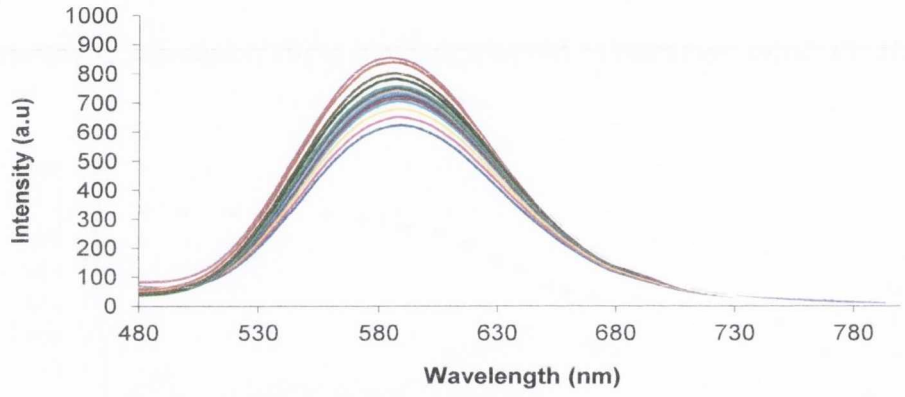

Figure A1.35: *Emission spectrum of* ***106*** *as a function of pH (excitation at 405 nm).*

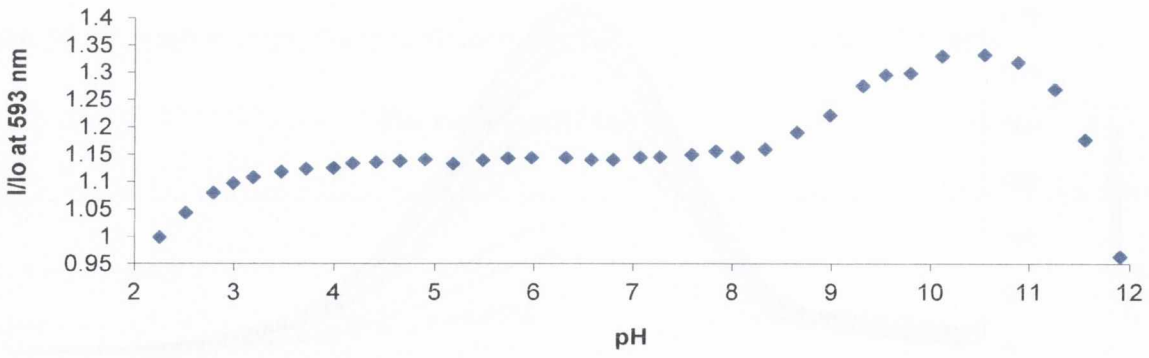

Figure 1A.36: *Plot of changes in the emission spectrum of* ***106*** *as a function of pH.*

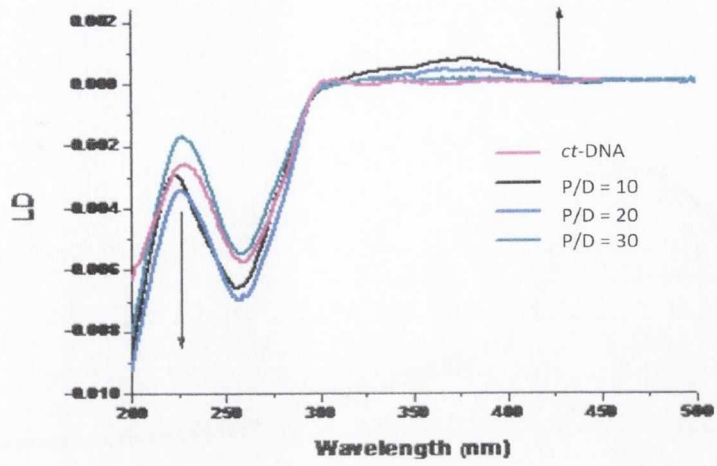

Figure A2.1: *Linear dichroism spectra of ct-DNA in the absence and presence of* ***81*** *at a variety of P/D ratios.*

Molecular Mechanics Modelling

Molecular mechanics (also called MM2-3 calculation) is a mathematical method, which models molecular geometries and their energies by adjusting bond lengths and, bond and torsion angles to an equilibrium, dependent on the hybridisation of the atoms and their bonding capacities.[289] This method relies on the laws of classical Newtonian physics and experimental parameters, manually introduced into the calculation, in order to predict the geometry of the molecules as a function of its steric energy.[289] The resulting set of equations and empirical parameters taken into account for these calculations is called field force and the MM2 and MM3 field forces are expressed in equation (1), in which E_p corresponds to the potential energy of the molecule is defined as the difference between the molecule and the ideal molecule.

$$E_p = \sum E_{bd} + \sum E_{ang} + \sum E_{tor} + \sum E_{bend} + \sum E_{wi} \qquad (1)$$

Consequently, the building of the molecular model consists of the minimisation of E_p, monitored by its gradient, *via* the adjustment of the E_{bd} (bonding energy), E_{ang} (dihedral angle energy), E_{tor} (molecular torsion energy), E_{bend} (bending energy) and E_{wi} (energy of weak interactions such as Van der Waals interactions, ππ-stacking and H-bonding). Consequently, the molecular mechanics approach, which in contrast to semi-empirical methods such as the quantum mechanics and *ab-initio* methods, does not take into account any electronic effects and offers an efficient method in order to predict the shape of supramolecules.[290] These calculations were performed in the MM2 force field using Chem3D version 11.

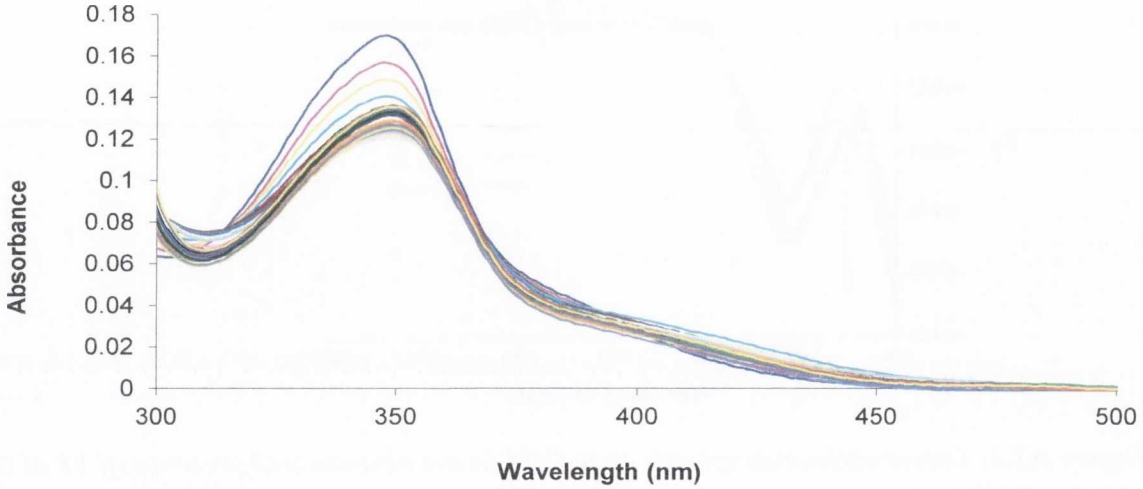

Figure A2.2: *Absorption spectrum of* ***88*** *upon increasing [ct-DNA] IN 10 mM phosphate buffer at pH 7.4.*

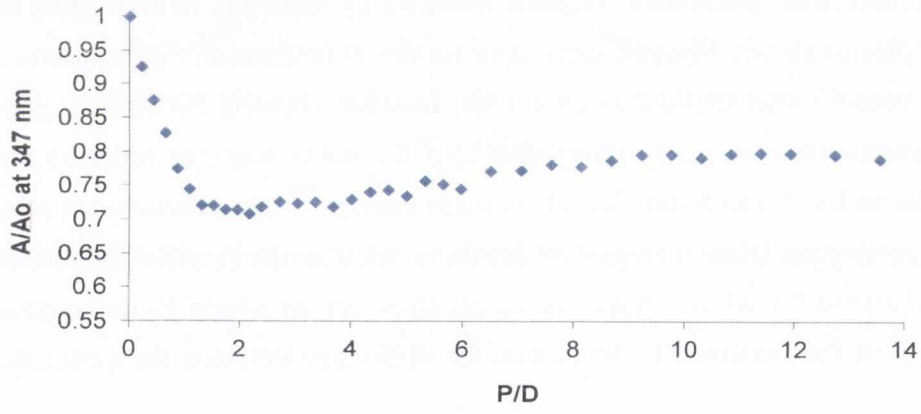

Figure A2.3: Plot of changes in the *absorption spectrum of* ***88*** *as a function of P/D.*

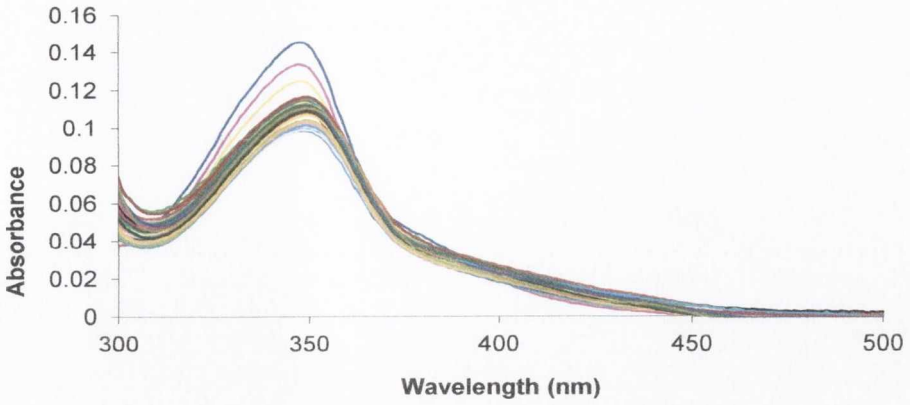

Figure A2.4: *Absorption spectrum of* ***89*** *upon increasing [ct-DNA] in 10 mM phosphate buffer at pH 7.4.*

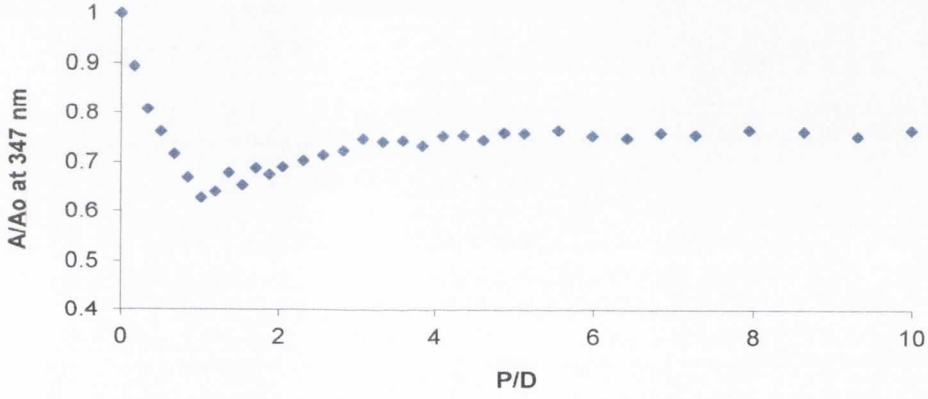

Figure A2.5: *Changes in the absorption spectrum of* ***89*** *as a function of P/D.*

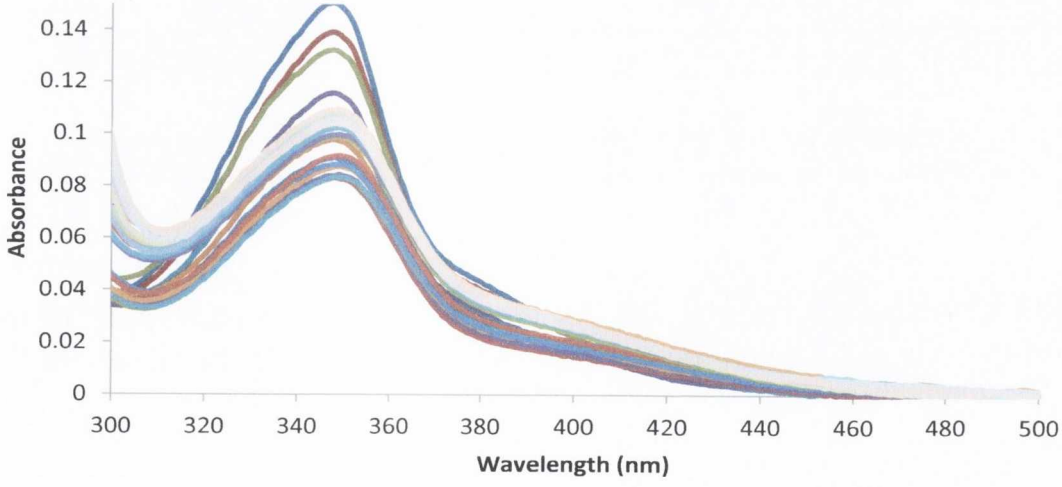

Figure A2.6: *Absorption spectrum of* ***90*** *upon increasing [ct-DNA].*

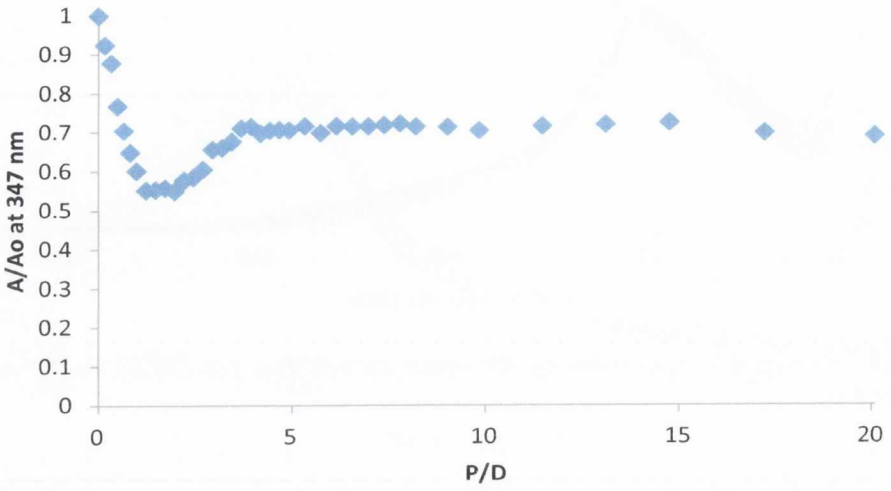

Figure A2.7: Changes in the *absorption spectrum of* ***90*** *as a function of P/D.*

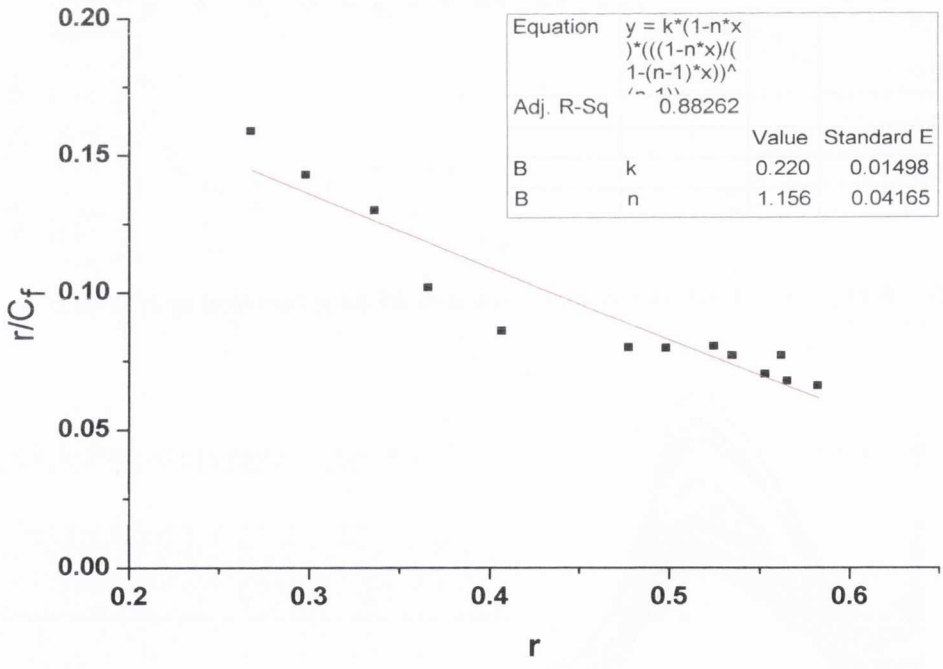

Figure A2.8: *Scatchard plot(◆) and best fit(-) for the emission data for* ***87*** *in 10 mM phosphate buffer (pH 7.4) according to the McGhee and von Hippel binding model.*[195]

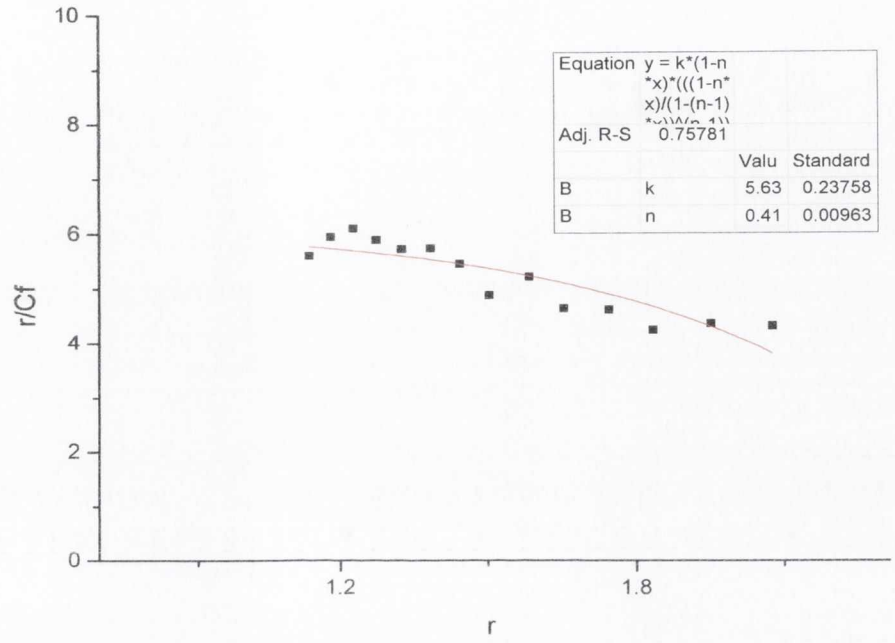

Figure A2.9: *Scatchard plot(◆) and best fit(-) for the emission data for* ***89*** *in 10 mM phosphate buffer (pH 7.4) according to the McGhee and von Hippel binding model.*[195]

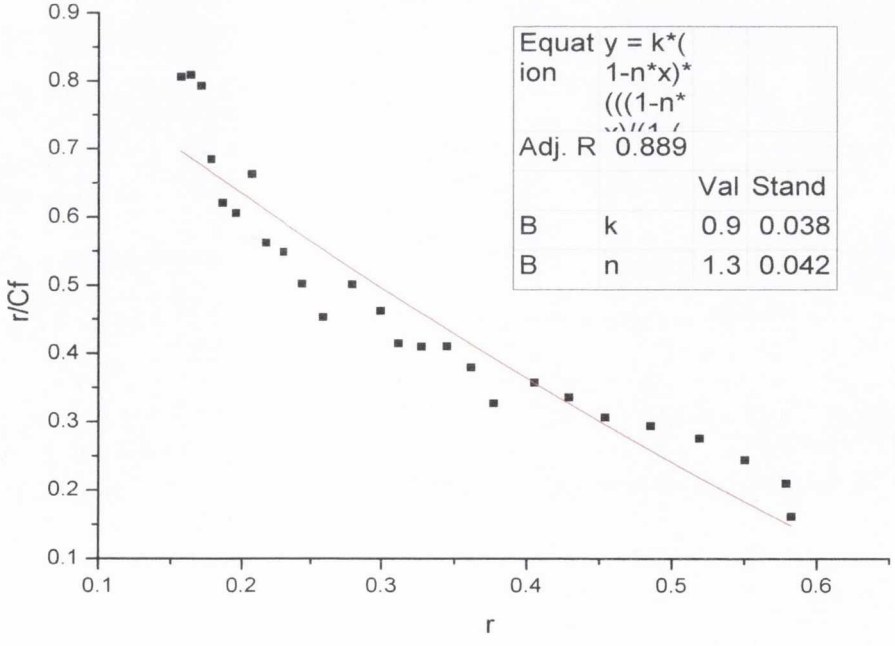

Figure A2.10: *Scatchard plot(◆) and best fit(-) for the emission data for* ***90*** *in 10 mM phosphate buffer (pH 7.4) according to the McGhee and von Hippel binding model.*[195]

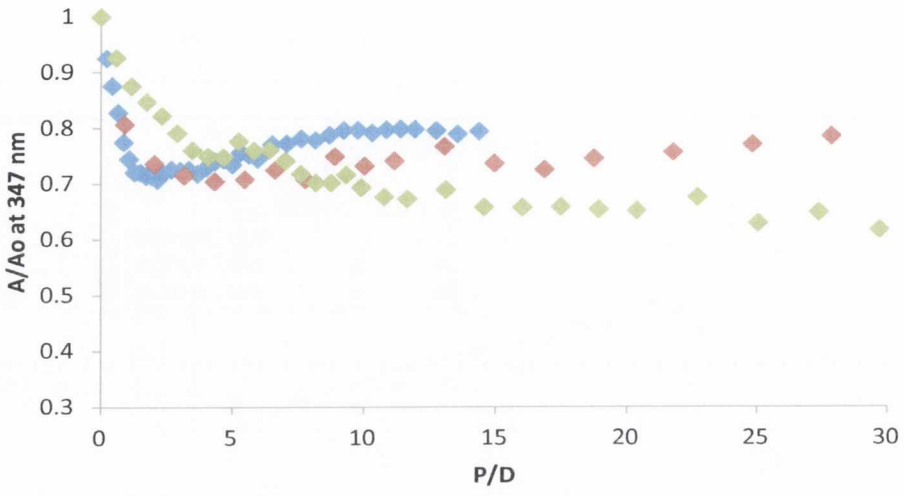

Figure A2.11: *Changes in* the *absorption spectrum of* ***88*** *as a function of P/D in the absence of NaCl (◆), the presence of 50 mM NaCl (◆) and the presence of 160 mM NaCl (◆).*

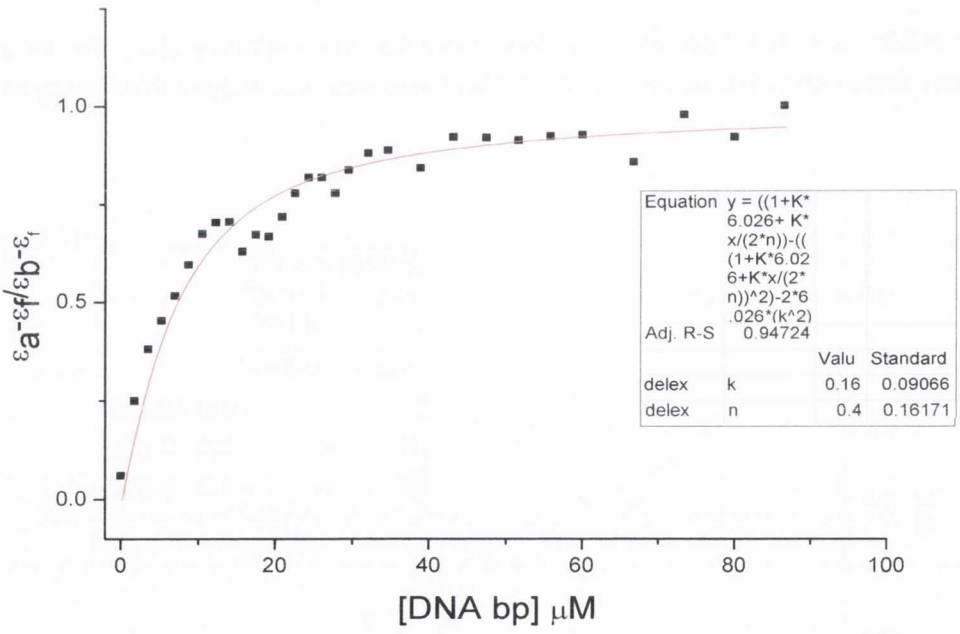

Figure A2.12: *Plot of* $(\varepsilon_a - \varepsilon_f)/(\varepsilon_a - \varepsilon_f)$ *versus [ct-DNA] in base pairs (◆) and the best fit for the data (-) for* ***88*** *in 10 mM phosphate buffer + 50 mM NaCl according to the Bard binding model.*[194]

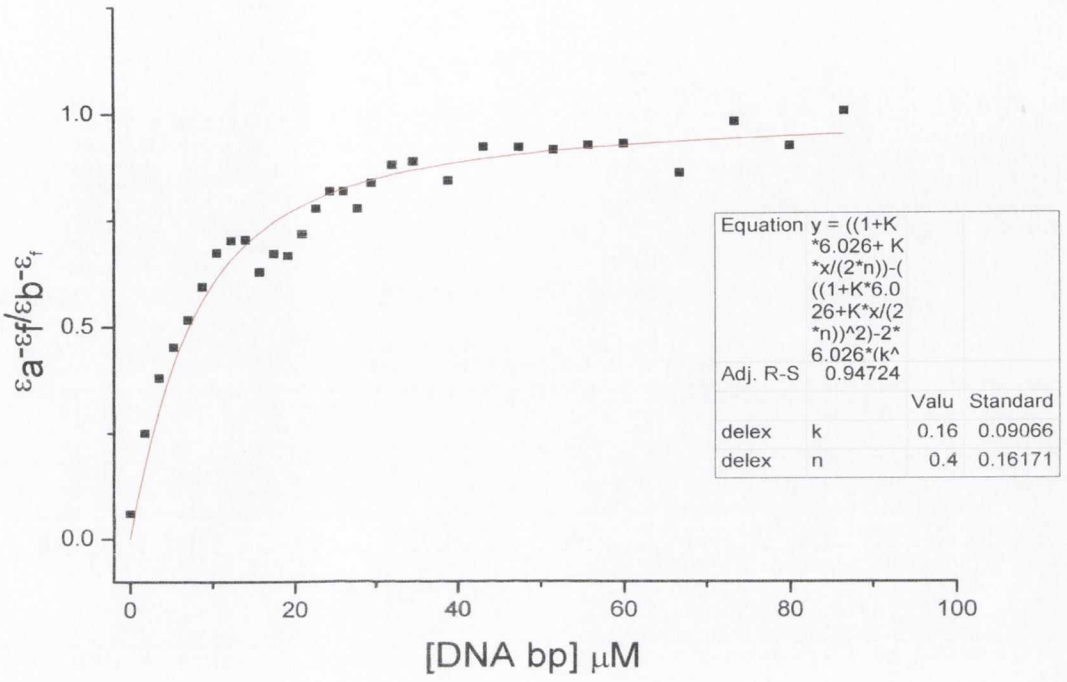

Figure A2.13: *Plot of* $(\varepsilon_a - \varepsilon_f)/(\varepsilon_a - \varepsilon_f)$ *versus [ct-DNA] in base pairs (◆) and the best fit for the data (-) for* ***88*** *in 10 mM phosphate buffer + 160 mM NaCl according to the Bard binding model.*[194]

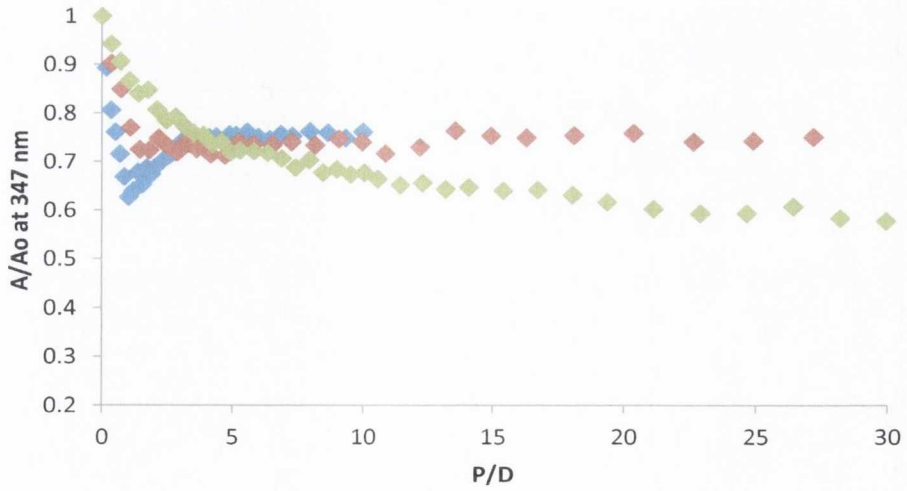

Figure A2.14: *Changes in* the *absorption spectrum of* ***89*** *as a function of P/D in the absence of NaCl (◆), the presence of 50 mM NaCl (◆) and the presence of 160 mM NaCl (◆).*

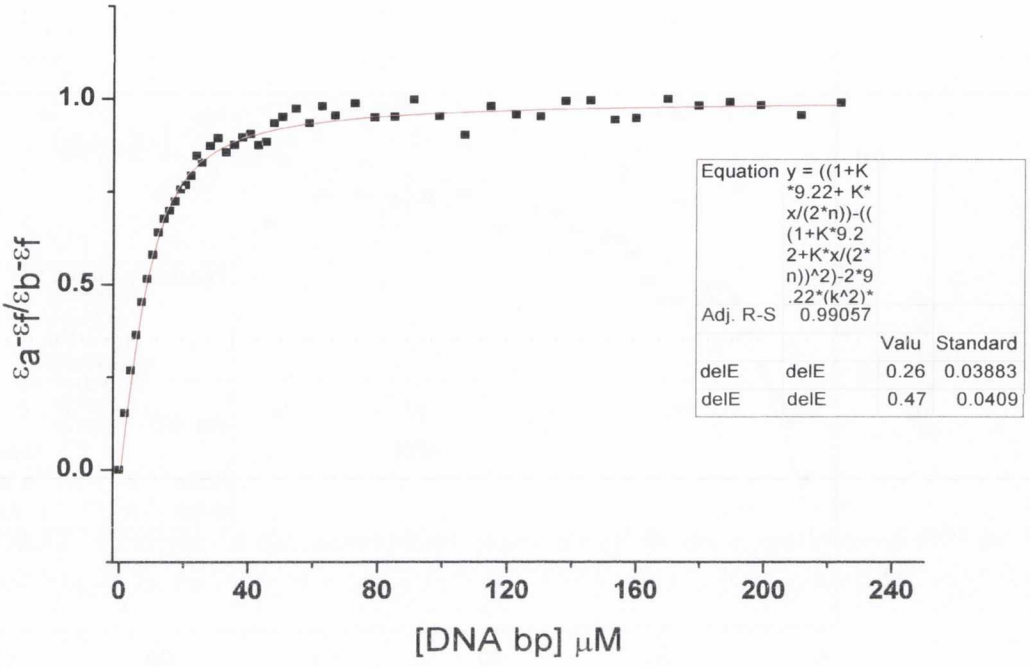

Figure A2.15: *Plot of* $(\varepsilon_a - \varepsilon_f)/(\varepsilon_a - \varepsilon_f)$ *versus [ct-DNA] in base pairs (◆) and the best fit for the data (-) for* ***89*** *in 10 mM phosphate buffer + 50 mM NaCl according to the Bard binding model.*[194]

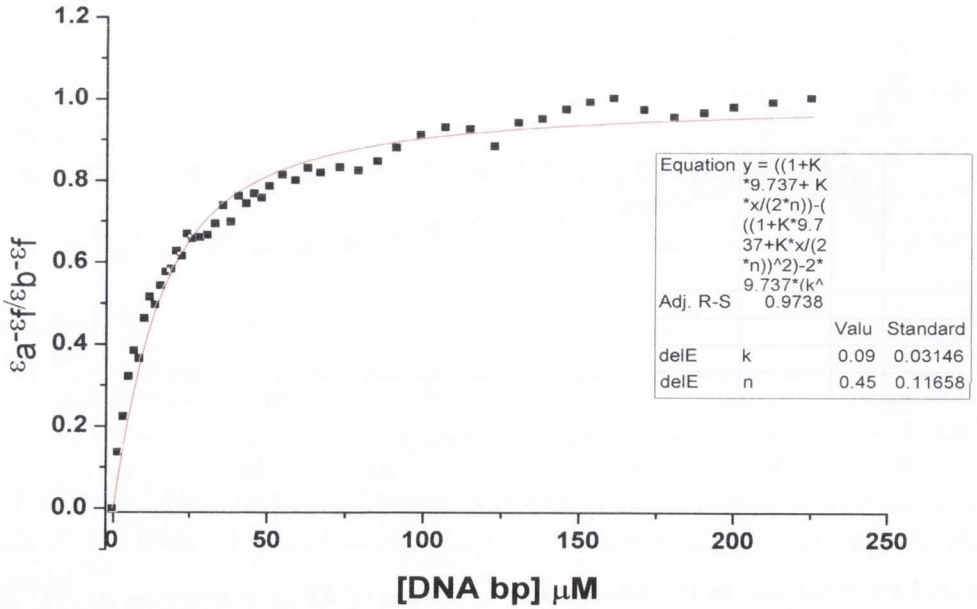

Figure A2.16: *Plot of* $(\varepsilon_a - \varepsilon_f)/(\varepsilon_a - \varepsilon_f)$ *versus [ct-DNA] in base pairs (◆) and the best fit for the data (-) for* ***89*** *in 10 mM phosphate buffer + 160 mM NaCl according to the Bard binding model.*[194]

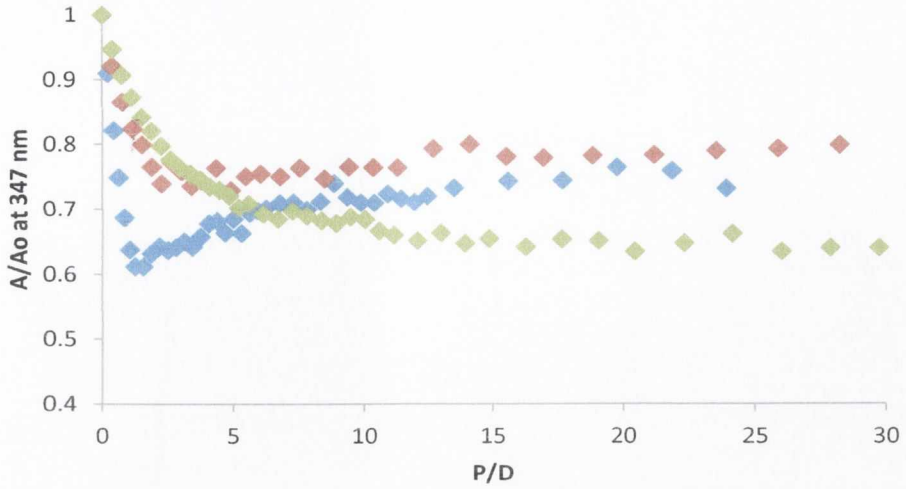

Figure A2.17: *Changes in* the *absorption spectrum of* ***90*** *as a function of P/D in the absence of NaCl (◆), the presence of 50 mM NaCl (◆) and the presence of 160 mM NaCl*

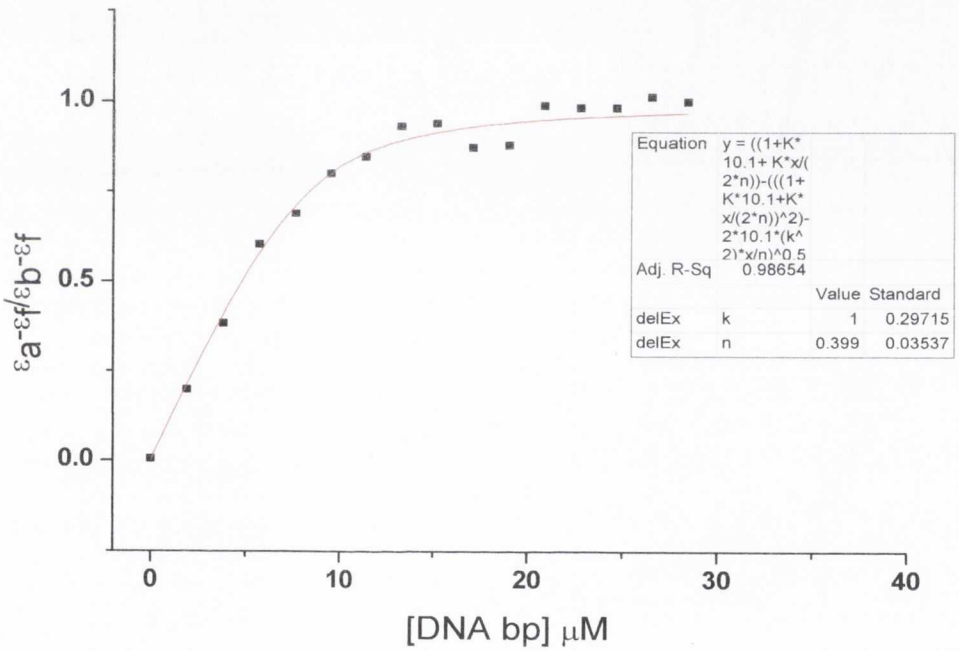

Figure A2.18: *Plot of* $(\varepsilon_a - \varepsilon_f)/(\varepsilon_a - \varepsilon_f)$ *versus [ct-DNA] in base pairs (◆) and the best fit for the data (-) for* ***90*** *in 10 mM phosphate buffer + 50 mM NaCl according to the Bard binding model.*[194]

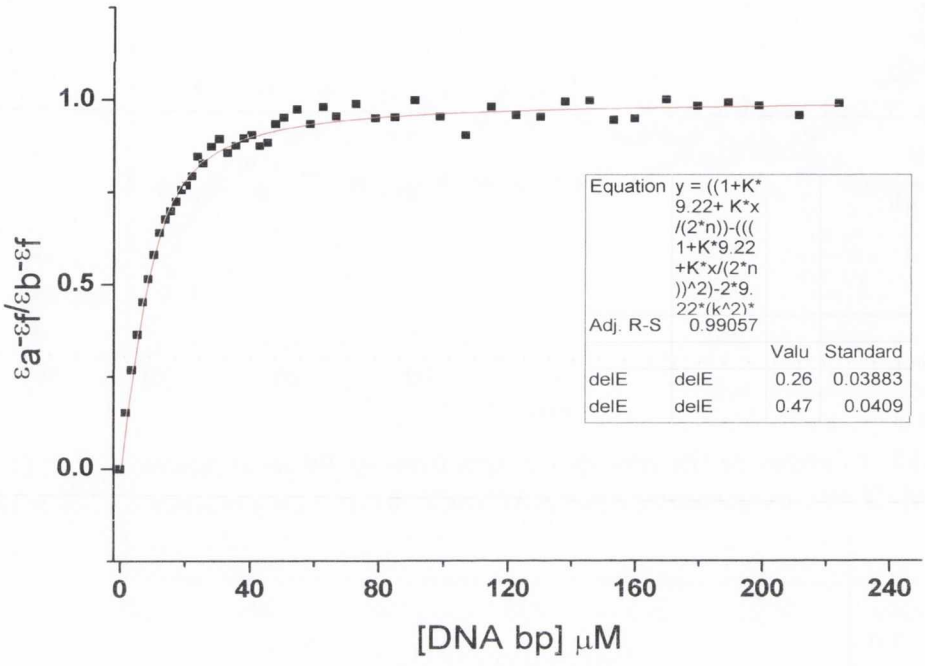

Figure A2.19: *Plot of* $(\varepsilon_a - \varepsilon_f)/(\varepsilon_a - \varepsilon_f)$ *versus [ct-DNA] in base pairs (◆) and the best fit for the data (-) for* ***90*** *in 10 mM phosphate buffer + 160 mM NaCl according to the Bard binding model.*[194]

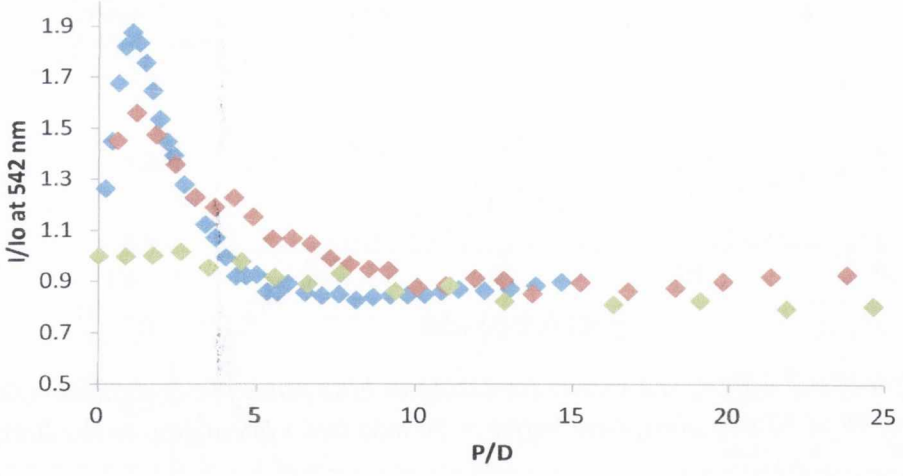

Figure A2.20: *Changes in* the *absorption spectrum of* ***88*** *as a function of P/D in the absence of NaCl (◆), the presence of 50 mM NaCl (◆) and the presence of 160 mM NaCl (◆).*

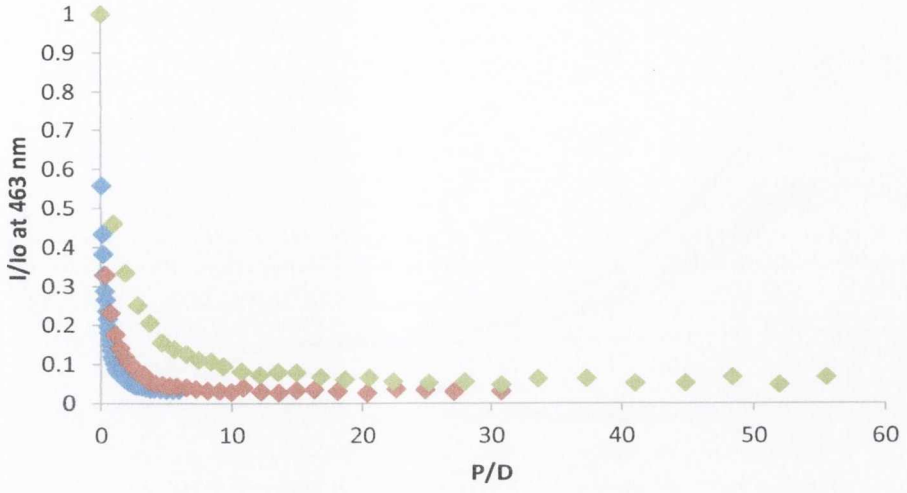

Figure A2.21: *Changes in* the *absorption spectrum of* ***89*** *as a function of P/D in the absence of NaCl (◆), the presence of 50 mM NaCl (◆) and the presence of 160 mM NaCl (◆).*

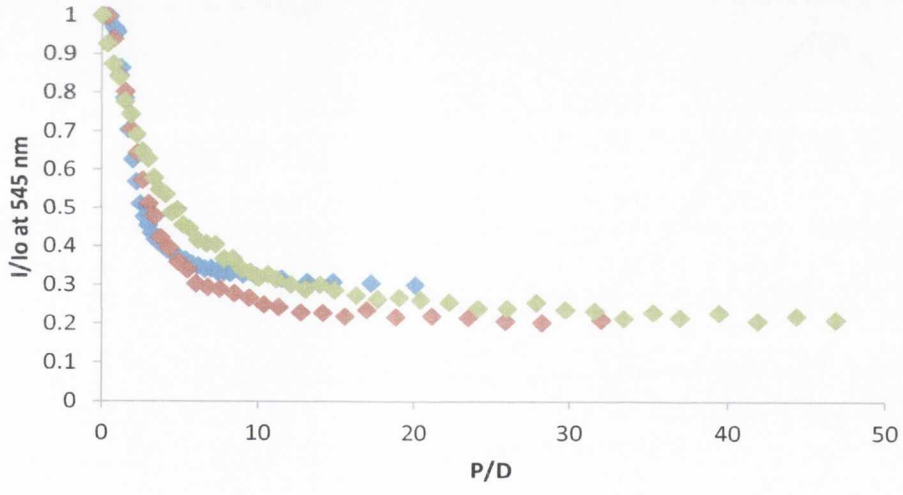

Figure A2.22: *Changes in* the *absorption spectrum of* ***90*** *as a function of P/D in the absence of NaCl (◆), the presence of 50 mM NaCl (◆) and the presence of 160 mM NaCl (◆).*

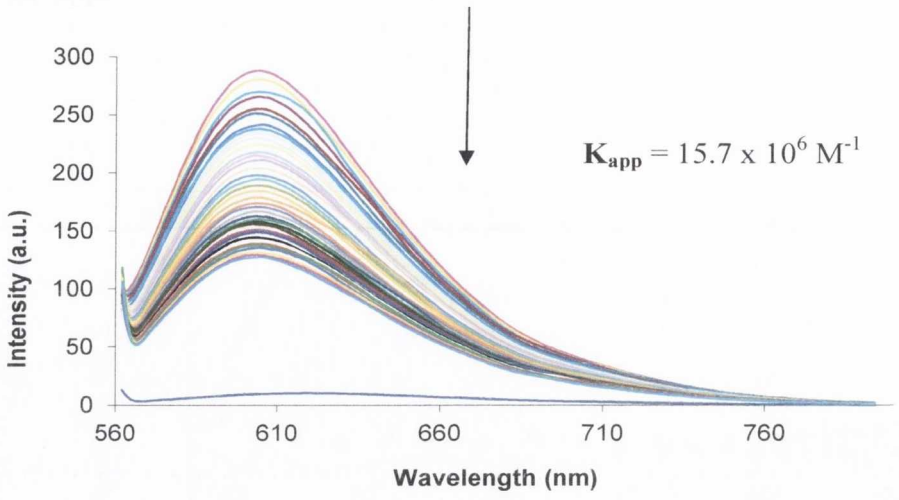

Figure A2.23: *The emission spectra of ethidium bromide, free and bound to ct-DNA (0.44 μM: 0.88 μM) in 10 mM phosphate buffer (pH 7.4) upon the addition of* ***86*** *with an excitation at 545 nm*

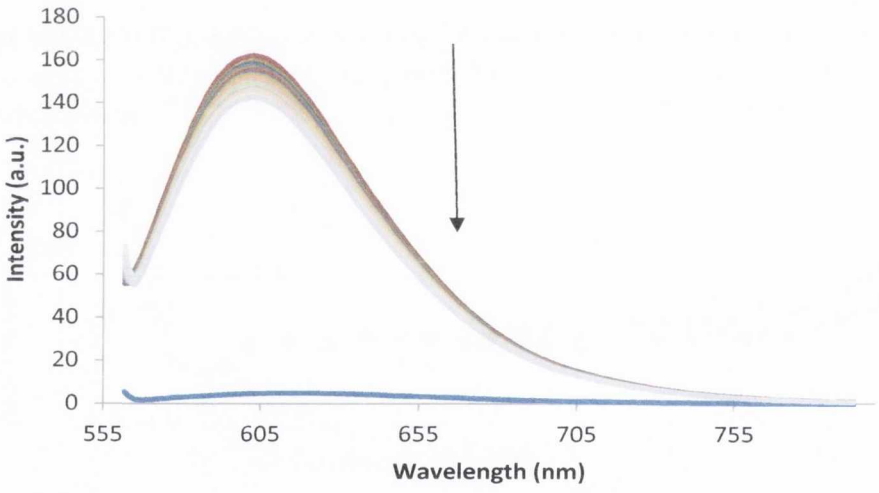

Figure A2.24: *The emission spectra of ethidium bromide, free and bound to ct-DNA (0.44 μM: 0.88 μM) in 10 mM phosphate buffer (pH 7.4) upon the addition of* ***87*** *with an excitation at 545 nm*

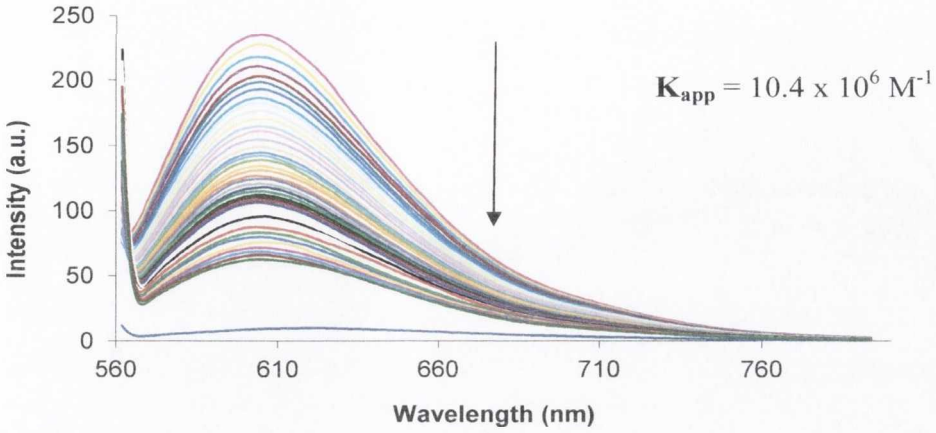

Figure A2.25: *The emission spectra of ethidium bromide, free and bound to ct-DNA (0.44 μM: 0.88 μM) in 10 mM phosphate buffer (pH 7.4) upon the addition of* ***88*** *with an excitation at 545 nm*

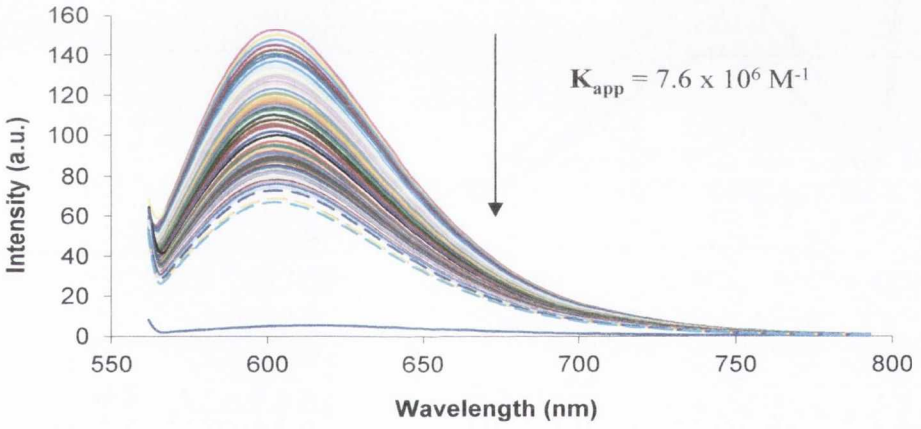

Figure A2.26: *The emission spectra of ethidium bromide, free and bound to ct-DNA (0.44 μM: 0.88 μM) in 10 mM phosphate buffer (pH 7.4) upon the addition of* ***89*** *with an excitation at 545 nm*

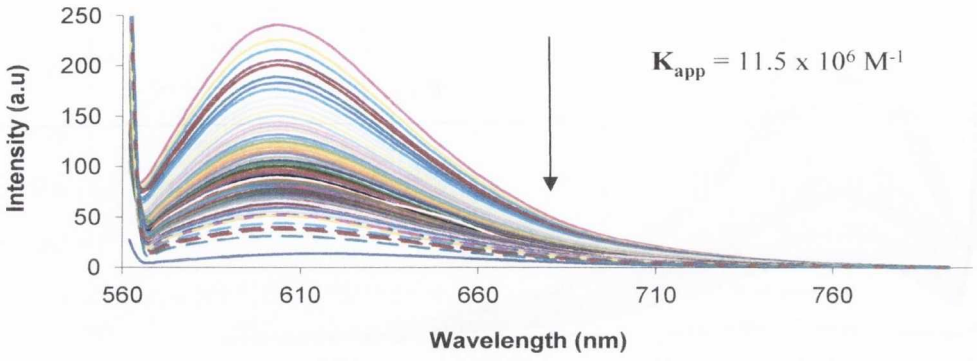

Figure A2.27: *The emission spectra of ethidium bromide, free and bound to ct-DNA (0.44 μM: 0.88 μM) in 10 mM phosphate buffer (pH 7.4) upon the addition of* ***90*** *with an excitation at 545 nm*

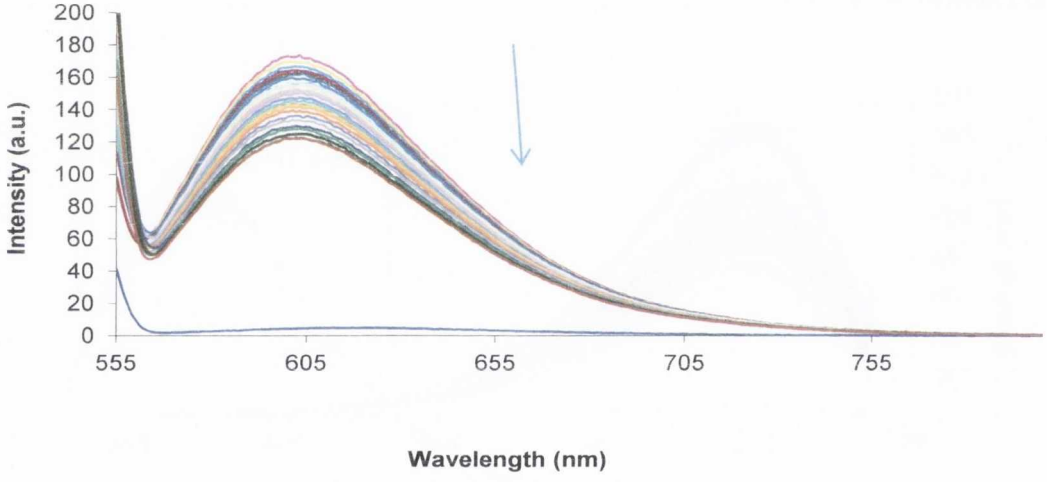

Figure A2.28: *The emission spectra of ethidium bromide, free and bound to ct-DNA (0.44 μM: 0.88 μM) in 10 mM phosphate buffer (pH 7.4) upon the addition of* ***20*** *with an excitation at 545 nm*

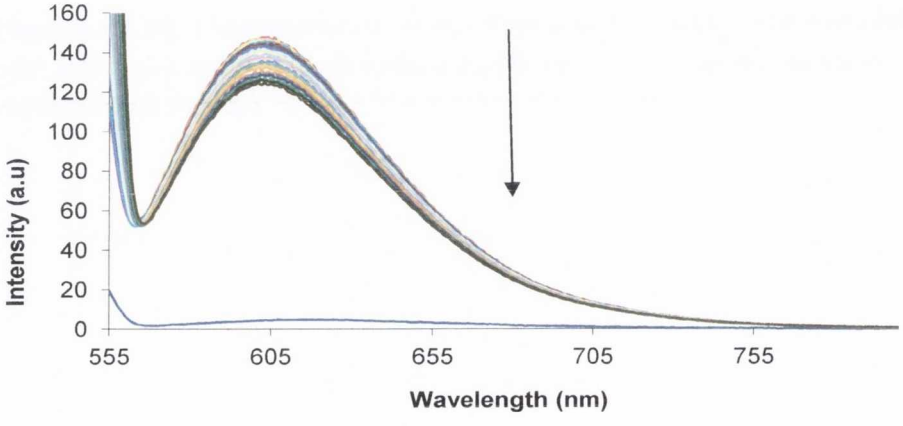

Figure A2.29: *The emission spectra of ethidium bromide, free and bound to ct-DNA (0.44 μM: 0.88 μM) in 10 mM phosphate buffer (pH 7.4) upon the addition of* ***103*** *with an excitation at 545 nm*

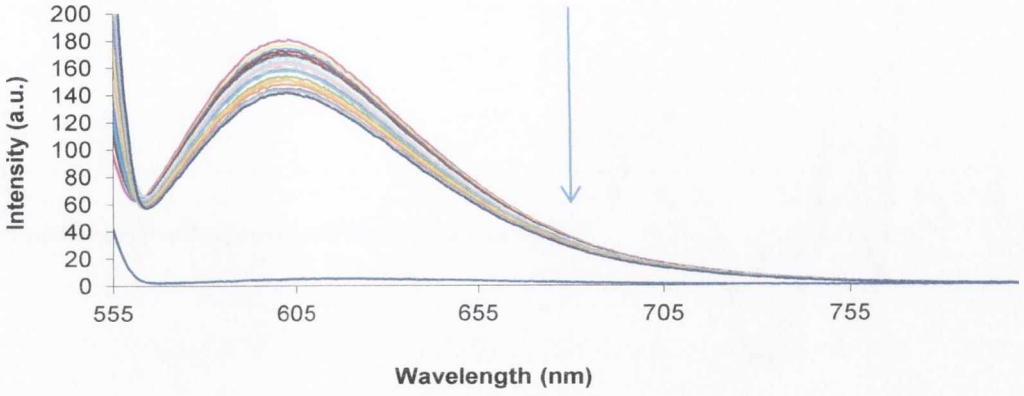

Figure A2.30: *The emission spectra of ethidium bromide, free and bound to ct-DNA (0.44 μM: 0.88 μM) in 10 mM phosphate buffer (pH 7.4) upon the addition of* ***104*** *with an excitation at 545 nm*

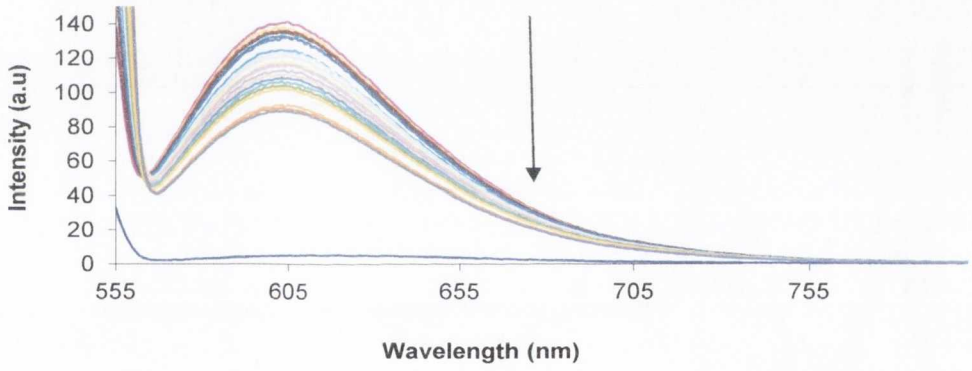

Figure A2.31: *The emission spectra of ethidium bromide, free and bound to ct-DNA (0.44 μM: 0.88 μM) in 10 mM phosphate buffer (pH 7.4) upon the addition of* ***105*** *with an excitation at 545 nm*

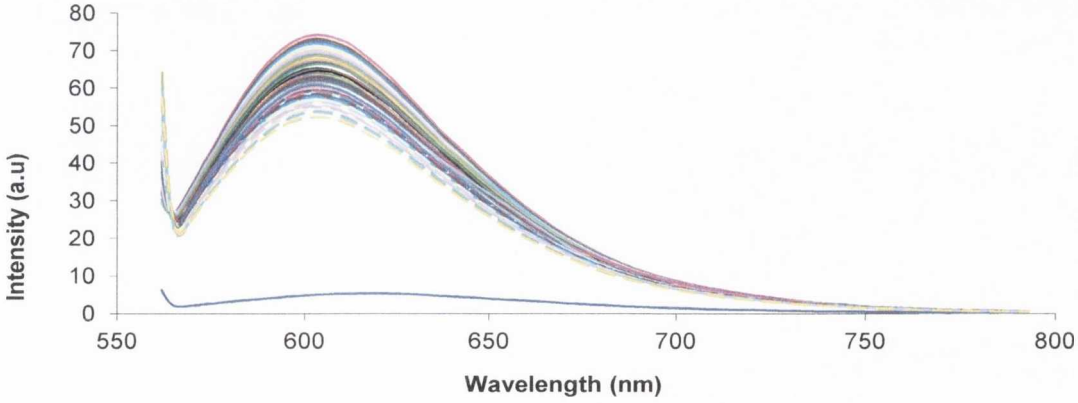

Figure A2.32: *The emission spectra of ethidium bromide, free and bound to ct-DNA (0.44 μM: 0.88 μM) in 10 mM phosphate buffer (pH 7.4) upon the addition of* ***106*** *with an excitation at 545 nm*

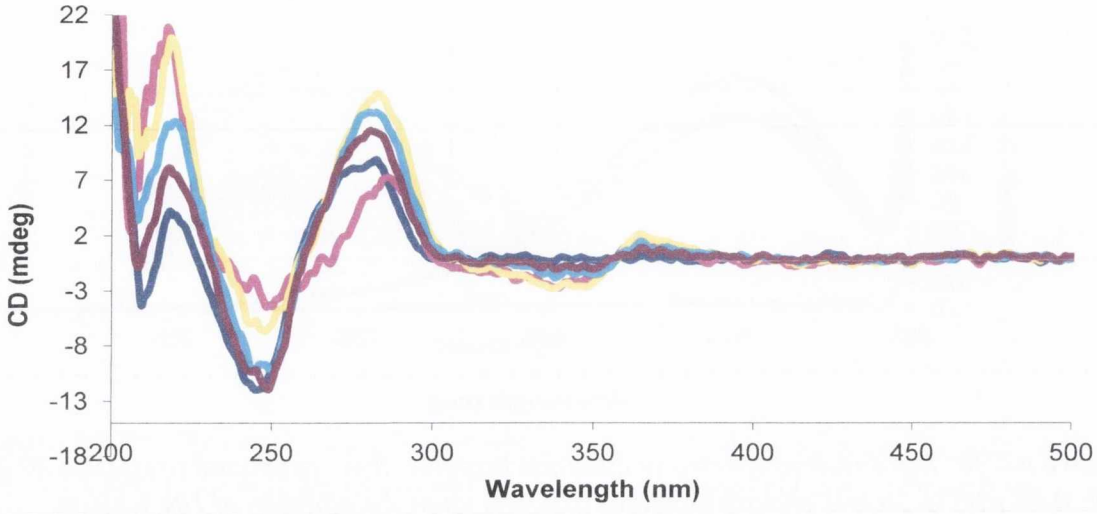

Figure 2A.33: *CD spectra of ct-DNA (150 μM) (-) in the presence of* ***86*** *at P/D ratios of 2.5 (-), 5 (-), 10(-) and 20 (-).*

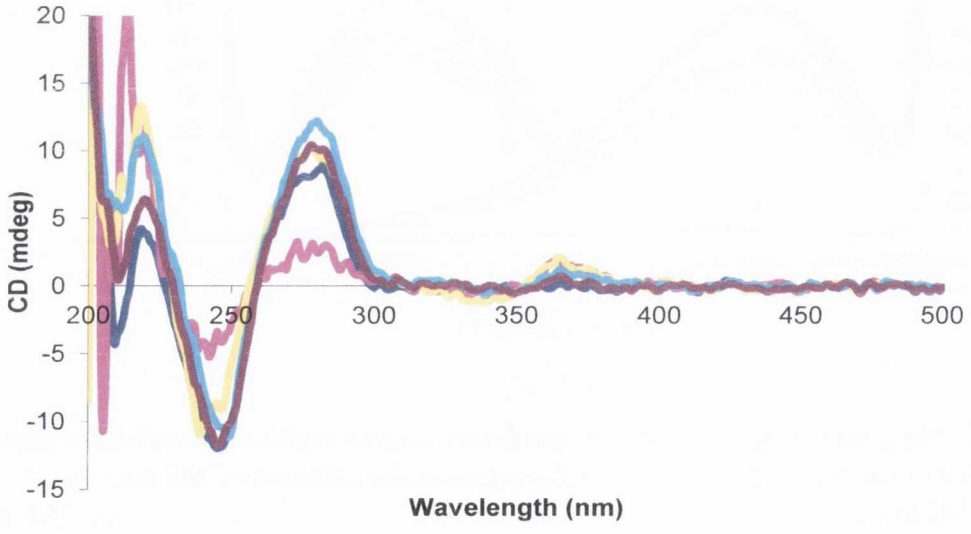

Figure 2A.34: *CD spectra of ct-DNA (150 μM) (-) in the presence of* ***88*** *at P/D ratios of 2.5 (-), 5 (-), 10(-) and 20 (-).*

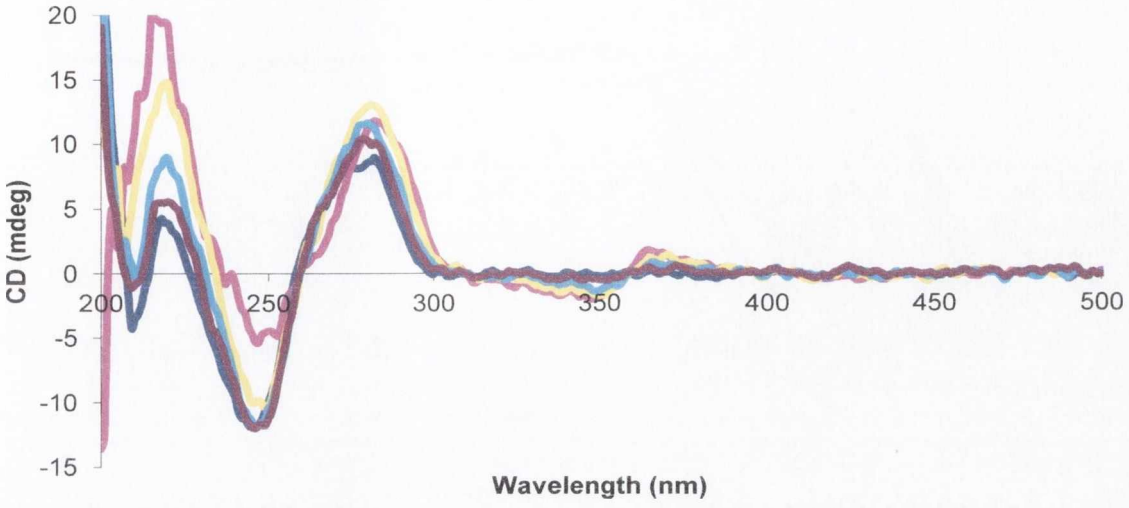

Figure 2A.35: *CD spectra of ct-DNA (150 μM) (-) in the presence of* ***89*** *at P/D ratios of 2.5 (-), 5 (-), 10(-) and 20 (-) in phosphate buffer (pH 7.4)*

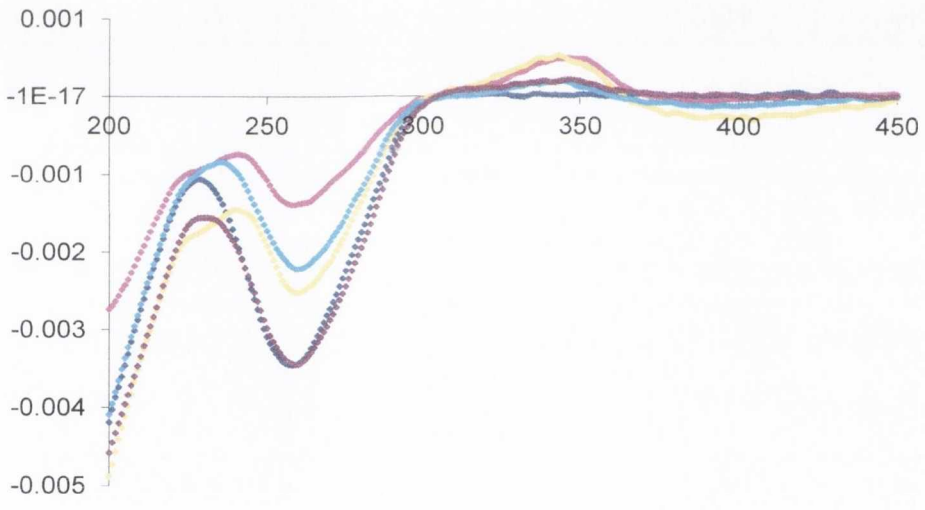

Figure 2A.36: *LD spectra of ct-DNA (379 μM) (◆) in the presence of* ***86*** *at P/D ratios of 2.5 (◆), 5 (◆), 10(◆) and 20 (◆) in phosphate buffer (pH 7.4).*

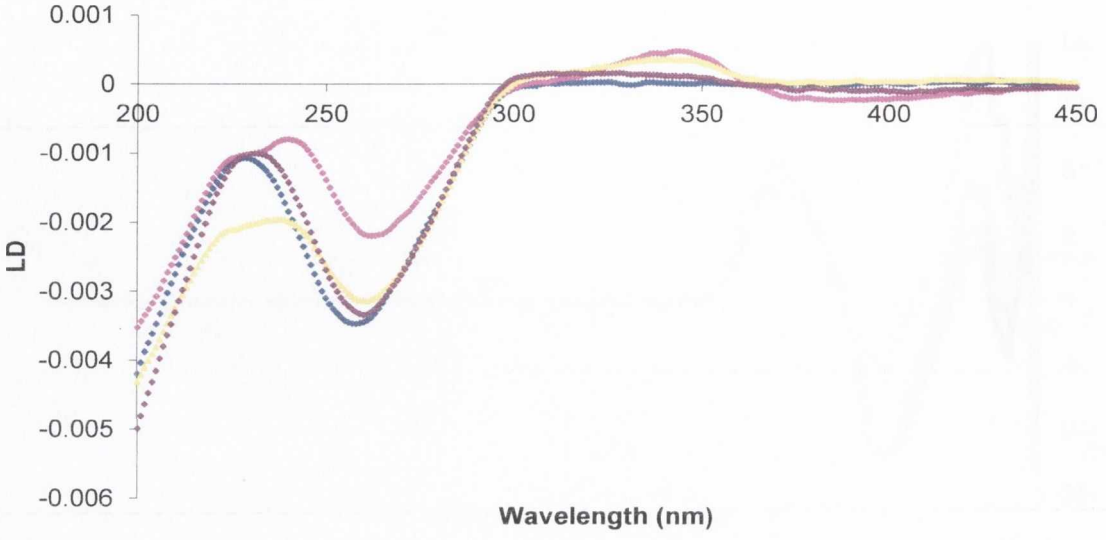

Figure 2A.37: *LD spectra of ct-DNA (379 μM) (◆) in the presence of* ***89*** *at P/D ratios of 2.5 (◆), 5 (◆), and 20 (◆) in phosphate buffer (pH 7.4).*

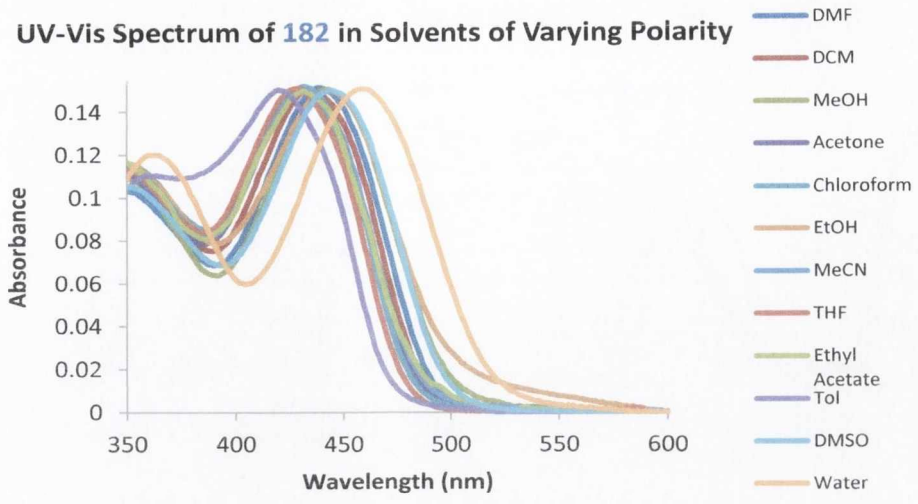

Figure A3.1: *Absorption spectra of 182 in solvents of varying polarity.*

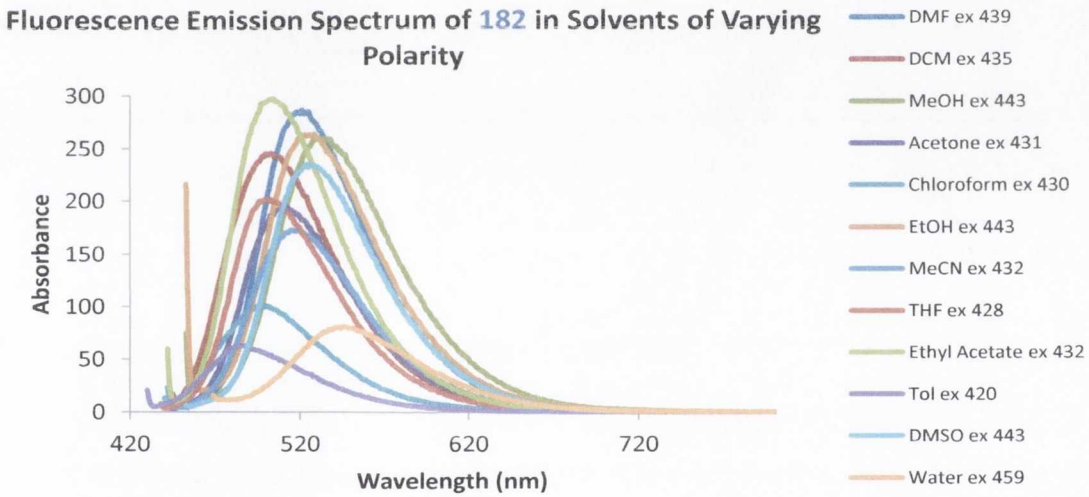

Figure A3.2: *Emission spectra of 182 in solvents of varying polarity. Excitation wavelengths can be found in the legend.*

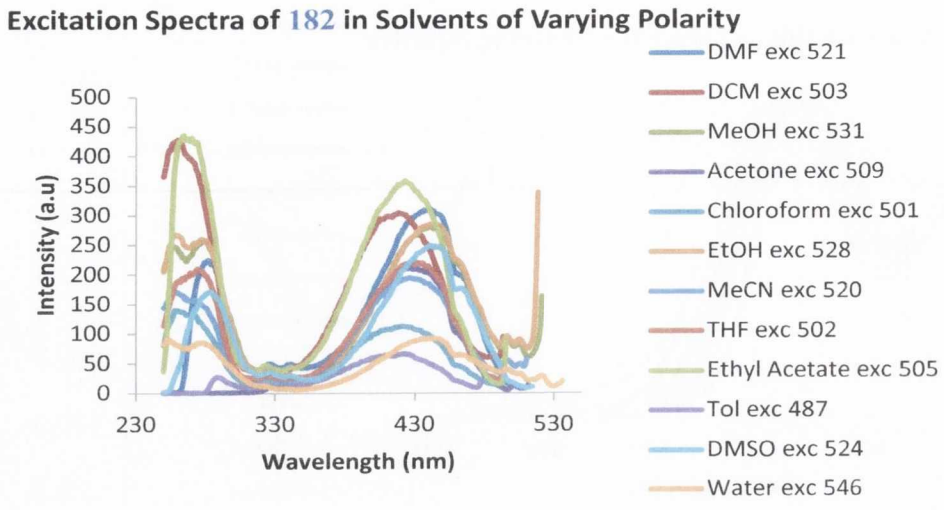

Figure A3.3: *Excitation spectra of 182 in solvents of varying polarity.*

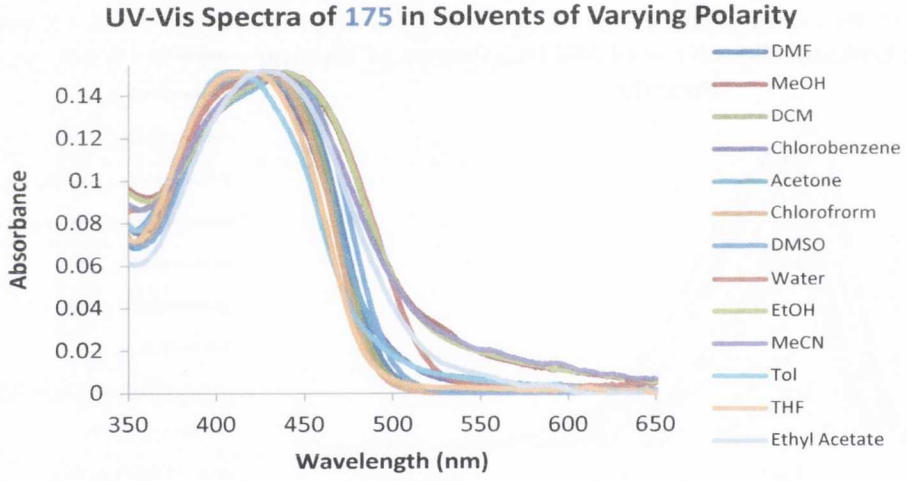

Figure A3.4: *Absorption spectra of 175 in solvents of varying polarity.*

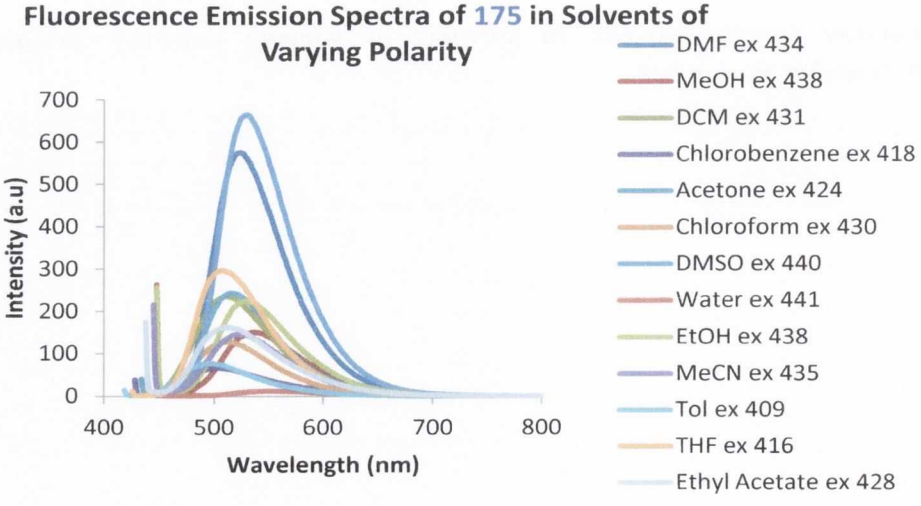

Figure A3.5: *Emission spectra of 175 in solvents of varying polarity. Excitation wavelengths can be found in the legend.*

Table 3.A.1: *Summary of the photophysical properties of 175.*

Solvent	$\lambda_{max\ UV}$ (nm)	$\lambda_{max\ FLU}$ (nm)	τ (ns)
DMF	434	524	2.07, 6.22
MeOH	438	535	2.19, 5.97
DCM	431	513	No accurate determination was achieved.
Chlorobenzene	418	503	No accurate determination was achieved.
Acetone	424	515	1.22, 8.22
Chloroform	430	511	No accurate determination was achieved.
DMSO	440	530	2.52, 6.87
Water	441	554	No accurate determination was achieved.
EtOH	438	529	2.24, 5.97
MeCN	435	521	1.55, 8.40
Tol	409	496	0.96, 7.95
THF	416	507	1.30, 6.93
Ethyl Acetate	428	513	0.74, 9.24

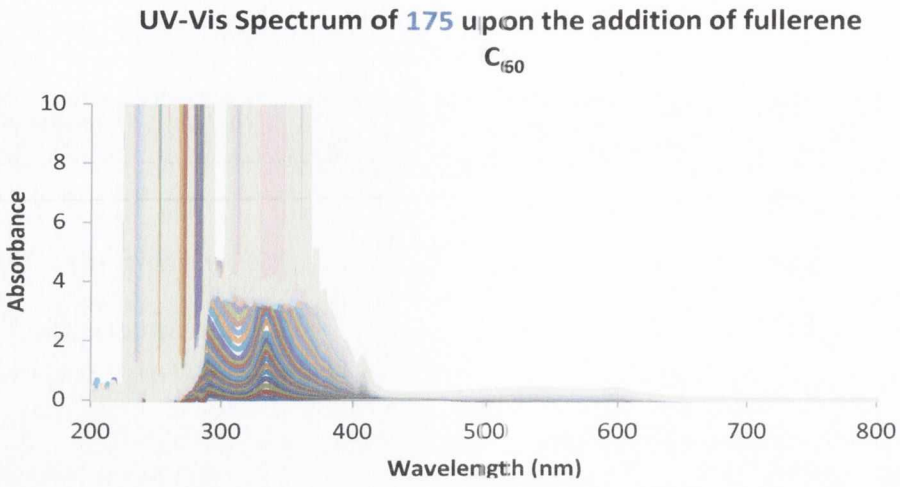

Figure A3.6: *Absorption spectrum of 175 upon the addition of* C_{60}.